THE JOURNAL OF

PHYSICAL CHEMISTRY

Volume 72

SEPTEMBER—DECEMBER 1968

PAGES 3073—4758

EASTON, PA.
MACK PRINTING COMPANY
1968

THE JOURNAL OF

PHYSICAL CHEMISTRY

Volume 72, Number 9 September 1968

Surface Tension of Some Binary Liquid Mixtures . . . . . **S. K. Suri and V. Ramakrishna** 3073

Ionic Reactions in Unsaturated Compounds. II. Ethylene . . . . **Thomas O. Tiernan and Jean H. Futrell** 3080

Raman Spectra of Fused Indium and Bismuth Chlorides . . . . . **J. T. Kenney and F. X. Powell** 3094

Water Adsorption and Dielectric Properties of Lyophilized Hemoglobin . . . **G. Brausse, A. Mayer, T. Nedetzka, P. Schlect, and H. Vogel** 3098

The Photolysis of Carbon Suboxide in the Presence of Hydrogen . . . . . **Alain Forchioni and Clive Willis** 3105

A Proton Magnetic Resonance Study of Hydrogen Bonding in Aliphatic Secondary Amines . . . **Ruth Ann Murphy and Jeff C. Davis, Jr.** 3111

The Crystal Structures of Bismuth Halide Complex Salts. III. Tris(dimethylammonium) Hexabromobismuthate(III), $[(CH_3)_2NH_2]_3BiBr_6$ . . . . . **W. Gant McPherson and Edward A. Meyers** 3117

Ionization Equilibria in Ammonia–Water Solutions to 700° and to 4000 Bars of Pressure . . . **Arvin S. Quist and William L. Marshall** 3122

Continuum Emission from Xenon in the Vapor Phase Induced by Absorption of 1470-Å Radiation . . . **L. Wayne Sieck** 3129

Carbon Monoxide Oxidation with an Oxygen Tracer over a Vanadium Pentoxide Catalyst . . . **Kozo Hirota, Yoshiya Kera, and Shousuke Teratani** 3133

Kinetics and Mechanism of the Decarboxylation of Anthranilic Acid in Aqueous Solution . . . **Alfred V. Willi, Chong Min Won, and Paul Vilk** 3142

Kinetics of the Bromine-Exchange Reaction of Gallium Bromide with Ethyl Bromide in 1,2,4-Trichlorobenzene and in Nitrobenzene . . . . . **Oh Cheun Kwun and Sang Up Choi** 3148

The Paramagnetic Species from Titanous Salts and Hydrogen Peroxide . . . **Roland E. Florin, Fred Sicilio, and Leo A. Wall** 3154

Infrared Study of the Surface Properties of Phosphoric Acid Impregnated Silica . . . **M. J. D. Low and P. Ramamurthy** 3161

The Kinetics of the Hydrogen–Fluorine Reaction. III. The Photochemical Reaction . . . **Joseph B. Levy and B. K. W. Copeland** 3168

Ultrasonic Absorption and the Kinetics of Conformational Change in Poly-L-lysine . . . **R. C. Parker, L. J. Slutsky, and K. R. Applegate** 3177

Electron Spin Resonance Studies of Carbon Dispersed on Alumina . . . . **Pierre A. Berger and James F. Roth** 3186

Proton-Transfer Complexes. I. Preferential Solvation of *p*-Nitrophenol–Amine Complexes in Nonaqueous-Solvent Mixtures . . . . . **Ronald Scott, Dennis De Palma, and Serge Vinogradov** 3192

The Sintering of Porous Glass: Benzene Adsorption by Heat-Treated Porous Glasses . . . **D. A. Cadenhead and D. H. Everett** 3201

The Thermochemistry of the Gas-Phase Equilibria *trans*-1,2-Diiodoethylene $\rightleftarrows$ Acetylene + I_2 and *trans*-1,2-Diiodoethylene $\rightleftarrows$ *cis*-1,2-Diiodoethylene . . . **Shozo Furuyama, David M. Golden, and Sidney W. Benson** 3204

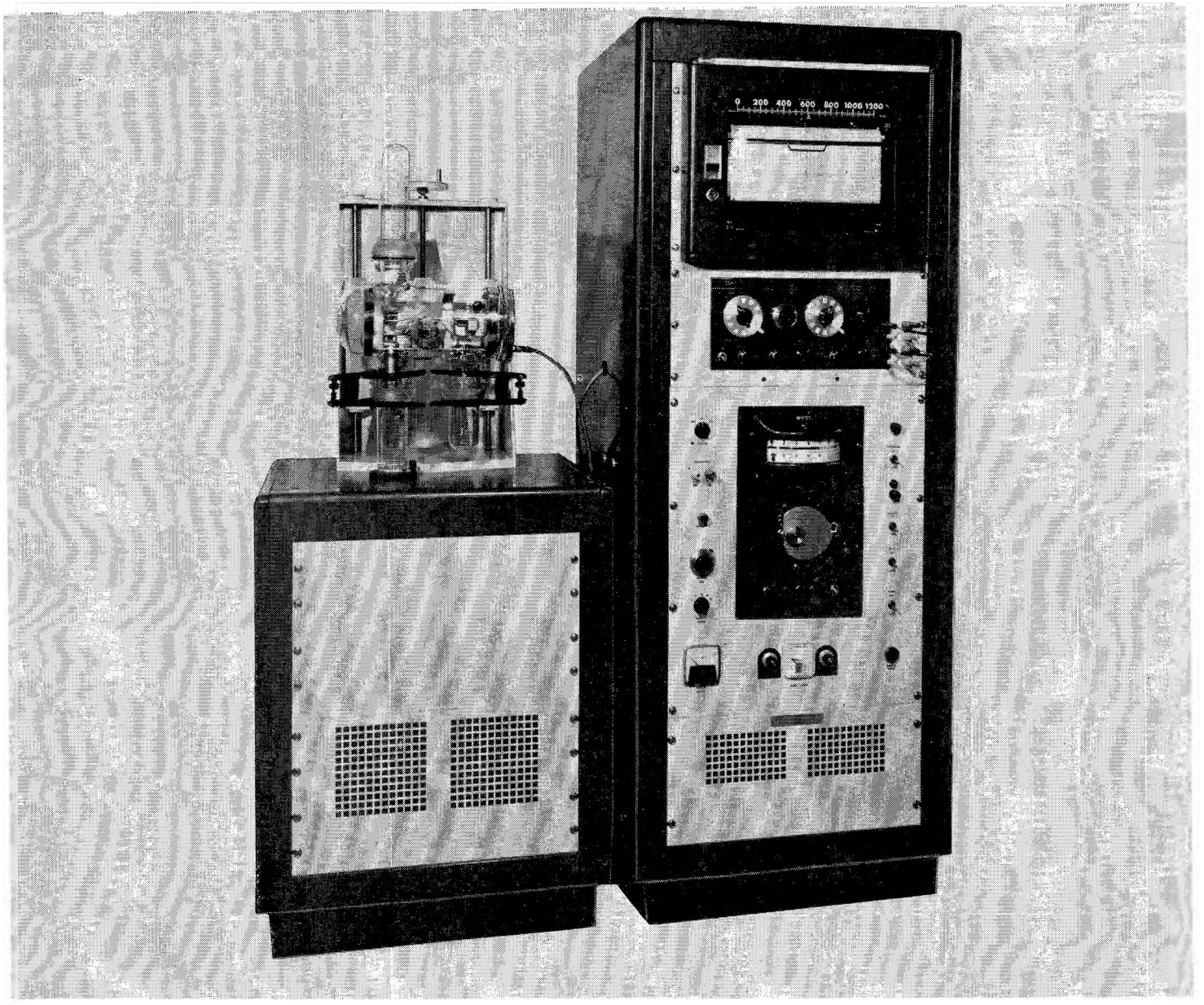

Measure thermal weight-loss... PRECISELY!

TEM-PRES Thermogravimetric Systems permit precision determinations of the effect of heat on the weight of materials over a wide range of conditions. Total weights up to 100 grams, with weight changes up to 20 grams, can be recorded on a single chart traverse. The balance has a precision of 1×10^{-7} grams and a sensitivity of 1×10^{-3} grams.

A resistance-wound furnace and a precision, semi-micro analytical balance comprise the heart of the system, with power supplies, programmer, controller, and strip-chart recorder as operational components. Standard furnaces are available for use to 1200°C., base-metal-wound, or to 1750°C., noble-metal-wound. Furnaces are designed to take a hermetically-sealed, drop-down tube permitting studies in vacuum to 10^{-3} torr, to 1500°C. and small positive pressures with various controlled atmospheres.

TEM-PRES RESEARCH

1401 S. Atherton, State College, Pa. 16801 (814) 237-7631

CARBORUNDUM

Relative Viscosity and Apparent Molal Volume of N-Methylpropionamide Solutions at Various Temperatures . . . **Frank J. Millero** 3209

Paramagnetic Resonance Study of the Triplet States of Various Aromatic Nitrogen Heterocycles, Biphenyl, and Acenaphthene . . . **Yasuhiko Gondo and August H. Maki** 3215

The Hydration of Pyridine in Organic Solvents . . . **James R. Johnson, Paul J. Kilpatrick, Sherril D. Christian, and Harold E. Affsprung** 3223

Spectroscopic Characterization of a New Polymorph of Metal-Free Phthalocyanine . . . **James H. Sharp and Marcel Lardon** 3230

The Sorption of Orthophosphate on Crystalline Metal Oxides . . . **D. R. Vissers** 3236

Nuclear Magnetic Resonance Studies of Weak Intermolecular Forces: Medium Effects in Saturated Heterocyclic Rings . . . **Harold Finegold** 3244

Fluorescence Yields of Aromatic Compounds . . . **William R. Dawson and Maurice W. Windsor** 3251

The Krypton-Radiosensitized Reaction of Deuterium Atoms with Ethylene . . . **A. Tewarson and F. W. Lampe** 3261

Tautomerism and Geometric Isomerism in Arylazophenols and Naphthols. IV. Spectra and Reversible Photoreactions of *m*- and *p*-Hydroxyazobenzene . . . **Gavriella Gabor, Yael F. Frei, and Ernst Fischer** 3266

Dielectric Study of Intermolecular Association in Sterically Hindered Octanol Isomers . . . **Gyan P. Johari and Walter Dannhauser** 3273

Spatial Distribution of Trapped Radicals in γ-Irradiated Ethylene Glycol Dimethacrylate Polymers . . . **John Zimbrick, Frank Hoecker, and Larry Kevan** 3277

Transport Processes in Hydrogen-Bonding Solvents. I. The Conductance of Tetraalkylammonium Salts in Ethanol and Propanol at 25° . . . **D. Fennell Evans and Philip Gardam** 3281

Transient Convective Diffusion in Capillaries . . . **Allen R. Overman** 3286

Solubility and Complex Formation Equilibria of Silver Chloride in Anhydrous Dimethylformamide . . . **James N. Butler** 3288

The Thermodynamics of the Vanadium Pentoxide (Solid or Liquid)–Water Vapor System . . **L. N. Yannopoulos** 3293

Intramolecular Hydrogen Bonding in the Lowest Excited Singlet States of Some Substituted Salicylic Acids . . . **Stephen G. Schulman and Herman Gershon** 3297

Absorption Maxima of the Visible Band of Iodine in Different Groups of Solvents . . . **E. M. Voigt** 3300

Reactions of Hydrocarbons with Mixtures of Active Nitrogen and Hydrogen Atoms. II. "Anomalous" Reactions: the Reactions of Cyanogen, Hydrogen Cyanide, and Acetylene . . . **David R. Safrany and Walter Jaster** 3305

The Effect of Additives upon the Reaction of Cyanogen with Active Nitrogen: Reactions of Carbon Atoms, CN Radicals, and the Chemiluminescent Reaction of C_2N Radicals with Atomic Oxygen . . . **David R. Safrany and Walter Jaster** 3318

NOTES

Reactions of Hydrocarbons with Mixtures of Active Nitrogen and Hydrogen Atoms. III. The Reactions of Methylacetylene and Allene . . . **David R. Safrany and Walter Jaster** 3323

Solid-State Reactions of $SrCO_3 + TiO_2$ . . . **N. H. Harris and R. L. Cook** 3326

$Hg(6^3P_1)$-Photosensitized Isomerization of Octafluorobutene-2 . . . **D. M. Graham and Takumi Hikida** 3328

Formation Constants of Some 2:2 and 3:3 Ion Pairs . . . **R. A. Matheson** 3330

Estimation of the Critical Surface Tension for Polymers from Molecular Constitution by a Modified Hildebrand–Scott Equation . . . **Souheng Wu** 3332

Absorption Spectra of Sodium–Ammonia Mixtures in the Gas Phase . . . **Irving Warshawsky** 3334

Kinetics of the Thermal $\alpha \rightarrow \beta$ Polymorphic Conversion in Metal-Free Phthalocyanine . . . **James H. Sharp and Roger L. Miller** 3335

Cobalt-60 Radiolysis of Aqueous Eosin . . . **A. F. Rodde, Jr., and L. I. Grossweiner** 3337

Thermodynamic Values for the Dimerization of 2-Pyridone and 2-Thiopyridone . . **N. Kulevsky and W. Reineke** 3339

Kinetics of the Gas-Phase Reactions of Diborane with Methylphosphines and Trimethylamine . . . **H. Brumberger and W. H. Smith** 3340

Contact Angles and Transition Regions in Soap Films . . . **H. M. Princen** 3342

Isobutane Chemisorption on Synthetic Faujasites . . . **P. Donald Hopkins and R. L. Stoffer** 3345

Dielectric Study of the Molecular Complexes Formed between Triethylamine and Acetic and Monochloracetic Acid . . . **S. R. Gough and A. H. Price** 3347

NEW PERIODICAL

JOURNAL OF MAGNETIC RESONANCE

edited by **WALLACE S. BREY, JR.,** *University of Florida, Gainesville, Florida*

This new bimonthly Journal, scheduled to appear in January of 1969, will include original papers dealing with the theory, techniques, methods of spectral analysis, and results of magnetic resonance spectroscopy. The subject matter of the Journal includes as primary areas both nuclear and electron magnetic resonance, extending to such related fields as quadrupole resonance, cyclotron resonance, the Mossbauer effect, and magnetic properties of the solid state.

In the field of nuclear magnetic resonance, papers concerned with wide-line and transient methods, as well as with high-resolution spectroscopy, will be included. Interpretative correlations of data and discussions of the relation of structure to magnetic resonance parameters are also within the scope of this Journal.

Description of developments in instrumentation, computational procedures, and theoretical approaches will be included, as will papers concerning the improvement and application of new techniques such as multiple resonance, direct computerization of spectrometer output, quantitative analytical procedures, and time-averaging of spectra.

FIRST ISSUES WILL CONTAIN:

J. Martin Anderson, The 'Direct Method': Application to Nuclear Magnetic Double Resonance

S. Brownstein and **L. Lunazzi,** Proton and Fluorine Resonance Spectra of Some Complexes of PF_5 and AsF_5

Hideaki Chihara, Magnetic Resonance Studies of the Disorder in Lithium Iodide Monohydrate and Monodeuterate

P. Diehl and **H. P. Kellerhals,** Unique Determination of Parameters from NMR Spectra of Oriented Molecules

Richard R. Ernst, Numerical Hilbert Transform and Automatic Phase Correction in Magnetic Resonance Spectroscopy

Charles S. Johnson, Jr., Some Comments on the Calculation of NMR Line Shapes for Exchanging AB Spin Systems

Bruce McGarvey and **J. Pearlman,** N^{14} NMR of Paramagnetic Transition Metal Complexes

Forrest S. Mortimer and **C. A. Reilly,** NMR Spectrum Types for Non-rigid Molecules

D. E. Woessner, B. S. Snowden, Jr., R. A. McKay, and **E. Thomas Strom,** Proton and Deuteron Spin-Lattice Relaxation in n-Dodecane

Shizuo Fujiwara, Fumikazu Yajima and **Akira Yamasaki,** Chemical Shift of NMR of Cobalt-59 in Some Inorganic Complex Compounds

Tokuko Watanabe and **Shizuo Fujiwara,** EPR Studies of Ti(III) Chelates in Aqueous Solution: The Nature of Chemical-Bonding and EPR Relaxation Mechanism

G. B. Savitsky, H. G. Spencer, and **J. F. Geldard,** Proton Chemical Shifts of Some Hydroxy-Benzenes Determined by Massive Deuteration

E. A. Cohen, A. J. R. Bourn, and **S. L. Manatt,** NMR Studies of Some Pentafluorobenzenes.

F. A. L. Anet and **J. L. Sudmeier,** Determination of the Relative Signs of Coupling Constants in Some Organomercuric Compounds by Internuclear Double and Triple Magnetic Resonance

Gerd N. LaMar, Proton Magnetic Resonance Studies of Magnetic Anisotropy in Di-Adducts of Cobalt(II)-*bis*(Acetylacetonate)

☐ *VOLUME 1, 1969 (Bimonthly), $25.00*

☐ *Personal Subscription°, $15.00*

☐ *STANDING ORDER*

°Personal subscriptions at a reduced rate are available on orders placed directly with the Publishers certifying that the subscription is paid for by the subscriber for his personal use.

ACADEMIC PRESS NEW YORK AND LONDON
111 FIFTH AVENUE, NEW YORK, N. Y. 10003

Viscosities of Some Organic Glasses Used as Trapping Matrices. II . . **A. Campbell Ling and John E. Willard** 3349

COMMUNICATIONS TO THE EDITOR

Intramolecular Elimination Reactions in the Photolysis of Fluoroaldehydes . . **E. R. Morris and J. C. J. Thynne** 3351

A Reply to "Intramolecular Elimination Reactions in the Photolysis of Fluoroaldehydes" . . . **G. O. Pritchard and M. J. Perona** 3352

Charged Square-Well Model for Ionic Solutions . . . . . **Jayendran C. Rasaiah and Harold L. Friedman** 3352

Experimental Method for Determining the Intersystem Crossing Rate Constant from Lowest Excited Singlet to Lowest Triplet State . . . . . **Donald R. Scott and Otto Maltenieks** 3354

A Note on the Dissolving of Stationary Spheres, Especially Gas Bubbles . . . . . **M. Cable** 3356

Reply to Communication by M. Cable . . . . . **Irvin M. Krieger** 3357

A Further Note on the Rate of Dissolving of Spherical Gas Bubbles . . . . . **L. E. Johns, Jr.** 3357

The Extent of Association in Liquid Dimethyl Sulfoxide . . . . . **Ralph L. Amey** 3358

On Radical Recombination Rates in SO_2-Doped Flames . . . . . **Robert Wheeler** 3359

AUTHOR INDEX

Affsprung, H. E., 3223
Amey, R. L., 3358
Applegate, K. R., 3177

Benson, S. W., 3204
Berger, P. A., 3186
Brausse, G., 3098
Brumberger, H., 3340
Butler, J. N., 3288

Cable, M., 3356
Cadenhead, D. A., 3201
Choi, S. U., 3148
Christian, S. D., 3223
Cook, L. R., 3326
Copeland, B. K. W., 3168

Dannhauser, W., 3273
Davis, J. C., Jr., 3111
Dawson, W. R., 3251
De Palma, D., 3192

Evans, D. F., 3281
Everett, D. H., 3201

Finegold, H., 3244
Fischer, E., 3266
Florin, R. E., 3154
Forchioni, A., 3105
Frei, Y. F., 3266
Friedman, H. L., 3352
Furuyama, S., 3204
Futrell, J. H., 3080

Gabor, G., 3266
Gardam, P., 3281
Gershon, H., 3297
Golden, D. M., 3204
Gondo, Y., 3215
Gough, S. R., 3347
Graham, D. M., 3328
Grossweiner, L. I., 3337

Harris, N. H., 3326
Hikida, T., 3328
Hirota, K., 3133
Hoecker, F., 3277
Hopkins, P. D., 3345

Jaster, W., 3305, 3318, 3323
Johari, G. P., 3273
Johns, L. E., Jr., 3357
Johnson, J. R., 3223

Kenney, J. T., 3094
Kera, Y., 3133
Kevan, L., 3277
Kilpatrick, P. J., 3223
Krieger, I. M., 3357
Kulevsky, N., 3339
Kwun, O. C., 3148

Lampe, F. W., 3261
Lardon, M., 3230
Levy, J. B., 3168
Ling, A. C., 3349
Low, M. J. D., 3161

Maki, A. H., 3215
Maltenieks, O., 3354
Marshall, W. L., 3122
Matheson, R. A., 3330
Mayer, A., 3098
McPherson, W. G., 3117
Meyers, E. A., 3117
Miller, R. L., 3335
Millero, F. J., 3209
Morris, E. R., 3351
Murphy, R. A., 3111

Nedetzka, T., 3098

Overman, A. R., 3286

Parker, R. C., 3177
Perona, M. J., 3352
Powell, F. X., 3094
Price, A. H., 3347
Princen, H. M., 3342
Pritchard, G. O., 3352

Quist, A. S., 3122

Ramakrishna, V., 3073
Ramamurthy, P., 3161
Rasaiah, J. C., 3352
Reineke, W., 3339
Rodde, A. F., Jr., 3337
Roth, J. F., 3186

Safrany, D. R., 3305, 3318, 3323
Schlect, P., 3098
Schulman, S. G., 3297
Scott, D. R., 3354
Scott, R., 3192
Sharp, J. H., 3230, 3335
Sicilio, F., 3154
Sieck, L. W., 3129
Slutsky, L. J., 3177
Smith, W. H., 3340
Stoffer, R. L., 3345
Suri, S. K., 3073

Teratani, S., 3133
Tewarson, A., 3261
Thynne, J. C. J., 3351
Tiernan, T. O., 3080

Vilk, P., 3142
Vinogradov, S., 3192
Vissers, D. R., 3236
Vogel, H., 3098
Voigt, E. M., 3300

Wall, L. A., 3154
Warshawsky, I., 3334
Wheeler, R., 3359
Willard, J. E., 3349
Willi, A. V., 3142
Willis, C., 3105
Windsor, M. W., 3251
Won, C. M., 3142
Wu, S., 3332

Yannopoulos, L. N., 3293

Zimbrick, J., 3277

THE JOURNAL OF

PHYSICAL CHEMISTRY

Volume 72, Number 10 October 1968

Vaporization Characteristics of Zinc Chloride, Bromide, and Iodide . . . . **Donald W. Rice and N. W. Gregory** 3361

Formation of Hydrogen in the Photolysis of Diborane at 1849 Å . . . . . **Marijon Bufalini and J. E. Todd** 3367

Mixed Ligand Chelates of Copper(II) with 8-Quinolinol and Arylhydroxycarboxylic Acids. I. Electronic Absorption Spectra . . . . **Stephen G. Schulman, William P. Kilroy, and Herman Gershon** 3372

The Vapor Pressure, the Heat of Sublimation, and the Evaporation Coefficient of Praseodymium Trifluoride . . . **Harry B. Skinner and Alan W. Searcy** 3375

Spectrum and Kinetics of the Hydroxynitromethane Anion Radical in Pulse-Irradiated Alkaline Nitromethane Solutions . . . . . **K.-D. Asmus and Irwin A. Taub** 3382

Electron Spin Resonance Studies of Radiolytically Produced Radicals in Aqueous Nitroalkane Solutions . . . **K. Eiben and Richard W. Fessenden** 3387

The Reactions of Hydrogen Atoms in Aqueous Solutions. Some Amino Acids . . . **Wynn A. Volkert and Robert R. Kuntz** 3394

Kinetics of Fluorination. III. The Unimolecular Decomposition of Chemically Activated *sec*-2,3-Dichloroperfluorobutyl Radicals . . . . . **Alan S. Rodgers** 3400

Kinetics of Fluorination. IV. The Unimolecular Decomposition of Chemically Activated *sec*-1,4-Dichloroperfluorobutyl Radicals . . . . . **Alan S. Rodgers** 3407

Equilibria in Pyridine. I. Determination of Absolute pK Values of Several Uncharged Acids and Investigation of a Few Typical Acid–Salt Mixtures . . . **L. M. Mukherjee, John J. Kelly, William Baranetzky, and Jerry Sica** 3410

Nuclear Magnetic Resonance in Thallium Borate Glasses. I. The Thallium-205 Chemical Shift . . . **Robert K. Momii and Norman H. Nachtrieb** 3416

The Interaction of Antagonistic and Cooperative Electrolytes in Water at 25°. A Hypothesis Concerning Anion-Exchange Resins . . . . . **Joseph Steigman and Jay Dobrow** 3424

Vapor Pressure Lowering and Light Scattering in Benzene Solutions of Alkylammonium Salts . . . **P. R. Danesi, M. Magini, and G. Scibona** 3437

Carbon-13 Kinetic Isotope Effect in the Thermal Isomerization of Methyl Isocyanide . . . **John F. Wettaw and L. B. Sims** 3440

The Heats of Formation of $AlClF_2$ and $AlCl_2F$ from Subliming AlF_3 in the Presence of $AlCl_3$ Vapor . . . **Ralph F. Krause, Jr., and Thomas B. Douglas** 3444

Mass Spectrometry and Ionization Energies of Some Condensed-Ring Aromatic and Heterocyclic Compounds . . . **E. J. Gallegos** 3452

Radiolysis of Liquid and Solid Dimethylmercury . . . . . **Clarence J. Wolf and John Q. Walker** 3457

The Pyrolysis of Tetrafluoroethylene . . . . . **George A. Drennan and Richard A. Matula** 3462

The Photoperoxidation of Unsaturated Organic Molecules. II. The Autoperoxidation of Aromatic Hydrocarbons . . . **B. Stevens and B. E. Algar** 3468

Infrared Spectral Shifts and Heats of Adsorption of Vapors on Silica Gel. . . **P. A. Elkington and G. Curthoys** 3475

A Thermodynamic Study of Hydrogen Bonding by Means of Gas–Liquid Chromatography . . . **Daniel E. Martire and Peter Riedl** 3478

Thermodynamics of Solutions with Liquid-Crystal Solvents. I. A Gas–Liquid Chromatographic Study of Cholesteryl Myristate . . . . . **D. E. Martire, P. A. Blasco, P. F. Carone, L. C. Chow, and H. Vicini** 3489

Reactions of Ions in the Radiolysis of Liquid Isobutane, Isopentane, and 2,3-Dimethylbutane . . . **Kuniyasu Tanno, Shoji Shida, and Tetsuo Miyazaki** 3496

The Extraction of Perchloric Acid by 1-Decanol . . . . . **D. J. Turner and R. M. Diamond** 3504

Ultraviolet Absorption Spectra of Gaseous SnF_2 and PbF_2 . . **R. H. Hauge, J. W. Hastie, and J. L. Margrave** 3510

Calorimetric Studies of Bis(fluoroxy)perfluoromethane . . . . . **G. D. Foss and D. A. Pitt** 3512

Lanthanide Ions as Sensitive Probes in Organic Photochemistry. I. Collisional Sensitization of Fluorescence by Triplet Donors . . . . . **Nicolae Filipescu and George W. Mushrush** 3516

Lanthanide Ions as Sensitive Probes in Organic Photochemistry. II. Photoreduction of *p,p'*-Dimethoxybenzophenone in Isopropyl Alcohol . . . . . **Nicolae Filipescu and George W. Mushrush** 3522

The Low-Frequency Spectra of Lithium Halide Molecular Species . . . **M. Freiberg, A. Ron, and O. Schnepp** 3526

Electronic Properties of Perfluorocarbons. Fluorescence and Phosphorescence in Perfluorobiphenyl, Perfluoronaphthalene, and Perfluorotoluene . . . . . **Herbert M. Rosenberg and Susan D. Carson** 3531

Influence of Heterogeneous Chemical Reactions upon Potentiostatic Current–Time Curves . . **Rolando Guidelli** 3535

Kinetics of the Reaction $NO_2(g) + I^-$ in Molten Alkali Metal Nitrates . . . **R. F. Bartholomew and D. W. Donigian** 3545

The Radiolysis of Colloidal Sulfur . . . . . **G. William Donaldson and Francis J. Johnston** 3552

Corresponding States of Argon and Methane . . . . . **Eugene M. Holleran and Gary J. Gerardi** 3559

Mössbauer Spectroscopy of Supported Gold Catalysts . . . . **W. N. Delgass, M. Boudart, and G. Parravano** 3563

Etherate Formation in Organoaluminum Compounds. Complex-Formation Tendency in a Series of Trialkylaluminum, Dialkylaluminum Chloride, Alkylaluminum Dichloride, and Aluminum Chloride Aryl Etherates . . . . . **G. H. Smith and F. J. Hamilton** 3567

Lattice Anharmonicity and the Thermal Accommodation Coefficient . . . . . **P. Feuer** 3573

On the Variational Principle for the Poisson–Boltzmann Equation . . . . **A. D. MacGillivray and J. D. Swift** 3575

The Mechanism of Isomerization of Methyl Nitrite . . . . . **P. A. Temussi and T. Tancredi** 3581

The Vapor Pressure of *p*-Xylene and Solutions of Tetra-*n*-pentylammonium Thiocyanate in *p*-Xylene . . . **John A. O'Malley, Clifford Owens, Carl Schmid, Daniel Quimby, and Charles M. King** 3584

Crystal Field–Spin Orbit Treatment in d^1 and d^9 Trigonal Bipyramidal Complexes . . . **Clifford A. L. Becker, Devon W. Meek, and T. M. Dunn** 3588

Ion Cyclotron Resonance of Olefins. I. A Study of the Ion–Molecule Reactions in Electron-Impacted Ethylene . . . **M. T. Bowers, D. D. Elleman, and J. L. Beauchamp** 3599

Hydrogen Ion Equilibria of Soybean Protein . . . . . **W. U. Malik and M. R. Jindal** 3612

The Reduction of Aromatic Hydrocarbons. II. Polarographic Study of the Effect of Proton Donors . . . **Jiri Janata and Harry B. Mark, Jr.** 3616

Simultaneous Kinetic and Infrared Spectral Studies of Carbon Monoxide Oxidation on Palladium under Steady-State Conditions . . . . . **Rayond F. Baddour, Michael Modell, and Ulrich K. Heusser** 3621

A Rotating Disk Electrode Study of the Catalytic Wave Produced by the Reduction of Iodine in the Presence of Iodate . . . . . **Premysl Beran and Stanley Bruckenstein** 3630

Electron Spin Resonance Spectroscopy of the Xanthyl Free Radicals. I. Xanthyl Radical: a Planar Diphenylmethyl . . . . . **Michael D. Sevilla and Gershon Vincow** 3635

Electron Spin Resonance Spectroscopy of the Xanthyl Free Radicals. II. 9-Phenylxanthyl: Spatial Configuration . . . . . **Michael D. Sevilla and Gershon Vincow** 3641

Electron Spin Resonance Spectroscopy of the Xanthyl Free Radicals. III. 9-Alkylxanthyls: Torsional Oscillation of the Alkyl Groups . . . . . **Michael D. Sevilla and Gershon Vincow** 3647

Differentiation between Tryptophan Residues in Proteins . . . . . **Yehudit Elkana** 3654

The Electrical Conductivity of Silica Gel in the Presence of Adsorbed Water . . . **J. H. Anderson and G. A. Parks** 3662

NOTES

Pulse Radiolysis of Aqueous Solutions of Thymine and Triacetoneamine N-Oxyl . . . **Peter T. Emmerson and Robin L. Willson** 3669

The Ultraviolet Absorption Spectra of Chlorine, Bromine, and Bromine Chloride in Aqueous Solution . . . **Hilda Gutmann, Menachem Lewin, and Berta Perlmutter-Hayman** 3671

The Universal Nitrogen Isotherm . . . . . **Conway Pierce** 3673

Dielectric Relaxation in Pure Chloroform . . . . . **Thirumalai V. Gopalan and Prasad K. Kadaba** 3676

Electron Affinities and the Electron-Capture Method for Aromatic Hydrocarbons . . . **L. E. Lyons, G. C. Morris, and L. J. Warren** 3677

Inhibition by C_3O_2 of the Explosive Combustion of CO . . . **Jean Lebel, Pierre Michaud, and Cyrias Ouellet** 3678

The Photochemical Decomposition of Methanethiol. Hot Hydrogen Atom Reaction with Deuterium . . . **G. P. Sturm, Jr., and John M. White** 3679

Spectroscopic Studies of Isotopically Substituted 4-Pyridones . . . . **Robert A. Coburn and Gerald O. Dudek** 3681

Hydrogen and Oxygen Isotope Fractionation between Ice and Water . . . . . **James R. O'Neil** 3683

A Measurement of the Heterogeneous Rate Constant for the Thiocyanate-Catalyzed Polarographic Reduction of Trivalent Gallium . . . . . **E. D. Moorhead and G. M. Frame, II** 3684

The Effect of Micelles on the Kinetics of the Cannizzaro Reaction . . . . . **L. R. Cramer and J. C. Berg** 3686

Nuclear Magnetic Resonance Dynamic Determination of Boron–Fluorine Internuclear Distances in Alkali Metal Fluoroborates . . . . . **H. J. C. Yeh and J. L. Ragle** 3688

Interruption and Evaporation Effects for the Reaction of Atomic Hydrogen with Solid Olefins at 77°K . . . **R. L. Espino, J. P. Jones, R. C. Reid, and M. W. P. Strandberg** 3689

The Absence of Fluorescence in 5-Nitro-8-quinolinol . . . . . **Stephen G. Schulman and Herman Gershon** 3692

Calorimetric Determination of the Distribution Coefficient and Thermodynamic Properties of Bromine in Water and Carbon Tetrachloride . . . . . **John O. Hill, Ian G. Worsley, and Loren G. Hepler** 3695

Applications of McLachlan's Theory to Physical Adsorption . . . . . **J. D. Johnson** 3697

COMMUNICATIONS TO THE EDITOR

Comment on "Current Dependence of Water Transport in Cation-Exchange Membranes" . . . **A. S. Tombalakian** 3698

Reply to "Comment on 'Current Dependence of Water Transport in Cation-Exchange Membranes'" . . . **N. Lakshminarayanaiah** 3699

Comments on "The Calculation of Cohesive and Adhesive Energies," by J. F. Padday and N. D. Uffindell . . . **F. M. Fowkes** 3700

Reply to Comments of F. M. Fowkes on "The Calculation of Cohesive and Adhesive Energies" . . . **J. F. Padday and N. D. Uffindell** 3700

Formation of Electronically Excited Species in Nitrogen Atom–Oxygen Atom Recombination Reactions Catalyzed by Carbon Compounds: NO($A^2\Sigma$, $B^2\Pi$) and O(^1S) . . . . **Arthur Fontijn and Roy Ellison** 3701

The Inefficiency of Triplet Energy Transfer from Ketones to Trivalent Rare Earth Ions . . . **Peter J. Wagner and Herbert N. Schott** 3702

Oxidation of Cerium(III) in Sulfuric Acid Solutions Induced by Cobalt-60 γ Radiation . . . **R. W. Matthews, H. A. Mahlman, and T. J. Sworski** 3704

Singlet Methylene in the Photolysis of Mercury–Ketene–Butene Systems . . . **Derek C. Montague and F. S. Rowland** 3705

Electron Spin Resonance Study of the Neopentyl Radical from the Radiolysis of Solid Neopentane in the Presence of Nitrous Oxide . . . . . **Jacob Lin and Ffrancon Williams** 3707

AUTHOR INDEX

Algar, B. E., 3468
Anderson, J. H., 3662
Asmus, K.-D., 3382

Baddour, R. F., 3621
Baranetzky, W., 3410
Bartholomew, R. F., 3545
Beauchamp, J. L., 3599
Becker, C. A. L., 3588
Beran, P., 3630
Berg, J. C., 3686
Blasco, P. A., 3489
Boudart, M., 3563
Bowers, M. T., 3599
Bruckenstein, S., 3630
Bufalini, M., 3367

Carone, P. F., 3489
Carson, S. D., 3531
Chow, L. C., 3489
Coburn, R. A., 3681
Cramer, L. R., 3686
Curthoys, G., 3475

Danesi, P. R., 3437
Delgass, W. N., 3563
Diamond, R. M., 3504
Dobrow, J., 3424
Donaldson, G. W., 3552
Donigian, D. W., 3545
Douglas, T. B., 3444
Drennan, G. A., 3462
Dudek, G. O., 3681
Dunn, T. M., 3588

Eiben, K., 3387
Elkana, Y., 3654
Elkington, P. A., 3475
Elleman, D. D., 3599
Ellison, R., 3701
Emmerson, P. T., 3669
Espino, R. L., 3689

Fessenden, R. W., 3387
Feuer, P., 3573
Filipescu, N., 3516, 3522
Fontijn, A., 3701
Foss, G. D., 3512
Fowkes, F. M., 3700
Frame, G. M., II, 3684
Freiberg, M., 3526

Gallegos, E. J., 3452
Gerardi, G. J., 3559
Gershon, H., 3372, 3692
Gopalan, T. V., 3676
Gregory, N. W., 3361
Guidelli, R., 3535
Gutmann, H., 3671

Hamilton, F. J., 3567
Hastie, J. W., 3510
Hauge, R. H., 3510
Hepler, L. G., 3695
Heusser, U. K., 3621
Hill, J. O., 3695
Holleran, E. M., 3559

Janata, J., 3616
Jindal, M. R., 3612
Johnson, J. D., 3697
Johnston, F. J., 3552
Jones, J. P., 3689

Kadaba, P. K., 3676
Kelly, J. J., 3410
Kilroy, W. P., 3372
King, C. M., 3584
Krause, R. F., Jr., 3444
Kuntz, R. R., 3394

Lakshminarayanaiah, N., 3699
Lebel, J., 3678
Lewin, M., 3671
Lin, J., 3707
Lyons, L. E., 3677

MacGillivray, A. D., 3575
Magini, M., 3437
Mahlman, H. A., 3704
Malik, W. U., 3612
Margrave, J. L., 3510
Mark, H. B., Jr., 3616
Martire, D. E., 3478, 3489
Matthews, R. W., 3704
Matula, R. A., 3462
Meek, D. W., 3588
Michaud, P., 3678
Miyazaki, T., 3496
Modell, M., 3621
Momii, R. K., 3416
Montague, D. C., 3705
Moorhead, E. D., 3684
Morris, G. C., 3677
Mukherjee, L. M., 3410
Mushrush, G. W., 3516, 3522

Nachtrieb, N. H., 3416

O'Malley, J. A., 3584
O'Neil, J. R., 3683
Ouellet, C., 3678
Owens, C., 3584

Padday, J. F., 3700
Parks, G. A., 3662
Parravano, G., 3563
Perlmutter-Hayman, B., 3671
Pierce, C., 3673
Pitt, D. A., 3512

Quimby, D., 3584

Ragle, J. L., 3688
Reid, R. C., 3689
Rice, D. W., 3361
Riedl, P., 3478
Rodgers, A. S., 3400, 3407
Ron, A., 3526
Rosenberg, H. M., 3531
Rowland, F. S., 3705

Schmid, C., 3584
Schnepp, O., 3526
Schott, H. N., 3702
Schulman, S. G., 3372, 3692
Scibona, G., 3437
Searcy, A. W., 3375
Sevilla, M. D., 3635, 3641, 3647
Shida, S., 3496
Sica, J., 3410
Sims, L. B., 3440
Skinner, H. B., 3375
Smith, G. H., 3567
Steigman, J., 3424
Stevens, B., 3468
Strandberg, M. W. P., 3689
Sturm, G. P., Jr., 3679
Swift, J. D., 3575
Sworski, T. J., 3704

Tancredi, T., 3581
Tanno, K., 3496
Taub, I. A., 3382
Temussi, P. A., 3581
Todd, J. E., 3367
Tombalakian, A. S., 3698
Turner, D. J., 3504

Uffindell, N. D., 3700

Vicini, H., 3489
Vincow, G., 3635, 3641, 3647
Volkert, W. A., 3394

Wagner, P. J., 3702
Walker, J. Q., 3457
Warren, L. J., 3677
Wettaw, J. F., 3440
White, J. M., 3679
Williams, F., 3707
Willson, R. L., 3669
Wolf, C. J., 3457
Worsley, I. G., 3695

Yeh, H. J. C., 3688

THE JOURNAL OF
PHYSICAL CHEMISTRY

Volume 72, Number 11 October 1968

Symposium on Photochemistry and Radiation Chemistry, U. S. Army Natick Laboratories, April 22-24, 1968

Introductory Remarks . . . . . **Elie Hayon** 3709

Chemiluminescence in Gases: Reactions Yielding Electronically Excited Sulfur Dioxide . . . **B. A. Thrush, C. J. Halstead, and A. McKenzie** 3711

Production of Electronically Excited Atoms. II. $H + HI \rightarrow H_2 + I^*(^2P_{1/2})$ . . **P. Cadman and J. C. Polanyi** 3715

Chemiluminescent Emission in Gaseous Reactions at Low Concentrations . . . **John Emerson, Robert Reeves, and Paul Harteck** 3721

Liquid Benzene Luminescence Quenching by Carbon Tetrachloride. Consideration of the Presence of Solvent Excimers in the Interpretation of the Observed Rates of Quenching . . . **P. K. Ludwig and C. D. Amata** 3725

Yield of Free Ions in Irradiated Liquids; Determination by a Clearing Field . . . **Werner F. Schmidt and A. O. Allen** 3730

Primary Processes in the Photolysis of SO_2 at 1849 Å . . . . . **J. N. Driscoll and Peter Warneck** 3736

Production of $N_2(A^3\Sigma_u^+)$ and $CO(a^3\pi)$ by $Hg(^1P_1)$ Photosensitization: Evidence from 2537-Å Mercury Scintillation . . . **Albrecht Granzow, Morton Z. Hoffman, Norman N. Lichtin, and Satish K. Wason** 3741

Higher Order Ion–Molecule Reactions. I. Theoretical Basis . . . . . **G. G. Meisels and H. F. Tibbals** 3746

The Gas-Phase Oxidation of Photochemically Generated Isopropyl Radicals . . **Graeme S. Milne and Colin Steel** 3754

A Pulse-Radiolysis System for the Observation of Short-Lived Transients . . . **M. J. Bronskill and J. W. Hunt** 3762

A New Flash-Photolysis System for the Investigation of Fast Reactions . . . . **E.-G. Niemann and M. Klenert** 3766

I^- Photosensitized Reactions in Metaphosphate Glass . . . . . **T. Feldmann and A. Treinin** 3768

An Efficient and Highly Selective Radiation-Induced Isomerization in the Crystalline State . . . **David C. Walker** 3772

A Mixed Triplet-Excimer Intermediate in the Photooxidation of N,N′-Diphenyl-*p*-phenylenediamine by the Diimine . . . **Michael Ottolenghi and René Bensasson** 3774

Photoreduction of Aminobenzophenones in Nonpolar Media. Effects of Tertiary Amines . . . **Saul G. Cohen and Jacob I. Cohen** 3782

The Photoperoxidation of Unsaturated Organic Molecules. III. Autoperoxidation in Polymer Films . . . **B. Stevens and B. E. Algar** 3794

Mechanisms of Photochemical Reactions in Solution. LVI. A Singlet-Sensitized Reaction . . . **Steven Murov and George S. Hammond** 3797

Transient Species in the Radiolysis of Solutions of Stilbene . . . **F. S. Dainton, C. T. Peng, and G. A. Salmon** 3801

Energy Transfer in Radiolysis of Rare Gas–Propane Liquid Mixtures . . . . . **R. D. Koob and Larry Kevan** 3808

Nature of the Transient Species in the Photochemistry of Negative Ions in Aqueous Solution . . . **R. Devonshire and J. J. Weiss** 3815

Flash Photolysis in the Vacuum Ultraviolet Region of the Phosphate Anions $H_2PO_4^-$, HPO_4^{2-}, and $P_2O_7^{4-}$ in Aqueous Solutions . . . . . **J. Robert Huber and E. Hayon** 3820

Photochemistry of Aqueous $Cr(CN)_6^{3-}$ . . . . . **A. Chiang and A. W. Adamson** 3827

Substituent Effects in Cyclohexadienyl Radicals as Studied by Pulse Radiolysis . . . . . **B. Cercek** 3832

The Absorption Spectra and Kinetics of Hydrogen Sesquioxide and the Perhydroxyl Radical . . . **Benon H. J. Bielski and Harold A. Schwarz** 3836

Pulse-Radiolysis and Flash-Photolysis Study of Aqueous Solutions of Simple Pyrimidines. Uracil and Bromouracil . . . **R. M. Danziger, E. Hayon, and M. E. Langmuir** 3842

Electrons, Ions, and Excited States in the Pulse Radiolysis of Dioxane . . . **J. H. Baxendale and M. A. J. Rodgers** 3849

Pulsed Radiolysis of Liquid Cyclohexane and *n*-Hexane. I. Yield of Hydrogen Atoms Measured by the Cyclohexadienyl Radical Absorption in Solutions Containing Benzene. II. Absorption Spectra and Reactions of Cyclohexyl and Hexyl Radicals . . . . . **Myran C. Sauer, Jr., and Inder Mani** 3856

The Photochemistry of Charge-Transfer Systems. I. Complexes of Iodine with Amines . . . **Arthur M. Halpern and Karl Weiss** 3863

The Pulse Radiolysis of Benzene–Biacetyl Solutions . . . **R. B. Cundall, G. B. Evans, P. A. Griffiths, and J. P. Keene** 3871

Positive Charge Migration in γ-Irradiated Organic Solids and Trapping by Alkanes at 77°K . . . **Pieter W. F. Louwrier and William H. Hamill** 3878

Comparison of Photo- and γ-Induced Ionization Processes in the Condensed Phase by Means of Electron Spin Resonance Spectroscopy . . . . . **Kozo Tsuji and Ffrancon Williams** 3884

Low-Energy, High-Angle Electron-Impact Spectrometry . . . **Aron Kuppermann, J. K. Rice, and Sandor Trajmar** 3894

Gas-Phase Photolysis of Cyclohexane in the Photoionization Region . . . **P. Ausloos, R. E. Rebbert, and S. G. Lias** 3904

The Photolysis of Ammonia at 2062 Å in the Presence of Propane . . . **W. E. Groth, U. Schurath, and R. N. Schindler** 3914

A Pulsed-Radiolysis Study of Atomic Oxygen Reactions in the Gas Phase . . . **G. M. Meaburn, D. Perner, J. LeCalvé, and M. Bourène** 3920

The Point of Attack of a Chlorine Atom on Trichloroethylene . . . **L. Bertrand, J. A. Franklin, P. Goldfinger, and G. Huybrechts** 3926

A Flash-Photolysis Study of Chromyl Chloride . . . **Rolf Halonbrenner, J. Robert Huber, Urs Wild, and Hans H. Günthard** 3929

AUTHOR INDEX

Adamson, A. W., 3827
Algar, B. E., 3794
Allen, A. O., 3730
Amata, C. D., 3725
Ausloos, P., 3904

Baxendale, J. H., 3849
Bensasson, R., 3774
Bertrand, L., 3926
Bielski, B. H. J., 3836
Bourène, M., 3920
Bronskill, M. J., 3762

Cadman, P., 3715
Cercek, B., 3832
Chiang, A., 3827
Cohen, J. I., 3782
Cohen, S. G., 3782
Cundall, R. B., 3871

Dainton, F. S., 3801
Danziger, R. M., 3842
Devonshire, R., 3815
Driscoll, J. N., 3736

Emerson, J., 3721
Evans, G. B., 3871

Feldmann, T., 3768
Franklin, J. A., 3926

Goldfinger, P., 3926
Granzow, A., 3741
Griffiths, P. A., 3871
Groth, W. E., 3914
Günthard, H. H., 3929

Halonbrenner, R., 3929
Halpern, A. M., 3863
Halstead, C. J., 3711
Hamill, W. H., 3878
Hammond, G. S., 3797
Harteck, P., 3721
Hayon, E., 3820, 3842
Hoffman, M. Z., 3741
Huber, J. R., 3820, 3929
Hunt, J. W., 3762
Huybrechts, G., 3926

Keene, J. P., 3871
Kevan, L., 3808
Klenert, M., 3766
Koob, R. D., 3808
Kuppermann, A., 3894

Langmuir, M. E., 3842
LeCalvé, J., 3920
Lias, S. G., 3904
Lichtin, N. N., 3741
Louwrier, P. W. F., 3878
Ludwig, P. K., 3725

Mani, I., 3856
McKenzie, A., 3711
Meaburn, G. M., 3920
Meisels, G. G., 3746
Milne, G. S., 3754
Murov, S., 3797

Niemann, E.-G., 3766

Ottolenghi, M., 3774

Peng, C. T., 3801
Perner, D., 3920
Polanyi, J. C., 3715

Rebbert, R. E., 3904
Reeves, R., 3721
Rice, J. K., 3894
Rodgers, M. A. J., 3849

Salmon, G. A., 3801
Sauer, M. C., Jr., 3856
Schindler, R. N., 3914
Schmidt, W. F., 3730
Schurath, U., 3914
Schwarz, H. A., 3836
Steel, C., 3754
Stevens, B., 3794

Thrush, B. A., 3711
Tibbals, H. F., 3746
Trajmar, S., 3894
Treinin, A., 3768
Tsuji, K., 3884

Walker, D. C., 3772
Warneck, P., 3736
Wason, S. K., 3741
Weiss, J. J., 3815
Weiss, K., 3863
Wild, U., 3929
Williams, F., 3884

THE JOURNAL OF

PHYSICAL CHEMISTRY

Volume 72, Number 12 November 1968

Thermodynamics of Aqueous Mixtures of Electrolytes and Nonelectrolytes. VI. Transfer of Hydrochloric Acid from Water to Aqueous Ethylene Glycol at 25° . . . . . **J. H. Stern and J. M. Nobilione** 3937

Fluorescence and Absorption Studies on Chlorophyll a *in Vitro* at 77°K . . . . **G. S. Singhal, W. P. Williams, and E. Rabinowitch** 3941

Photolysis of Ketene by 2139-Å Radiation . . . . . **G. B. Kistiakowsky and Theodore A. Walter** 3952

Dissociation Pressures in the System LaH_2–LaH_3, 250–450° . . **Charles E. Messer and Gilbert Wan-hoi Hung** 3958

A Mass Spectrometric Study of the Rhenium–Oxygen System . . . . **J. E. Battles, G. E. Gundersen, and R. K. Edwards** 3963

An Infrared Study of Internal-Rotational Barriers in Solid π Complexes of Methylbenzenes. I. Hexamethylbenzene–Tetracyanoethylene . . . . **Bennie Ware, Ken Williamson, and J. Paul Devlin** 3970

Semiempirical Calculations on Sulfur-Containing Heterocycles . . **J. Fabian, A. Mehlhorn, and R. Zahradník** 3975

Ultraviolet and Ultrasonic Absorption Spectral Studies of the Association of $CuSO_4$ and $Cu(en)_2S_2O_3$ in Water at 25° . . . . **Paul Hemmes and Sergio Petrucci** 3986

Mechanism of Gaseous Siloxane Reaction with Silica. II . . . . . **William Hertl** 3993

The Crystal Structure of Racemic α,α'-Dimethylglutaric Acid . . . **Paolo Ganis, Piero Andrea Temussi, Maurits G. Northolt, and Leroy E. Alexander** 3997

Kinetics and Mechanism of the Thermal Decomposition of Nitronium Perchlorate . . . **J. N. Maycock and V. R. Pai Verneker** 4004

Thermal Decomposition of $LiAlH_4$ . . . . . **M. McCarty, Jr., J. N. Maycock, and V. R. Pai Verneker** 4009

Effects of Intentional Impurities on the Thermal Stability of Nitronium Perchlorate . . . **J. N. Maycock, V. R. Pai Verneker, and C. S. Gorzynski, Jr.** 4015

Gas–Liquid Chromatographic Study of the Thermodynamics of Solution of Some Aromatic Compounds. III. Solutions and Associative Interaction with Tetrachloroterephthalate Esters . . . **Stanley H. Langer, Bruce M. Johnson, and John R. Conder** 4020

Electrical Conductance Studies in Anhydrous Formic Acid Solutions . . . **Thomas C. Wehman and Alexander I. Popov** 4031

Vacuum Ultraviolet Photolysis of the C_4H_6 Isomers. I. 1,3-Butadiene . . . . . **Richard D. Doepker** 4037

Three- and Four-Bond ^{31}P–^1H Coupling Constants and Geminal Proton Nonequivalence in Ethyl Esters of Phosphorus Acids . . . . . **M. P. Williamson and C. E. Griffin** 4043

Osmotic and Activity Coefficients for Binary Mixtures of Sodium Chloride, Sodium Sulfate, Magnesium Sulfate, and Magnesium Chloride in Water at 25°. I. Isopiestic Measurements on the Four Systems with Common Ions . . . **Y. C. Wu, R. M. Rush, and G. Scatchard** 4048

Isopiestic Measurements on the System Water–Sodium Chloride–Magnesium Chloride at 25° . . . **R. F. Platford** 4053

Anisotropy of Proton Fluctuations and the Kerr Effect of Protein Solutions. Theoretical Considerations . . . **William H. Orttung** 4058

Anisotropy of Proton Fluctuations in Proteins. Calculations for Simple Models . . . . . **William H. Orttung** 4066

A Study of the Noise Generated during Ion Transport across Membranes . . . **M. E. Green and Masao Yafuso** 4072

The Interpretation of Heat Capacity Measurements through Two-Component, Liquid–Liquid Critical Regions . . . **Robert E. Barieau** 4079

an instrument for simultaneous DTA/TGA at half the cost of other, comparable instruments

The Shimadzu DT-2B Thermal Analysis apparatus (at right) features simultaneous DTA/TGA capability to 1200°C, a transistorized three-pen recorder especially designed for use in thermal analysis, and a universal furnace which rapidly responds to control.

The DT-2B exceeds the differential thermal analysis and thermogravimetry capabilities of instruments costing twice as much. And it is a thoroughly reliable apparatus with an extremely stable base line, high sensitivity and reproducibility.

Accessories are available: to expand its DTA operation to a range of −150° to 1500°C; perform dilatometric measurements to 1200°C; and make high performance specific heat measurements to 850°C utilizing a double relative adiabatic system (Sykes-Jones method).

THE SHIMADZU DT-20B

Soon to be available is the companion DT-20B for micro TGA and DTA analyses. Ideal for samples ranging in size from a few tenths of a milligram to as high as 50 mg., this instrument offers unrivaled baseline stability and high sensitivity.

Write to Aminco to receive literature describing the DT-2B and DT-20B in detail.

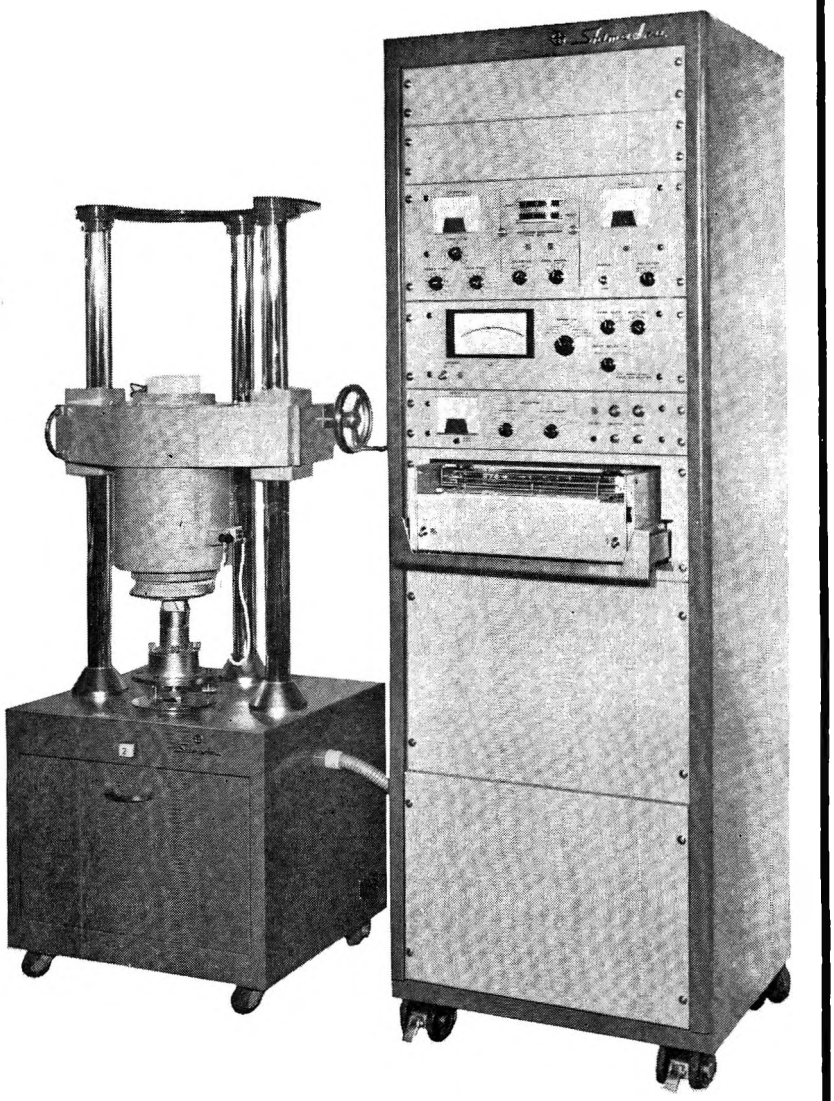

AMINCO IS SOLE DISTRIBUTOR IN U.S. AND CANADA

The Shimadzu DT-2B and DT-20B Thermal Analyzers are distributed exclusively in North America by American Instrument Co., Inc. To arrange for a demonstration and/or demonstration sample analysis, contact the Materials Technology Laboratory at Aminco.

AMINCO®

AMERICAN INSTRUMENT CO., INC.

8030 Georgia Avenue, Silver Spring, Maryland 20910

Polymorphism in *n*-Alkylammonium Halides. A Differential Scanning Calorimetric Study . . . **J. Tsau and D. F. R. Gilson** 4082

The Ion-Exchange Properties of Zeolites. IV. Alkaline Earth Ion Exchange in the Synthetic Zeolites Linde X and Y . . . **Howard S. Sherry** 4086

An X-Ray Study of Strontium–Sodium Ion Exchange in Linde X. An Example of a Two-Phase Zeolite System . . . **David H. Olson and Howard S. Sherry** 4095

Temperature Dependence of the Limiting Viscosity Number of the Solutions of Acrylonitrile–Styrene Copolymers in Dimethylformamide . . . **Yuko Shimura-Kambe** 4104

Substituent Effects on the Tautomerism of Schiff Bases . . . **John W. Ledbetter, Jr.** 4111

Electron Paramagnetic Resonance Studies of Complex Ion Formation between Mn^{2+} and F^-, Cl^-, Br^-, I^-, or SO_4^{2-} . . . **Douglas C. McCain and Rollie J. Myers** 4115

Conductance of the Alkali Halides. XII. Sodium and Potassium Chlorides in Water at 25° . . . **Yin-Chech Chiu and Raymond M. Fuoss** 4123

Electron Spin Resonance of Solubilized Long-Chain Nitroxides . . . **A. S. Waggoner, A. D. Keith, and O. H. Griffith** 4129

Raman Spectroscopy of Sulfur, Sulfur–Selenium, and Sulfur–Arsenic Mixtures . . . **A. T. Ward** 4133

A Theory of Interfacial Tension of Two-Phase Ternary Liquid Systems . . . **Donald J. Cotton** 4139

Solvolysis of Benzyl Chloride in Glycerol–Water Mixtures: Relation between Activation Parameters and Thermal Expansivity . . . **D. L. Gay and E. Whalley** 4145

Measurement of the Average Surface Stress of Gold as a Function of Temperature in the Temperature Range 50–985° . . . **J. S. Vermaak and Doris Kuhlmann-Wilsdorf** 4150

The Significant Structure and Properties of Molten Mercuric Halides . . . **Mu Shik Jhon, Gerardo Clemena, and E. R. Van Artsdalen** 4155

Kinetics of Elemental Boron Chlorination by Chlorine Atoms and Chlorine Molecules . . . **Daniel E. Rosner and H. Donald Allendorf** 4159

Surface Interactions of NaY and Decationated Y Zeolites with Nitric Oxide as Determined by Electron Paramagnetic Resonance Spectroscopy . . . **Jack H. Lunsford** 4163

Convective Diffusion across a Porous Diaphragm . . . **Allen R. Overman** 4168

Surface Dipole Moments of Adsorbed Organic Films on Chromium . . . **P. Martin, Jr., and B. J. Bornong** 4172

Ion-Exchange Equilibria between Glass and Molten Salts . . . **H. M. Garfinkel** 4175

Quadrupolar Relaxation of Aluminum-27 Nuclear Magnetic Resonance in Aluminum Alkyls . . **Leonidas Petrakis** 4182

Deuteron Spin-Lattice Relaxation of D_2O in Organic Solvents . . . **J. C. Hindman, A. Svirmickas, and M. Wood** 4188

Thermochemical Investigations of the Water–Triethylamine System . . . **Gary L. Bertrand, John W. Larson, and Loren G. Hepler** 4194

The Oxidation of Hydrazine by Molybdenum(VI) . . . **T. Huang and J. T. Spence** 4198

Activity Coefficients, Aggregation, and Thermodynamics of Tridodecylammonium Salts in Nonpolar Solvents . . . **A. S. Kertes and G. Markovits** 4202

A Spectroscopic Study of the Surface of Zeolite Y. II. Infrared Spectra of Structural Hydroxyl Groups and Adsorbed Water on Alkali, Alkaline Earth, and Rare Earth Ion-Exchanged Zeolites . . . **John W. Ward** 4211

The Conductance of Dilute Solutions of Sodium in Liquid Ammonia at −33.9, −45, and −65° . . . **Robert R. Dewald and John H. Roberts** 4224

Cross-linking of Polystyrene by High-Energy Radiation. II. Molecular Weight Changes in the Pregel Region . . . **Louis M. Alberino and William W. Graessley** 4229

The Vaporization Thermodynamics of Trieuropium Tetroxide . . . **John M. Haschke and Harry A. Eick** 4235

The Kinetics of the Reaction of Trifluoromethyl Radicals with Hydrogen Sulfide . . . **Jayavant D. Kale and Richard B. Timmons** 4239

Nuclear Magnetic Resonance Studies of the Competition between Inter- and Intramolecular Hydrogen Bonding. I. Determination of Equilibrium Constants . . . **Thomas A. Wittstruck and John F. Cronan** 4243

On the Slope of Free Energy Plots in Chemical Kinetics . . . **Audrey O. Cohen and R. A. Marcus** 4249

Apparent and Partial Molal Volumes of Water in Organic Solvents . . . **W. L. Masterton and H. K. Seiler** 4257

The Standard Potential of the Lithium Electrode in Aqueous Solutions . . **Rima Huston and James N. Butler** 4263

Ionization of Liquids by Radiation Studied by the Method of Pulse Radiolysis. I. Solutions of N,N,N′,N′-Tetramethyl-*p*-phenylenediamine in Hydrocarbons . . . **C. Capellos and A. O. Allen** 4265

Most Used ...because it's most useful.

It leads in editorial pages (230) and advertising pages (240). No wonder it generates far more inquiries (68,000) from laboratory chemists, life scientists, physicists, and engineers than any other guide.

The LAB GUIDE is where manufacturers say, "Here we are. Compare us with all our competitors, and our products with theirs."

It's the true one-stop buying source.

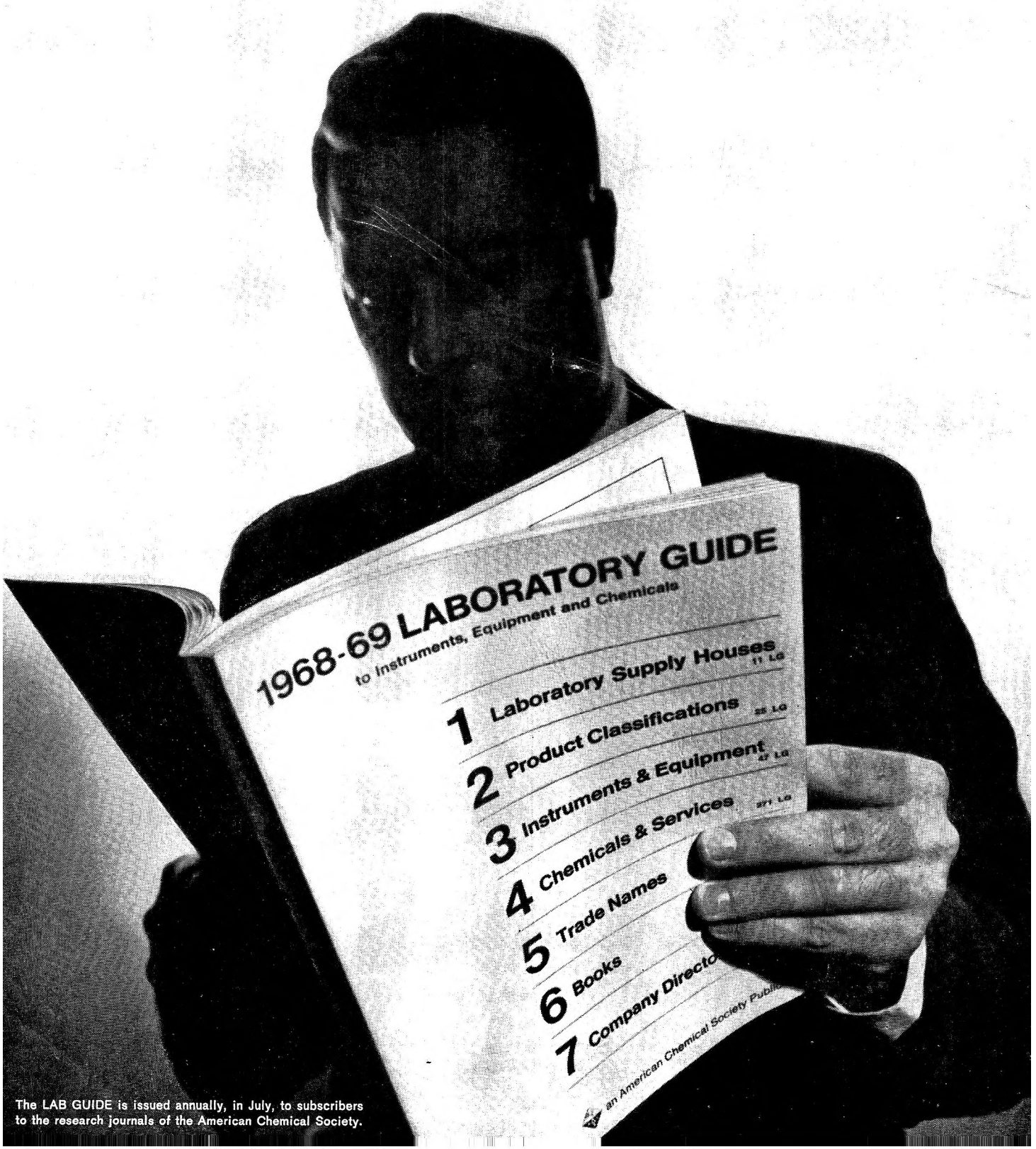

The LAB GUIDE is issued annually, in July, to subscribers to the research journals of the American Chemical Society.

Endor of Methyl, Matrix, and α Protons in Amorphous and Polycrystalline Matrices . . . **James S. Hyde, Günther H. Rist, and L. E. Göran Eriksson** 4269

Combined Endor and Electron Paramagnetic Resonance Techniques in a Study of Some Low-Symmetry Triphenylmethyl Derivatives . . . **Lowell D. Kispert, James S. Hyde, Charles de Boer, Douglas LaFollette, and Ronald Breslow** 4276

The Reaction of Sulfur Hexafluoride with Hydrated Electrons . . . . . **K.-D. Asmus and J. H. Fendler** 4285

The Osmotic and Activity Coefficients of Some Bolaform Electrolytes . . . **O. D. Bonner, Carey Rushing, and Arnold L. Torres** 4290

The Swelling of Alkylammonium Montmorillonites . . . . . **W. H. Slabaugh and P. Anne Hiltner** 4295

Internal Rotation in Liquid 1,2-Difluorotetrachloroethane . . . . . **R. A. Newmark and R. E. Graves** 4299

Molybdovanadophosophoric Acids and Their Salts. II. Investigation of Solution Properties . . . **C. J. Hallada, G. A. Tsigdinos, and B. S. Hudson** 4304

Thermal Conductivity of Binary Liquid Solutions . . . . . **Z. Losenicky** 4308

NOTES

Nitrogen-15 Magnetic Resonance Spectroscopy. Coupling Constants in Hydrogen Cyanide . . . **Gerhard Binsch and John D. Roberts** 4310

The Crystal Structure of Benzophenone . . . . . **Everly B. Fleischer, Nako Sung, and Stuart Hawkinson** 4311

Determination of Critical Temperature by Differential Thermal Analysis . . . **Horst W. Hoyer, Angelo V. Santoro, and Edward J. Barrett** 4312

A Rapid Method for the Determination of Electrical Conductance of Ion-Exchange Membranes . . . **V. Subrahmanyan and N. Lakshminarayanaiah** 4314

Thermal Conductivity and Diffusion Parameter: Critical-Point Behavior . . . . . **L. Seigel** 4316

H_2O–D_2O Isotope Effect in Partial Molal Volumes of Alkali Metal and Tetraalkylammonium Salts . . . **B. E. Conway and L. H. Laliberté** 4317

An Analysis of the Particle Size Distribution of Ammonium Chloride Formed by Rhythmic Precipitation of Ammonia and Hydrogen Chloride . . . . . **G. A. Davies, A. B. Ponter, and S. Singh** 4320

Possible Error in the Calibration of Knudsen Cells by Mercury Effusion . . . . . **David A. Northrop** 4323

A New Method for Studying Ion Adsorption . . . . . **Ying-Chech Chiu and M. A. Genshaw** 4325

Entropy and Thermodynamic Functions of $As_4(g)$ . . . . . **Robert J. Capwell, Jr., and Gerd M. Rosenblatt** 4327

Solvation Numbers of Some Ions in Sulfolane by Conductance Measurements . . . **Mario Della Monica and Ugo Lamanna** 4329

Solubilization Behavior of a Polyoxyethylene Sulfate Type of Surfactant in Connection with the Micellar Charge . . . **Fumikatsu Tokiwa** 4331

The Chloride Catalysis of the Np(III)–Fe(III) Reaction in Aqueous Acid Sclutions . . . **T. W. Newton, Gloria E. McCrary, and W. G. Clark** 4333

Electrochemical and Electron Paramagnetic Resonance Investigation of Nitrotriphenylamine Reductions . . . **Robert F. Nelson and Ralph N. Adams** 4336

Hydrogen Isotope Equilibria in the System Hydrogen–Water . . . . . **Yan Bottinga** 4338

Ion Exchange of Montmorillonite at High Pressures . . . . . **H. L. Chang and H. C. Custard** 4340

COMMUNICATIONS TO THE EDITOR

Light Emission from Shock-Heated Carbon Disulfide–Argon Mixtures . . . **S. J. Arnold, W. G. Brownlee, and G. H. Kimbell** 4344

Effect of Water on Chlorophyll–Quinone Interactions in the Solid State . . . **Gwendolyn Sherman and Eiji Fujimori** 4345

Spin–Spin Coupling in Di-*t*-butylcarbinol. An Alternate Interpretation . . . **R. M. Hammaker, Larry K. Patterson, and Kenneth C. Lin** 4346

Trapped Electrons in γ-Irradiated Polycrystalline *n*-Hydrocarbons Studied by Electron Spin Resonance Spectroscopy . . . **Machio Iwasaki, Kazumi Toriyama, and Toshio Ohmori** 4347

Electrogenerated Chemiluminescence. II. The Rotating-Ring–Disk Electrode and the Pyrene–N,N,N′,N′-Tetramethyl-*p*-phenylenediamine System . . . **J. T. Maloy, Keith B. Prater, and Allen J. Bard** 4348

AUTHOR INDEX

Adams, R. N., 4336
Alberino, L. M., 4229
Alexander, L. E., 3997
Allen, A. O., 4265
Allendorf, H. D., 4159
Arnold, S. J., 4344
Asmus, K.-D., 4285

Bard, A. J., 4348
Barieau, R. E., 4079
Barrett, E. J., 4312
Battles, J. E., 3963
Bertrand, G. L., 4194
Binsch, G., 4310
Bonner, O. D., 4290
Bornong, B. J., 4172
Bottinga, Y., 4338
Breslow, R., 4276
Brownlee, W. G., 4344
Butler, J. N., 4263

Capellos, C., 4265
Capwell, R. J., Jr., 4327
Chang, H. L., 4340
Chiu, Y.-C., 4123, 4325
Clark, W. G., 4333
Clemena, G., 4155
Cohen, A. O., 4249
Conder, J. R., 4020
Conway, B. E., 4317
Cotton, D. J., 4139
Cronan, J. F., 4243
Custard, H. C., 4340

Davies, G. A., 4320
de Boer, C., 4276
Della Monica, M., 4329
Devlin, J. P., 3970
Dewald, R. R., 4224
Doepker, R. D., 4037

Edwards, R. K., 3963
Eick, H. A., 4235
Eriksson, L. E. G., 4269

Fabian, J., 3975
Fendler, J. H., 4285
Fleischer, E. B., 4311
Fujimori, E., 4345
Fuoss, R. M., 4123

Ganis, P., 3997
Garfinkel, H. M., 4175
Gay, D. L., 4145
Genshaw, M. A., 4325
Gilson, D. F. R., 4082
Gorzynski, C. S., Jr., 4015
Graessley, W. W., 4229
Graves, R. E., 4299
Green, M. E., 4072
Griffin, C. E., 4043
Griffith, O. H., 4129
Gundersen, G. E., 3963

Hallada, C. J., 4304
Hammaker, R. M., 4346
Haschke, J. M., 4235
Hawkinson, S., 4311
Hemmes, P., 3986
Hepler, L. G., 4194
Hertl, W., 3993
Hiltner, P. A., 4295
Hindman, J. C., 4188
Hoyer, H. W., 4312
Huang, T., 4198
Hudson, B. S., 4304
Hung, G. W., 3958
Huston, R., 4263
Hyde, J. S., 4269, 4276

Iwasaki, M., 4347

Jhon, M. S., 4155
Johnson, B. M., 4020

Kale, J. D., 4239
Keith, A. D., 4129
Kertes, A. S., 4202
Kimbell, G. H., 4344
Kispert, L. D., 4276
Kistiakowsky, G. B., 3952
Kuhlmann-Wilsdorf, D., 4150

LaFollette, D., 4276
Lakshminarayanaiah, N., 4314
Laliberté, L. H., 4317
Lamanna, U., 4329
Langer, S. H., 4020
Larson, J. W., 4194
Ledbetter, J. W., Jr., 4111
Lin, K. C., 4346
Losenicky, Z., 4308
Lunsford, J. H., 4163

Maloy, J. T., 4348
Marcus, R. A., 4249
Markovits, G., 4202
Martin, P., Jr., 4172
Masterton, W. L., 4257
Maycock, J. N., 4004, 4009, 4015
McCain, D. C., 4115
McCarty, M., Jr., 4009
McCrary, G. E., 4333
Mehlhorn, A., 3975
Messer, C. E., 3958
Myers, R. J., 4115

Nelson, R. F., 4336
Newmark, R. A., 4299
Newton, T. W., 4333
Nobilione, J. M., 3937
Northolt, M. G., 3997
Northrop, D. A., 4323

Ohmori, T., 4347
Olson, D. H., 4095
Orttung, W. H., 4058, 4066
Overman, A. R., 4168

Pai Verneker, V. R., 4004, 4009, 4015
Patterson, L. K., 4346
Petrakis, L., 4182
Petrucci, S., 3986
Platford, R. F., 4053
Ponter, A. B., 4320
Popov, A. I., 4031
Prater, K. B., 4348

Rabinowitch, E., 3941
Rist, G. H., 4269
Roberts, J. D., 4310
Roberts, J. H., 4224
Rosenblatt, G. M., 4327
Rosner, D. E., 4159
Rush, R. M., 4048
Rushing, C., 4290

Santoro, A. V., 4312
Scatchard, G., 4048
Seigel, L., 4316
Seiler, H. K., 4257
Sherman, G., 4345
Sherry, H. S., 4086, 4095
Shimura-Kambe, Y., 4104
Singh, S., 4320
Singhal, G. S., 3941
Slabaugh, W. H., 4295
Spence, J. T., 4198
Stern, J. H., 3937
Subrahmanyan, V., 4314
Sung, N., 4311
Svirmickas, A., 4188

Temussi, P. A., 3997
Timmons, R. B., 4239
Tokiwa, F., 4331
Toriyama, K., 4347
Torres, A. L., 4290
Tsau, J., 4082
Tsigdinos, G. A., 4304

Van Artsdalen, E. R., 4155
Vermaak, J. S., 4150

Waggoner, A. S., 4129
Walter, T. A., 3952
Ward, A. T., 4133
Ward, J. W., 4211
Ware, B., 3970
Wehman, T. C., 4031
Whalley, E., 4145
Williams, W. P., 3941
Williamson, K., 3970
Williamson, M. P., 4043
Wittstruck, T. A., 4243
Wood, M., 4188
Wu, Y. C., 4048

Yafuso, M., 4072

Zahradník, R., 3975

THE JOURNAL OF

PHYSICAL CHEMISTRY

Volume 72, Number 13 December 1968

Temperature Dependence of Nuclear Magnetic Resonance Coupling Constants and Chemical Shifts of the Vinyl Halides and Some Vinyl Ethers . . . **Wallace S. Brey, Jr., Katherine Nasfay Scott, and Donald R. Whitman** 4351

The Acetylene-Photosensitized Reaction of Methane at 1470 Å . . **Seiki Takita, Yuji Mori, and Ikuzo Tanaka** 4360

Crystal Structure of the Zeolite Nickel Faujasite . . . . . **D. H. Olson** 4366

The Dielectric Behavior of Aqueous Solutions of Bovine Serum Albumin from Radiowave to Microwave Frequencies . . . . **Edward H. Grant, Susan E. Keefe, and Shiro Takashima** 4373

Multicomponent Equilibria in Exchange of Substituents between the Dimethylsilicon and Dimethylgermanium Moieties . . . **Kurt Moedritzer, Leo C. D. Groenweghe, and John R. Van Wazer** 4380

The Thermal Decomposition of Solid Hexaamminecobalt(III) Azide. The Cobalt(II) Reaction . . . **T. B. Joyner** 4386

New Method for Determining Magnetic Susceptibility and Magnetic Moment . . . **Toshio Ikeda and Hisashi Yoshioka** 4392

Statistical Theory for the Equilibrium Distribution of Rigid Molecules in Inert Porous Networks. Exclusion Chromatography . . . **J. Calvin Giddings, Eugene Kucera, Christopher P. Russell, and Marcus N. Myers** 4397

Electromotive Force Studies in Aqueous Solutions at Elevated Temperatures. X. The Thermodynamic Properties of HCl–KCl, HCl–RbCl, HCl–CsCl, HCl–$MgCl_2$, HCl–$CaCl_2$, HCl–$SrCl_2$, and HCl–$AlCl_3$ Mixtures . . . . . **M. H. Lietzke and H. A. O'Brien, Jr.** 4408

Phase Transformations in the Praseodymium Oxide–Oxygen System: High-Temperature X-Ray Diffraction Studies . . . **D. Arthur Burnham and LeRoy Eyring** 4415

High-Temperature X-Ray Diffraction Studies of the Terbium Oxide–Oxygen and Mixed Cerium Terbium Oxide–Oxygen Systems . . . . . **D. Arthur Burnham, LeRoy Eyring, and J. Kordis** 4424

Anomalous Temperature Dependence of Kinetic Carbon Isotope Effects and the Phenomenon of Crossover . . . **Thomas T.-S. Huang, William J. Kass, Warren E. Buddenbaum, and Peter E. Yankwich** 4431

Solid-State Reactivity of Picric Acid and Substituted Hydrocarbons . . . . . **R. P. Rastogi and N. B. Singh** 4446

Adsorption Characteristics of Water-Soluble Polymers. I. Poly(vinyl alcohol) and Poly(vinylpyrrolidone) at the Aqueous–Air Interface . . . . . **J. E. Glass** 4450

Adsorption Characteristics of Water-Soluble Polymers. II. Poly(ethylene oxide) at the Aqueous–Air Interface . . . **J. E. Glass** 4459

Absorptions and Fluorescences of 2-Phenylnaphthalene, 2′-Methyl-2-phenylnaphthalene, and 1-Fluoro-2-phenylnaphthalene. Spectroscopic Evidence for the Equilibrium Conformation of the Lowest Excited States . . . . . **Homer E. Holloway, Robert V. Nauman, and James H. Wharton** 4468

The Electronic Structure and Spectra of 2-Phenylnaphthalene. Ground- and Excited-State Potential Energies as Functions of Molecular Conformation . . . **Homer E. Holloway, Robert V. Nauman, and James H. Wharton** 4474

Heterogeneous Activation in Thermal Unimolecular Reaction . . . **Kenneth M. Maloney and B. S. Rabinovitch** 4483

The Experimental Evaluation of k_∞ in Unimolecular Reaction Systems . . . . . **I. Oref and B. S. Rabinovitch** 4488

Infrared Vibrational Properties of GeF_2 . . . . . **J. W. Hastie, R. Hauge, and J. L. Margrave** 4492

Thermodynamics of Binary Solutions of Nonelectrolytes with 2,2,4-Trimethylpentane. III. Volumes of Mixing with Cyclohexane (10–80°) and Carbon Tetrachloride (10–80°) . . . **Elmer L. Washington and Rubin Battino** 4496

Thermodynamics of Binary Solutions of Nonelectrolytes with 2,2,4-Trimethylpentane. IV. Vapor–Liquid Equilibrium (35–75°) and Volume of Mixing (25°) with Carbon Tetrachloride . . **Rubin Battino** 4503

Steric Effect in the Radiolysis of *cis*- and *trans*-1,2-Dimethylcyclohexane . . . . . **Manfred K. Eberhardt** 4509

Photoelectric Effects in Thin and Bilayer Lipid Membranes in Aqueous Media . . . . . **H. T. Tien** 4512

A Kinetic Study of the Reactions of Water and *t*-Butyl Alcohol with Sodium in Liquid Ammonia . . . **Robert R. Dewald and Richard V. Tsina** 4520

Vaporization Equilibria in the Sodium Chloride–Zinc Chloride System . . . . **Donald W. Rice and N. W. Gregory** 4524

Reactions in the Cobalt-60 Irradiation of Pyridine and Methylpyridines . . . . **J. J. Duvall and H. B. Jensen** 4528

The Chemical Model as Applied to Associated Liquid Solutions. The Ethanol–Heptane System . . . **R. W. Haskell, H. B. Hollinger, and H. C. Van Ness** 4534

Ionic Polymerization under an Electric Field. XII. Living Anionic Polymerization of Styrene in the Binary Mixtures of Benzene and Tetrahydrofuran . . . **Norio Ise, Hideo Hirohara, Tetsuo Makino, and Ichiro Sakurada** 4543

The Gibbs Free Energy of Transfer of the Alkali Perrhenates and Perchlorates between Pure Water and Pure Nitromethane . . . . . **G. R. Haugen and H. L. Friedman** 4549

Tracer Studies of Acid-Catalyzed Reactions. VIII. Langmuir Kinetics in Cycloalkane Isomerization over Silica–Alumina . . . . . **Joe W. Hightower and W. Keith Hall** 4555

Cooperative Binding to a One-Dimensional Lattice. The Amylose–Iodine–Iodide Complex . . . **Friedemann W. Schneider, Charles L. Cronan, and Sunil K. Podder** 4563

Kinetics of the Li(Hg)–Li^+ Reaction in Dimethyl Sulfoxide . . . . . **David R. Cogley and James N. Butler** 4568

The Molybdenum(VI)-Catalyzed Oxidation of Hydrazine by Methylene Blue . . . . **T. Huang and J. T. Spence** 4573

The Fluorescence of Protonated Azulenoid Systems . . . . . **R. C. Dhingra and J. A. Poole** 4577

Standard Potentials of Potassium Electrodes and Activity Coefficients and Medium Effects of Potassium Chloride in Ethanol–Water Solvents . . . **Aloys J. Dill, Leonard M. Itzkowitz, and Orest Popovych** 4580

Activation of Hydrogen at 79°K by Supported Copper . . . . **J. E. Benson, Arden B. Walters, and M. Boudart** 4587

Apparent Molal Expansibilities of Some Divalent Chlorides in Aqueous Solution at 25° . . . . . **Frank J. Millero** 4589

Electronic Oscillator Strength of CF_2 . . . . . **A. P. Modica** 4594

Effects of Matrix Polarity on the Optical and Electron Spin Resonance Spectra of Trapped Electrons in Organic Glasses . . . . . **Alfred Ekstrom and John E. Willard** 4599

Radical Decay Kinetics in Organic Glasses. Spatial Effects and Isotope Effects . . . **William G. French and John E. Willard** 4604

Homolytic Hydroxylation of Naphthalene in Oxygenated Aqueous Solutions by γ Radiolysis at Higher Temperatures . . . . . **I. Balakrishnan and M. P. Reddy** 4609

Polymer Studies by Gel Permeation Chromatography. IV. The Degradation of Polystyrene by Ultrasonics and by Benzoyl Peroxide . . . . . **William B. Smith and Harold W. Temple** 4613

Association in Mixed Alkali Halide Vapors . . . . . **J. Guion, D. Hengstenberg, and M. Blander** 4620

Infrared Spectra of Gaseous Protio- and Deuteriooxalic Acids . . . . . **Bruce M. Pava and Fred E. Stafford** 4628

Spectra of Metal β-Ketoenolates. The Electronic Spectrum of Monomeric Nickel(II) Acetylacetonate and the Infrared Spectra of Matrix-Isolated Acetylacetonates of Cobalt(II), Nickel(II), Copper(II), and Zinc(II) . . . **J. P. Fackler, Jr., M. L. Mittleman, H. Weigold, and G. M. Barrow** 4631

Catalytic Polarographic Current of a Metal Complex. IV. Effect of the Electrode Double Layer on the Ni(II)–*o*-Phenylenediamine Prewave . . . **Lowell R. McCoy, Harry B. Mark, Jr., and Lucien Gierst** 4637

Brillouin Spectra of Dilute Solutions and the Landau–Placzek Formula . . . **George A. Miller and Ching S. Lee** 4644

The Solubility of Helium, Nitrogen, Argon, and Ethane in N-Methylacetamide, a High Dielectric Solvent without Anomalous Structural Effects . . . . . **R. H. Wood and D. E. DeLaney** 4651

Thermodynamics of Ionization of Deuterium Oxide . . . . . **Robert N. Goldberg and Loren G. Hepler** 4654

Potentials of Cells with Liquid Junctions . . . . . **William H. Smyrl and John Newman** 4660

A Shock Tube Study of the Pyrolysis of Propylene. Kinetics of the Vinyl–Methyl Bond Rupture . . . **G. A. Chappell and H. Shaw** 4672

Hydrogen Bonding between Adsorbed Gases and Surface Hydroxyl Groups on Silica . . **W. Hertl and M. L. Hair** 4676

NOTES

A Proposed Viscosity–Concentration Equation beyond Einstein's Region . . . . . **S. P. Moulik** 4682

Gas-Phase Photolysis of Mixtures of Cyclohexane with Benzene and with Nitrous Oxide at 1470 Å . . . **Robert R. Hentz and Ronald J. Knight** 4684

The Vapor-Phase Infrared Spectra of the Niobium Oxotrihalides, $NbOCl_3$, $NbOBr_3$, and $NbOI_3$ . . . **Carl O. Schulz and Fred E. Stafford** 4686

Some Comments on Cohesion Energies of Liquids . . . . . **Vojtech Fried and Garry B. Schneier** 4688

Acidic Sites on Mordenite. An Infrared Study of Adsorbed Pyridine . . . . . **F. R. Cannings** 4691

An Apparatus for Degassing Liquids by Vacuum Sublimation . . . **T. N. Bell, E. L. Cussler, K. R. Harris, C. N. Pepela, and Peter J. Dunlop** 4693

Phase Separation in the Palladium–Hydrogen System . . . . . **Y. Ebisuzaki and M. O'Keeffe** 4695

Mass Spectra and Sublimation Pressures of IF_7 and IOF_5 . . . **C. J. Schack, D. Pilipovich, S. N. Cohz, and D. F. Sheehan** 4697

The Diffusion of Gases in Nonpolar Liquids. The Open-Tube Method . . . **Lorna Bennett, Wing Y. Ng, and John Walkley** 4699

Quantum Yield of the Photonitrosation of Cyclohexane . . . . . **Hajime Miyama, Noriho Harumiya, Yoshikazu Ito, and Shigeru Wakamatsu** 4700

Electron Magnetic Resonance Spectra of $MnCl_2$—LiCl–KCl Eutectic Mixtures . . . . . **Terry B. Swanson** 4701

Ion Exchange in Molten Salts. III. The Ion-Exchange Properties of Sodium Zeolite A in Molten $NaNO_3$. The Exchange with Calcium and Strontium Cations . . . . . **M. Liquornik and Y. Marcus** 4704

The Formation of the $S_2O_4^-$ Free Radical in Dimethylformamide . . . . . **R. G. Rinker and S. Lynn** 4706

Crystal Structure Effect in the γ Radiation of *p*-Dichlorobenzene . . . . . **F. K. Milia and E. K. Hadjoudis** 4707

The Effect of Neighboring Magnetic Anisotropy on NH Proton Chemical Shifts . . . . . **B. M. Fung** 4708

Conductance of Thallous Nitrate in Dioxane–Water Mixtures at 25° . . . **Alessandro D'Aprano and Raymond M. Fuoss** 4710

The Thermochemistry of the Gas-Phase Equilibrium $2CH_3I \rightarrow CH_4 + CH_2I_2$. The Heat of Formation of CH_2I_2 . . . **Shozo Furuyama, David M. Golden, and Sidney W. Benson** 4713

COMMUNICATIONS TO THE EDITOR

On Carbonyl Carbon-13 Hyperfine Splitting in Free Radicals and the Possible Nonplanarity of Certain Ketyls . . . **E. Thomas Strom** 4715

The Measurement of Rotary Power and Rotary Dispersion Using Polarized Rayleigh Scattering of Laser Radiation . . . **J. N. Gayles and A. W. Lohmann** 4716

Interpretation of the High-Resolution Electron Spin Resonance Spectrum of the 2,4,5-Triphenylimidazolyl Radical . . . **M. A. J. Wilks and M. R. Willis** 4717

Effect of Dimer Formation on the Triplet States of Organic Dyes . . **Richard W. Chambers and David R. Kearns** 4718

Correlation of ΔH and ΔS for the Association of the Rare Earth(III) Ions with Fluoride . . . **R. E. Mesmer and C. F. Baes, Jr.** 4720

On the Radiation-Induced Reduction of Amide and Peptide Functions in Aquoorganic Systems . . . **John Holian and Warren M. Garrison** 4723

Additions and Corrections 4724

Author Index to Volume 72, 1968 4726

Subject Index to Volume 72, 1968 4749

AUTHOR INDEX

Baes, C. F., Jr., 4720
Balakrishnan, I., 4609
Barrow, G. M., 4631
Battino, R., 4496, 4503
Bell, T. N., 4693
Bennett, L., 4699
Benson, J. E., 4587
Benson, S. W., 4713
Blander, M., 4620
Boudart, M., 4587
Brey, W. S., Jr., 4351
Buddenbaum, W. E., 4431
Burnham, D. A., 4415, 4424
Butler, J. N., 4568

Cannings, F. R., 4691
Chambers, R. W., 4718
Chappell, G. A., 4672
Cogley, D. R., 4568
Cohz, S. N., 4697
Cronan, C. L., 4563
Cussler, E. L., 4693

D'Aprano, A., 4710
DeLaney, D. E., 4651
Dewald, R. R., 4520
Dhingra, R. C., 4577
Dill, A. J., 4580
Dunlop, P. J., 4693
Duvall, J. J., 4528

Eberhardt, M. K., 4509
Ebisuzaki, Y., 4695
Ekstrom, A., 4599
Eyring, L., 4415, 4424

Fackler, J. P., Jr., 4631
French, W. G., 4604
Fried, V., 4688
Friedman, H. L., 4549
Fung, B. M., 4708
Fuoss, R. M., 4710
Furuyama, S., 4713

Garrison, W. M., 4723
Gayles, J. N., 4716
Giddings, J. C., 4397
Gierst, L., 4637
Glass, J. E., 4450, 4459
Goldberg, R. N., 4654
Golden, D. M., 4713
Grant, E. H., 4373
Gregory, N. W., 4524
Groenweghe, L. C. D., 4380
Guion, J., 4620

Hadjoudis, E. K., 4707
Hair, M. L., 4676
Hall, W. K., 4555
Harris, K. R., 4693
Harumiya, N., 4700
Haskell, R. W., 4534
Hastie, J. W., 4492
Hauge, R., 4492
Haugen, G. R., 4549
Hengstenberg, D., 4620
Hentz, R. R., 4684
Hepler, L. G., 4654
Hertl, W., 4676
Hightower, J. W., 4555
Hirohara, H., 4543
Holian, J., 4723

Hollinger, H. B., 4534
Holloway, H. E., 4468, 4474
Huang, T., 4573
Huang, T. T.-S., 4431

Ikeda, T., 4392
Ise, N., 4543
Ito, Y., 4700
Itzkowitz, L. M., 4580

Jensen, H. B., 4528
Joyner, T. B., 4386

Kass, W. J., 4431
Kearns, D. R., 4718
Keefe, S. E., 4373
Knight, R. J., 4684
Kordis, J., 4424
Kucera, E., 4397

Lee, C. S., 4644
Lietzke, M. H., 4408
Liquornik, M., 4704
Lohmann, A. W., 4716
Lynn, S., 4706

Makino, T., 4543
Maloney, K. M., 4483
Marcus, Y., 4704
Margrave, J. L., 4492
Mark, H. B., Jr., 4637
McCoy, L. R., 4637
Mesmer, R. E., 4720
Milia, F. K., 4707
Miller, G. A., 4644
Millero, F. J., 4589
Mittleman, M. L., 4631
Miyama, H., 4700

Modica, A. P., 4594
Moedritzer, K., 4380
Mori, Y., 4360
Moulik, S. P., 4682
Myers, M. N., 4397

Nauman, R. V., 4468, 4474
Newman, J., 4660
Ng, W. Y., 4699

O'Brien, H. A., Jr., 4408
O'Keeffe, M., 4695
Olson, D. H., 4366
Oref, I., 4488

Pava, B. M., 4628
Pepela, C. N., 4693
Pilipovich, D., 4697
Podder, S. K., 4563
Poole, J. A., 4577
Popovych, O., 4580

Rabinovitch, B. S., 4483, 4488
Rastogi, R. P., 4446
Reddy, M. P., 4609
Rice, D. W., 4524
Rinker, R. G., 4706
Russell, C. P., 4397

Sakurada, I., 4543
Schack, C. J., 4697
Schneider, F. W., 4563
Schneier, G. B., 4688
Schulz, C. O., 4686
Scott, K. N., 4351

Shaw, H., 4672
Sheehan, D. F., 4697
Singh, N. B., 4446
Smith, W. B., 4613
Smyrl, W. H., 4660
Spence, J. T., 4573
Stafford, F. E., 4628, 4686
Strom, E. T., 4715
Swanson, T. B., 4701

Takashima, S., 4373
Takita, S., 4360
Tanaka, I., 4360
Temple, H. W., 4613
Tien, H. T., 4512
Tsina, R. V., 4520

Van Ness, H. C., 4534
Van Wazer, J. R., 4380

Wakamatsu, S., 4700
Walkley, J., 4699
Walters, A. B., 4587
Washington, E. L., 4496
Weigold, H., 4631
Wharton, J. H., 4468, 4474
Whitman, D. R., 4351
Wilks, M. A. J. 4717
Willard, J. E., 4599, 4604
Willis, M. R., 4717
Wood, R. H., 4651

Yankwich, P. E., 4431
Yoshioka, H., 4392

NOTICE TO AUTHORS

I. General Considerations

The Journal of Physical Chemistry is devoted to reporting both experimental and theoretical research dealing with fundamental aspects of physical chemistry. Space limitations necessitate giving preference to research articles dealing with previously unanswered basic questions in physical chemistry. Acceptable topics are those of general interest to physical chemists, especially work involving new concepts, techniques, and interpretations. Research that may lead to reexaminations of generally accepted views is, of course, welcome.

The Journal of Physical Chemistry publishes three types of manuscripts: *Articles*, *Notes*, and *Communications to the Editor*.

Authors reporting data should include, if possible, an interpretation of the data and its relevance to the theories of the properties of matter. However, the discussion should be concise and to the point and excessive speculation is to be discouraged. Papers reporting redeterminations of existing data will be acceptable only if there is reasonable justification for repetition: for example, if the more recent or more accurate data lead to new questions or to a reexamination of well known theories. Manuscripts that are essentially applications of chemical data or reviews of the literature are, in general, not suitable for publication in *The Journal of Physical Chemistry*. Detailed comparisons of methods of data analysis will be considered only if the paper also contains original data, or if such comparison leads to a genesis of new ideas.

Authors should include an introductory statement outlining the scientific rationale for the research. The statement should clearly specify the questions for which answers are sought and the connection of the present work with previous work in the field. All manuscripts are subject to critical review. It is to be understood that the final decision relating to a manuscript's suitability rests solely with the editorial staff.

Symposium papers are sometimes published as a group, but only after special arrangement with the editor.

Authors' attention is called to the "Handbook for Authors," available from the Special Issues Sales Department, American Chemical Society, 1155 Sixteenth St., N.W., Washington, D. C. 20036, in which pertinent material is to be found.

II. Types of Manuscripts

A. Articles should cover their subjects with thoroughness, clarity and completeness. However, authors should also strive to make their *Articles* as concise as possible, avoiding unnecessary historical background. Abstracts to *Articles* should be brief—300 words is a maximum—and should serve to summarize the significant data and conclusions. The abstract should convey the essence of the *Article* to the reader.

B. Notes. Papers submitted in the category of *Notes* should report work that represents a complete and self-contained study of limited nature. *Notes* are a luxury in the present scientific literature; authors should not use a *Note* to report work that is part of a continuing study. *Notes* are not to be used for reporting preliminary results; reports of such work should be postponed until the work is completed or should be submitted as *Communications* if the results are of immediate or unusual interest to physical chemists. The same criteria of suitability for publication apply to *Notes* as to *Articles* (see General Considerations). The length of a *Note*, including tables, figures, and text, must not exceed 1.5 journal pages (1500 words or the equivalent). A *Note* should not be accompanied by an abstract.

C. Communications to the Editor are of two types, *Letters* and *Comments*. Both types are restricted to three-quarters of a page (750 words or the equivalent) including tables, figures, and text, and both types of *Communications* are subject to critical review, but special efforts will be made to expedite publication.

Letters should report preliminary results whose immediate availability to the scientific community is deemed important, and whose topic is timely enough to justify the double publication that usually results from the publication of a *Letter*.

Comments include significant remarks on the work of others. The editorial staff will generally permit the authors of the work being discussed to reply.

III. Introduction

All manuscripts submitted should contain brief introductory remarks describing the purpose of the work and giving sufficient background material to allow the reader to appreciate the state-of-knowledge at the time when the work was done. The introductory remarks in an *Article* should constitute the first section of the paper and should be labeled accordingly. In *Notes* and *Communications*, the introductory material should not be in such a separate section. To judge the appropriateness of the manuscript for *The Journal of Physical Chemistry*, the editorial staff will place considerable weight on the author's intentions as stated in the Introduction.

IV. Functions of Reviewers

The editorial staff requests the scientific advice of reviewers who are active in the area of research covered by the manuscript. The reviewers act only in an advisory capacity and the final decision concerning a manuscript is the responsibility of the editorial staff. The reviewers are asked to comment not only on the scientific content, but also on the manuscript's suitability for *The Journal of Physical Chemistry*. With respect to *Communications*, the reviewers are asked to comment specifically on the urgency of publication. All reviews are anonymous and the reviewing process is most effective

if reviewers do not reveal their identities to the authors. An exception arises in connection with a manuscript submitted for publication in the form of a comment on the work of another author. Under such circumstances the first author will, in general, be allowed to review the communication and to write a rebuttal, if he so chooses. The rebuttal and the original communication may be published together in the same issue of the journal. Revised manuscripts are generally sent back to the original reviewers, who are asked to comment on the revisions. If only minor revisions are involved, the editorial staff examines the revised manuscript in light of the recommendations of the reviewers and without seeking further opinions. For the convenience of reviewers, authors are advised to indicate clearly, either in the manuscript or in a covering letter, the specific revisions that have been made.

V. Submission of Manuscripts

All manuscripts must be submitted in duplicate, including an original typewritten double-spaced copy. All original data which the author deems pertinent must be submitted along with the manuscript. For example, a paper reporting a crystal structure should include structure factor tables for use by the reviewers. Manuscripts must be submitted on $8^1/_2 \times 11$ in. paper; legal-sized paper is not acceptable. Authors submitting figures must include original drawings or photographs thereof. Xerographic copies of figures are acceptable for review purposes only. Graphs must be black ink on white or blue paper. Lettering at the sides of graphs may be penciled in and will be typeset. Figures and tables should be held to a minimum consistent with adequate presentation of information.

Footnotes and references to the literature should be numbered consecutively within the paper; the number should also be placed in parentheses in the left margin opposite the line in which the reference first appears. A complete list of references should appear at the end of the paper. Initials of the authors referred to in the citations should be included in the complete reference at the back of the paper. Nomenclature should conform to that used in *Chemical Abstracts* and mathematical characters should be underlined for italics, Greek letters should be annotated, and subscripts and superscripts clearly marked.

Papers should not depend for their usefulness on unpublished material, and excessive reference to material in press is discouraged. References not readily available (*e.g.*, private technical reports, preprints, or articles in press) that are necessary for a complete review of the paper must be included with the manuscript for use by the reviewers.

VI. Revised Manuscripts

A manuscript sent back to an author for revision should be returned to the editor within 6 months; otherwise it will be considered withdrawn and treated as a new manuscript when and if it is returned. Revised manuscripts returned to the editor must be submitted in duplicate, and all changes must be made by typewriter, since handwritten additions or corrections are unacceptable. Unless the changes are very minor, all pages affected by revision must be retyped. If revisions are so extensive that a new typescript of the manuscript is necessary, it is requested that a copy of the original manuscript be submitted along with the revised one.

VII. Supplementary Material

By arrangement with the National Auxiliary Publications Service (NAPS) of the American Society for Information Science (ASIS), supplementary material, such as extensive tables, graphs, spectra, and calculations, can be distributed in the form of microfiche copies or photoprints readable without optical aids. This material should accompany the manuscript for review by the editors and reviewers. Upon acceptance, it will be sent by the editor to NAPS where it is assigned a document number. A deposit fee of $6.50 (for 60 manuscript pages or less) is required and should be included with the material sent to the editor. The check must be made payable to ASIS-NAPS. Further details may be obtained from NAPS c/o CCM Information Sciences, Inc., 22 W. 34 St., New York, N. Y. 10001.

VIII. Proofs and Reprints

Galley proofs, original manuscript, cut copy, and reprint order form are sent by the printer directly to the author who submitted the manuscript. The attention of the authors is directed to the instructions which accompany the proof, especially the requirement that all corrections, revisions, and additions be entered on the proof and not on the manuscript. Proofs should be checked against the manuscript (in particular all tables, equations, and formulas, since this is not done by the editor) and returned as soon as possible. No paper is released for printing until the author's proof has been received. Alterations in an article after it has been set in type are made at the author's expense, and it is understood that by entering such alterations on proofs the author agrees to defray the cost thereof. The filled-out reprint form must be returned with the proof, and if a price quotation is required by the author's organization a request for it should accompany the proof. Since reprinting is generally done from the journal press forms, all orders must be filed before press time. None can be accepted later, unless a previous request has been made to hold the type. Reprint shipments are made a month or more after publication, and bills are issued by the printer subsequent to shipment. Neither the editors nor the Washington office keeps any supply of reprints. Therefore, only the authors can be expected to meet requests for single copies of papers.

A page charge is assessed to cover in part the cost of publication. Although payment is expected, it is not a condition for publication. Articles are accepted or rejected only on the basis of merit, and the editor's decision to publish the paper is made before the charge is assessed. The charge per journal page is $35.

THE JOURNAL OF
PHYSICAL CHEMISTRY

VOLUME 72, NUMBER 9 SEPTEMBER 16, 1968

Surface Tension of Some Binary Liquid Mixtures

by S. K. Suri and V. Ramakrishna[1]

Chemistry Department, Indian Institute of Technology, New Delhi, India *(Received May 5, 1968)*

Surface tension of binary solutions containing dioxane, benzene, cyclohexane, and nitrobenzene, has been determined. The systems dioxane + benzene and dioxane + nitrobenzene show linear dependence of surface tension on the composition at 20–30°, while the others follow the expected trend. Two models for the surface layer, based on the regular-solution theory, have been applied to the data. The nature of the resulting X_1^{σ}–X_1^{l} plots has been discussed in terms of the parameters f_1^{l}, A, and ω^{l} of the systems.

Introduction

A reasonable analysis of the nature of the surface layer of binary liquid mixtures can be made in terms of some recent theories.[2–7] In almost all such analyses a knowledge of the following factors is necessary: (i) activity coefficients of the components in bulk solution, (ii) surface occupancy of the individual molecules, and (iii) a suitable model for the surface layer to obtain surface concentrations. Uncertainties involved in the use of bulk activity coefficients can be reduced by choosing mixtures of hydrocarbons which behave nearly like ideal solutions, as has been done by Schmidt, Clever, and coworkers.[8,9] They found, however, that in some cases, *viz.*, solutions of *n*-dodecane in isooctane[8a] and in *n*-hexane and 2,2,4-trimethylpentane,[9] unexpected surface tension curves were obtained, which were attributed to the comparatively larger molecular size of the first component and orientation effects at the surface. We have shown recently[10] that in the system benzene + cyclohexane, the use of cross-sectional areas assuming spherical molecules is less satisfactory than the assumption of flat-lying molecules at the free surface as well as at a solid–liquid interface. Like benzene and cyclohexane, 1,4-dioxane has a six-membered ring and is also nonpolar. In the light of the above observations, surface tensions of binary solutions containing dioxane, for which the available data are scanty, assume particular significance. In this article we present the surface tensions of binary solutions of dioxane in benzene and in cyclohexane, and we also compare the influence of one polar molecule, nitrobenzene, in these solvents.

Experimental Section

The liquids were purified according to standard procedures.[10,11] Particular care was taken to keep dioxane free of moisture; thus it was distilled over metallic

(1) To whom all correspondence may be addressed.

(2) J. H. Hildebrand and R. L. Scott, "The Solubility of Non-Electrolytes," 3rd ed, Dover Publications Inc., New York, N. Y., 1964.

(3) R. Defay, I. Prigogine, A. Bellemans, and D. H. Everett, "Surface Tension and Adsorption," Longmans, Green & Co. Ltd., London, 1966.

(4) J. J. Kipling, "Adsorption from Solutions of Non-Electrolytes," Academic Press Inc., New York, N. Y., 1965.

(5) T. P. Hoar and D. A. Melford, *Trans. Faraday Soc.*, **53**, 315 (1957).

(6) F. B. Sprow and J. M. Prausnitz, *Can. J. Chem.*, **45**, 25 (1967); *Trans. Faraday Soc.*, **62**, 1105 (1966); C. A. Eckert and J. M. Prausnitz, *Amer. Inst. Chem. Eng. J.*, **10**, 677 (1964).

(7) J. C. Eriksson, *Advan. Chem. Phys.*, **6**, 145 (1964); *Ark. Kemi.*, **26**, 49 (1966).

(8) (a) H. B. Evans and H. L. Clever, *J. Phys. Chem.*, **68**, 3433 (1964); (b) R. L. Schmidt, J. C. Randall, and H. L. Clever, *ibid.*, **70**, 3912 (1966).

(9) R. L. Schmidt and H. L. Clever, Abstracts, 153rd National Meeting of the American Chemical Society, Miami Beach, Fla., April 1967.

(10) S. K. Suri and V. Ramakrishna, *J. Phys. Chem.*, **72**, 1555 (1968).

(11) A. Weissberger, "Organic Solvens," Vol. VII, 2nd ed, Interscience Publishers, Inc., New York, N. Y., 1960.

Table I: Some Physical Properties of the Liquids Used[a]

Liquid (i)	Fp, °C	ρ_i, g/ml 20°	ρ_i, g/ml 30°	γ_i, dyn/cm 20°	γ_i, dyn/cm 30°	$10^{10}A_i$ (30°),[b] cm²/mol
Benzene	5.50 (5.53)	0.8790 (0.8790)	0.8685 (0.8685)	28.85 (28.88)	27.55 (27.57)	0.169
Cyclohexane	6.60 (6.68)	0.7786 (0.7785)	0.7694 (0.7690)	25.00 (25.20)	23.85 (23.82)	0.193
1,4-Dioxane	11.75 (11.80)	1.0338 (1.0337)	1.0220 (1.0223)	33.75 (33.74)	32.20 (32.20)	0.165
Nitrobenzene	5.70 (5.70)	1.2035 (1.2032)	1.1933 (1.1936)	43.40 (43.35)	42.20 (42.17)	0.185

[a] All values in parentheses indicate the literature values.[12] [b] Calculated from $A_i = V_i^{2/3}N^{1/3}$.

Table II: Surface Tension (dyn/cm) of Some Binary Solutions at 30°

Benzene (1) + cyclohexane (2) X_1^1	γ	Benzene (1) + dioxane (2) X_1^1	γ	Cyclohexane (1) + dioxane (2) X_1^1	γ	Benzene (1) + nitrobenzene (2) X_1^1	γ	Cyclohexane (1) + nitrobenzene (2) X_1^1	γ	Dioxane (1) + nitrobenzene (2) X_1^1	γ
0.1332	24.10	0.1769	31.49	0.1456	30.17	0.1152	39.15	0.1232	35.49	0.1258	41.00
0.2405	24.36	0.3304	30.74	0.2885	28.60	0.2228	37.05	0.1826	33.47	0.2116	40.20
0.3380	24.50	0.4860	29.87	0.4335	27.32	0.3335	35.43	0.2883	30.52	0.3459	38.85
0.4426	24.80	0.5330	29.75	0.4857	26.64	0.4374	34.07	0.3648	29.07	0.4414	37.92
0.5621	25.32	0.6552	29.12	0.6006	25.92	0.5333	32.82	0.4766	27.30	0.5446	36.98
0.6373	25.65	0.8175	28.42	0.7807	25.00	0.6320	31.65	0.5729	26.27	0.6445	35.90
0.7491	26.13	...	...	...	...	0.7285	30.61	0.6776	25.41	0.7355	35.05
0.8277	26.56	...	...	...	...	0.8217	29.58	0.7572	24.91	0.8269	34.19
0.9136	27.05	...	...	...	...	0.9118	28.54	0.8842	24.32	0.9124	33.30

Table III: Surface Tension (dyn/cm) of the Binary Solutions at 20°

Benzene (1) + cyclohexane (2) X_1^1	γ	Benzene (1) + dioxane (2) X_1^1	γ	Cyclohexane (1) + dioxane (2) X_1^1	γ	Benzene (1) + nitrobenzene (2) X_1^1	γ	Cyclohexane (1) + nitrobenzene (2) X_1^1	γ	Dioxane (1) + nitrobenzene (2) X_1^1	γ
0.2236	25.25	0.1769	32.92	0.1456	32.29	0.1152	40.72	0.1137	39.38	0.2116	41.31
0.4495	25.70	0.3304	32.08	0.2885	30.63	0.2003	39.13	0.2084	36.32	0.3350	39.98
0.5510	25.97	0.4860	31.33	0.4335	29.45	0.3335	36.97	0.3884	31.51	0.4414	39.09
0.6601	26.52	0.5330	31.09	0.4857	28.64	0.4254	35.68	0.5854	28.80	0.5213	38.28
0.7436	26.86	0.6552	30.34	0.6006	28.01	0.5333	34.25	0.7932	26.83	0.6623	36.82
0.8474	27.47	0.8175	29.83	0.7807	26.49	0.6320	33.01	0.8988	25.81	0.7355	36.25
...	...	...	...	...	...	0.7285	31.75	...	...	0.7711	35.77
...	...	...	...	...	...	0.8177	30.78	...	...	0.9124	34.51
...	...	...	...	...	...	0.9117	29.67	...	...	...	...

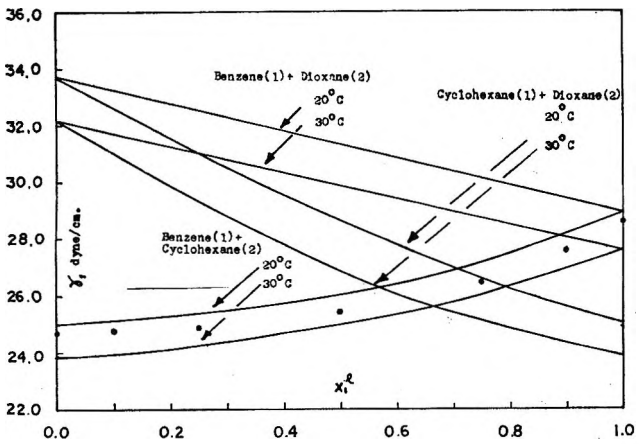

Figure 1. Surface tension–composition diagram at 20 and 30°: ●, benzene (1) and cyclohexane (2), 20° (see ref 13).

sodium just before use. Nitrobenzene was purified in the last stages through five to nine cycles of fractional crystallization followed by vacuum distillation. Some physical properties of these liquids are recorded in Table I and are compared with the literature values. The method of determining surface tension has already been described.[10] The results obtained for the binary solutions at 20 and 30° are recorded in Tables II and III and are compared with some available literature values in Figures 1 and 2.

Results and Discussion

The data shown in Figure 1 generally agree well with the available literature values.[13] For the nitrobenzene systems, some differences at the nitrobenzene end are noticeable; this might be due to the more rigorous

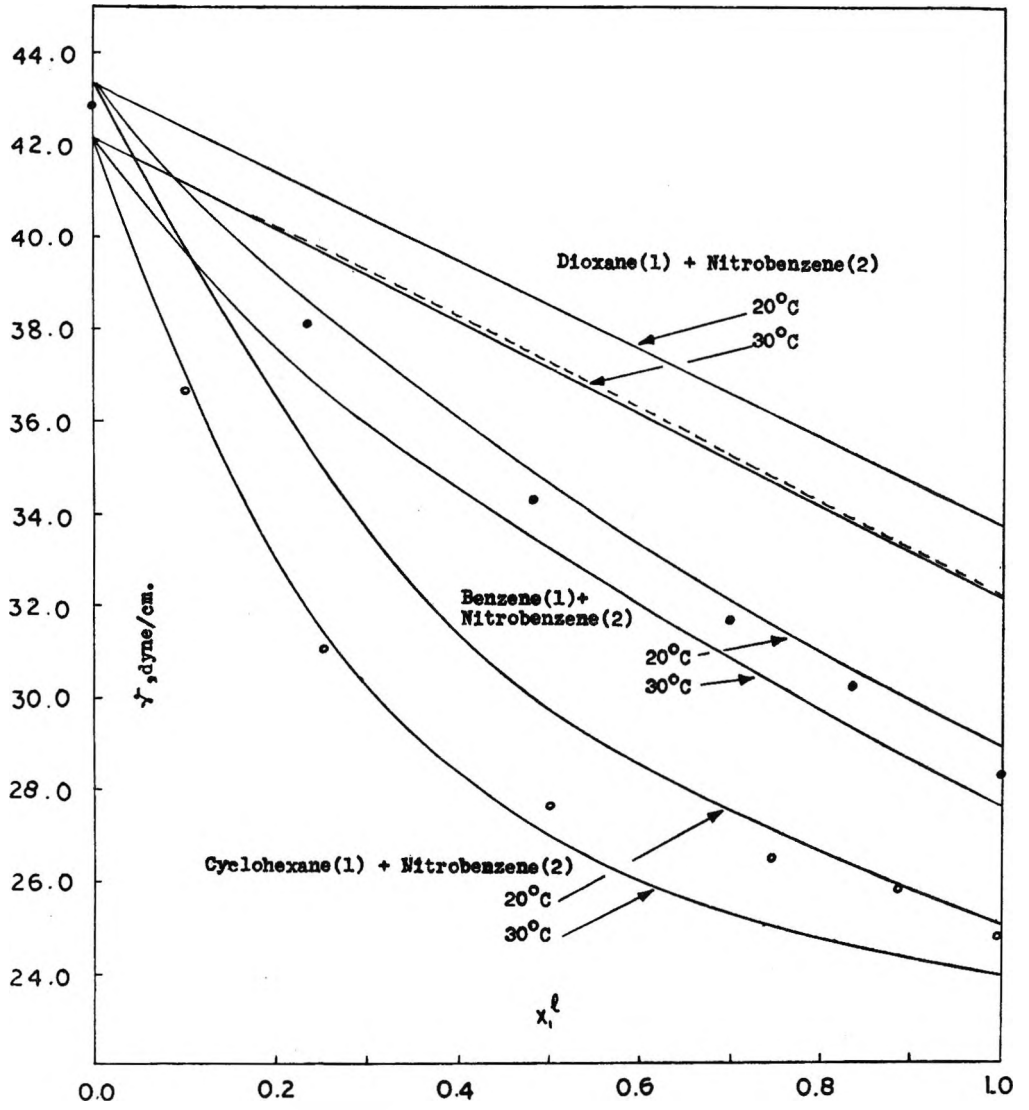

Figure 2. Surface tension–composition diagram at 20 and 30°: O, cyclohexane (1) and nitrobenzene (2), 20°: ●, benzene (1) and nitrobenzene (2), 25°. (See ref 13.)

purification cycles followed for our sample of liquid. The data for binary solutions containing dioxane follow the expected trend, except in two cases (Figures 1 and 2), where $\gamma^E = 0$. Indeed, for the system dioxane + nitrobenzene, the experimental data show a slight tendency to convexity toward the composition axis (broken line in Figure 2). The linear surface tension curves are of interest and cannot be attributed in our systems to size effects, as the molecules of benzene, dioxane, and nitrobenzene are quite close to one another in their surface occupancy (Table I).

In Table IV are recorded the excess surface tension, defined by

$$\gamma^E = \gamma - X_1^l\gamma_1 - X_2^l\gamma_2 \quad (1)$$

where γ is the surface tension of the mixture and γ_i and X_i^l are the surface tension and mole fraction, respectively, of the individual components.

The surface tensions of the solutions were calculated in three different ways for comparison with the experimental values.[12]

(i) First they were calculated by assuming that both the bulk liquid and the surface layer form ideal solutions and using the form of the equation given by Hildebrand[2]

$$\gamma = X_1^l\gamma_1 + X_2^l\gamma_2 - (A/2RT)(\gamma_1 - \gamma_2)^2X_1^lX_2^l \quad (2)$$

where A is the surface occupancy of the molecules (cm^2/mol). We have used the approximation $A_1 \cong A_2 \cong (A_1 + A_2)/2 = A$ in the above equation.

(ii) The second theoretical model is due to Hoar and Melford (HM),[5] and was developed for nonpolar solutions with the assumption that the bulk liquid and the surface layer behave like regular solutions and that the molecules approximate to hard spheres. Thus

(12) J. Timmermans, "Physico-Chemical Constants of Pure Organic Compounds," Elsevier Publishing Co., New York, N. Y., 1950.

Table IV: Excess Surface Tension (dyn/cm) at Various Compositions of Binary Solutions at 30°

System 1 + 2		γ^E at X_1^1 = 0.1	0.2	0.4	0.5	0.6	0.8	0.9
Benzene + cyclohexane	Exptl	−0.20	−0.37	−0.62	−0.67	−0.68	−0.45	−0.26
	Ideal-solution model	−0.05	−0.08	−0.12	−0.14	−0.12	−0.08	−0.05
	HM model	−0.15	−0.28	−0.46	−0.51	−0.53	−0.38	−0.22
	SP model	−0.43	−0.82	−1.33	−1.62	−1.72	−1.37	−0.90
Benzene + dioxane	Exptl	0.00	0.00	0.00	0.00	0.00	0.00	0.00
	Ideal-solution model	−0.07	−0.11	−0.17	−0.18	−0.17	−0.11	−0.07
	HM model	−0.16	−0.28	−0.42	−0.42	−0.39	−0.24	−0.13
	SP model	−1.06	−1.54	−1.94	−1.80	−1.62	−1.00	−0.54
Cyclohexane + dioxane	Exptl	−0.52	−0.93	−1.35	−1.33	−1.20	−0.69	−0.36
	Ideal-solution model	−0.21	−0.38	−0.60	−0.62	−0.60	−0.38	−0.21
	HM model	−1.11	−1.71	−1.99	−1.89	−1.65	−0.92	−0.47
	SP model	−3.48	−4.93	−5.95	−5.95	−5.63	−4.24	−2.92
Benzene + nitrobenzene	Exptl	−0.61	−1.09	−1.54	−1.51	−1.38	−0.84	−0.45
	Ideal-solution model	−0.65	−1.20	−1.80	−1.89	−1.80	−1.20	−0.65
	HM model	−1.00	−1.47	−1.82	−1.79	−1.58	−0.92	−0.47
	SP model	−0.55	−0.98	−1.31	−1.37	−1.31	−0.80	−0.43
Cyclohexane + nitrobenzene	Exptl	−3.37	−5.45	−6.20	−5.77	−4.98	−2.77	−1.43
	Ideal-solution model	−1.15	−1.95	−2.97	−3.15	−2.97	−1.95	−1.15
	HM model	−3.12	−4.51	−4.82	−4.35	−3.56	−1.80	−0.89
	SP model	−9.32	−11.50	−10.73	−9.75	−8.47	−5.15	−3.10
Dioxane + nitrobenzene	Exptl	0.00	0.00	0.00	0.00	0.00	0.00	0.00
	Ideal-solution model	−0.31	−0.55	−0.83	−0.87	−0.83	−0.55	−0.31
	HM model	−0.22	−0.38	−0.56	−0.57	−0.54	−0.33	−0.18
	SP model	−0.11	−0.22	−0.41	−0.44	−0.44	−0.30	−0.15

Table V: Constants for Evaluating Activity Coefficients of Solutions

System 1 + 2	Constants of RK Eq (10) B	C	D	ω^1 (calcd), cal: Solubility parameter	RK Eq	ω^1 (HM model), cal	η, ergs/cm²
Benzene + cyclohexane[a]	0.209	0.013	0.017	89	308	90	0.68
Benzene + dioxane	0.169	−0.027	0.065	63	197	60	0.07
Cyclohexane + dioxane	0.594	0.271	0.218	312	1200	310	1.18
Benzene + nitrobenzene	...	...	...	69	...	70	0.28
Cyclohexane + nitrobenzene	1.156	−0.409	0.348	344	1036	340	1.84
Dioxane + nitrobenzene	...	...	...	0	...	0	0.08

[a] Constants B, C, and D are from B. C. Y. Lu and R. F. Lama, *Trans. Faraday Soc.*, **63**, 727 (1967).

$$\gamma = \gamma_1 + (RT/A_1) \ln (X_1^\sigma f_1^\sigma / X_1^1 f_1^1) = \gamma_2 + (RT/A_2) \ln (X_2^\sigma f_2^\sigma / X_2^1 f_2^1) \quad (3)$$

and

$$\ln f_i^1 = (\omega^1/RT)(1 - X_i^1)^2 \quad (4a)$$

$$\ln f_i^\sigma = (l'\omega^1/RT)(1 - X_i^\sigma)^2 \quad (4b)$$

The parameter ω^1 is taken as constant for an isothermal solution[5] and is related to the heat of mixing, ΔH_m, by the relation $\omega^1 = \Delta H_m / X_1^1 X_2^1$. The factor l' in eq 4b is supposed to vary between 0.5 and 0.75, the lower values tending to make the calculated surface tension curve of binary mixtures slightly more negative with respect to the $\gamma^E = 0$ line. Keeping this effect of l' in

view, we have used a fixed value of $l' = 0.5$ in our calculations and have evaluated the parameter ω^1(HM) from the Hildebrand solubility parameters of the liquids.[2] These values were directly used in eq 3 and 4 for the calculation of γ^E (Table V).

(iii) The third theoretical approach used by us for the calculation of the surface tension of binary solutions is due to Prausnitz and coworkers[6] and was originally applied to nonpolar cryogenic systems consisting of nearly spherical molecules. They obtained

$$RT \ln f_i^\sigma = A_i(1 - \theta_i)^2\eta \quad (5)$$

where

$$\theta_i = X_i^\sigma A_i / \sum(X_i^\sigma A_i) \quad (6)$$

and

$$\eta = C_1^\sigma + C_2^\sigma - 2\sqrt{C_1^\sigma C_2^\sigma} \quad (7)$$

where C_i^σ is the configurational energy density of the components in the surface layer. Prausnitz and coworkers[6] have indicated how η can be calculated from the experimental data for the enthalpies and surface tensions of the pure components. The values of η thus calculated for the binary systems are recorded in Table V. The authors have further shown that the surface concentration, X_i^σ, and the surface tension of the binary mixtures can be evaluated from

$$X_2^\sigma/X_1^\sigma = (X_2^l f_2^l / X_1^l f_1^l) \times \exp\left[\frac{\gamma_1 A_1 - \gamma_2 A_2 - (\theta_1^2 A_2 - \theta_2^2 A_1)\eta}{RT}\right] \quad (8)$$

and

$$\gamma = \theta_1\gamma_1 + \theta_2\gamma_2 + \theta_1\theta_2\eta + [RT/(X_1^\sigma A_1 + X_2^\sigma A_2)][X_1^\sigma \ln (X_1^\sigma/X_1^l f_1^l) + X_2^\sigma \ln (X_2^\sigma/X_2^l f_2^l)] \quad (9)$$

For the application of eq 8 and 9, the activity coefficients in the bulk solution, f_i^l, are required. We have estimated these values from the available liquid–vapor equilibrium data[13] for these systems by fitting a Redlich–Kister-type (RK) equation

$$\log f_i^l = (1 + X_1^l)^2[B + C(1 - 4X_i^l) + D(1 - 2X_i^l)(1 - 6X_i^l)] \quad (10)$$

A thermodynamic consistency test, as pointed out by Lu, Spinner, and Ho,[14] was applied in all cases. The constants B, C, and D calculated for the systems are recorded in Table V, as are the ω^l values, ω^l(RK), corresponding to eq 10 at $X_i^l = 0.5$ for comparison. It will be observed that the ω^l(RK) values are consistently higher than the corresponding ω^l(HM). For the benzene + nitrobenzene and dioxane + nitrobenzene systems suitable liquid–vapor equilibrium data are not available.

As a first measure, in the use of all these equations,

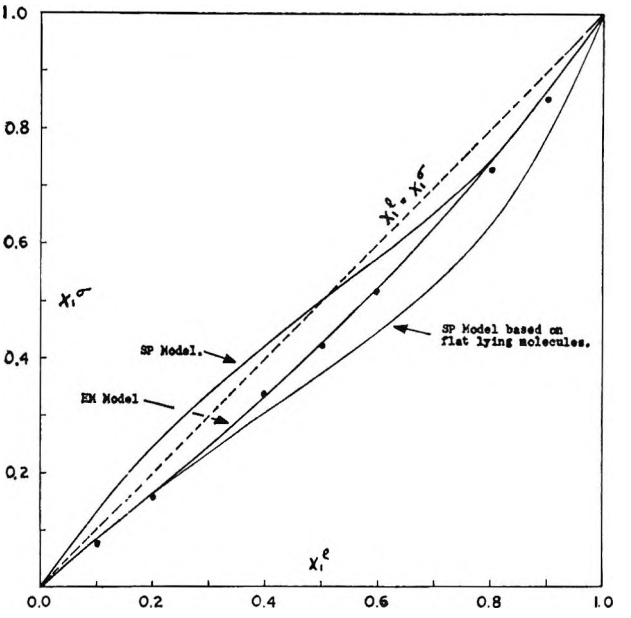

Figure 3. Benzene (1) and cyclohexane (2): ●, Gibbs.

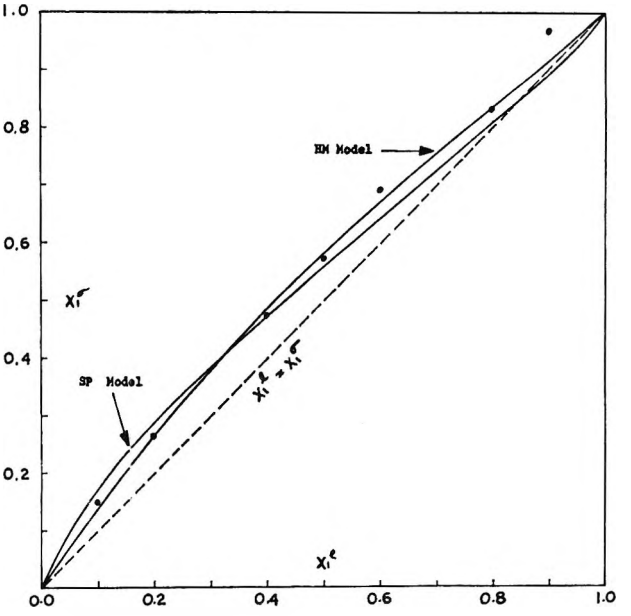

Figure 4. Benzene (1) and dioxane (2): ●, Gibbs.

A_i has been evaluated from $V_i^{2/3}N^{1/3}$ assuming spherical molecules. The theoretically calculated values for the excess surface tensions of the binary mixtures are included in Table IV with the experimental data.

The first point to note is that the surface tension of the binary solutions of the nonpolar solvents benzene, cyclohexane, and dioxane is not described by the single-parameter eq 2, using an average value for A, the sur-

(13) J. Timmermans, "The Physico-Chemical Constants of Binary Systems in Concentrated Solutions," Vol. 1, Interscience Publishers, New York, N. Y., 1959.

(14) B. C. Y. Lu, I. H. Spinner, and J. C. K. Ho, *Can. J. Chem. Eng.*, 40, 16 (1962).

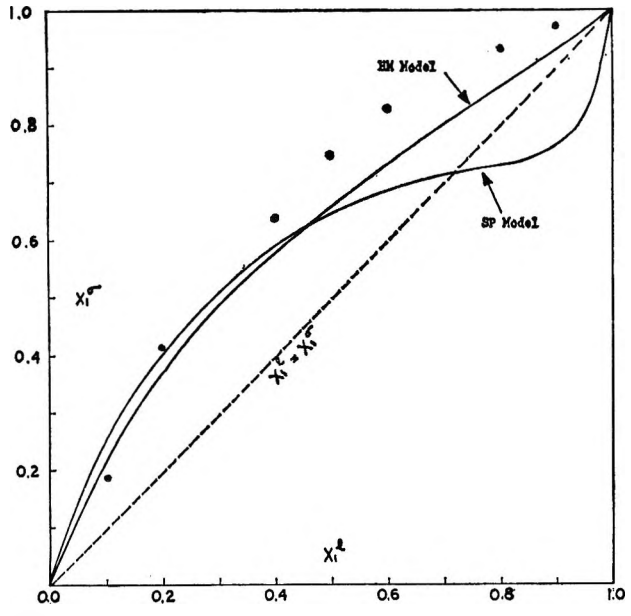

Figure 5. Cyclohexane (1) and dioxane (2): ●, Gibbs.

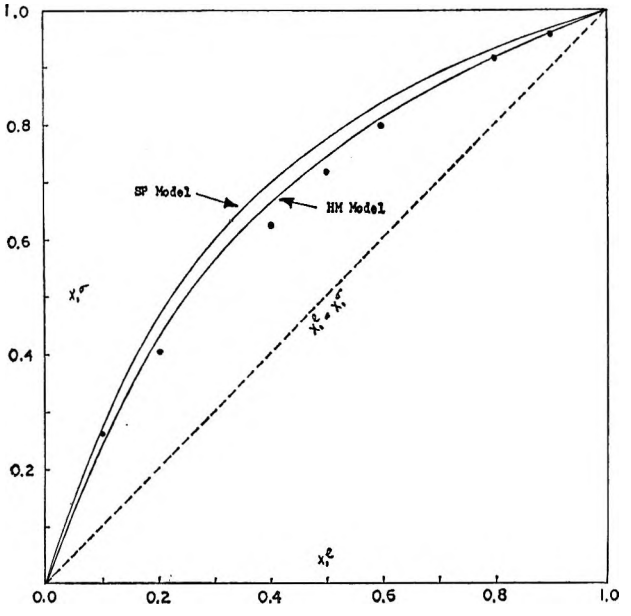

Figure 6. Benzene (1) and nitrobenzene (2): ●, Gibbs.

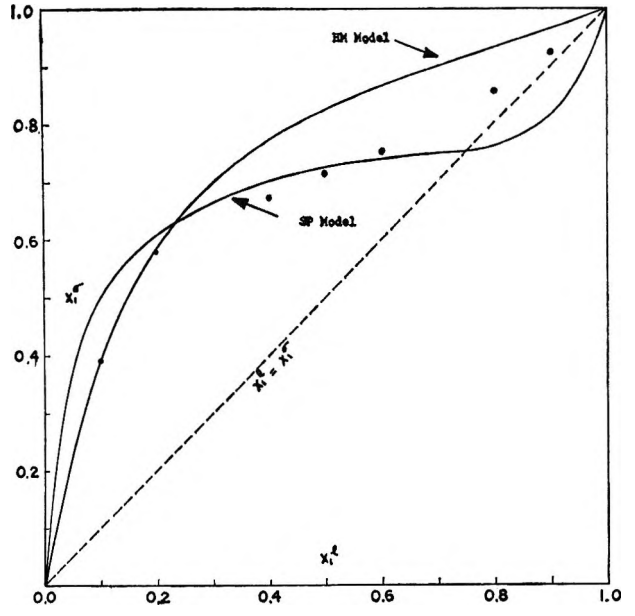

Figure 7. Cyclohexane (1) and nitrobenzene (2): ●, Gibbs.

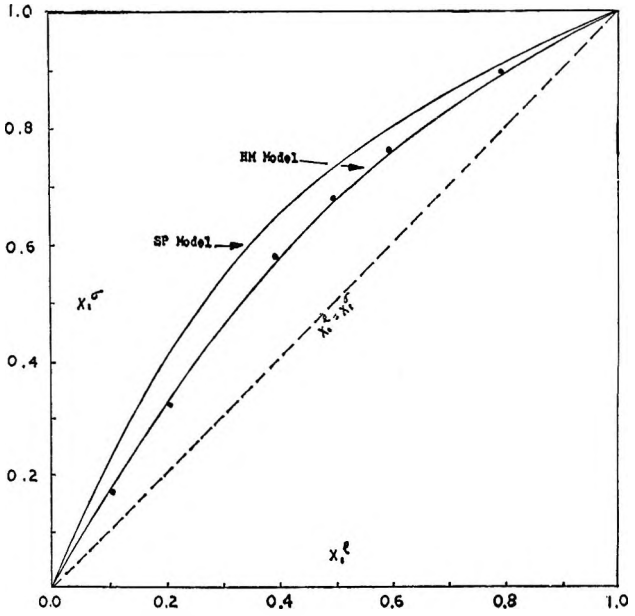

Figure 8. Dioxane (1) and nitrobenzene (2): ●, Gibbs.

face occupancy of the molecules. For the systems benzene + cyclohexane and cyclohexane + dioxane, the required values of A to obtain a better fit of eq 2 with the experimental data would be unreasonably high, and for the benzene + dioxane system, it would be negligibly small.

The application of the regular-solution model to the binary solutions studied here, particularly those containing nitrobenzene which has a strong dipolar character, needs some justification. There is good reason to believe that the dipole in nitrobenzene is "buried," being physically displaced toward the middle of the benzene ring and not located in the NO bonds.[15] Hildebrand and Scott[16] have also observed that, in spite of its strong dipolar character, nitrobenzene acts more nearly like an ideal solvent, such as chlorobenzene (a moderate dipole), for naphthalene, in the sense of the regular-solution theory. Our data also appear to support this view.

The application of the HM model to these binary

(15) (a) R. J. Good, "Treatise on Adhesion and Adhesives," Vol. I, R. L. Patrick, Ed., Marcel Dekker, Inc., New York, N. Y., 1966, p 25; (b) C. P. Smyth, "Dielectric Behavior and Structure," McGraw-Hill Book Co., Inc., New York, N. Y., 1955.

(16) J. H. Hildebrand and R. L. Scott, "Regular Solutions," Prentice-Hall, Inc., Englewood Cliffs, N. J., 1962, p 130.

solutions, using ω^1(HM) calculated from solubility parameters and individual A_i values given in Table I, yields satisfactory values, in good agreement with the experiments. However, as has been pointed out already, the ω^1(HM) values are lower than the ω^1(RK) obtained from vapor–liquid equilibrium data (Table V). We would like to repeat our previous remark[10] that ω^1(HM) may be considered only as an adjustable parameter in the application of eq 3 and 4. Nevertheless, it is interesting to note that the HM model gives extremely satisfactory agreement when extended to binary solutions containing nitrobenzene, using ω^1(HM) calculated from solubility parameters.

The SP model (eq 5–9), which is also based essentially on the regular-solution theory, gives γ^E estimates which are more divergent from the experimental data than the HM model, this difference being particularly marked for those very systems which have high ω^1 values. Interestingly enough, in the two cases, benzene + nitrobenzene and dioxane + nitrobenzene, where the vapor–liquid equilibrium data are not available and f_i^1 has been approximated as unity, the SP model gives γ^E estimates closer to the experimental than the HM model.

It is of interest to calculate the surface composition, X_i^σ, predicted by the two models discussed above and to compare them with values obtained from an independent procedure, namely, by applying the Gibbs adsorption isotherm to the surface tension data of the binary solutions. We will use the convention[4,9]

$$\Gamma_1^N = \Gamma_1 X_2^1 - \Gamma_2 X_1^1 = (X_1^1/RT)(\mathrm{d}\gamma/\mathrm{d} \ln a_2) \quad (11)$$

where Γ_1^N is the adsorption or excess concentration at the free liquid surface and Γ_i is the actual concentration of the component. Combining eq 11 with

$$\Gamma_1 A_1 + \Gamma_2 A_2 = 1 \quad (12)$$

the surface concentrations Γ_i and hence X_i^σ can be calculated. The use of eq 12 restricts the surface to a monolayer but does not preclude the simultaneous use of eq 11 or the earlier equations for surface tensions. Indeed, Eriksson[17] prefers this method for calculating Γ_i and X_i^σ if A_i (eq 12) can be given suitable values. The data for X_i^σ for the systems studied are plotted in Figures 3–8. It will be observed that the solid curves shown in Figures 3–8 for X_i^σ from the HM model are generally in good agreement with the values calculated from eq 11 and 12 (solid circles). In the case of binary mixtures of the nonpolar solvents and cyclohexane + nitrobenzene (Figures 3–5 and 7), where f_i^1 based on eq 10 are used in the application of the Sprow–Prausnitz (SP) model, the X_i^σ values cross the $X_i^\sigma = X_i^1$ line (solid lines marked SP model). This is rather unexpected. For the two other nitrobenzene systems, where f_i^1 has been approximated as unity and η is low, the predictions of the SP model for X_i^σ are in satisfactory agreement with the estimates from eq 11 and 12 (Figures 6 and 7). We believe, as stated earlier,[10] that this condition arises because of the use of spherical shape for the molecules and not solely due to the calculation of f_i^1 from eq 10, to account for the nonideality of the bulk liquid. If in eq 9 we consider A_i as an adjustable parameter and use $A = (A_1 + A_2)/2$, as has been done for eq 2, it will have the effect of decreasing the calculated surface occupancy of the larger molecules while increasing, correspondingly, that of the smaller—the maximum difference introduced in A_i for the binary systems studied here would be ~8.5%. We then find that X_i^σ calculated from the SP model shows a lesser tendency to cross the $X_i^\sigma = X_i^1$ line.

It appears to us that while f_i^1 is more appropriately obtained from vapor–liquid equilibria by using an equation of the type of eq 10, rather than from the solubility parameters, the use of the former for calculating surface tension of binary mixtures of even simple nonpolar solvents necessitates the application of A_i as an adjustable parameter when the molecules are not spherical. The possibility of A_i being variable with respect to the composition of the binary liquid mixture has been pointed out earlier by Eriksson.[7] On the other hand, if ω^1 is used as an adjustable parameter, γ^E can be calculated satisfactorily using A_i calculated from $(V_i^{2/3})(N)^{1/3}$.

Acknowledgment. S. K. S. wishes to thank the Council of Scientific and Industrial Research for financial grants during a part of this work.

(17) J. C. Eriksson, private communication, 1967.

Ionic Reactions in Unsaturated Compounds. II. Ethylene[1]

by Thomas O. Tiernan and Jean H. Futrell

Aerospace Research Laboratories, Office of Aerospace Research, Wright-Patterson Air Force Base, Ohio 45433
(Received September 12, 1967)

Ionic polymerization in ethylene was investigated at pressures up to 1 torr using a modified time-of-flight mass spectrometer. Reactions of individual ions participating in the reaction sequence were identified by studies with a tandem mass spectrometer. Experiments utilizing perdeuterioethylene were employed to determine various details of the condensation mechanism. The results indicate that even in the pressure region below 50 μ, the reaction of the parent molecule ion involves the formation of an intermediate collision complex of substantial lifetime, the dissociation rate being of the order of 3×10^8 sec^{-1}. The data strongly suggest, however, that at these low pressures, the propagation of the ionic chain occurs principally *via* fragment ions rather than by means of undissociated reaction complexes. From tandem experiments with impacting ions having a 0.3-eV energy, it was deduced that charge transfer is an important mode of reaction for all the major primary ionic species in addition to the other concurrent ion–molecule processes in which these ions participate. An ionic reaction which has not previously been detected in the ethylene system has been observed for ethyl ions in this investigation, and the implications of this reaction sequence for radiolysis experiments are discussed. Threshold behavior in the energy dependence of the endothermic ion–molecule reaction, $C_2H_4^+ + C_2H_4 \rightarrow C_3H_3^+ + CH_3 + H_2$, analogous to that observed in certain endothermic charge-transfer and atom-exchange processes is also reported and discussed qualitatively.

Introduction

As a continuation of our studies of ionic reactions in unsaturated compounds, we have examined the ethylene system. Ionic processes in ethylene have already been extensively studied and several laboratories have previously reported the results of mass spectrometric investigations of this compound.[2-9] In addition, a considerable amount of information relating to ion–molecule reactions in ethylene has been derived from radiation chemistry studies.[10] The latter have provided important evidence concerning the role of intermediate ions in the reaction sequence. Mass spectrometric studies conducted at high pressures approaching typical radiolysis conditions, in which some of the ionic intermediates in ethylene have been directly identified and their lifetimes estimated,[6,7] are especially pertinent to this question. Additional insight into the reactions of the parent molecule ion has been provided by a recently reported investigation of the photoionization of ethylene.[11]

Among the several authors who have considered the ethylene system, there seems to be general agreement as to the identification of the reactions occurring. There are two notable exceptions, however, these being the early results obtained by Melton and Rudolph[2] and the more recently reported investigation of Szabo.[8] Both of the latter papers postulate a number of ionic reactions for ethylene which were not suggested by the other investigators and which would appear to be energetically prohibited in some cases. In the investigation by Szabo, the reactant ethylene ions were generated using the charge-exchange techniques developed by Lindholm. This difference in the mode of preparation of reactant ions and the fact that the Stockholm apparatus discriminates strongly against ions formed with momentum in the forward direction may contribute to some of the discrepancies.

There remain several questions regarding the ionic reaction mechanism for ethylene, and, in addition, there is considerable controversy regarding the reactivity and lifetime of intermediate collision complexes formed in such processes.[12] In an attempt to resolve the conflicting data which are still evident in the literature and to establish unequivocally the reactions of significance for the ethylene system, we have undertaken the present study, which is somewhat analogous to that which we previously reported for acetylene.[13] It was also our purpose to obtain more definitive information relative

(1) Presented, in part, at the 15th Annual Meeting of the Radiation Research Society, San Juan, Puerto Rico, May 1967.

(2) C. E. Melton and P. S. Rudolph, *J. Chem. Phys.*, **32**, 1128 (1960).

(3) F. H. Field, *J. Amer. Chem. Soc.*, **83**, 1523 (1961).

(4) A. G. Harrison, *Can. J. Chem.*, **41**, 236 (1963).

(5) S. Wexler and R. Marshall, *J. Amer. Chem. Soc.*, **86**, 781 (1964).

(6) P. Kebarle and A. M. Hogg, *J. Chem. Phys.*, **42**, 668 (1965).

(7) P. Kebarle, R. M. Haynes, and S. Searles, Advances in Chemistry Series, No. 58, American Chemical Society, Washington, D. C., 1966, p 210.

(8) I. Szabo, *Ark. Fysik*, **33**, 57 (1966).

(9) P. Kebarle and R. M. Haynes, *J. Chem. Phys.*, **47**, 1676 (1967).

(10) G. G. Meisels, Advances in Chemistry Series, No. 58, American Chemical Society, Washington, D. C., 1966, p 243.

(11) R. Gorden, Jr., and P. Ausloos, *J. Chem. Phys.*, **47**, 1799 (1967).

(12) G. G. Meisels and H. F. Tibbals, Proceedings of the 15th Annual Conference on Mass Spectrometry and Allied Topics, American Society for Testing and Materials, Committee E-14, Denver, Colo., May 1967, p 11.

(13) J. H. Futrell and T. O. Tiernan, *J. Phys. Chem.*, **72**, 158 (1968).

to the participation and lifetime of reaction complexes for unsaturated systems such as this.

Experimental Section

The experimental approach employed for this study is essentially the same as that described for the first paper of this series.[13] Consecutive ion–molecule reactions in ethylene were studied at pressures up to 1 torr using a high-pressure time-of-flight mass spectrometer which was developed in this laboratory and which has already been described in detail.[14] The source dimensions of this instrument are such that the distance from the collimated electron beam to the source exit aperture is 0.29 cm. For all the experiments reported here, the source field strength was maintained at 10 V/cm, the ionizing voltage at 100 eV, and electron-trap currents were kept below 10^{-7} A to minimize space-charge phenomena. The pressure differential between the ion source and surrounding vacuum envelope for this instrument is approximately 1000:1. The source pressure is maintained constant for a given experiment by means of a Granville-Phillips automatic pressure controller (Series 213), for which the reference signal is provided by an MKS Baratron Model 77H1 pressure transducer. From appropriate plots of ion-intensity data as a function of pressure which were obtained with this instrument, reaction cross sections were derived.

Elementary reaction steps for the condensation sequence in ethylene were established by use of the ARL tandem mass spectrometer,[15] in the manner which has been indicated by previous studies.[16] In these experiments, a given ion is mass and energy selected from the fragments produced in the first stage of the tandem instrument and impacted on the gas of interest in the collision chamber. The product ions are then analyzed in a second-stage spectrometer. Unless otherwise noted, all such studies reported here were accomplished with impacting ions of kinetic energy 0–0.4 eV. The intensities of secondary ions were measured using pulse-counting techniques.

Reaction orders for various ions which are reported in this paper were determined from logarithmic plots of ion intensity as a function of the collision-chamber pressure in the tandem mass spectrometer. The measured intensities were corrected for scattering and attenuation of the primary beam by normalizing the data to the summation of product-ion intensities with the requirement that this total ion intensity be proportional to collision-chamber pressure.

Ethylene used in these experiments was Phillips research grade and, except for removal of gases noncondensable at liquid nitrogen temperature, was not subjected to further purification. Gas chromatographic analysis indicated only negligible amounts of other impurities. Deuterated compounds were obtained from Merck Sharp and Dohme, Ltd. All other chemicals were obtained from the Matheson Co. and were used as received except for purification as noted above.

Results

The mass spectrum of ethylene as a function of pressure, at source pressures up to 1 torr, was determined using the modified time-of-flight instrument. Figure 1 shows the observed variation for some of the more prominent ions in the spectrum. A large number of data points were obtained, and to avoid confusion, only the smooth curves drawn through these points are exhibited in this figure. In Figure 2, where the scale is enlarged for clarity, the pressure plots for several of the ions of minor intensity are presented. Kinetic data for the major primary and secondary ions were obtained from semilogarithmic plots of normalized ion intensity as a function of pressure (Figures 3 and 4). Total reaction cross sections were deduced from the slopes of the linear portions of these plots by the usual methods. The values so obtained are tabulated in Table I. For purposes of comparison, previously reported data from other sources are also listed in this table.

Table I: Total Cross Sections for Reactions of Ions with Ethylene

	Total cross sections, $\times 10^{16}$ cm^2 molecule^{-1}			
Ion	This work	Ref 4	Ref 5[a]	Ref 6
$C_2H_2^+$	110	18	37	93
$C_2H_3^+$	50	17	...	47
$C_2H_4^+$	33	13	40	62
$C_2H_5^+$	30	...	...	28
$C_3H_5^+$	37	...	...	19
$C_4H_7^+$	13	...	...	26
Source field strength, V/cm	10	12.5	10	12
Reaction path length (l), cm	0.28	0.20	0.12	0.32

[a] Total cross sections were obtained by summing the partial cross sections listed in cases where a single reactant yields more than one product.

Reactions with the parent molecule of individual ions produced by primary fragmentation of ethylene were also examined in the tandem mass spectrometer as reported in Tables II–VI. In order to confirm the reactions of higher order ions which were suggested by the single-source experiments at elevated pressures, several experiments were conducted in which these ions were used as impacting species in the tandem mass spectrometer. Pressure limitations prevent the introduction of ethylene into the first stage of the tandem spec-

(14) J. H. Futrell, T. O. Tiernan, F. P. Abramson, and C. D. Miller, *Rev. Sci. Instrum.*, **39**, 340 (1968).

(15) J. H. Futrell and C. D. Miller, *ibid.*, **37**, 1521 (1966).

(16) F. P. Abramson and J. H. Futrell, *J. Chem. Phys.*, **45**, 1925 (1966).

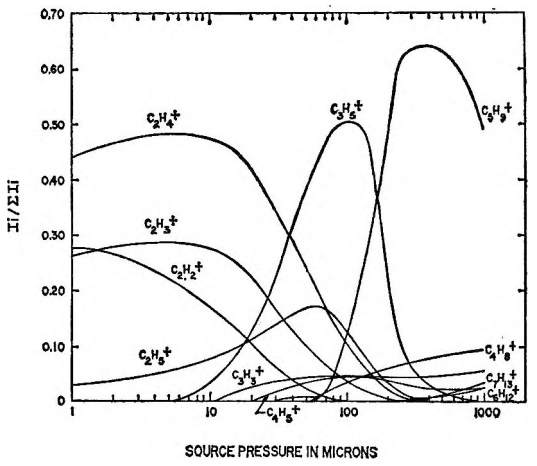

Figure 1. The dependence of the relative intensities of major ionic species in ethylene on the source pressure in the time-of-flight mass spectrometer.

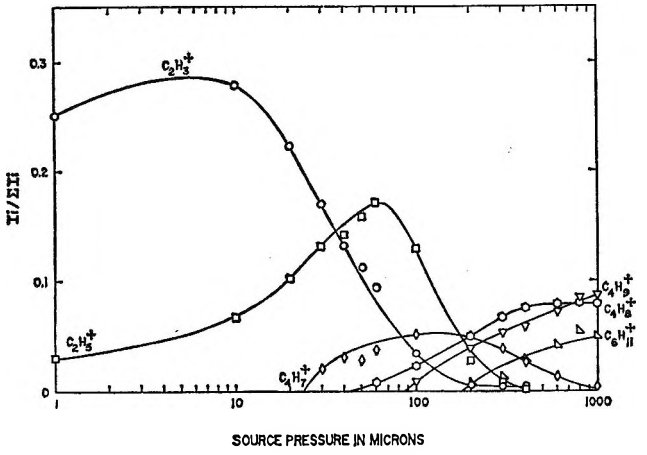

Figure 2. Variations of the relative intensities of several minor ions with the pressure of ethylene in the mass spectrometer ion source.

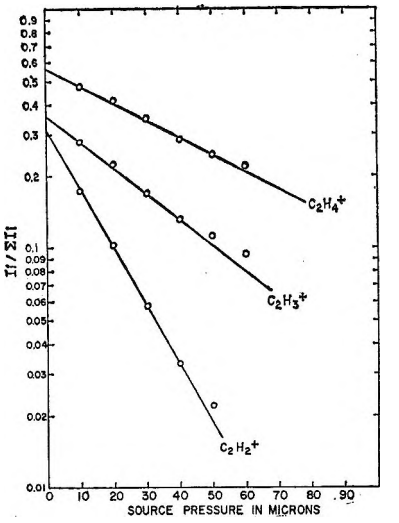

Figure 3. Semilogarithmic plots of the relative intensities of $C_2H_2^+$, $C_2H_3^+$, and $C_2H_4^+$ as functions of ethylene pressure.

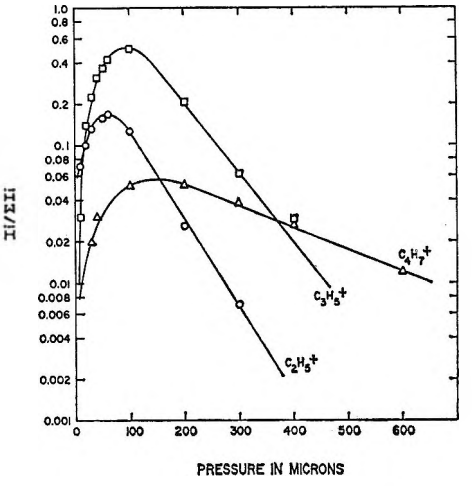

Figure 4. Semilogarithmic plots of the relative intensities of $C_2H_5^+$, $C_3H_5^+$, and $C_4H_7^+$ as functions of ethylene pressure.

Table II: Ionic Products from the Reaction of $C_2H_4^+$ with C_2H_4

m/e (product ion)	Species	Relative intensity 5 μ	Relative intensity 60 μ
29	$C_2H_5^+$, $^{12}C^{13}CH_4^+$	0.023	0.019
30	$C_2H_6^+$	0.002	0.001
38	$C_3H_2^+$	0.002	0.001
39	$C_3H_3^+$	0.006	0.007
40	$C_3H_4^+$	0.009	0.011
41	$C_3H_5^+$	0.84	0.80
42	$C_3H_6^+$	0.013	0.013
53	$C_4H_5^+$	...	0.002
54	$C_4H_6^+$	0.004	0.004
55	$C_4H_7^+$	0.10	0.094
56	$C_4H_8^+$	0.002	0.005
67	$C_5H_7^+$	...	0.005
69	$C_5H_9^+$	0.0008	0.031
70	$C_5H_{10}^+$	...	0.001
82	$C_6H_{10}^+$	...	0.0001

Table III: Ionic Products from the Reaction of $C_2H_3^+$ with C_2H_4

m/e (product ion)	Species	Relative intensity 5 μ	Relative intensity 50 μ
28	$C_2H_4^+$, $^{12}C^{13}CH_3^+$	0.020	0.019
29	$C_2H_5^+$	0.85	0.78
39	$C_3H_3^+$	0.039	0.040
40	$C_3H_4^+$	0.002	0.002
41	$C_3H_5^+$	0.002	0.069
51	$C_4H_3^+$	0.001	0.001
53	$C_4H_5^+$	0.080	0.075
54	$C_4H_6^+$	0.003	0.005
55	$C_4H_7^+$	...	0.004
57	$C_4H_9^+$	...	0.0004

trometer in sufficient quantities to produce secondary ions for use as impacting species. Therefore, for these experiments, ions of empirical formula corresponding

Table IV: Isotopic Products from the Reaction of $C_2H_3^+$ with C_2D_4

Product	Relative intensity 5 μ	Relative intensity 50 μ
$C_3DH_2^+$	0.044	0.036
$C_2D_2H^+$	0.057	0.053
$C_2D_3^+$	0.029	0.020
$C_2D_3H_3^+$	0.11	0.085
$C_2D_4^+$, $C_2D_3H_2^+$	0.13	0.19
$C_2D_4H^+$	0.56	0.46
$C_3DH_2^+$	0.015	0.014
$C_3D_2H^+$	0.017	0.020
$C_3D_3^+$	...	0.008
$C_3D_2H_3^+$	...	0.001
$C_3D_3H_2^+$	...	0.006
$C_3D_4H^+$	...	0.027
$C_3D_5^+$	...	0.029
$C_4D_2H_3^+$	0.010	0.010
$C_4D_3H_2^+$	0.017	0.022
$C_4D_4H^+$	0.011	0.010

Table V: Ionic Products from the Reaction of $C_2H_2^+$ with C_2H_4

m/e (product ion)	Species	Relative intensity 5 μ	Relative intensity 50 μ
27	$C_2H_3^+$	0.039	0.031
28	$C_2H_4^+$	0.70	0.56
29	$C_2H_5^+$	0.004	0.010
39	$C_3H_3^+$	0.082	0.096
41	$C_3H_5^+$	0.007	0.12
52	$C_4H_4^+$	0.011	0.010
53	$C_4H_5^+$	0.15	0.14
55	$C_4H_7^+$	...	0.013
69	$C_5H_9^+$	...	0.0024

Table VI: Ionic Products from the Reaction of C_2H^+ with C_2H_4

m/e (product ion)	Species	Relative intensity 5 μ
26	$C_2H_2^+$	0.063
27	$C_2H_3^+$	0.10
28	$C_2H_4^+$	0.42
38	$C_3H_2^+$	0.035
39	$C_3H_3^+$	0.030
50	$C_4H_2^+$	0.10
51	$C_4H_3^+$	0.18
52	$C_4H_4^+$	0.062

to the secondary species were obtained in the first stage by primary fragmentation of appropriate molecules. Thus for the reactions listed in Table XI, $C_2H_5^+$ was obtained from propane, $C_3H_5^+$ from 1-butene, and $C_4H_7^+$ from 1-chloro-2-butene. It should be mentioned that for the case of the parent-ion reaction with ethylene, reported in Table II, there is a certain amount of $C_2H_4^+$ produced by charge exchange and there will, therefore, be a ^{13}C isotope contribution from this component of the $C_2H_4^+$ to the (parent + 1) peak in the spectrum. Since it is impossible to distinguish the $C_2H_4^+$ produced by charge exchange from the primary beam, it is not possible to make an isotope correction to the (parent + 1) peak. In the studies with C_2D_4, the charge-exchange product appears at a mass different from that of the primary beam, so this correction is obvious. For the purpose of determining mechanistic details for the specific reactions, some of the studies in the tandem instrument were accomplished with C_2D_4 in the collision chamber. Conversely, some experiments were conducted in which deuterated ionic species derived from C_2D_4 or other deuterated compounds were impacted on C_2H_4 in the collision chamber. The data derived from these isotopic studies are given in Tables IV and VII–XIII.

Table VII: Isotopic Products from the Reaction of $C_2H_4^+$ with C_2D_4

Product	Relative intensity 5 μ	Relative intensity 50 μ
$C_2DH_3^+$	0.019	0.012
$C_2DH_4^+$	0.042	0.029
$C_2D_3H^-$	0.024	0.017
$C_2D_4^+$	0.28	0.25
$C_2D_4H^+$	0.019	0.012
$C_3DH_2^-$	...	0.002
$C_3D_2H^-$	...	0.004
$C_3DH_4^+$	0.049	0.044
$C_3D_2H_3^+$	0.23	0.19
$C_3D_3H_2^+$	0.23	0.21
$C_3D_4H^-$	0.051	0.078
$C_3D_5^+$	0.010	0.070
$C_4D_3H_4^+$	0.015	0.017
$C_4D_4H_3^+$	0.034	0.032
$C_4D_4H_4^+$	0.001	0.003
$C_4D_7^+$	...	0.004
$C_4D_7H^+$	...	0.001
$C_5D_5H_4^+$	...	0.001
$C_5D_6H_3^+$	...	0.004
$C_5D_7H_2^+$	...	0.005
$C_5D_8H^+$	...	0.001
$C_6D_9^+$	...	0.003

Evidence concerning the origin of product ions observed in the ethylene system can also be obtained by determining the reaction order of these ions. Since the intensity of a product ion of order n is proportional to the nth power of the pressure,[17] the reaction order of a particular ion is given directly by the slope of a plot of the logarithm of its intensity as a function of the logarithm of the pressure in the collision chamber. Figures 5 and 6 are representative of such plots for the products from the reactions of ethylene parent ions with ethylene and perdeuterioethylene, respectively.

(17) I. Szabo, *Phys. Rev. Lett.*, **A24**, 702 (1967).

Table VIII: Isotopic Products from the Reaction of $C_2D_4^+$ with C_2H_4

Product ion[a]	Relative intensity 5 μ	Relative intensity 50 μ
$C_3H_5^+$	0.024	0.193
$C_3H_4D^+$	0.088	0.113
$C_3H_3D_2^+$	0.364	0.252
$C_3H_2D_3^+$	0.368	0.220
$C_3HD_4^+$	0.074	0.045
$C_4H_7^+$	...	0.018
$C_4H_8^+$	...	0.004
$C_4H_7D^+$	...	0.004
$C_4H_4D_3^+$	0.028	0.022
$C_4H_3D_4^+$	0.054	0.038
$C_4H_4D_4^+$	...	0.008
$C_5H_7^+$	...	0.004
$C_5H_9^+$	...	0.029
$C_5H_8D^+$	...	0.012
$C_5H_7D_2^+$	...	0.020
$C_5H_6D_3^+$	...	0.015
$C_5H_5D_4^+$	...	0.003

[a] Products having a mass lower than $C_2D_4^+$ (m/e 32) could not be estimated in this experiment because metastable fragments from decomposition of the primary beam obscure this region of the spectrum.

Table IX: Comparison of Observed and Calculated Distributions of $C_3X_5^+$ Isotopic Products from Ethylene Parent-Ion Reactions Using Deuterated Reactants

Product	Relative intensity Calcd	Relative intensity Exptl 5 μ	Relative intensity Exptl 50 μ
Reactants: $C_2H_4^+ + C_2D_4$			
$C_3H_4D^+$	0.071[a]	0.087	0.085
$C_3H_3D_2^+$	0.43	0.41	0.37
$C_3H_2D_3^+$	0.43	0.41	0.40
$C_3HD_4^+$	0.071	0.091	0.15
$C_5H_4D_5^+$	0.25[b]	...	0.090
$C_5H_3D_6^+$	0.51	...	0.38
$C_5H_2D_7^+$	0.22	...	0.40
$C_5HD_8^+$	0.018	...	0.12
Reactants: $C_2D_4^+ + C_2H_4$			
$C_3H_4D^+$	0.071[a]	0.097	0.19
$C_3H_3D_2^+$	0.43	0.41	0.40
$C_3H_2D_3^+$	0.43	0.42	0.35
$C_3HD_4^+$	0.071	0.083	0.069
$C_5H_8D^+$	0.018[c]	...	0.24
$C_5H_7D_2^+$	0.22	...	0.40
$C_5H_6D_3^+$	0.51	...	0.30
$C_5H_5D_4^+$	0.25	...	0.055

[a] Assuming complete randomization of an intermediate $C_4H_4D_4^+$ complex. [b] Assuming complete randomization of an intermediate $C_6H_4D_8^+$ complex. [c] Assuming complete randomization of an intermediate $C_6H_8D_4^+$ complex.

It should be noted that these experiments measure directly the reaction order with respect to neutral molecules of a particular ion; single-gas, single-source experiments analyzed in the same manner at appropriate pressures should be higher by an order of 1, since primary ions are formed by a first-order process.

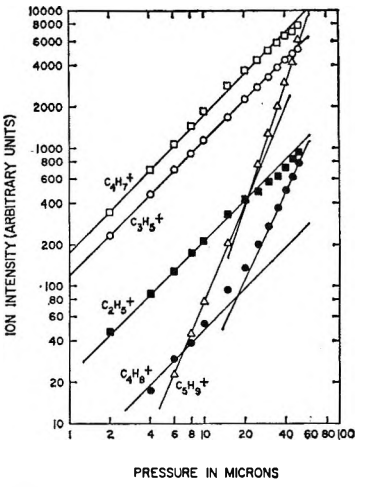

Figure 5. Logarithmic plots of ion intensities as a function of the collision-chamber presure for products from the reaction of $C_2H_4^+$ with ethylene as observed in the tandem mass spectrometer.

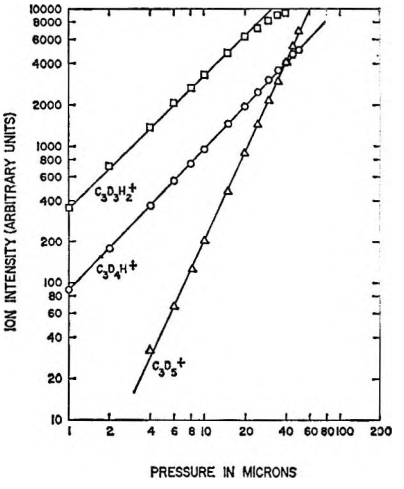

Figure 6. Logarithmic plots of ion intensites as a function of ethylene pressure for $C_3X_5^+$ products from the reaction of $C_2H_4^+$ with C_2D_4 as observed in the tandem mass spectrometer.

In another series of experiments in the tandem mass spectrometer, $C_2H_4^+$ ions were produced in the collision chamber by charge-transfer reactions between ions of appropriate recombination energy and ethylene. Ion–molecule reactions of the parent ion with C_2H_4 were then induced by elevating the collision-chamber pressure. This technique is similar to that employed by Szabo,[8] although there are some significant differences in the instrumentation used in the two cases. The spectrometer utilized by Szabo is constructed so that product ions are extracted from the collision chamber at right angles to the direction of the impacting ion beam. This geometry discriminates against products which have appreciable momenta in the forward direction.

Table X: Isotopic Distribution of Three-Carbon Ionic Products from the Reaction of $C_2H_4^+$ with C_2D_4 at a Collision-Chamber Pressure of 5 μ as a Function of the Kinetic Energy of the Impacting Ion

Energy ($C_2H_4^+$), eV	Relative intensities							
	$C_3DH_2^+$	$C_3D_2H^+$	$C_3DH_4^+$, $C_3D_3^+$	$C_3D_2H_3^+$	$C_3D_3H_2^+$	$C_3D_4H^+$	$C_3D_5^+$	$C_3H_3^+ : C_3H_5^+$ [a]
0.8	...	0.006	0.085	0.40	0.38	0.092	0.026	...
1.5	0.008	0.010	0.088	0.34	0.31	0.11	0.15	0.059
2.0	0.013	0.018	0.092	0.29	0.25	0.11	0.22	0.077
3.0	0.012	0.040	0.11	0.23	0.17	0.14	0.30	0.20
5.0	0.083	0.092	0.14	0.15	0.12	0.14	0.27	0.44
10	0.25	0.24	0.14	0.034	0.032	0.044	0.26	2.9

[a] Determined in a separate experiment in which $C_2H_4^+$ ions were impacted on C_2H_4.

Table XI: Isotopic Products from the Reactions of $C_2H_5^+$, $C_3H_5^+$, and $C_4H_7^+$ with C_2D_4 Observed in the Tandem Mass Spectrometer at a Collision-Chamber Pressure of 5 μ

Product ion	Relative intensity, Reactant ion		
	$C_2H_5^+$	$C_3H_5^+$	$C_4H_7^+$
$C_2D_3^+$	0.14	...	0.20
$C_2D_3H^+$, $C_2D_2H_3^+$	0.32	...	...
$C_2D_4^+$	0.15	0.022	...
$C_2D_4H^+$	0.20	...	...
$C_3DH_4^+$	0.023	0.17	...
$C_3D_2H_3^+$	0.088	0.43	...
$C_3D_3H_2^+$	0.065	0.27	...
$C_3D_4H^+$	0.017	0.039	...
$C_4H_6D^+$	...	...	0.18
$C_4H_5D_2^+$	...	...	0.21
$C_4H_4D_3^+$	...	...	0.24
$C_4H_3D_4^+$	...	...	0.071
$C_5H_5D_4^+$	...	0.066	...
$C_6H_7D_4^+$	...	...	0.095

Table XII: Comparison of Observed and Calculated Distributions of $C_3X_5^+$ Isotopic Products from Reactions of Ethyl Ions with Ethylene Using Deuterated Reactants

Product	Relative intensity, Reactants			
	$C_2H_5^+ + C_2D_4$		$C_2D_5^+ + C_2H_4$	
	Calcd[a]	Exptl (5 μ)	Calcd[b]	Exptl 5 μ
$C_3H_4D^+$	0.16	0.12	0.04	0.05
$C_3H_3D_2^+$	0.48	0.46	0.32	0.31
$C_3H_2D_3^+$	0.32	0.33	0.48	0.45
$C_3HD_4^+$	0.04	0.08	0.16	0.19

[a] Assuming complete randomization of an intermediate $C_4H_5D_4^+$ complex. [b] Assuming complete randomization of an intermediate $C_4H_4D_5^+$ complex.

On the other hand, the in-line geometry of our tandem instrument, in which product ions from the collision chamber are detected in the same direction as the impacting ions, maximizes the collection of momentum-transfer products, such as those which result from ion–molecule reactions. The reaction-order plots for product ions produced by this charge transfer–ion molecule reaction sequence in our study are shown in Figures 7 and 8. In this case, the reaction orders observed in the tandem should be the same as those determined in single-source experiments, since, with this technique, the reagent ethylene ions are produced in the collision chamber by a first-order reaction, that is, the charge-transfer process.

The remaining figure (Figure 9) shows a kinetic plot from which data for the $C_4H_8^+$ complex are derived as discussed in the next section. Certain ionic reactions of significance to the radiation chemistry of ethylene have also been explored in this study and these are also treated more fully in the following section.

Discussion

Variation of Ion Intensities with Pressure. The observed variations of ion intensities with pressure in the mass spectrum of ethylene, as shown in Figures 1 and 2, are in close agreement with the trends previously reported by Wexler and Marshall.[5] If the reaction sequence

$$C_2H_4^+ \longrightarrow C_3H_5^+ \longrightarrow C_5H_9^+ \qquad (1)$$

is assumed, as the pressure-dependence plots suggest, then there is an apparent excess of the $C_5H_9^+$ ion. Wexler and Marshall observed a similar excess of this ion which they attributed to the fact that a portion of the $C_2H_4^+$ precursor of this ion is formed by a charge-transfer reaction between $C_2H_2^+$ and ethylene. The plausibility of this reaction sequence is substantiated by our study of $C_2H_2^+$ reactions in the tandem mass spectrometer which is reported in Table V.

Figure 1 also indicates the increasing prominence of $C_4H_8^+$ and $C_6H_{12}^+$ at higher pressures, although neither ion is detected below 50 μ. Since these ions correspond to the species which would be formed as intermediate complexes in the condensation sequence of the $C_2H_4^+$ ion, this behavior suggests a stabilization of these intermediates at higher pressures as a result of collisional deactivation. Collisional stabilization of ionic intermediates has also been observed by other investi-

Table XIII: Ionic Products from the Reaction of $C_4H_8^+$ Ions from Different Source Molecules with C_2H_4 at a Collision-Chamber Pressure of 5 μ

Product ion	m/e (product ion)	Relative intensity: Source of $C_4H_8^+$ 1-Butene	*cis*-2-Butene	*trans*-2-Butene	Isobutene	Cyclobutane
$C_4H_7D^+$	57	0.11	...	...	0.52	...
$C_4H_6D_2^+$	58	0.21	...	...	0.30	...
$C_4H_5D_3^+$	59	0.20	...	...	0.12	...
$C_4H_4D_4^+$	60	0.096	...	...	0.028	...
$C_5H_8D^+$	70	0.011	...	...	0.012	0.29
$C_5H_7D_2^+$	71	0.10	...	...	...	...
$C_5H_6D_3^+$	72	0.12	1.00	1.00	0.018	0.57
$C_5H_5D_4^+$	73	0.15	...	...	...	...
$C_6H_8D_4^+$	88	0.0024	...	...	...	0.14
Relative rate constant		1.00	0.006	0.005	0.73	0.02

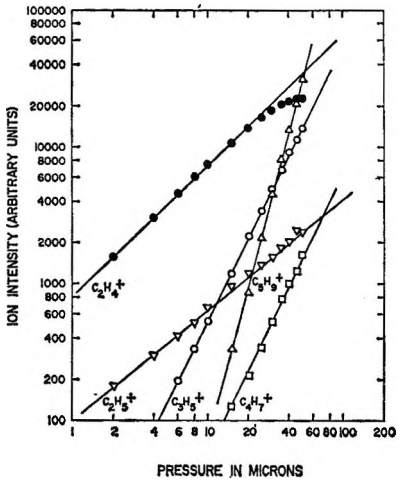

Figure 7. Logarithmic plots of product-ion intensities from the reaction of H_2S^+ with ethylene as a function of the collision-chamber pressure in the tandem mass spectrometer.

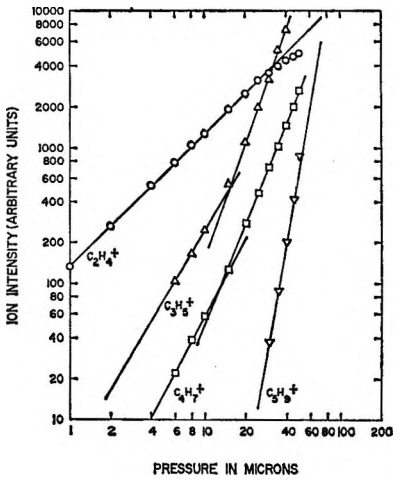

Figure 8. Logarithmic plots of product-ion intensities from the reaction of N_2O^+ with ethylene as a function of the collision-chamber pressure in the tandem mass spectrometer.

gators,[3,5,6] and additional evidence supporting this phenomenon will be presented later in this paper.

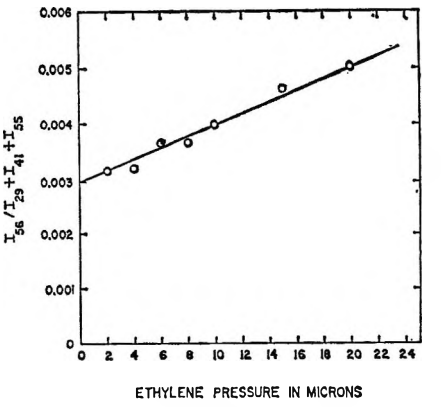

Figure 9. Plot of the ratio $I_{56}/(I_2 + I_{41} + I_{55})$ for the reaction of $C_2H_4^+$ ions with ethylene as a function of the collision-chamber pressure in the tandem mass spectrometer.

The experimental reaction cross sections listed in Table I are in reasonably good agreement with the previously reported data.[3-5] The data of Field[3] seem to be systematically lower than the values obtained by other workers and perhaps represent small errors in the pressure measurement or reaction length in these early experiments. With the exception of Harrison's experiments,[4] the range of ion energies is approximately the same in all these cases, and the spread of values obtained in these recent experiments probably is indicative of the precision of rate measurements by this method for highly reactive organic molecules. Obviously, in view of the magnitude of some of the observed ionic reaction cross sections, the ethylene system should be classed as very reactive. Also, the large differences in cross sections observed for the reactions of fragment ions suggest the probable importance of chemical factors in defining reaction channels for ion–molecule reactions. As many others have already noted, the collision model of Gioumousis and Stevenson[18] does not treat this problem, and the present ex-

(18) G. Gioumousis and D. P. Stevenson, *J. Chem. Phys.*, **29**, 294 (1958).

periments provide no information on the validity of this model.

Reactions of Individual Ions. $C_2H_4^+$ and Sequential Product Ions. The products from the reaction of low-energy (~0.3 eV) $C_2H_4^+$ ions with ethylene which were observed in the tandem mass spectrometer at two collision-chamber pressures are given in Table II. At the lower pressure, some 94% of the total product spectrum consists of $C_3H_5^+$ and $C_4H_7^+$ with trace amounts of several other ions. In the spectrum at 60 μ of pressure, the growth of the products $C_4H_8^+$ and $C_5H_9^+$ is evident. These results are in agreement with the reaction products from $C_2H_4^+$ which Field[3] deduced from single-source experiments in which appearance-potential measurements were used as the principal means of identifying the reactions. Employing similar techniques, Wexler and Marshall[5] found much the same reaction sequence but failed to include $C_4H_7^+$ as a product of the $C_2H_4^+$ and instead attributed this ion to the reaction of the $C_2H_3^+$ primary ion.

The reaction-order plots obtained with the tandem instrument which are shown in Figure 5 provide further support for the indicated reaction sequence of $C_2H_4^+$. It is seen from these plots that the $C_2H_5^+$, $C_3H_5^+$ and $C_4H_7^+$ ions all exhibit first-order dependence upon collision-chamber pressure, as would be expected if they were produced directly from $C_3H_4^+$. The $C_4H_8^+$ and $C_5H_9^+$ plots are particularly interesting, because they show two linear segments. The lower segment of the $C_4H_8^+$ plot corresponds to first-order dependence, while the upper segment indicates second-order behavior. Since the reaction of $C_2H_4^+$ with ethylene produces a $(C_4H_8^+)^*$ product with about 1.7 eV of excess energy (if the $C_2H_4^+$ is assumed not to be vibrationally excited and the product ion is assumed to have the 1-$C_4H_8^+$ structure), this product is expected to decompose almost entirely unless this excess energy is removed by a third body. And indeed, the order dependence just noted for $C_4H_8^+$ clearly demonstrates such a collisional stabilization of this product at higher pressures.

$$C_2H_4^+ + C_2H_4 \longrightarrow (C_4H_8^+)^* \xrightarrow{M} C_4H_8^+ \qquad (2)$$

Presumably the lower order $C_4H_8^+$ product is formed by some process which is less exothermic, or the excess energy is degraded in some way other than third-body collisions. The $C_5H_9^+$ product exhibits a second-order pressure dependence at lower pressures, but the upper segment indicates that this is a third-order product. Thus while $C_5H_9^+$ is produced in part by the further reaction of a product or products from the initial $C_2H_4^+$ interaction, it also results from a higher order process. Field's earlier data for this ion[4] also hinted that it was produced from more than one source.

It is appropriate to note, at this point, that in spite of general agreement on the final products resulting from reaction of the parent ion with ethylene, there is still considerable uncertainty with regard to the participation of intermediate complexes in the condensation sequence. Wexler and Marshall,[5] for example, propose for the low-pressure (up to 10 mm) gas-phase ionic polymerization of ethylene a sequence which is propagated by carbonium ion fragments,[19] as shown in reactions 3–5, rather than by undissociated molecular ions

$$C_2H_4^+ + C_2H_4 \longrightarrow C_3H_5^+ + CH_3 \qquad (3)$$

$$C_3H_5^+ + C_2H_4 \longrightarrow C_5H_9^+ \qquad (4)$$

$$C_5H_9^+ + C_2H_4 \longrightarrow C_7H_{13}^+ \qquad (5)$$

Such a reaction sequence implies that the intermediate complexes are of comparatively short lifetime and decompose prior to further reaction. On the other hand, Field[3] proposes that the ionic condensation proceeds through reactions of undissociated intermediate reaction complexes, as indicated in reactions 6–9c, and he has estimated that the rate of decomposition of $(C_4H_8^+)^*$ is 4×10^7 sec^{-1}

$$C_2H_4^+ + C_2H_4 \longrightarrow (C_4H_8^+)^* \qquad (6)$$

$$(C_4H_8^+)^* \longrightarrow C_3H_5^+ + CH_3 \qquad (7a)$$

$$(C_4H_8^+)^* \longrightarrow C_4H_7^+ + H \qquad (7b)$$

$$(C_4H_8^+)^* + C_2H_4 \longrightarrow (C_6H_{12}^+)^* \qquad (8)$$

$$(C_6H_{12}^+)^* \longrightarrow C_3H_5^+ + C_3H_7 \qquad (9a)$$

$$(C_6H_{12}^+)^* \longrightarrow C_4H_8^+ + C_2H_4 \qquad (9b)$$

$$(C_6H_{12}^+)^* \longrightarrow C_5H_9^+ + CH_3 \qquad (9c)$$

Quite recently, Kebarle[9] has obtained data which have an important bearing on these reaction sequences. From a study of the xenon-sensitized radiolysis of ethylene in his high-pressure mass spectrometric apparatus, this investigator has determined approximate rate constants for reactions 6 and 8 of $k_6 = 10^{-9}$ cm^3 molecule^{-1} sec^{-1} and $k_8 = 2 \times 10^{-12}$ cm^3 molecule^{-1} sec^{-1}, respectively. Kebarle also observed that no $C_3H_5^+$ ions were present in his spectra, while $C_5H_9^+$ was found in high abundance. He therefore suggested the possibility that the $C_3H_5^+$ ions might react rapidly with ethylene to yield the $C_5H_9^+$ product and would, therefore, not be detected. This would only require that reaction 4 have a rate constant comparable with that for reaction 6, since no ethylene ions were observable in his experiments either, except at very low pressures. Unfortunately, Kebarle could not actually confirm this reaction path on the basis of his data.

Several experiments which we have accomplished

(19) While it is recognized that all positive ions in which the charge is presumed to reside on the carbon are formally designated "carbonium" ions, it is convenient for purposes of distinguishing different classes of ionic reactants to restrict this term to fragment ions such as $C_3H_3^+$, whereas ions of stable molecular species such as $C_4H_8^+$ are identified as "molecular" ions. This terminology is used in the discussion presented in this paper.

using the tandem mass spectrometer address the question of possible reaction paths which has been considered above. First, we have examined the reactions of both $C_3H_5^+$ and $C_4H_8^+$ with ethylene in order to identify the actual products of these reactions and to compare the reactivity of these species. These ions have also been impacted on perdeuterioethylene for the purpose of obtaining more insight into the reaction mechanism. Unfortunately, in its present configuration the tandem spectrometer cannot be operated with sufficiently high pressure in the ion source to produce usable intensities of $C_3H_5^+$ and $C_4H_8^+$ *via* ion–molecule reactions of ethylene. Accordingly, reactant ions for these experiments were derived from several molecular sources. $C_3H_5^+$ was derived from both 1-butene and neopentane, while $C_4H_8^+$ ions were obtained from the entire series of butenes and cyclobutane. The data for these experiments, presented in Tables XI, XIII, and XIV, indicate that both $C_3H_5^+$ and $C_4H_8^+$ do, in fact, react with ethylene to yield $C_5H_9^+$.

Table XIV: Products from the Reactions of $C_2H_5^+$, $C_3H_5^+$, and $C_4H_7^+$ with C_2H_4 Observed in the Tamden Mass Spectrometer at a Collision-Chamber Pressure of 5 μ

Product ion	Relative intensity — Ionic reactant $C_2H_5^+$	$C_3H_5^+$	$C_4H_7^+$
$C_2H_3^+$	...	...	0.68
$C_2H_4^+$	...	0.22	...
$C_2H_6^+$	0.030	...	...
$C_3H_5^+$	0.85	...	...
$C_3H_6^+$	0.070	...	...
$C_4H_7^+$	0.053	...	...
$C_5H_9^+$	...	0.78	...
$C_6H_{11}^+$	...	...	0.32

The important question, of course, concerns the relative rates with which these species react. A comparison of the two ions under consideration is complicated by the fact that the reactions of butene ions show a pronounced dependence on the structure of the molecule from which they are derived. This is indicated by the data presented in Table XIII, in which are listed the rate constants for reactions of butene ions from the various sources with C_2D_4, relative to the reaction of 1-butene ions which is taken as unity. For $C_4H_8^+$ ions derived from both 1-butene and isobutene, it can be seen that the major reaction process is simply a back-reaction yielding isotopically scrambled reactant ions. If only the rate constant for the production of $C_5X_9^+$ products is considered, (X = H or D), it is evident that $C_4H_8^+$ from 1-butene reacts with ethylene at a significant rate to form this product. The rate constant for $C_4H_8^+$ obtained from *trans*-2-butene, the least reactive of the isomeric butene sources, was smaller by a factor of about 75. It seems apparent from these results that the various butene ions do not achieve equivalent structures prior to reaction.

Although $C_5X_9^+$ is also produced, the products from the reaction of $C_3H_5^+$ ions with ethylene and perdeuterioethylene (Tables XI and XIV) show that back-reaction is the predominant reaction mode. Table XV presents a comparison of the relative rate constants for the production of $C_5H_9^+$ from $C_3H_5^+$ and the various butene ions. These rate measurements are based on isotopic experiments in the tandem spectrometer for which the several reaction paths can be distinguished. The data indicate that only $C_4H_8^+$ ions with the 1-butene structure could compete effectively with $C_3H_5^+$ as a source of $C_5H_9^+$. Since we are, of course, unable to specify the structure of the $C_4H_8^+$ ions produced by ion–molecule reaction of $C_2H_4^-$ with ethylene, this information is not conclusive in determining the principal source of the $C_5H_9^+$ product in experiments at higher pressures. It is plausible, however, since the $C_4H_8^+$ ion is collisionally stabilized at higher pressure, that this ion will ultimately rearrange to the most thermodynamically stable 2-butene ion structure regardless of its original configuration.

Table XV: Relative Rate Constants for Reactions of Various Ions with Ethylene as Determined in the Tandem Mass Spectrometer

Reactant ion	Reactant source	Product ion	Relative rate constant
$C_2H_4^+$	Ethylene	$C_3H_5^+$	1.0
$C_3H_5^+$	1-Butene	$C_5H_9^+$	0.0078
	Neopentane	$C_5H_9^+$	0.0075
$C_4H_7^+$	1-Chloro-2-butene	$C_2H_3^+$	0.0039
	1-Chloro-2-butene	$C_6H_{11}^+$	0.0018
$C_4H_8^+$	1-Butene	$C_5H_9^+$	0.059
	cis-2-Butene	$C_5H_9^+$	0.00091
	trans-2-Butene	$C_5H_9^+$	0.00072
	Isobutene	$C_5H_9^+$	0.0039
	Cyclobutane	$C_5H_9^+$	0.0018

The low reactivity with ethylene of $C_4H_8^+$ ions obtained from 2-butene has also been observed by Kebarle and Haynes,[7,9] who studied this reaction in a conventional ion–molecule mass spectrometer. These authors reported that the cross section for the reaction

$$C_4H_8^+ + C_2H_4 \longrightarrow C_5H_9^+ + CH_3 \qquad (10)$$

is 400 times smaller than the cross section for the parent-ion reaction

$$C_2H_4^+ + C_2H_4 \longrightarrow C_3H_5^+ + CH_3 \qquad (11)$$

Also, as we have already mentioned, these same workers observed that the rate constant for the parent-ion reaction is some 500 times lower than that for the

$C_4H_8^+$ species produced in the xenon-sensitized radiolysis of ethylene. Our own data listed in Table XV indicate that the rate constants for these two reactions differ by a factor of about 1200 (taking the rate for $C_4H_8^+$ from 2-butene). This large decrease in the rate constant for the secondary addition reaction may well be due to combined structural and steric effects.[9] Using ground-state energetic values[20] for the ions involved, calculations indicate that reaction 10 is approximately thermoneutral for 1-butene ions but endothermic by at least 12 kcal/mol for the other isomeric butene ions.

Another set of experiments accomplished in the dual-stage mass spectrometer are more definitive regarding the mechanism for production of $C_5H_9^+$ in ethylene. In these experiments, for which the data are given in Tables VII and VIII, the distributions of isotopic products resulting from the reactions of $C_2H_4^+$ ions with C_2D_4 and $C_2D_4^+$ ions with C_2H_4 have been determined. In Table IX, the relative distributions of the $C_3X_5^+$ and $C_5X_9^+$ species (X = H or D) are compared with the distributions of these products which are calculated on the basis of a mechanism which involves sequential additions of the molecule ion forming intermediate complexes in which the hydrogen species are completely randomized prior to dissociation of the complex. The isotopic product distribution is calculated on a purely statistical basis ignoring possible isotope effects for loss of fragments containing carbon. The agreement between the calculated and experimental distributions for the $C_3X_5^+$ products at a collision-chamber pressure of 5 μ is shown to be quite good for both reactions. We interpret this agreement as indicative of the fact that an intermediate $C_4H_4D_4^+$ complex is formed in these reactions and that it is sufficiently long lived to permit essentially complete randomization of the hydrogen species. A more significant observation can be made from the distributions obtained at a collision-chamber pressure of 50 μ at which the $C_5X_9^+$ products can be detected. It is seen that the distribution of $C_5X_9^+$ species closely approximates the distribution for the $C_3X_5^+$ products at the same pressure but is distinctly different from the distribution of $C_5X_9^+$ products which can be calculated by assuming that these ions result from decomposition of a $C_6X_{12}^+$-complex intermediate. These observations strongly suggest that for the pressure range employed in these studies, the $C_5X_9^+$ product is formed by the carbonium ion reaction sequence (reactions 3 and 4) rather than through the sequence involving undissociated complexes (reactions 6, 8, and 9c), in spite of the fact that the $C_4H_8^+$ apparently has a lifetime sufficient to allow considerable rearrangement and presumably sufficient to undergo further reaction.

Estimates of the rate constant for decomposition of the $(C_4H_8^+)^*$ complex have now been made from several experimental investigations. In addition to the early mass spectrometric determination[3] of $k_7 = 4 \times 10^7$ sec^{-1}, which has already been mentioned, a value of 5×10^7 sec^{-1} for this rate constant was determined from radiolysis experiments,[10] and a recent photolytic investigation has yielded a value of $k_7 = 2 \times 10^7$ sec^{-1}. From experiments in the tandem mass spectrometer, we are able to estimate this rate constant in the low-pressure region, where further reactions of the ionic dissociation products from $(C_4H_8^+)^*$ or of the complex itself are negligible and do not complicate the kinetic analysis. In these experiments, the product-ion intensities from the reaction of $C_2H_4^+$ ions with ethylene were determined as a function of collision-chamber pressure. The experimental data for this reaction, which have already been discussed, indicate that at pressures below about 20 μ a mechanism which adequately accounts for the products may be represented as

$$C_2H_4^+ + C_2H_4 \xrightarrow{k_6} (C_4H_8^+)^* \quad (6)$$

$$(C_4H_8^+)^* \xrightarrow{k_{7a}} C_3H_5^+ + CH_3 \quad (7a)$$

$$(C_4H_8^+)^* \xrightarrow{k_{7b}} C_4H_7^+ + H \quad (7b)$$

$$(C_4H_8^+)^* \xrightarrow{k_{7c}} C_2H_5^+ + C_2H_3 \quad (7c)$$

$$(C_4H_8^+)^* + C_2H_4 \xrightarrow{k_{12}} C_4H_8^+ + C_2H_4 \quad (12)$$

From this reaction scheme, the kinetic expression

$$\frac{k_{12}}{k_{7a} + k_{7b} + k_{7c}} = \frac{I_{C_4H_8^+}}{I_{C_2H_5^+} + I_{C_3H_5^+} + I_{C_4H_7^+}} \frac{1}{[C_2H_4]} \quad (13)$$

is deduced, and it is apparent that the slope of a plot of the indicated ion-intensity ratio as a function of ethylene pressure will yield the required rate-constant ratio. Such a plot for the reaction in question is shown in Figure 9 and yields a slope of $k_{12}/(k_{7a} + k_{7b} + k_{7c}) = 3.5 \times 10^{-18}$ cm^3 $molecule^{-1}$. If it is then assumed that the stabilization process, reaction 12, occurs at every collision, the simple orbiting-complex theory[18] can be applied to calculate k_{12}, using the relation

$$k = 2\pi\left(\frac{e^2\alpha}{\mu}\right)^{1/2} \quad (14)$$

where α is the polarizability of the neutral molecule and μ is the reduced mass of the reaction pair. This calculation yields a value of $k_{12} = 1.1 \times 10^{-9}$ cm^3 $molecule^{-1}$ sec^{-1}, and from the above ratio, one obtains a rate constant for the over-all dissociation of $(C_4H_8^+)^*$ of $k_7 = 3.2 \times 10^8$ sec^{-1}. This rate is somewhat higher than that determined by other workers and this may reflect differences in the energy content of the $(C_4H_8^+)^*$ complex formed in our experiments as compared with the other cases. It is interesting to note that the rate-

(20) F. H. Field and J. L. Franklin, "Electron Impact Phenomena," Academic Press Inc., New York, N. Y., 1957.

constant ratio, $k_{12}/(k_{7a} + k_{7b} + k_{7c}) = 3.5 \times 10^{-18}$ cm^3 molecule^{-1}, obtained in our experiments is effectively the ratio of stabilization to decomposition for the $(C_4H_8^+)^*$ entity. Kebarle and coworkers[7,9] have observed that xenon is an efficient deactivating agent for excited ions in ethylene and has determined an over-all stabilization-to-decomposition ratio for the ethylene system of 3.4×10^{-17} cm^3 molecule^{-1} at an ethylene pressure of 40 μ. This implies that xenon is a more efficient stabilizing agent than ethylene itself, although there is obviously considerable uncertainty in both sets of measurements.

Some other interesting points remain to be considered with regard to the isotopic distributions of $C_3X_5^+$ products from the parent-ion reactions which are reported in Table IX. It is noticed that in the reaction of $C_2H_4^+$ with C_2D_4, the heavier $C_3X_5^+$ ions are slightly more abundant than the lighter ions, while the reverse is true for the reaction of $C_2D_4^+$ with C_2H_4. In both cases these trends become more pronounced as the collision-chamber pressure increases. Although there is some scatter in the experimental data, the relative ion intensities measured in ten separate experiments with two different observers were in agreement within about 1% in all cases.

It would be difficult to explain these observations on the basis of simple isotope effects. In our experience, such shifts in relative product distribution at higher pressures usually indicate contributions to these products from higher order reactions. An examination of the secondary product ions from the parent-ion reaction with ethylene (Tables II, VII, and VIII) shows that there are only two products, namely $C_2H_5^+$ and $C_4H_7^+$, which might undergo further reaction with increasing pressure to yield $C_3H_5^+$. In separate experiments, each of these ions was impacted on ethylene and perdeuterioethylene, and the results, reported in Tables XI and XIV implicate the ethyl ion as a source of $C_3H_5^+$. The $C_4H_7^+$ ion apparently does not produce $C_3H_5^+$.

The reaction

$$C_2H_5^+ + C_2H_4 \longrightarrow (C_4H_9^+) \xrightarrow{*} C_3H_5^+ + CH_4 \quad (15)$$

has not been detected in earlier investigations of the ethylene system. It would be difficult to observe in conventional ion–molecule reaction studies. From the data shown in Tables VII and VIII, it is evident that the ethyl ion is produced from the ethylene parent ion by both proton-transfer and hydrogen atom abstraction reactions. Thus at higher pressures this ethyl ion product reacts further, contributing to the $C_3X_5^+$ products (in the isotopic experiments) and effecting the shift in distribution reported for these products in Table IX. It is also interesting that the $C_2H_5^+$ reaction with C_2D_4 and the analogous reaction of the deuterated ethyl species both yield distributions of $C_3X_5^+$ products which are in remarkable agreement with the distributions which can be calculated by assuming that these ions are formed from the decomposition of the appropriate randomized intermediate complexes. These comparisons are shown in Table XII and it can be seen that the $C_3X_5^+$ distributions in this case are quite different from the corresponding distributions which are produced by the parent-ion reaction.

It should be mentioned that the distribution of $C_3X_5^+$ products resulting from the reaction of ethylene parent ions with the deuterated molecule has also been determined by Meisels.[10] This investigator observed a distribution $C_3H_4D^+:C_3H_3D_2^+:C_3H_2D_3^+:C_3HD_4^+ = 10.6:39.8:39.9:9.6$, which he interpreted to be substantially different from statistical predictions. These experiments, however, were conducted with a conventional single-source mass spectrometer and required the introduction into the ion source of an equimolar mixture of C_2H_4 and C_2D_4. Thus the reactions of $C_2H_4^+$ with C_2D_4 and of $C_2D_4^+$ with C_2H_4 occur simultaneously in such an experiment, and the observed $C_3X_5^+$ product results from superposition of both distributions. It is interesting to observe that if we combine the distributions of $C_3X_5^+$ determined in our experiments for each of these processes at 50 μ, as reported in Table IX (assuming equal cross sections for both reactions), and renormalize, we arrive at a distribution of $C_3H_4D^+:C_3H_3D_2^+:C_3H_2D_3^+:C_3HD_4^+ = 0.13:0.39:0.38:0.10$, in very close agreement with the single-source experiments.[10] We conclude, therefore, that our interpretation that the $C_3H_5^+$ produced by the ethylene parent ion is formed by decomposition of a randomized $(C_4H_8^+)^*$ intermediate is correct. The departure of the $C_3X_5^+$ product distribution from statistical at higher pressures, which was observed both in our isotopic experiments and in single-source experiments, results from a complicating reaction. This reaction is the formation of isotopic $C_3X_5^+$ from the further reaction of ethyl ions produced by the initial parent-ion interaction.

In earlier discussion, it was suggested that the somewhat larger rate of decomposition for the $(C_4H_8^+)^*$ complex which we observe in this work as compared with previous estimates may reflect differences in the internal energy of the complex as formed in the various experiments. It can be readily demonstrated that internal energy of the reaction complex has a dramatic influence on the fragmentation modes. Thus Table X shows the distributions of the C_3 products from the reaction of $C_2H_4^+$ with C_2D_4 as a function of the kinetic energy of the impacting ion. As the reactant-ion energy increases, the $C_3X_5^+$ distribution is complicated by the appearance of $C_3X_3^+$ products. That more extensive fragmentation of the complex is actually occurring with increasing energy of the bombarding ion was confirmed by examination of the corresponding reaction with C_2H_4. The results of this separate experi-

ment, reported in the last column of Table X, show that the $C_3H_3^+$ fragment increases rapidly at the expense of the $C_3H_3^+$ ion when the parent-ion energy is raised. Since no $C_3H_3^+$ product is observed for the reaction of quasi-thermal energy $C_2H_4^+$ ions, these facts demonstrate clearly the conversion of translational energy of the impacting ion into internal energy of the reaction complex. With this increased internal energy, the distribution of $C_3X_5^+$ fragments produced by decomposition of the reaction complex in the isotopic experiments departs rapidly from a statistical distribution. This probably results because of the reduced lifetime for the complex at higher relative energies.

The dependence of the cross sections for production of $C_3H_3^+$ and $C_3H_5^+$ from the $C_2H_4^+$ reaction on the reactant-ion energy is itself quite interesting. Calculations on the basis of ground-state energetics show that the reaction producing $C_3H_5^+$ is exothermic by about 0.4 eV, while the reaction forming $C_3H_3^+$ is endothermic by 1.7–2.2 eV, depending on the structure of the ion formed and the identity of the neutral products. By analogy with the observations of Maier[21,22] of the cross section dependence for exothermic and endothermic charge-transfer and for endothermic atom-transfer ion–molecule reactions, one would expect that the cross section for the exothermic process yielding $C_3H_5^+$ would fall off somewhat with increasing reactant-ion energy, while that for the endothermic production of $C_3H_3^+$ should exhibit a threshold, followed by a rapid rise. This is, in fact, exactly the behavior observed for the cross sections of these two processes.

In order to estimate the threshold for production of $C_3H_3^+$, the ratio $C_3H_3^+$:$C_3H_5^+$ was plotted as a function of the $C_2H_4^+$ kinetic energy on the laboratory scale. Since only a few points were obtained, this plot is not presented here, but a few of its features will be noted. The plot exhibits a small tail in the region near threshold, but at energies in excess of $E_{lab} = 4$ eV, the ratio rises very sharply to a maximum. If the linear portion of this latter, rapidly changing segment of the plot is extrapolated, then a threshold for appearance of $C_3H_3^+$ of $E_{lab} = 4.1$ eV is determined. This corresponds to a barycentric energy of 2.1 eV. While it is perhaps fortuitous, in view of the precision of our experimental determination, the calculated endothermicity of the reaction yielding $C_3H_3^+$ is exactly 2.1 eV, if the product ion has the $CH_2{=}C{=}CH^+$ structure and the neutral products are CH_3 and H_2. In any event, we believe this to be the first reported case in which such threshold behavior has been observed for an endothermic ion–molecule reaction which involves such a considerable amount of rearrangement.

One remaining aspect of the product distribution reported in Table VII for the reaction of $C_2H_4^+$ ions with perdeuterioethylene requires clarification. It is observed that there is a rather substantial yield of $C_2D_4^+$ from this reaction, as well as smaller amounts of $C_3D_5^+$, $C_4D_7^+$, and $C_5D_9^+$. The appearance of these products is explained on the basis of a charge-transfer reaction producing $C_2D_4^+$, which then undergoes the same reaction sequence as $C_2H_4^+$. Such an explanation was confirmed by reacting $C_2D_4^+$ with C_2H_4, which produces the analogous products $C_2H_4^+$, $C_3H_5^+$, $C_4H_7^+$, and $C_5H_9^+$, as reported in Table VIII. Further support for the charge-transfer mechanism is presented in Figure 6, which compares the order of the $C_3D_5^+$ product from the $C_2H_4^+$–C_2D_4 reaction with the orders of the $C_3D_4H^+$ and $C_3D_3H_2^+$ products in the low-pressure region where contributions from ethyl ions to these products are minimal. The order plots in Figure 6 show that the $C_3D_5^+$ ion is produced by a reaction one order higher than the process yielding the other two ions, as would be expected from the proposed reaction sequence. It seems clear from these data that $C_3D_5^+$ and $C_5H_9^+$ result from an entirely different reaction process than that by which the other $C_3X_5^+$ and $C_5X_9^+$ ions are formed, and therefore, the former ions were not included as part of the distributions resulting from intermediate-complex dissociation and subsequent reaction. This means, however, that $C_3H_5^+$ in the ethylene system is produced simultaneously by reactions of different orders, a possibility which was suggested by Field[3] some time ago.

$C_2H_3^+$ and Sequential Products. The products from the reaction of $C_2H_3^+$ with C_2H_4 are shown in Table III. It can be seen that the ethyl ion is essentially the only product at low pressures, although very small amounts of $C_2H_4^+$, $C_3H_3^+$, and $C_4H_5^+$ are also detected. From a study of the reaction of vinyl ions with C_2D_4, which is reported in Table IV, it was established that the ethyl ion is formed for the most part by the proton-transfer reaction

$$C_2H_3^+ + C_2D_4 \longrightarrow C_2D_4H^+ + C_2H_2 \qquad (16)$$

The competing hydride ion transfer process is also observed

$$C_2H_3^+ + C_2D_4 \longrightarrow C_2D_3^+ + C_2H_3D \qquad (17)$$

but is of much less significance than the former reaction, the relative rate constants being in the ratio $k_{16}/k_{17} = 19{:}1.0$. It is also apparent that a minor portion of the $C_2H_3^+$ reactant undergoes condensation reactions with ethylene. Thus a small fraction of the observed product ions must result from a process which involves the formation of a $(C_4H_7^+)^*$ intermediate. The lifetime and relative abundance of such a complex are important questions, as we shall see, for the radiation chemistry of ethylene. Several facts lead us to believe that, in the pressure range of the experiments reported in this work, the $(C_4H_7^+)^*$ complex is quite short lived and of relatively minor importance in the

(21) W. B. Maier, II, *J. Chem. Phys.*, **42**, 1790 (1965).
(22) W. B. Maier, II, *ibid.*, **46**, 4991 (1967).

reaction sequence. First, a comparison of the observed distributions of isotopic products for a particular ionic species with that calculated on a statistical basis gives very poor agreement. Thus decomposition of a randomized $(C_4H_3D_4^+)^*$ complex would be expected to yield a $C_4X_5^+$ distribution corresponding to $C_4D_2H_3^+:C_4D_3H_2^+:C_4D_4H^+ = 0.29:0.57:0.14$, whereas the data in Table IV indicate that these products are of the order 0.26:0.45:0.29.

The experimental distribution of $C_2X_5^+$ products is somewhat complicated by the fact that the $C_2D_3H_2^+$ product coincides with the charge-transfer product $C_2D_4^+$. Even if this ion is ignored, however, it is still apparent that the experimental distribution is quite different from the statistical. The observed ratio of $C_2D_2H_3^+:C_2D_4H^+ = 0.20:1.0$, while the predicted statistical ratio is 2.1:1.0. It seems clear, therefore, that the major product of the vinyl ion reaction with ethylene, namely ethyl ion, is formed almost entirely by a discrete transfer process which does not involve a randomized intermediate collision complex. Further evidence is provided by the over-all condensation sequence determined in the time-of-flight mass spectrometer. As Figure 2 demonstrates, the $C_4H_7^+$ product actually passes through a maximum at about 150 μ of pressure and then decays effectively to zero relative intensity at 1000 μ. Simultaneously, a small amount of $C_6H_{11}^+$ product is formed. Such behavior for the $C_4H_7^+$ ion would not be expected if this species were the complex formed in the vinyl ion reaction, because such a complex should be stabilized to an increasing extent at higher pressures, just as is observed for the $(C_4H_8^+)^*$ complex resulting from the parent-ion reaction. On the other hand, such a pressure dependence for $C_4H_7^+$ is readily explained if this ion is produced by decomposition of the $(C_4H_8^+)^*$ complex, a decomposition mode which might disappear as the latter ion is stabilized. Therefore, it appears that in the pressure range to which our study is limited, up to 1000 μ, the $C_4H_7^+$ ion is formed by the $C_2H_4^+$ reactant, a reaction which we have already confirmed. The reaction complex $(C_4H_7^+)$ has such a short lifetime that it cannot be stabilized and does not participate in the reaction sequence over our accessable pressure range.

Since the reaction of vinyl ions with ethylene to produce $(C_4H_7^+)^*$ is exothermic by about 4 eV, this reaction complex is highly excited. Stabilization of this intermediate at elevated pressures is apparently possible, however, because Kebarle[7,9] has observed relatively large abundances of $C_4H_7^+$ and $C_6H_{11}^+$ in the argon-sensitized radiolysis of ethylene (under conditions which produce mainly $C_2H_3^+$ as the primary reactant) using his ultrahigh-pressure mass spectrometric device. This same investigator also detects $C_6H_{11}^+$ in significant abundance in pure ethylene at pressures of several torr. Our tandem experiments appear to confirm this, since the reaction of $C_4H_7^+$ ions with ethylene (Tables XII and XIV) does produce the condensation product. At the lower pressures which characterize our experiments, however, the hydride-transfer reaction

$$C_4H_7^+ + C_2D_4 \longrightarrow C_2D_3^+ + C_4H_7D \qquad (18)$$

is the dominant mode of reaction. Relative rate constants measured for these processes are cited in Table XV.

The observations just discussed have important implications for the radiation chemistry of ethylene because, as Meisels has noted, a reaction sequence involving the formation of $C_4H_7^+$ by the vinyl ion interaction with ethylene, followed by the reactions

$$C_4H_7^+ + C_2H_4 \longrightarrow (C_6H_{11}^+)^* \qquad (19)$$

$$(C_6H_{11}^+)^* \longrightarrow C_5H_7^+ + CH_4 \qquad (20)$$

provides a possible radiolysis mechanism for forming molecular methane. The results of the present investigation suggest an alternate pathway for molecular methane production, namely, the reaction of ethyl ion to yield $C_3H_5^+$ (reaction 15). Moreover, this reaction is probably important in radiolysis, since Kebarle's experiments[7] show a large concentration of $C_4H_9^+$ ions in ethylene at higher pressures. This species undoubtedly represents the stabilized complex formed in reaction 15. Indeed, Kebarle attributed his observation of this $C_4H_9^+$ product to the ethyl ion reaction but was unable to specify the decomposition products of the complex. Under the conditions of his experiments, any $C_3H_5^+$ formed reacts rapidly to yield $C_5H_9^+$ and is, therefore, not detected. As already noted, our experiments confirm reaction 19, but we observe no $C_5H_7^+$ product which would result from reaction 20. We therefore consider reaction 15 to be a much more likely source of the molecular methane product observed in ethylene radiolysis. It is also possible, of course, that the $(C_4H_9^+)^*$ complex which is stabilized at the higher pressures characteristic of the radiolysis experiments reacts directly with ethylene under these conditions to yield the methane product

$$C_4H_9^+ + C_2H_4 \longrightarrow C_6H_{13}^+ \longrightarrow C_5H_9^+ + CH_4 \qquad (21)$$

These considerations indicate that the actual methane-forming step will depend upon the lifetimes and rates of stabilization of the various intermediate complexes involved. The latter factors are, in turn, dependent upon the total system pressure and may be strongly influenced by the presence of sensitizers such as rare gases.

$C_2H_2^+$ and C_2H^+. Some 70% of the reacting $C_2H_2^+$ yields the charge-transfer product $C_2H_4^+$ at the lower collision-chamber pressure indicated in Table V, in agreement with the postulates of several earlier authors.[3,5] That this reaction is indeed simple charge transfer was confirmed by using C_2D_4 as the neutral species, since $C_2D_4^+$ was the observed product in this

case. At 50 μ of pressure, the higher order products from reaction of $C_2H_4^+$ begin to appear. The reaction of C_2H^+ with C_2H_4, for which the products are indicated in Table VI, is also mainly a charge-transfer process, although in this case there are also substantial amounts of other products which result from a condensation reaction. Since charge transfer is endothermic for ground state C_2H^+, this observation is evidence for the formation of the long-lived excited ions $(C_2H^+)^*$ from ethylene by electron impact.

Production of $C_2H_4^+$ by Charge-Transfer Reactions. In an earlier section of this paper it was mentioned that Szabo,[8] using charge exchange to generate the appropriate ethylene ions, has studied ion–molecule reactions for these species by elevating the pressure in the collision chamber of a tandem mass spectrometer. For the case where charge-transfer reagents with recombination energies appropriate to produce only $C_2H_4^+$ were used, Szabo observed as products $C_4H_8^+$, $C_3H_5^+$, $C_4H_7^+$ and other minor ions, in general agreement with the findings of the present study. However, Szabo's results indicated that $C_3H_5^+$ and $C_4H_7^+$ were tertiary products, whereas previously proposed reaction schemes predicted second-order dependence for these ions. On the basis of this order dependence, several reaction processes were proposed which are not observed in our experiments. As we have already established in this investigation, $C_3H_5^+$ is actually formed by both second- and third-order reactions. However, Szabo's studies were conducted at such low pressures that the higher order process should not have been observed. The discrepancies indicated by Szabo's work prompted us to conduct a series of experiments in which charge exchange was utilized to produce $C_2H_4^+$ ions in the collision chamber of our tandem mass spectrometer at such pressures that ion–molecule reactions of the ions initially produced were probable. The reaction order of the product ions was then determined by the pressure dependence of the products. Figures 7 and 8 show the reaction-order plots for product ions from the impact of H_2S^+ and N_2O^+, respectively, on ethylene. With H_2S^+ as the reactant, $C_2H_4^+$ was observed to exhibit first-order dependence as expected, while $C_3H_5^+$ and $C_4H_7^+$ were determined to be second-order products. This clearly supports our findings reported in the earlier sections of this paper. The plots in Figure 6, for which N_2O^+ was the impacting ion, indicate reaction orders which are in agreement with those deduced from the H_2S^+ reaction plots. There is apparently a transition in order for $C_3H_5^+$ and $C_4H_7^+$ formation, as would be expected if the higher order reaction yielding $C_3H_5^+$ and the collisional stabilization of the $C_4H_7^+$ complex become dominant at higher pressures. Since Szabo worked in the very low pressure range, it would not be expected that his experiments should show this transition. It should also be noted that the $C_5H_9^+$ species exhibit peculiarly high orders in our plots, and the reason for this behavior is not clear.

The differences between our charge-transfer data and those of Szabo are not readily explained. However, as pointed out in previous discussion, isotopic experiments show that a fraction of the $C_3H_5^+$ product is actually produced by the parent ion which results from charge exchange even at quite low collision-chamber pressure. This contribution to $C_3H_5^+$ is, therefore, one reaction order higher than the parent ion produced directly by electron impact. We have also noted that the Lindholm instrument is constructed with a geometry which discriminates strongly against momentum-transfer products. If this charge transfer is conjectured to take place mainly *via* an orbiting complex (*i.e.*, is appropriately considered as a competing reaction channel in an ion–molecule collision complex), the product ion and any subsequent ion–molecule reaction product referenced to that ion would exhibit varying degrees of mass discrimination. It is possible that such a discrimination effect might explain the $C_4H_7^+$ and $C_3H_5^+$ discrepancies. This conjecture cannot, of course, be confirmed on the basis of existing evidence. In any case, the disparity between the results obtained by Szabo and those reported in this and other work suggests that one should be very cautious about using reaction orders as the principal criteria for establishing ion–molecule reaction mechanisms.

Acknowledgment. The authors wish to acknowledge with gratitude the assistance of Mr. C. D. Miller who accomplished some of the experimental measurements reported in this paper.

Raman Spectra of Fused Indium and Bismuth Chlorides

by J. T. Kenney and F. X. Powell

Department of Chemistry, The Catholic University of America, Washington, D. C. 20017 *(Received September 20, 1967)*

Raman spectra have been obtained from molten $BiCl_3$ and from $BiCl_3$ in the LiCl–KCl eutectic. The spectra give some indication that the eutectic melt contains $BiCl_4^-$ and $BiCl_5^{2-}$ with little $BiCl_6^{3-}$. Molten $BiCl_3$ probably does not consist of $BiCl_3$ units. Raman spectra obtained from $InCl_2$ indicate that it exists in the pure melt as $In(InCl_4)$ and in a chloride melt as a mixture of $InCl_4^-$ and $InCl_5^{2-}$. A chloride melt of $InCl_3$ contains the species $InCl_5^{2-}$ and $InCl_6^{3-}$.

Introduction

This paper extends the study by Raman spectroscopy of the chlorides of bismuth and indium in the molten state. The object in the case of bismuth is to determine whether any significant structural changes occur as the result of changing chloride concentration. In the case of indium we attempt to assign the oxidation state in fused salt media by determining the structures present in the molten state.

Experimental Section

The samples used in these studies were prepared by filtration into the Raman tube. This technique is similar to the one described by Janz.[1] After filtration the tube was sealed off under vacuum and kept molten for several months to allow sedimentation of any fine particles. This period of sedimentation resulted in samples which were optically void, and the measurement of weak Raman lines was therefore facilitated by this procedure.

The pure $BiCl_3$ was prepared from Fisher reagent grade $BiCl_3 \cdot H_2O$ by removal of the water with HCl gas. This was accomplished by passing the HCl up through the filtering frit and sample for 4 hr at room temperature. The temperature was then slowly raised to 120°, and the passage of HCl gas was continued until no further water collected downstream. The sample was then fused, the HCl was shut off, and the system was evacuated. The sample was then filtered with a positive pressure of HCl, was evacuated, and was sealed off. Samples of $BiCl_3$ in the LiCl–KCl eutectic were prepared by mixing the solid reagents and treating in a similar fashion.

Indium dichloride was prepared by passing HCl through molten indium metal in the same manner as above. The dark red color of InCl persisted until all the indium metal was used. When the sample was free of metal, it was filtered with a positive pressure of HCl, was evacuated, and was sealed off. $InCl_2$ in the LiCl–KCl eutectic was prepared by mixing solid $InCl_2$ prepared in the above fashion with the solid eutectic. This mixture was dried overnight at 150° under vacuum. The sample was then fused and HCl was passed through the solution for 4 hr. The sample was then filtered and sealed off as before.

Indium trichloride in the LiCl–KCl eutectic was prepared by mixing indium metal with the eutectic which was fused and then was dried by passing HCl through the melt overnight. Chlorine was then passed through the melt, which changed from colorless to yellow. The sample was then filtered and sealed off.

It was found that standard Raman tubes would often break under the thermal and mechanical stresses encountered with molten salt samples. A satisfactory tube was prepared by flaring out a Pyrex tube (15 mm o.d.) and inserting a 0.5 in. in diameter window in the end of the tube. The tube was then collapsed onto the window and the excess glass was drawn off. This procedure gave a strong seal with a rounded joint and no distortion in the window.

The sample holder used for the molten salt spectra runs is quite similar to others in the literature.[2] A shielded thermocouple was brought into the bottom of the sample compartment and allowed a temperature control of ±2° with a gradient of less than 5° along the sample tube.

The exposures were obtained with an $f/6.3$ Jarrell-Ash grating spectrograph with exposure times up to 70 hr. All spectra were obtained on Eastman-Kodak backed spectrographic plates, and tracings were recorded using a Joyce Mark IIIC densitometer. The positions of the lines were determined by calibrating the plate with an Fe–Ne hollow cathode discharge lamp.

The Raman spectra were obtained from mercury, cadmium, and rubidium electrodeless discharge lamps. These lamps will be described in a separate paper.

Results

Bismuth Trichloride. Bismuth trichloride in the vapor phase has been shown by electron diffraction to have a trigonal pyramid structure.[3] The Raman spec-

(1) G. J. Janz, T. R. Kozlowski, and S. C. Wait, *J. Chem. Phys.*, **39**, 1809 (1963).

(2) G. J. Janz and D. W. James, *ibid.*, **35**, 739 (1961).

(3) H. A. Skinner and L. A. Sutton, *Trans. Faraday Soc.*, **36**, 681 (1940).

trum of the solid has been interpreted as a trigonal pyramid with C_{3v} symmetry.[4] Molten $BiCl_3$ has an equivalent conductance of 0.44, indicating the formation of a large number of ion pairs and/or conjugation.[5]

The system $BiCl_3$–LiCl gives a simple eutectic and shows no evidence for compound formation.[6] $BiCl_3$ with NaCl and with KCl displays compound formation of the type 3KCl–$BiCl_3$, 2KCl–$BiCl_3$, and KCl–$BiCl_3$ first appearing at some 25 mol % of $BiCl_3$.[6] The freezing point depression indicates compound formation for both NaCl and KCl with $BiCl_3$, but no appreciable complexing in the liquid is indicated from the volume of mixing.[6]

Optical spectra of Bi^{3+} in aqueous chloride solution show formation of the series $BiCl^{2+}$, $BiCl_2^+$, $BiCl_3$, $BiCl_4^-$, and $BiCl_5^{2-}$ with increasing chloride concentration.[7] Optical spectra have also been obtained from molten KCl–LiCl eutectics[8] and in solid NaCl and KCl,[9] but the principal species giving rise to the spectra were not identified.

A four-line Raman spectrum of $BiCl_3$ in aqueous HCl has also been interpreted as coming from a trigonal pyramid molecule with C_{3v} symmetry.[10] The Raman spectrum of the solid $BiCl_6^{3-}$ has been reported,[11] and the values are listed in Table I.

Table I: Reported Raman Shifts (K) of Bi^{3+} Chlorides

$BiCl_3$ in HCl(aq)[10]	96 (ν_4)	130 (ν_2)	242 (ν_3)	288 (ν_1)
$BiCl_3$(s)[4]	146 (ν_4)	169 (ν_2)	242 (ν_3)	288 (ν_1)
$BiCl_6^{3-}$[11]	108 (ν_5)	222 (ν_2)		259 (ν_1)

Raman spectra were obtained from molten $BiCl_3$ at 260, 330, and 400° and from $BiCl_3$ 2 and 4 *M* in the LiCl–KCl eutectic at 470 and 510° off both the Cd 6438- and Rb 7479-Å lines. The pure sample was yellow-orange in color and the eutectic solutions were yellow. The densitometer tracings are shown in Figure 1, and Table II gives the observed line positions.

Table II: Observed Raman Shifts (K) of $BiCl_3$

$BiCl_3$ (fused)	123	264	315
$BiCl_3$ (LiCl–KCl)	120	244	281

The spectrum of $BiCl_3$ in the LiCl–KCl eutectic is a three-line spectrum which shows no change on going from a 2 to a 4 *M* solution (from 13 to 25 mol % in $BiCl_3$). The line centered at 281 K is the strongest and is partially overlapping the weak line at 244 K. The line centered at 120 K is intermediate in intensity between the other two lines and shows some trailing to the high-frequency side.

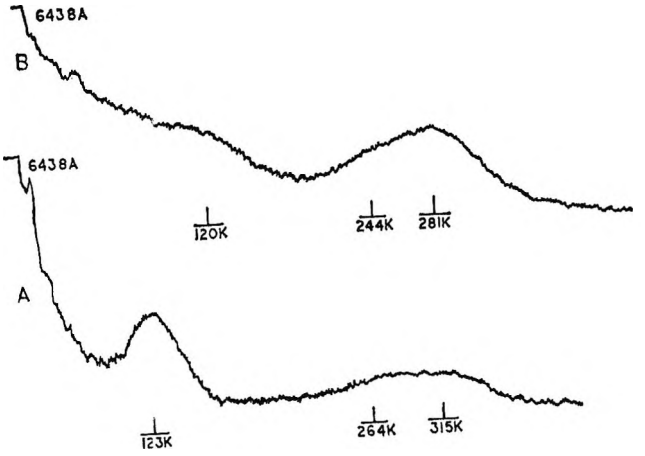

Figure 1. Raman spectra: A, molten $BiCl_3$; B, $BiCl_3$ in the molten LiCl–KCl eutectic.

Molten $BiCl_3$ gives three lines, with the strongest the low-frequency line at 123 K. This line shows a trailing toward the high-frequency side. Two lines at 264 and 315 K are partially overlapping and nearly equal in intensity.

The Raman spectrum of $BiCl_3$ in aqueous HCl shows four lines, with one line, the ν_2 line, very weak and the high-frequency line most intense.[10] This has been interpreted as the spectra of a trigonal C_{3v} molecule. The spectrum from the eutectic solution is similar to that of aqueous HCl, though the fourth line does not appear. The optical spectra have shown, however, the presence of other species in an aqueous chloride medium, *e.g.*, $BiCl_4^-$ and $BiCl_5^{2-}$.[7] Thus the earlier Raman interpretation must be corrected to allow for the presence of species of other than C_{3v} symmetry. In addition, the interpretation of the eutectic spectrum which is similar to the aqueous must allow for the presence of several species.

In Raman spectra the most intense line is usually the symmetric stretch or ν_1 line. In the eutectic the highest frequency line is most intense, in agreement with the aqueous spectra and also in agreement with the solid hexachloride ion. However, the ν_1 line of $BiCl_6^{3-}$ at 259 K is lower in frequency than either the 281 K line in the eutectic or the 288 K line in the aqueous solution. Since the ν_1 line usually shifts to lower frequencies as the

(4) P. Krishnamurti, *Indian J. Phys.*, **5**, 1 (1930).

(5) A. Klemm in "Molten Salt Chemistry," M. Blander, Ed., Interscience Publishers, Inc., New York, N. Y., 1964, p 535.

(6) C. C. Addison and W. D. Halstead, *J. Chem. Soc., A*, 1236 (1966).

(7) L. Newman and D. H. Hume, *J. Amer. Chem. Soc.*, **79**, 4576 (1957).

(8) G. P. Smith, D. W. James, and C. R. Boston, *J. Chem. Phys.*, **42**, 2249 (1965).

(9) A. Glasner and R. Reisfeld, *ibid.*, **32**, 956 (1960).

(10) S. Bhagavantam, *Indian J. Phys.*, **5**, 66, 86 (1930).

(11) T. Barrowcliffe, I. R. Beattie, P. Day, and K. Livingston, *J. Chem. Soc., A*, 1810 (1967).

coordination number increases, the eutectic solution probably does not contain much of the $BiCl_6^{3-}$ species. From the chloride ion concentration, which is about 22 *M*, the eutectic solution would be expected to have a higher coordination number than 3, which is the coordination number in the neutral species. The position of the ν_1 line indicates that Bi^{3+} in the eutectic has a higher coordination number than in the aqueous HCl used to obtain the Raman spectrum but probably less than the 6 of the solid ion. The width of the lines indicates that more than one species is present and that this is probably caused by species with different ionic charges.[12]

The Raman spectra of the pure melt are not similar to that of the aqueous, eutectic, or solid $BiCl_6^{3-}$. The ionic conductance of the melt and the width of the lines[12] would indicate that multiply charged species are present in the melt. The Raman spectra in this case cannot identify the species giving rise to the Raman effect, except to note what species could not give this pattern. $BiCl_2^+$ is not the principal species present, since it would be of C_{2v} symmetry and thus give a three-line Raman pattern with the central line most intense. $BiCl_3$ should be a trigonal pyramid with C_{3v} symmetry, but the intensity pattern is incorrect, since the ν_1 line would be of highest frequency for this symmetry, and this is not the case here. The possibility remains that the melt could be a mixture of $BiCl_2^+$ and $BiCl_4^-$ or chlorine bridged dimers. It is doubtful that the melt is a bridged chain structure of many units, since this would be expected to show a temperature dependence in the Raman spectrum corresponding to chain degradation. However, no temperature effect was observed. The Raman spectra indicate the presence of different species in the pure melt than in the chloride solution, but we are unable at present to identify these species.

Indium Dichloride and Trichloride. A number of studies have been made on the halides of indium, particularly the chlorides. Phase studies give conflicting results, with one proposing that the substance $InCl_2$ is a mixture of $InCl_3$ and In_4Cl_6.[13] Another showed that $InCl_2$ exists in the liquid and the vapor,[14] with a third showing that the series InCl, In_2Cl_3, $InCl_2$, and $InCl_3$ forms in the system In–Cl.[15]

Indium in the ground state has two 5s electrons and one 5p electron. The species In^{2+} would therefore be expected to be paramagnetic. Magnetic susceptibility studies on the solid indicate no unpaired electrons,[16,17] and to account for this either the dimeric species In_2Cl_4 with an In–In bond or the mixed oxidation state $In(InCl_4)$ was proposed. X-Ray diffraction studies on the solid failed to show the presence of $In(InCl_4)$.[18] Magnetic susceptibility measurements on a quenched melt of $InCl_{1.65}$ showed it to be paramagnetic, indicating the presence of monomeric $InCl_2$;[18] however, the results were not confirmed.[19]

Gallium is directly above indium in the periodic table, and some similarity between the properties of the dichlorides was expected. Raman spectral studies have shown that $GaGl_2$ exists in the melt as the mixed oxidation state ($Ga(GaCl_4)$ rather than as the simple triatomic or its dimer.[20] Fused $GaCl_2$ has a specific conductance of 0.27,[5] reflecting the presence of the ion pairs Ga^+ and $GaCl_4^-$. $InCl_2$ has a conductance of 0.47,[5] which is indicative of ion pairs, either from autoionization or a mixed oxidation state.

Raman spectra have shown the presence of a tetrahedral $InCl_4^-$ in an ether extract of aqueous HCl and $InCl_3$.[21] An aqueous HCl system of $InCl_3$ contains the ions $InCl_5^{2-}$ and $InCl_6^{3-}$, in addition to the tetrachloride.[21] The spectra are listed in Table III along with the values for $InCl_6^{3-}$ in the solid.

Table III: Raman Shifts (K) of Indium Chlorides

$InCl_4^-$ (ether extract)[21]	321 (ν_1)	89 (ν_2)	337 (ν_3)	112 (ν_4)
$InCl_3$ (HCl(aq))[21]	283 (ν_1)	130[a]	175[a]	
$InCl_6^{3-}$(s)[11]	277 (ν_1)	193 (ν_2)	149 (ν_5)	

[a] No assignment has been made.

Raman spectra have been obtained from $InCl_2$ at 330, 350, and 380°, from $InCl_2$ 2 and 4 *M* in LiCl–KCl at 480 and 510°, and from $InCl_3$ 3 *M* in the LiCl–KCl eutectic at 480 and 510°. The Raman shifts are shown in Figures 2 and 3; the frequencies are given in Table IV.

Table IV: Observed Raman Shifts (K) of $InCl_2$ and $InCl_3$

$InCl_2$ (pure)	317	110
$InCl_2$ (2 *M* in LiCl–KCl)	295	106
$InCl_2$ (4 *M* in LiCl–KCl)	294	107
$InCl_3$ (3 *M* in LiCl–KCl)	285	95

$InCl_2$ was yellow when molten and white when solid. In water it disproportionated to indium metal and

(12) G. J. Janz and D. W. James, *J. Chem. Phys.*, **38**, 902, 905 (1963).

(13) R. J. Clark, E. Griswold, and J. Kleinberg, *J. Amer. Chem. Soc.*, **80**, 4764 (1958).

(14) U. N. Fadeef and P. I. Fedorov, *Zh. Neorgan. Khim.*, **9**, 378 (1964).

(15) U. N. Fadeef and P. I. Fedorov, *ibid.*, **9**, 381 (1964).

(16) W. Klemm and W. Tilk, *Z. Anorg. Chem.*, **207**, 175 (1932).

(17) A. P. Palkin and N. V. Ostrikova, *Zh. Neorgan. Khim.*, **8**, 2566 (1963).

(18) E. I. Krylou and A. K. Shtol'ts, *ibid.*, **2**, 1753 (1957).

(19) G. Brauer and H. Morawietz, *Z. Anorg. Allg. Chem.*, **340**, 133 (1965).

(20) L. A. Woodward, G. Garton, and H. L. Roberts, *J. Chem. Soc.*, 3727 (1956).

(21) L. A. Woodward and M. J. Taylor, *ibid.*, 4473 (1960).

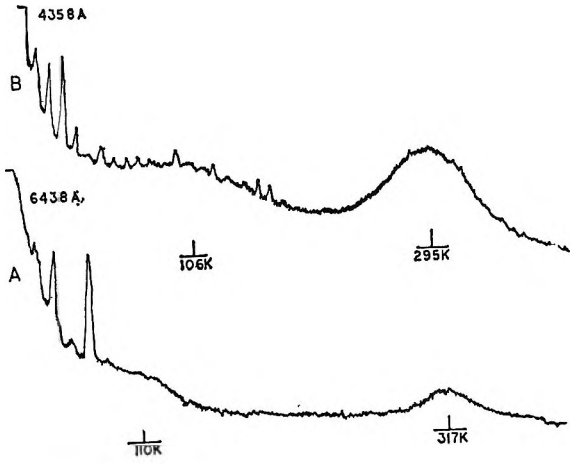

Figure 2. Raman spectra: A, molten $InCl_2$; B, $InCl_2$ in the molten LiCl–KCl eutectic.

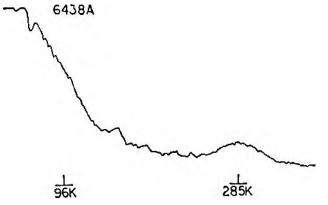

Figure 3. Raman spectrum of molten $InCl_3$ in the LiCl–KCl eutectic.

In^{3+}, with the colored In^{+} appearing as an intermediate. The $InCl_2$ solutions in the eutectic were colorless. $InCl_3$ in the eutectic was yellow in color. The spectra of $InCl_2$ in the eutectic were obtained from the Hg 4047- and 4358-Å lines, while the $InCl_2$ and $InCl_3$ eutectic spectra were obtained from the Cd 6438- and Rb 7947-Å lines.

All samples gave weak two-line spectra, with the higher frequency component the stronger in all cases. The lines were broad and symmetrical, with the width similar to that from melts possessing a number of ion pairs.

Since the spectra are weak, they are undoubtedly incomplete, but some statements about the species and structures may still be made. The symmetric stretching mode, the ν_1 line, is usually the most intense Raman line. For the pure melt of $InCl_2$, the strong line at 317 K is very close in position to the ν_1 line of the tetrachloroindate ion at 321 K. The weaker line at 110 K is broad and could include the ν_2 and ν_4 lines of the tetrachloroindate species at 89 and 112 K, respectively. The remaining line of the tetrachloroindate species is much weaker and would probably not appear in our weak spectra. The similarity of the spectrum of the pure melt with the spectrum of the ether extract of $InCl_3$ in aqueous HCl indicates that similar species are present, *viz.*, that $In(InCl_4)$ is the principal species in the melt. The observed spectrum of $InCl_2$ is weaker than the spectrum of $GaCl_2$[20] where the full tetrahedral spectrum is obtained. This is because the higher equivalent conductance of the $InCl_2$ melt causes the lines of the spectrum to appear broader and weaker.

When the chloride concentration is increased by placing $InCl_2$ in a eutectic, the ν_1 line shifts to lower frequency. We interpret this shift to be the result of a change in coordination, because an increase in coordination usually results in a shift of ν_1 to lower frequency. Thus the decrease in frequency of the ν_1 line in our experiments is indicative of the formation of $InCl_5^{2-}$ and possibly $InCl_6^{3-}$.

The $InCl_3$ in the chloride eutectic shows a further lowering in the ν_1 frequency closer to the value of 277 K for $InCl_6^{3-}$. Its spectra can be compared with that of $InCl_3$ in aqueous HCl. The close comparison of the spectra, in addition to the width of the lines, indicates that $InCl_6^{3-}$ and $InCl_5^{2-}$ are the predominant species present in the $InCl_3$ eutectic.

Acknowledgments. We thank Professor E. R. Lippincott for the use of the Joyce densitometer and also Dr. J. B. Hunt for many helpful discussions. In addition, we appreciate the financial support provided by the Naval Ordnance Laboratory, White Oak, Md.

Water Adsorption and Dielectric Properties of Lyophilized Hemoglobin

by G. Brausse, A. Mayer, T. Nedetzka, P. Schlecht, and H. Vogel

Physik-Department der Technischen Hochschule München, Germany

Accepted and Transmitted by The Faraday Society (October 13, 1967)

The adsorption of water on lyophilized horse hemoglobin and the dielectric properties have been investigated simultaneously up to a hydration degree of $h = 0.352$ g of H_2O/g of protein. Critical hydration values of $h_c = 0.12$ and 0.165 g of H_2O/g of protein were found. The first BET monolayer was calculated to be complete at $h_m = 0.0576$ g of H_2O/g of protein. This quantity appears to be correlated to the hydration value $h = 0.0695$ g of H_2O/g of protein of monomolecular adsorption on polar sites. From the ratio of these two quantities, the percentage of polar groups of the hemoglobin molecule available for hydration is estimated to be 0.83%. The dielectric dispersion of lyophilized hemoglobin is compared with that of dilute aqueous hemoglobin solution. Possible polarization mechanisms are discussed.

Introduction

The phenomenon that the physical and chemical properties of proteins strongly depend on the degree of hydration has been experienced in a variety of experiments. The characteristic feature of this behavior is the existence of a critical hydration value. Above and below that value different physical or chemical conditions appear to prevail. It was recognized that this critical hydration value, h_c, must correspond to a characteristic stage in the hydration process of the protein molecule.

The adsorption of water on various lyophilized proteins has been studied by Bull,[1] Shaw,[2] Pauling,[3] and more recently for the case of hemoglobin by Cardew and Eley.[4] It was recognized that the shape of the adsorption isotherms of proteins can be described (a) for low hydration degrees in terms of the BET theory of Brunauer, Emmett, and Teller[5] and (b) for high hydrations in terms of the solution theory of Flory.[6] It is generally believed that the first BET monolayer value, h_m, accounts for the first step in the adsorption process. The deviation from linearity of the BET plot above a critical hydration value, h_c, is attributed to the fact that at large water content solution conditions for the protein–water system prevail.[1] Since it was noted that the ratio h_c/h_m was nearly 2 for several proteins, Bull[1] suggested that h_m and $h_c - h_m$ represent the completion of a first and second layer of water molecules between the hydrophilic regions of neighboring protein molecules. This basic concept has initiated investigations on the correlation between the critical hydration and the protein composition and conformation.[7-12]

The electrical properties of hydrated proteins have been investigated by Bailey,[13] Spivey and Taylor,[14] Rosenberg,[15] Rosen,[11] Maračić, Pivat, and Pravdić,[16] Eley and Leslie,[17] and Takashima and Schwan.[18] The drastic increase of the electric conductance as well as of the permittivity of proteins at a certain critical hydration has been attributed to changes in the conduction and the polarization mechanisms, respectively.

The purpose of this work was to establish the critical hydration of hemoglobin by the simultaneous investigation of the sorption process and the determination of the dielectric parameters.

Experimental Section

Hemoglobin was prepared from horse blood. The red cells were separated, were washed several times with a 0.9% NaCl solution, and were hemolized by distilled water, and the stroma was removed. The hemoglobin solution then was dialyzed against distilled water at 4° for about 24 hr in order to remove electrolytes. The concentrated hemoglobin solution then was freeze dried by the following procedure: 50 ml of a concentrated

(1) H. B. Bull, *J. Amer. Chem. Soc.*, **66**, 1499 (1944).

(2) T. M. Shaw, *J. Chem. Phys.*, **12**, 391 (1944).

(3) L. Pauling, *J. Amer. Chem. Soc.*, **67**, 555 (1945).

(4) M. H. Cardew and D. D. Eley, "Fundamental Aspects of the Dehydration of Foodstuffs," The Chemical Society, London, 1958.

(5) S. Brunauer, P. H. Emmett, and E. Teller, *J. Amer. Chem. Soc.*, **60**, 309 (1938).

(6) P. J. Flory, *J. Chem. Phys.*, **10**, 51 (1942).

(7) O. L. Sponsler, J. D. Bath, and J. W. Ellis, *J. Phys. Chem.*, **44**, 996 (1940).

(8) R. W. Green, *Trans. Roy. Soc. New Zealand*, **77**, 313 (1949).

(9) S. R. Hoover and E. F. Mellon, *J. Amer. Chem. Soc.*, **72**, 2562 (1950).

(10) A. D. McLaren and J. W. Rowen, *J. Polym. Sci.*, **7**, 289 (1951).

(11) D. Rosen, *Trans. Faraday Soc.*, **59**, 2178 (1963).

(12) H. F. Fischer, *Biochim. Biophys. Acta*, **109**, 544 (1965).

(13) S. T. Bailey, *Trans. Faraday Soc.*, **47**, 509 (1951).

(14) D. I. Spivey and C. P. S. Taylor, *Discussions Faraday Soc.*, **27**, 239 (1959).

(15) B. Rosenberg, *J. Chem. Phys.*, **36**, 816 (1962).

(16) S. Maračić, G. Pivat, and V. Pravdić, *Biochem. Biophys. Acta*, **79**, 293 (1964).

(17) D. D. Eley and R. B. Leslie, *Advan. Chem. Phys.*, **7**, 238 (1964).

(18) S. Takashima and H. P. Schwan, *J. Phys. Chem.*, **69**, 4176 (1965).

horse blood solution was poured into a 1-l. spherical flask and was frozen in a thin layer over the whole inner surface. The flask was evacuated to 0.1 torr by a vacuum pump *via* a cold trap, which was cooled by an acetone–Dry Ice mixture to −70°. The water content of the lyophilized hemoglobin was *ca.* 5%. The absolute dry state of a protein is somewhat difficult to define. Generally, the approach to a constant value after a procedure of drying under vacuum or heating, up to about 100°, during a period of time is taken as a standard of dryness.[1,4,11,15,19] Procedures of drying at 0.1 torr and 23° and heating at 120° in air gave similar results. The error of such a standard is, however, that one does not know how much water in spite of drying remains bound and how much material is lost during heating by exhaust. The best procedure appeared to be heating under vacuum at 105°. The portion of methemoglobin was determined spectrophotometrically in the range 500–700 mμ of the absorption spectrum. Freshly lyophilized hemoglobin contained 60% met- and 40% oxyhemoglobin. With increasing age and degree of hydration of the material, the portion of methemoglobin increased. After a period of 5 weeks, about 80% methemoglobin was obtained at a medium degree of hydration. It is advisable to perform future experiments with CO-hemoglobin, which is known to be resistant against the oxidation of Fe and against denaturation. The degree of denaturation of the lyophilized material was determined by dissolving it in distilled water, centrifuging the unsoluble components, and determining their percentage. Freshly lyophilized hemoglobin had a degree of denaturation of about 4–8%. If stored at a cool temperature over P_2O_5, the denaturation does not exceed 10–12% during some months. The progress of denaturation with temperature and the degree of hydration is summarized in Table I. The hemoglobin samples were sealed in tubes over solutions of H_2SO_4 to obtain a predetermined relative water vapor pressure and were stored for a period of time in a thermostat-controlled environment, maintained to within 0.2°.

In order to determine adsorption isotherms, two approaches have been tried. (a) Using a light powder of hemoglobin and applying the weighing-bottle method for different vapor pressures, the adsorption isotherm with just one sample could be determined (Cardew and Eley[4] used different samples for different humidities!). (b) For the dielectric experiments, solid pellets must be used in order to avoid embedded air. Finely powdered hemoglobin was pressed with a continuously increasing pressure up to a maximum of 470 kg/cm² by a hydraulic-pressure tool. During the procedure of pressing, air could be withdrawn by a vacuum pump, so that holes within the pellets were avoided. The pellets had a diameter of 13 mm and a thickness of 1.5–2.5 mm; they had plane and parallel surfaces and smooth borders. Since the pellet is weighed directly, errors due to water adsorption on the weighing bottle thus are avoided. The adsorption isotherms of several samples were determined. Each sample was stored for 1 week over H_2SO_4 solutions. This short period (Cardew and Eley[4] used 7 months!) seems to be satisfying, since from adsorption kinetics it follows that at low relative pressures saturation is adjusted within some hours and at high relative pressures within 2–3 days. The deviation from the actual saturation equilibrium after an adjustment of 1 week proved to be within the error of measurement. In view of the aging and the increasing denaturation of the material (Table I), it appeared more reasonable to keep the time of adjustment in limits at the expense of a definite approach to equilibrium. It was proved that the adsorption isotherms of solid pellets lie only slightly below those of light powders. For the dry pellets, a packing factor, which is defined by the sum of the partial volumes of the hemoglobin molecules per sample volume of nearly 100%, is estimated. The assumed axial ratios of the molecule are 64 × 55 × 50 Å.[20] The density of a dry pellet was calculated to be 1.16 g/cm³, in good agreement with the value of 1.17 g/cm³ suggested by Edsall.[21] Hydrations are defined as the grams of H_2O per gram of protein and have been varied between 0 and 0.352.

The capacitance and the conductance of the hemoglobin pellets were determined with two impedance bridges, one covering the frequency range from 120 cps to 100 kcps, with a reproducibility of 0.01 pF and 0.01 μmho, the other covering the range from 100 kcps to

Table I: Progress of Denaturation with Temperature and the Degree of Hydration

Temp, °C	Time, weeks	Degree of hydration, g of H_2O/g of protein	Degree of denaturation, weight fraction
10.5	0	0	0
	1	0.02	0.10
	5	0.087	0.17
	7	0.128	0.21
	11	0.345	0.30
20.5	0	0	0.08
	2	0.02	0.10
	4	0.06	0.11
	7	0.123	0.29
	11	0.328	0.40
25.0	0	0	0.08
	7	0.124	0.25
	9	0.192	0.44
	11	0.315	0.58

(19) S. W. Benson and D. A. Ellis, *J. Amer. Chem. Soc.*, **72**, 2095 (1950).

(20) A. F. Cullis, H. Muirhead, M. F. Perutz, and M. G. Rossman, *Proc. Roy. Soc.*, **A191**, 83 (1949).

(21) J. T. Edsall, "The Proteins," Vol. 1B, Academic Press Inc., New York, N. Y., 1953.

30 Mcps, with an accuracy of 0.1 pF and 1 μmho. The pellet was situated in a plate condenser of Au or Pt electrodes and was pressed together by the electrodes with a pressure of about 5 kg/cm². The whole electrode arrangement could be isolated from air in order to avoid changes of the water content of the pellet during measurements. The temperature of the cell was controlled by a thermostat. Correction for electrode-polarization effects in the low-frequency range is crucial in order to obtain the true dielectric dispersion. Three methods have been applied to eliminate the nonreproducible electrode polarization at the interface between the electrode and the sample: (a) a correction according to the method of Schwan,[22] (b) the comparison of two equivalent samples of different thickness, and (c) the measurement with isolating electrodes (an isolating foil (0.1 mm thick Teflon) between the electrode and the sample completely prevents an exchange of charge carriers).

Results

(*a*) *Sorption Data.* The adsorption isotherms of lyophilized hemoglobin for different temperatures are shown in Figure 1, where the degree of hydration, expressed as per cent regain, is plotted *vs.* the water vapor pressure. For comparison, the data of Cardew and Eley are included. The errors of the data are less than 1%. In Figure 2 the isotherms have been replotted in terms of the BET equation

$$\frac{p/p_0}{h[1 - (p/p_0)]} = \frac{1}{h_m C} + \frac{C - 1}{h_m C}\frac{p}{p_0}$$

which is known to describe the adsorption of water in many cases over a range of 0.05–0.5 of relative water vapor pressure. In the above equation, h_m is the quantity of adsorbed water corresponding to the first BET monolayer and C is a constant related to the heat of adsorption. From this plot, h_m and C can be obtained from the slope and intercept. Table II shows the values of h_m for different temperatures. That our values differ from the values obtained by Cardew and Eley[4] results from the fact that our values are based on the adsorption isotherms, whereas Cardew and Eley[4] calculated h_m from a smoothed curve. They may, however, also result from the different degree of denaturation. Deviations from a straight line occur at about $p/p_0 = 0.5$. Our data indicate a dependence of the critical limits of the BET equation on temperature; *i.e.*, with increasing temperature, the deviations from linearity occur at lower partial vapor pressure. The hysteresis phenomenon of adsorption and desorption isotherms is shown for two different temperatures in Figure 3. The maximum value of the hysteresis at $p/p_0 = 0.5$ is about 0.02–0.03. With increasing hydration there is a small increase in the volume of the hemoglobin pellet, as shown in Figure 4. It is, however, remarkable that this dependence does not follow a straight line but has a kink at about $h = 0.12$.

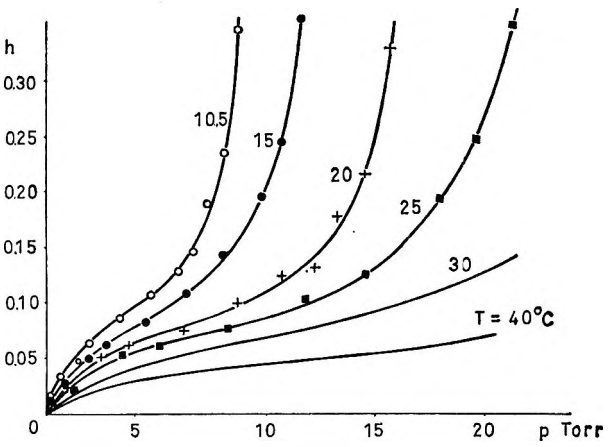

Figure 1. Adsorption isotherms of lyophilized hemoglobin at different temperatures. The degree of hydration is plotted *vs.* the water vapor pressure. The data of Cardew and Eley[4] (30 and 40°) are included.

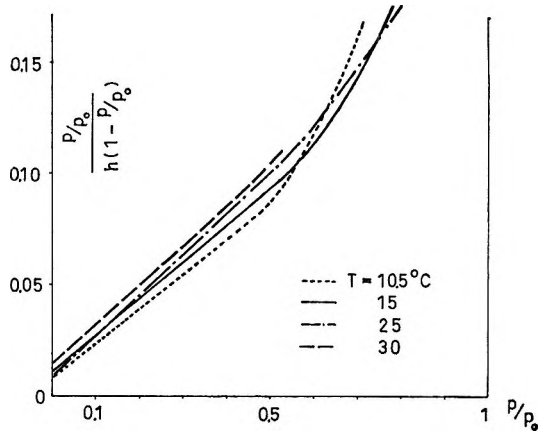

Figure 2. The BET plot of the adsorption isotherms of lyophilized hemoglobin (p/p_0 is the relative water vapor pressure).

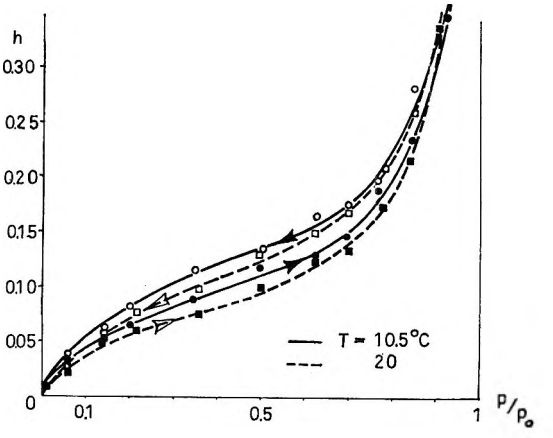

Figure 3. Hysteresis of the adsorption and desorption isotherms of lyophilized hemoglobin.

(22) H. P. Schwan, *Biophysik*, **3**, 181 (1966).

Table II: First BET Monolayer Values, h_m, at Different Temperatures

Temp, °C	h_m, g of water/ g of protein	Ref
10.5	0.0625	This work
15.0	0.0576	This work
25.0	0.0530	This work
30	0.0576	4
40	0.0572	4

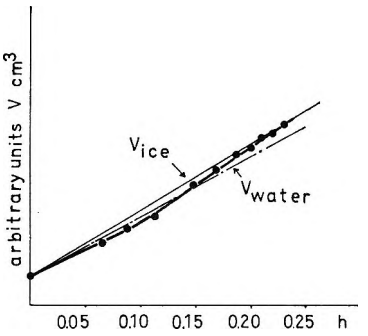

Figure 4. The volume of lyophilized hemoglobin plotted *vs.* the degree of hydration.

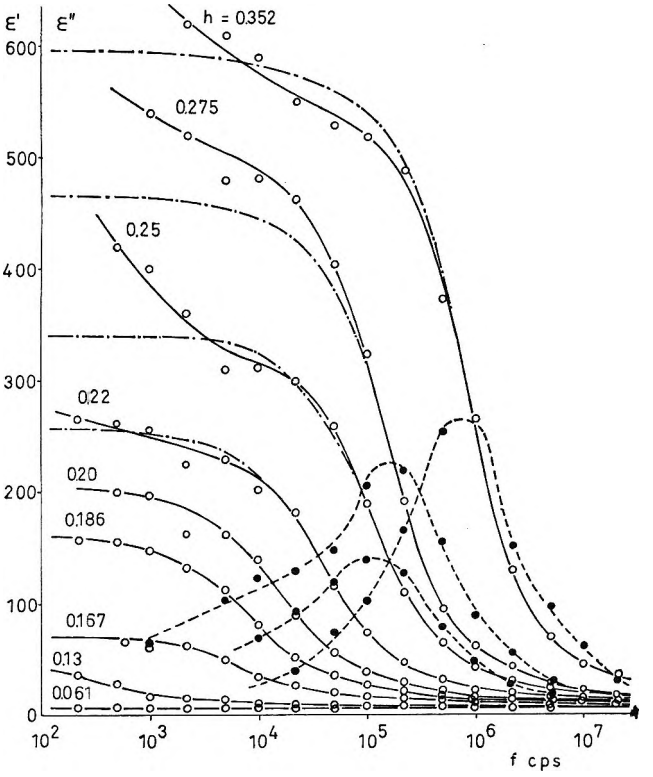

Figure 5. Dielectric dispersion of lyophilized hemoglobin at various hydration degrees. The real and imaginary parts of the complex dielectric constant $\epsilon = \epsilon' - i\epsilon''$ are plotted *vs.* the frequency of the electric field.

(*b*) *Dielectric Data.* Lyophilized hemoglobin exhibits a dielectric dispersion in the frequency range from 1 kc to 10 Mcps which strongly depends on the degree of hydration of the protein, Figure 5. At a constant temperature the dispersion stage is increased with increasing hydration and the corresponding relaxation frequencies are shifted toward higher frequencies. The dependence of the dielectric increment on the degree of hydration indicates the following behavior. A slow increase of the increment up to about $h = 0.165$ is fol-

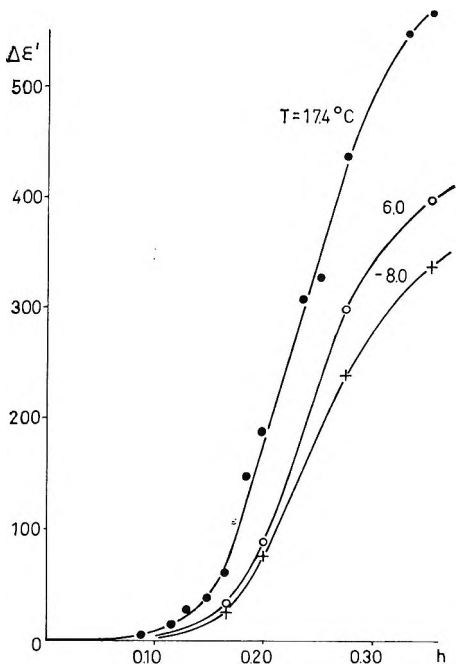

Figure 6. The dependence of the dielectric increment on the degree of hydration at different temperatures.

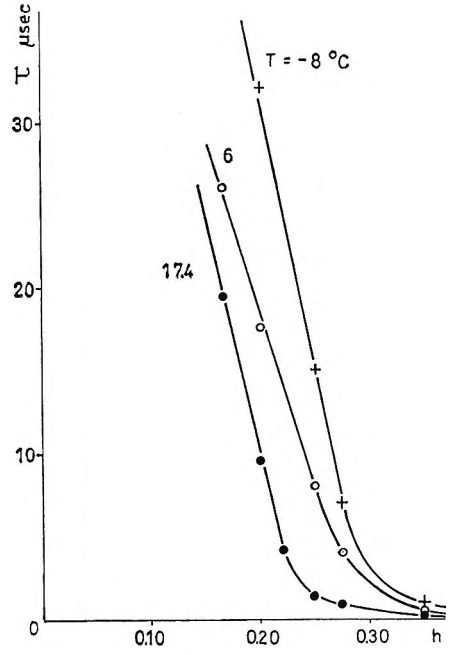

Figure 7. The dependence of the relaxation time on the degree of hydration at different temperatures.

lowed by a steep increase in the region h = 0.165–0.27, while above h = 0.27 the curve levels off, Figure 6. The relaxation time, τ, of the dispersion falls off with increasing hydration nearly exponentially and levels out at a hydration value, h, of about 0.25–0.30, Figure 7. The Cole–Cole parameter α is not zero; *i.e.*, not a single relaxation time but a distribution of relaxation times controls the dispersion mechanism. The Cole–Cole parameter, α, was found to decrease with an increase in the degree of hydration. Two typical Cole–Cole plots are shown in Figure 8. The dielectric dispersion exhibits a pronounced temperature dependence. With increasing temperature the dielectric increment increases while the relaxation time decreases (Figures 6 and 7). From the plot of ln τ *vs.* $1/T$ an activation energy, E_a, for the dispersion of about 0.22 ± 0.06 eV can be estimated. This value was calculated for degrees of hydration between h = 0.168 and 0.352. A significant trend of the activation energy within this hydration range was not observed. Denaturation of the protein reduces the dielectric increment considerably (Figure 9).

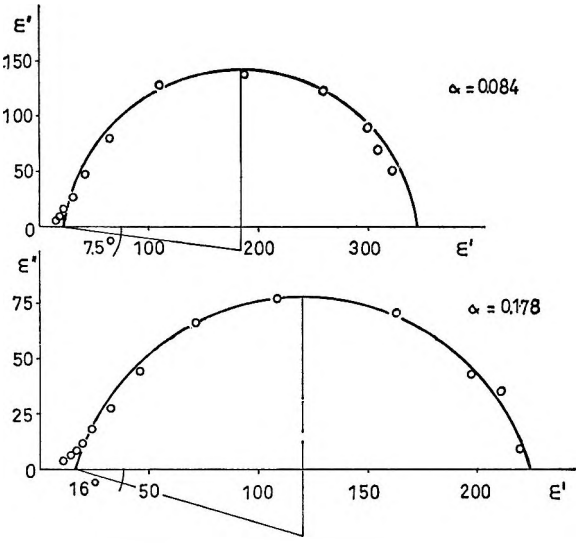

Figure 8. A Cole–Cole plot: (a) h = 0.253, T = 17.4°, α = 0.084; (b) h = 0.220, T = 17.4°, α = 0.178.

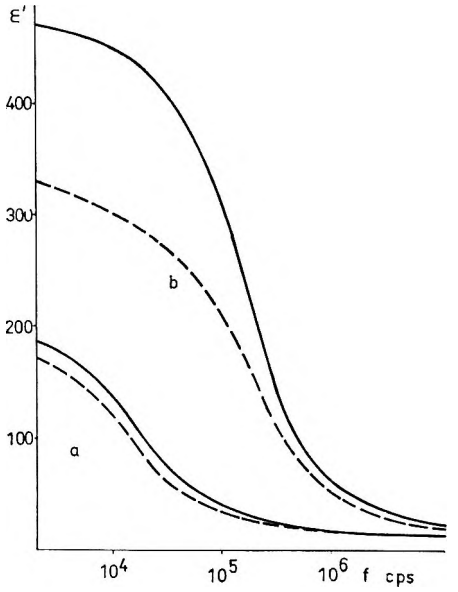

Figure 9. Dielectric dispersion of lyophilized hemoglobin at different degrees of denaturation: —, 20%; – – –, 90%; (a) h = 0.20; (b) h = 0.275.

Discussion

For lyophilized hemoglobin, critical hydration values, h_c, observed from the dependence of various physical properties on the degree of hydration are summarized in Table III. For comparison, estimated hydration values of hemoglobin in aqueous solution are included.

Table III: Observed Critical Hydration Values

Expt	h_c, g of H_2O/ g of protein	Ref
(a) Lyophilized Hemoglobin		
Adsorption isotherms	0.12	This work
Dielectric dispersion (100-kcps range)	0.165	This work
Conductivity	0.18	16
(b) Aqueous Hemoglobin Solution		
Dielectric dispersion (100-Mcps range)	0.30 ± 0.10	*a*
Dielectric dispersion (10-Gcps range)	0.24	*b*

[a] H. P. Schwan, *Ann. N. Y. Acad. Sci.*, **125**, 344 (1965). [b] B. P. Schoenborn, R. M. Featherstone, P. O. Vogelhut, and C. Süsskind, *Nature*, **202**, 695 (1964).

The adsorption isotherms indicate a critical hydration, h_c, at approximately 0.12. Above that value, solution conditions appear to prevail. The volume change of the lyophilized hemoglobin during water adsorption increases less in the range up to about h = 0.12; however, they increase more steeply in the range h = 0.12 to 0.24 than would be expected if this change were merely due to the added amount of liquid water or ice. In a completely (artificial) dry state, the protein presumably has a conformation different from that of a native fully hydrated state, as the hydration shell is considered to be (in addition to the hydrophobic interactions of the peptide chain) the skeleton of the tertiary structure of the protein. An argument for this conception is, for example, the strong hydration dependence of the magnetic susceptibility of hemoglobin observed by Havemann and Haberditzl.[23] As the electronic state of Fe is believed to be determined by the protein conformation

(23) R. Havemann and W. Haberditzl, *Z. Physik. Chem.* (Leipzig), **210**, 267 (1959).

and *vice versa*,[24] a change in the Fe state implies a change in the tertiary structure pertinent to a change in the degree of hydration. A volume change as observed is then expected to be made up of three processes: (a) diffusion of water molecules into the sample and hydration on specific sites, (b) increased reconstitution of the quasi-denatured protein molecules to hydrated native ones, and (c) dissolving of the hydrated protein molecules in more or less liquid water.

In the view of such a hypothesis, a plausible explanation for the phenomenon of the adsorption–desorption hysteresis may also be given. Two processes could be involved: (a) at low hydrations and (b) at high hydrations. (a) After the procedure of freeze and heat drying, the hemoglobin molecules are quasi-denatured, and a number of hydrophilic groups are buried within the polypeptide chains and might be not accessible to hydration. Upon increasing hydration, the protein molecules reconstitute themselves in the native conformation where the far larger number of hydrophilic groups is situated on the surface of the macromolecule. If now desorption takes place, a hysteresis should occur, as the mild procedure of lowering the water vapor pressure will not influence the protein conformation; *i.e.*, the desorption isotherms must lie above the adsorption isotherms. (b) Upon proceeding to high humidities, *i.e.*, to solution conditions, mutual orientation of the protein molecules will be possible and exactly in such a way as to facilitate the formation of H bridges so that upon desorption for energetical reasons a hydration as high as possible will maintain. Different explanations for the hysteresis have been given by Seehof, Keilin, and Benson[25] and Eley and Leslie.[17]

For several proteins a similar characteristic dependence of the dielectric increment on the degree of hydration has been observed. While Rosen[11] found for bovine serum albumin and whale myoglobin critical hydrations of $h_c = 0.246$ and 0.235, respectively, we found for horse hemoglobin $h_c = 0.165$ and Takashima and Schwan[18] found for ovalbumin $h_c = 0.10$. These different critical hydrations may be due to the specific protein composition and conformation. The enormous discrepancy between the absolute values of the dielectric increments of the hydrated proteins is amazing. While Rosen[11] obtained dielectric increments of the magnitude of 1–10, Takashima and Schwan[18] found at same degrees of hydration a value of 200, and we obtained figures of about 300–600. This discrepancy could be due to the fact that samples of light powder, as used by Rosen[11] and Takashima and Schwan,[18] contain a larger amount of embedded air capacitance, which falsifies the true dielectric constant, than do solid pellets that we have used. On the other hand, this discrepancy could also be due to a Maxwell–Wagner effect being more or less present in the samples.

It appears that three polarization mechanisms are mainly involved in the performance of the observed dielectric dispersion, namely the Maxwell–Wagner effect and the orientational polarization of the molecular hemoglobin dipoles and water molecules.

(*a*) *The Maxwell–Wagner Effect.* A Maxwell–Wagner effect of the protein–water system probably accounts for some or all of the dispersion observed. This effect is due to the inhomogeneity of the material, *i.e.*, due to the fact that the protein–water system consists of non- or semiconducting protein molecules, of conducting hydration layers enveloping the macromolecule, and (at higher degrees of hydration) of more or less "free" bulk conducting water between adjacent hydrated protein molecules. Wagner[26] and Miles and Robertson[27] have treated the case of a nonconducting sphere surrounded by a thin concentric conducting shell embedded in a nonconducting medium and have derived the following relation for the relaxation time, τ, of the dielectric polarization

$$\tau = \frac{3\epsilon_1\epsilon_0 a}{2\lambda d}$$

where a is the radius of the sphere, d is the thickness of the shell, λ is the conductivity of the shell, ϵ_1 is the dielectric constant of the sphere, $\epsilon_3 = \epsilon_1$ and is the dielectric constant of the outer medium, and ϵ_0 is the dielectric constant in a vacuum. If applied to our problem, the range of validity of this relation must be limited to low degrees of hydration in order to fulfill the requirement of $\epsilon_3 = \epsilon_1$. Taking reasonable figures for the parameters, $d = 3 \times 10^{-8}$ cm, $a = 30 \times 10^{-8}$ cm, $\lambda \approx 10^{-8}$ ohm^{-1} cm^{-1}, and $\epsilon_1 \approx 4$, a relaxation time of the order of 10^{-3} to 10^{-4} sec is estimated, which is in good agreement with the observed order of relaxation times at low degrees of hydration (Figure 5). The parameters a, d, and λ will, in general, depend upon the degree of hydration, and in particular, λ will depend upon the temperature. A spread of relaxation times at a given temperature and hydration as expressed by a nonvanishing Cole–Cole parameter must then be due to a spread of the parameters a, d, and λ, *i.e.*, due to an inhomogenously hydrated material. With increasing hydration, when all hemoglobin molecules of the sample have completed their hydration shell, the spread of relaxation times is expected to decrease, owing to the increasing homogenity of the material. The observed dependence of the Cole–Cole parameter of the hemoglobin hydration (Figure 8) might thus be interpreted. The alternating current and direct current conductivities of proteins exhibit a typical dependence on hydration.[11,28] The ac conductivity of hydrated hemoglobin

(24) R. Lumry, *Japan. J. Phys.*, 1, 2 (1961).

(25) J. M. Seehof, B. Keilin, and S. W. Benson, *J. Amer. Chem. Soc.*, 75, 2428 (1953).

(26) K. W. Wagner, *Ann. Phys.*, 40, 817 (1913); *Arch. Elektrotech.*, 2, 371 (1914).

(27) J. B. Miles and H. P. Robertson, *Phys. Rev.*, 40, 583 (1932).

(28) D. D. Eley and D. I. Spivey, *Nature*, 26, 725 (1960).

increases rapidly above a critical hydration of $h = 0.18$, whereas the dc conductivity levels out to a saturation value at a critical hydration of $h = 0.12$. This behavior indicates that different conduction mechanisms appear to prevail below and above a critical hydration degree. It has been suggested[16,28] that at low hydration the dc conduction is due to an electronic intrinsic or an impurity mechanism, while at higher coverages of adsorbed water an H-bonded network of water is built up and a dc proton conductivity is expected to set in along lines proposed by Riehl.[29] It appears plausible to assume that an ac proton conduction mechanism is responsible for the observed increase of the ac conductivity. The hydration dependence of the ac conductivity of hemoglobin is reflected in that of the dielectric polarization, for which a critical hydration of $h = 0.165$ has been observed. For a Maxwell–Wagner polarization, one would expect that (a) with increasing hydration the Maxwell–Wagner polarization should approach a maximum and decrease again, owing to the decrease of the protein concentration (Figure 6 indeed indicates some sort of saturation behavior above $h \approx 0.3$), and (b) with decreasing temperature the Maxwell–Wagner polarization should decrease and the relaxation time should increase, since the protonic conductivity is known to decrease with decreasing temperature.[28] Such a behavior was also observed (Figures 6 and 7).

(*b*) *Hindered Dipole Orientation of the Macromolecule.* The dielectric dispersion of aqueous protein solutions is believed to be due to an orientational polarization of the permanent or quasi-permanent dipole moment of the macromolecule.[30] At a sufficient high water content this mechanism should, therefore, be possible also for lyophilized hydrated protein and should contribute to the observed dielectric polarization. The hydration shell of hemoglobin is complete at about $h \approx 0.24$.[31,32] Above this value the relaxation time of hydrated hemoglobin approaches the relaxation time of aqueous solution. This concept is supported by the following observations. (a) The relaxation time levels out with increasing hydration near $h = 0.3$ to an asymptotical value of about 10^{-6} sec (Figure 7). The same order of magnitude is found for the relaxation time in diluted aqueous hemoglobin solutions.[30b] The dependence of the relaxation time on hydration (Figure 7) could be due in part to a hydration-dependent microscopic viscosity of the water which is known to determine also the relaxation time of aqueous hemoglobin solutions.[30b] (b) The activation energy derived from the temperature dependence of the dielectric dispersion of both lyophilized hemoglobin (0.22 ± 0.06 eV in the range $0.17 < h < 0.35$) and aqueous hemoglobin solution (0.20 ± 0.02 eV) are within error the same as the activation energy of the viscosity of water (0.22 eV).

(*c*) *Polarization of the Water Molecules.* Rosen[11] has suggested that the drastic increase of the permittivity at a critical hydration was pertinent to different polarization mechanisms of the adsorbed water molecules. At low hydrations the water molecules forming the first tightly bound hydration layer on the protein contribute by their electronic and molecular polarizability, whereas at higher hydrations the more loosely bound water molecules contribute by dipolar orientation. An extension of this conception is suggested by the striking fact that pure ice exhibits a dielectric dispersion in about the same frequency range, namely, 1–10 kcps,[33,34] as hydrated proteins at low degrees of hydration. The ice dispersion has been attributed to polarization by molecular reorientation of water molecules brought about by lattice imperfections.[35,36] Owing to the possibility of proton jumps, these imperfections easily can move within the lattice of ice.[29] If the protein hydration is considered to resemble a disturbed ice structure, the concentration of lattice imperfections is expected to be increased largely and might compensate the smaller volume concentration of icelike water in the hydrated material. The activation energy of the dispersion of single-crystal ice (13.5 kcal/mol[29]) is somewhat different from that of hydrated hemoglobin (5 kcal/mol); however, the activation energy for a molecular-reorientation mechanism might well be considerably smaller in the disturbed ice structure of the protein hydration than in a single-crystal structure of ice.

The common way of analysis was followed and the expected hydration values calculated on the basis of the hemoglobin composition were compared with the experimentally obtained critical hydration values. The hydration of (a) monomolecular adsorption on polar sites (ionic and nonionic: arg, his, lys, asp, glu, cys, met, ser, thr, tyr, and try), (b) multimolecular adsorption on specified sites with certain coordination numbers, as suggested by Sponsler, Bath, and Ellis[7] (OH (3): ser, tyr, and hypro; COOH (4): asp and glu; NH_2 (3): lys; =NH (2): arg, his, and try; =N (1): his), and (c) a monolayer of water covering the whole surface of the hemoglobin molecule are summarized in Table IV. The mean value of the first BET monolayer, h_m, is remarkably close to the hydration values calculated for monomolecular adsorption on polar sites. This underlines the fact that these two quantities are

(29) N. Riehl, *Zh. Fiz. Khim.*, **29**, 1372 (1955).

(30)(a) J. L. Oncley, *Chem. Rev.*, **30**, 433 (1942); (b) W. Goebel and H. Vogel, *Z. Naturforsch.*, **19b**, 292 (1964).

(31) H. P. Schwan, *Ann. N. Y. Acad. Sci.*, **125**, 344 (1965).

(32) B. P. Schoenborn, R. M. Featherstone, P. O. Vogelhut, and C. Süsskind, *Nature*, **202**, 695 (1964).

(33) P. Wintsch, *Helv. Phys. Acta*, **5**, 126 (1932).

(34) R. P. Auty and R. H. Cole, *J. Chem. Phys.*, **20**, 1309 (1952).

(35) N. Bjerrum, *Kgl. Danske Videnskab. Selskab, Mat. Fys. Medd.*, **27**, 1 (1951).

(36) J. A. Schellmann and W. Kauzmann, *Phys. Rev.*, **82**, 325 (1951).

meaningfully related. It is known from the X-ray diffraction data of Perutz[37,38] that nearly all the polar groups of the hemoglobin molecule are situated on the surface. At least those polar groups which establish contact between the four subunits and also the four proximal histidines will not be available for hydration. This percentage is estimated from the data of Perutz[37] to be about 0.12–0.155%. From the adsorption data, an independent way for determination of this percentage is possible. If it is assumed that one polar site can bind one molecule water during the first step of the adsorption process, the percentage of polar sites lying on the surface and accessible to hydration can be estimated from the ratio of the first BET monolayer value to the monomolecular adsorption value. From our data a ratio of about 0.83 is obtained, *i.e.*, about 0.17 of the total number of polar sites are hidden within the hemoglobin molecule. The calculated hydration values, assuming either a monolayer of water or multimolecular adsorption on specified sites, are considerably larger than the experimentally observed critical hydration values of lyophilized hemoglobin; however, those calculated values agree with the hydration values observed for aqueous hemoglobin solutions[31,32] and with the degrees of hydration where both in the water adsorption and in the dielectric dispersion solution conditions are approached.

Table IV: Calculated Hydration Values

	h, g of H_2O/g of protein
Monomolecular adsorption on polar sites	0.0695
Multimolecular adsorption on specified sites	0.24
Monolayer on a spheroid (64 × 55 × 50 Å)	0.29
First BET monolayer (at 15°)	0.0576
Estimation of Fisher[12]	0.25

Acknowledgment. We wish to thank Professor N. Riehl and Dr. H. Engelhardt for valuable discussions. This work was supported by a grant from the Stiftung Volkswagenwerk.

(37) M. F. Perutz, *J. Mol. Biol.*, **13**, 646 (1965).

(38) M. F. Perutz, J. C. Kendrew and H. C. Watson, *ibid.*, **13**, 669 (1965).

The Photolysis of Carbon Suboxide in the Presence of Hydrogen

by Alain Forchioni

Centre d'Etudes Nucléaires de Saclay, Gif-sur-Yvette, Essonne, France

and Clive Willis

Research Chemistry Branch, Atomic Energy of Canada Limited, Chalk River, Ontario, Canada

Accepted and Transmitted by The Faraday Society (October 13, 1967)

Carbon suboxide has been photolyzed in the presence of hydrogen at 2537, 1470, and 1236 Å. At all wavelengths virtually identical results are obtained and the gaseous products formed are carbon monoxide, methane, and ethane with traces of propane. A mechanism involving methylene is proposed to explain the results. The relative rate constant for the reaction of ^1C_2O with carbon suboxide compared with hydrogen was found to be 160 ± 30. The possibilities for the primary species and subsequent reactions are discussed.

Introduction

The photolysis of carbon suboxide in the presence of hydrogen has been studied at wavelengths above and below 2000 Å, as the reactions occurring may be of importance in reactor chemistry, radiation chemistry, and upper-atmosphere chemistry. The photolysis of carbon suboxide in the presence of olefins, (C_nH_{2n}), has been fairly extensively studied,[1-6] and it is now generally accepted that above 2000 Å photolysis of

(1) K. D. Bayes, *J. Amer. Chem. Soc.*, **83**, 3412 (1961).

(2) K. D. Bayes, *ibid.*, **85**, 1730 (1963).

(3) C. Willis and K. D. Bayes, *ibid.*, **88**, 3203 (1966).

(4) R. T. K. Baker, J. A. Kerr, and A. F. Trotman-Dickenson, *J. Chem. Soc., A*, 975 (1966).

carbon suboxide leads to the production of the molecule C_2O, which subsequently reacts with the olefin. The major product of this reaction is $C_{n+1}H_{2n}$, which is measured as a mixture of the allene and acetylene isomers.

In the present paper the reactions of C_2O with hydrogen are discussed. The final products of the reactions are methane, ethane, and propane, and it is proposed that these are due to the intermediate formation of methylene, CH_2, and its subsequent reactions with hydrogen.

Photolyzing light of a wavelength below 2000 Å is energetically capable of giving a carbon atom from a carbon suboxide molecule in a single-photon process. The results we have obtained for this wavelength region are essentially identical with those for the longer wavelength region where only C_2O can be formed. However, we are unable to differentiate between a carbon atom and a C_2O molecule on kinetic grounds.

Experimental Section

Carbon suboxide was prepared by dehydration of malonic acid with phosphorus pentoxide at 40–50° followed by successive vacuum distillations to yield a product with a purity of 99.95%. The hydrogen used was ultrapure U grade (99.998% or better) obtained from Air Liquide Co. The methods of analysis used in the present experiments showed no hydrocarbon impurity in this hydrogen.

Gaseous products were identified and measured by gas chromatography, the hydrocarbons with a hydrogen flame ionization detector and the carbon monoxide by a hot-wire thermal-conductivity detector. Quantitative calibration of the analysis technique was determined with synthetic samples. No attempt was made to measure the yield of the carbon suboxide polymer.

Photolyses at 2537 Å were carried out in a quartz cell using a helical, low-pressure mercury arc which gave a uniform radial intensity within the helix. The cylindrical photolysis cell was placed at the center of the helical arc and small variations in the positioning of the cell did not significantly affect the incident intensity. A very thin Pyrex filter was used to eliminate 1849-Å radiation and to attenuate the 2537-Å radiation. No intensity effects on product ratios were observed.

For 1470 and 1236 Å, xenon and krypton resonance lamps, of the type described by Okabe,[7] were used. The lamps were equipped with lithium fluoride windows and were excited by a microwave generator. The photolysis cells used at these wavelengths were short Pyrex tubes of the same diameter as the lamps, equipped with a lithium fluoride front window. The windows were sealed to the cell and lamp with either black wax or epoxy resin. For a photolysis run the windows of the cell and the lamp were butted against each other in a fixed position.

Mercury-free gas systems were used throughout the studies and no evidence was found for any mercury-sensitized reactions occurring.

Results

Photolysis at 2537 Å. The observed products from the photolysis of carbon suboxide in the presence of hydrogen at 2537 Å were carbon monoxide, methane, ethane, propane, and the carbon suboxide polymer. Other hydrocarbons, if produced, were below the limits of detection of the analytical techniques used. During a photolysis run, the yellow-brown carbon suboxide polymer coated out on the wall of the cell. This polymer was removed after each run by filling the cell with an atmosphere of oxygen and flaming to red heat.

The yields of gaseous products are given in Table I. Some yields obtained from the photolysis of 30 torr of carbon suboxide in the presence of 600 torr of hydrogen are plotted as a function of photolysis time in Figure 1. The falloff in the rate of production of gaseous products with time is due both to the consumption of carbon suboxide and to the change of light transmission of the quartz cell due to the polymer deposition.

Photolysis at 1470 and 1236 Å. The products observed from photolysis at these wavelengths were carbon monoxide, ethane, methane, and carbon suboxide polymer. Carbon suboxide has a very high extinction coefficient at these wavelengths[8] and photolysis occurred only in the first few millimeters of the gas mixture. This led to a very rapid deposition of polymer on the lithium fluoride windows and eliminated further photolysis, so that only low conversions were possible. The yields of gaseous products are given in Table II. Prolonged exposure of the gas mixture in the cell after the first few minutes led to no further products, even though the windows were not opaque to radiation above 2000 Å. This indicates that any radiation emitted by the rare gas resonance lamps above this wavelength did not contribute significantly to the results obtained.

Discussion

Photolysis at 2537 Å. Initially photolysis of carbon suboxide with 2537-Å radiation gives a C_2O molecule. Theoretical considerations of the molecular orbitals for C_2O predict a $^3\Sigma$ ground state with low-lying $^1\Delta$ and $^1\Sigma$ excited states.[2] Photolysis of carbon suboxide[3] at 3000 Å appears to give uniquely the triplet state of C_2O. At shorter wavelengths, a species of different reactivity is formed which is presumably C_2O in a singlet electronic state. At wavelengths in the region

(5) R. B. Cundall, A. S. Davies, and T. F. Palmer, *J. Phys. Chem.*, **70**, 2503 (1966).

(6) C. Devillers, *Compt. Rend.*, **262c**, 1485 (1966).

(7) J. Okaba, *J. Opt. Soc. Amer.*, **54**, 478 (1964).

(8) M. M. Kim and J. L. Roebber, *J. Chem. Phys.*, **44**, 1709 (1966).

Table 1: Photolysis Yields at 2537 Å[a]

Sample photolyzed	Photolysis time, sec	Yields, torr				
		CO	CH_4	C_2H_6	C_3H_8	$\Sigma n[C_nH_{2n+2}]$
30 torr of C_3O_2,	10	1.3	...	0.03	...	0.06
600 torr of H_2	15	2.1	...	0.05	...	0.10
	20	2.8	...	0.07	...	0.14
	30	4.0	...	0.11	...	0.23
	30	5.4	...	0.14	...	0.28
	30	5.0	...	0.13	...	0.26
	30[b]	19.8	0.041	0.50	0.02	1.10
	30[b]	21.5	0.030	0.53	0.03	1.18
	60	10.5	0.005	0.27	...	0.54
	60	8.05	0.014	0.20	...	0.41
	60	10.0	0.020	0.25	0.005	0.53
	60[c]	29.2	0.074	0.80	0.04	1.79
	105	17.0	0.020	0.45	0.005	0.93
	120	19.7	0.023	0.47	0.01	0.99
	180	21.3	0.032	0.53	0.01	1.11
	210	28.0	0.020	0.75	0.02	1.58
	240	26.7	0.046	0.67	0.02	1.45
	300	27.8	0.053	0.70	...	1.45
	420	32.0	0.069	0.82	0.02	1.79
	510	33.8	0.078	0.91	0.03	2.00
	570	37.0	0.110	1.14	0.05	2.52
	720	37.5	0.105	1.19	0.05	2.78
3 torr of C_3O_2,	100	1.6	...	0.10	0.005	0.22
600 torr of H_2	180	2.7	0.018	0.18	0.005	0.39
	200	3.3	0.020	0.25	0.01	0.55
	240	4.0	0.030	0.28	0.02	0.65
	300	4.3	0.060	0.36	0.03	0.88
	510	4.7	0.21	0.39	0.05	1.13

[a] All photolyses were carried out using a thin Pyrex filter which reduced the 2537-Å intensity and eliminated any 1849-Å radiation. [b] Using a thick Vycor quartz filter instead of the Pyrex filter. [c] Foil neutral density filter instead of the Pyrex filter.

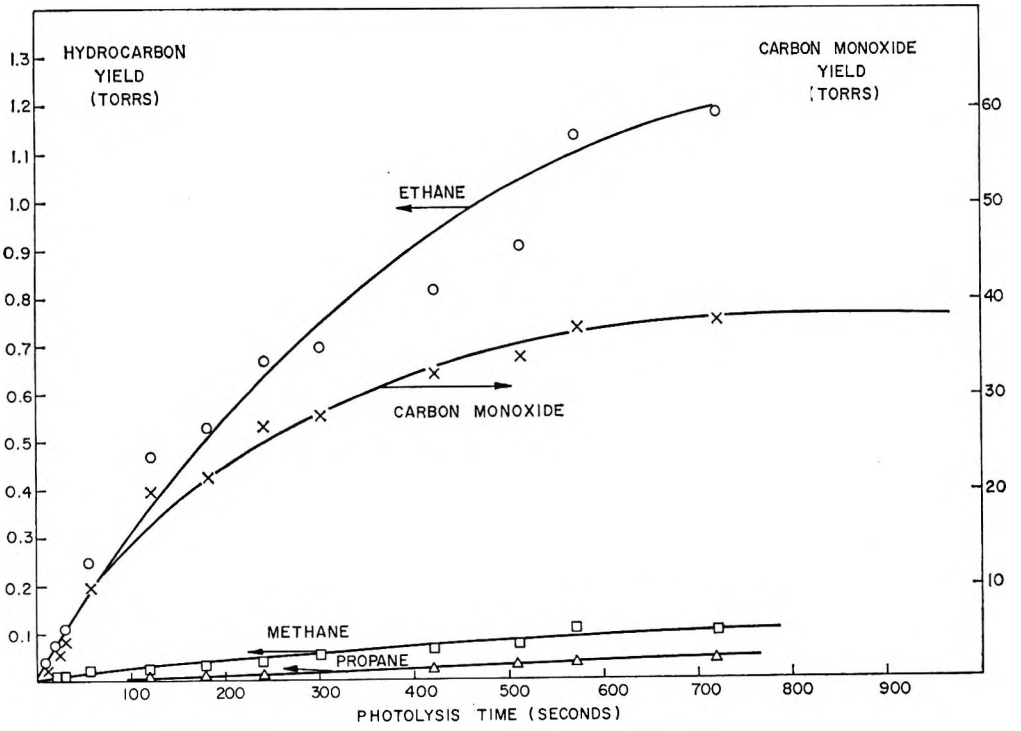

Figure 1. Product yields as a function of time for 2537 Å: O, ethane; ×, carbon monoxide; □, methane; △, propane.

Table II: Photolysis Yields at 1236 and 1470 Å from 30 Torr of C_3O_2 and 600 Torr of H_2

Wavelength, Å	Photolysis time[a] min	Yields, torr CO	CH_4[b]	C_2H_6[b]	$\Sigma n[C_nH_{2n+2}]$
1236	10	0.54	...	0.007	0.014
	43	1.0	0.004	0.018	0.031
	45	1.0	0.004	0.017	0.035
	30	1.2	...	0.022	0.044
	90	2.8	0.03	0.066	0.19
	120	1.8	0.02	0.042	0.086
	330	1.7	...	0.033	0.066
1470	15	0.13	...	0.0024	0.005
	180	1.9	0.01	0.045	0.10
	270	3.1	0.03	0.052	0.137

[a] Photolysis time is rather arbitrary, owing to the change of transmission of LiF with polymer formation. [b] The limit of sensitivity for detection under these conditions is less than for the photolysis at 2537 Å, owing to the much smaller volume being photolyzed, and any propane yield was below this limit of detection.

2200–2900 Å, both triplet and singlet states are formed, and about 2500 Å, the proportion of singlet reaches a maximum[2] of more than 90%. At 2537 Å then, the primary transient species can be considered to be the molecule C_2O in a singlet excited state. Reactions of this molecule with hydrogen must eventually lead to the hydrocarbon products observed.

There is a strong similarity between the yields of saturated hydrocarbons formed in the present study and those from studies of methylene–hydrogen reactions.[9-11] A reaction scheme involving methylene can be written to explain qualitatively the hydrocarbon yields observed

$$C_3O_2 + h\nu(2537\ \text{Å}) \longrightarrow {}^1C_2O + CO \quad (1)$$

$${}^1C_2O + H_2 \longrightarrow {}^1CH_2 + CO \quad (2)$$

$${}^1CH_2 + H_2 \longrightarrow CH_4^* \quad (3)$$

$$CH_4^* + M \longrightarrow CH_4 + M \quad (4)$$

$$CH_4^* \longrightarrow CH_3 + H \quad (5)$$

$$CH_3 + CH_3 \longrightarrow C_2H_6 \quad (6)$$

$$CH_3 + H_2 \longrightarrow CH_4 + H \quad (7)$$

$$CH_3 + H + M \longrightarrow CH_4 + M \quad (8)$$

$$H + H + M \longrightarrow H_2 + M \quad (9)$$

Reactions 3–9 are essentially the same used to explain the results from methylene–hydrogen reactions.

The direct formation of methylene by reaction 2 is thermodynamically possible. Probably the best value for the heat of formation of C_2O ($X^3\Sigma$) is 93 ± 5 kcal mol,[12] with about 15 kcal/mol of excitation energy associated with the singlet state.[2] The heat of formation of CH_2 (^1A) is 95 ± 5 kcal/mol,[13,14] and reaction 2, therefore, is exothermic by some 40 kcal/mol.

While methane and ethane are primary products, it appears that propane is a secondary product. This could be formed by a reaction of the type

$$CH_2 + C_2H_6 \longrightarrow C_3H_8 \quad (10)$$

Not all the ^1C_2O formed reacts with the hydrogen present. Some must react with carbon suboxide to form the polymer. If only hydrocarbons were formed, the total methylene yield, $\sum n[C_nH_{2n+2}]$ (this assumes that each carbon atom of the hydrocarbons originates from a C_2O molecule), should be half the carbon monoxide yield

$$nC_3O_2 + nh\nu + (n+1)H_2 \longrightarrow C_nH_{2n+2} + 2nCO$$

The measured methylene yields are much less than half the carbon monoxide yield.

The reaction of C_2O with the carbon suboxide can be written

$$C_2O + C_3O_2 \xrightarrow{[C_3O_2]} yCO + \text{polymer} \quad (11)$$

A kinetic treatment of the reactions as written leads to the expression

$$\left(\frac{1}{1+y}\right)\left\{\frac{\frac{d}{dt}[CO]}{\frac{d}{dt}\sum n[C_nH_{2n+2}]} - 2\right\} = \frac{k_{11}}{k_2}\frac{[C_3O_2]_t}{[H_2]_t} \quad (I)$$

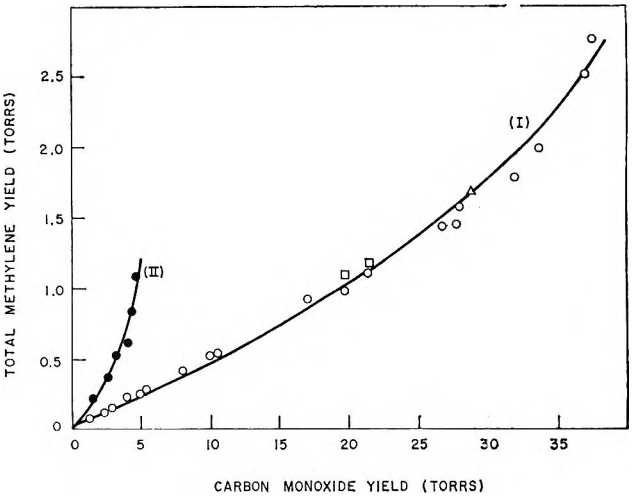

Figure 2. Total methylene plotted against carbon monoxide for 2537 Å: curve I (600 torr of H_2, 30 torr of C_3O_2): ○, thin Pyrex filter; □, thick Vycor filter; △, foil filter; curve II (600 torr of H_2, 3 torr of C_3O_2), ●.

(9) H. Gesser and E. W. R. Steacie, *Can. J. Chem.*, **34**, 113 (1956).
(10) J. A. Bell and G. B. Kistiakowsky, *J. Amer. Chem. Soc.*, **84**, 3417 (1962).
(11) J. Chanmugan and M. Burton, *ibid.*, **78**, 509 (1956).
(12) C. Willis and K. D. Bayes, *J. Phys. Chem.*, **71**, 3367 (1967).
(13) H. M. Frey, *Reaction Kinetics*, **2**, 131 (1964).
(14) D. W. Setser and B. S. Rabinovitch, *Can. J. Chem.*, **40**, 1425 (1962).

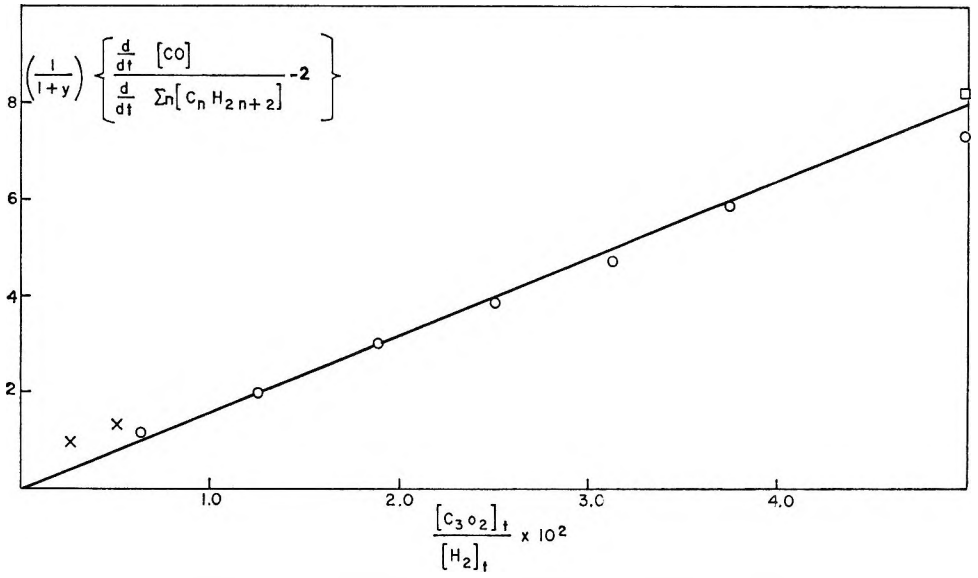

Figure 3. Plot of function I using values derived from Figure 2: O, 600 torr of H_2, 30 torr of C_3O_2 at 2537 Å; ×, 600 torr of H_2, 3 torr of C_3O_2 at 2537 Å; □, 600 torr of H_2, 30 torr of C_3O_2 at 1470 and 1236 Å (*i.e.*, value derived from Figure 4).

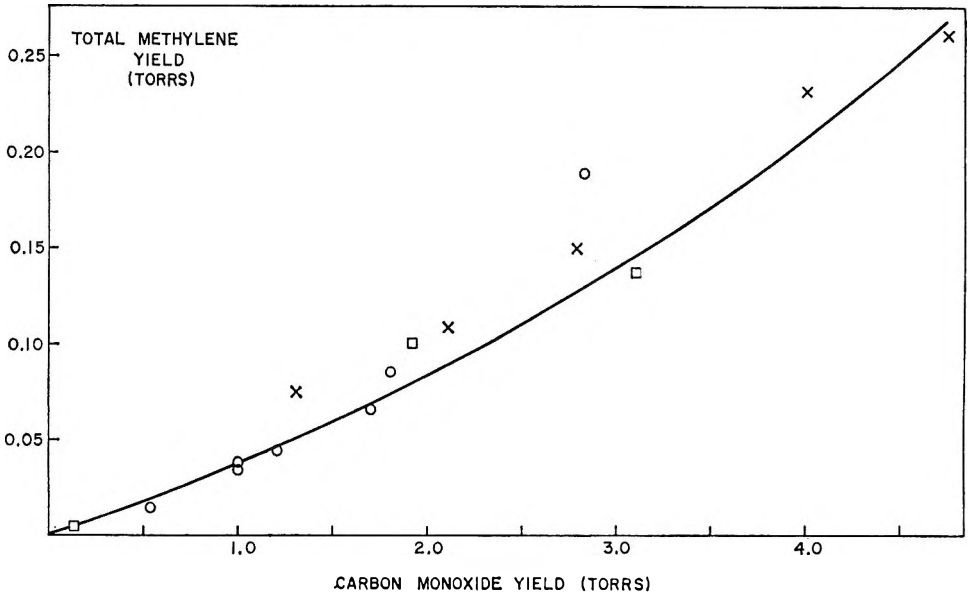

Figure 4. Total methylene plotted against carbon monoxide for 1236-, 1470-, and 2537-Å photolyses, 600 torr of H_2 and 30 torr of C_3O_2: ×, 2537 Å; O, 1236 Å; □, 1470 Å.

where $y + 1$ is effectively the quantum yield of carbon monoxide. A value for y was estimated by comparing the photolysis of carbon suboxide–ethylene mixtures under identical conditions and containing identical pressures of carbon suboxide. If it can be assumed for photolysis in the presence of ethylene that the quantum yield of carbon monoxide is 2,[2] then the ratio of the initial rates of production of carbon monoxide in the two systems gives $2/(y + 1)$. A value of 2.5 ± 0.5 was found for y.

In Figure 2, the yield of carbon monoxide [CO] is plotted against the yield of methylene, $\sum n[C_nH_{2n+2}]$. The reciprocal slopes of these curves give $(d/dt)[CO]/(d/dt)\sum n[C_nH_{2n+2}]$. Taking the slopes of these curves at various points, the left-hand side of expression I can be calculated. In Figure 3, the left-hand side of expression I is plotted against $[C_3O_2]_t/[H_2]_t$. The hydrogen concentrations were considered to be constant throughout the photolysis, and the carbon suboxide concentrations were interpolated assuming a zero concentration of carbon suboxide at a carbon monoxide pressure of 39 torr, the limit shown in Figure 1. The slope of the line plotted in Figure 3 gives $k_{11}/k_2 = 160 \pm 30$.

Photolysis at 1470 and 1236 Å. Although the formation of a carbon atom in the photolysis of carbon sub-

oxide is not energetically possible above 2000 Å, between 2000 and 1400 Å C(^{3}P), C(^{1}D), and C(^{1}S) progressively become thermodynamically possible.[15] It was hoped, by comparing the reactivities of the photochemically generated species produced at different wavelengths above and below 2000 Å, to confirm the conclusion of Stief and De Carlo, who have indicated[16] that a carbon atom is the primary product at wavelengths shorter than 1500 Å.

The plot of $\sum n[C_nH_{2n+2}]$ *vs.* [CO] for results from photolyses at 1470 and 1236 Å is shown in Figure 4. No real differences between these values and those from 2537 Å photolyses are apparent.

If carbon atoms were initially formed at these wavelengths then

$$C_3O_2 + h\nu(1470 \text{ or } 1236 \text{ Å}) \longrightarrow C + 2CO \quad (12)$$

$$C + H_2 \longrightarrow CH_2 \quad (13)$$

$$C + C_3O_2 \xrightarrow{[C_3O_2]} xCO + \text{polymer} \quad (14)$$

This leads to the expression

$$\left(\frac{1}{2+x}\right)\left\{\frac{\frac{d}{dt}[CO]}{\frac{d}{dt}\sum n[C_nH_{2n+2}]} - 2\right\} = \frac{k_{14}}{k_{13}}\frac{[C_3O_2]_t}{[H_2]_t} \quad (II)$$

At 1470 and 1236 Å, the carbon suboxide absorbs all incident radiation and x was estimated using nitrous oxide and carbon dioxide actinometry compared with the initial rate of carbon monoxide production. A good estimate was difficult to obtain, owing to the rapidity at which the polymer rendered the lithium fluoride window opaque, but it was found that $2 < 2 + x < 4$. This gives $k_{14}/k_{13} = 150 \pm 50$. (A value of 3.5 for $2 + x$ was used to calcultate this.)

At first sight, the almost identical relative rate constants k_{11}/k_2 and k_{14}/k_{13} would seem to indicate that the same species is formed at all wavelengths studied, the molecule C_2O. However, without more kinetic evidence about the reactions of carbon atoms, this equivalence cannot be used as a criterion to prove or disprove the production of carbon atoms in the photolysis of carbon suboxide with short-wavelength light.

Conclusions

The presence of methylene has been indicated in the photolysis of carbon suboxide in the presence of hydrogen at 1236, 1470, and 2537 Å. This is formed by reaction of a C_2O molecule in a singlet state with hydrogen and perhaps by the reaction of a carbon atom at the short wavelengths. A differentiation between these two species in the photolysis of carbon suboxide must await further kinetic information on reactions of carbon atoms in well defined electronic states.

Acknowledgments. We are happy to thank Dr. H. Hering and Mr. J. Sutton for their encouragement and interest in this work. C. W. wishes to thank the French Commissariat à l'Energie Atomique for a fellowship during which this work was carried out.

(15) Using the heat of formation of carbon suboxide reported by B. D. Kybett, G. K. Johnson, C. K. Baker, and J. L. Margrave, *J. Phys. Chem.*, **69**, 3603 (1965), and other values from standard tables.

(16) L. J. Stief and V. T. De Carlo, *J. Chem. Phys.*, **43**, 2552 (1965).

A Proton Magnetic Resonance Study of Hydrogen Bonding in Aliphatic Secondary Amines

by Ruth Ann Murphy[1]

Department of Chemistry, University of Texas, Austin, Texas

and Jeff C. Davis, Jr.

Department of Chemistry, University of South Florida, Tampa, Florida *(Received November 13, 1967)*

Chemical shift measurements of the amine proton of several secondary aliphatic amines, diethylamine, di-*n*-propylamine, di-*i*-propylamine, di-*n*-butylamine, piperidine, and 2-pipecoline in cyclohexane have been analyzed in terms of a monomer–dimer association model. Although the linear variation of the chemical shifts with concentration indicated such an equilibrium in all the cases studied, it was not possible to obtain unambiguous values for equilibrium constants for each system. For di-*n*-butylamine at 34° and piperidine at 38°, values of 0.20 and 0.18 mol fraction^{-1}, respectively, were calculated. Values obtained for ΔH of association for these two amines were -1.5 ± 0.5 and -2.1 ± 0.4 kcal mol^{-1}, respectively. Discrepancies in chemical shifts and calculated parameters are discussed in terms of steric hindrance and other factors.

Introduction

A nmr investigation of the NH···N hydrogen bond was undertaken to determine effects of various conditions upon its formation. A series of aliphatic secondary amines was chosen for this investigation, because they possess the NH group and yet have only one proton and only one acceptor site which can be expected to participate in hydrogen bonding. Cyclohexane was selected as the solvent, since it is highly inert.

The only previously reported work of this nature using a highly inert solvent is that of Happe,[2] who observed the self-association of pyrrole in cyclohexane, and that of Springer and Meek,[3] who observed the self-association of diethylamine in cyclohexane.

Experimental Section

Reagents. Diethylamine, di-*i*-propylamine, di-*n*-butylamine, and di-*i*-butylamine were Eastman grade. Di-*n*-propylamine (bp 108–110°), piperidine (bp 105–106.5°), and 2-pipecoline (bp 117–119°) were from Matheson Coleman and Bell. The amines were dried over KOH and then distilled from CaO through a Hempel column packed with 5 × 5 mm glass rings.

Precautions were taken to prevent exposure of the compounds to atmospheric moisture; the distilled amines were stored in Teflon FEP bottles under dry nitrogen or in a desiccator over NaOH. The position of the NH signal (relative to the methyl signal or, in the case of piperidine, to the highest point in the high-field methylene signal) in the pmr spectrum of the stored amine could be compared with its value when freshly distilled to check for absorption of moisture.

Phillips research grade cyclohexane was used without further treatment.

Sample Preparation. Samples were prepared by weight in volumes of approximately 10 ml or less, transfer of reagents being done with syringes and pipet. All samples were kept in a desiccator until the spectra had been obtained, which did not exceed 26 hr from the time of preparation.

Spectra were obtained on a Varian A-60 pmr spectrometer with a V-6031 variable-temperature probe, using nmr tubes of 5 mm o.d. Sweep widths were maintained essentially constant for each run by calibration with samples containing compounds having signals of known frequency separation. The temperature readings were measured as a function of the signal separation of an anhydrous ethylene glycol sample, the calibration of which was checked with a copper–constantan thermocouple. Spectra were obtained at ambient temperature after the sample had been in the probe a minimum of 12 min. Each chemical shift obtained at low amine concentrations was evaluated from at least four determinations, and as no trend in the successive values was observed, it is assumed that the sample temperatures did not change during the chemical shift measurements. The chemical shift of the methyl signal of the dialkylamines, relative to the cyclohexane signal, varied only a few tenths of 1 cps with dilution of the amine and showed no change at the lower amine concentrations at which it has been assumed that only monomers and dimers are present in significant concentrations. These methyl signals were used as references for measurement of the chemical shift of the NH signal of the dialkylamines. The cyclohexane signal was used as the reference in the studies of piperidine and 2-pipecoline. The probe temperature was checked

(1) This work is taken in part from a thesis by R. A. Murphy, submitted in partial fulfillment of the requirements for the Ph.D. degree, University of Texas, Austin, Texas, Jan 1967.

(2) J. A. Happe, *J. Phys. Chem.*, 65, 72 (1961).

(3) C. S. Springer, Jr., and D. W. Meek, *ibid.*, 70, 481 (1966).

at the beginning and end of each run; its maximum variation was 2.5°.

Results

For all compounds studied, with the exception of di-*i*-propylamine, which did not display a signal that could be positively attributed to the NH proton, one and only one signal arising from the NH proton was observed. The spectrum of di-*i*-propylamine was obtained at different temperatures, at varying concentrations of cyclohexane, and in acetone in the attempt to move the signal to higher or lower field strength to determine if the missing signal had been hidden by other signals. None of these spectra had a signal comparable with those arising from the NH protons in the other amines studied; although at a much higher instrument gain setting than is needed to observe the signals of the protons bonded to carbon atoms in this molecule, a very broad signal, about 20 cps at half-height, is observed approximately 57 cps to the high-field side of the cyclohexane signal.

Tables I–V give the chemical shift of the NH protons (ν) as a function of the mole fraction of the amine in cyclohexane (X) for the other amines in this study, with the exception of diethylamine, for which these data already have been reported.[4] In general, concentrations sufficiently low that the effects of higher polymers can be neglected received greater attention. With the exception of piperidine, for which the NH signal was not obscured by the ^{13}C satellite from the solvent at any

Table I: Chemical Shift of the Di-*n*-propylamine NH Proton as a Function of Concentration in Cyclohexane

Mole fraction of $(CH_3CH_2CH_2)_2NH$	Chemical shift of the NH-proton signal, cps from the center of the methyl signal 38°	52°	64°
1.0000	14.0	...	...
0.7257	16.5	...	...
0.4728	19.5	...	...
0.3089	21.9	...	...
0.1554	24.8	24.9	25.1
0.1340	24.9	24.8	25.6
0.1221	25.1	25.5	26.4
0.1153	25.4	25.4	26.2
0.0869	26.4	26.9	27.0
0.0771	26.4	27.1	27.0

Table II: Chemical Shift of the Di-*n*-butylamine NH Proton as a Function of Concentration in Cyclohexane

Mole fraction of $(CH_3CH_2CH_2CH_2)_2NH$	Chemical shift of the NH-proton signal, cps from the center of the methyl signal 34°	45°	59°
1.000	19.0	...	...
0.699	21.0	...	...
0.519	22.8	...	...
0.303	25.6	...	...
0.165	28.0	...	...
0.156	27.6	27.9	28.4
0.136	28.3	...	28.9
0.129	28.4	28.9	28.6
0.114	28.6	29.4	29.6
0.0973	29.5	29.6	29.7
0.0794	29.7	29.6	...
0.0697	30.2	30.5	...

Table III: Chemical Shift of the Di-*i*-butylamine NH Proton as a Function of Concentration in Cyclohexane

Mole fraction of $((CH_3)_2CHCH_2)_2NH$	Chemical shift of the NH-proton signal, cps from the center of the methyl signal 37°	52°	64°
1.0000	15.6	...	...
0.7204	16.7	...	...
0.4934	17.3	...	...
0.3078	18.8	...	...
0.1671	20.3	19.8	21.5
0.1546	20.5	20.6	21.2
0.1337	21.5	20.7	23.3
0.1309	20.9	...	...
0.1242	20.8	21.2	22.2
0.1142	21.3	21.6	24.4
0.0770	22.8	23.4	24.6

Table IV: Chemical Shift of the Piperidine NH Proton as a Function of Concentration in Cyclohexane

Mole fraction of $CH_2(CH_2)_3CH_2NH$	Chemical shift of the NH-proton signal, cps from the cyclohexane signal 38°	50°	64°
0.3923	5.7	...	...
0.1906	15.6	...	...
0.1581	17.2	...	...
0.1151	19.8	21.7	23.1
0.0892	21.5	22.8	24.3
0.0732	22.4	23.8	25.2
0.0631	23.5	24.6	25.6
0.0534	23.8	25.1	26.3
0.0529	24.1	25.3	26.4
0.0422	25.6	25.9	26.5

Table V: Chemical Shift of the 2-Pipecoline NH Proton as a Function of Concentration in Cyclohexane

Mole fraction of $CH_3CH_2(CH_2)_3CH_2NH$	Chemical shift of NH-proton signal (34°), cps from cyclohexane
0.802	4.7
0.684	7.9
0.520	12.3
0.379	16.4
0.334	17.2
0.280	18.8
0.252	21.4
0.233	21.5

(4) R. A. Murphy and J. C. Davis, Jr., *J. Phys. Chem.*, **71**, 3361 (1967).

Table VI: Line Parameters for Chemical Shifts of NH Protons as a Function of Concentration and Values Obtained for $K\Delta_D$, ν_1, and $\nu_{1,c}$

Cmpd	Temp, °C	Slope, cps/mol fraction	Y intercept, cps	Root-mean-square error	$K\Delta_D$, cps/mol fraction	ν_1, cps	$\nu_{1,c}$, cps
Diethylamine	31	−48.6 ± 1.3	43.0 ± 0.1	0.22	−24.3	43.0	67.8
Di-*n*-propylamine	38	−29.3 ± 0.8	28.8 ± 0.1	0.11	−14.6	28.8	61.5
	52	−41.2 ± 1.1	30.4 ± 0.1	0.14	−20.6	30.4	63.1
	64	−25.1 ± 0.9	29.1 ± 0.1	0.18	−12.6	29.1	61.8
Di-*n*-butylamine	34	−29.0 ± 0.5	32.2 ± 0.1	0.13	−14.5	32.1	64.8
	45	−25.5 ± 1.1	32.1 ± 0.1	0.24	−12.8	32.1	64.7
	59	−24.1 ± 1.9	32.1 ± 0.2	0.21	−12.0	32.1	64.7
Di-*i*-butylamine	37	−26.4 ± 1.3	24.5 ± 0.2	0.30	−13.2	24.5	57.9
	52	−29.8 ± 1.6	24.9 ± 0.2	0.18	−14.9	24.9	58.2
	64	−31.6 ± 2.3	26.8 ± 0.3	0.70	−15.8	26.8	60.1
Piperidine	38	−65.3 ± 0.4	27.4 ± 0.03	0.14	−32.6	27.4	27.4
	50	−59.1 ± 0.7	28.3 ± 0.05	0.15	−29.5	28.3	28.3
	64	−49.9 ± 0.6	28.8 ± 0.05	0.13	−24.9	28.8	28.8

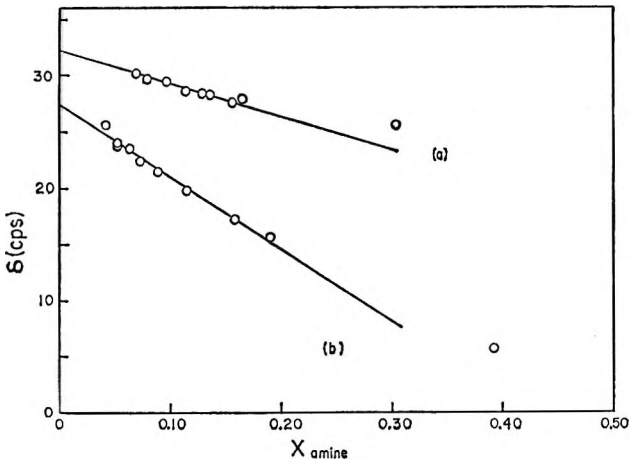

Figure 1. Variation of the NH chemical shift with the mole fraction of amine in cyclohexane: (a) di-*n*-butylamine at 34°; (b) piperidine at 38°.

observed concentration, the lowest concentration studied was approximately $0.07X$. At lower X values the size and position of the satellite made measurements of ν unfeasible.[4] It was not possible to study 2-pipecoline at concentrations lower than about $0.23X$, as the position of the methyl doublet prevented observations of the NH signal.

Data appearing below about $X = 0.16$ gave linear plots of ν *vs.* X. This linearity is illustrated in Figure 1. The parameters of these lines, as determined by the method of least squares, are given in Table VI. The broadness of the di-*i*-butylamine signal made it extremely difficult to determine chemical shifts, and this effect is probably responsible for the greater scatter of the data for this compound. Temperature work for diethylamine is not presented here, as its relatively low boiling point of 55.5°[5] tends to make high-temperature work subject to error from evaporation, and at low temperatures the signals were too broad for accurate determination of their position. The latter effect is probably due to viscosity effects arising from approaching the freezing point of cyclohexane (6.5°)[6] and also possibly decreased instrument resolution.

Treatment

Assuming that only monomers and dimers are present

$$\nu = \frac{n_1}{n_t}(\nu_1) + \frac{n_2}{n_t}(2\nu_2) \tag{1}$$

where n refers to number of moles and the subscripts 1, 2, and t represent moles of monomer, moles of dimer, and total moles, respectively. From the equilibrium-constant expression, the dimer concentration can be written

$$D = \frac{(4AK + A + S) - [(4AK + A + S)^2 - 4A^2K(4K + 1)]^{1/2}}{2(4K + 1)} \tag{2}$$

in which A represents the stoichiometric number of moles of amine, D is the number of moles of the dimeric form present, S is the number of moles of solvent, and K is the equilibrium constant of dimerization. From expressions 1 and 2, ν can be expressed as

$$\nu = \nu_1 + \left\{\frac{(4AK + A + S) - [(4AK + A + S)^2 - 4A^2K(4K + 1)]^{1/2}}{A(4K + 1)}\right\}(\nu_2 - \nu_1)$$

(5) C. D. Hodgman, *et al.*, Ed., "Handbook of Chemistry and Physics," 45th ed, The Chemical Rubber Co., Cleveland, Ohio, 1964, p C-109.

(6) See ref 5, p C-267.

or as

$$\nu = \nu_1 + \left\{ \frac{[(4K+1)/X] - \{[(4K+1)/X^2] - 4K(4K+1)\}^{1/2}}{4K+1} \right\} (\nu_2 - \nu_1)$$

As reported by Huggins, Pimentel, and Shoolery[7] in their work with phenols, at concentrations of hydrogen-bonding species such that only monomers and dimers are present in appreciable quantities, the plot of ν *vs.* X is linear, the y intercept being ν_1 and the slope being $2K(\nu_2 - \nu_1)$. This has been applied to the line-parameters in Table VI, which gives the values obtained for ν_1 and $2K(\nu_2 - \nu_1)$, subject to the foregoing assumptions. As the reference signal used varied with the compounds, the ν_1 values cannot be compared without adjustment to a common reference. Thus $\nu_{1,c}$ refers to ν_1 relative to the cyclohexane signal.

In their study of chloroform dimerization, Jumper, Emerson, and Howard[8] calculated dimer concentrations for various values of K and selected the value of K best fitting the data. Then ν_1 and ν_2 were calculated by expression 3. Here again the assumption that only monomers and dimers are present in appreciable concentrations was made. This method selected values for ν_1, ν_2, and K for di-*n*-butylamine and piperidine (Table VII).[8b] The other sets of data did not give conclusive results when programmed in this manner. The method was tested with a set of model data, calculated for preset values of $K = 2$, $\nu_1 = 30$, $\nu_2 = -2.5$, which were of the order of values expected for these compounds, to check the FORTRAN program used on a CDC1604 computer. It was found that the correct value of K is selected only if the chemical shifts have been very accurately calculated. Thus the program seems to be quite sensitive to errors in the data, which may explain the large value for ν_2 in the di-*n*-butylamine data and in the piperidine data at 38°, as well as the increase of K with temperature in the piperidine data.

Table VII: Values Obtained for ν_1, ν_2 and H by Curve Fitting[8b]

Cmpd	Temp, °C	ν_1, cps	ν_2, cps	K, (mol fraction)$^{-1}$
Di-*n*-butylamine	34	32.4	−52.7	0.20
Piperidine	38	27.7	−178.5	0.18
	50	30.1	−5.1	1.8

Although the enthalpy for the hydrogen-bond formation cannot be determined directly from the data presented here, due to uncertainty in the value of K obtained, ΔH can be calculated by the method of Davis, *et al.*,[9] in which $K\Delta_D$ is plotted *vs.* T^{-1}. The slope obtained is then $-\Delta H/R$, subject to the assumptions that (1) only monomers and dimers are present in significant concentrations, (2) that the concentrations of the species closely approximate their activities, and (3) that both ΔH and Δ_D are constant over the temperature range considered. Values of ΔH of -2.1 ± 0.4 kcal/mol for piperidine and -1.5 ± 0.5 kcal/mol for di-*n*-butylamine are obtained by this method, where mole implies mole of hydrogen bond. The scatter of the di-*i*-butylamine data, shown by the errors given in Table VI, was too great to determine ΔH for this compound. The di-*n*-propylamine data are unusual in that the points do not progress with temperature in the expected manner. Equilibrium constants for hydrogen-bond formation generally decrease with temperature; however, the di-*n*-propylamine data exhibit an increase of $K\Delta_D$ with the first increase of temperature, and then a decrease of $K\Delta_D$ with a further rise of temperature.

A possible explanation for this phenomenon would be the simultaneous existence of open and closed dimers in the di-*n*-propylamine solutions. The ratio of the equilibrium constant for formation of the open species to the equilibrium constant for the closed species would be expected to increase with increasing temperature, since the greater energy of the molecules would oppose the formation of a closed dimer relative to the less restricted configuration of an open form.

Thus the ΔH values presented for piperidine and di-*n*-butylamine are subject to the assumption that only one type of dimer is formed. The di-*n*-propylamine data do seem to indicate the possible existence of two forms of dimers.

Extremely accurate values of Δ_D would give a clue as to the actual situation here. In the first place, one could test the assumption that Δ_D is essentially temperature independent. Secondly, an open dimer has only one associated proton, while a closed dimer has two; thus Δ_D for a closed dimer could be expected to be greater than that for the open form. The question cannot be answered at present, however, due to the lack of data.

Discussion

Spectra of Pure Amines. All spectra except that of di-*i*-propylamine show readily identifiable NH signals. A possible explanation for the difficulty in observing the di-*i*-propylamine signal would be the existence of relatively few hydrogen bonds in this compound at room temperature, relative to the other amines used in this study. This is indicated by the boiling point of di-*i*-

(7) C. M. Huggins, G. C. Pimentel, and J. N. Shoolery, *J. Phys. Chem.*, **60**, 1311 (1956).

(8) (a) C. F. Jumper, M. T. Emerson, and B. B. Howard, *J. Chem. Phys.*, **35**, 1911 (1961); (b) R. A. Murphy, Ph.D. Thesis, University of Texas, Austin, Texas, Jan 1967.

(9) J. C. Davis, Jr., K. S. Pitzer, and C. N. R. Rao, *J. Phys. Chem.*, **64**, 1744 (1960).

propylamine, which is lower than those of its structural isomers.[10-12]

One would expect that if appreciable hydrogen bonding in di-*i*-propylamine were present at temperatures near 80°, its boiling point would be higher, and not lower, than that of triethylamine, which does not have a proton capable of hydrogen bonding. The boiling point of di-*n*-propylamine, which has a readily identifiable NH-proton signal, is well above that of triethylamine. Similarly, while the melting point of di-*i*-propylamine is above that of triethylamine, it is still more than 20° below that of di-*n*-propylamine, suggesting that at these low temperatures some hydrogen bonding does occur in the di-*i*-propyl compound, although not as much as in the di-*n*-propyl compound.

Further, the Cenco–Petersen molecular model of di-*i*-propylamine shows that the NH proton is blocked by the *i*-propyl groups. Thus the broad signal observed at high gain may be the signal characteristic of the NH proton in the monomeric species. One would expect that any proton exchange in the di-*i*-propyl compound would occur much more slowly than in the other amines studied, and this exchange could be of such a rate as to account for the width of the signal. The room temperature shift of this broad signal, 57 cps relative to cyclohexane, compared well with the value of $\nu_1 = 57.9$ cps for di-*i*-butylamine. As the NH signal of di-*i*-butylamine is broader than the corresponding signals of the other amines which had obvious NH signals, the possibility exists that the *i*-butyl groups shield the NH group, slowing exchange sufficiently for the NH signal to be broadened somewhat, although to a lesser extent than in di-*i*-propylamine. This seems to be consistent with the fact that in di-*i*-propylamine the branched carbon atom is bonded directly to the nitrogen atom, while in di-*i*-butylamine an unbranched carbon atom is between the branched carbon and the nitrogen.

ν_1, ν_2, and K. The ν_1 value for piperidine is markedly different from that for the dialkylamines, falling 30 cps or more to lower field strength. The diethylamine ν_1 is at a somewhat higher field than the values for the other dialkylamines, although the lower temperature at which this measurement was made could account for at least part of the difference. The other dialkylamines appear to have similar values for ν_1, that of di-*i*-butylamine being the lowest. Thus no trend was observed such as in the investigation of alcohols in CCl_4 by Davis *et al.*,[9] in which ν_1 for *t*-butyl alcohol and *i*-propyl alcohol were about equal and less than ν_1 for ethanol, which was less than ν_1 for methanol. A slight trend of ν_1 to higher field strength with temperature is indicated for piperidine and di-*i*-butylamine by the data in Table VI, although ν_1 for di-*n*-butylamine appears to be temperature independent. The ν_1 values for di-*n*-propylamine show the same trend with temperature as do the values of $K\Delta_D$ for this compound. None of the changes of ν_1 with temperature is very large, although there appears to be some variation.

An obvious feature of Table VI is the magnitude of $K\Delta_D$ for piperidine, compared with the other compounds. Diethylamine has the second largest value for $K\Delta_D$, although this comparison cannot be made too rigidly, as data for the other compounds were obtained at somewhat higher temperatures than was that for diethylamine. The values of $K\Delta_D$ for di-*n*-propylamine, di-*n*-butylamine, and di-*i*-butylamine are not too different, but the trend with temperature of the $K\Delta_D$ values for the *n*-propyl compound is striking. Even though the trend for the *i*-butyl compound is in a direction opposite to that predicted by assuming a simple monomer–dimer equilibrium, the error in these values is large enough that a variation with temperature cannot be established.

Because of the lack of steric hindrance, the NH proton of piperidine would be expected to form hydrogen bonds more readily than that of the other amines studied and thus has a larger K. This is supported by the data, which indicate that $K\Delta_D$ for piperidine is somewhat greater than the value for the other amines, although Δ_D cannot be assumed to be the same for the various compounds. It is reasonable, however, to assume that K for piperidine would be at least as large as K for the other compounds, *e.g.*, di-*n*-propylamine. If it is assumed, then, that the K's for these two compounds are equal, Δ_D for piperidine is more than twice as great as the corresponding value for di-*n*-propylamine. It is possible that the different values of ν_1 cause part of this difference. Although Δ_D for piperidine could be larger than that of di-*n*-propylamine, it is a reasonable assumption that K for piperidine is also greater than for di-*n*-propylamine and, therefore, for the other amines studied as well.

Muller and Reiter[13] have done calculations to account for the temperature variation of the chemical shift of a hydrogen-bonded proton. They state that the chemical shift in this case is a function of the quantum state of the stretching vibration of the hydrogen bond, and since this is of a very low frequency, a slight change in temperature could alter the vibrational states. This effect in turn could cause the resonance frequency of the hydrogen-bonded proton to shift, even though the association remains.

Another mechanism which could result in a ν_2 which is apparently temperature dependent would arise from the simultaneous presence of open and closed dimers. A change in temperature would alter the relative concentrations of the two associated species, and since each would have characteristic value of ν_2, there would be a

(10) See ref 5, p C-110.
(11) See ref 5, p C-113.
(12) See ref 5, p C-111.
(13) N. Muller and R. C. Reiter, *J. Chem. Phys.*, 42, 3265 (1965).

difference in the ν_2 observed at the initial and final temperatures. It is possible that both this process and that suggested by Muller and Reiter contribute to a variation of Δ_D with temperature. Since the ν_1 values show only slight variation with temperature, any sizable variation of Δ_D would most likely result from a change in ν_2 with temperature.

Happe's nmr study of pyrrole dimerization in cyclohexane[2] obtained a value for $K = 4.3$ (mol fraction)$^{-1}$, which is somewhat larger than any of the values for either piperidine or di-*n*-butylamine obtained in this work. The far-infrared investigation of pyrrole autoassociation in CCl_4 by Lorenzelli and Alemagna[14] revealed bands which they interpreted as being indicative of hydrogen-bonded chains.

Springer and Meek interpreted the results of their nmr investigation of ethylamine association in cyclohexane in terms of a monomer–tetramer equilibrium, obtaining 1.75×10^{-3} (mol/l.)$^{-3}$ for the equilibrium constant for tetramer formation. Their assumption that the apparently constant value of ν for $X < 0.092$, is ν_1 has, however, been questioned.[4] Feeney and Sutcliffe[15] did a similar study of diethylamine in CCl_4, obtaining 2.5×10^{-4} (mol/l.)$^{-3}$ for the equilibrium constant of tetramer formation.

A monomer–dimer equilibrium was assumed in this investigation, because it is believed that fewer assumptions are required for this case. The monomer–tetramer case requires numerous assumptions regarding the rates of formation and dissociation of dimers and trimers as well as of tetramers. Further, the linear variation of ν with concentration provides evidence for the monomer–dimer system.

Enthalpy. The enthalpy values presented here for piperidine and di-*n*-butylamine fall within the range suggested by Orgel;[16] further, it is reasonable that the value for piperidine should exceed that for di-*n*-butylamine. It would be desirable to obtain values for other amines, however, as well as to pursue the study at lower concentrations. This would test the assumptions made in this study and aid in determining any trends which may exist in the relative NH$\cdots$N energies.

Acknowledgment. The authors wish to express their appreciation to the National Science Foundation and to the Office of Saline Water, U. S. Department of the Interior, for support of this work.

(14) V. Lorenzelli and A. Alemagna, *Compt. Rend.*, **257**, 2977 (1963).
(15) J. Feeney and L. H. Sutcliffe, *J. Chem. Soc.*, 1123 (1962).
(16) L. E. Orgel, *Rev. Mod. Phys.*, **31**, 100 (1959).

The Crystal Structures of Bismuth Halide Complex Salts. III. Tris(dimethylammonium) Hexabromobismuthate(III), $[(CH_3)_2NH_2]_3BiBr_6$

by W. Gant McPherson[1] and Edward A. Meyers

Department of Chemistry, Texas A & M University, College Station, Texas 77843 *(Received November 22, 1967)*

$[(CH_3)_2NH_2]_3BiBr_6$ is rhombohedral, $R\bar{3}$, with $z = 12$ in the unit cell indexed on a hexagonal basis; $a = b = 29.25$ (6) Å and $c = 8.45$ (2) Å. The structure was determined from the intensities of 1160 independent (hkl) reflections, $l = 0$–4, collected with a Weissenberg camera, with (Ni-filtered) Cu Kα radiation (λ 1.5418 Å) and multiple-film packs. The crystal was treated as a cylinder, $\mu R = 3.12$ for absorption corrections. Full-matrix least-squares refinement of the parameters gave $R_1 = \Sigma|F_o - F_c|/\Sigma|F_o| = 0.11$ with isotropic temperature factors, and $R_1 = 0.08$ with anisotropic temperature factors for Bi and Br. In the least-squares refinement, 80 reflections with $|F_o| \gtrsim 325$ were given zero weight and the remaining 1080 reflections were given unit weight. Two crystallographically independent Bi(III)Br_6 octahedra, (A) and (B), are present in the structure. For (A), Bi(A)–Br(A) = 2.849(7) Å and Br(A)–Bi(A)–Br(A) = 92.5 (3)°. For (B), Bi(B)–Br(1)(B) = 2.822 (9) Å, Bi(B)–Br(2)(B) = 2.852 (8) Å, Bi(B)–Br(3)(B) = 2.839 (8) Å, Br(1)(B)–Bi(B)–Br(2)(B) = 91.9 (3)°, Br(1)(B)–Bi(B)–Br(3)(B) = 87.2 (2)°, and Br(2)(B)–Bi(B)–Br(3)(B) = 90.1 (2)°. Thus the Bi–Br bond distances do not appear to differ significantly from their average, 2.840 Å, but the angular deviations from 90.0° indicate that the octahedra are not regular. The total Pauling bond order is 2.7 for the Bi–Br bonds in an octahedron. (No satisfactory corrections were made for the effects of thermal motion on bond distances, so that the values cited may be too small and less reliable than indicated.) Two crystallographically independent cations, A and B, are present in the structure. The mean C–N bond distance is 1.56 Å, the mean C–N–C bond angle is 118°, with no significant deviations from these values. The van der Waals contacts are greater than 3.6 Å, except for Br(3)(B)–C(2)(B) = 3.47 (9) Å. There are short N···Br contacts. For N(A), N(A)–Br(A) = 3.44 (7) Å and N(A)–Br(2)(B) = 3.48 (7) Å, and these contacts couple the two types of Bi(III)Br_6 octahedra together. For N(B), N(B)–Br(1)(B) = 3.49 (6) Å and N(B)–Br(2)(B) = 3.44 (6) Å, and these contacts are exclusively to the Bi(III)Br_6 octahedron, (B).

Introduction

In two earlier studies[2,3] we have reported the structures of organic ammonium salts of Bi(III)Br_4, Bi(III)-I_4, and Bi(III)Br_5. Several regularities were observed in these structures. In each case, the Bi atom was surrounded by a distorted octahedron of halogen nearest neighbors and linked into infinite chains *via* halogen bridges. Moreover, the total Bi–halogen Pauling bond order[4] was close to 3. In the present study, the structure of $[(CH_3)_2NH_2]_3BiBr_6$ was determined in order to obtain structural parameters for the anion units which were expected to be Bi(III)Br_6 octahedra.

Experimental Section

$[(CH_3)_2NH_2]_3BiBr_6$ was prepared by Osborne.[5] Single crystals were grown by recrystallization from a 1:1 water–propanol mixture, approximately 1 M in HBr. A nearly cylindrical needle-shaped crystal 0.2 mm in diameter was selected and mounted in a 0.2-mm thin-walled Lindemann glass capillary. Precession photographs with (Zr-filtered) Mo Kα radiation (λ 0.7107 Å) were obtained and the unit cell was found to be rhombohedral. When indexed on the basis of a hexagonal cell with the c axis along the needle direction, $a = b = 29.25$ (6) Å, $c = 8.45$ (2) Å, $d_{measd} = 2.5$ (1) g/cc, $d_{calcd} = 2.63$ (1) g/cc for $z = 12$.

The crystal was transferred to the Weissenberg camera and (hkl) data were collected for $l = 0$–4 with (Ni-filtered) Cu Kα radiation (λ 1.5418 Å) and a multiple-film pack. The value $\mu R = 3.12$ was used for the absorption corrections for the cylindrical sample, and Lorentz and polarization corrections were also applied to the approximately 1160 reflections measured with a Welch Densichron, Model 10. Only reflections for which $-h + k + l = 3N$ were observed, which indicated a rhombohedral space group.

Refinement was begun in space group $R\bar{3}m$.[6] Three Bi atoms were generated from Bi(A) placed in special

(1) Submitted to the Graduate College of Texas A & M University in partial fulfillment of the requirements for the degree of Doctor of Philosophy, Jan 1967.

(2) B. K. Robertson, W. G. McPherson, and E. A. Meyers, *J. Phys. Chem.*, 71, 3531 (1967).

(3) W. G. McPherson and E. A. Meyers, *ibid.*, 72, 532 (1968).

(4) L. Pauling, *J. Amer. Chem. Soc.*, 69, 542 (1947).

(5) J. F. Osborne, Master's Thesis, Texas A & M University, College Station, Texas, 1960.

(6) "International Tables for X-Ray Crystallography," Vol. I, Kynoch Press, Birmingham, England, 1952, pp 272–273, 252–253.

Table I: Atomic Coordinates of $[(CH_3)_2NH_2]_3BiBr_6$ Obtained in the Isotropic Refinement (Standard Deviations Are Given in Parentheses and Apply to the Last Digit of a Number)

		x	y	z	B, Å^2
Bi(A)	*a*	0	0	0	3.50 (10)
	b	0	0	0	3.31 (11)
	c	0	0	0	4.07 (8)
	d	0	0	0	3.87 (8)
Bi(B)	*a*	1/6	1/3	1/3	3.00 (5)
	b	1/6	1/3	1/3	2.80 (5)
	c	1/6	1/3	1/3	3.55 (5)
	d	1/6	1/3	1/3	3.35 (5)
Br(A)	*a*	0.0852 (2)	0.0766 (2)	0.1860 (9)	4.36 (13)
	b	0.0852 (2)	0.0766 (2)	0.1860 (9)	4.55 (13)
	c	0.0852 (2)	0.0763 (2)	0.1868 (7)	5.01 (10)
	d	0.0852 (2)	0.0763 (2)	0.1868 (7)	5.21 (10)
Br(1)(B)	*a*	0.1487 (3)	0.2525 (3)	0.5496 (10)	5.14 (15)
	b	0.1486 (3)	0.2525 (3)	0.5496 (10)	5.33 (15)
	c	0.1489 (2)	0.2524 (2)	0.5481 (8)	5.77 (11)
	d	0.1488 (2)	0.2524 (2)	0.5481 (8)	5.98 (11)
Br(2)(B)	*a*	0.1433 (2)	0.2642 (2)	0.0697 (9)	4.47 (13)
	b	0.1433 (2)	0.2642 (2)	0.0698 (9)	4.65 (13)
	c	0.1434 (2)	0.2644 (2)	0.0686 (7)	5.21 (10)
	d	0.1435 (2)	0.2643 (2)	0.0687 (7)	5.39 (10)
Br(3)(B)	*a*	0.0581 (2)	0.3016 (2)	0.3620 (9)	4.17 (12)
	b	0.0581 (2)	0.3016 (2)	0.3620 (9)	4.35 (12)
	c	0.0579 (2)	0.3015 (2)	0.3615 (6)	4.79 (9)
	d	0.0579 (2)	0.3015 (2)	0.3615 (7)	4.97 (10)
C(1)(A)	*a*	0.020 (3)	0.139 (3)	0.413 (11)	6.7 (17)
	b	0.020 (3)	0.139 (3)	0.413 (11)	7.0 (18)
	c	0.021 (2)	0.138 (2)	0.413 (8)	7.3 (13)
	d	0.021 (2)	0.138 (2)	0.412 (8)	7.7 (13)
N(A)	*a*	0.037 (3)	0.160 (3)	0.263 (9)	8.1 (17)
	b	0.037 (3)	0.160 (3)	0.262 (9)	8.6 (17)
	c	0.036 (2)	0.159 (2)	0.250 (7)	9.2 (13)
	d	0.036 (2)	0.158 (2)	0.248 (7)	9.4 (13)
C(2)(A)	*a*	0.000 (3)	0.167 (3)	0.149 (11)	8.1 (21)
	b	0.000 (3)	0.167 (3)	0.149 (11)	8.6 (22)
	c	0.001 (2)	0.163 (2)	0.138 (7)	7.4 (13)
	d	0.001 (2)	0.163 (2)	0.138 (7)	7.7 (13)
C(1)(B)	*a*	0.434 (3)	0.125 (3)	0.105 (9)	6.3 (16)
	b	0.434 (3)	0.125 (3)	0.105 (9)	6.7 (17)
	c	0.430 (2)	0.123 (2)	0.104 (7)	6.9 (12)
	d	0.430 (2)	0.123 (2)	0.105 (7)	7.2 (12)
N(B)	*a*	0.373 (2)	0.118 (2)	0.118 (7)	6.1 (13)
	b	0.373 (2)	0.118 (2)	0.119 (7)	6.4 (13)
	c	0.375 (1)	0.117 (1)	0.102 (5)	6.1 (9)
	d	0.375 (1)	0.117 (1)	0.103 (5)	6.4 (9)
C(2)(B)	*a*	0.328 (3)	0.060 (3)	0.174 (10)	8.4 (21)
	b	0.328 (3)	0.060 (3)	0.174 (11)	8.9 (22)
	c	0.332 (3)	0.062 (3)	0.176 (8)	10.0 (18)
	d	0.332 (3)	0.063 (3)	0.176 (8)	10.6 (18)

[a] Unit weights, all data, uncorrected for anomalous dispersion (ad). [b] Unit weights, all data, corrected for ad. [c] Unit weights, selected data ($|F_o| \lesssim 325$), uncorrected for ad. [d] Unit weights, selected data ($|F_o| \lesssim 325$), corrected for ad.

position *a* (0, 0, 0), and nine Bi atoms from Bi(B), in a special position directly related to *e*, (1/2, 0, 0), (0, 1/2, 0), and (1/2, 1/2, 0). A Fourier synthesis was constructed[7] from (*hk*0) data with the Bi atoms included in the calculations.[8] Only four Br peaks appeared in the vicinity of Bi(B). The space group $R\bar{3}m$ was

Table II: Bond Distances and Angles for $((CH_3)_2NH_2)_3BiBr_6$ (Standard Deviations Are Given in Parentheses and Apply to the Last Digit of a Number)

	Table I		Table III	
	From *b* rows	From *d* rows	From *a* rows	From *b* rows
	Bond distance, Å			
Bi(A)–Br(A)	2.849 (7)	2.850 (6)	2.851 (5)	2.851 (5)
Bi(B)–Br(1)(B)	2.822 (9)	2.818 (7)	2.817 (6)	2.818 (6)
Bi(B)–Br(2)(B)	2.852 (8)	2.858 (7)	2.867 (6)	2.867 (6)
Bi(B)–Br(3)(B)	2.839 (8)	2.844 (8)	2.843 (7)	2.843 (7)
C(1)(A)–N(A)	1.40 (9)	1.48 (7)	1.47 (5)	1.47 (5)
C(2)(A)–N(A)	1.54 (10)	1.46 (7)	1.50 (5)	1.49 (5)
C(1)(B)–N(B)	1.68 (8)	1.54 (6)	1.55 (4)	1.56 (4)
C(2)(B)–N(B)	1.61 (9)	1.59 (7)	1.59 (5)	1.58 (5)
	Bond angles, deg			
Br(A)–Bi(A)–Br(A)	92.5 (3)	92.3 (2)	92.3 (2)	92.3 (2)
Br(1)(B)–Bi(B)–Br(2)(B)	91.9 (3)	91.8 (2)	91.9 (2)	91.9 (2)
Br(1)(B)–Bi(B)–Br(3)(B)	87.7 (2)	88.0 (1)	88.1 (2)	87.9 (1)
Br(2)(B)–Bi(B)–Br(3)(B)	90.1 (2)	90.1 (1)	90.1 (1)	90.1 (1)
C(1)(A)–N(A)–C(2)(A)	121 (7)	124 (5)	124 (3)	124 (3)
C(1)(B)–N(B)–C(2)(B)	115 (5)	111 (4)	110 (3)	109 (3)

discarded, and $R\bar{3}$[6] was selected for all further calculations. The Bi positions were not affected by the change in the choice of space group. The atoms Bi(A), Bi(B), and Br(A), the bromine atom close to Bi(A), were included in the electron density calculation with (*hk*0) data, and it was apparent that two of the four peaks around Bi(B) were exceptionally large. This indicated that each of the larger peaks was made up of the contribution of two Br atoms superposed along [001]. The *z* coordinate of each Br atom was obtained with the assumptions that Bi–Br = 2.8 Å and that the $Bi(III)Br_6$ group was a regular octahedron. The Bi and Br coordinates were refined by least squares,[9] with unit weights, isotropic temperature factors, and no correction for anomalous dispersion, $R_1 = \Sigma \| F_o - F_c \| / \Sigma | F_o | = 0.14$ and $R_2 = [\Sigma(F_o - F_c)^2/\Sigma F_o]^{1/2} = 0.16$.

In order to locate the positions of the light atoms (C and N) of the two crystallographically distinct dimethylammonium groups required, a three-dimensional difference Fourier synthesis was calculated, with the contributions of the heavy atoms (Bi and Br) subtracted. Additional least-squares refinement was carried out, with C and N coordinates permitted to vary. Improvement was noted, $R_1 = 0.120$ and $R_2 = 0.128$. A similar set of calculations were made, with anomalous-dispersion corrections included,[10] $R_1 = 0.120$ and $R_2 = 0.129$. The results of these refinements are given in Table I, rows *a* and *b*, and the values of some relevant bond angles and distances calculated[11] from the *b* rows are given in Table II. From the calculations, it may be seen that there were no significant differences between the results obtained with or without the inclusion of anomalous-dispersion corrections for the least-squares refinement of all of the data observed, with isotropic temperature factors and unit weights. The ratio of scale factors for corresponding zones in rows *a* and *b* varied from 1.035 to 1.045.

During the estimation of intensities, it had been observed that the more intense reflections, $|F_o| \gtrsim 325$, were difficult to read, even on the lightest films. Also, the reflection (113) was found to be partially in the shadow of the beam stop support. This reflection was discarded and the least-squares refinement of the atomic parameter and zonal scale factors for the 1080 reflections that remained was carried out with isotropic temperature factors and unit weights. The results are given in Table I in the *c* rows for which no corrections were made for anomalous dispersion and in the *d* rows for which corrections were made for anomalous dispersion. $R_1 = 0.108$ and $R_2 = 0.119$ and $R_1 = 0.109$ and $R_2 = 0.120$ for rows *c* and *d*, respectively. The ratio of corresponding zonal scale factors between rows *c* and *d* varied from 1.035 to 1.038. The scale factors were then fixed at the values obtained in the isotropic refinements in *c* and *d* rows of Table I and the anisotropic refinement of Bi and Br was carried out to give the results in rows *a* and *b* in Table III and in the last two columns of Table II; $R_1 = 0.079$, $R_2 = 0.090$, $R_1 =$

(7) W. G. Sly, D. P. Shoemaker, and J. H. Van den Hende, Two, and Three-Dimensional Crystallographic Fourier Summation Program for the IBM 7090 Computer, CBRL-22M-62, Massachusetts Institute of Technology, Esso Research and Engineering Co., 1962.

(8) Atomic scattering factors for Bi, Br, N, and C were taken from "International Tables for X-Ray Crystallography," Vol. III, Kynoch Press, 1962, pp 212, 206–207, 202–203.

(9) W. R. Busing, K. O. Martin, and H. A. Levy, "ORFLS, A FORTRAN Crystallographic Least-Squares Program," ORNL-TM-305, Oak Ridge National Laboratory, Oak Ridge, Tenn., 1962.

(10) "International Tables for X-Ray Crystallography," Vol. III, Kynoch Press, 1962, pp 214–216.

(11) W. R. Busing, K. O. Martin, and H. A. Levy, "ORFFE, A FORTRAN Crystallographic Function and Error Program," ORNL-TM-306, Oak Ridge National Laboratory, Oak Ridge, Tenn., 1964.

Table III: Atomic Coordinates of $[(CH_3)_2NH_2]_3BiBr_6$ Obtained in the Anisotropic Refinement (Standard Deviations Are Given in Parentheses and Apply to the Last Digit of a Number; Values of β_{ij} Listed Have Been Multiplied by 10^4)

		x	y	z	β_{11}	β_{22}	β_{33}	β_{12}	β_{13}	β_{23}
Bi(A)	*a*	0	0	0	16.6 (4)	16.6	139	8.3	0	0
	b	0	0	0	15.7 (4)	15.7	131	7.9	0	0
Bi(B)	*a*	1/6	1/3	1/3	14.0 (2)	12.9 (2)	132 (6)	6.4 (2)	0.8 (8)	0.5 (7)
	b	1/6	1/3	1/3	13.3 (2)	12.2 (2)	121 (6)	6.0 (2)	0.8 (8)	0.5 (7)
Br(A)	*a*	0.0852 (1)	0.0763 (1)	0.1868 (5)	20.1 (6)	20.3 (6)	175 (11)	10.1 (5)	−17.1 (18)	−13.2 (18)
	b	0.0852 (1)	0.0764 (1)	0.1867 (5)	20.7 (6)	20.9 (6)	190 (12)	10.4 (5)	−17.5 (18)	−13.4 (19)
Br(1)(B)	*a*	0.1487 (1)	0.2523 (1)	0.5478 (6)	25.2 (7)	21.6 (7)	270 (14)	13.9 (6)	12.1 (22)	30.3 (21)
	b	0.1487 (1)	0.2523 (1)	0.5480 (6)	25.8 (7)	22.3 (7)	284 (14)	14.2 (6)	12.4 (22)	30.9 (21)
Br(2)(B)	*a*	0.1434 (1)	0.2643 (1)	0.0673 (5)	22.2 (6)	20.4 (6)	160 (12)	10.8 (5)	−4.5 (18)	−17.8 (19)
	b	0.1434 (1)	0.2643 (1)	0.0673 (6)	22.8 (6)	21.0 (6)	172 (12)	11.1 (5)	−4.8 (19)	−18.0 (19)
Br(3)(B)	*a*	0.0579 (1)	0.3016 (1)	0.3614 (5)	13.3 (5)	24.0 (6)	194 (11)	9.1 (5)	1.5 (16)	−1.2 (19)
	b	0.0579 (1)	0.3016 (1)	0.3614 (5)	13.8 (5)	24.7 (7)	209 (12)	9.4 (5)	1.5 (16)	−1.1 (19)
C(1)(A)	*a*	0.021 (1)	0.140 (1)	0.417 (6)	26 (5)	26	230	13	0	0
	b	0.021 (1)	0.140 (1)	0.416 (6)	26 (5)	26	236	13	0	0
N(A)	*a*	0.036 (1)	0.158 (1)	0.253 (4)	25 (4)	25	227	13	0	0
	b	0.036 (1)	0.157 (1)	0.252 (4)	26 (4)	26	237	13	0	0
C(2)(A)	*a*	0.000 (2)	0.162 (2)	0.137 (5)	27 (5)	27	244	14	0	0
	b	0.000 (2)	0.162 (2)	0.137 (5)	28 (5)	28	253	14	0	0
C(1)(B)	*a*	0.431 (1)	0.124 (1)	0.102 (5)	26 (5)	26	232	13	0	0
	b	0.431 (1)	0.124 (1)	0.102 (5)	27 (5)	27	243	14	0	0
N(B)	*a*	0.376 (1)	0.118 (1)	0.104 (4)	26 (4)	26	237	13	0	0
	b	0.376 (1)	0.118 (1)	0.104 (4)	27 (4)	27	247	14	0	0
C(2)(B)	*a*	0.334 (2)	0.063 (2)	0.176 (6)	34 (7)	34	302	17	0	0
	b	0.334 (2)	0.063 (2)	0.176 (6)	35 (7)	35	317	18	0	0

[a] Unit weights, selected data ($|F_o| \lesssim 325$), uncorrected for ad. [b] Unit weights, selected data ($|F_o| \lesssim 325$), corrected for ad.

0.079, and $R_2 = 0.090$, respectively. The net result of these computations is to show that neither the inclusion of corrections for anomalous dispersion, the removal of intense reflections, nor the introduction of anisotropic temperature factors produces significant changes in bond distances or angles in this structure, although there is the expected apparent improvement in the estimated standard deviation that accompanies a reduction in R_2. The discussion will be based primarily upon the values given in rows *a* and *b* of Table I. A table of observed and calculated structure factors may be obtained from the authors upon request.

Discussion

Two crystallographically independent $Bi(III)Br_6$ octehedra and two crystallographically independent dimethylammonium groups are present in the structure. The Bi–Br bond distances given in Table III, in the *b* rows, vary from 2.822 to 2.852 Å, with an average value of 2.840 Å. The Br–Bi–Br bond angles (for Br atoms *cis* to one another in the octahedra) vary from 87.7 to 92.5°, and thus there appear to be small but significant angular distortions from the value of 90° expected for a regular octahedron. The octahedron around Bi(A) is flattened in the *c* direction. The mean C–N distance is 1.56 Å, and the mean C–N–C bond angle is 118°, with no significant deviations from these values. The van der Waals contacts are normal, greater than 3.6 Å, except for Br3(B) – C2(B) = 3.47 (9) Å. There are several short N···Br contacts: N(A)–Br(A) = 3.44(7) Å, N(A)–Br(2)(B) = 3.48 (7) Å, N(B)–Br(1)(B) = 3.49 (6) Å, and N(B)–Br(3)(B) = 3.44 (6) Å. The $(CH_3)_2NH_2$ group that contains N(A) links the two crystallographically different $Bi(III)Br_6$ octahedra together through N(A)–Br(A) and N(A)–Br(2)(B). The second $(CH_3)_2NH_2$ group is associated closely only with the octahedron centered on Bi(B) and is coupled to Br(1)(B), Br(3)(B), and less closely to Br2(B), with N(B)–Br2(B) = 3.65 (6) Å. The values of the van der Waals and N···Br contacts fluctuate considerably in the several refinements. Schematic diagrams of the structure are given in Figures 1 and 2.

The total BiBr bond order for a $Bi(III)Br_6$ octahedron was estimated as 2.7 from Pauling's equation[3] $d_n = d_1 - 0.6 \log n$, where $d_1 = 2.64$ Å and $d_n = 2.84$ Å (average). This is lower than the values estimated for the total BiBr bond order, 2.9, obtained from the $Bi(III)Br_4$ and $Bi(III)Br_5$ structures. If d_n were 2.81 Å, the bond order would be 3.0, so that the expansion of the octahedron here is quite small. The individual BiBr bond orders are 0.45. The expansion may be associated with the increased charge of the ion. The corrections for the Bi–Br bond distances for the "riding-motion" model[12] were calculated, for rows *a* and *b* of Table III, and varied between 0.01 and 0.02 Å. The coupling between octahedra through N(A), and with

(12) W. R. Busing and H. A. Levy, *Acta Crystallogr.*, 17, 142 (1964).

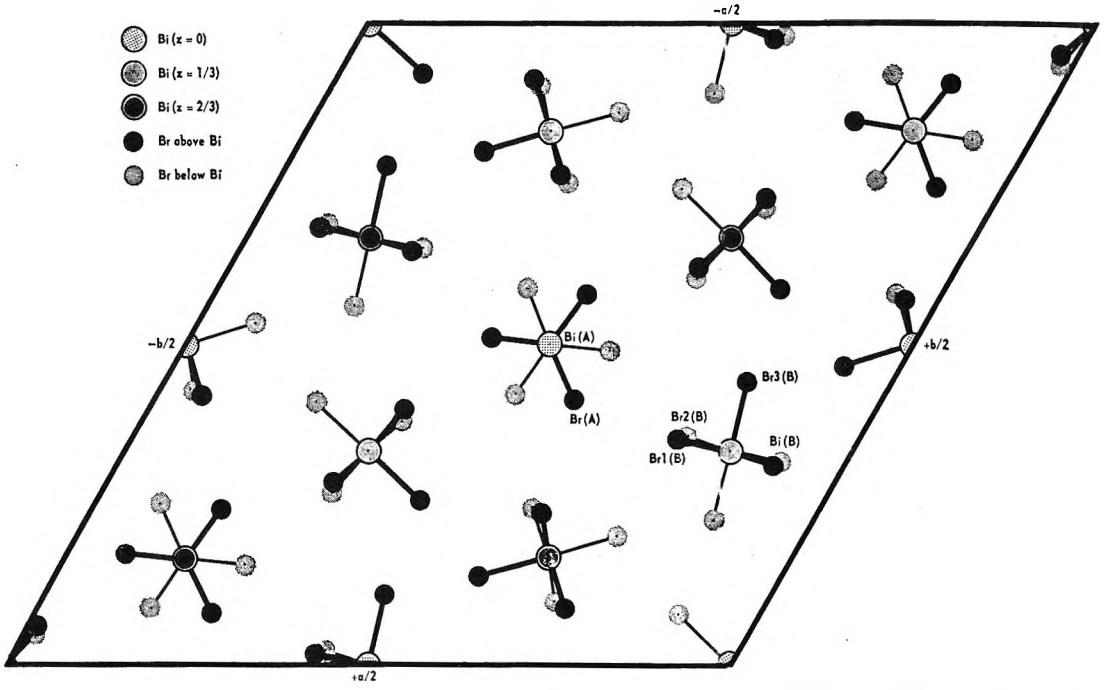

Figure 1. Projection of the structure of $((CH_3)_2NH_2)_3BiBr_6$ along (001): larger circles, Bi atoms; smaller circles, Br atoms.

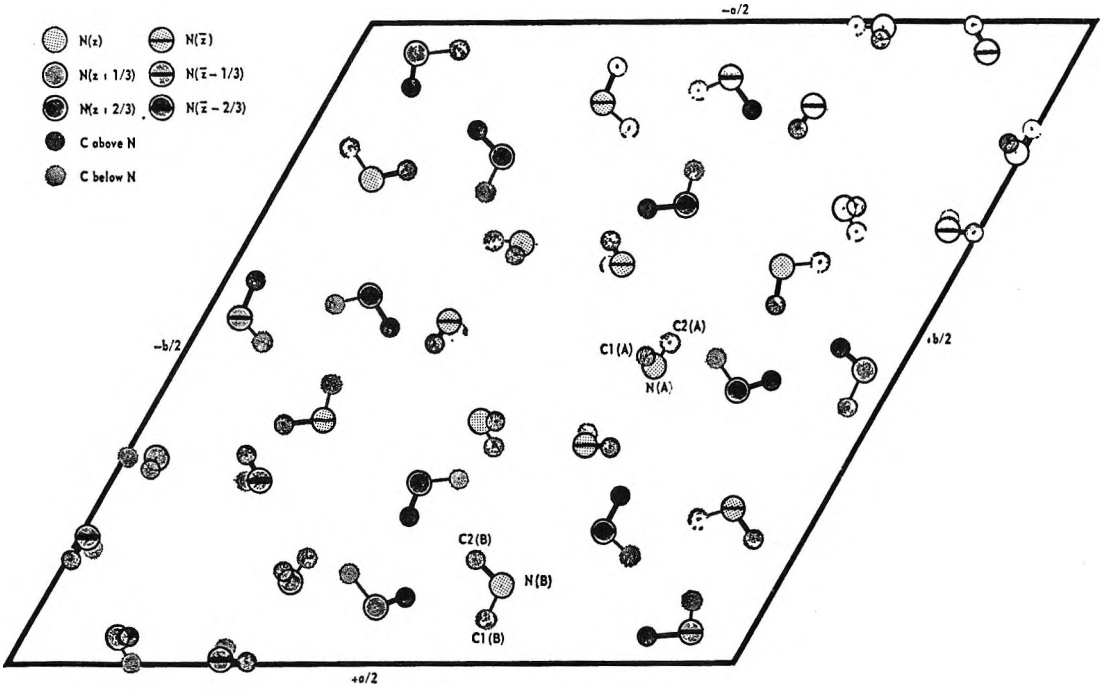

Figure 2. Projection of the structure of $((CH_3)_2NH_2)_3BiBr_6$ along (001): larger circles, N atoms; smaller circles, C atoms.

the N(B)-containing $(CH_3)_2NH_2$ group, makes the correction uncertain.

The angular distortions of the octahedra are small, but, on the basis of the estimated standard deviations (0.2–0.3°), appear to be real. In a recent study[13] of $(NH_4)_2SbBr_6$, it was found that the Sb(V)Br_6 octahedron was distorted, whereas the Sb(III)Br_6 group was undistorted. It may be that the group V halide anions are, in general, rather easily distorted and that the unsymmetrically charged organic units in the present structure are responsible for the distortions observed. It is also possible that a "lone-pair" effect upon coordination may be responsible for the distortion in Bi(III)Br_6.

Acknowledgments. The financial support of The

(13) S. L. Lawton and R. A. Jacobsen, *Inorg. Chem.*, 5, 743 (1966).

Robert A. Welch Foundation is gratefully acknowledged. The facilities of the Data Processing Center of the Texas A & M University System have been used extensively in this research. Dr. Roger D. Whealy has kindly supplied us with a sample of the compound studied.

Ionization Equilibria in Ammonia–Water Solutions to 700° and to 4000 Bars of Pressure[1]

by Arvin S. Quist and William L. Marshall

Reactor Chemistry Division, Oak Ridge National Laboratory, Oak Ridge, Tennessee 37830 *(Received December 6, 1967)*

The electrical conductances of 0.0100 and 0.0501 *m* aqueous ammonia solutions were measured to 800° and 4000 bars. Measurements are also reported for 0.0098 *m* NaOH solutions to 300°, together with estimates of Λ_0(NaOH) over the same temperature range. From the measurements on the ammonia solutions and estimates of the limiting equivalent conductances of ammonium hydroxide, conventional equilibrium constants for the hydrolysis of ammonia were calculated. From these values and their isothermal variation with the concentration of water, the complete constants, K^0, were obtained that are independent of changes in dielectric constant or in density.

Introduction

A convenient method for studying equilibria involving ions in aqueous electrolyte solutions at supercritical temperatures and pressures is the measurement of their electrical conductances. Equilibrium constants for ionic dissociation reactions have been calculated from measurements of this kind over wide ranges of temperature and density. Recent studies in our laboratory have included those of NaCl,[2a] NaBr,[2b] and HBr.[3] This present paper gives conductance measurements on 0.01 and 0.05 *m* solutions of ammonia to 700°. Measurements were also performed at 800°, but the conductances at this temperature were essentially zero even at 4000 bars. From these measurements and with estimates for the limiting equivalent conductance of $NH_4^+ + OH^-$ at several temperatures and densities, conventional equilibrium constants for the hydrolysis of ammonia were calculated to 700°.

The present paper also includes some measurements on 0.0098 *m* NaOH solutions to 300°. From these measurements, estimates were made of the limiting equivalent conductances of NaOH as a function of density to 300°. By using these limiting conductances along with assumptions based on the previously observed behavior of other strong electrolytes at high temperatures and pressures, estimates were made of the limiting equivalent conductance of NaOH to 800°.

Experimental Section

The equipment and procedures used for these measurements have been described previously.[2a] All conductance measurements were made with the cell containing no pressure seals in the high-temperature region. A stock solution of approximately 1 *m* ammonia was prepared from reagent grade ammonium hydroxide (J. T. Baker Chemical Co., Phillipsburg, N. J., 30% NH_3) and conductivity water. This stock solution was standardized, by using weight buret techniques, against potassium acid phthalate. From the stock solution, 0.0100 and 0.0501 *m* ammonia solutions were prepared and their conductances were measured to 800° and 4000 bars.

A 0.0098 *m* NaOH solution was prepared from a standard 1.0 *N* NaOH solution (Fisher Scientific Co., Fair Lawn, N. J.) and standardized in the same manner as described for the stock solution of ammonium hydroxide. Reliable measurements on the NaOH solution were obtained only at temperatures below 300°. At 400° and above, the solution concentration changed rapidly because of the reaction of NaOH with the Al_2O_3 insulation tube in the high-temperature region of the cell. Thorough flushing of the conductance cell was carried out at the temperature and pressure of the experiment, but even then reliable values of conductances could not be obtained above 300°.

(1) Research sponsored by the U. S. Atomic Energy Commission under contract with Union Carbide Corporation.

(2)(a) A. S. Quist and W. L. Marshall, *J. Phys. Chem.*, **72**, 684 (1968); (b) A. S. Quist and W. L. Marshall, *ibid.*, **72**, 2100 (1968).

(3) A. S. Quist and W. L. Marshall, *ibid.*, **72**, 1545 (1968).

Two different inner electrodes were used with the conductance cell. Their cell constants were 0.495 and 0.525 cm^{-1} as determined from measurements on 0.01 Demal KCl solutions at 25.00 ± 0.01°. Conductivity water obtained from a quartz still was used to prepare all solutions.

The experimental measurements on these alkaline solutions were not as accurate as those for the previous electrolytes.[2,3] Reaction with the Al_2O_3 tube, mentioned above, and pickup of CO_2 from the air in transferring these solutions from the stock bottle to the apparatus introduced errors not found in studying acidic or neutral solutions. Also, with the ammonia solutions the conductances were very low at high temperatures, and therefore the effects of ionic impurities became appreciable. Thus, although the measurements at low temperatures can be considered reliable to within approximately 2%, the uncertainty was much greater at high temperatures and low pressures.

Results and Discussion

Results. The measured conductances were converted to both specific and equivalent conductances by the methods described previously.[2a] Figures 1 and 2 show specific conductances of the ammonia solutions as a function of pressure at the temperatures of the experiments. Figure 3 presents isobaric specific conductances as a function of temperature for a 0.0100 *m* ammonia solution. The maxima in these curves near 150° and the subsequent sharp decrease with increasing temperature as compared with the behavior of NaCl[2a] and NaBr[2b] indicate that these solutions contain relatively few ions at high temperatures. Hydrolysis constants for ammonia were calculated and are presented in a later section of this paper.

Figure 4 gives isotherms of equivalent conductances as a function of density for the 0.0501 *m* ammonia solution. Again, comparison of these results with the NaCl and NaBr data[2] indicates that aqueous ammonia is an extremely weak electrolyte at high temperatures. Tables I and II contain smoothed values of the conductances of the ammonia solutions at integral temperatures and densities. The values in parentheses represent conductances at saturation vapor pressure at that temperature.

Figure 5 presents the results for the NaOH solutions, given as the specific conductance as a function of pressure at temperatures to 285°. From these measurements, NaOH appears to behave as a strong electrolyte at least to 300°. Equivalent conductances of 0.0098 *m* NaOH at integral temperatures and densities are given in Table III.

Estimation of the Limiting Equivalent Conductances of NH_4OH and NaOH to 800°. Limiting equivalent conductances for ammonium hydroxide could not be calculated from the experimental measurements. Since it is a very weak electrolyte, accurate measurements could not be made at low enough concentrations to permit reliable extrapolations of the conductances to infinite dilution. Therefore, the limiting equivalent conductances for ammonium hydroxide necessary for the calculation of ionization constants from the conductance measurements were obtained indirectly. Estimates of $\Lambda_0(NH_4OH)$ were calculated as described below and were based primarily on assumed similarities in the behavior of $\Lambda_0(NaOH)$ and $\Lambda_0(NH_4OH)$.

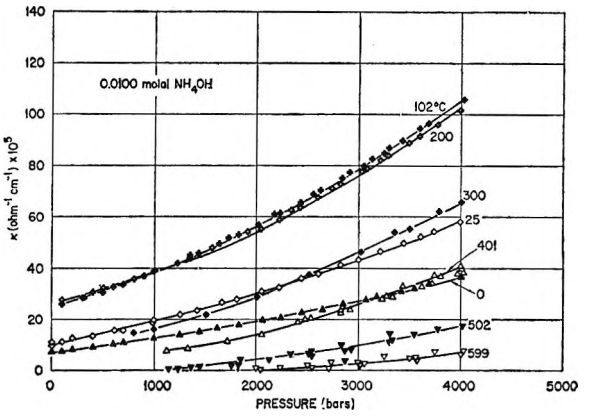

Figure 1. Specific conductances of 0.0100 *m* solutions of NH_4OH as a function of pressure at several temperatures.

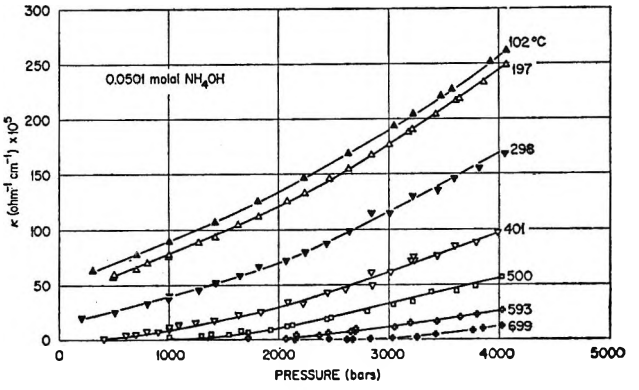

Figure 2. Specific conductances of 0.0501 *m* NH_4OH solutions as a function of pressure at several temperatures.

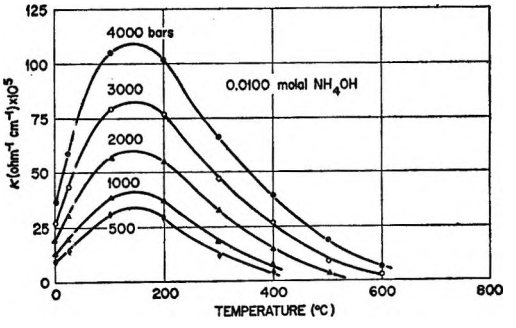

Figure 3. Isobaric variation of specific conductances of 0.0100 *m* NH_4OH solutions as a function of temperature. Pressures of 500 to 4000 bars.

Table I: The Equivalent Conductances (cm^2 ohm^{-1} $equiv^{-1}$) of 0.0100 *m* NH_4OH Solutions at Integral Temperatures and Densities

Temp, °C	Density, g cm^{-3}									
	0.70	0.75	0.80	0.85	0.90	0.95	1.00	1.05	1.10	1.15
0							7.1	13.0	22.5	36.0
25						(10.7)	11.0	21.5	39.7	
100						(25.0)	38.4	66.6	113	
150						...	56.0	...	...	
200					31.0	45.6	70.4			
250					33.6	52.0	78.8			
300			17.0	23.0	36.4	56.0	83.0			
350			18.4	26.0	39.2					
400	10.0	13.0	18.8	28.8	42.0					
450	8.0	11.0	17.5							
500	6.0	9.0	15.0							
550	...	7.0								
600	...	6.0								

Table II: The Equivalent Conductances (cm^1 ohm^{-1} $equiv^{-2}$) of 0.0501 *m* NH_4OH Solutions at Integral Temperatures and Densities

Temp, °C	Density, g cm^{-3}												
	0.50	0.55	0.60	0.65	0.70	0.75	0.80	0.85	0.90	0.95	1.00	1.05	1.10
100										(11.2)	17.5	32	56
150										...	25.5	45	
200								(9.9)	13.1	20.3	32.0	58	
250									15.3	24.3	37.2		
300						5.4	7.7	11.2	17.4	27.6	41.7		
350						5.4	8.0	12.3	19.5				
400	0.2	0.7	1.2	2.0	3.1	5.4	8.2	13.5	21.2				
450	0.2	0.7	1.1	1.9	3.1	5.4	8.6	14.5					
500	0.2	0.7	1.0	1.8	3.0	5.4	8.8	15.5					
550	...	...	0.8	1.6	3.0	5.4	9.0						
600	...	...	0.6	1.5	3.0	5.4	9.4						
650	...	...	0.5	1.4	2.9								
700	...	...	0.4	1.2	2.8								

Table III: The Equivalent Conductances of 0.0098 *m* NaOH Solutions at Integral Temperatures and Densities

Temp, °C	Density, g cm^{-3}									
	0.70	0.75	0.80	0.85	0.90	0.95	1.00	1.05	1.10	1.15
0							134	144	142	134
25						(236)	236	239	235	
100						(563)	563	557	547	
200				(908)	904	890	872			
300	(1100)	1090	1085	1074	1060	1050	1040			

Wright, Lindsay, and Druga[4] reevaluated the conductance measurements of Noyes[5] on aqueous NaOH solutions to 218° and obtained limiting equivalent conductances at saturated vapor pressures. These Λ_0 values were later extrapolated to 300°.[6] Estimates of limiting conductances of NaOH from our present data to 300° were obtained by solving the Onsager conductance equation[7]

$$\Lambda = \Lambda_0 - (\alpha\Lambda_0 + \beta)\sqrt{C} \qquad (1)$$

for Λ_0, using the measured equivalent conductance of 0.0098 *m* NaOH. Values for α and β were calculated at each temperature and density from reported dielectric constants[8] and viscosities[9,10] of water. These esti-

(4) J. M. Wright, W. T. Lindsay, Jr., and T. R. Druga, Report No. WAPD-TM-204, Bettis Atomic Power Laboratory, Westinghouse Electric Corp., Pittsburgh, Pa., June 1961.

(5) A. A. Noyes, *et al.*, Publication No. 63, Carnegie Institution of Washington, Washington, D. C., 1907.

(6) A. S. Quist and W. L. Marshall, *J. Phys. Chem.*, 69, 2984 (1965).

(7) L. Onsager, *Physik. Z.*, 28, 277 (1927).

(8) A. S. Quist and W. L. Marshall, *J. Phys. Chem.*, 69, 3165 (1965).

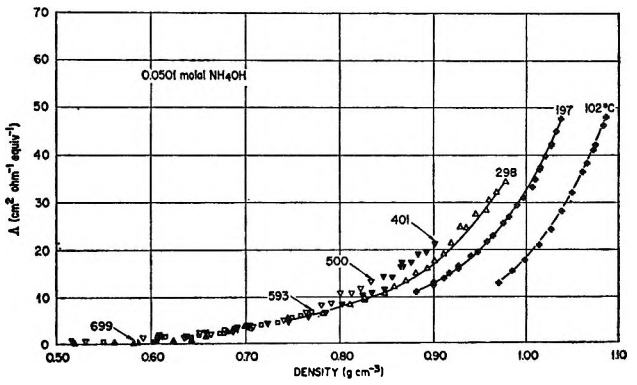

Figure 4. Equivalent conductances of 0.0501 *m* NH_4OH solutions as a function of density at several temperatures.

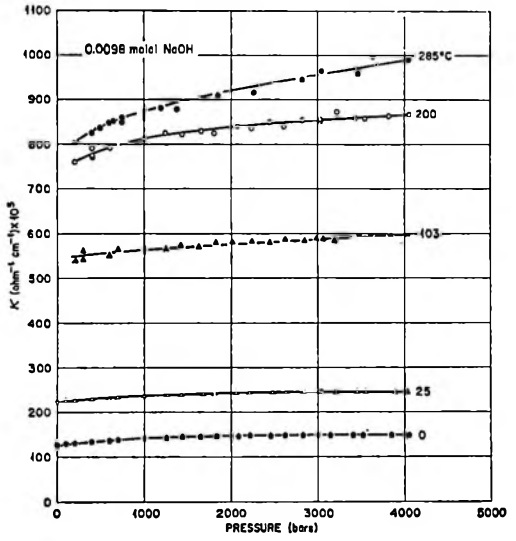

Figure 5. Specific conductances of 0.0098 *m* NaOH solutions as a function of pressure at several temperatures.

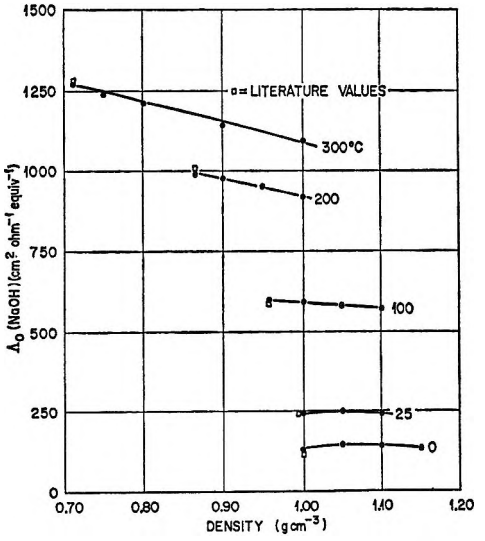

Figure 6. Limiting equivalent conductances of NaOH as a function of density at temperatures from 0 to 300°.

mated limiting equivalent conductances are shown in Figure 6 as a function of solvent density. The values at saturation vapor pressure agree very well with the previously reported values,[6] except at 0° where the present values are approximately 7% higher.

The linear relationship between limiting equivalent conductance and density shown in Figure 6 at 100–300° for NaOH has been observed previously at temperatures from 100 to 800° for $KHSO_4$,[11] NaCl,[2a] NaBr,[2b] and HBr.[3] Moreover, at temperatures above 400°, the limiting equivalent conductances for several electrolytes[2,11] have been observed to be independent of temperature at constant density. In these instances, the slope of the line (Λ_0 *vs.* density) was the same at 400° as at 300°. Therefore, by assuming that NaOH behaves like the previously reported electrolytes, by using the slope of the 300° isotherm from Figure 6, and by using an estimated Λ_0(NaOH) at 400° at a particular density, an equation can be written that will give a value for Λ_0(NaOH) at all densities at 400° and above. When log Λ_0(NaOH) values at a density of 0.8 and 0.9 g cm^{-3} were plotted against $T(°K)^{-1}$ at temperatures to 300° and then extrapolated to 400° in a manner consistent with the observed behavior of NaCl to 400°,[2a] values of Λ_0(NaOH) of 1260 and 1205 were obtained at 400°, 0.8 and 0.9 g cm^{-3}, respectively. With these values, together with the relationship of Λ_0 *vs.* density observed at 300° (Figure 6), the following equation was obtained to represent the limiting equivalent conductance of NaOH at 400° and above

$$\Lambda_0(\text{NaOH}) = 1770 - 630d \qquad (2)$$

where d is the density of the solution.

Limiting equivalent conductances for NH_4OH to 300° were estimated by assuming that the relationship between $\Lambda_0(NH_4OH)$ and solvent density would be the same as that observed for Λ_0(NaOH). From the slopes of the lines for Λ_0(NaOH) *vs.* density at 0–300° shown in Figure 6 and the Λ_0's for NH_4OH at saturation vapor pressure at these same temperatures,[6] values of $\Lambda_0(NH_4OH)$ were calculated and are presented in Table IV. Limiting equivalent conductances at 150, 250, and 350° were obtained by interpolation and extrapolation of plots of log Λ_0 *vs.* $T(°K)^{-1}$ (at constant density). Estimates for limiting equivalent conductances of ammonium hydroxide from 400 to 800° are given by the equation

$$\Lambda_0(NH_4OH) = 1910 - 630d \qquad (3)$$

which was obtained by a procedure similar to that used in calculating the corresponding equation for NaOH (eq 2).

(9) K. H. Dudziak and E. U. Franck, *Ber. Bunsenges. Phys. Chem.*, **70**, 1120 (1966).

(10) K. E. Bett and J. B. Cappi, *Nature*, **207**, 620 (1965).

(11) A. S. Quist and W. L. Marshall, *J. Phys. Chem.*, **70**, 3714 (1966).

Table IV: Estimates of the Limiting Equivalent Conductances of NH_4OH to 350°

Temp, °C	Density, g cm^{-3}									
	0.70	0.75	0.80	0.85	0.90	0.95	1.00	1.05	1.10	1.15
0							145	155	153	144
25						(272)	272	275	270	
100						(653)	648	640	632	
150						865	835	805		
200				(1095)	1075	1045	1015			
250					1200	1165	1140			
300	(1400)	1375	1345	1310	1280	1250	1220			
350		1420	1385	1355	1325	1290	1260			

Table V: Negative Logarithm of the Conventional Equilibrium Constant, K, for the Hydrolysis of Ammonia in Water $[NH_3(H_2O) \rightleftharpoons NH_4^+ + OH^-]$[a]

Temp, °C	Density, g cm^{-3}													
	0.50	0.55	0.60	0.65	0.70	0.75	0.80	0.85	0.90	0.95	1.00	1.05	1.10	1.15
0											4.60	4.10	3.55	3.05
25										(4.80)	4.80	4.15	3.55	
100										(4.85)	4.45	3.90	3.35	
150											4.35	3.80		
200								(5.45)	5.20	4.75	4.30	3.75		
250									5.15	4.70	4.30			
300						6.25	5.90	5.55	5.10	4.65	4.25			
350						6.30	5.90	5.50	5.05					
400	9.4	8.3	7.75	7.25	6.75	6.30	5.90	5.40	5.00					
450	9.4	8.3	7.80	7.30	6.80	6.30	5.85	5.35						
500	9.4	8.3	7.90	7.35	6.85	6.35	5.85	5.30						
550	...	...	8.10	7.45	6.85	6.35	5.80							
600	...	...	8.35	7.50	6.85	6.35	5.75							
650	...	...	8.50	7.55	6.90									
700	...	...	8.70	7.70	6.90									

[a] The standard state is the hypothetical 1 M solution.

Calculation of the Hydrolysis Constants for Aqueous Ammonia to 800°. The hydrolysis of aqueous ammonia can be represented by the equations

$$NH_3(H_2O)_j + kH_2O \rightleftharpoons NH_4(H_2O)_m^+ + OH(H_2O)_n^- \quad (4a)$$

$$K^0 = \frac{a_{NH_4(H_2O)_m^+} a_{OH(H_2O)_n^-}}{a_{NH_3(H_2O)_j} a_{H_2O}^{\,k}} \quad (4b)$$

$$K^0 = K/a_{H_2O}^{\,k} \quad (4c)$$

$$\log K = \log K^0 + k \log a_{H_2O} \quad (4d)$$

where K^0 is the complete equilibrium constant, including waters of hydration, and is independent of changes in dielectric constant or in density,[12,13] K is the conventional equilibrium constant, a represents activity, and j, m, and n are hydration numbers. The conventional constant can be calculated from the experimental data by the equations

$$K = \frac{\theta^2 C_0}{1 - \theta} f_\pm^2 \quad (5)$$

$$\theta = \frac{\Lambda}{\Lambda_0} S(z) \quad (6)$$

where θ is the fraction ionized, C_0 is the stoichiometric NH_3 molarity, $S(z)$ is a function defined by Shedlovsky[14] that is based on an empirical extension to the Onsager limiting-conductance equation, and $f_\pm$ is the mean molar activity coefficient of NH_4^+ and OH^- calculated by the equation

$$\log f_\pm = \frac{-AI^{1/2}}{1 + I^{1/2}} \quad (7)$$

In eq 7, A is the theoretical Debye–Hückel limiting slope for a 1:1 electrolyte and I is the ionic strength calculated from the equation

$$I = \theta C_0 \quad (8)$$

(12) W. L. Marshall and A. S. Quist, *Proc. Nat. Acad. Sci.*, **58**, 901 (1967).

(13) A. S. Quist and W. L. Marshall, *J. Phys. Chem.*, **72**, 1536 (1968).

(14) T. Shedlovsky, *J. Franklin Inst.*, **225**, 739 (1938).

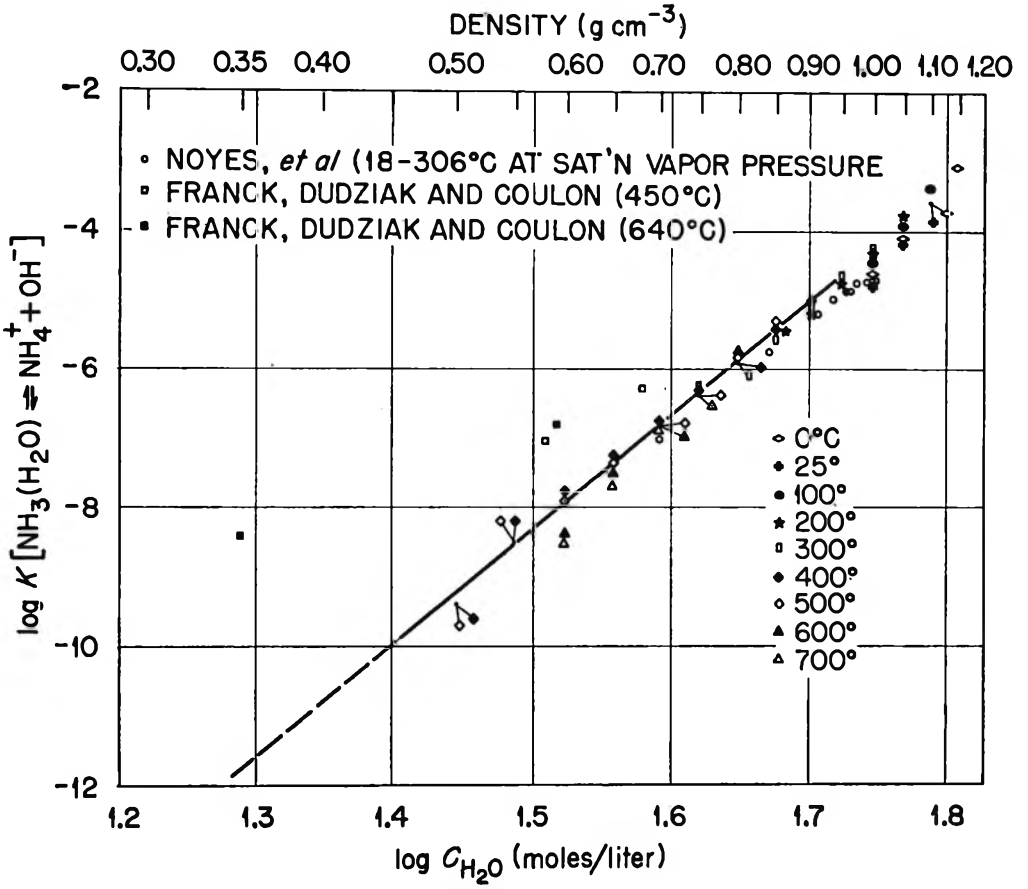

Figure 7. Log K(molar units) for the equilibrium $NH_3(H_2O) \rightleftharpoons NH_4^+ + OH^-$ as a function of the logarithm of the molar concentration of water at temperatures from 0 to 700°.

In order to obtain the best value of K when it was calculated from more than one concentration of NH_4OH, the above equations were used in the form[14]

$$\frac{1}{\Lambda S(z)} = \frac{1}{\Lambda_0} + \frac{C_0 \Lambda S(z) f_\pm^2}{K \Lambda_0^2}$$

A nonlinear least-squares method[15] was used to fit the data to the above equation. Values of the negative logarithm of the conventional equilibrium constant for the hydrolysis of ammonia calculated from the equivalent conductances in Tables I–II (and by using the $\Lambda_0(NH_4OH)$ values from Table IV and eq 3) are given in Table V. Since the $\Lambda_0(NH_4OH)$ values are estimates, it is of interest to consider the effect of a change in Λ_0 upon the calculated K. In general, it was found that a 10% decrease in Λ_0 caused approximately a 20% increase in K.

If the activity of water in eq 4d is taken to be equal to its molar concentration,[12,13] then isothermal plots of log K *vs.* log C_{H_2O} (where C_{H_2O} is the molar concentration of water) might give straight lines with slope k. This behavior is observed generally, as shown in Figure 7. The slopes of the isotherms decrease with increasing temperature, but seem to reach a constant value near 16–17 between 400 and 500°. Values of k of 31, 29, 25, 21, and 18 were obtained for temperatures of 0, 25, 100, 200, and 300°, respectively. Previously, NaCl was found to have a constant value of k equal to 10.2 from 400 to 800°.[2a] For HBr this value of k increased from 12 to 16 with increasing temperature from 400 to 800°.[3]

By using a constant value of $k = 16.5$, values of the logarithm of the complete constant $K°$ were calculated to be −34.0, −33.0, −32.9, and −33.1 at temperatures of 400, 500, 600, and 700°, respectively. These results indicate that $\Delta E_v°$ approaches zero at temperatures above 400°.

Plots of the conventional log K *vs.* $T(°K)^{-1}$ at several constant densities are given in Figure 8. The slopes of these lines give some graphic indications of the behavior of $\Delta E_v°$ for the complete equilibrium over a wide range of temperature. Thus at low temperatures $\Delta E_v°$ will be positive and appears to approach the value of zero at high temperatures. The sharp decrease in log K above 500° at densities of 0.65 and 0.60 g cm^{-3} is believed not to be real but only gives an indication of the uncertainty in the values of K at high temperatures and low den-

(15) M. H. Lietzke, United States Atomic Energy Commission Report ORNL-3259, Oak Ridge National Laboratories, Oak Ridge, Tenn., 1962.

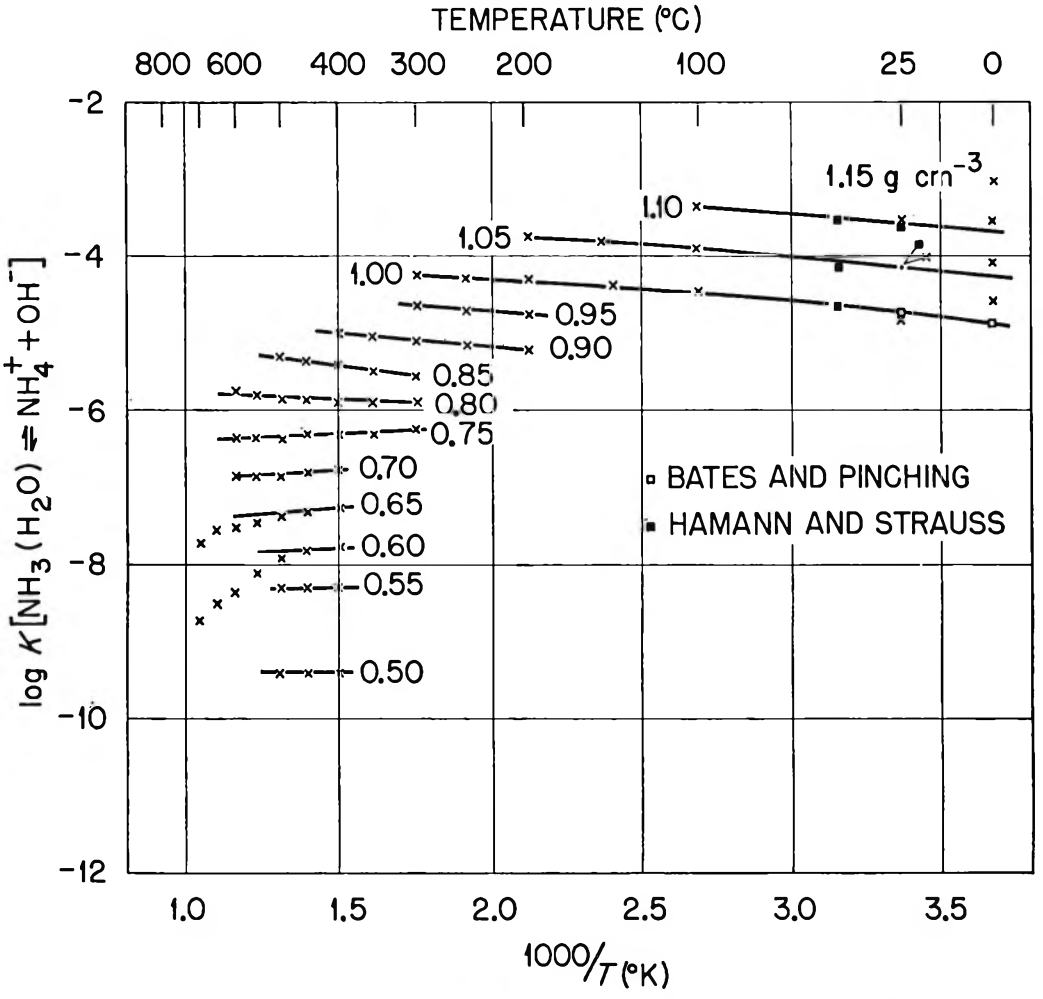

Figure 8. Log K(molar units) for the equilibrium $NH_3(H_2O) \rightleftharpoons NH_4^+ + OH^-$ as a function of $T(°K)^{-1}$ at solvent densities from 0.50 to 1.15 g cm^{-3}.

sities. It should be noted that in the region (0–400°) where k changes with temperature, $K°$ does not represent precisely the same equilibrium at each temperature.[3]

Previous determinations of the ionization constant of ammonium hydroxide include the results of Bates and Pinching[16] from 0 to 50° at 1 atm by an emf method. Our value of −4.80 for log K at 25°, 1 atm, agrees well with their value of −4.751, but our value of −4.60 at 0°, 1 atm, is considerably higher than the Bates and Pinching value of −4.862. The comparative results are included in Figure 8 and indicate that our own value at 0° may not be reliable. This graph also contains a comparison of our results with those reported by Hamann and Strauss[17] at 25 and 45° at pressures to 12,000 atm; both results are in good agreement. The present results may also be compared in Figure 7 with values estimated previously by Franck[18,19] to 640°. Figure 7 also includes the values obtained by Noyes[5] to 306° at saturation vapor pressure. Our results appear to be in very good agreement with the earlier work of Noyes.

Acknowledgment. The technical assistance of Wiley Jennings in making the conductance measurements is gratefully acknowledged.

(16) R. G. Bates and G. D. Pinching, *J. Amer. Chem. Soc.*, **72**, 1393 (1950).

(17) S. D. Hamann and W. Strauss, *Trans. Faraday Soc.*, **51**, 1684 (1955).

(18) E. U. Franck, *Angew. Chem.*, **73**, 309 (1961).

(19) E. U. Franck, K. H. Dudziak, and G. Coulon, *Abstr. Int. Congr. Pure Appl. Chem., 18th, Montreal*, 94 (1961).

Continuum Emission from Xenon in the Vapor Phase Induced by Absorption of 1470-Å Radiation

by L. Wayne Sieck

Radiation Chemistry Section, National Bureau of Standards, Washington, D. C. 20234 *(Received December 14, 1967)*

When xenon is exposed to a source of its own lowest energy resonance radiation (1470 Å) in the vapor phase, a symmetric continuum is observed in emission which exhibits a maximum at approximately 1715 Å. The addition of excess krypton to low pressures of xenon increases the continuum intensity substantially, and the "quenching" effects of other additives which are transparent to the resonance radiation are also reported.

Introduction

The origin and characteristics of the vacuum ultraviolet continua observed in emission when the heavier rare gases are exposed to electron bombardment at elevated pressures have been the subject of continuing study in several laboratories.[1,2] These luminescence features have been ascribed to radiative transitions in excited rare gas molecules generated by a molecular ion–electron combination ($A_2^+ + e \rightarrow A_2^*$) and mechanisms of the type $A^* + nA \rightarrow A_2^* + (n-1)A$, where A^* is a metastable rare gas atom formed directly by electron impact or following collisions of atoms excited to resonance levels. However, since the usual optical-selection rules for electronic excitation are not applicable in electron impact, the direct or indirect role of excited resonance levels in generating this luminescence is difficult to establish unambiguously. In the present study, selective excitation of a resonance level was achieved by exposing xenon to a source of its resonance radiation (1470 Å, 8.4 eV). This method, which has not been reported previously in a luminescence study, uniquely defines the starting material, and any resulting continua can be traced to the subsequent interactions of atoms initially excited to the $5p^5(^2P_{1/2})6s$ $[I_{1/2}]_1^0$ level.

Experimental Section

The apparatus consisted of three components: (1) a 1470-Å xenon lamp, (2) a spherical photolysis vessel, and (3) a vacuum uv monochromator.[3] All components were coaxially aligned such that the output of the lamp was directed through the vessel (the total path length was 26 cm) directly onto the entrance slit of the monochromator (the slit width was 200–500 μ). Transmitted resonance radiation as well as any emission situated in the wavelength region 1100–5500 Å was monitored by operating the monochromator as a scanning spectrograph. The amplified signal from the photomultiplier was displayed directly on a chart recorder. The xenon microwave-powered discharge lamp, which was fitted with a lithium fluoride window (12 mm in diameter), was of the general type described previously[4] and provided a flux of approximately 10^{15} quanta/sec at 1470 Å. A second lithium fluoride window (8 mm in diameter) was also attached to the photolysis vessel at the point of connection to the entrance-slit housing of the monochromator.

Volatile impurities were removed from xenon (Airco assayed reagent) by outgassing at −196° and trap-to-trap distillation *in vacuo*. Filling of the photolysis vessel was carried out by volatilization from a reservoir of previously condensed xenon which was slowly warmed from liquid nitrogen temperatures. Methane-d_4 was purified by gas chromatography. Airco assayed reagent grade H_2, N_2, and krypton were used without further purification, except for passage through a cold trap maintained at −196° prior to usage. A cold finger attached to the photolysis vessel was also maintained at −78° in all experiments.

Results

Absorption of Incident 1470-Å Radiation. The 1470-Å light source was operated at two different pressures during the course of these experiments. For convenience, the operating pressures will subsequently be distinguished by the following notation: lamp I (70 μ) and lamp II (700 μ). Figure 1 indicates the transmitted 1470-Å intensity as a function of xenon pressure in the photolysis vessel. The transmission curve for lamp I may be clearly resolved into two components. The rapid decrease at low cell pressures, indicated by curve A (lamp I), appears to be a composite associated with the absorption of true resonance radiation and slightly shifted fringe components. The other distinct component, curve B (lamp I), which exhibits essentially the same slope as the transmission

(1) P. G. Wilkinson, *Can. J. Phys.*, **45**, 1715 (1967).

(2) R. Turner, *Phys. Rev.*, **158**, 121 (1967).

(3) For a description of the monochromator, see H. Okabe, *J. Chem. Phys.*, **47**, 101 (1967).

(4) See, for example, J. R. McNesby and H. Okabe, *Advan. Photochem.*, **3**, 6 (1964).

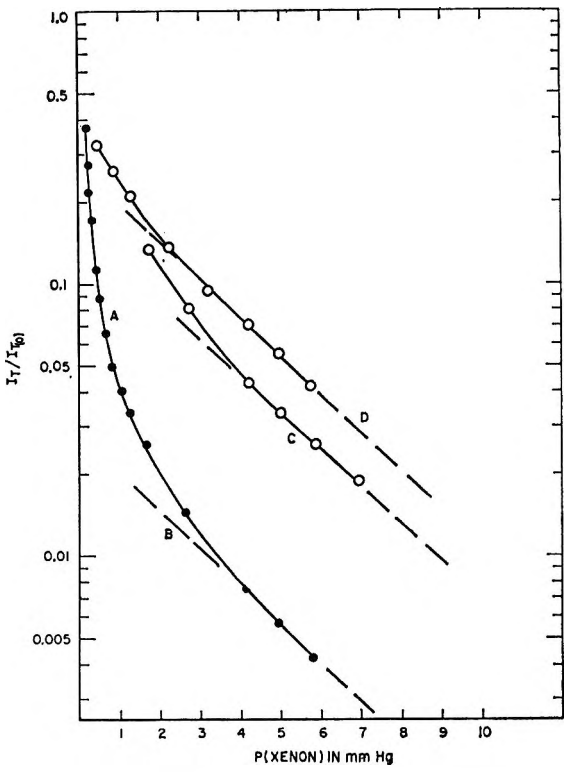

Figure 1. Typical transmission curves for 1470-Å radiation through xenon for the two lamps. Data plotted *vs.* xenon pressure, where I_{T_0} denotes the transmitted intensity obtained when the cell was evacuated. Curves A and B were obtained for lamp I (70 μ), while curves C and D were obtained for lamp II (700 μ). Curve C reflects transmission properties when the discharge region is close to the window when compared with curve D.

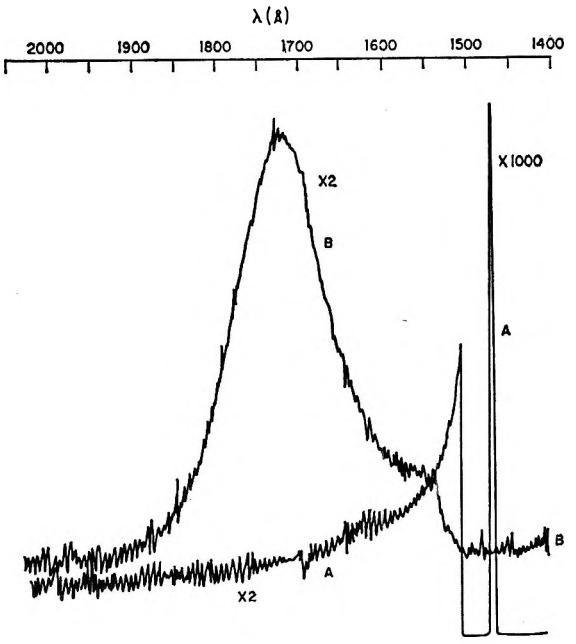

Figure 2. Typical photomultiplier tracing of the continuum emission from xenon. Tracing A indicates the signal obtained with the cell evacuated. Tracing B indicates the signal obtained when the vessel was filled with xenon at a pressure of 150 mm using lamp II. (Note the change of the scale during the scan.)

curves indicated for lamp II, reflects absorption of radiation exhibiting significant wavelength shifts due to Holtsmark broadening. The fact that absorption is much more efficient at low lamp pressures is not surprising, since less reversal of true resonance radiation and less line broadening would be anticipated under these conditions. At a constant lamp pressure, the intercept obtained following extrapolation of the absorption curve due to fringe radiation (curves B–D) to zero cell pressure was found to depend somewhat on the path length between the discharge region and the window of the lamp. The net effect of decreasing this distance was to increase the apparent absorption coefficient of xenon.

Luminescence from Xenon; Production of Continua. As the pressure of xenon was increased in the photolysis vessel, a continuum appeared in emission which exhibited a maximum at approximately 1715 Å. Figure 2 contains a reproduction of a typical photomultiplier tracing (B) of this system obtained at a pressure of 150 mm with lamp II. For comparison, the intensity of the 1470-Å radiation transmitted through the evacuated vessel is also included (A). Increasing the instrument resolution to 2.5 Å (half-width for an atomic line) failed to reveal any structure, and no other emission features were detected in the wavelength region 1450–5500 Å at any pressure. The general contour of the continuum and the position of the maximum was found to be independent of the pressure of both xenon in the cell and in the 1470-Å lamps. The shoulder at approximately 1500 Å (curve B) is transmitted fringe radiation from the lamp which was not being absorbed in the cell. As expected, the shoulder was relatively more intense when the xenon lamp was operated at 700 μ, since broadening of atomic resonance radiation was more pronounced. The intensity of this virtual component of the continuum decreased exponentially with cell pressure, and the apparent maximum was also shifted to longer wavelengths. The wavelength shift and the concurrent decrease in intensity was due to absorption of this incident fringe radiation by xenon dimers of the type reported by McLennan, *et al.*, as early as 1933.[5]

The effect of cell pressure on the continuum intensity is indicated in Figure 3 for lamps I and II. The increase in intensity was found to be second order below ~40 torr (see the insert in Figure 3). As the pressure was increased further, the intensity increased more or less linearly and approached a high-pressure asymptote.

It was also found that extrapolation of the linear segment of an intensity *vs.* pressure plot did not pass through the origin but gave a slight positive inter-

(5) J. C. McLennan and R. Turnball, *Proc. Roy. Soc.*, **A139**, 683 (1933).

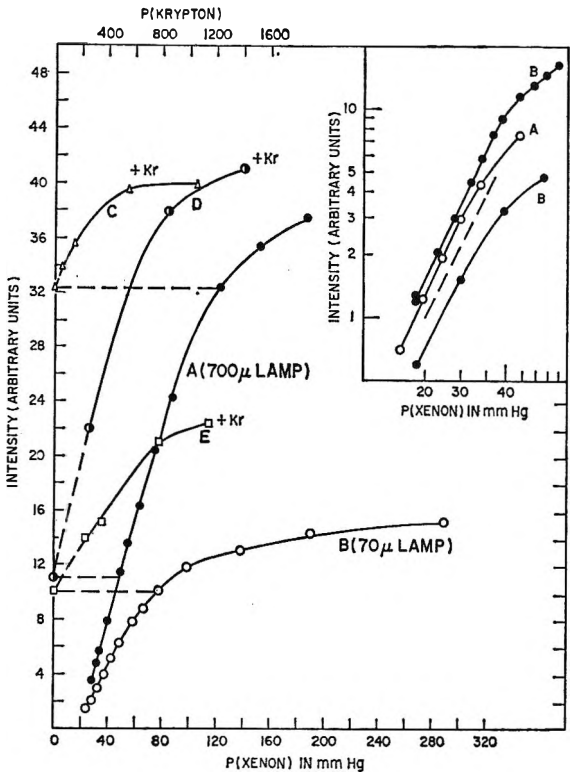

Figure 3. Effect of xenon pressure and added krypton on the continuum intensity: curve A, effect of xenon pressure using lamp II; curve B, intensity obtained with lamp I; curve C, intensity obtained when krypton was added to a constant pressure (120 mm) of xenon using lamp II; curve D, intensity observed when krypton was added to 50 mm of xenon using lamp II; curve E, intensity observed when krypton was added to 80 mm of xenon using lamp I. All intensities were normalized to a constant value for the incident flux of a 1470-Å radiation. The insert is the log–log plot of typical data obtained in the low-pressure region for pure xenon: curve A, lamp II; curves B, lamp I. Dotted line drawn with a slope of 2.0. Intensities are integrated values taken over the entire continuum range.

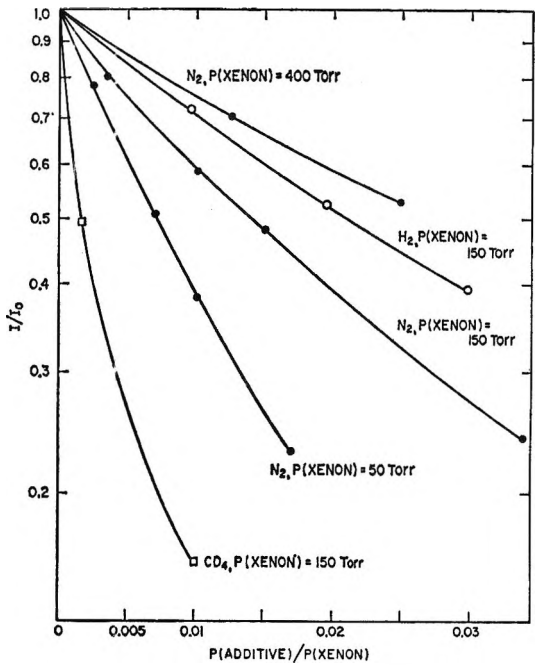

Figure 4. Effect of added N_2, H_2, and CD_4 on the continuum intensity at constant pressures of xenon. Data plotted as I/I_0 *vs.* additive concentration, where I/I_0 is the intensity observed in the presence of the additive divided by the intensity observed from pure xenon at that pressure of xenon. Intensities are integrated values taken over the entire continuum range.

cept on the P axis, which varied depending on the lamp used and the discharge conditions. This result was not surprising, in view of the transmission curves shown in Figure 1. At $P > 150$ torr, the emission level was relatively constant over a wide range, although a gradual decrease was observed at pressures greater than 400–500 torr. The luminescence efficiency, when defined as the number of counted photons at 1715 Å divided by the number of 1470-Å photons transmitted through the evacuated cell, was approximately a factor of 2 higher when lamp II was used.

Effect of Additives on the Continuum Intensity. The effect of added CD_4, N_2, and H_2 on the intensity of the continuum was determined at a constant xenon pressure of 150 torr using lamp II. These data are shown in Figure 4. Also included are data obtained with added N_2 at xenon pressures of 50 and 400 torr. The additives (with the exception of CD_4, which exhibited an extinction coefficient approximately 0.1 atm^{-1} cm^{-1} at 1470 Å) were found to be transparent in the wavelength region 5500–1450 Å, and no new emission features were found in any of the mixtures investigated. The continuum intensities obtained for Xe–CD_4 mixtures were found to be dependent upon the time lapse between the introduction of CD_4 and the measurement of the luminescence intensity. This effect can be attributed to modification of the over-all mechanism by accumulated decomposition products of CD_4.

A variation in slit width did not affect the observed percentage decrease in the continuum emission in any mixture, as long as the comparison was made with pure xenon at the same setting.

When excess krypton was added to a constant low pressure of xenon, the intensity of the 1715-Å continuum increased substantially. Typical data obtained with lamps are given in Figure 3. When lamp II was used, the luminescence intensity obtained when 600–900 torr was added to 120 torr of xenon (curve C) was essentially equal to that measured when the vessel was charged with 300–400 torr of pure xenon (curve A). More krypton was required to reach this maximum value when the partial pressure of xenon was maintained at 50 mm (curve D). One set of data taken with lamp I is indicated by curve E in Figure 3. In this case the limiting high-pressure intensity was substantially higher than the maximum level obtained from the photolysis of pure xenon. The contour of the

1715-Å continuum was insensitive to introduction of krypton in all experiments, and no new continua were detected in these mixtures at any wavelength in the region 1400–5500 Å.

When a considerable excess was introduced, however, the shoulder on the continuum (which, in the absence of krypton, was simply transmitted fringe radiation from the lamp) appeared to increase substantially and a new feature with the same contour but degraded to shorter wavelengths was detected at approximately 1450 Å. This continuous system, which was a true emission feature, is attributed to Lorentzian broadening of trapped xenon resonance radiation rather than the formation of bound upper states of XeKr*.

As mentioned earlier, no new emission features were detected in mixtures of xenon with N_2, H_2, and CD_4. It is, however, very difficult to establish conclusively whether or not the presence of 1–3 mol % of these additives modifies the bulk absorption characteristics of xenon at pressures greater than 30 torr. Typical photomultiplier tracings obtained from Xe–N_2 mixtures in the wavelength region 1450–1700 Å are given in Figure 5. The curve indicated by the notation "vacuum" indicates the contour of the transmitted fringe radiation associated with the 1470-Å source obtained with the cell evacuated. When xenon was admitted at a pressure of 150 torr, curve B (containing component A) was obtained. The effect of adding increasing amounts of N_2 to 150 torr of xenon is indicated by curves C–E. All of these curves share a common, superimposable portion indicated by A. The dotted line, which was not obtained experimentally, gives an approximate indication of the intensity distribution which one might expect to obtain when the continuum is completely quenched (infinite dilution with N_2). It follows that xenon was itself absorbing that portion of the monitored signal indicated by the shaded area at a pressure of 150 torr and was, in fact, actually absorbing a small fraction of its own continuum radiation in the wavelength region 1500–1600 Å. However, in all of the xenon-additive mixtures investigated, that portion of the monitored signal indicated by curve A was exactly superimposable, indicating that the presence of N_2, H_2, and CD_4 in relatively small amounts did not affect the bulk absorption characteristics of xenon.

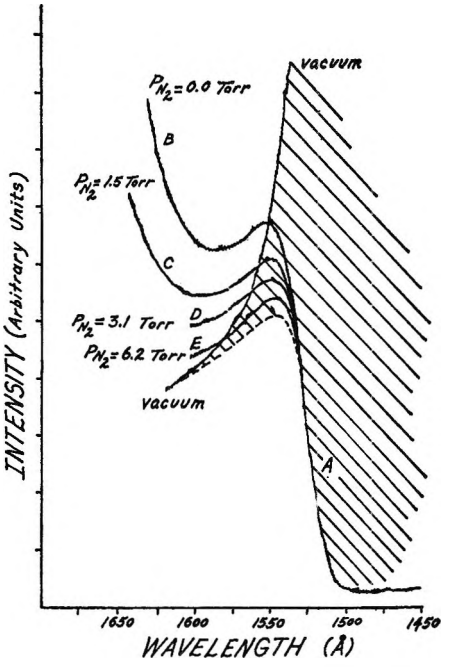

Figure 5. Typical photomultiplier tracings obtained for xenon and xenon–nitrogen mixtures. The xenon pressure was 150 torr. All curves were obtained at a constant incident flux of 1470-Å radiation, with the resolution equivalent to a 1.5-Å half-width for an atomic line.

Discussion

Effect of Pressure. In order to discuss the data, the following general formalization must be considered

$$Xe(^1S_0) + h\nu\ (1470\ Å) \longrightarrow Xe(^3P_1) \quad (1)$$

$$Xe(^3P_1) \longrightarrow Xe(^1S_0) + h\nu \quad (2)$$

$$Xe(^3P_1) + nXe(^1S_0) \longrightarrow Xe_2^* + (n-1)Xe(^1S_0) \quad (3)$$

Processes 1 and 2 reflect absorption and emission of resonance radiation without stipulating whether or not the emitted photon exhibits a wavelength (energy) shift due to Holtsmark broadening at higher pressures. Reaction 3 denotes an over-all sequence(s) for formation of Xe_2^*, which may eventually emit the 1715-Å continuum.

Unfortunately, any photolysis experiment suffers from the consequences of Beer's law, namely, that initial absorption of the incident photons is localized in the window region as the pressure of the absorbing gas is increased. This situation, as well as resonance diffusion away from the sampling volume, will always tend to obscure the significance of an observed pressure dependence when sampling takes place from a small portion of the vessel. Consequently, it is extremely difficult to relate unambiguously the observed second-order behavior observed at lower pressures to any fundamental step in reaction 3. Only in those cases where the spatial distribution of excited species is relatively uniform (as in high-energy electron impact) will such data give any insight into the mechanism.

The fact that the normalized continuum intensity in the range 200–400 torr was substantially lower when lamp I was used as the excitation source is not surprising. This effect is directly related to the transmission curves shown in Figure 1. At any given pressure, absorption of the incident radiation was relatively more efficient with lamp I. Consequently, the initial concentration of $Xe(^3P_1)$ near the lamp window was higher and the probability for a wall reaction resulting in de-excitation of any of the precursors for Xe_2^* (or Xe_2^*

itself) was enhanced. The absorption characteristics of the system when the high-pressure lamp was used were such that the spatial distribution of intermediates was more homogeneous and energy loss at the window was reduced. Deexcitation of precursors for Xe_2^* may also have occurred *via* removal (at the window) of the photon emitted in process 2. The present data are not sufficient to define the exact mechanism(s).

Effect of Additives. It has already been established that the addition of excess krypton increased the continuum intensity to essentially the same level as was obtained from pure xenon at higher pressures (lamp II). The same behavior was observed with lamp I, but the intensity was considerably greater than that obtained from pure xenon (see Figure 3). This behavior (lamp I) is related to the wall effect just discussed. A higher intensity was obtained with added krypton relative to pure xenon, because the measurements with the mixture were taken at lower pressures of xenon where the distance of average penetration of the incident light beam was greater. This condition tends to reduce wall effects, and the continuum intensity (curve E, Figure 3) increased over the limiting high-pressure value (curve B, Figure 3).

The quenching data may be treated rigorously, since the kinetic analysis may be carried out without consideration of wall effects and complications due to radiation diffusion. A steady-state approximation incorporating excited Xe atoms and a quenching step which is first order in the additive yields a family of quenching curves (depending on the value of n in reaction 3) which may be compared with the data obtained with added N_2. Assuming that the additive does not react with Xe_2^*, the only consistent solution yields a value nearly equal to 2. This result may be interpreted in several ways. It may be taken as evidence for production of metastable $^3P_2$ atoms, direct three-body conversion of $Xe(^3P_1)$ to Xe_2^*, two concurrent mechanisms which exhibit a different pressure dependence, etc. Turner[2] has recently concluded that the rate of production of a molecular emission in krypton can be explained by two mechanisms, each of which involves metastable atoms. As indicated above, the results of the quenching analysis can neither confirm nor deny the analogous situation for this system.

Carbon Monoxide Oxidation with an Oxygen Tracer over a Vanadium Pentoxide Catalyst

by Kozo Hirota, Yoshiya Kera, and Shousuke Teratani

Department of Chemistry, Faculty of Science, Osaka University, Toyonaka, Osaka, Japan *(Received January 2, 1968)*

The oxidation reaction of carbon monoxide with gaseous oxygen on a powdered V_2O_5 catalyst was studied over the temperature range from 345 to 410°, using heavy oxygen ^{18}O (about 3 atom %) as the tracer. When the lattice oxygen of the catalyst was partially substituted by concentrated heavy oxygen before the experiment, the percentage of ^{18}O in the produced carbon dioxide changed gradually during the oxidation, in accordance with the ^{18}O concentration in the catalyst, even though the percentage of ^{18}O in oxygen and in carbon monoxide was practically invariant. When a mixture of oxygen and carbon dioxide, both containing about 60 atom % of ^{18}O, was brought into contact with the catalyst at 370°, only the oxygen in carbon dioxide was found to be exchangeable with the lattice oxygen. The exchange rate of carbon dioxide was increased by the presence of carbon monoxide. The oxidation of carbon monoxide on vanadium pentoxide was explained by the oxidation–reduction mechanism. The relative rate of each elementary step and the surface intermediates during the reaction are discussed, and a detailed reaction scheme is proposed.

Introduction

Vanadium pentoxide, supported or unsupported, has been used extensively for the catalytic oxidation of hydrocarbons or sulfur dioxide. Most of the mechanisms of these oxidation reactions have been discussed assuming a regeneration process of oxygen in the catalysts,[1] *i.e.*, by a oxidation–reduction mechanism.

Basing their conclusions on the kinetic study of

(1) (a) C. E. Senseman and O. A. Nelson, *Ind. Eng. Chem.*, **15**, 521 (1923); (b) J. M. Weiss, C. R. Downs, and R. M. Burns, *ibid.*, **15**, 965 (1923); (c) B. Neumann, *Z. Elektrochem.*, **41**, 589, 821 (1935); (d) G. L. Simard, J. F. Steger, R. J. Arnot, and L. A. Siegel, *Ind. Eng. Chem.*, **47**, 1424 (1955).

oxidation of carbon monoxide on vanadium pentoxide, Hughes and Hill[2] supported the regeneration mechanism. Tarama and Teranishi[3] more conclusively gave the catalyst the same role in this reaction system. Roiter[4] attempted to obtain direct evidence for the behavior of the catalyst by using a heavy-oxygen tracer, but he reached the conclusion that the oxygen in the catalyst does not participate in the oxidation reaction of naphthalene over the temperature range from 320 to 390° and in the oxidation of sulfur dioxide at 580°. Recently, one of the authors[5] studied the carbon monoxide oxidation on vanadium pentoxide by the use of highly concentrated heavy oxygen as a tracer. Since the oxygen in the oxide is found to be exchangeable during the oxidation, this author favored the regeneration mechanism. Moreover, the presence of exchangeable oxygen in vanadium pentoxide was confirmed by using an infrared technique.[6]

The purposes of this study are to confirm the above results and to obtain information in order to give a deeper understanding of the oxidation mechanism of carbon monoxide.

Experimental Section

Materials. Heavy oxygen used in the oxidation reaction (*ca.* 3% ^{18}O) was produced by the electrolysis of heavy water containing ^{18}O, followed by passage through a liquid nitrogen trap. (If not otherwise described, atom per cent is used; *e.g.*, the per cent of ^{18}O equals $([^{18}O_2] + {}^1/_2\,[^{16}O^{18}O])/([^{18}O_2] + [^{16}O^{18}O] + [^{16}O_2])$). Carbon monoxide (99.5%) from Takachiho Trading Co. was used without further purification. The mixture of oxygen and carbon dioxide, both containing about 60% ^{18}O, was prepared by the thermal-diffusion method in our laboratory.[7] (As will be understood in Table II, isotopic equilibration of this mixture is not established with respect to both oxygen and carbon dioxide.)

Catalyst. Vanadium pentoxide powders (Mitsuwa Chemical Co., special grade) were used without any treatment. The surface area of the powders was determined to be 2.5 m^2/g from BET plots of carbon dioxide adsorption at −78°. The amount of vanadium pentoxide was 0.300 g in each experiment.

Apparatus and Procedure. The results of experiment A were obtained with the reaction apparatus A shown in Figure 1. In each run, fresh catalyst powders were placed in the reaction tube, R. Prior to each experiment, a calcium chloride tube, which had an open end to the air, was attached to the joint, J, and R was heated with an electric furnace, F, at 490° for 1 hr. After the calcium chloride tube was replaced by the gas reservoir G, containing a mixture of heavy oxygen and carbon monoxide, R was degassed with an oil diffusion pump at 490° for 2 hr. The trap, T, was cooled at −78° during the evacuation. The degree of vacuum reached about 10^{-6} mm after the degassing, according to an ionization gauge. A thermostat was used to keep the temperature in the reaction tube within ±5°.

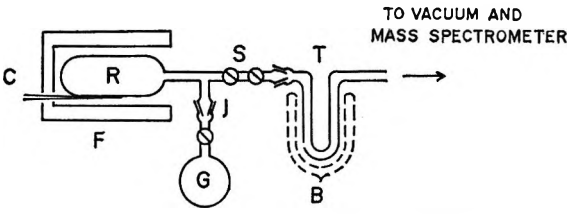

Figure 1. Reaction apparatus A: R, reaction tube; G, gas reservoir; S, sampling part; T, trap; B, Dry Ice–acetone bath; F, electric furnace; C, chromel–alumel thermocouple; J, joint.

The oxidation reaction was begun by expanding the mixture of heavy oxygen and carbon monoxide in G into R. At a given time, about 1% of the gas reacting in R was expanded into the sampling part S (*ca.* 1 cm^3) and was immediately analyzed with a mass spectrometer (Hitachi RMU-5B), installed at the Institute for Protein Research, Osaka University. The sampling was repeated several times in each experiment.

Generally, the accuracy of each determination of the isotopic composition depended on the partial pressure of the gas. The mean errors of the ^{18}O concentration of each component varied from ±0.02 to ±0.1%. (When highly enriched heavy oxygen was used, ^{17}O became measurable but was neglected in the calculation for simplicity's sake.)

In order to perform the oxidation experiment on the ^{18}O-enriched catalyst (*cf.* experiment C), reaction apparatus B was used, which is slightly different from apparatus A, as Figure 2 shows. The gas reservoirs G_1 and G_2 contained given amounts of the gas for the substitution and the oxidation, respectively. After the catalyst was treated as mentioned above, this substitution was carried out by means of the isotopic-exchange reaction between the catalyst and a mixture of oxygen and carbon dioxide in G_1 at 370°. Both components of this mixture contained about 60% ^{18}O. After 31 hr, the reaction was stopped and the gaseous product was pumped out. Then the oxidation experiment was carried out immediately at the same temperature.

The total inner volume of the reaction apparatus was about 110 cm^3 for apparatus A and about 130 cm^3 for apparatus B. Pressure during the reaction was indirectly determined from that of the sample.

(2) M. F. Hughes and G. R. Hill, *J. Phys. Chem.*, **59**, 388 (1955).

(3) K. Tarama, S. Teranishi, and A. Yasui, *Nippon Kagaku Zasshi*, **81**, 1034 (1960); K. Tarama, S. Teratani, S. Yoshida, and N. Tamura, *Proc. Int. Congr. Catal. 3rd, Amsterdam*, 1964, 262 (1965).

(4) V. A. Roiter, *Kinet. Katal.*, **1**, 63 (1960).

(5) K. Hirota, T. Imanaka, M. Chono, and K. Kishimoto, *Shokubai* (Tokyo), **6**, 48 (1964).

(6) Y. Kera, S. Teratani, and K. Hirota, *Bull. Chem. Soc. Jap.*, **40**, 2458 (1967).

(7) K. Hirota, Y. Kobayashi, M. Takahashi, and Y. Yoshikawa, *Daitai to Hoshasen*, **2**, 235 (1959).

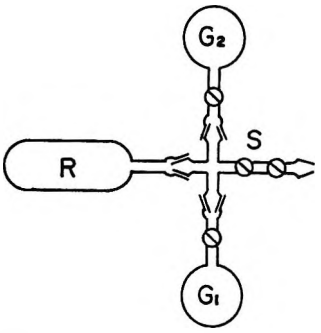

Figure 2. Reaction apparatus B.

Results

Experiment A. The Distribution of ^{18}O among the Components in the Oxidation Reaction. The oxidation reaction of carbon monoxide with gaseous oxygen (*ca.* 3% ^{18}O) was carried out at 345, 370, 390, and 410°, partial pressures of carbon monoxide and heavy oxygen in the initial mixture being nearly stoichiometric (35.0 and 18.0 mm, respectively). Heavy oxygen was transferred gradually to carbon dioxide in the course of the oxidation, as shown by Figure 3. The relative oxidation rate may be understood by the dotted lines and arrows, which indicate the ratio of the produced carbon dioxide to its equilibrium value.

The initial oxidation rate is shown in Table I, and the activation energy of the oxidation was estimated from the rate to be 14.3 kcal/mol. The per cent of ^{18}O in carbon monoxide remained practically the same as its initial value (*ca.* 0.3%), and the per cent of ^{18}O in oxygen increased, though only slightly, while the per cent of $C^{16}O^{18}O$ in the produced carbon dioxide always remained at less than the per cent of ^{18}O in oxygen and reached a maximum at every temperature except at 345°. This tendency of the curve was more marked at higher temperatures.

The stoichiometric change was observed, within experimental error, in each run. Nevertheless, it became clear from the material balance on the heavy oxygen that some heavy oxygen was caught by the catalyst during the reaction, suggesting that the lattice oxygen takes part in the reaction. This is an example of the evidence against Roiter's conclusion.

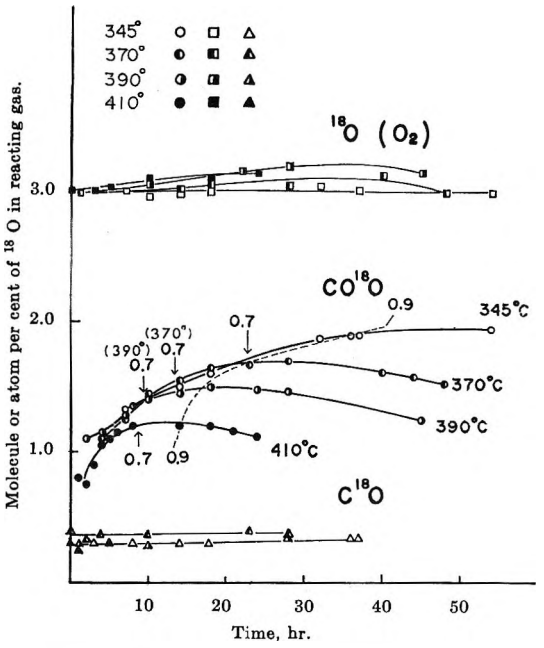

Figure 3. The temperature effects of the distribution of ^{18}O among the reactants and products during the carbon monoxide oxidation. The numbers 0.7 and 0.9 and the dotted line indicate the fraction of conversion.

Table I: The Initial Oxidation Rate of Carbon Monoxide and the Initial Isotopic Exchange Rate between Carbon Dioxide and Vanadium Pentoxide

Expt no.	Temp, °C	P_{CO_2}, mm	P_{O_2}, mm	P_{CO}, mm	Oxidation rate (molecule) 10^{11} cm^{-2} sec^{-1}	Exchange rate (atoms) 10^{11} cm^{-2} sec^{-1}
A-1	410	...	34.5	18	5.5	
A-2	390	...	33.5	18.5	3.9	
A-3	370	...	34.5	18	2.6	
A-4	345	...	35	18	1.8	
C	370	...	28	15	1.4	
D-1	370	11.5	...	...		2.1
D-2	370	11.5	...	31		4.6
D-3	370	11.5	16	...		2.4
B	370	10.5	13.5	1.5		3.7

Experiment B. The Isotopic-Exchange Reaction between Oxygen, Carbon Dioxide, and the V_2O_5 Catalyst. In order to confirm such exchangeability of lattice oxygen as deduced by experiment A, the isotopic-exchange reaction between gaseous oxygen, carbon dioxide, and vanadium pentoxide was carried out at 370°. Actually, a small amount of carbon monoxide was present in the mixture. The partial pressures of oxygen, carbon dioxide, and carbon monoxide were 13.5, 10.5, and 1.5 mm, respectively, and the initial ^{18}O were 59.8, 66.6, and *ca.* 60%, respectively. For each molecular species, the per cent present as each of its isotopic isomers is plotted as a function of reaction time in Figure 4.

The constancy of the percentage of ^{18}O *vs.* time in oxygen is shown by experiment B more clearly than by experiment A, but the per cent of ^{18}O in carbon dioxide, averaged on CO_2, $C^{16}O^{18}O$, and $C^{18}O_2$, decreased markedly in Experiment B. This decrease of the percentage of ^{18}O indicates the presence of some exchangeable oxygen in the oxide. Judging from the curve of the per cent of ^{18}O in carbon dioxide, the isotopic equilibrium between carbon dioxide and the lattice oxygen near the surface seems to be practically established after 31 hr at 370°. This point will be discussed later, with reference to the reaction order of the ^{18}O exchange. Therefore, from the per cent of ^{18}O in carbon dioxide after 31 hr, the per cent of ^{18}O of the surface layer oxygen in contact

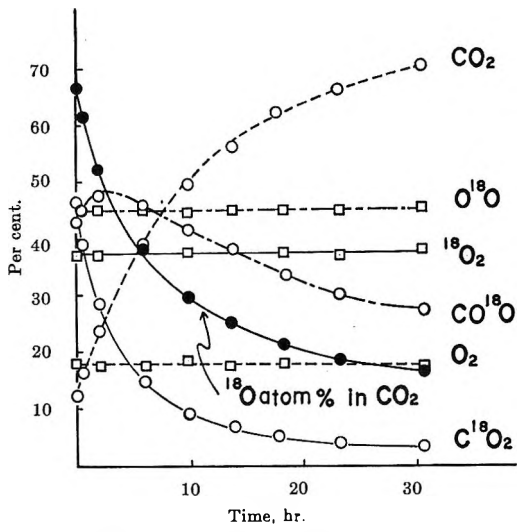

Figure 4. The isotopic exchange of the mixture of heavy oxygen and heavy carbon dioxide with V_2O_5 at 370°.

with carbon dioxide can be estimated to be 16%, assuming that the isotopic concentration in the lattice oxygen is the same as that in carbon dioxide at this time.

Another important fact, that gaseous oxygen does not exchange with lattice oxygen at 370°, can be obtained from Figure 4, and this finding may be expected from the result obtained by Cameron, Farkas, and Litz[8] and also by Margolis,[9] who reported that the exchange reaction became measurable only at 435°. This finding may be supported by the data in Table II, where the "equilibrium" constants, K_I and K_{II} of isotopic equilibrium, defined by eq 1 during the course of experiment B, are described.

$$K_I = \frac{(^{16}O^{18}O)^2}{(^{16}O_2)(^{18}O_2)} \qquad K_{II} = \frac{(C^{16}O^{18}O)^2}{(C^{16}O_2)(C^{18}O_2)} \qquad (1)$$

Though the experimental errors are a little large, Table I indicates that K_I is invariant, while K_{II} reaches its true equilibrium constant, 4.0, after 10–20 hr. This suggests that the desorption of oxygen is very difficult, even if its adsorption is easy, while both processes by carbon dioxide are easily performed.

Table II: "Equilibrium" Constants *vs.* Time in Experiment B

	Time, hr.						
	0	2	10	14	18	23.5	31
K_I	3.2	3.2	2.9	3.2	3.2	3.0	3.3
K_{II}	3.4	3.5	3.9	3.9	4.0	4.0	3.9

Experiment C. The Oxidation Reaction on the ^{18}O-Enriched Catalyst. The ^{18}O-enriched V_2O_5 catalyst which was prepared by the above exchange reaction (experiment B) was degassed for 30 min and was used immediately for the oxidation reaction at 370°. The

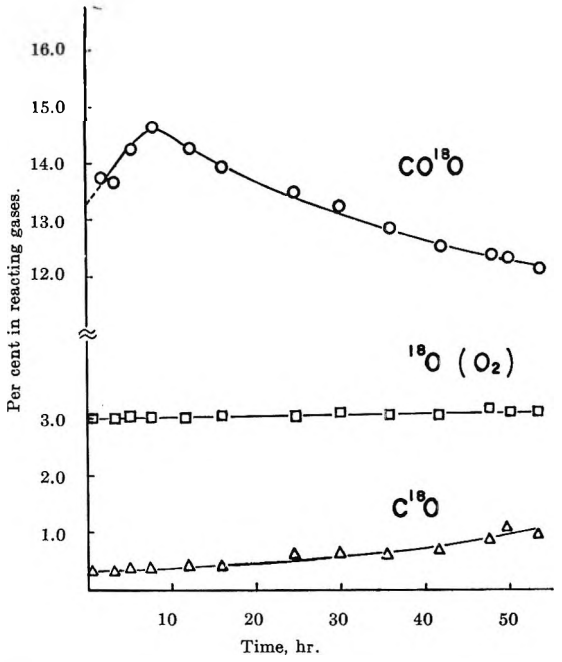

Figure 5. Oxidation of carbon monoxide on ^{18}O-enriched V_2O_5 at 370°. The initial percentage of $C^{16}O^{18}O$ is estimated to be 13.3%.

initial partial pressures of carbon monoxide and oxygen were 28.0 and 15.0 mm, respectively, and the oxygen gas initially contained about 3.0% of ^{18}O. The percentage of ^{18}O is plotted against time in Figure 5. (The initial percentage of $C^{16}O^{18}O$ was estimated to be 13.3% by the result obtained in Table III.)

The curves indicate clearly that in spite of the slight increase of per cent ^{18}O in oxygen, $C^{16}O^{18}O$ in the produced carbon dioxide shows a marked change, a maximum, and the curve reaches as high a value at the maximum as the ^{18}O concentration of the surface layers. The gradual increase of the per cent of ^{18}O in carbon monoxide will have some connection with the reaction mechanism, as will be mentioned.

Experiment D. The Effect of Oxygen or Carbon Monoxide on the Exchange Rate between Heavy Carbon Dioxide and the Catalyst. In order to obtain some knowledge on the exchangeability of lattice oxygen, the following three experiments were carried out at 370° on a fresh catalyst, using $C^{18}O_2$ as a component: for D-1, the pressure of CO_2 is 11.5 mm; for D-2, the partial pressures of CO_2 and CO are 11.5 and 31 mm, respectively; for D-3, the partial pressures of CO_2 and O_2 are 11.5 and 16 mm, respectively.

The carbon dioxide initially contained about 46.6% of ^{18}O in each experiment. Percentages of ^{18}O are plotted against time, as shown in Figure 6, where the three curves, D-1, D-2, and D-3, correspond to the above

(8) W. C. Cameron, A. Farkas, and L. M. Litz, *J. Phys. Chem.*, **57**, 229 (1953).

(9) L. J. Margolis, *Izv. Akad. Nauk SSSR, Otd. Khim. Nauk*, 225 (1959).

PLACE
STAMP
HERE

American Chemical Society

1155 Sixteenth Street, N.W.
Washington, D.C. 20036

ATTN. H. C. SPENCER

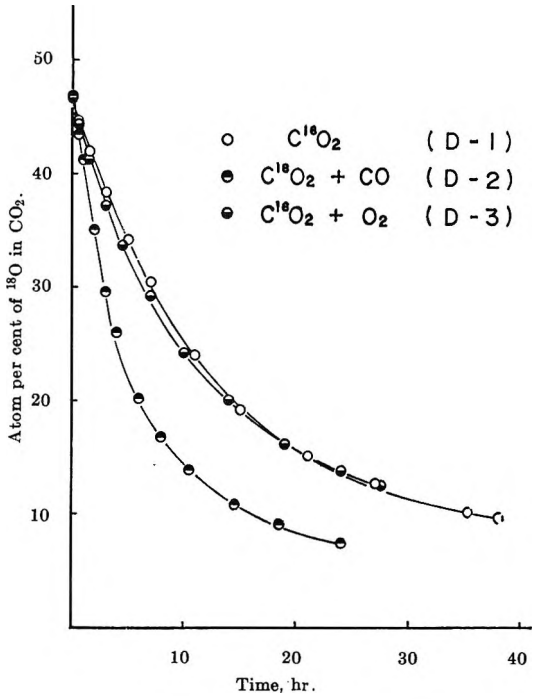

Figure 6. The effect of oxygen or carbon monoxide on the exchange rate between heavy carbon dioxide and V_2O_5 at 370°.

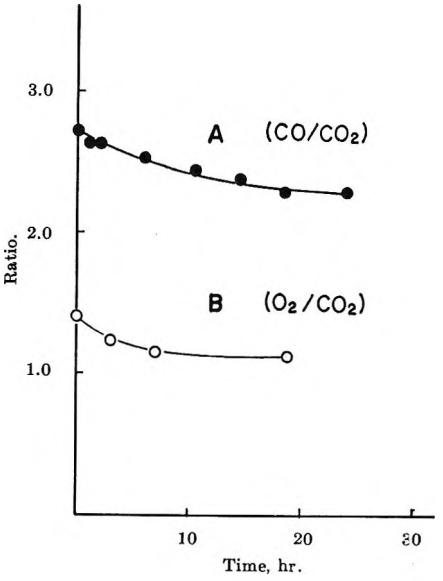

Figure 7. Ratios of the amount of $CO:CO_2$ and $O_2:CO_2$ *vs.* time during the exchange shown by Figure 6.

three experiments. From the initial slope of each curve, the exchange rate was calculated in atoms per second per unit area of catalyst. The rates are compared in the last column of Table I, where the last one is the exchange rate of experiment B done at 370°. It was clearly shown that carbon monoxide promotes the exchange rate while oxygen does not promote it. Experiment B shows a value intermediate between the values of experiments D-2 and D-3, probably due to the presence of a small amount of carbon monoxide.

For reference to the discussion of the oxidized amount of carbon monoxide, the ratio of the amount of $CO:CO_2$ in D-2 are shown *vs.* time in curve A in Figure 7. The curve of D-2 represents the upper limit of the amount of oxidized carbon monoxide *vs.* carbon dioxide, because this relative decrease of carbon monoxide *vs.* carbon dioxide can be also ascribed to the larger chemisorbed amount of carbon monoxide. By simple calculation, the amount of the oxidized carbon monoxide after 24 hr is found to be less than 1.3 mm. This amount is too small to explain the catalytic effect of carbon monoxide by the exchange rate. Curve B of D-3 in Figure 7 indicates that the surface is oxidized to some extent during the exchange, considering that much less carbon dioxide than oxygen can be chemisorbed.

Discussion

Experiment A shows that the per cent ^{18}O both in carbon monoxide and in oxygen remained nearly constant during the reaction and also that the per cent of $C^{16}O^{18}O$ in the produced carbon dioxide was always less than the per cent of ^{18}O in gaseous oxygen. Both results clearly indicate that most of the oxygen species which participate directly in the oxidation are not gaseous or physically adsorbed oxygen molecules but are oxide catalysts. If otherwise, per cent of the $C^{16}O^{18}O$ in the produced carbon dioxide must be equal to the per cent of ^{18}O in gaseous oxygen.

It was shown by experiment C (Figure 5) that the per cent of ^{18}O in gaseous oxygen remains much less than that of the oxygen species in the surface layers, while the per cent of ^{18}O in carbon monoxide depends on it very slightly, and the per cent of ^{18}O in the produced carbon dioxide markedly depends on it. From the curve of the percentage of $C^{16}O^{18}O$, in Figure 5, the maximum ^{18}O concentration is estimated to be 14.7%, which is very close to 16%, the initial per cent of ^{18}O in the surface layers, as described before. By this reasoning, experiment C is regarded as evidence of the important role of the lattice oxygen in the oxidation on the V_2O_5 catalyst. Accordingly, the gradual decrease of the per cent of $C^{16}O^{18}O$ in the produced carbon dioxide from 14 to 12% in the course of the oxidation may give other evidence that the oxidation proceeds through the extraction of the surface-layer oxygen with carbon monoxide, because the gradual decrease of the curve can be explained by the shortage of ^{18}O in the surface as the reaction proceeds. The fractions of oxygen which come from the lattice to carbon dioxide can be calculated easily, if it is assumed that the ^{18}O concentration in the catalyst was 16% during the entire process, up to 54 hr. The fractions $O_L:CO_2$, are shown *vs.* time in Table III, by which *ca.* 80% of the primary oxidative species is found to be lattice oxygen and only *ca.* 20% is found to be gaseous oxygen; *i.e.*, the lattice oxygen plays an important role in the oxidation, while the gaseous oxygen plays a secondary role, gradually supplying the

lattice oxygen consumed by the oxidation. These results are completely inconsistent with Roiter's conclusion.[4]

Table III: Oxygen Source in the Produced Carbon Dioxide in Experiment C

Time, hr	P, mm	Molecules of CO_2 × 10^{19}	$O_L:CO_2$[a]	Time, hr	P, mm	Molecules of CO_2 × 10^{18}	$O_L:CO_2$[a]
1.5	1.2	0.54	0.82	24.5	14.7	6.59	0.81
3	2.3	1.03	0.82	30	17.1	7.66	0.79
5	3.8	1.70	0.87	37	19.0	8.52	0.76
8	5.8	2.60	0.90	42	20.4	9.14	0.74
12	8.4	3.76	0.87	50	22.0	9.86	0.72
16	10.7	4.79	0.85	54	22.5	10.08	0.71

[a] O_L denotes the oxygen in the lattice.

Since the oxidation reaction proceeds stoichiometrically according to experiment A, it can be considered that the composition of vanadium and oxygen in the surface layers of catalyst is kept constant during the reaction; *i.e.*, the transfer of oxygen from the gaseous phase to the surface layers occur as a step of the steady reaction, thus introducing heavy oxygen into the catalyst in the course of experiment A. On the basis of these findings, the regeneration mechanism which has been presented by many authors[1] can be supported.

In experiment A, as the reaction temperature became high, the per cent of ^{18}O in the produced CO_2 became small. This temperature effect is explained as follows. The activation energy of the diffusion of oxygen from surface layers into bulk is larger than the activation energy of the oxidation, so that with the increase of the reaction temperature, the per cent of ^{18}O in the reactive surface layers becomes relatively smaller, because of dilution with normal oxygen from the bulk.

Figure 3 indicates also that when the oxidation reaction came near to the final stage, the per cent of ^{18}O in the produced carbon dioxide reached a maximum and then decreased at higher temperatures. This finding is interpreted to mean that the percentage of ^{18}O decreases at the surface layers, because the partial pressure of oxygen at the final stage was reduced to less than 0.1–0.3 of the initial value. This means that the transfer of ^{18}O from the gaseous oxygen decreased, and the fraction of oxygen supplied by the transfer of normal oxygen in the bulk to the surface became larger, thus producing the decrease of the per cent of ^{18}O in the carbon dioxide produced.

Reaction Order of the Carbon Dioxide Exchange with the Surface. In order to obtain further evidence for the presence of different kinds of surface oxygen species exchangeable with carbon dioxide, the kinetic treatment was applied to the decrease in the per cent of ^{18}O in carbon dioxide of experiment B, using

$$-\ln \frac{X - X_\infty}{X_0 - X_\infty} = kt \qquad (2)$$

where X_0 and X_∞ represent the initial and the equilibrium values of X (the per cent of ^{18}O in carbon dioxide), respectively, and k is the rate constant.

Since the X_∞ value cannot be determined experimentally, several trial values were selected between the uppermost value of 16% at a time of 31 hr and the lowest value of 0.015%, which corresponds to the case when all the lattice oxygen was equally exchangeable. The plots of $-\log (X - X_\infty)/(X_0 - X_\infty)$ *vs.* time are shown in Figure 8. Curve A indicates that 16% is still much larger than the equilibrium value, while curve E suggests that all the lattice oxygen does not participate in the exchange. Any one of the intermediate values also does not give a good straight line, as shown by curves B–D. From such a result it may be concluded that this exchange reaction does not obey the first-order law over the entire range of time.

The above deviation from the law, as shown in Figure 8, may be explained as follows. According to the literature,[10] as far as all atoms in the molecule are the same in exchangeability and the kinetic isotope effect can be neglected,[11] the first-order law must be applied whether the reaction is homogeneous or heterogeneous. Considering the fact that the isotopic effect has to be small in the cases of oxygen isotopes, different kinds of

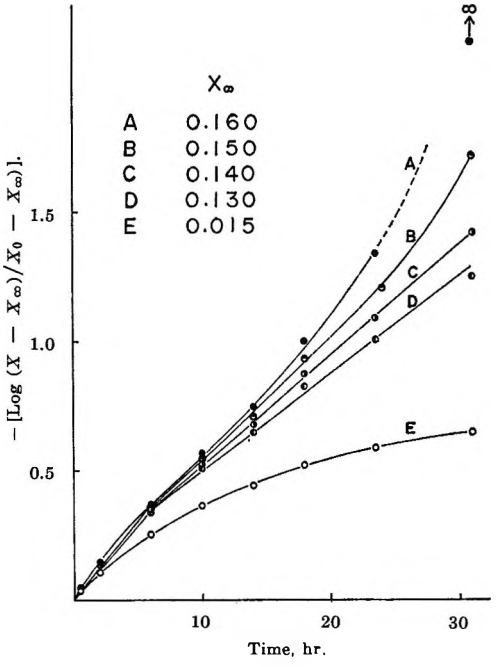

Figure 8. The analysis of the isotopic-exchange reaction shown by Figure 4 following the first-order law.

(10) (a) J. N. Wilson and R. G. Dickinson, *J. Amer. Chem. Soc.*, **59**, 1358 (1937); (b) H. A. C. McKay, *Nature*, **142**, 997 (1938); (c) N. Morita, *Bull. Chem. Soc. Jap.*, **15**, 166 (1940); (d) R. B. Duffield and M. Calvin, *J. Amer. Chem. Soc.*, **68**, 557 (1946).

(11) G. M. Harris, *Trans. Faraday Soc.*, **57**, 716 (1951).

oxygen species may be present in the vanadium pentoxide catalyst. Actually, it is shown that all the oxygen atoms in the catalyst do not have equal exchangeability, judging from the tendency that a selection of any value of X_∞ always deviates from a straight line. However, the nature of the different kinds of oxygen species in the oxide cannot be determined at present.

This conclusion seems to be contrary to the results of Cameron, Farkas, and Litz,[8] who found the exchange rate of gaseous oxygen with lattice oxygen in the noncrystalline oxide to agree with the first-order law very well and ascribed this finding to the fast diffusion of oxygen in the oxide bulk, so that the exchange on the surface becomes the rate-determining step. However, since their experiment was carried out at more than 445° and the activation energy of the exchange was as high as 45 kcal/mol, a reaction of this kind would not be observed at 370°, at which the present research was carried out. In other words, the rate of exchange may be different from the rate of the diffusion depending on the temperature, and this explains the apparently different behavior mentioned above.

Surface Intermediates. In order to discuss the mechanism in detail, it is necessary to know the surface intermediates of the oxidation; there is still no agreement among the researchers concerning this point, despite the importance of these intermediates in understanding the mechanism of the oxidation.

For instance, the existence of the carbonate ion[12] or the "CO_3 complex"[13] has been presented by several authors as a species observable during the catalytic oxidation reaction of carbon monoxide on several metal oxides. Eischens and Pliskin[14] first observed infrared absorption bands during the carbon monoxide oxidation on nickel and/or nickel oxide (Carb-o-sil-supported nickel whose surface was oxided by exposing it to oxygen) and supported the possibility of the formation of two ionic species, I and II, from the bands observed, as well as the formation of nonionic species, III.

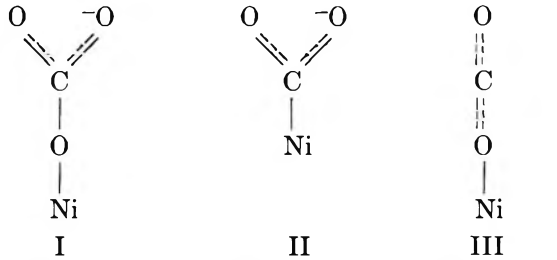

I 1390 cm^{-1} II 1530 cm^{-1} III 2193 cm^{-1}

The existence of the CO_3^{2-} species on vanadium pentoxide was deduced by Tarama, *et al.*,[15] but conclusive evidence of this as the necessary intermediate does not seem to have been obtained from their research.

Experiment D will give us some important knowledge of this problem, because the rate of oxygen exchange of $C^{16}O^{18}O$ with the V_2O_5 catalyst becomes larger when carbon monoxide is added (in D-2), while the rate of the experiment when oxygen is added (in D-3) remains practically the same as that of D-1. The result of experiment D may be explained by reaction 3; *i.e.*, carbon dioxide is dissociatively chemisorbed on a special site of the surface, composed of a vanadyl group and a vacant V̇ atom, in the first step, and then produces species IV. However, oxygen in the desorbing carbon dioxide may be different from that of the chemisorbed one.

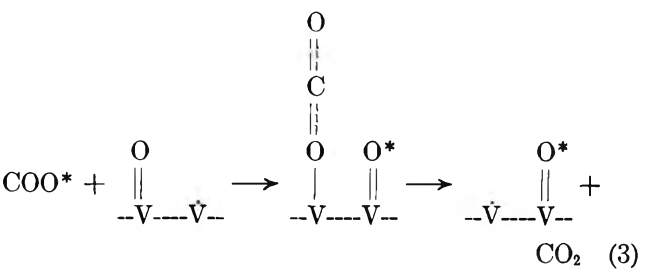

CO_2 (3)

IV

The catalytic effect of carbon monoxide in no. D-2 can be explained by its oxidation, as indicated by curve A in Figure 7, because, as reaction 4 shows, carbon monoxide produces species IV, similar to that in reaction 3, as a result of chemisorption on a vanadyl group, and then carbon dioxide, which does not contain ^{18}O, desorbs in the second step, producing a vacant V̇ atom. Such processes increase the occurrence of reaction 3, because the special sites which are composed of a vanadyl group and a vacant V̇ atom are increased in number.

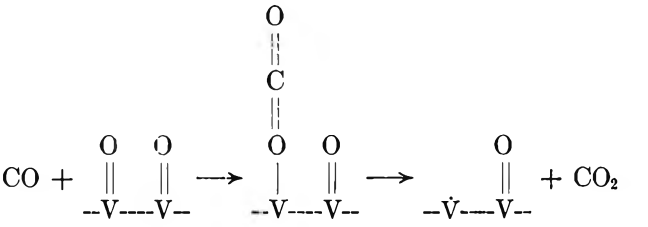

(4)

IV

It might be well to mention the peculiar chemisorption behavior of oxygen. The finding that the percentage of ^{18}O did not decrease during the oxidation must not necessarily be ascribed to the nondissociative state of the oxygen adsorbed but rather to the large heat of chemisorption of oxygen, and for this reason the desorption could not occur practically. Actually, the rate of chemisorption of oxygen on V_2O_4, a reduced species of V_2O_5, was estimated to be faster than that on V_2O_5,[16]

(12) W. E. Garner and F. J. Veal, *J. Chem. Soc.*, 1487 (1935).

(13) R. M. Dell and F. S. Stone, *Trans. Faraday Soc.*, **50**, 501 (1954); W. E. Garner, F. S. Stone, and P. F. Tiley, *Proc. Roy. Soc.*, **A211**, 472 (1952); F. S. Stone, *Advan. Catal.*, **13**, 8 (1962).

(14) R. P. Eischens and W. A. Pliskin, *ibid.*, **9**, 662 (1957).

(15) K. Tarama, S. Teranishi, K. Hattori, and A. Yasui, *Nippon Kagaku Zasshi*, **81**, 1038 (1960).

and the dissociative chemisorption of oxygen on vanadium pentoxide at 370–450° was suggested.[17]

According to experiment B, the isotopic exchange of gaseous oxygen with vanadium pentoxide was slow at 370°, so that the reaction could not be measured at that temperature. Such a different exchangeability may be explained by assuming that gaseous oxygen is chemisorbed on such special sites which are composed of two adjacent vacant V̇ atoms, as reaction 5 shows. This is why the rate of formation of the vanadyl groups on the partly reduced oxide is not as fast as expected.

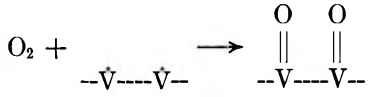

(5)

By reactions 3 and 5, the effect of oxygen in no. D-3, that oxygen does not become an obstacle to the chemisorption of carbon dioxide, can be explained easily. Additional support of the presence of vacant V̇ atoms on the surface is the appearance of an esr signal, which can be ascribed to the V̇ atom, on the vanadium pentoxide produced from ammonium *m*-vanadate at 450° or from the oxide sintered at 700°.[18] For the case in which the oxide was kept at 100° for several hours, this signal did not decrease very much.[19] These findings suggest that the site chemisorbed by gaseous oxygen is not a single vacant V̇ atom. On the other hand, Boreskov's suggestion[20] that the exchange of molecular oxygen occurs without dissociation is not ruled out by reaction 5 as a perfect independent process of the dissociative chemisorption.

Moreover, reaction 5 can explain why the $O_L:CO_2$ values at 1.5 and 3 hr in Table III are smaller than the others. At the initial stage of the reaction, owing to the evacuation treatment, there are adjacent pairs of vacant V̇ atoms on the surface, so that oxygen chemisorption occurs very quickly, and the per cent of ^{18}O on the surface becomes almost that of the gaseous oxygen. However, the percentage of ^{18}O increases gradually, owing to the diffusion from the catalyst bulk, and the fraction of ^{18}O in the carbon dioxide thus becomes larger.

From the above reasoning, it may be understood that the CO_3 species are species V and VI, which are easily transferrable forms of species IV, as shown by reaction 6. Formation of such species as VII, however, will be ruled out by this consideration, because this kind of species has not been hitherto reported.

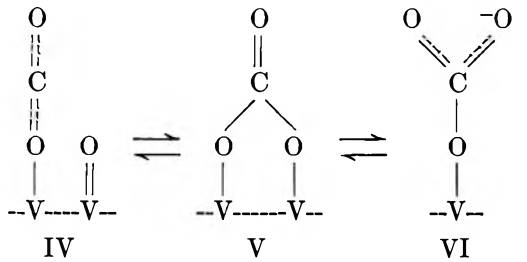

(6)

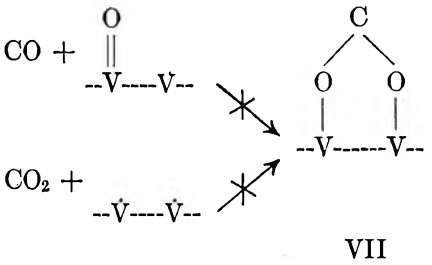

(7)

Mechanism of Oxidation. During the above discussion, the outline of the scheme of both the carbon monoxide oxidation and the carbon dioxide exchange has been obtained. The scheme is summarized by Figure 9, which may be called classical. The relative rate of each step at 370° will be discussed in more detail.

In experiment B, which concerns the isotopic exchange with the lattice oxygen (Figure 4), carbon dioxide was found to exchange more easily than gaseous oxygen. Therefore, the backward rate of the first step (dissociation of gaseous oxygen) is estimated to be much slower than both the backward rates of the third step (formation of adsorbed carbon dioxide) and the fourth step (desorption of carbon dioxide). According to experiment C (Figure 5), since the per cent of ^{18}O in carbon monoxide increased only slightly after contact with the ^{18}O in the surface layers of the catalyst, the backward rate of the second step (desorption of carbon monoxide) must also be slow in the oxidation, even though faster than the backward rate of the first step. Therefore, only the forward rate of the first step (I) is described in Figure 9, and the rate must be the same with the net rates of the second (II), third (III), and fourth (IV) steps, respectively; *i.e.*, since the net reaction rate of each step must be equal in the steady state of reaction, it can be estimated that the first and second steps are much slower than the third and fourth steps, as was expressed by the length of the arrows in Figure 9.

Hughes and Hill,[2] basing their conclusions on the kinetic data, seem to indicate that either the third or the fourth step was slower than the first step. Tarama,

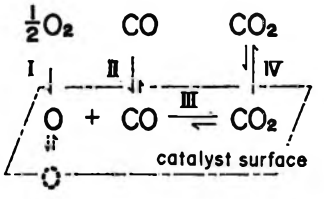

Figure 9. A classical reaction scheme.

(16) L. Ya. Margolis, *Izv. Akad. Nauk SSSR, Otd. Khim. Nauk*, 225 (1952).

(17) Private communication from Professor S. Teranishi, 1967.

(18) K. Tarama, *et al.*, *Bull. Chem. Soc. Jap.*, **34**, 1195 (1961).

(19) K. Hirota and K. Kuwata, *ibid.*, **36**, 229 (1963).

(20) G. K. Boreskov, *Advan. Catal.*, **15**, 285 (1964); see especially pp 296 and 310.

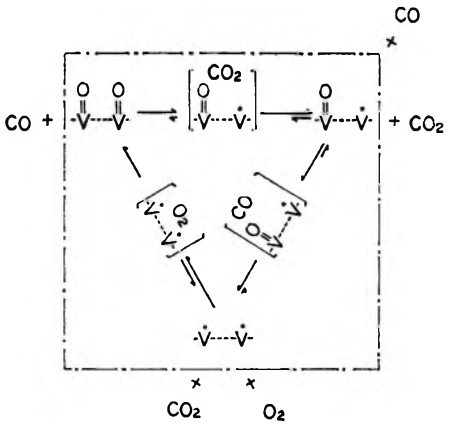

Figure 10. The proposed "triangular" reaction scheme.

et al.,[3] pointed out that the third step was the rate-determining step. In the present study, it was concluded that the first and second steps are rather slower than the third and the fourth steps.

Such discrepancies can be understood if a new reaction scheme, shown by Figure 10, is proposed, based on reactions 3–7. According to this triangular scheme, it is evident that the rate of chemisorption of gaseous oxygen and the rate of oxidation of carbon monoxide are intimately connected; *e.g.*, oxygenc an be chemisorbed only when adjacent vacant V̇ atoms are present or are produced by the reduction of carbon monoxide, and gaseous oxygen can indirectly oxidize carbon monoxide. In the case of the oxygen-exchange reaction between carbon dioxide and a catalyst, the processes occur only along the horizontal side of the triangle, contrary to the cyclic processes for the cases of oxidation. It is interesting to study whether this triangular mechanism based on the data collected mainly at 370° may be applied to the reaction at higher temperatures.

Finally, it might be added that, according to experiment A, the per cent of ^{18}O in the gaseous oxygen increases slightly at every temperature, while the total amount of ^{18}O decreased. This rare example of enrichment of ^{18}O may be regarded as a result of the kinetic isotopic effect, which is brought about by the process of the first step (dissociative adsorption of oxygen on the catalyst), as already pointed out,[5] considering that its backward rate is negligibly slow. Another point to be discussed is the exchangeability of the oxygen in the V=O group with that in the V—O—V group, because the oxygen exchange proceeds easily into the bulk of the oxide. This problem will be discussed in a future report now in progress.

Conclusions

(1) The classical oxidation–reduction mechanism on the catalytic oxidation of carbon monoxide with gaseous oxygen has been confirmed for vanadium pentoxide powders.

(2) A more detailed mechanism based on the experimental result obtained by using a ^{18}O tracer of high concentration has been proposed for the reaction as shown by the triangular scheme in Figure 10.

(3) Participation of the lattice oxygen in the reaction has been concluded definitely, contrary to the result of Roiter, who used also the oxygen-tracer method in his research.

Acknowledgment. The authors wish to express their sincere thanks to the Institute for Protein Research, Osaka University, for permission to use their mass spectrometer for carrying out this research and to Professor Shi-Ichiro Teranishi, Faculty of Engineering Science, Osaka University, for constructive discussion with him about this research.

Kinetics and Mechanism of the Decarboxylation of Anthranilic Acid in Aqueous Solution[1]

by Alfred V. Willi, Chong Min Won, and Paul Vilk[2]

The College of Pharmaceutical Sciences, Columbia University, New York, New York 10023 *(Received January 17, 1968)*

The kinetics of decarboxylation of anthranilic acid (HA) has been studied at 70 and 85° in weakly acidic solutions (pH 4.7–1.4) of a constant ionic strength of $\mu = 0.1$ *N*, and at 85° in 0.1–3.9 *N* aqueous hydrochloric acid. The results in weakly acidic solutions supply evidence for two parallel reactions of H_3O^+ with HA and of H_3O^+ with A^-. The mechanisms of both pathways involve predominant rate-determining proton transfer from H_3O^+ to the carbon atom in the position 1 of the aromatic ring. In strongly acidic solutions, above $[H_3O^+] = 0.5$ *N*, the pseudo-first-order rate constant, k, decreases with increasing $[H_3O^+]$, which indicates a change of mechanism. A quantitative treatment of the pH dependence of k has been carried out on the basis of the stationary state principle and with the aid of the Hammett acidity function. For sufficiently high $[H_3O^+]$, there is a linear relationship between $1/k$ and h_0 with a high precision. It may be derived solely from a mathematical analysis of the experimental rate data that in weakly acidic solutions the total rate is mainly governed by the rates of the proton-transfer steps; while with increasing acidity of the solution, a gradual change takes place to complete rate control by the C–C bond-cleavage steps.

Introduction

The decarboxylation kinetics of aromatic acids with electron-releasing substituents has been studied in some detail by several research workers.[3-8] On the basis of the empirical rate law (eq 1) found in aqueous solutions, the reactions could be formulated either as first-order decompositions of the unionized acid HA or as second-order reactions of the anion A^- with the hydroxonium ion[5,6]

$$\text{rate} = k_{HA}[HA] = k_H{}^A[A^-][H_3O^+] \quad (1)$$

In the examples of *p*-aminosalicylic and *p*-aminobenzoic acids, decarboxylation proceeds *via* two parallel pathways according to the rate equation[6]

$$\text{rate} = k_{H_2A}[H_2A^+] + k_{HA}[HA] = k_H{}^{HA}[HA][H_3O^+] + k_H{}^A[A^-][H_3O^+] \quad (2)$$

Experimental evidence for mechanism A-Se2 was supplied with the aid of data on substituent effects, general acid catalysis, and solvent isotope effects. It was concluded that the slow step involves a proton transfer from H_3O^+ to the carbon atom in position 1 of the aromatic ring of either the acid, HA, or the anion, A^-.[5,6] The two-step nature of the mechanism was first established by Lynn and Bourns,[9] who measured carbon-13 isotope effects in the decarboxylation of 2,4-dihydroxybenzoic acid in various acetate buffers.

A new development was indicated by the findings of Dunn, Leggate, and Scheffler,[7] who observed that the decarboxylation rates of *p*-methoxy- and *p*-methylanthranilic acids decrease with increasing $[H_3O^-]$ for hydroxonium ion concentrations above 0.1 *N*. In this pH range, however, the substrate is not involved in any further acid–base equilibrium beyond the addition of a proton to the amino group. Similar results have been reported recently by Los, Rekker, and Tonsbeek[8] for a few 2-substituted 4-aminobenzoic acids. These findings support a change of the slow step in the mechanism, from rate-determining proton transfer to rate-determining C–C bond cleavage.[7,8]

Though experimental results are available for *p*-aminobenzoic acid as well as for a few substituted anthranilic acids,[7] no previous work has been published on the decarboxylation kinetics of unsubstituted anthranilic acid in aqueous solutions of various pH values. Since the absence of a carbon isotope effect has been established for this reaction in 1 *N* (=0.5 *M*), aqueous sulfuric acid,[10] it was desirable to obtain information on

(1) The major portion of this material has been taken from a thesis submitted by C. M. Won to the College of Pharmaceutical Sciences, Columbia University, New York, N. Y., in partial fulfillment of the requirements for the Master of Sciences degree, 1967.

(2) Undergraduate research participant at the College of Pharmaceutical Sciences, Columbia University, New York, N. Y., 1967.

(3) For a review of earlier work, see A. V. Willi, "Säurekatalytische Reaktionen der organischen Chemie—Kinetik und Mechanismen," F. Vieweg und Sohn, Braunschweig, West Germany, 1965.

(4) W. M. Schubert, *J. Amer. Chem. Soc.*, **71**, 2639 (1949); W. M. Schubert, J. Donahue, and J. D. Gardner, *ibid.*, **76**, 9 (1954); W. M. Schubert, R. E. Zahler, and J. Robins, *ibid.*, **77**, 2293 (1955).

(5) W. M. Schubert and J. D. Gardner, *J. Amer. Chem. Soc.*, **75**, 1401 (1953).

(6) A. V. Willi and J. F. Stocker, *Helv. Chim. Acta*, **37**, 1113 (1954); A. V. Willi, *ibid.*, **40**, 1053 (1957); **43**, 644 (1960); *Z. Naturforsch.*, **13a**, 997 (1958); *Trans. Faraday Soc.*, **55**, 433 (1959); *Z. Physik. Chem.* (Frankfurt), **27**, 221 (1961).

(7) G. E. Dunn, P. Leggate, and I. E. Scheffler, *Can. J. Chem.*, **43**, 3080 (1965).

(8) R. F. Rekker and W. Th. Nauta, *J. Med. Pharm. Chem.*, **2**, 281 (1960); J. M. Los, R. F. Rekker, and C. H. T. Tonsbeek, *Rec. Trav. Chim. Pays-Bas*, **86**, 622 (1967).

(9) K. R. Lynn and A. N. Bourns, *Chem. Ind.* (London), 782 (1963).

(10) W. H. Stevens, J. M. Pepper, and M. Lounsbury, *Can. J. Chem.*, **30**, 529 (1952).

the rate equation in order to supply sufficient evidence to establish a mechanism. It was expected that a change of mechanism in strongly acidic solutions would occur also in this example and that this reaction might be well suited for a complete mathematical analysis of the kinetic data in the region of the change of mechanism.

A detailed kinetic study of the decarboxylation of anthranilic acid in aqueous solution has been carried out and the results are reported in this article. Experiments have been done in weakly acidic solutions at a constant ionic strength of $\mu = 0.1\ N$, as well as in 0.1–3.9 N aqueous hydrochloric acid solutions.

Experimental Section

The ionization constant K_1 (definition below) of anthranilic acid at 70 and 85° and at a constant ionic strength of 0.1 N was determined by potentiometric measurements in a thermostated cell without liquid junction with a glass electrode Metrohm Type H and a silver–silver chloride electrode. pcH values[11] were measured with a Metrohm Type E388 pH meter.

Kinetic measurements were carried out as described previously[6] by following the decrease of the uv absorption at 310 and 315 mμ. The concentration of the substrate in the kinetic solutions (in the ampoules) was $3 \times 10^{-4}\ M$. The solutions contained 0.9% ethanol which had been used to dissolve the organic acid. Samples of the solutions were neutralized with NaOH solution, were buffered to a pH of 7.8, and were diluted fivefold before measuring the optical densities (D) in 5-cm quartz cells with a Beckman DU spectrophotometer. (Neutralization and buffering were omitted in the experiments with solutions in dilute hydrochloric acid ($\geq 0.1\ N$), and optical densities were measured at 275 and 280 mμ.)

Ampoules had been treated with 2 N hydrochloric acid for 4 weeks before use. A stream of nitrogen was passed through the kinetic solutions for the "slow" experiments with acetate buffers, before filling them into ampoules.

In all kinetic experiments, log $(D - D_\infty)$ decreased linearly with time, indicating that the reaction followed a first-order course at a constant pH. The reactions were followed through 2–3 half-lives. D_∞ was obtained from the optical density after 10 half-lives; usually there was good agreement with the theoretical value (obtained from the uv spectra of aniline). For the very slow reactions, the theoretical value of D_∞ was used. Pseudo-first-order rate constants were calculated from the experimental data with the aid of the least-squares method. Their estimated precision is within ±2%.

Results

Ionization Constants. It is necessary for a discussion of the pH dependence of the rate to have available values of the ionization constants K_1 and K_0 of anthranilic acid

$$[H_3O^+][HA]/[H_2A^+] = K_0$$

$$[H_3O^+][A^-]/[HA] = K_1$$

Determinations of these constants are to be done at the same temperature and ionic strength as the kinetic measurements. Results for K_1 from potentiometric determinations are

$$K_1 = (2.53 \pm 0.12) \times 10^{-5} \quad (70°, \mu = 0.1\ N)$$

$$K_1 = (2.81 \pm 0.10) \times 10^{-5} \quad (85°, \mu = 0.1\ N)$$

(The accuracy of the pK determinations at high temperatures is discussed in the Appendix.)

K_0 is in the order of magnitude of 10^{-2}. Under these circumstances it is not possible to obtain reliable values with the potentiometric method.

Rate Constants. Experimental results of pseudo-first-order rate constants, k, for various hydroxonium ion concentrations at a constant ionic strength of $\mu = 0.1\ N$ are given in Table I. The data exhibit a similar pH dependence as found in the decarboxylation of p-aminobenzoic acid: k increases parallel to an increasing concentration of the cation, H_2A^+, in the acid–base equilibrium of the amino acid. The experimental values can be fitted into eq 3, which has been derived from rate equation 2. (The pseudo-first-order

$$k = \frac{K_0 k_H^{HA}[H^+]^2 + K_0 K_1 k_H^{A}[H^+]}{[H^+]^2 + K_0[H^+] + K_0 K_1} \qquad (3)$$

rate constant is defined by the equation k = rate/$[A_{total}]$, with $[A_{total}] = [H_2A^+] + [HA] + [A^-]$.) Empirical values for the parameters of eq 3 are given in Table II. K_0, $k_{H_2A} = K_0 k_H^{HA}$, and $k_{HA} = K_1 k_H^{A}$ are obtained from the rate data by a method of successive approximations, which has been described previously. Pseudo-first-order rate constants are calculated from these parameters with the aid of eq 3 and are compared with the experimental data in Table I. The agreement is satisfactory. Approximate Arrhenius parameters for k_H^{HA} and k_H^{A} are reported in Table III and a comparison is done with the corresponding results obtained for the decarboxylation reactions of 4-aminobenzoic and 2,4-dihydroxybenzoic acids.

Table IV contains results of kinetic measurements in acetate buffers. If buffer ratio and ionic strength are kept constant, the rate constant, k, does not depend on the buffer concentration. Consequently, there is no indication of general acid catalysis for this buffer system.

Results for k in strongly acidic solutions are reported in Table V. The first-order rate constant decreases by

(11) R. G. Bates, "Determination of pH," John Wiley and Sons, Inc., New York, N. Y., 1964.

Table I: Pseudo-First-Order Rate Constants for the Decarboxylation of Anthranilic Acid in Water (μ = 0.1 N KCl)

Temp, °C	$[H_3O^+]$	10^6k, sec^{-1} Obsd	Calcd
70.07 ± 0.04	3.89×10^{-2}	1.39	1.44
	2.90×10^{-2}	1.35	1.36
	1.91×10^{-2}	1.25	1.22
	9.87×10^{-3}	0.81	0.97
	4.92×10^{-3}	0.70	0.75
	2.95×10^{-3}	0.63	0.63
	7.53×10^{-5}[a]	0.30	0.30
	2.51×10^{-5}[a]	0.20	0.20
84.97 ± 0.04	3.98×10^{-2}	7.57	7.53
	2.98×10^{-2}	6.95	6.90
	1.98×10^{-2}	5.97	6.02
	9.89×10^{-3}	4.22	4.52
	4.93×10^{-3}	3.38	3.44
	2.96×10^{-3}	2.99	2.85
	2.05×10^{-5}[a]	0.78	0.77

[a] In acetate buffer.

Table II: Equilibrium and Rate Constants in Water (μ = 0.1 N)

Temp, °C	10^2K_0	k_{H_2A}, sec^{-1}	k_{HA}, sec^{-1}	10^4 k_H^{HA}, sec^{-1} mol^{-1}	$10^2k_H^A$, sec^{-1} mol^{-1}
70.07	1.57	1.88×10^{-6}	4.05×10^{-7}	1.20	1.60
84.97	2.29	1.08×10^{-5}	1.82×10^{-6}	4.72	6.48

Table III: Arrhenius Parameters for the Decarboxylation in Water (μ = 0.1 N)

Substrate	k_H^{HA} log A	k_H^{HA} E_a, kcal	k_H^A log A	k_H^A E_a, kcal
Anthranilic acid[a]	10.3	22.4	12.8	22.9
p-Aminobenzoic acid[b]	10.3	21.7	12.5	22.8
2,4-Dihydroxybenzoic acid[b]	...	...	13.06	23.3

[a] This work. [b] Reference 6.

Table IV: Decarboxylation of Anthranilic Acid in Aqueous Acetate Buffers (μ = 0.1 N KCl)

Temp, °C	10^2C_{HOAc}, N	10^2C_{NaOAc}, N	10^7k, sec^{-1}
70.07 ± 0.04	1	1	2.10
	2	2	2.08
	3	3	2.04
	3	1	3.01
	6	2	3.05
84.97 ± 0.04	2	2	7.88
	3	3	7.70

Table V: Decarboxylation of Anthranilic Acid in Aqueous Hydrochloric Acid Solutions at 84.97°

C_{HCl} (= [H$^+$]), N	h_0, N	10^6k, sec^{-1}	$10^{-5}Y$, sec
0.100	0.105	7.28	1.13
0.478	0.60	7.54	1.28
0.991	1.59	6.58	1.50
1.92	4.68	4.00	2.49
2.94	11.0	2.16	4.62
3.91	24.6	1.11	9.01

a factor of 7 when the hydrochloric acid concentration is increased from 0.5 to 3.9 N

Discussion

The apparent absence of general catalysis by acetic acid does not generally exclude the possibility of a rate-determining proton transfer. General catalysis may remain undetectable if the Brønsted α coefficient is close to unity. A well-known example of such a case is the acid-catalyzed hydration of alkenes.[12] An α value of 0.9 was found in the decarboxylation of p-aminosalicylic acid. It may be expected that α is even higher for less reactive substrates (which indicates more complete proton transfer in the transition state). General catalysis by acetic acid was still detectable in the decarboxylation of 2-hydroxy-1-naphthoic acid and p-aminobenzoic acid.[6] (However, the rate increases with increasing buffer concentration were not very much beyond the limits of experimental error.) It appears that in the decarboxylation of anthranilic acid, general acid catalysis has passed below the limit of detectability, possibly as a consequence of weak steric hindrance caused by the o-NH_2 group.

The rate maximum of the anthranilic acid decarboxylation is at a pH value between 0.2 and 0.5 (Table V), which is far away from the isoelectric point, $^1/_2$ (pK_0 + pK_1) = 3.10. Consequently, the observed rate–pH profile cannot be explained solely by assuming either rate-determining formation or rate-determining decomposition of a tautomer of HA, such as X (see below), whose rate of formation or equilibrium concentration, respectively, would be at a maximum value at the isoelectric point. The same conclusion has been drawn already by Dunn, *et al.*,[7] for the decarboxylation of p-methoxyanthranilic acid. Actually, the observed validity of eq 3, with $k_{H_2A} = k_H^{HA}K_0 > k_{HA}$, in the pH region above 1.5, is also sufficient to exclude such a simple mechanism. Therefore, the presence of the rate maximum in the high-acidity region must indicate a change of the rate-determining step.

It has been postulated[3,4,9] that in the two reaction

(12) F. G. Ciapetta and M. Kilpatrick, *J. Amer. Chem. Soc.*, 70, 639 (1948); R. W. Taft, E. L. Purlee, P. Riesz, and C. A. deFazio, *ibid.*, 77, 1584 (1955). For further references, see ref 3, Chapter VI.

pathways corresponding to rate equation 2, the σ complex intermediates X and HX^+ are formed

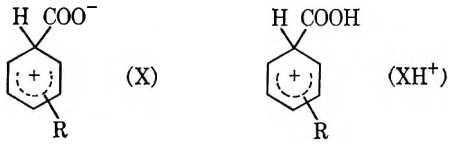

Since it may be expected that COO^- is a much better leaving group than COOH, the intermediate HX^+ presumably undergoes a fast acid–base reaction to form X, which then splits off carbon dioxide rapidly.[7] A complete scheme of all possible reaction steps is

$$\begin{array}{ccccc} HA + H_3O^+ & \underset{k_{-I}^0}{\overset{k_I^0}{\rightleftharpoons}} & HX^+ & \xrightarrow{k_{II}^0} & \text{product} + COOH^+ \\ \uparrow\downarrow K_1 & & \uparrow\downarrow K_0^* & & \\ A^- + H_3O^+ & \underset{k_{-I}^-}{\overset{k_I^-}{\rightleftharpoons}} & X & \xrightarrow{k_{II}^-} & \text{product} + CO_2 \end{array}$$

As has been shown previously,[7,8,13,14] eq 4 may be derived by applying the principle of the stationary state to the sum of concentrations of X and HX^+

$$k = \frac{k_I^0 K_0[H^+]^2 + k_I^- K_0 K_1[H^+]}{[H^+]^2 + K_0[H^+] + K_0K_1} \times \frac{k_{II}^- + k_{II}^0[H^+]/K_0^*}{k_{-I}^- + k_{II}^- + (k_{-I}^0 + k_{II}^0)[H^+]/K_0^*} \quad (4)$$

The first factor in this equation is essentially identical with the right side of eq 3. The second factor takes care of the decrease of the total rate due to return from the intermediates. If the two conditions $k_{II}^0 \gg k_{-I}^0$ and $k_{II}^- \gg k_{-I}^-$ are fulfilled simultaneously, the second factor will be equal to unity. It will be equal to a constant for low values of $[H^+]$ if $k_{II}^- \lesssim k_{-I}^-$. If on the other hand, the conditions $k_{II}^0 \ll k_{-I}^0$ and $k_{II}^- \ll k_{-I}^-$ are fulfilled at the same time, eq 4 can then be rearranged in such a way that it will have again the same mathematical form as eq 3. (In such a case, acid–base equilibria between HA, HX^+, X, and A^- are established at all times, and the slow step involves C–C bond cleavage.) A strong pH dependence of the second factor is to be expected for examples with either $k_{II}^0 \gg k_{-I}^0$ and $k_{II}^- \ll k_{-I}^-$ or $k_{II}^0 \ll k_{-I}^0$ and $k_{II}^- \gg k_{-I}^-$. (However, these extreme cases are not the only possibilities.)

The first derivative with respect to $[H^+]$ of the second factor, f_2, of eq 4 is equal to

$$\frac{df_2}{d[H^+]} = \frac{(k_{-I}^- k_{II}^0 - k_{II}^- k_{-I}^0)/K_0^*}{[k_{-I}^- + k_{II}^- + (k_{-I}^0 + k_{II}^0)[H^+]/K_0^*]^2} \quad (5)$$

The sign of $df_2/d[H^+]$ does not depend on $[H^+]$; it is determined by the sign of the expression in the parentheses in the numerator. For hydroxonium ion concentrations below 4×10^{-2} N, the second factor of eq 4 appears to be constant, since the pH dependence of the experimental rate constants, k, can be represented by the first factor of eq 4. For $[H^+] \geqq 1$ N, the first factor attains a constant value because $[H^+] \gg K_0 \gg K_1$ and $k_I^0 K_0 > k_I^- K_1$

$$f_1 = k_I^0 K_0 \quad (\text{if } [H^+] \geqq 1\ N)$$

According to the experimental data (Table V), k decreases if $[H^+]$ is increased to 1 N and higher. Consequently, the derivative of the second factor must be negative. It follows from eq 5 that

$$k_{-I}^- k_{II}^0 - k_{II}^- k_{-I}^0 < 0$$

$$k_{II}^0/k_{-I}^0 < k_{II}^-/k_{-I}^-$$

For the reasons discussed above, both ratios of rate constants cannot be on the same side with respect to unity, except if both are relatively close to unity. Consequently

$$k_{II}^0/k_{-I}^0 \lesssim 1 \quad (6a)$$

$$k_{II}^-/k_{-I}^- \gtrsim 1 \quad (6b)$$

As k_{II}^0 and k_{-I}^0 become more important with increasing $[H^+]$, eq 6a and 6b indicate a partial or complete change of the rate-determining step from proton transfer to the carbon at low $[H^+]$ to cleavage of the bond between the ring and carboxylic (or carboxylate) group at high $[H^+]$.

For a quantitative treatment of the rate data in strongly acidic solutions, it is advantageous to split off $k_{II}^-/(k_{II}^- + k_{-I}^-)$ from the second factor of eq 4. Furthermore, since in strongly acidic solutions $K_1 \ll [H^+]$ the term K_0K_1 may be neglected in the denominator of the first factor. Consequently, we obtain[13]

$$k = \frac{[H^+] + k_I^- K_1/k_I^0}{[H^+] + K_0} \frac{k_I^0 K_0 k_{II}^-}{k_{II}^- + k_{-I}^-} \times \frac{1 + k_{II}^0[H^+]/k_{II}^- K_0^*}{1 + (k_{-I}^0 + k_{II}^0)[H^+]/(k_{-I}^- + k_{II}^-)K_0^*} \quad (7)$$

As recently shown[13] this equation may be transformed into eq 9 by introducing thermodynamic equilibrium and rate constants, activity coefficients, and the Hammett acidity function[15] $h_0 = 10^{-H_0}$

$$[H^+] = a_H/f_H = h_0 f_{BH}/f_B f_H \quad (8)$$

$$k = \frac{(h_0 + a)d}{h_0 + b} \frac{1 + mh_0}{1 + ph_0} \quad (9)$$

The coefficients a, b, d, m, and p correspond to the ones in the equivalent positions of eq 7, except for the following: (i) all equilibrium and rate constants in the coefficients are thermodynamic constants valid for $\mu = 0$;

(13) A. V. Willi and P. Vilk, *Z. Phys. Chem.* (Frankfurt), in press.

(14) A. A. Frost and R. G. Pearson, "Kinetics and Mechanism," John Wiley and Sons, Inc., New York, N. Y., 1961.

(15) L. P. Hammett, "Physical Organic Chemistry," McGraw-Hill Book Co., Inc., New York, N. Y., 1940; M. A. Paul and F. A. Long, *Chem. Rev.*, 57, 1 (1957).

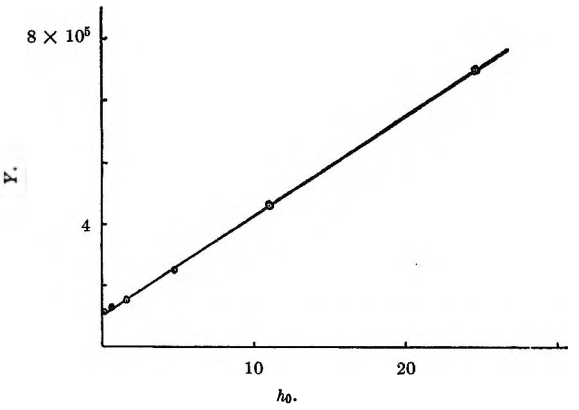

Figure 1. Y (eq 11) as a function of h_0.

(ii) each coefficient contains an activity coefficient ratio as a factor, for example

$$b = {}_0K_0(f_B f_{H_2A}/f_{BH} f_{HA}) \qquad (10)$$

The activity coefficients in a, b, m, and p occur as ratios of the type $f_+f_0'/f_+'f_0$. Only d contains the simple ratio $f_{H2A}/f_{\pm I}{}^0$. ($f_{\pm I}{}^0$ refers to the transition state of the formation of HX^+.)

If, according to eq 11, the variable Y is plotted as a function of h_0, a straight line is obtained[16] (Figure 1). This result indicates that

$$Y = \frac{h_0 + a}{k(h_0 + b)} = \frac{1 + ph_0}{d(1 + mh_0)} \qquad (11)$$

in the h_0 range of the experimental data mh_0 must be small in comparison to unity. A least-squares treatment of the data leads to the following empirical values for the coefficients

$$A = p/d = (3.24 \pm 0.03) \times 10^4 \text{ sec l. mol}^{-1}$$

$$B = 1/d = (1.04 \pm 0.06) \times 10^5 \text{ sec}$$

with a correlation coefficient of $R = 0.9998$.

Such a good correlation may be due to the fact that the particles involved in this reaction are similar to the nitroanilines, or their conjugate acids, respectively, which have been used to establish the h_0 scale. Furthermore, it follows that $d = 0.96 \times 10^{-5}$ sec^{-1} and $p = 0.311$ mol^{-1} l. d corresponds to $k_H{}^{HA}K_0 = k_{H_2A}$ in eq 3. The value of k_{H_2A} in Table II refers to an ionic strength of 0.1 N and it is 12% higher than the d value obtained in an extrapolation to $h_0 = 0$.

Since mh_0 is negligible, it follows from a comparison of eq 4 and 9 that the reaction step $HX^+ \rightarrow$ aniline + $COOH^+$ (which refers to $k_{II}{}^0$) does not appreciably contribute to the total reaction

$$h_0 k_{II}{}^0/k_{II}{}^- K_0{}^* = mh_0 \ll 1$$

$$k_{II}{}^0 \ll k_{II}{}^- K_0{}^*/h_0$$

Consequently

$$k_{II}{}^0 \ll k_{II}{}^-[X]/[HX^+]$$

A high limit for m may be computed on the basis of the assumption that the error of the k value for $h_0 = 24.6$ may be 10%. (This is much higher than the experimental error of k, but we have to consider that the assumption of the constancy of the activity coefficient ratios may not be valid with a very high precision. Furthermore, it is a matter of some doubt whether or not h_0 values determined at 25° can be precisely correlated with rate constants measured at 85°.) If $h_0 = 24.6$ and $k \leq 1.22 \times 10^{-6}$ [$= (1.11 \times 10^{-6}) + 10\%$] sec^{-1} are inserted into eq 9, it follows that $m \leq 0.00407$ mol^{-1} l.

A very important relation[13] may be derived by comparison of eq 7 and 9 if the activity coefficient ratios are set equal to unity

$$p/m = \frac{k_{-I}{}^0 + k_{II}{}^0}{k_{II}{}^0} \frac{k_{II}{}^-}{k_{II}{}^- + k_{-I}{}^-}$$

The lower limit of $p/m = 0.311/0.00407 = 76.5$ and the higher limit of $k_{II}{}^-/(k_{II}{}^- + k_{-I}{}^-) = 1$. Thus it follows that

$$\frac{k_{-I}{}^0 + k_{II}{}^0}{k_{II}{}^0} = k_{-I}{}^0/k_{II}{}^0 + 1 \geq 76.5$$

$$k_{-I}{}^0/k_{II}{}^0 \geq 75.5$$

This indicates that the return step from the intermediate HX^+ is much faster than the C–C bond-cleavage step with elimination of $COOH^+$. A sufficient increase of the acidity of the solution to fulfil the condition $k_{II}{}^- K_0{}^*/[H^+] \gtrsim k_{-I}{}^0$ (in order to decrease the rate *via* the pathway $HX^+ \rightarrow X \rightarrow$ products) will then lead to complete control of the total rate by the C–C bond-cleavage steps. In the range of the experimental data of Table V, however, the rate of cleavage of the C–C bond (*via* X) is still comparable to the rate of return from the intermediates HX^+ and X, and it is not yet completely rate determining. On the other hand, it is not precisely known whether or not there is still some return in weakly acidic solutions. If there is none (*i.e.*, if $k_{-I}{}^- \lesssim 0.01 k_{II}{}^-$), return in 3.9 N hydrochloric acid will amount to approximately 90%.

It should be emphasized that all these conclusions have been drawn solely on the basis of an analysis of the experimental data about the pH dependence of the rate. No use has been made of any structural argument (concerning the better leaving group, for instance) or of any additional experimental information, such as the absence of carbon isotope effects or the similarities of rate constants and Arrhenius parameters for anthranilic acid, 4-aminobenzoic acid, and 2,4-dihydroxybenzoic acid (Table III). Both findings are in agreement with the conclusions drawn from the pH

(16) a and b are relatively small in comparison to h_0. The errors will be insignificant if instead of the thermodynamic constants the values of the constants at $\mu = 0.1$ N are used ($a \approx k_I{}^- K_I/k_I{}^0$ and $b \approx K_0$).

dependence of the rate: at low [H+], the C protonation step is predominantly (or perhaps completely) rate determining. We cannot expect a pronounced primary carbon isotope effect in dilute solutions of strong acids up to 1 *N*.

The high limit of the over-all reaction rate is given by the rate of proton transfer from H_3O^+ to HA

$$\text{rate} = k_H^{HA}[H^+][HA] = k_H^{HA}K_0[H_2A^+] \quad (k_H^{HA} = k_I^0)$$

The rate must have attained its maximum value when practically all of the substrate is present as the cation, H_2A^+, provided that the rate of product formation, $k_{II}[X]$, is fast in comparison to the sum of the rates of the reverse reactions, $k_{-I}^-[X] + k_{-I}^0[HX^+]$ (The intermediate HX^+, after it has been formed from HA and H^+, loses the carboxylic proton in a fast step, and product formation always takes place *via* the intermediate X.)

In the high-acidity region ($[H^+] > 0.5$ *N*), the rate decreases with increasing h_0 as the rates of the reverse reactions become comparable with the decreased rate of product formation, $k_{II}^-[X]$. This is caused by the decrease of [X] due to the shift of the equilibrium $X + H^+ \rightleftharpoons HX^+$ in favor of HX^+.

Since the step $HX^+ \rightarrow$ product + $COOH^+$ (k_{II}^0) can be neglected in this example, the second factor of eq 4 becomes more simple, and we obtain for the pseudo-first-order rate constant

$$k = \frac{k_I^0 K_0 k_{II}^-}{k_{-I}^- + k_{II}^- + k_{-I}^0[H^+]/K_0^*}$$

The fraction $k/k_I^0K_0$ (the observed rate constant divided by maximum rate constant) must be equal to the ratio (rate of product formation of X):(total rate of conversion of X or HX^+).

$$k/k_I^0K_0 = k_{II}^-/(k_{II}^- + k_{-I}^- + k_{-I}^-[H^+]/K_0^*)$$

It follows that in 3.9 *N* HCl, 12% of the intermediate X goes over to the products immediately after it has been formed. Consequently, C–C cleavage is only partially rate determining even in 3.9 *N* HCl.

Experimental data have become available recently in this laboratory on the decarboxylation kinetics of *p*-aminobenzoic acid and *p*-aminosalicylic acid in strongly acidic solutions.[13] The method of treatment of the data is the same, and in Table VI results for p and m are compared with the ones obtained in this study. It may be expected that substituents at the aromatic ring cause approximately equal effects on k_{-I}^0, k_{II}^0, and k_{II}^-. Consequently the ratios k_{II}^0/k_{II}^- and $k_{-I}^0/(k_{II}^- + k_{-I}^-)$ may exhibit relatively little change when going from one substrate to another. Therefore, the values of p and m are governed mainly by the relative order of magnitude of K_0^*. If K_0^* increases, p and m must decrease (see eq 7 and 9). It is understandable that in the σ complex intermediates a substantial fraction of the positive charge is localized (by resonance) on the NH_2 group, and the repulsive electrostatic effect on the carboxylic proton is stronger if the NH_2 group is in the *ortho* position.

Table VI: Empirical Values for Parameters of Eq 9

Substrate	Temp, °C	10^5d, sec^{-1}	p, mol^{-1} l.	m, mol^{-1} l.
Anthranilic acid[a]	85.0	0.96	0.311	($\leq$0.00407)
p-Aminobenzoic acid[b]	85.0	1.30	4.35	0.024
p-Aminosalicylic acid[b]	30.0	0.240	1.84	

[a] This work. [b] Reference 13.

The experimental data for the decarboxylation of anthranilic acid do not supply evidence for a significant contribution of the reaction step $HX^+ \rightarrow$ aniline + $COOH^+$. In the example of *p*-aminobenzoic acid, however, the plot of Y *vs.* h_0 is curved, and the most likely explanation for this finding is the occurrence of such a reaction step with the rate constant k_{II}^0.[13,16a]

Appendix

The Accuracy of pH and pK_c Values Measured at High Temperatures. Since a referee questioned the accuracy of the pH and pK measurements at high temperatures, a discussion of the problem of pH measurement is given in this paragraph.

In this work, the pcH scale was used at a constant ionic strength of 0.1 *N* KCl. Calibration of the cell was carried out at the temperature of the measurements with a solution of 0.0100 *N* HCl and 0.0900 *N* KCl (pcH = 2.000). It has been shown previously in the example of the acid-catalyzed decomposition of ethyl diazoacetate at 20° that this type of pH measurement leads to very satisfactory results. In the pH region between 2.0 and 5.2, the simple linear equation log k = constant − pcH was fulfilled within ±0.017 pH unit or better.[17] It may be recommended very strongly to apply the pcH scale also for other correlations of kinetic data with pH values (provided these are in the region of 1.5–12.5).

As far as the pcH measurements at high temperatures are concerned, a special glass electrode was applied (Metrohm Type H) which has been developed for use

(16a) NOTE ADDED IN PROOF. Longridge and Long recently found evidence of a similar change of mechanism with increasing acidity in the decarboxylation of azulene-1-carboxylic acid. This example does not involve the complication of the protonation of an amino group. Therefore, k does not decrease with increasing acidity in the pH region in which the change of mechanism occurs since the reactive intermediate (comparable with X) contains the same number of protons as the substrate (J. L. Longridge and F. A. Long, *J. Amer. Chem. Soc.*, **90**, 3092 (1968)).

(17) A. V. Willi and R. E. Robertson, *Can. J. Chem.*, **31**, 493 (1953).

in the temperature region of 50–100°. Special care was taken that the solution and all essential parts of the cell were on the desired temperature.

An independent check of the accuracy of the high temperature pcH measurements can be made by comparison of our results for the pK_c of acetic acid with precision data published by other authors (emf measurements with a hydrogen electrode and electric conductance measurements). We obtained, for an ionic strength of 0.1 N, pK_c = 4.60 (70°) and 4.69 (85°). With the aid of the Debye–Hückel equation

$$\log \gamma_{\pm} = -A\sqrt{\mu}/(1 + \sqrt{\mu})$$

the following approximate thermodynamic pK values could be calculated: pK_a = 4.87 (70°) and 4.97 (85°).

As far as we know pK_a determinations of acetic acid have not been carried out at 70 and 85°. Extrapolation of the Harned and Ehlers pK_a data[18] in the temperature range 0–55° (5° intervals, H electrode) leads to pK_a = 4.85 (70°) and 4.91 (85°). Similar results are obtained by interpolation of Ellis' electric-conductance data[19] (25°, 50–200° (50° intervals), 225°): pK_a = 4.85 (70°) and 4.89 (85°).

The agreement of our result with these values is excellent at 70° and fair at 85°, if it is considered that errors of a few 0.01 pH unit may be caused by the inaccuracy of the Debye–Hückel equation as well as by the inaccuracies of the extrapolation or interpolation procedures.

(18) H. S. Harned and R. W. Ehlers, *J. Amer. Chem. Soc.*, **54**, 1350 (1932); **55**, 652 (1933).

(19) A. J. Ellis, *J. Chem. Soc.*, 2299 (1963).

Kinetics of the Bromine-Exchange Reaction of Gallium Bromide with Ethyl Bromide in 1,2,4-Trichlorobenzene and in Nitrobenzene[1]

by Oh Cheun Kwun and Sang Up Choi

Department of Chemistry, Hanyang University, Seoul, Korea *(Received January 18, 1968)*

The rate of the bromine-exchange reaction between gallium bromide and ethyl bromide in 1,2,4-trichlorobenzene and in nitrobenzene has been determined, utilizing ethyl bromide labeled with radioactive bromine. The results indicate that the exchange reaction is second order with respect to gallium bromide and first order with respect to ethyl bromide in each of the two solvents. The third-order rate constant determined at 19° is $(2.8 \pm 0.1) \times 10^{-2}$ l.^{2} mol^{-2} sec^{-1} in 1,2,4-trichlorobenzene and $(1.9 \pm 0.1) \times 10^{-3}$ l.^{2} mol^{-2} sec^{-1} in nitrobenzene. The activation energy, the enthalpy of activation, and the entropy of activation for the exchange reaction have been determined. It has also been observed that gallium bromide exchanges bromine faster with ethyl bromide than with methyl bromide. A reaction mechanism for the bromine exchange is proposed.

Introduction

A kinetic study of the bromine-exchange reaction of gallium bromide with methyl bromide in 1,2,4-trichlorobenzene and nitrobenzene solutions was carried out previously.[2] The results indicated that the exchange reaction was second order with respect to gallium bromide and first order with respect to methyl bromide in both solvents utilized. The third-order rate constants obtained at 19° in the two solvents were 0.82×10^{-2} and 2.4×10^{-5} l.^{2} mol^{-2} sec^{-1}, respectively.

A similar study was carried out by Sixma, Hendriks, and Holtzapffel on the system of aluminum bromide with ethyl bromide in carbon disulfide.[3] They reported that the bromine-exchange reaction between aluminum bromide and ethyl bromide was also second order with respect to aluminum bromide and first order with respect to ethyl bromide. The third-order rate constant obtained at 0.1° was 8.5×10^{-2} l.^{2} mol^{-2} sec^{-1}.

Thus the two groups of authors carried out exchange studies using different metal bromides and different alkyl bromides, and they observed same third-order

(1) Based on Ph.D. Thesis of O. C. Kwun, Kyungpook University, Taegu, Korea, 1968.

(2) S. U. Choi and J. E. Willard, *J. Amer. Chem. Soc.*, **87**, 3072 (1965).

(3) F. L. J. Sixma, H. Hendriks, and D. Holtzapffel, *Rec. Trav. Chim.*, **75**, 127 (1956).

kinetics for the exchange reactions. In order to make a closer comparison, it appeared important to extend the exchange studies to the system of gallium bromide with ethyl bromide. Furthermore, no decisive mechanism for the exchange reactions was proposed by both groups of authors mentioned above. Thus in the hope of presenting a reasonable mechanism, the present study on the bromine exchange between gallium bromide and ethyl bromide in 1,2,4-trichlorobenzene and nitrobenzene solutions was undertaken.

Experimental Section

Apparatus. The apparatus used in the present study was essentially the same as that used previously,[2] except for minor modifications.[4] All experiments were carried out in a high-vacuum system where the materials came in contact with glass and mercury, and more rarely with stopcock grease. The general vacuum-line techniques were similar to those described by Sanderson.[5]

Materials. Gallium bromide was prepared by the direct combination of metallic gallium with bromine in a vacuum line.[2,6] It was resublimed several times *in vacuo* and was collected in small ampoules with fragile tips.[2] Nitrobenzene (reagent grade, Merck, Germany) and 1,2,4-trichlorobenzene (special grade, Wako, Japan) were dried with Drierite, were fractionated in a 100-cm Todd column packed with glass helices, and were stored over Drierite.

Preparation of Ethyl Bromide (^{82}Br). A small quantity of solid potassium bromide (reagent grade, Merck, Germany) was irradiated with neutrons to induce (n,γ) reaction of bromine.[7] The irradiated potassium bromide was mixed with an appropriate amount of inactive potassium bromide. The mixture was then used to synthesize ethyl bromide labeled with ^{82}Br by the reaction of potassium bromide with ethanol in the presence of concentrated sulfuric acid.[8] After ethyl bromide was distilled from the reaction mixture, it was dried with calcium chloride. It was then introduced into and fractionated inside the vacuum line. The ethyl bromide (^{82}Br) thus prepared and purified was stored in the vacuum line.

Procedures Used in the Study of the Exchange Reactions. The experimental procedures used in the present study and the method of calculation of the exchange rates were similar to those described previously.[2]

Gallium bromide was introduced into the reaction vessel of the vacuum line. The weight of gallium bromide introduced was determined by weighing the ampoule and its fragments before and after the transfer. A known quantity of solvent, 1,2,4-trichlorobenzene or nitrobenzene, was then introduced into the reaction vessel from a side tube of the reaction vessel. Thus a solution of gallium bromide in 1,2,4-trichlorobenzene or nitrobenzene of known concentration was prepared inside the vacuum line.

The reaction vessel was maintained at the desired temperatures, 19, 15, 11, or 25°, by a water bath whose temperature was constant within ±0.05°. Vapors were circulated continuously over the surface of the magnetically stirred solution, with the aid of a small heating coil, as described previously.[2]

A known quantity of labeled ethyl bromide vapor was introduced to the reaction vessel by expanding the vapor from the storage system to the reaction vessel. This was taken to be time zero. Radioactivity of the ethyl bromide vapor near the scintillation detector was measured at constant time intervals. The concentration of ethyl bromide in solution was evaluated by knowing the total quantity of ethyl bromide present in the entire reaction vessel and by measuring the Henry's law constants for ethyl bromide over the solutions of gallium bromide in the two solvents.

The measured radioactivity should be proportional to the radioactivity of ethyl bromide present in the entire vapor phase of the reaction vessel, which should, in turn, be proportional to the radioactivity of ethyl bromide in solution. Hence from the measured counting rates as a function of time, the rate of exchange, R, of bromine between gallium bromide and ethyl bromide in solution was determined by the usual Guggenheim method[2,9]

$$R = -2.303\left(\frac{3ab}{3a+b}\right)\frac{d}{dt}\log\left(A_t - A_{t+\nu}\right) \qquad (1)$$

where a denotes the molar concentration of gallium bromide and b denotes that of ethyl bromide in solution. The term $A_t - A_{t+\nu}$ represents the change in counting rate during a constant time interval, ν, starting at a different time, t, after the reaction started. Counting rates were ordinarily in the range of 10,000–150,000 counts/min.

Procedures for the Solubility Determinations. In order to calculate the rates of the exchange reactions, the solubilities of ethyl bromide in the solution of gallium bromide in both 1,2,4-trichlorobenzene and nitrobenzene were measured. The apparatus and procedures for the solubility determinations were similar to those described previously.[2,10]

(4) Modifications involved the use of a scintillation detector instead of a Geiger tube and the use of an ordinary glass tubing in the place of the annular vessel used previously (vessel F of Figure 2 in ref 2).

(5) R. T. Sanderson, "Vacuum Manipulation of Volatile Compounds," John Wiley and Sons, Inc., New York, N. Y., 1948.

(6) W. C. Johnson and J. B. Parson, *J. Phys. Chem.*, **34**, 1210 (1930).

(7) The irradiation was carried out in a nuclear reactor, TRIGA-II, of the Atomic Energy Research Institute, Seoul, Korea. This assistance is gratefully acknowledged.

(8) R. Q. Brewster, C. A. Vanderwerf, and W. E. McEwen, "Unitized Experiments in Organic Chemistry," D. Van Nostrand Co., Inc., Princeton, N. J., 1963, p 62.

(9) See, for example, A. A. Frost and R. G. Pearson, "Kinetics and Mechanism," John Wiley and Sons, Inc., New York, N. Y., 1953, p 48.

(10) S. U. Choi, *J. Korean Chem. Soc.*, **7**, 65 (1963).

Results

Solubility Determinations. The solubilities of ethyl bromide in 1,2,4-trichlorobenzene and nitrobenzene were determined at several temperatures in the presence and absence of gallium bromide. The results are summarized in Table I. In each determination, good linearity was observed between equilibrium pressures of ethyl bromide and mole fractions of ethyl bromide in solution.

Table I: Solubilities of Ethyl Bromide in 1,2,4-Trichlorobenzene and in Nitrobenzene in the Presence and Absence of Gallium Bromide

Solvent	Temp, °C	[$GaBr_3$], M	Henry's law constant,[a] mm
$C_6H_3Cl_3$	19	0	560[b]
		0.321	547
		0.242	542
		0.104	550
		0.072	549[b]
		0.070	547[b]
		0.069	550[b]
		0.068	545[b]
	15	0	481
		0.319	448
	25	0	685
		0.206	667
$C_6H_5NO_2$	19	0	552[b]
		0.193	541[b]
		0.191	537[b]
		0.186	530[b]
		0.184	534[b]
	11	0	375
		0.333	345

[a] Henry's law constant is the equilibrium pressure of the gas (in mm) divided by its mole fraction in the solution. [b] Reference 10.

Table I shows that the Henry's law constants for ethyl bromide over gallium bromide solutions are smaller than those observed in pure solvents at each temperature. This indicates that ethyl bromide dissolves better in the gallium bromide solutions than in the pure solvents. This agrees with our previous observation that ethyl bromide has an interaction with gallium bromide both in 1,2,4-trichlorobenzene solution and in nitrobenzene solution.[10]

Bromine Exchange between Gallium Bromide and Ethyl Bromide in 1,2,4-Trichlorobenzene. The rates of bromine exchange between gallium bromide and ethyl bromide in 1,2,4-trichlorobenzene were measured at 19, 15, and 25°. The results are summarized in Table II. In each run good linearity was observed between log $(A_t - A_{t+\nu})$ and time. A typical result is shown in Figure 1. From slopes of these lines and molar concentrations of gallium bromide and ethyl bromide, the rate of the bromine exchange, R, was calculated with the aid of eq 1. The observed values of R are listed in the fourth column of Table II.

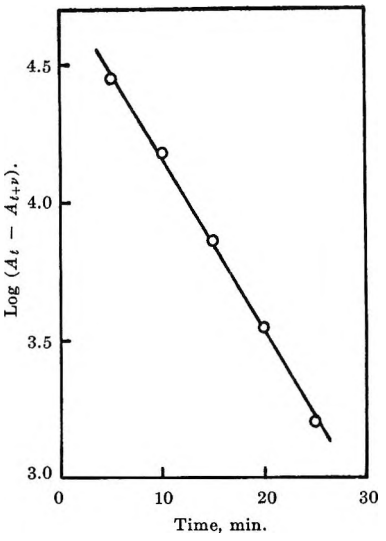

Figure 1. Plots of log $(A_t - A_{t+\nu})$ *vs.* time for the system of gallium bromide (0.230 M) with ethyl bromide (0.397 M) in 1,2,4-trichlorobenzene at 19°.

Table II: Rates of Exchange of Bromine between Ethyl Bromide and Gallium Bromide in 1,2,4-Trichlorobenzene

Reaction temp, °C	[$GaBr_3$], M	[C_2H_5Br], M	Rate × 10^4, mol $l.^{-1}$ sec^{-1}	10^2k_2, $l.^2$ mol^{-2} sec^{-1}
19	0.239	0.171	2.62	2.69
	0.239	0.304	4.79	2.76
	0.230	0.113	1.62	2.72
	0.230	0.231	3.43	2.81
	0.230	0.336	4.98	2.80
	0.230	0.397	6.03	2.87
	0.230	0.613	9.06	2.80
	0.135	0.406	1.96	2.64
	0.130	0.297	1.38	2.75
	0.106	0.209	0.673	2.87
	0.106	0.344	1.06	2.74
			Av	2.8 (±2%)
15	0.308	0.158	3.40	2.24
	0.308	0.269	5.48	2.15
			Av	2.2
25	0.313	0.364	11.9	3.35
	0.202	0.345	5.02	3.57
	0.177	0.158	1.83	3.70
	0.073	0.173	0.336	3.65
			Av	3.6

The exchange-reaction rate may also be expressed as

$$R = k[GaBr_3]^n[C_2H_5Br]^m$$

When the values of log R obtained at given $GaBr_3$ concentration were plotted against log [C_2H_5Br], good

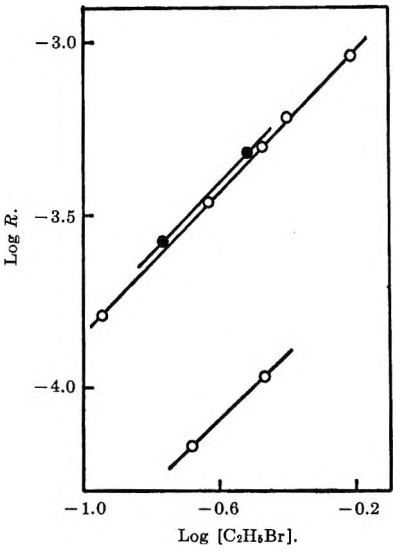

Figure 2. The effect of concentration of ethyl bromide on the rate of bromine exchange between ethyl bromide and gallium bromide in 1,2,4-trichlorobenzene at 19°: upper line, 0.239 *M* $GaBr_3$; middle line, 0.230 *M* $GaBr_3$; lower line, 0.106 *M* $GaBr_3$.

linearity was observed. Since the slope of each line (Figure 2) was approximately equal to 1, it was concluded that $m = 1$. Hence

$$R = k[GaBr_3]^n[C_2H_5Br]$$

When the values of log $\{R/[C_2H_5Br]\}$ were plotted against log $[GaBr_3]$, good linearity was again observed. Since the slope of the line (Figure 3) was approximately equal to 2, $n = 2$, and the following equation was obtained

$$R = k_3[GaBr_3]^2[C_2H_5Br] \quad (2)$$

It is concluded, therefore, that the bromine exchange in 1,2,4-trichlorobenzene is second order with respect to gallium bromide, and first order with respect to ethyl bromide.

The third-order rate constant, k_3, was evaluated by dividing the observed rate of exchange by $[GaBr_3]^2 \cdot [C_2H_5Br]$. The values of k_3 are listed in the last column of Table II. The k_3 values show good constancy at each temperature examined.

Good linearity was obtained by plotting the values of log k_3 against the reciprocal of the absolute temperature T (Figure 4). From the slope and intercept of this line, the activation energy E_a and the logarithm of the frequency factor log A of the bromine exchange were calculated to be 8.2 ± 0.9 kcal/mol and 4.6 ± 0.6, respectively.

In order to obtain other activation parameters for the exchange reaction, such as enthalpy of activation $\Delta H^{\pm}$ and entropy of activation $\Delta S^{\pm}$, the value of log (k_3/T) were plotted against the reciprocal of absolute temperature. Good linearity was again observed (Figure 5). From the slope and intercept of the line,

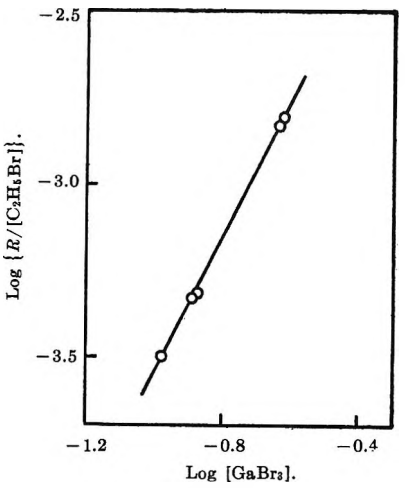

Figure 3. The effect of concentration of gallium bromide on the rate of bromine exchange between ethyl bromide and gallium bromide in 1,2,4-trichlorobenzene at 19°.

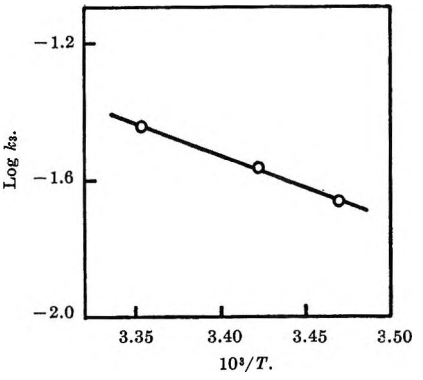

Figure 4. Temperature dependence of log k_3 of the bromine exchange reaction in 1,2,4-trichlorobenzene.

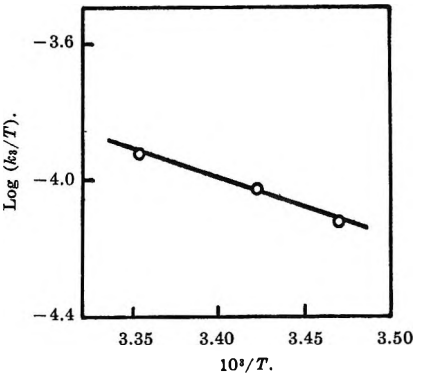

Figure 5. Temperature dependence of log (k_3/T) of the bromine exchange reaction in 1,2,4-trichlorobenzene.

the values of $\Delta H^{\pm}$ and $\Delta S^{\pm}$ for the exchange reaction were calculated to be 7.6 ± 0.9 kcal/mol and −40 ± 3 eu, respectively.

Bromine Exchange between Gallium Bromide and Ethyl Bromide in Nitrobenzene. The rates of bromine exchange between gallium bromide and ethyl bromide

in nitrobenzene were also measured at 19 and 11°. The results are summarized in Table III.

Table III: Rates of Exchange of Bromine between Ethyl Bromide and Gallium Bromide in Nitrobenzene

Reaction temp, °C	$[GaBr_3]$, M	$[C_2H_5Br]$, M	Rate × 10^5, mol $l.^{-1}$ sec^{-1}	10^2k_3, $l.^2$ mol^{-2} sec^{-1}
19	0.225	0.383	3.36	1.73
	0.225	0.428	3.55	1.64
	0.225	0.910	8.59	1.86
	0.225	1.25	12.6	2.00
	0.225	1.82	17.7	1.92
	0.191	0.261	1.90	2.00
	0.191	0.641	4.78	2.04
	0.191	0.937	6.88	2.01
	0.175	0.246	1.19	1.58
	0.144	0.216	0.852	1.90
	0.0920	0.469	0.867	2.17
	0.0835	0.127	0.177	2.00
	0.0835	0.401	0.565	2.02
			Av	1.9 (±7%)
11	0.342	0.467	5.17	0.95
	0.325	2.28	25.4	1.05
	0.162	0.868	2.51	1.10
			Av	1.0

Values of log R at given $GaBr_3$ concentration were plotted against log $[C_2H_5Br]$ (Figure 6), and values of log $\{R/[C_2H_5Br]\}$ were plotted against log $[GaBr_3]$ (Figure 7). Again, good linearity was observed. From the slopes of these lines, the following rate equation was obtained for the exchange reaction in nitrobenzene solution

$$R = k_3[GaBr_3]^2[C_2H_5Br]$$

The activation parameters for the exchange reaction in nitrobenzene solution were also estimated from the temperature dependence of the rate constant, although experimental data were taken only at two different temperatures. From the variation of log k_3 with the reciprocal of absolute temperature, the activation energy and the logarithm of the frequency factor of the exchange reaction were estimated to be 13 ± 2 kcal/mol and 6.7 ± 1.5, respectively. From the variation of log (k_3/T) with the reciprocal of absolute temperature, the values of $\Delta H^{\pm}$ and $\Delta S^{\pm}$ for the exchange reaction were estimated to be 12 ± 2 kcal/mol and −29 ± 7 eu, respectively.

Discussion

As a result of the present study, it is concluded that the reaction of bromine exchange between gallium bromide and ethyl bromide is second order with respect to gallium bromide and first order with respect to ethyl bromide. Similar kinetics were observed earlier on the systems of methyl bromide–gallium bromide[2] and ethyl bromide–aluminum bromide.[3] Thus it seems reasonable to consider a similar reaction mechanism for the bromine exchange between the two Friedel–Crafts catalysts and the alkyl bromides in solution.

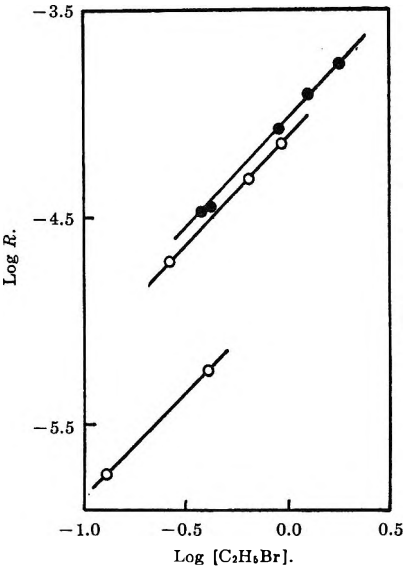

Figure 6. The effect of concentration of ethyl bromide on the rate of bromine exchange between ethyl bromide and gallium bromide in nitrobenzene at 19°: upper line, 0.225 M $GaBr_3$; middle line, 0.191 M $GaBr_3$; lower line, 0.0835 M $GaBr_3$.

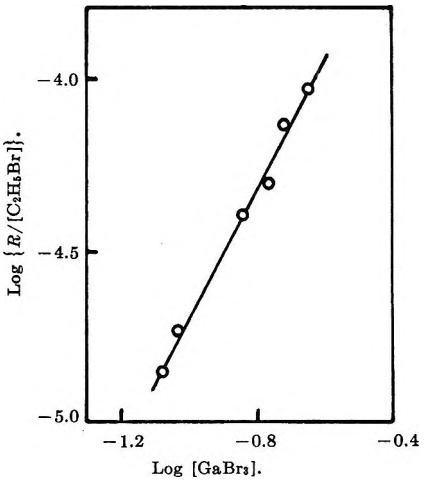

Figure 7. The effect of concentration of gallium bromide on the rate of bromine exchange between ethyl bromide and gallium bromide in nitrobenzene at 19°.

The results of the present study are compared with those of the earlier study on the corresponding system with methyl bromide (Table IV). It can be seen in Table IV that gallium bromide exchanges bromine faster with ethyl bromide than with methyl bromide. On the other hand, it has been noted that benzene and toluene react faster with ethyl bromide than with methyl bromide in the Friedel–Crafts alkylation reactions (Table V).[11,12] Hence, it appears reasonable

Table IV: Summary of Data Obtained for the Reactions of Bromine Exchange between Gallium Bromide and Alkyl Bromides

Solvent	Alkyl bromide	Kinetics (order)	k_3 (at 19°), l.² mol⁻² sec.⁻¹	E_a, kcal mol⁻¹	Log A	$\Delta H^{\ddagger}$, kcal mol⁻¹	$\Delta S^{\ddagger}$, eu
$C_6H_3Cl_3$	CH_3Br[a]	3rd	0.82×10^{-2}	14	7.9[c]	13[c]	−24[c]
	C_2H_5Br[b]	3rd	2.8×10^{-2}	8.2	4.6	7.6	−40
$C_6H_5NO_2$	CH_3Br[a]	3rd	2.4×10^{-5}	18	8.4[c]	12[c]	−37[c]
	C_2H_5Br[b]	3rd	1.9×10^{-3}	13	6.7	12	−29

[a] Reference 2. [b] The present study. [c] Evaluated from data reported in ref 2.

Table V: Summary of Data Obtained for the Friedel–Crafts Alkylation Reactions of Aromatic Hydrocarbons in 1,2,4-Trichlorobenzene

Catalyst	Aromatic	Alkyl bromide	$10^3 k_3$, l.² mol⁻² sec⁻¹	Ref
$GaBr_3$	Benzene	CH_3Br	0.0689	11
		C_2H_5Br	4.3	11
	Toluene	CH_3Br	0.673	11
		C_2H_5Br	28	11
$AlBr_3$	Benzene	CH_3Br	3.58	12
		C_2H_5Br	227	12
	Toluene	CH_3Br	18.3	12
		C_2H_5Br	653	12

to presume similarity in reaction mechanisms of both the bromine exchange and the alkylation reactions.

Reaction mechanism for the gallium bromide catalyzed alkylation reaction of benzene and toluene in 1,2,4-trichlorobenzene was previously postulated in the scheme (S, solvent molecules)

$$S + Ga_2Br_6 \rightleftharpoons S\text{–}Ga_2Br_6 \quad (3)$$

$$S + S\text{–}Ga_2Br_6 \rightleftharpoons 2S\text{–}GaBr_3 \quad (4)$$

$$RBr + S\text{–}GaBr_3 \rightleftharpoons R^{\delta+}Br^{\delta-}\text{–}GaBr_3 + S \quad (5)$$

$$ArH + R^{\delta+}Br^{\delta-}\text{–}GaBr_3 \xrightarrow{\text{slow}} \left[Ar{<}\begin{matrix}H\\R\end{matrix}\right]^{+} GaBr_4^{-} \quad (6)$$

$$S + \left[Ar{<}\begin{matrix}H\\R\end{matrix}\right]^{+} GaBr_4^{-} \rightleftharpoons ArR + HBr + S\text{–}GaBr_3 \quad (7)$$

In step 5 the formation of a polarized alkyl bromide–gallium bromide addition compound, $R^{\delta+}Br^{\delta-}\text{–}GaBr_3$, was assumed. The breaking of the carbon–bromine bond in the alkyl bromide was assumed to contribute significantly to stability of the transition state of the alkylation reaction. Thus the relative rates of alkylation of the alkyl bromides were attributed to the varying abilities for the alkyl radicals to tolerate positive charge. In step 6 the formation of a σ complex was assumed to be the rate-determining step of the alkylation reaction.

The reaction mechanism for the bromine-exchange reactions of gallium bromide with alkyl bromides is now assumed in a similar way to that described above for the Friedel–Crafts alkylation reactions

$$RBr + S\text{–}GaBr_3 \rightleftharpoons R^{\delta+}Br^{\delta-}\text{–}GaBr_3 + S \quad (5)$$

$$R^{\delta+}Br^{\delta-}\text{–}GaBr_3 + S\text{–}GaBr_3 \xrightarrow{\text{slow}} R^{+}Ga_2Br_7^{-} + S \quad (6')$$

$$S + R^{+}Ga_2Br_7^{-} \rightleftharpoons RBr + S\text{–}Ga_2Br_6 \quad (7')$$

In this mechanism again, the breaking of the carbon–bromine bond in the alkyl bromide molecules was assumed to take an important part in determining the stability of the transition state of the exchange reaction. Thus the experimental observation that gallium bromide exchanges bromine faster with ethyl bromide than with methyl bromide could be explained by the greater ability of ethyl group to tolerate positive charge than methyl group.

It has been previously observed that in the presence of hydrogen bromide aromatic hydrocarbons form σ complexes more readily with dimeric molecules of aluminum and gallium bromides than with monomeric aluminum and gallium bromides.[13,14] Now it is assumed that alkyl bromides interact more strongly with dimeric gallium bromide than with monomeric gallium bromide. Thus in step 6′ the formation of an ion-pair intermediate is assumed to proceed with the aid of a second molecule of gallium bromide monomer associated with solvent molecules.

Finally, it is assumed that step 6′ is the rate-determining step of the exchange reaction. Then this proposed mechanism leads to the kinetic expression

$$\text{rate} = k[S\text{–}GaBr_3]^2[C_2H_5Br]$$

which compares well with the experimental observations.

(11) S. U. Choi and H. C. Brown, *J. Amer. Chem. Soc.*, **85**, 2596 (1963).

(12) H. Jungk, C. R. Smoot, and H. C. Brown, *ibid.*, **78**, 2185 (1956).

(13) H. C. Brown and W. J. Wallace, *ibid.*, **75**, 6268 (1953).

(14) S. U. Choi and H. C. Brown, unpublished results.

The Paramagnetic Species from Titanous Salts and Hydrogen Peroxide

by Roland E. Florin, Fred Sicilio, and Leo A. Wall

National Bureau of Standards, Washington, D. C. 20234 *(Received January 22, 1968)*

The radical species giving esr spectra on mixing titanous salts and hydrogen peroxide cannot be hydroxyl as formerly supposed. Observed kinetics are inconsistent with simple generation and disappearance schemes. In organic-substrate mixtures the species increases with time, while organic radicals decrease. The two "hydroxyl" species are probably forms of HO_2 complexed with Ti^{4+}. The rate constant k_1 of the initial reaction, $Ti^{3+} + H_2O_2 \rightarrow OH + OH^- + Ti^{4+}$, is estimated as equal to or greater than 200 M^{-1} sec^{-1} from the appearance rate of Ti^{4+}–H_2O_2 and as 800–1800 M^{-1} sec^{-1} from indirect analysis of radical concentration–time curves.

Introduction

Upon mixing aqueous hydrogen peroxide and titanium trichloride in a flow system, Dixon and Norman observed an esr spectrum which they ascribed tentatively to hydroxyl.[1] Organic additives were attacked to yield plausible hydroxyl abstraction products

$$Ti^{3+} + H_2O_2 \longrightarrow Ti^{4+} + \cdot OH + OH^- \quad (1)$$

$$\cdot OH + RH \longrightarrow R\cdot + H_2O \quad (2)$$

Later investigators[2-5] found complicating features and proposed modifications in the structure. We have made further observations bearing on the rate of reaction 1, the stoichiometry and incidental products of the over-all reaction, and the kinetics of organic-substrate mixtures. According to our results, which are related to those of Fischer[5] and Turkevich, *et al.*,[4] it is now very unlikely that the observed spectra are those of a primary reactive species such as OH.

Experimental Section

Esr Spectra and Kinetics. The general experimental arrangements have been described[2] and resemble those used elsewhere.[1-5] In the present work, the only "dead volume" used was 0.10 cm^3.

Titanium Kinetics. A T-shaped mixer, followed by a uniform cylindrical downstream region housed in a sliding comparator block, was used to observe the rate of appearance of the deep yellow Ti^{4+}–H_2O_2 complex and also, for concentrated solutions in stoichiometric ratio only, the rate of disappearance of the purple Ti^{3+} color. Reference solutions, containing known concentrations of the Ti^{4+} complex in tubes of the same diameter, were moved up and down stream until a visual match was obtained. Note was taken of the downstream distance matching half the final Ti^{4+} concentration, as a function of flow rate. The time corresponding to this distance was computed with the aid of the measured cross section πr^2 by the formula $t = \pi r^2 s/F$, where s is the downstream distance and F is the flow rate. Although static comparisons could distinguish concentration differences of $\pm 10\%$ of the usual final concentration of the yellow complex, it is unlikely that times are more reproducible than $\pm 20\%$, which was the probable error of the apparent rate constant in one series of observations at different flow rates.

Titrations. Approximately 0.05 M hydrogen peroxide and 0.01 M $TiCl_3$ were made up by dilution with 0.1 M sulfuric acid. Titrations were done to the first appearance or final disappearance of a faint yellow peroxide-complex color. The titanium solution was standardized immediately after use with acid permanganate. The peroxide concentrations are relative to an assumed consumption ratio of 2.00 Ti/1.00 H_2O_2 in the usual titration, which agrees with the prepared concentration within 10%. In the more careful work, the $TiCl_3$ solution was stored in a deep container and was withdrawn from the bottom into a nitrogen-flushed buret, and the titrations were done in flasks, in a flowing nitrogen stream to guard against the fairly rapid oxidation of titanous chloride by atmospheric oxygen.[6]

Detection of Chemical Products. Solutions of equal molarity ($\pm 5\%$) in titanous chloride and hydrogen peroxide, containing methanol at several molar concentrations and 0.1 M sulfuric acid, were passed through a mixer into a receiver at 10 $\pm$ 5 cm^3 sec^{-1}. The product was adjusted to a colorless end point with one of the two solutions, usually 1–4% of the total volume. After a delay of 1 hr, formaldehyde was estimated in a portion of product by a Schiff's reagent method.[7]

(1) W. T. Dixon and R. O. C. Norman, *Nature*, **196**, 891 (1962); *J. Chem. Soc.*, 3119 (1963).

(2) F. Sicilio, R. E. Florin, and L. A. Wall, *J. Phys. Chem.*, **70**, 47 (1966).

(3) L. H. Piette, Preprint, Petroleum Division, 147th National Meeting of the American Chemical Society, Philadelphia, Pa., April 1964.

(4) Y. S. Chiang, J. Craddock, D. Mickewich, and J. Turkevich, *J. Phys. Chem.*, **70**, 3509 (1966).

(5) H. Fischer, *Ber. Bunsenges. Phys. Chem.*, **71**, 685 (1967).

(6) H. A. E. Mackenzie and F. C. Tompkins, *Trans. Faraday Soc.*, **38**, 465 (1942).

(7) J. E. Walker, "Formaldehyde," 3rd ed, Reinhold Publishing Corp., New York, N. Y., 1954, p 458; for an evaluation, see C. N. Satterfield, R. E. Wilson, R. M. LeClair, and R. C. Reid, *Anal. Chem.*, **26**, 1792 (1954).

The remainder was neutralized to pH 7 ± 0.5 with concentrated NaOH. A 5–10-ml portion was separated from salts by 5 hr of vacuum sublimation, room temperature to liquid-nitrogen temperature, followed by 30 min of heating of the residue at 100°. After storage of the condensate, 1–10-days at 10°, samples were analyzed by vapor chromatography, using a 10-ft by $^3/_{16}$-in. stainless steel column, containing 20% Carbowax 20M on 60–80 mesh Chromosorb W (acid washed) with a programmed column temperature of 100–180°, and a dual flame ionization detector. The column was calibrated with a synthetic mixture of 2 *M* methanol, 0.01 *M* formaldehyde, 0.01 *M* glycol and water; however, recovery efficiency in the complete experiments is uncertain. The flame-ionization detector was not sensitive to formaldehyde.[8]

Results

Radical Concentration–Time Curves. When large amounts of an organic reactant are present, the curves of the logarithm of radical concentration against time can be regarded as somewhat distorted straight lines. The slope is primarily governed by the hydrogen peroxide concentration, provided a large excess is present, and the general location is rather insensitive to substrate concentration provided that this is high. This interpretation is illustrated in Figure 1 and will be discussed in greater detail elsewhere.[9,10,10a] The gross behavior can be rationalized by the reaction sequence

$$Ti^{3+} + H_2O_2 \longrightarrow \cdot OH + OH^- + Ti^{4+} \quad (1)$$

$$\cdot OH + RH \longrightarrow R\cdot + H_2O \quad (2)$$

$$R\cdot + R\cdot \longrightarrow \text{products} \quad (3)$$

From the steady-state condition

$$k_1(H_2O_2)(Ti^{3+}) = kR^2$$

the slope of the plot of log [*R*] *vs. t* should approach the value

$$-k_1(H_2O_2)/(2 \times 2.303)$$

The rather indefinite k_1's thus deduced are in the range 880–1840 M^{-1} sec^{-1}. Other interpretations are also possible; the curves of Figure 1 suggest that the simple picture needs at least minor modification.

Concentration–Time Curves at Lower Substrate Concentration. At methanol concentrations typically below 0.05 *M* but dependent upon peroxide concentration, both the organic radical and the radical previously identified as ·OH are present, Figure 2. In the range of shorter times, the "OH" concentration grows while the $\dot{C}H_2OH$ concentration is falling. Others have reported the same changes.[4] A possible explanation is that the substrate becomes exhausted, which, in view of the relative amounts of Ti^{3+} and CH_3OH, would necessitate a chain reaction. A chain reaction is not too unlikely *per se*,[11] but an objection to the exhaustion hypothesis

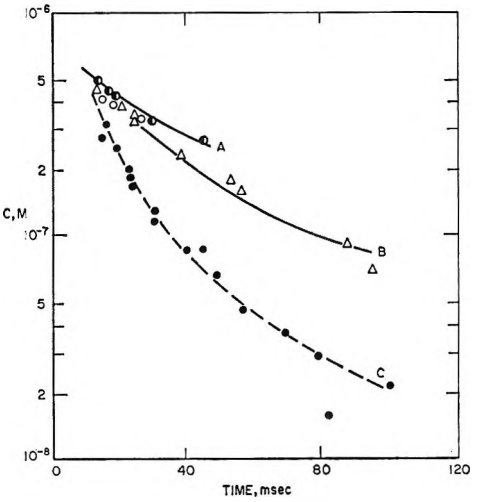

Figure 1. Concentrations of $\cdot CH_2OH$ as a function of time: temperature, 22°; concentration of $TiCl_3$, 0.005 *M*; concentration of CH_3OH and H_2O_2, respectively: (A) ◐, 1.25 *M*, 0.05 *M*; (B) ○, 0.125 *M*, 0.05 *M*; (B) △, 0.25 *M*, 0.05 *M*; (C) ●, 1.0 *M*, 0.10 *M*.

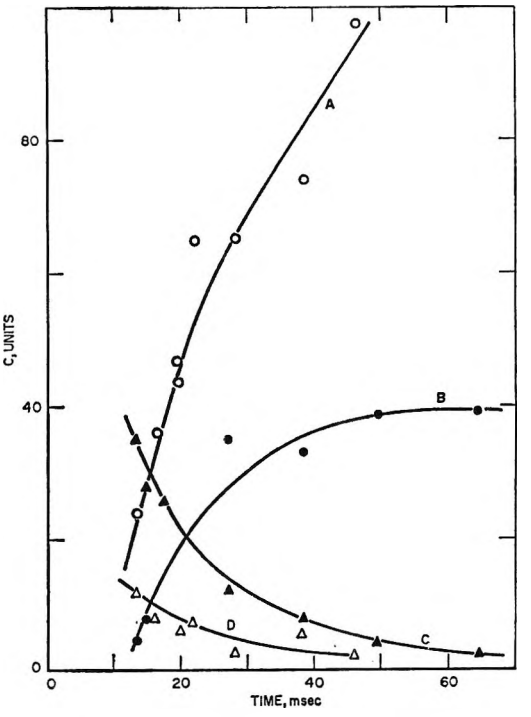

Figure 2. Radicals and "·OH" at intermediate substrate concentrations: temperature, 22°; 0.05 *M* H_2O_2; 0.005 *M* $TiCl_3$; (A) ○, "·OH;" (B) ●, "·OH;" (C) ▲, CH_2OH from 0.025 *M* CH_3OH; (D) △, CH_2OH from 0.017 *M* CH_3OH. One concentration unit equals 3.9×10^{-9} *M* $\cdot CH_2OH$ or 3.3×10^{-9} *M* "·OH."

(8) Thanks are extended to Dr. J. M. Antonucci, National Bureau of Standards, and Dr. E. Ragelis, Food and Drug Administration, for the chromatographic determinations.

(9) R. E. Florin, F. Sicilio, and L. A. Wall, *J. Res. Nat. Bur. Stand.*, A72, 49 (1968).

(10) R. E. Florin, F. Sicilio, and L. A. Wall, unpublished data.

(10a) NOTE ADDED IN PROOF. In all figures concentrations must be increased by the factor 35/3, related to quantum mechanics of the calibration with aqueous manganese. This does not affect the derived values of k_1.

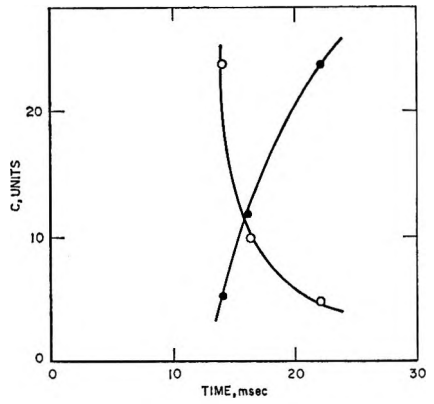

Figure 3. Radicals in 0.5 M acetic acid at 22°: 0.05 M H_2O_2, 0.005 M $TiCl_3$; ●, "·OH;" ○, $\cdot CH_2COOH$. The units are arbitrary, the concentration of "·OH" is greater than $\cdot CH_2COOH$.

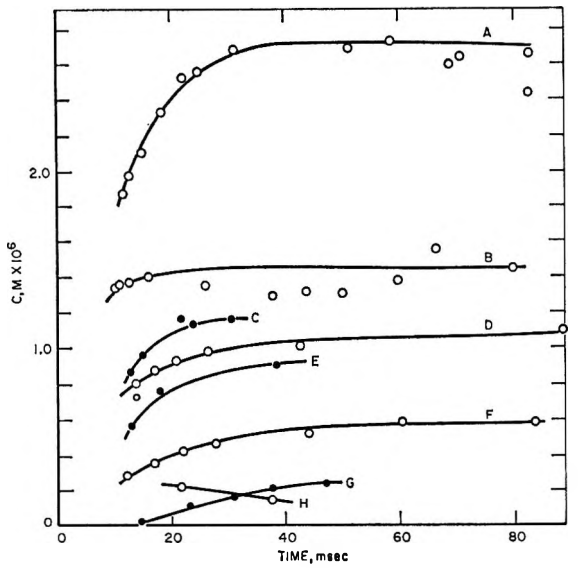

Figure 4. Concentration of the supposed "·OH" radicals produced at small or zero organic-substrate concentration: temperature, 22°; (A) 0.05 M H_2O_2, titanous sulfate 0.005 M in Ti^{3+}; (B) 0.1 M H_2O_2, 0.05 M $TiCl_3$, no substrate; (C) 0.005 M CH_3OH, 0.05 M H_2O_2, 0.005 M $TiCl_3$; (D) 0.05 M H_2O_2, 0.005 M $TiCl_3$, no substrate; (E) 0.01 M CH_3OH, 0.05 M H_2O_2, 0.005 M $TiCl_3$; (F) 0.025 M H_2O_2, 0.005 M $TiCl_3$, no substrate; (G) 0.015 M CH_3OH, 0.05 M H_2O_2, 0.005 M $TiCl_3$; (H) 0.05 M H_2O_2, titanous sulfate 0.114 M in Ti^{3+}.

is that the same behavior occurs with massive concentrations of the less reactive substrate acetic acid, which could not change appreciably during reaction, Figure 3. At the lowest substrate concentrations, the "OH" alone is seen. Its concentration grows more slowly and to lower maximum levels than in pure H_2O_2, Figure 4. These results are difficult to reproduce. It seems established that at some substrate concentrations the concentration of "OH" can reach higher maximum levels than in pure hydrogen peroxide.[4]

Titanium and Peroxide without Substrate. The growth of the hydroxyl-like radical for several conditions is shown in Figure 4. Results are not directly comparable with those of ref 2 because of the incompatible time scales, as discussed there. The most striking result is the much higher concentration reached in the sulfate system, curve A, although spectra are qualitatively similar.[2]

Unsuccessful attempts were made to produce radicals by the reaction of titanium trichloride with oxygen (saturated, 1.3×10^{-3} M) in 0.1 M sulfuric acid. No trace of the "hydroxyl" spectrum was seen and no $\dot{C}H_2OH$ spectrum was seen when methanol was present, although hydrogen peroxide at similar concentrations, 10^{-3} M, produced spectra several times above noise level. The reaction

$$Ti^{3+} + O_2 + H^+ \longrightarrow Ti^{4+} + HO_2\cdot$$

is a conceivable path for the obviously rapid consumption of Ti^{3+} exposed to oxygen and could be a factor in the nonappearance of O_2 when Ti^{3+} and H_2O_2 react. If the reaction occurs, either it is too slow for detection of the $HO_2\cdot$ produced or else the spectrum of the latter is broader than those seen with $Ti^{3+} + H_2O_2$. Some related reaction is likely, however, since dilute solutions of polyvinyl alcohol with $TiCl_3$ are rapidly degraded when oxygen is bubbled through them.[10]

Titanium Consumption Rates and k_1. The k_1 values computed from the downstream distance for half color change, flow speed, and tube diameter, are assembled in Table I. The uncertainty is great, but the order of magnitude agrees with the old instrumental determination by Chance,[12] whose result, 430–750 M^{-1} sec^{-1}, is probably the one to be preferred. The rate of color formation was apparently the same in the presence or absence of substrate, but the result is not very firmly established because of the large uncertainty. The significance of these values and of the value given by Chance is ambiguous in several ways. The reactions in question are

$$Ti^{4+} + H_2O_2 \longrightarrow Ti^{4+}\text{–}H_2O_2 \qquad (4)$$

and

$$OH + Ti^{3+} \longrightarrow Ti^{4+} + OH^- \qquad (5)$$

If eq 4 is always rapid, then the result measures k_1 provided eq 5 does not occur. If eq 1 is always followed rapidly by eq 5, at least up to half-consumption, then the k_1 of Table I really represents $2k_1$; on more careful investigation, the titanium consumption might show a change of regime, being governed initially by k_1 (OH low), soon after by $2k_1$ (Ti^{3+} and OH both high), and finally again by k_1 (Ti^{3+} low). If eq 4 is comparable with or slower than eq 1, the result merely states that k_1 (or $2k_1$) is at least as great as the tabulated value. It should be noted that the k_1 of Table I are only about

(11) J. H. Merz and W. A. Waters, *J. Chem. Soc.*, 515 (1949).
(12) B. Chance, *J. Franklin Inst.*, 229, 737 (1940).

Table I: Titanium Color Kinetics

Cross section (mixer), cm^2	Temp, °C	(H_2O_2), M	(CH_3OH), M	Half-life, sec	k_1, M^{-1} sec^{-1}
0.036	22	0.05	0	0.048–0.070	280–580
0.048	22	0.0125	0	0.260–0.310	200–240
0.048	48	0.0125	0	0.070–0.087	780–1180
0.036	22	0.05	0	0.036–0.076	186–386
0.036	22	0.05	1.0	0.051–0.070	198–272
0.036	22	0.05	0	0.025–0.040	350–555
0.036	22	0.05	2.0	0.038–0.049	284–370
0.129	22	0.025	0	0.106–0.130	210–260
0.129	22	0.025	2.0	0.129–0.129	210

one-fifth as great as those deduced from slopes in Figure 1, which range from 880 to 1840 M^{-1} sec^{-1}. If the interpretation of Figure 1 is correct, then reaction 4 is slow and rate determining.

Stoichiometry. A 1-mol amount of hydrogen peroxide consumes roughly 2 g-atoms of titanium when no substrate is present and consumes nearly 1 g-atom with a high concentration of substrate present, as shown in Table II. These results were obtained in a nitrogen atmosphere; in air the titanium consumption tends to be higher. The low result indicated in the second column of the first row was accompanied by a strong smell of chlorine in the effluent nitrogen stream. In 0.5 M polyethylene oxide, titrated in air, an approximate 1:1 consumption ratio was also obtained.

Table II: Titration of Titanous Chloride with Hydrogen Peroxide (g-atoms of Ti^{3+} per mole of H_2O_2)

	Peroxide into titanium	Titanium into peroxide
Pure (in 0.1 M sulfuric acid)	2.00	1.50
Methanol added (2 M)	1.24	0.96
Polyethylene oxide added (0.5 M), titration in air	...	1.0

Chemical Products. Ethylene glycol and formaldehyde were recovered from the rapid mixing of equimolar amounts of titanous chloride and hydrogen peroxide, containing methanol substrate. The amounts reported in Table III may be low by a large factor if recovery was inefficient.

Table III: Chemical Product Recovered from Methanol Oxidation[a]

	Concn of titanous chloride and hydrogen peroxide (prepared)				
	0.03	0.03	0.01	0.01	0.01
	Concn of methanol (prepared)				
	2.0	2.0	2.0	2.0	0.67
	Concn of product (found)				
Glycol	*b*	0.0038, 0.0054	*b*	0.0012	*b*
Formaldehyde	0.0023	0.0013	0.0005	0.0004	0.0005

[a] All concentrations are in moles per liter of the final mixture volume (0.1 M H_2SO_4). [b] Not determined.

Discussion

Previous measurements[2] indicated a possible disappearance rate constant of 4.5×10^5 M^{-1} sec^{-1} for the supposed "hydroxyl," which is very much less than the value for ordinary OH deduced from pulsed and steady-state radiolysis.[13–16] The discrepancy of rates alone is not completely conclusive, since it could be brought about by complexing and consequent charge effects. Possible complexing of the OH in metal ion–hydrogen peroxide systems is also suggested by the variations of the relative reactivity of α- and β-hydrogen atoms, *e.g.*, in ethanol, as one changes the source of the hydroxyl.[1,17,18] However, several features of the kinetics reported here are incompatible with the identification of the spectrum with any form of reactive hydroxyl.

The steady-state interpretation of radical concentration–time curves at high substrate concentrations, advanced in connection with Figure 1, agrees conceptually with that of Fischer,[19] although the latter does not need to consider explicit time dependence. Second-order curves taken individually, $1/c$ *vs.* t, actually make a better fit to the data, but they are mutually inconsistent, unlike those of Shiga[18] with ferrous systems.

Other interpretations of Figure 1 are difficult to exclude. For example, other reactions beside eq 3 could consume radicals

$$R\cdot + Ti^{4+} \longrightarrow Q \text{ (nonradical)} \quad (6)$$

$$R\cdot + Ti^{4+} \longrightarrow R^+ + Ti^{3+} \quad (7)$$

$$R^+ + H_2O \longrightarrow ROH + H^+ \quad (8)$$

$$R\cdot + HO\text{–}OH \longrightarrow Q \text{ (nonradical)} \quad (9)$$

$$R\cdot + HO\text{–}OH \longrightarrow ROH + \cdot OH \quad (10)$$

Several mechanisms involving one or more of reactions 6–10 as well as eq 1–3 yield closed-form equations reproducing the behavior shown in Figure 1. In most of these cases the slope and the color-appearance rates of Table I lose their simple significance. Reaction 10, once advocated for the Fenton's-reagent system, was

(13) H. A. Schwartz, *J. Phys. Chem.*, **66**, 255 (1962).
(14) G. Czapski and L. M. Dorfman, *ibid.*, **68**, 1169 (1964).
(15) J. H. Baxendale, "Pulse Radiolysis," Academic Press Inc., New York, N. Y., 1965, pp 17, 25.
(16) M. Anbar and P. Neta, *Int. J. Appl. Radiat. Isotopes*, **16**, 227 (1965).
(17) R. Livingston and H. Zeldes, *J. Chem. Phys.*, **44**, 1245 (1966).
(18) T. Shiga, *J. Phys. Chem.*, **69**, 3805 (1965).
(19) H. Fischer, *Makromol. Chem.*, **98**, 179 (1966).

abandoned in part by Waters[20] in favor of a combination involving analogs of eq 1 and eq 7, *e.g.*

$$R\cdot + Fe^{3+} \longrightarrow Fe^{2+} + R^+$$

Reactions such as eq 7 have been discussed in terms of redox potentials[21,22]

$$R\cdot \rightleftharpoons R^+ + e \quad (E_{-e})$$
$$R\cdot + e \rightleftharpoons R:^- \quad (E_{+e})$$

By observing the occurrence or failure of reduction in reference systems such as Fe^{3+}–Fe^{2+}, Sn^{4+}–Sn^{2+}, and methylene blue, it was estimated that E_{-e} was less than 0.4 V for a cyanoalkyl radical[22] and perhaps −0.2 V for a radical RĊHOH.[21] Since the value for TiO^{2+}–Ti^{3+} is near 0.1 V,[23] at pH 0, by the convention in which more positive values indicate stronger oxidants, reaction 7 seems thermodynamically possible for some radicals.[24] However, if eq 7 or 10 occurs, the rate cannot be a large multiple of the rate of reactions 1 and 3. Both reactions would increase the consumption of peroxide relative to titanium beyond the limits of Table II. The glycol yield, Table III, demonstrates the occurrence of the combination reaction (eq 3) to some extent, possibly much greater than indicated; the recovery of formaldehyde, a possible primary product of eq 7 or 10, is no greater. Thus although the reactions 7 and/or 10 may modify the set of eq 1–3 appreciably, they do not seem to be constituents of a long chain reaction.

Unlike curves of radical concentration, our previous "OH"-disappearance curves[2] cannot describe a steady-state concentration of the species, since in their time range the titanous ion is almost completely consumed and the radical formation rate is negligibly small.

When both the "OH" and R are present, the changes with time, Figure 2, are contrary to reasonable expectations for the true OH. The reactions involving radicals can be consolidated as

$$d(R)/dt = k_2(RH)(OH) - k_{11}(R)(OH) - k_3R^2$$

which includes

$$R + OH = ROH \qquad (11)$$

The steady state in R involves

$$\frac{(R)^2}{(OH)} = \frac{k_2(RH)}{k_3} - \frac{k_{11}(R)}{k_3}$$

The ratio on the left should give a linear plot against (R) with slope $-k_{11}/k_3$ and intercept $k_2(RH)/k_3$. Without the need for a plot, the data of Figure 2 are enough to show that this relation is incorrect; with increasing (R) (shorter time), $(R)^2/(OH)$ does not decrease but increases.

The behavior at intermediate concentrations, Figure 2, seems too complex to account for at present; in the example just given, the supposed (OH) and (R) are related very strangely for any simple mechanism.

In the pure Ti^{3+}–H_2O_2 system, two of the simpler mechanisms involving OH can be shown to be inadequate

$$Ti^{3+} + H_2O_2 \longrightarrow OH + OH^- + Ti^{4+} \qquad (1)$$
$$OH + Ti^{3+} \longrightarrow OH^- + Ti^{4+} \qquad (5)$$

and

$$Ti^{3+} + H_2O_2 \longrightarrow OH + OH^- + Ti^{4+} \qquad (1)$$
$$OH + OH \longrightarrow H_2O_2 \qquad (12)$$

These two cases have been developed completely in the literature.[25,26] Assuming that we can identify the radical species of ref 1–5 with OH, the experimental data to be accommodated are: the maximum concentration, 1.6×10^{-6} *M* in chloride or 10^{-5} *M* in sulfate; $k_1(H_2O_2)$, 12.5 sec^{-1} colorimetric or 44 sec^{-1} by log-plot slope; disappearance rate constant, 4.5×10^5 M^{-1} sec^{-1} at 28° or 3.2×10^5 M^{-1} sec^{-1} at 20°; and the initial concentrations, $(Ti^{3+}) = 0.005$ *M* and $(H_2O_2) = 0.05$ *M*. The three major types of data—maximum, $k_1(H_2O_2)$, and disappearance—cannot simultaneously be fitted to the Chien mechanism[25]

$$A \xrightarrow{"k_1"} B \qquad 2B \xrightarrow{"k_2"} C$$

Taking $(A)_0 = (Ti)_0 = 5 \times 10^{-3}$ *M*, "k_1" = $k_1(H_2O_2)$ = 50 sec^{-1} (*cf.* 44 sec^{-1}), "k_2" = 4.5×10^5 M^{-1} sec^{-1}, the intermediate parameter $\eta = (A_0)k_2/k_1$ has a value of 45. A solution for the choice is shown in Figure 5, where a normalized reciprocal concentration is plotted for easier comparison with ref 2. Some qualitative features are similar. The theoretical rate of rise to the maximum is too great relative to the experimental rate. The theoretical concentration at the maximum is much too high, approximately 6×10^{-4} *M*. In the approach of $1/c$ *vs.* t to second-order behavior, the slope theoretically approaches the final within 50% at $k_1(H_2O_2)t = 5.7$ and within 20% at $k_1(H_2O_2)t = 9.2$. The times are long, not absolutely but relative to the time at maximum, and they correspond to very small fractions of the initial titanium remaining, 3×10^{-3} and 10^{-4}, respectively. If we retain the same $(A)_0$ and $k_1(H_2O_2)$ but reject the experimentally derived k_2 in favor of more normal values, *e.g.*, 10^9 M^{-1} sec^{-1}, as found in pulsed radiolysis,[13–16] then the concentration at maximum is lower, 1.6×10^{-5} *M*, the time to reach maximum becomes very short, 1.6×10^{-4} sec, and the second-order slope is approached within 50% at $k_1(H_2O_2)t = 10$ (*i.e.*,

(20) W. A. Waters, "Vistas in Free-Radical Chemistry," Pergamon Press Inc., New York, N. Y., 1959, pp 155–160.

(21) D. J. Mackinnon and W. A. Waters, *J. Chem. Soc.*, 323 (1953).

(22) R. M. Haines and W. A. Waters, *ibid.*, 4256 (1955).

(23) W. M. Latimer, "Oxidation Potentials," Prentice-Hall, Inc., Englewood Cliffs, N. J., 1938.

(24) The authors are indebted to a reviewer for suggesting the possibility of reactions 6–10.

(25) J. Y. Chien, *J. Amer. Chem. Soc.*, **70**, 2256 (1948).

(26) S. Benxon, *J. Chem. Phys.*, **20**, 1605 (1952).

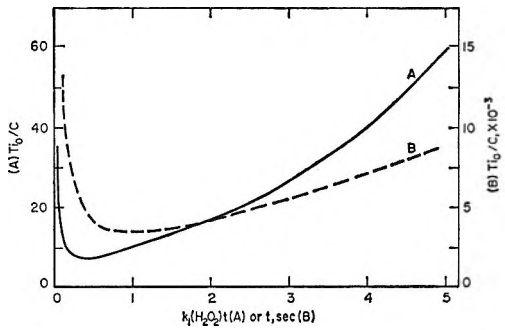

Figure 5. Comparison of "·OH"-radical kinetics with the Chien scheme,[25] $Ti^{3+} + H_2O_2 \xrightarrow{k_1} \cdot OH + OH^-$ and $2 \cdot OH \xrightarrow{k_2} H_2O_2$: (A) theoretical, $(A)_0 = (Ti)_0 = 5 \times 10^{-3}$ *M*, "k_1" $\equiv k_1(H_2O_2) = 50$ sec^{-1}, "k_2" $= 4.5 \times 10^6$ M^{-1} sec^{-1}; (B) experimental,[2] $(Ti)_0 = 5 \times 10^{-3}$ *M*, $(H_2O_2) = 0.05$ *M*, 20°.

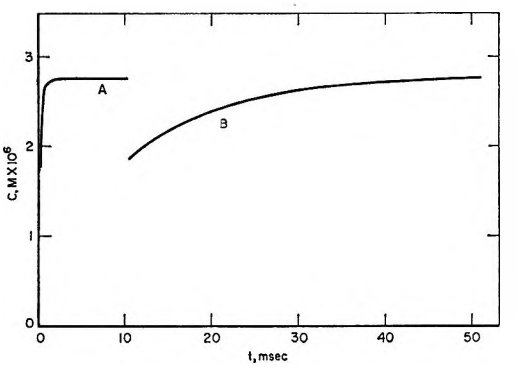

Figure 6. Comparison of "·OH"-radical kinetics with Benson's scheme,[26] $Ti^{3+} + H_2O_2 \xrightarrow{k_1} \cdot OH$ and $\cdot OH + Ti^{3+} \xrightarrow{k_2} Ti^{2+} + OH^-$: (A) theoretical, $(A)_0 = (Ti^{3+})_0 = 0.0014$ *M*, $K \cong (\cdot OH)_{max} = 2.75 \times 10^{-6}$ *M* from sulfate data, $(A)_0/K = 500$; (B) experimental, Figure 4.

0.2 sec), corresponding to concentrations near 3×10^{-8} *M*. In this latter case, an approximate first-order plot holds within a few per cent up to $k_1(H_2O_2)t = 7$.

Choices of parameters matching a low maximum concentration will demand a high k_2/k_1 and, therefore, a prolonged steady state, essentially first order and governed by k_1. Apparently in Chien's system a second-order regime can always be reached in principle, but for a larger η the region recedes to impractically long times and low concentrations. The limiting equations are obtained by applying to Chien's solution the properties of the Bessel and Hankel functions at small values of the argument.

$$\frac{1}{B} \cong \frac{k_2}{k_1} \frac{k_1 t - \ln\left(\frac{4(A_0)k_2}{k_1}\right) + \frac{\pi}{\beta}\sqrt{\frac{(A_0)k_2}{k_1}} e^{-k_1 t/2}}{1 - \frac{\pi}{\beta} e^{-k_1 t}}$$

$$\frac{1}{B} \cong k_2 t - \ln\left(\frac{4(A_0)k_2}{k_1}\right) + \epsilon$$

Here ϵ is a small quantity, and

$$\beta = \frac{kJ_1(2i\sqrt{\eta})}{H_1^1(2i\sqrt{\eta})}$$

is a parameter used by Chien, and the other symbols have been defined already. In the Benson mechanism[26]

$$A \xrightarrow{k_1} B$$

$$A + B \xrightarrow{k_2} C \quad (k_1/k_2 = K \cong B_{max})$$

K is close to 10^{-5} *M*, making $(A)_0/K = 5000$. Calculations after Benson's method show (Figure 6) that the high steady level is 92% attained at $k_1(H_2O_2)t = 0.005$ and 98% attained at $k_1(H_2O_2)t = 0.008$, *i.e.*, in a very small fraction of a reagent half-life. With the present $k_1(H_2O_2)$, the corresponding times would be immeasurably small. The disagreement would be greater for $K = 1.6 \times 10^{-6}$ *M*. More general objections are that the high level should remain forever (not serious, since it actually falls off very gradually compared with the growth rate) and that it should be nearly independent of the initial titanium concentration.

A modification of Benson's scheme involving $HO_2\cdot$ differs only in the identification of the constants, provided that OH is present in a low steady-state concentration

$$Ti^{3+} + H_2O_2 \xrightarrow{k_1} \cdot OH$$

$$\cdot OH + H_2O_2 \xrightarrow{k_{13}} HO_2\cdot \qquad (13)$$

$$HO_2\cdot + Ti^{3+} + H^+ \xrightarrow{k_{14}} H_2O_2 \qquad (14)$$

More complex systems can be devised, some of which are tractable. The observed species evidently has a low disappearance rate when alone, but the low maximum level suggests that something present during earlier stages of reaction either destroys the species or competes with its formation. If Ti^{3+} reacts with undetected ·OH as well as observed complexed $HO_2\cdot$, the low ultimate level, lowered formation rate, and dependence of level upon the initial $(Ti^{3+})_0$ can be accommodated. The difference between the sulfate and chloride results can be explained along two lines. (1) Ionic species in the $TiCl_3$ system differ generally in reactivity from those in the $Ti_2(SO_4)_3$ system; to illustrate, perhaps a $TiCl(H_2O)_5^{2+}$ ion reacts more slowly with H_2O_2 and more rapidly with ·OH than does $Ti(SO_4)(H_2O)_4^+$. (2) The chloride ion content of $TiCl_3$ acts as a competitive substrate or inhibitor, according to the sequence

$$H^+ + \cdot OH + Cl^- \longrightarrow Cl + H_2O \qquad (15)$$

$$Cl + Cl \longrightarrow Cl_2 \qquad (16)$$

Reaction 15, reported by Taube and Bray, is discussed in ref 21. Its effect will be somewhat offset by resemblances between OH and Cl reactions. This second

explanation is in accord with the reported unfavorable effect of added chloride in this system[1] and with the pronounced smell of chlorine observed when the reagents are mixed in a beaker. An oxidation–reduction cycle on chloride may play some part

$$H^+ + \cdot OH + Cl^- \longrightarrow Cl + H_2O \quad (15)$$

$$Cl + Cl \longrightarrow Cl_2 \quad (16)$$

$$Ti^{3+} + Cl_2 \longrightarrow Ti^{4+} + Cl + Cl^- \quad (17)$$

or

$$Ti^{3+} + Cl \longrightarrow Ti^{4+} + Cl^- \quad (18)$$

It seems unprofitable to attempt an exact kinetic account. Relying on Fischer's strongly supported suggestion[5] that one kind of "·OH" is Ti–O–O·$^{3+}$ and is formed by the reaction

$$\cdot OH + Ti(O^{2+})O \xrightarrow{k_{19}} OH^- + Ti{-}O{-}O\cdot^{3+} \quad (19)$$

and allowing for some inhibitor action by such substances as the Cl^- content of $TiCl_3$ as well as by added substrates, the following outline accounts for some features at intermediate substrate concentration

$$Ti^{3+} + H_2O_2 \xrightarrow{k_1} \cdot OH + OH^- + Ti^{4+}$$

$$Ti^{4+} + H_2O_2 \xrightarrow{k_4} Ti(O^{2+})O$$

(rapid; nearly all Ti^{4+} present as $Ti(O^{2+})O$)

$$\cdot OH + Ti(O^{2+})O \xrightarrow{k_{10}} Ti{-}O{-}O\cdot^{3+} + OH^-$$

$$\cdot OH + S' \xrightarrow{k_{20}} R' \quad (20)$$

$$R' + Ti{-}O{-}O\cdot^{3+} \xrightarrow{k_{21}} \text{inert products} \quad (21)$$

$$Ti{-}O{-}O\cdot^{3+} + Ti^{3+} \xrightarrow{k_{22}} Ti(O^{2+})O + Ti^{4+} \quad (22)$$

$$\frac{d(R')}{dt} = 0; \quad k_{20}(S')(OH) = k_{21}(R')(Ti{-}O{-}O\cdot^{3+})$$

$$\frac{d(OH)}{dt} = 0 = k_1(H_2O_2)(Ti^{3+}) - k_{20}(S')(OH) - k_{19}[(Ti^{3+})_0 - (Ti^{3+})](OH)$$

$$(OH) = \frac{k_1(H_2O_2)(Ti^{3+})}{k_{20}(S') + k_{19}[(Ti^{3+})_0 - (Ti^{3+})]}$$

$$(Ti)_0 e^{-k_1(H_2O_2)t} > (Ti^{3+}) > (Ti)_0 e^{-2k_1(H_2O_2)t}$$

$$\frac{d(Ti{-}O{-}O\cdot^{3+})}{dt} = \frac{\{k_{19}[(Ti)_0 - (Ti^{3+})] - k_{20}(S')\}k_1(H_2O_2)(Ti^{3+})}{k_{19}[(Ti)_0 - (Ti^{3+})] + k_{20}(S')} - k_{22}(Ti^{3+})(Ti{-}O{-}O\cdot^{3+})$$

If no reaction with inhibitor or substrate ($k_{20}(S')$, $k_2(S)$, or $k_{15}(Cl^-)$) is allowed, the initial rate of growth becomes $k_1(H_2O_2)(Ti^{3+})$, which appears too rapid, as discussed under the Benson scheme above. The $k_{20}(S')$ term in the denominator permits a lower initial rate of growth. Moreover, with a reactive substrate in the right intermediate amount, the growth rate can be zero initially but large later because of the increasing term $k_{19}[(Ti^{3+})_0 - (Ti^{3+})]$, dependent upon oxidized titanium. This is consistent with certain growth curves of Turkevich, *et al.*,[4] as well as with the present Figures 2 and 3. The acceleration of growth by the smallest substrate concentrations must still be explained along the lines of Turkevich, *et al.*;[4] *i.e.*, the reactivity of Ti^{4+}, its peroxide complex, and Ti–O–O·$^{3+}$ varies with the additional ligands such CH_3OH or SO_4^{2-}.

Numerical values of many of the rate constants above, or of close analogs, have been estimated by various methods.[13–16,27,28] Thus Anbar tabulates rate constants (in M^{-1} sec^{-1}) for eq 2, 6×10^8; eq 5, 3×10^8 (assumed the same as for Fe^{2+}); eq 12, 6×10^9; eq 13, 10^7; eq 15, 2×10^7 and 4×10^9 (divergent); and eq 23, 4×10^5, and other workers[27,28] estimate rate

$$OH + HSO_4^- = SO_4\cdot^- + H_2O \quad (23)$$

constants for eq 3 of 10^9 M^{-1} sec^{-1}. Reactions 11 and 16 may be similar to reactions 3 and 12, reaction 14 and 18 may be similar to reaction 5, and reaction 19 may be similar to reaction 13.

According to these values, competition for OH among stable components of our mixtures would go as in Table IV. Barring interference from reactions 7–10 or unidentified reactions, it seems that at high concentrations the organic substrate should compete successfully (reaction 2). This would involve low (OH) and the possible applicability of the simple reaction scheme outlined in reference to Figure 1. In the absence of an organic substrate, reaction 15 could dominate if the high value of k_{15} applies.

The previously reported low values for the disappearance rate[2] are only an order of magnitude lower than

(27) S. J. Rand and R. L. Strong, *J. Amer. Chem. Soc.*, **82**, 5 (1960).
(28) I. A. Taub and L. M. Dorfman, *ibid.*, **84**, 4053 (1962).

Table IV: Competition for OH

Reaction no.	Reactant	k, M^{-1} sec^{-1}	Present concn, M	kC, sec^{-1}
2	CH_3OH	6×10^8	2.0	1×10^9
4	Ti^{3+}	3×10^8 [a]	$<5 \times 10^{-3}$	$<1.5 \times 10^6$
13	H_2O_2	1×10^7	5×10^{-2}	5×10^5
15	Cl^- high	4×10^9	1.5×10^{-2}	6×10^7
	Cl^- low	2×10^7		3×10^5
23	HSO_4^-	4×10^5	0.1	4×10^4

[a] Assumed equal to Anbar's Fe^{2+}.[16]

those found elsewhere for $HO_2\cdot$,[15] suggesting a very moderate effect on rates due to complexing as Ti–O–O$\cdot^{3+}$. This is in curious contrast to the very long lifetime of the related O_2^- in pyridine.[29]

Conclusion

The foregoing arguments show at least that the supposed "OH" violates the two simplest kinetic schemes for a system of H_2O_2, Ti^{3+}, and ·OH and that when a substrate is present the species grows while its expected secondary products are declining. At present the most likely structure is some form of complex as proposed by Turkevich, *et al.*,[4] and specifically the structure Ti–O–O$\cdot^{3+}$ due to Fischer.[5] Such structures appear consistent with our observed kinetics. The latter is essentially a complexed, ionized $HO_2\cdot$ radical. Weaker evidence against the OH structure may lie in the high g averages computed from presumed spectra of ·OH in various irradiated single crystals,[30] *e.g.*, 2.0267 in ice and $Li_2SO_4\cdot H_2O$ and 2.0388 in $CaSO_4\cdot 2H_2O$.

(29) W. Slough, *Chem. Commun.*, 184 (1965).

(30) T. E. Gunter, *J. Chem. Phys.*, **46**, 3818 (1967).

Infrared Study of the Surface Properties of Phosphoric Acid Impregnated Silica

by M. J. D. Low and P. Ramamurthy

Department of Chemistry, New York University, New York, New York 10453 *(Received January 23, 1968)*

Adsorbents were prepared by impregnating Cab-O-Sil silica with phosphoric acid solution. Infrared spectra were recorded of the dehydration, the H_2O sorption and desorption, and the reaction with D_2O, pyridine, and NH_3. In addition to the bands of surface silanol groups, a sharp band was observed at 3666 cm^{-1}. The latter could be formed by reacting with H_2O, exchanged with D_2O, exhibited the behavior typical of bands of surface OH groups, and was assigned to the OH fundamental of isolated POH groups which do not interact with their surface environment. A broad band near 2900 cm^{-1} was attributed to surface hydroxyls involving =PO(OH) and similar structures. Some H_2O was dissociatively adsorbed, as was NH_3, generating POH groups. Bands tentatively assigned to NH_4^+, PNH_2, and PNHP structures were observed on NH_3 sorption. Pyridinium ions were formed on the hydrated surface. The various reactions, as well as the fact that phosphorus oxide was retained on the silica even after degassing at 800°, indicate that the adsorbent was not simply a dispersion of phosphoric acid or P_4O_{10} on an otherwise inactive silica support.

Recent work with porous glass and impregnated silicas showed impurities to be important in determining the adsorptive and reactive properties of the adsorbents.[1-7] For example, boria produced adsorption sites[4,5] for H_2O and NH_3, while aluminum ions acted as adsorption sites and polymerization centers[7] for HCN. As trivalent oxides modified the reactivity of the silica skeleton, it was desirable to extend the studies to pentavalent oxides. Phosphorus was chosen because, in view of the well-known isostructural relations between silicates and phosphates,[8] some of the material might "build" into the surface of the silica.

Experimental Section

The general procedures are described elsewhere.[2-7] Silica adsorbents were prepared by impregnating

(1) M. J. D. Low and N. Ramasubramanian, *Chem. Commun.*, 499 (1965).

(2) M. J. D. Low and N. Ramasubramanian, *J. Phys. Chem.*, **70**, 2740 (1966).

(3) M. J. D. Low and N. Ramasubramanian, *ibid.*, **71**, 730 (1967).

(4) M. J. D. Low, N. Ramasubramanian, and V. V. Subba Rao, *ibid.*, **71**, 1726 (1967).

(5) M. J. D. Low and N. Ramasubramanian, *ibid.*, **71**, 3077 (1967).

(6) M. J. D. Low, N. Ramasubramanian, and P. Ramamurthy, *J. Vacuum Sci. Techr.*, **4**, 111 (1967).

Cab-O-Sil powder[9] with aqueous P_4O_{10} solution using the incipient wetness method. The mixture was air dried at 115° for 5 hr. The powder was pressed at 20 tons/in.^{2} to form disks approximately 20 mm in diameter, weighing approximately 50 mg.

Porous glass, Corning Code 7930, was purchased from Corning Glass Works in 1-mm thick sheets. Samples approximately 1 × 10 × 25 mm were boiled in 2 wt % of aqueous P_4O_{10} solution for 30 min and air dried at 110° for 30 min.

Spectra were recorded with a Perkin-Elmer Model 521 spectrophotometer, usually with standard operating procedures. Screens and the instrument's device were frequently used to provide ordinate scale expansion below 2000 cm^{-1}.

Results and Discussion

Figure 1 shows the results obtained when a sample containing 5 wt % P_4O_{10} was progressively degassed. The band generally ascribed to the OH stretching fundamental of surface "free" SiOH groups was initially detected near 3740 cm^{-1}. That band, hereafter termed the SiOH band, declined in intensity and half-width and shifted to 3747 cm^{-1} above 300°. An intense absorption occurred over the range 3700–2000 cm^{-1}, the sample being opaque over the range 3500–2900 cm^{-1} at 25°. The opaque region became transmitting on degassing the sample, and the absorption turned into a rather broad band centering near 2900 cm^{-1}, which then progressively decreased. The transmittance increased more rapidly near 3500 cm^{-1} than in the 3000-cm^{-1} region on degassing. A narrower band was also observed. Initially near 3663 cm^{-1}, that band became smaller and sharper with increasing degassing temperature and shifted to 3666 cm^{-1}.

Spectra recorded at various degassing stages of a sample containing 2 wt % P_4O_{10} are shown in Figure 2. The changes in the SiOH and 3666-cm^{-1} bands were like those described for the 5 wt % sample, although the 3666-cm^{-1} band was less intense. A wide absorption occurred from about 3700 to 2000 cm^{-1}, but, unlike that found with the 5 wt % sample, consisted of two strongly overlapping and broad absorptions centered near 2900 and 3500 cm^{-1}. The 2900-cm^{-1} absorption declined slightly more rapidly than the 3500-cm^{-1} one and was not distinct above 300°. The 3500-cm^{-1} band formed a wide shoulder on the low wave number side of the SiOH band, much as was found with the desorption of water from porous glass.[5] In the later stages of degassing, a third broad band was observed centered near 3300 cm^{-1}. Examples of this are shown in spectrum E, Figure 1, and spectrum F, Figure 2.

Some experiments were carried out to determine if the new bands could be produced by adsorbing water. Some results are shown in Figure 3. A highly degassed specimen was exposed to H_2O vapor at 25°. At low pressure, *e.g.*, spectrum B, Figure 3, the SiOH band

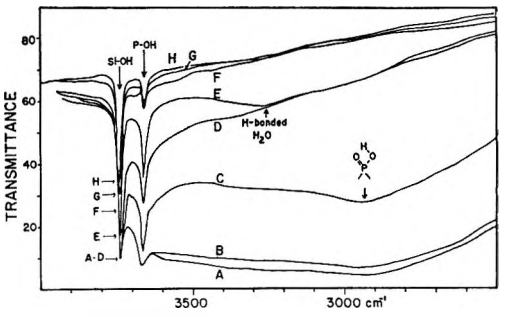

Figure 1. Dehydration of 5 wt % P_4O_{10}·SiO_2. After preparation the sample was degassed for 24 hr at 25° (A) and then for 2 hr at each of the following temperatures: B, 100°; C, 200°; D, 300°; E, 400°; F, 500°; G, 600°; H, 700°.

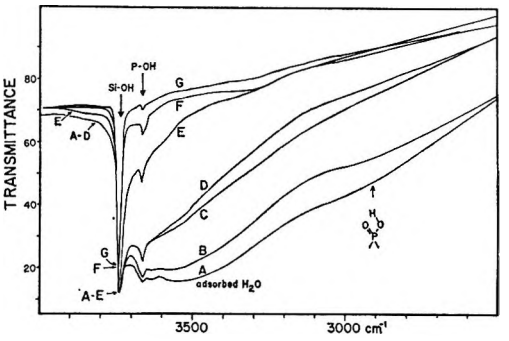

Figure 2. Dehydration of 2 wt % P_4O_{10}·SiO_2. After preparation the sample was degassed at the following temperatures and times, in hours: A, 25°, 12; B, 100°, 2: C, 200°, 2; D, 300°, 2; E, 400°, 5; F, 500°, 5; G, 600°, 5.

did not change significantly, but the 3666-cm^{-1} band increased and broadened. With increasing pressure, the SiOH band increased, broadened, and shifted to 3740 cm^{-1}; the 3666-cm^{-1} band declined; an ill-defined band appeared near 3700 cm^{-1}; and a broad absorption formed which was composed of two strongly overlapping broad bands centered near 3500 and 2900 cm^{-1}. The 3666-cm^{-1} band first increased, and then decreased, on degassing at progressively higher temperatures, *cf.* the sequence of spectra A–J of Figure 3. Much of the broad absorptions could be removed below 300°. At the end of the adsorption–desorption cycle, the SiOH band was significantly larger than at the beginning of the cycle. At intermediate stages of degassing the broad 3300-cm^{-1} band could be observed.

Treating a sample with D_2O caused changes in both the OH and OD regions. For example, a degassed sample of 5 wt % P_4O_{10} was treated with 5 torr of D_2O at 25°. Bands in the OH region declined and sharp bands were formed at 2754 and 2697 cm^{-1} in the OD region. Complete exchange could be effected by a fourfold

(7) M. J. D. Low, N. Ramasubramanian, P. Ramamurthy, and A. V. Deo, *J. Phys. Chem.*, in press.

(8) W. Eitel, "Silicate Science," Vol. I, Academic Press Inc., New York, N. Y., 1964, p 232 ff, and references therein.

(9) G. Cabot Co., Boston, Mass.

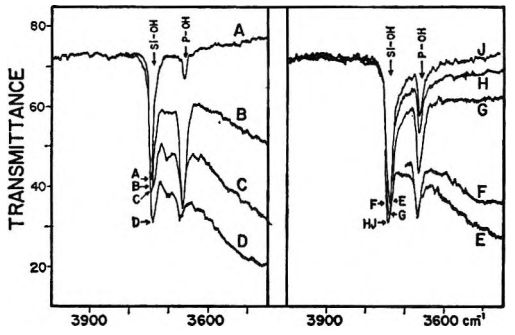

Figure 3. Reaction with H_2O. A specimen of 5 wt % P_4O_{10}·SiO_2 after degassing for 6 hr at 750° (spectrum A). The specimen was then exposed to H_2O at 25° and degassed at 25° for 5 min; the pressures, in torr, and exposure times, in hours, were, respectively: B, <1, 2; C, 4, 1; D, 18, 11. The specimen was then degassed at the following temperatures and times, in hours: E, 25°, 10; F, 100°, 2; G, 200°, 10; H, 350°, 4; J, 550°, 8.

repetition of heating in D_2O vapor at 200° for 2 hr and degassing at 350° for 1 hr, followed by a 3-hr degassing at 350°. The band positions with the fully deuterated surface were at 2754 and 2698 cm^{-1}. The ν_{OH}/ν_{OD} ratio of 1.359 for the 3666-cm^{-1} band closely approximates the theoretical value of the isomer shift expected for identical OH and OD structures and, with the observation that the decline of the 3666-cm^{-1} band accompanied the growth of the 2698-cm^{-1} band, indicates that OH groups were involved in the exchange reaction.

The adsorption of CCl_4 on a 5 wt % sample decreased the intensity of the SiOH band and shifted it to 3744 cm^{-1}, a band appeared near 3690 cm^{-1}, and the 3666-cm^{-1} band declined and broadened. The bands were restored when the CCl_4 was removed by pumping at 30°. Similar perturbations of the two hydroxyl bands were produced by NH_3 and pyridine adsorption and indicate that the OH groups were on the surface of the adsorbent.

Although the various experiments indicate that the sharp 3666-cm^{-1} band was caused by a surface OH species which was not the same as the silanol responsible for the 3747-cm^{-1} SiOH band, the possibility of a second silanol structure is not excluded. However, the band could be produced by impregnating pure silica with phosphoric acid, increased in intensity with increasing P_4O_{10} content, and occurred with adsorbents which had only been dried at 115°. In view of the low temperature, it seems unlikely that a structural modification of the adsorbent could have occurred which might give rise to a second silanol structure. The various observations thus lend some support to the suggestion that the 3666-cm^{-1} band (hereafter termed the POH band) was brought about by surface POH groupings.

It must be pointed out that the frequency of what has been termed the POH band is considerably higher than that generally found for P–OH stretching vibrations. As pointed out by Bellamy,[10] although the OH valency vibration is relatively independent of the nature of the group to which the OH is attached, with phosphorus compounds containing the =PO(OH) group, the hydrogen-bonding effects are even greater than those of carboxylic acids, so that the OH vibrations occupy a characteristic position; with acids, broad shallow bands appeared in the 2700–2560-cm^{-1} region. However, as shown by the various spectra, the POH band is relatively sharp, shows much of the behavior of the 3747-cm^{-1} silanol band, and is not strongly hydrogen bonded, so that the 2700–2560-cm^{-1} criterion need not apply. In view of this, the 3666-cm^{-1} band is ascribed to the OH stretching fundamental of surface POH groups which are "free" or interact only to a small extent with their environment, in direct analogy to free SiOH groups. This would imply that surface =PO(OH) structures are not responsible for the 3666-cm^{-1} band. The latter would be caused by OH on a portion of the P_4O_{10} surface where the interaction with neighboring P=O groups was minimal or perhaps by geminal hydroxyls formed by a reaction of H_2O with ≡P=O groups.

The simplest reaction of H_2O with the P_4O_{10} surface would be expected to result in the rupture of P–O–P linkages

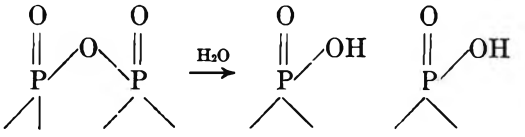

producing the hydrogen-bonded =PO(OH) species. These could then become further hydroxylated. The broad 2900-cm^{-1} absorption, which, as shown by Figures 1 and 2, increased with increasing P_4O_{10} concentration, is attributed to such species. The broad 3300-cm^{-1} band, which was also found with P_4O_{10}-impregnated porous glass, is attributed to H_2O bound to the hydroxylated P_4O_{10} surface. There was relatively little change of the SiOH band when appreciable amounts of water were removed from the surface, *e.g.*, spectra A–D of Figure 1 and spectra A–E of Figure 2. A substantial portion of the 3500-cm^{-1} absorption at relatively high stages of coverage is, therefore, attributed to the overlapping of the 3500- and 3300-cm^{-1} bands, *i.e.*, to H_2O hydrogen bonded to the hydroxylated P_4O_{10} surface. The 3500-cm^{-1} absorption and "tailing" in the 3700–3300-cm^{-1} region, *e.g.*, spectrum E of Figure 2, is attributed to H_2O adsorption on silanols. On H_2O sorption and desorption or on dehydration, it was found that the transmittance in the 2000–1400-cm^{-1} range changed by as much as 10%. However, distinct bands in the 1650–1600-cm^{-1} region, attributable to the H–O–H deformation of adsorbed

(10) L. J. Bellamy, "The Infrared Spectra of Complex Molecules," 2nd ed, John Wiley and Sons, Inc., New York, N. Y., 1960, p 319 ff.

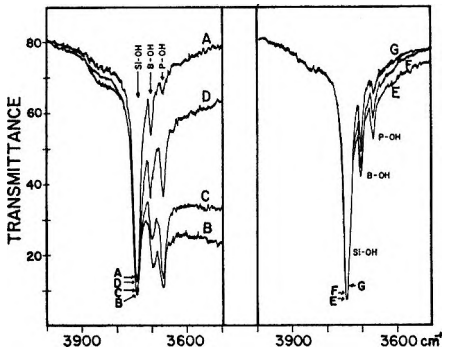

Figure 4. H_2O sorption on impregnated porous glass. A phosphoric acid impregnated porous glass specimen was degassed for 32 hr at 800° (spectrum A) and exposed to 3 torr of H_2O at 25° for 30 min and degassed for 5 min at 25° (spectrum B). The specimen was then degassed at the following temperatures and times, in hours: C, 100°, 12; D, 200°, 1.5; E, 300°, 3; F, 400°, 2; G, 500°, 2.

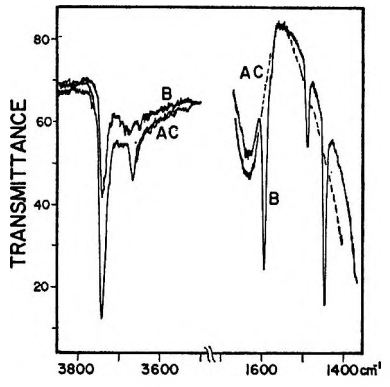

Figure 5. Pyridine sorption: A, a sample of 5 wt % P_4O_{10}·SiO_2 after degassing for 2 hr at 600°; B, after exposure to 10 torr of pyridine at 25° for 30 min and degassing for 5 min at 25°; C, after degassing for 10 hr at 100°.

H_2O, were not observed. The origin of the small band occasionally observed near 3700 cm^{-1}, *e.g.*, spectra C and D of Figure 3, is uncertain; loosely bound H_2O may be involved.

Porous Glass. A few experiments were carried out with phosphoric acid impregnated porous glass. Some results of H_2O sorption and desorption are shown in Figure 4. Broad bands were formed at 3500 and 3300 cm^{-1} when water was sorbed, but the most significant changes involved the POH band, *e.g.*, spectra B and C. The 3703-cm^{-1} band[1,2] was not appreciably affected, although surface boria is highly reactive to H_2O.[5] The results indicate that H_2O reacted preferentially with surface P_4O_{10}.

Pyridine Sorption. Some experiments were carried out with pyridine sorption to determine if the POH groups would readily act as Brønsted sites. Some results are shown in Figure 5. Pyridine sorption caused a large decrease of the SiOH and POH bands, and a broad absorption occurred from 3500 to 2000 cm^{-1}, centering near 3000 cm^{-1}. These effects are attributed to the hydrogen bonding of pyridine to silanol[11,12] and POH groups. The bands in the 3100–3000-cm^{-1} region of adsorbed pyridine[11,12] were weak and indistinct. However, sharp bands were observed at 1593, 1488, and 1443 cm^{-1}. These, using Parry's assignments[13] for the bands of physically and chemically adsorbed pyridine, are attributed to physically adsorbed pyridine. The spectrum of the adsorbent prior to pyridine sorption could be restored by degassing under mild conditions (spectrum C, Figure 5).

Bands attributable to the pyridinium ion[11,12] were not observed when pyridine was sorbed on a highly degassed specimen but were detected when pyridine was sorbed on a specimen which had been pretreated with water, as shown in Figure 6. Spectrum A of the hydrated surface exhibited a very broad absorption in the 3700–2000-cm^{-1} region similar to that of spectrum A of Figure 2. When pyridine was sorbed, bands were observed near 1591 cm^{-1}, with a shoulder near 1575 cm^{-1}, and at 1542, 1488, and 1440 cm^{-1}, and the broad absorption declined somewhat over the range 3700–2800 cm^{-1}. The 2591- and 1440-cm^{-1} bands declined appreciably on mild degassing (spectrum C, Figure 6). All bands were moved on degassing at 200°. Using Parry's analysis[13] again, the bands in the 1600–1400-cm^{-1} region are attributed to physically adsorbed pyridine and pyridinium ions. The results thus suggest that no appreciable quantity of pyridinium ions were formed on degassed surfaces by reaction with POH groups, although Farmer and Mortland's observations[14] that strong hydrogen bonding can diminish characteristic pyridinium ion bands make quantitation uncertain. However, pyridinium ions were formed by reaction with sorbed water.

Reaction with NH_3. The reaction of NH_3 with bulk P_4O_{10} has been studied many times, and the formation of a variety of products has been mentioned. Some of the work was reviewed by Becke-Goehring.[15] The sorption of NH_3 on phosphoric acid impregnated silica was consequently studied in order to determine if reactions other than physical adsorption would occur.

When a specimen was exposed to NH_3 at 25°, both the SiOH and POH bands declined and shifted to lower wave numbers, the POH band decreasing more rapidly than the SiOH band; and a broad absorption occurred from 3600 to 2000 cm^{-1} centering near 3000 cm^{-1}. When the sample was subsequently degassed, the SiOH band increased and then decreased at degassing temperatures

(11) M. R. Basila, T. R. Kantner, and K. H. Rhee, *J. Phys. Chem.*, **68**, 3197 (1964).

(12) M. J. D. Low and V. V. Subba Rao, *Can. J. Chem.*, in press.

(13) E. P. Parry, *J. Catal.*, **2**, 371 (1963).

(14) V. C. Farmer and M. M. Mortland, *J. Chem. Soc., A*, 344 (1966).

(15) M. Becke-Goehring, DDC Document No. AD 639932, 1958; M. Becke-Goehring and J. Sambeth, *Z. Anorg. Allg. Chem.*, **297**, 18 (1958).

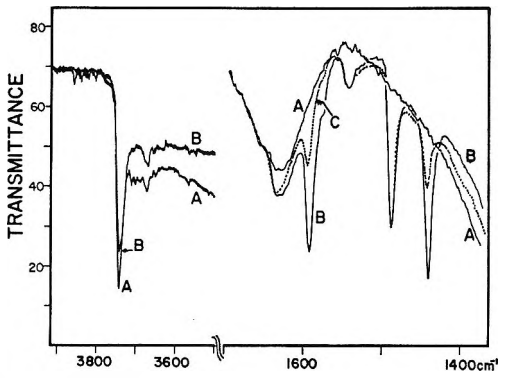

Figure 6. Pyridine sorption on a hydrated sample of 5 wt % $P_4O_{10}\cdot SiO_2$: A, after exposure to 1 torr of H_2O at 25° and degassing at 200° for 5 hr; B, after exposure to 10 torr of pyridine at 25° for 1 hr and degassing at 25° for 5 min; C, after degassing for 1 hr at 50°.

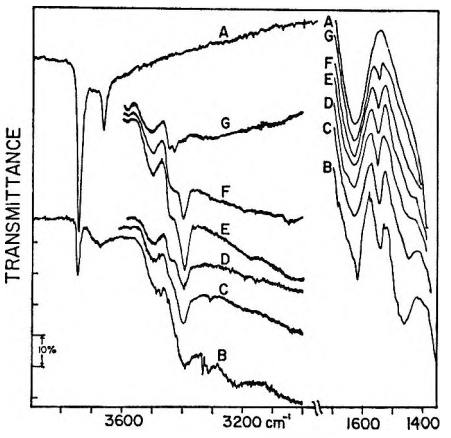

Figure 7. Reaction with NH_3: A, a specimen of 5 wt % $P_4O_{10}\cdot SiO_2$ after degassing for 5 hr at 600°; B, after exposure to 60 torr of NH_3 for 2 hr at 25°; C, after exposure to 60 torr of NH_3 for 48 hr at 25°, followed by 10 min degassing at 25°. The sample was then degassed at the following temperatures and times, in hours: D, 25°, 12; E, 100°, 1; F, 150°, 1; G, 200°, 1. The ordinates are displaced; the transmittance was 73% at 3900 cm^{-1} for each trace. Spectra E–G and others in the region below 1700 cm^{-1} are ordinate expanded.

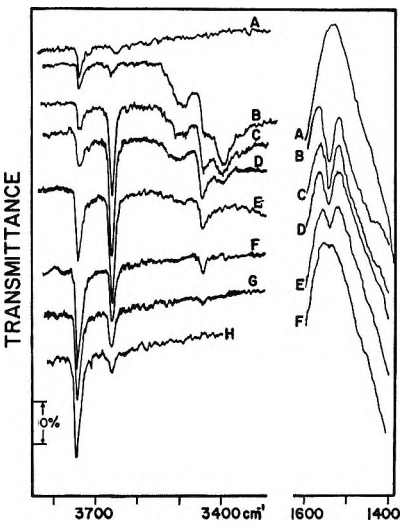

Figure 8. OH generation of dehydroxylated surface: A, a specimen of 5 wt % $P_4O_{10}\cdot SiO_2$ after degassing for 9 hr at 800°; B, after exposure to 40 torr of NH_3 at 25° for 1 hr and degassing at 25° for 10 min. The sample was then degassed at the following temperatures and times, in hours: C, 25°, 12; D, 100°, 1; E, 200°, 1.5; F, 250°, 1; G, 300°, 1; H, 300°, 2. The ordinates are displaced; the transmittance was 71–73% at 3800 cm^{-1}. The regions below 1600 cm^{-1} are ordinate expanded.

higher than 350°, the POH band increased until 200° was reached and declined at higher temperatures, and much of the broad absorption could be removed at room temperature, the rest disappearing near 200°. These over-all effects of NH_3 sorption and desorption on OH groups were similar to those observed on sorbing NH_3 on porous glass[4] and, in analogous fashion, are attributed mainly to perturbations of surface SiOH and POH groups by hydrogen bonding to physically adsorbed NH_3. Bands caused by more tightly bonded species were also observed. Some spectra of a degassing sequence are shown in Figure 7 (and also in Figure 8). The various results can be summarized as follows. (a) Bands near 3400, 3220, and 1620 cm^{-1} could be greatly diminished by pumping at room temperature. These are ascribed[16] to the asymmetric and symmetric NH stretching vibration and to the asymmetric deformation vibration of physically adsorbed NH_3. (b) A band at 3400 cm^{-1} decreased with increasing degassing temperature and disappeared above 200°; simultaneously, an absorption decreased in the 1500–1400-cm^{-1} region. At high surface coverage (spectrum B, Figure 7), the band was near 1460 cm^{-1}, shifted to 1450 cm^{-1} on mild degassing (spectrum C, Figure 7), and then became ill-defined because of the sloping background. After some further degassing, the absorption appeared to be caused by two overlapping bands near 1480 and 1450 cm^{-1} (spectrum D, Figure 7). (c) An absorption which at first was observed as a shoulder near 3430–3420 cm^{-1} on the 3400-cm^{-1} band became more distinct on degassing (spectrum F, Figure 7); it declined but became a distinct band at 3440 cm^{-1} and disappeared near 350°. Simultaneously, a band shifted from 1540 to 1549 cm^{-1}, declined, and disappeared near 350°. (d) A broad band near 3550 cm^{-1} declined with increasing temperature and disappeared above 200°.

Difficulties arise in attempting to make assignments for the observed bands, because groups containing NH linkages bound to phosphorus have not been studied extensively, and a variety of surface structures can be postulated. The bands in the 3500–3400-cm^{-1} region fall within the general range found for NH stretching vibrations but are higher than the range reported for

(16) V. N. Abramov, A. V. Kieselev, and V. I. Lygin, *Russ. J. Phys. Chem.*, **38**, 1020 (1964).

the NH_4^+ ion[17] and PNH_2 and PNHP groupings.[18,19] Although it is not possible to make definite assignments, the intensity changes of bands in the 3500–3400- and 1600–1400-cm^{-1} regions suggest that each of the pairs of bands observed (*i.e.*, 3400 and 1450, 3450 and 1549, and 3500 and 1480 cm^{-1}) was brought about by a different surface grouping.

The 1450-cm^{-1} band is quite close to the frequencies reported for the NH deformation mode of the NH_4^+ ion, as summarized by Little,[17] and is consequently assigned to the NH_4^+ deformation. Some support for this assignment comes from the following experiments. A 5 wt % $P_4O_{10}\cdot SiO_2$ sample was exposed to NH_3 and degassed at 25° for 6 hr; the spectrum showed bands at 3500, 3440, 3400, and 1549 cm^{-1}, a weak shoulder at 1450 cm^{-1}, and a shallow broad band centered near 3000 cm^{-1}. The NH_3-treated specimen was then exposed to 5 torr of H_2O at 25° for 30 min and was degassed at 25° for 5 min. After this treatment, the 3500-, 3440-, and 1549-cm^{-1} bands disappeared, and the 1450-cm^{-1} band was increased. The 3400-cm^{-1} band was smaller but was superimposed on a broad band due to adsorbed H_2O. The results suggest that NH_4^+ species had been produced by reaction of sorbed NH_3 with H_2O, although a band in the vicinity of 3300 cm^{-1} attributable[17] to the NH stretching mode of NH_4^+ was not observed. The band at 3400 cm^{-1} which appears and disappears in concert with the 1450-cm^{-1} band is assigned to the NH stretching vibration of the NH_4^+ ion, although its frequency is higher than that usually reported for that mode.[17]

For the 3450 and 1549 cm^{-1} pair, the 1549-cm^{-1} band falls well within the range of the NH deformation vibration for PNH_2 groups, but the 3450-cm^{-1} band is higher than the range of 3330–3100 cm^{-1} reported for the corresponding NH stretching vibrations found with solids.[18,19] The 3500-cm^{-1} band, which may be associated with the 1480-cm^{-1} shoulder, is similarly outside the range reported for P–NH_2 and P–NH–P vibrations. It is perhaps significant that in spectra of degassing sequences, such as those of Figures 7 and 8, the transmittance on the high wave number side of the 3400-cm^{-1} band increased, much as if an absorption located between the 3450- and 3400-cm^{-1} bands became weaker. If the 3500-cm^{-1} band is taken as the asymmetric band of PNH_2, the Bellamy and Williams relation[20] between the frequencies of asymmetric and symmetric NH_2 bands predicts the symmetric band to occur at 3411 cm^{-1}, *i.e.*, on the high wave number side of the 3400-cm^{-1} band. This would imply the assignment of 3500-, ~3411-, and ~1480-cm^{-1} absorptions to PNH_2 groups and the pair of bands at 3450 and 1549 cm^{-1} to PNHP structures. Although speculative, these assignments are tentatively adopted.

Some support for the formation of secondary or primary amines comes from other experiments. Spectra of sorption–desorption cycles suggest that additional SiOH and POH groups were generated, but the changes in the hydroxyl region were difficult to define because of the hydrogen-bonding effects and the continual intensity changes of both OH bands. Some further experiments were, therefore, carried out with highly dehydroxylated specimens. Some results are shown in Figure 8. The adsorbent was subjected to high-temperature degassing so that, as shown by the small OH bands in spectrum A, most of the surface OH groups had been removed. When the specimen was then exposed to NH_3 and mildly degassed (spectra B–D), the SiOH and POH groups grew in intensity. The largest change occurred in the POH groups (spectrum C) at 25°. The simplest reactions responsible for the hydroxyl generation would be

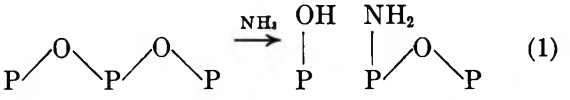

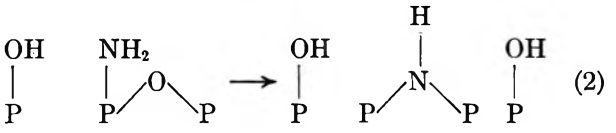

Reaction of PNH_2 and PNHP groups with H_2O could then lead to the formation of NH_4^+ ions

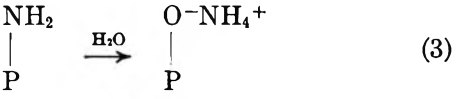

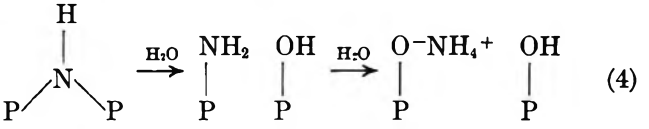

NH_4^+ ions could be formed by reaction with POH groups or by reaction with POP bridges

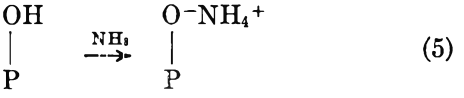

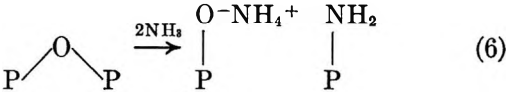

Such reactions imply a relatively easy movement of hydrogen atoms. The relative ease of exchange of NH_3 with surface OH groups supports this. A deuterated specimen which had been exhaustively exchanged was prepared. A prominent SiOH band formed when NH_3 was sorbed at 25°; simultaneously, the SiOD and POD bands decreased. Indistinct bands due to ND_3

(17) L. H. Little, "Infrared Spectra of Adsorbed Species," Academic Press Inc., New York, N. Y., 1966, pp 185 ff, 344 ff.

(18) J. V. Pustinger, W. T. Cave, and M. L. Nielsen, *Spectrochim. Acta*, 15, 909 (1959).

(19) Reference 10, p 322.

(20) L. J. Bellamy and R. L. Williams, *Spectrochim. Acta*, 9, 341 (1957).

were detected in the 2500–2400-cm^{-1} region. The results indicate that surface OD groups were rapidly converted to OH groups by exchange with sorbed NH_3.

Nature of the Adsorbent. It is important to note that POH groups could be regenerated with H_2O or NH_3 even after the adsorbent had been severely degassed. This means that at least a portion of the phosphoric acid with which the silica had been impregnated must have been retained after heating at 800°. (It is not known to what extent P_4O_{10} sublimed from the adsorbent, if at all; judging from the intensities of the POH band before and after a high-temperature treatment, there was no discernible decrease in P_4O_{10}.) Liquid phosphorus oxide would have a vapor pressure of several thousand torr[21] at the high temperatures used to degas the impregnated silicas and would, therefore, have been pumped away. At least some of the phosphorus oxide must, therefore, have been strongly bound to the silica surface and yet have retained much of the nature and reactivity of P_4O_{10}. The entire silica surface was not covered, because SiOH groups could be perturbed by adsorption. The structure of the material is not known; perhaps an orthorhombic $(P_2O_5)_n$ sheet polymer[21] became locked to the silica skeleton. However, the adsorbent cannot be considered simply as phosphoric acid or P_4O_{10} dispersed over the surface of silica, and the properties of the two constituents cannot be considered simply as additive.

The spectra of Figure 8 show that the initial OH generation involved POH groups. However, upon degassing above 100° the SiOH band grew and the POH band declined. As much of the adsorbed NH_3 had been removed from the surface, the likely source of the hydrogen required to form SiOH groups is the POH groups. As with the case of H_2O sorption on porous glass,[5] where surface boria acted as the reaction site and source of reactant, the present results indicate that surface phosphorus oxide acts as the source of the reactant required for the formation of SiOH groups. The spectra of Figure 3 show changes similar to those of Figure 8, although less clearly, because of the hydrogen-bonding effects. For both cases it is suggested that hydrogen atoms, formed through the disruption of POH groups, migrated to the silica portion of the surface and reacted there to form SiOH groups. As with the H_2O–$B_2O_3 \cdot SiO_2$ system, the apparent reactivity of the silica skeleton was modified.

Acknowledgment. Support by grants from the Center for Air Pollution Control of the Department of Health, Education, and Welfare, and the National Science Foundation (Grant GP 1434) is gratefully acknowledged.

(21) J. R. Van Wazer and C. F. Callis in "Inorganic Polymers,, F. G. A. Stone and W. A. G. Graham, Ed., Academic Press Inc. New York, N. Y., 1962, p 70 ff.

The Kinetics of the Hydrogen–Fluorine Reaction. III. The Photochemical Reaction[1]

by Joseph B. Levy and B. K. W. Copeland

Kinetics and Combustion Group, Atlantic Research Corporation, Alexandria, Virginia *(Received February 5, 1968)*

Mixtures of hydrogen, fluorine, oxygen, and nitrogen can be prepared which are stable in the dark at room temperature. On irradiation of such mixtures with a 3130-Å light, hydrogen and fluorine react at a measurable rate. The effects of light intensity, reagent pressures, oxygen pressure, and total pressure on reaction rates at 15° have been measured. The results show that oxygen inhibits the reaction through the step $H + O_2 + M \rightarrow HO_2 + M$ and allow an evaluation of the energy of activation for the step $H + F_2 \rightarrow HF + F$ as 1.5 ± 0.3 kcal mol^{-1}. Earlier results on the thermal oxygen-inhibited reaction are reinterpreted in the light of the present results.

Introduction

We have been studying the kinetics of the reaction of hydrogen and fluorine at reactant pressures of about 20–80 torr and have recently reported on the oxygen-inhibited reaction in the temperature range 122–162°.[2] We report here results of our study of the photochemical reaction at 15° in the same general reactant-pressure region.

Experimental Part

Chemicals. The fluorine used in this work was fluorine (General Chemical Co.) that was freed of hydrogen fluoride by passage through a potassium fluoride trap. The nitrogen was prepurified grade (Southern Oxygen Co.). Mass spectrographic analyses[3] showed it to contain 0.1% of oxygen as the only impurity. The hydrogen was dry electrolytic grade (Southern Oxygen Co.) containing no more than 0.2% impurities, consisting of nitrogen and oxygen. The helium was Southern Oxygen Co. Grade A, specified as being 99.99% pure. The hexafluoroethane was Freon 116 (Matheson Co.) specified as being 99.6% minimum purity.

The Reaction Cells. The reaction cells were fabricated as in our earlier work[2,4] except that the cell bodies were of aluminum rather than magnesium. Two cells were used, each had a 4.41-cm i.d.; one was 10 cm long and the other was 20 cm long. Temperature control was achieved by circulating water from a thermostatically controlled bath through copper tubing wrapped around the cell body. The runs reported here were performed at 15 ± 0.5°.

The Irradiation Apparatus. In the early part of this work, the light from a mercury arc lamp was passed through a solution, containing nickel sulfate and cobaltous sulfate, which cut off all light below about 3000 Å.[5] This arrangement was later replaced by a system utilizing a monochromator in place of the filter solution. All the data reported here refer to this later arrangement, unless otherwise specified.

In the later arrangement, the light from a mercury arc lamp was focused on the entrance slit of a 33-86-40 Bausch and Lomb grating monochromator by means of two quartz lenses. The monochromator was set at 3130 Å. The emergent beam was collimated by a quartz lens and the collimated beam passed through the cell, filling it. A quartz lens downstream of the cell served to focus the light onto an RCA 935 phototube. The output of this tube was continuously monitored by a microammeter. The monochromator, collimating lens, reaction cell, focusing lens, and phototube were all mounted on an optical bench. The initial experiments were performed with a Hanovia 100-W mercury arc lamp; the subsequent experiments which comprise the bulk of the results utilized a Westinghouse 1000-W mercury short-arc high-pressure lamp.

Procedure for Making a Run. The general procedure for making a run was to evacuate the cell and to admit into it oxygen, fluorine, nitrogen, and hydrogen in the order named. This was accomplished by using a manifold constructed from 0.25-in. heavy-wall Teflon tubing, which used Teflon tees and valves which were attached by Teflon fittings. At one end of the manifold was a glass mercury manometer with the exposed side of the mercury covered by a layer of fluorolube oil. A tilting McLeod gage was attached to one of the manifold valves.

(1) This work was supported by the Air Force Office of Scientific Research of the Office of Aerospace Research under Contract No. AF 49(638)-1131.

(2) J. B. Levy and B. K. W. Copeland, *J. Phys. Chem.*, 69, 408 (1965).

(3) We are indebted to Dr. Robert Nugent of this laboratory for this analysis.

(4) J. B. Levy and B. K. W. Copeland, *J. Phys. Chem.*, 69, 3700 (1965).

(5) M. Kasha, *J. Opt. Soc. Amer.*, 38, 929 (1948)

Oxygen pressures that were of the order of a few torr were measured using the McLeod gage, which had a 0–10-torr range. Higher pressures were read on the manometer. The other gases were added by building the pressure in the manifold up to an appropriate value with the cell valve closed and then admitting the gas to the cell, while building the pressure up to the desired final value. The manifold was evacuated and flushed with the next gas to be added before each addition. The fluorine pressure was measured optically at 2850 Å in a Beckman DU spectrophotometer whose cell compartment had been modified to allow insertion of the reaction cell. By adding oxygen first of all, it was possible to measure low pressures of it accurately with the McLeod gage. By adding fluorine before hydrogen it was possible to see if any dark reaction occurred by checking the 2850-Å absorption. It was necessary to add nitrogen before hydrogen to prevent reaction in the dark (see the Results). The order of addition was set by the above considerations.

In making a run, the cell was brought to the desired temperature, filled with the gases as described above, and was allowed to sit at least 15 min in the darkened laboratory. The voltage was adjusted on the light-source power supply to bring the reading on the phototube to a predetermined value. This seemed to keep the light intensity reproducible from day to day. The absorption at 2850 Å was then checked to see if any reaction had occurred. For all the runs below, no reaction occurred in this period. The cell was then put in place on the optical bench with a shutter blocking the light beam. The shutter was removed and the timer simultaneously was started. After the desired irradiation period, the shutter was replaced and the absorption at 2850 Å was measured in the Beckman spectrophotometer. The readings in the spectrophotometer were constant, which showed that the reaction ceased when the irradiation ceased. The above procedure was repeated as desired.

The Beer's law curve for fluorine was constructed by measuring the absorption at pressures ranging from 0 to 200 torr. A pressure of 20 torr in the 20-cm cell resulted in a value of $\log I_0/I = 0.160$. The 10-cm cell gave values in agreement with those of the 20-cm cell. The constant was checked each day at a few points and was found to be reproducible. In the experiments reported here, the fluorine pressures never exceeded 100 torr.

The Actinometric Measurements. Light-beam intensities were measured by means of uranyl oxalate actinometry.[6] A Pyrex cell, with quartz faces cemented on, placed downstream of the reaction cell, was filled with the actinometer solution. Phototube readings showed that the actinometer solution absorbed >99% of the light.

Results

The Dark Reaction. We have found in earlier work[2] that, for certain compositions of fluorine, hydrogen, helium, and oxygen, stable mixtures were obtained at room temperature. Thus mixtures prepared from partial pressures of fluorine, hydrogen, and oxygen at 50 torr each and a partial pressure of helium of 610 torr (to make the total pressure 1 atm) were stable at 25°. For lesser amounts of oxygen with the total pressure maintained at 760 torr with helium, the reaction occurred at a rate that increased as the proportion of oxygen decreased.

We have examined the question of preparing such mixtures in somewhat greater detail prior to conducting the photochemical experiments. The experiments were performed in a darkened room, but the cell was exposed to the light beam of the spectrophotometer.

In these experiments the cell was filled with fluorine to a partial pressure of 50 torr, an inert gas was added to some pressure, and hydrogen was admitted. Where no reaction occurred as the hydrogen was admitted, its partial pressure was built up to 50 torr and the fluorine absorption was monitored to see if reaction occurred. The results are shown in Table I.

Table I: The Dark Reactions of Hydrogen and Fluorine at 15°[a]

Run	Inert gas	Pressure of inert gas, torr	Observations
154-A	None	...	Fluorine consumed as hydrogen admitted
154-B	Helium	500	Fluorine consumed as hydrogen admitted
155	Helium	1470	Slow reaction
154-C	Nitrogen	300	Fluorine consumed as hydrogen admitted
154-C	Nitrogen	400	No reaction
154-E	Nitrogen	660	No reaction
154-F	Hexafluoroethane	100	Explosive reaction as hydrogen admitted
154-G	Hexafluoroethane	200	Very slow reaction
154-H	Hexafluoroethane	400	No reaction
162	Oxygen	50	No reaction

[a] $P_{F_2} = 50$ torr; a 10-cm reaction cell was used.

The above results are essentially qualitative in nature, but they establish that the presence of inert gas acts to stabilize hydrogen–fluorine mixtures and that the order of decreasing effectiveness is hexafluoroethane > nitrogen ≫ helium. Although hexafluoroethane is more effective on a volume basis than nitrogen, it is less available and, in addition, yielded carbonaceous

(6) C. R. Masson, V. Boekelheide, and W. A. Noyes, Jr., "Technique of Organic Chemistry," Vol. II, 2nd ed, A. Weissburger, Ed., Interscience Publishers, New York, N. Y., 1956, pp 289–299.

products in the case where an explosion occurred. We, therefore, chose nitrogen as our inert gas. It may be pointed out that since oxygen inhibits the reaction,[2] it should be possible to prepare mixtures richer in fluorine and hydrogen and leaner in the inert gas than indicated by Table I if oxygen is present.

The Photochemical Reaction. The kinetics of the photochemical reaction have been measured in detail at 15°. The effects of reagent concentration, light intensity, and total pressure have been determined. The results are presented below.

The Nature of the Reaction Products. We have demonstrated in our studies of the thermal oxygen-inhibited reaction of hydrogen and fluorine that hydrogen fluoride was the only reaction product. We have not performed additional analytical experiments but assume that this is so for the photochemical reaction at 15°. This assumption is supported by the absence of the rate acceleration that would be expected if oxygen were consumed in any way as the reaction progressed.

The Effect of the Hydrogen Pressure. The dependence of the rate on hydrogen pressure was one of the first aspects of this reaction that we investigated. This was done by keeping all other parameters constant and varying the hydrogen pressure. The results of a set of experiments are shown in Table II. Data for two duplicate experiments with a pressure of 100 torr of hydrogen and for experiments in which the hydrogen pressure was increased by factors of 2 and 4 are shown. There is some scatter in the data, but it is clear that the rate is independent of the hydrogen pressure. The above experiments were performed with the 100-W lamp. Data obtained with the 1000-W lamp, see below, also show that the rate of reaction is independent of the hydrogen pressure.

The Effect of Oxygen Pressure. The general inhibiting effect of oxygen on the reaction is shown in Figure 1. The curves show, qualitatively, that the inhibiting effect is most pronounced for small amounts of added oxygen—the drop in rate in going from 2.2 torr of O_2 to 5.0 torr is much more pronounced than that in going from 20 to 100 torr.

Table II: The Effect of Hydrogen Pressure on the Reaction Rate[a]

Time, min	P_{H_2}, torr				
	100			200	400
	Per cent reaction				
0	0	0	0	0	0
0.5	5.7	7.0	7.3	5.7	7.2
1.0	10.9	12.2	13.0	10.7	12.9
1.5	14.4	15.6	16.5	14.7	17.0
2.5	21.9	24.0	23.5	20.5	19.0
3.0	24.2	28.6	26.5	24.3	25.8
4.0	29.0	33.7	31.5	29.8	31.2
5.0	32.9	37.5	35.8	34.5	35.5
8.0	42.8	47.8	48.6	42.8	46.3
10.0	46.8	50.1	51.6	49.2	51.0

[a] The temperature was 15°; the cell length was 10 cm; the light source was a 100-W Hanovia lamp; the light was filtered through a nickel sulfate–copper sulfate filter solution; the total pressure was made up to 760 torr with nitrogen. The pressures of fluorine and oxygen were 100 and 5.2 ± 0.1 torr, respectively.

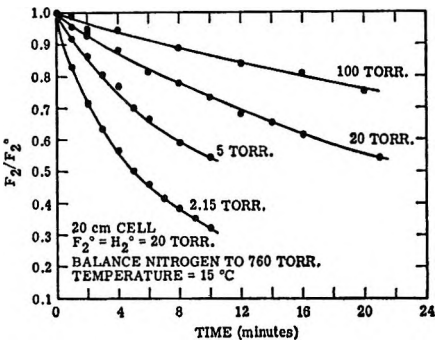

Figure 1. The dependence of rate on oxygen pressure.

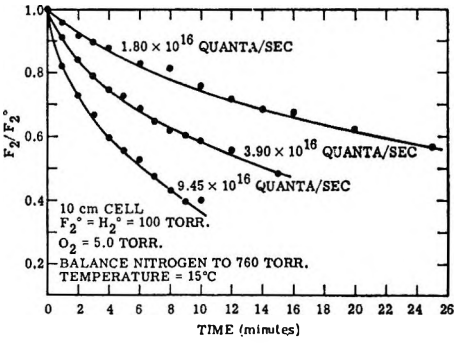

Figure 2. The dependence of rate on light intensity.

The Effect of Light Intensity. Experiments were performed with the 1000-W lamp and the 20-cm cell in which wire-gauze screens were introduced between the monochromator and the cell to reduce the light intensity to correspond to appropriate values as indicated by the phototube. The results are shown in Figure 2 and the dependence of rate on light intensity is evident. A fourfold range of light intensities is represented.

Tangents were taken to the curves at equal fluorine concentrations in order to investigate the quantitative dependence of rate on light intensity. If the Beer's law expression is written $I_0/I = 10^{\epsilon(F_2)}$, where ϵ is a constant for a given cell, then $I_a = I_0(1 - 10^{-\epsilon(F_2)})$ and at equal fluorine concentrations I_a is directly proportional to I_0. For a system where Beer's law is obeyed, I_a is thus directly proportional to I_0. The dependence of the rate on I_0, hence on I_a, is shown in Table III.

The data are compared in Table III by calculating the value of n in the equation $V_1/V_2 = (I_1/I_2)^n$, where V_1 and V_2 refer to the instantaneous rates at equal fluorine pressures. Values of n were calculated using the data for the highest intensity in combination with

Table III: The Dependence of Rate on Light Intensity[a]

P_{F_2}, torr	I_0 = 9.45 × 10¹⁶ quanta sec⁻¹ $-dP_{F_2}/dt$, torr/min	I_0 = 3.90 × 10¹⁶ quanta sec⁻¹ $-dP_{F_2}/dt$, torr/min	n	I_0 = 1.80 × 10¹⁶ quanta sec⁻¹ $-dP_{F_2}/dt$, torr/min	n
93.2	2.26	0.88	1.1	0.34	1.1
84.8	1.41	0.59	1.0	0.24	1.1
79.0	1.07	0.48	0.9	0.20	1.0
67.8	1.02	0.34	1.3	0.13	1.3
56.5	0.43	0.14	1.3	0.085	1.1

[a] The initial pressures were $F_2 = H_2 = 100$ torr, $O_2 = 5.0$ torr, and $N_2 = 555$ torr at a temperature of 15°. The cell length was 20 cm and the light source was a 1000-W lamp.

the corresponding values for each of the lower two densities. We conclude from the above that the rate depends on the first power of the absorbed light.

The Effect of Total Pressure. A series of four experiments was performed at 15° with standard pressures of fluorine and hydrogen equal to 20.0 torr, an oxygen pressure of 5.0 torr, and various pressures of nitrogen to yield total pressures varying from 95 to 760 torr. The results are shown in Figure 3. The data have been plotted as $(F_2)/(F_2)_0$. It is clear that the reaction rate increases as the total pressure is decreased.

Experiments at Other Temperatures. We have attempted to perform experiments at temperatures above 15° and below. It was clear that the reaction would not have a large temperature coefficient, so that it seemed necessary to have temperature intervals of significant magnitude if the rate change were to be significant. Accordingly, experiments were attempted at 50°. These were abandoned because reaction was observed in many cases in the dark for mixtures similar to those used in the experiments at 15°.

Experiments were then performed at −42°. Here a new phenomenon was observed. On irradiation of reaction mixtures, the optical density at 2850 Å decreased, but on standing in the dark the optical density increased again. For example, for a run with initial pressures of 20 torr each of hydrogen and fluorine, 5.3 torr of oxygen, and 715 torr of nitrogen, a 6-min irradiation period yielded a fluorine concentration corresponding to 26% reaction; the absorption increased as the cell sat in the dark and leveled off at a reading corresponding to 14.5% reaction after 3 min. This phenomenon was observed repeatedly. It can only be explained on the basis of the photochemical formation of a species that decomposes in the dark to give back fluorine and which absorbs the 2850-Å light less strongly than fluorine does. We cannot identify this species at this time, but because of its intrusion we have not pursued the kinetics at this temperature. We emphasize that no evidence for a species of this sort in the 15° experiments was ever found.

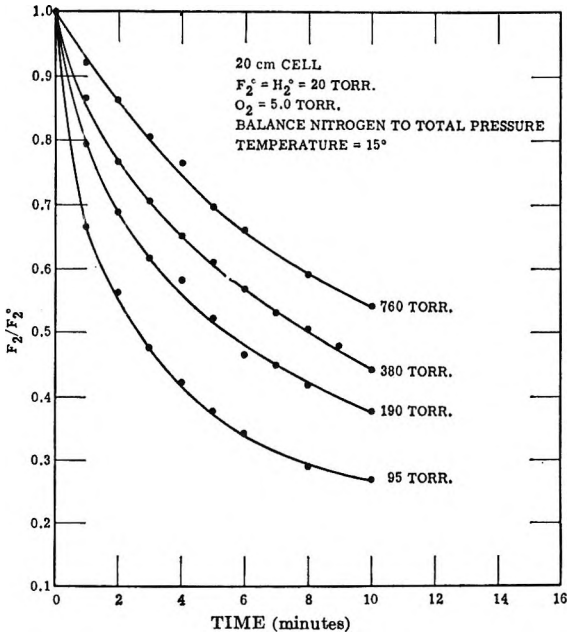

Figure 3. The dependence of rate on total pressure.

It is worth reporting the results of some collateral experiments at −42° in which fluorine and oxygen alone were irradiated. In these experiments a species more intensely absorbing at 2850 Å than fluorine was formed, and this species decayed in the dark to give back fluorine. This species was shown to be dioxygen difluoride by measuring its extinction coefficients. These measurements were made in the following way. A mixture of 20 torr each of fluorine and oxygen was irradiated for 1 hr at −42°, and the cell contents were pumped through a Teflon-tubing trap cooled in liquid nitrogen. A reddish orange solid which melted to a reddish orange liquid was observed in the trap. This is characteristic of F_2O_2. This material was readmitted to the cell, was allowed to decompose, and the absorption at 2850 Å was measured. The reading corresponded to 1.5 torr of fluorine. From the initial absorption due to fluorine, the increase in absorption on irradiation, and the final value, an approximate extinction coefficient of 8.5 (defined as ϵ in $I = I_0 \times 10^{-\epsilon pd}$, with p in atmospheres and d in centimeters) at 2850 Å was calculated. Similar readings were made over a range of wavelengths from 2250 to 3500 Å. The resulting curve of absorption *vs.* wavelength agreed well with that reported by Brodersen, Frisch, and Schumacher for F_2O_2.[7] These results led us to conclude that dioxygen difluoride is formed by the irradiation of oxygen–fluorine mixtures at −42°. We emphasize here that irradiation of such mixtures at 15° results in no observable changes.

The Dependence of the Rate on the Fluorine Concentration. The Mechanism of the Reaction. Discussion of

(7) P. H. Brodersen, P. Frisch, and H. J. Schumacher, *Z. Physik. Chem.* (Leipzig), B37, 25 (1937).

the dependence of the rate on the fluorine concentration is complicated by the fact that the fluorine concentration can enter the rate equation in two ways, *i.e.*, as a result of the dependence of I_a on fluorine and as a result of fluorine being involved directly in the kinetics as a reacting molecule. It is most convenient to discuss the effect on the rate of the fluorine concentration, or, what is more pertinent, of the fluorine to oxygen ratio, in terms of a reaction mechanism. The evidence which has been presented above placed certain restrictions on any mechanism, and the steps which seem most plausible suggest themselves rather readily. For these reasons we present a mechanism for the photochemical reaction at this point and consider thereafter how the predictions of the mechanism concur with our results. The mechanism is

$$F_2 + \text{light} \xrightarrow{k_1} 2F \quad (1)$$

$$F + H_2 \xrightarrow{k_2} HF + H \quad (2)$$

$$H + F_2 \xrightarrow{k_3} HF + F \quad (3)$$

$$H + O_2 + M \xrightarrow{k_4} HO_2 + M \quad (4)$$

$$HO_2 + F_2 \xrightarrow{k_5} HF + O_2 + F \quad (5)$$

$$F + HO_2 \xrightarrow{k_6} HF + O_2 \quad (6)$$

Step 5 has been postulated earlier[2] to explain our results with the thermal reaction at 132–162°. Step 6 has been chosen in preference to other termination steps that might be written for HO_2 because, as will be shown below, it is required for the results at the higher temperatures. This is not compelling evidence for this step at 15°; however, since any step that destroys HO_2 without continuing the chain or consuming oxygen gives the same result, we write step 6 for the sake of simplicity. From the above mechanism the reaction rate is

$$\frac{-d(F_2)}{dt} = {}^1/_2[k_2(F)(H_2) + k_3(H)(F_2) + k_5(F_2)(HO_2) + k_6(F)(HO_2)]$$

It is possible to obtain a useful rate expression from the above mechanism only for the two limiting cases (see the Appendix)

$$k_5(F_2)(HO_2) \gg k_6(F)(HO_2) \quad (7)$$

and

$$k_6(F)(HO_2) \gg k_5(F_2)(HO_2) \quad (8)$$

For the case of the inequality 7, the rate expression for $(F_2) >> (O_2)$ shows a dependence on $(F_2)(H_2)^{1/2}I_a^{1/2}$, and this is contrary to our results with regard to the dependence on (H_2) and on I_a. For this reason we reject inequality 7.

For the case of the inequality 8, the rate expression found is

$$\frac{-d(F_2)}{dt} = I_a + \frac{k_3 I_a(F_2)}{k_4(O_2)(M)} \quad (9)$$

This is consistent with our results on the lack of dependence on (H_2), on the direct dependence on I_a, and on the inverse dependence on (O_2). We, therefore, proceed to examine the expression quantitatively and to postulate inequality 8 for the photochemical reaction at 15°.

Quantitative Treatment of the Data. In order to examine the validity of expression 9 from a quantitative viewpoint, it is necessary to consider the dependence of I_a on fluorine concentration. We write the Beer's law expression for fluorine in the 20-cm cell in our irradiation apparatus as

$$\log \frac{I_0}{I} = \beta(F_2)$$

where the units of concentration are moles per liter and the units of β, the proportionality constant, are liters per mole. It then follows that

$$I_a = I_0(1 - 10^{-\beta(F_2)}) \quad (10)$$

Incorporation of this expression for I_a into expression 9 yields a differential rate equation containing the fluorine concentration as the only variable, but one that cannot be integrated to give a useful expression.

We have determined the relationship between I_a and (F_2) by measuring I_0, the intensity of the light beam passed by the empty cell, and values of I at fluorine pressures in the cell of 20 and 50 torr. From these values we calculate the Beer's law constant, and from Beer's law we calculate I_a as a function of (F_2) from 0 to 50 torr. Three determinations of I_0 yielded an average value of 1.06×10^{17} quanta sec^{-1}, with an average deviation of $\pm 0.07 \times 10^{17}$ quanta sec^{-1}. This value has been multiplied by 1.05 to allow for reflection losses,[8] so that we set $I_0 = (1.11 \pm 0.07) \times 10^{17}$ quanta sec^{-1}, equivalent to 3.69×10^{-5} einstein $l.^{-1}$ min^{-1}. The Beer's law constant calculated from the intensities at 20 and 50 torr was $\beta = (88 \pm 8)$ l. mol^{-1}.

The plot of I_a, calculated using the Beer's law constant, *vs.* (F_2) was found to be only slightly curved and was very closely approximated by a straight line for $(F_2) \leq 1.8 \times 10^{-3}$ mol. $l.^{-1}$ (30 torr). For this region of concentration, therefore, the relation $I_a = \gamma(F_2)$ can be introduced, where γ is the empirical slope obtained from the linear plot. Since the introduction of this expression for I_a leads to considerable simplification in treatment of the data, we have made use of it in our quantitative treatment of runs where fluorine pressures did not exceed 30 torr.

(8) J. G. Calvert and J. N. Pitts, Jr., "Photochemistry," John Wiley and Sons, Inc., New York, N. Y., 1966, p 794.

The reaction rate then becomes

$$\frac{-d(F_2)}{dt} = \gamma(F_2) + \frac{k_3\gamma}{k_4(O_2)(M)}(F_2)^2 \qquad (11)$$

which may be integrated[9] to obtain

$$e^{-\gamma t} = \frac{\gamma + \gamma\dfrac{k_3}{k_4(M)}r}{\alpha\gamma + \gamma\dfrac{k_3}{k_4(M)}r}$$

where $\alpha = (F_2)_0/(F_2)_t$ and $r = (F_2)_0/(O_2)$. The exponential may be replaced by the first two terms of the Taylor expansion, *i.e.*, by $1 - \gamma t$, to give, with rearrangement

$$\frac{\alpha - 1}{\gamma} - \alpha t = \frac{k_3 r}{k_4(M)}t \qquad (12)$$

It should be pointed out here that the value obtained actinometrically for γ was 0.00465; the third term in the expansion, $(\gamma t)^2/2$, represents a contribution of about 0.1% for $t = 10$ min and 0.4% for $t = 20$ min. Since a time of 10 min in most cases represented a considerable reaction, the neglecting of terms higher than the second in the expansion was deemed justifiable and data for the first 10–20 min of reaction were plotted.

The results for three representative experiments, plotted for expression 12, are shown in Figure 4. The data are obviously linear and the agreement of the values of $k_3/k_4(M)$ derived from the slopes is satisfactory. We have treated our runs where the initial fluorine pressure was $\leq$30 torr in the above manner and have derived values of $k_3/k_4(M)$ from the curves which were in all cases linear. The linearity was good enough to allow the slopes to be determined visually to within about 3%. The discrepancy between different runs exceeds this substantially. We have, therefore, determined slopes visually. These are shown in Table IV and yield $k_3/k_4(M) = 4.6 \pm 0.7$ as the average value and the average deviation from the average.

Although a substantial variation in the critical parameter $(F_2)_0/(O_2)$ is encompassed in these runs, *i.e.*, from 1.0 to 9.9, the variation in (F_2) itself was only about threefold, *i.e.*, 10 to 30 torr. Runs at higher fluorine pressures had been made but were not amenable to the above treatment for reasons mentioned above. To check the validity at higher fluorine pressures of the postulated rate expression, we have returned to the differential expression 9. By measuring tangents to the (F_2)–t curve directly with a half-silvered mirror and by calculating I_a from expression 10, we have evaluated $k_3/k_4(M)$ at discrete points on the curve. These are tabulated in Table V.

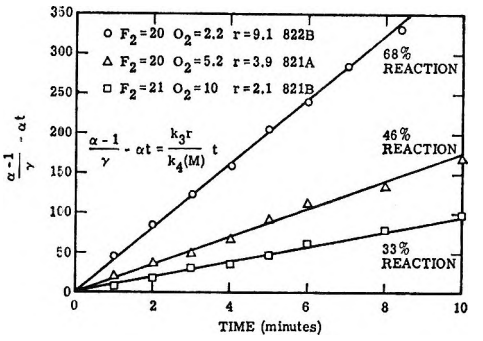

Figure 4. Test of the rate expression for the oxygen-inhibited photochemical hydrogen–fluorine reaction.

Table IV: Kinetic Results for the Photochemical Hydrogen–Fluorine Reaction at 15° from Integrated Rate Expressions

Expt no.	P_{F_2}, torr	P_{H_2}, torr	r	Slope	$k_3/k_4(M)$
822C	20	20	1.0	6.40	6.4
821B	21	10	2.1	9.60	4.6
824D	10	5	2.0	10.4	5.2
821A	20	5.2	3.9	18.0	4.7
815B	20	5.0	4.0	14.7	3.7
822A	20	5.0	4.0	17.0	4.3
823B	30	4.9	6.1	23.4	3.8
814A	20	2.2	9.1	30.0	3.3
822B	20	2.2	9.1	41.5	4.6
815A	20	2.2	9.1	48.0	5.3

Table V: Graphical Evaluation of $k_3/k_4(M)$

Expt no.	$(F_2)_0$, torr	(O_2), torr	$(F_2)_t$, torr	Slope, torr min^{-1}	I_a, torr min^{-1}	$k_3/k_4(M) =$ (slope $- I_a$)/$[I_a(F_2)_t/(O_2)]$
823A	50.0	5.9	38.7	5.95	0.17	4.5
824B	50.0	5.6	23.0	2.48	0.11	5.3
823A	50.0	5.9	29.3	2.84	0.14	3.9
824C	75.0	5.7	57.7	11.4	0.24	4.6
824C	75.0	5.7	50.5	8.00	0.23	3.8
824C	75.0	5.7	40.5	4.35	0.19	3.1
						Av 4.2

The agreement with the value for $k_3/k_4(M)$ obtained graphically is satisfactory and extends the range of (F_2) encompassed by the data to 57.7 torr, an over-all range of about 6 torr. It appears evident that the rate expression is supported by the experimental results and that $k_3/k_4(M)$ at 15° and 1 atm equals 4.6 ± 0.7.

Discussion

The Effect of Pressure on the Dark Reaction. Two explanations can be proposed for the effect of inert gases on the stability of hydrogen–fluorine mixtures in the dark. One explanation is that the inert gases

(9) K. B. Yerrick and M. E. Russell, *J. Phys. Chem.*, **68**, 3752 (1964).

quench energy chains. Recently, evidence has been presented to show that explosions in this system proceed by an energy-chain mechanism.[10] It is difficult to distinguish energy chains from thermal chains; moreover, we know of no other case where the energy-chain mechanism has been proved.[11] Judgment must be reserved as to the validity of the above explanation.

An alternative explanation is that the added gases serve to increase the heat capacity of the mixture and prevent a temperature rise, resulting from trace amounts of dark reaction, that would lead to a thermal explosion. The efficiencies of the inert gases examined rise with increasing heat capacity, and we consider this explanation more likely. It may be pointed out that there is no reason to believe that the order of increasing heat capacity should bear any relation to the order of efficiency in deactivating an excited hydrogen fluoride molecule, *i.e.*, in quenching energy chains.

The Oxygen Inhibition of the Reaction. The kinetics serve to rule out as a step of any significance

$$F + O_2 + M \longrightarrow FO_2 + M \qquad (I)$$

This conclusion does not mean that step I does not occur but only that, if it does occur, it is followed by steps that lead to chain propagation rather than chain termination.

In order to discuss step I it is necessary to discuss the strength of the O_2–F bond formed. In an earlier publication[2] we advanced arguments that led to a value of 15 kcal for that bond. We are no longer convinced of the correctness of our premise in that argument, to wit that the first step in the decomposition of O_2F_2 is the cleavage of an O–F bond, but it still seems plausible that the value we proposed for this bond is at least approximately correct. It may be pointed out that from the heat of formation of $O_2F_2(g)$[12] of 4.73 kcal mol^{-1} the process of $O_2F_2 \rightarrow O_2 + 2F$ is endothermic by $\sim$32 kcal mol^{-1}. Since there is good evidence that FOO· has some stability,[13] it is clear that cleavage of both the first and second O–F bonds must be significantly endothermic and it is doubtful that the F–O_2 bond strength differs substantially from 15 kcal mol^{-1}. A similar value has been deduced from mass spectrographic experiments.[14]

If the bond formed in step I has a dissociation energy of about 15 kcal/mol, then we see no reason why step I should not occur. Further support for this step is given by the results at −42° with oxygen–fluorine mixtures. The only reasonable route for the formation of the observed dioxygen difluoride is *via*

$$F + O_2 + M \longrightarrow FO_2 + M$$

$$FO_2 + F + M \longrightarrow F_2O_2 + M$$

The presumption is that at the lower temperature the rate of reaction of FO_2 with hydrogen is much slower than it is at 15° and the FO_2 species can persist until it collides with a fluorine atom. This suggests the possibility that at temperatures significantly lower than −42° the main route of reaction of FO_2 would be to form O_2F_2, which in turn might be a stable species at this temperature.[15] If this were so, the inhibition of the reaction by oxygen could proceed predominantly *via* eq 1 and a kinetic analysis would allow the evaluation of the rate constant for step 2. We plan to investigate this possibility.

At 15° the further reaction of FO_2 cannot be *via* the above step nor *via*

$$H + FO_2 \longrightarrow HF + O_2$$

$$F + FO_2 \longrightarrow F_2 + O_2$$

since all three would lead to chain termination, contrary to the observed kinetics. We conclude, therefore, that the step

$$FO_2 + H_2 \longrightarrow HF + O_2 + H \qquad (II)$$

must be occurring. The value of 15 kcal mol^{-1} for the O_2–F bond allows the above step to be exothermic by about 19 kcal/mol. One way of viewing the above reaction is to consider that the O_2–F bond is so weak that the fluorine atom retains almost as much reactivity as it had when it was free. It can be readily demonstrated that inclusion of steps I and II in the mechanism written earlier would not change the final rate expression, since the hydrogen atom reactions are unaffected.

Step 4 thus leads to inhibition, while step I does not because the species HO_2 is much less reactive than FO_2. The reactivity of HO_2 is also a factor in the consideration of the differences between our thermal results[2] and the present photochemical results. The O_2–H bond strength of 46 kcal mol^{-1} [16] is so much higher than that of O_2–F that we feel the postulated difference in behavior between these two species is reasonable.

Reexamination of the Results for the Oxygen-Inhibited Thermal Hydrogen–Fluorine Reaction. The thermal reaction at 122–162°[2] was also inhibited by oxygen but reached a limiting rate at high oxygen to fluorine ratios. The limiting rate obeyed very well an expression first order in fluorine and half-order in hydrogen. At that time the interpretation was complicated by the belief, now abandoned, that FO_2 played a role. The situation in the absence of FO_2 is much simpler.

(10) G. A. Kapralova, E. M. Trofimova, and A. J. Shilov, *Kinet. Katal.*, **6**, 972 (1965).

(11) S. W. Benson and W. B. DeMore in "Annual Review of Physical Chemistry," Vol. 16, H. Eyring, C. J. Christensen, and H. S. Johnston, Ed., Annual Reviews, Inc., Palo Alto, Calif., 1965, p 402.

(12) A. D. Kirshenbaum, A. V. Grosse, and J. G. Aston, *J. Amer. Chem. Soc.*, **81**, 6398 (1959).

(13) A. Arkell, *ibid.*, **87**, 4057 (1965).

(14) T. J. Malone and H. A. McGee, Jr., *J. Phys. Chem.*, **69**, 4338 (1965).

(15) H. S. Schumacher and P. Frisch, *Z. Physik. Chem.* (Leipzig), **B37**, 1 (1937).

(16) A. J. B. Robertson, *Trans. Faraday Soc.*, **48**, 229 (1952).

For the thermal reaction, step 1 in the photochemical mechanism is replaced by a first-order dissociation of fluorine, *i.e.*

$$F_2 + M \xrightarrow{k_1} 2F + M \qquad (13)$$

It is necessary to assume that inequality 7 is valid at these temperatures or the rate would not reach a limit at low $(F_2)/(O_2)$ but would go to zero.

For this mechanism (see the Appendix) the rate expression found is

$$\frac{-d(F_2)}{dt} = \left(\frac{k_1k_2k_5(M)}{k_6}\right)^{1/2}(F_2)(H_2)^{1/2}\left[\frac{k_3}{k_4(M)}\frac{(F_2)}{(O_2)} + 1\right]^{1/2} \qquad (14)$$

For the limiting case where $(F_2)/(O_2) \ll 1$, the expression reduces to

$$\frac{-d(F_2)}{dt} = \left(\frac{k_1k_2k_5(M)}{k_6}\right)^{1/2}(F_2)(H_2)^{1/2}$$

which agrees with the experimental results. It should be pointed out that step 6 is required as the termination step, since other possibilities yield a rate expression of a different form.

Measurements of the variation of rate with oxygen pressure at fixed fluorine and hydrogen pressures were reported earlier for cases where $(F_2)/(O_2)$, see ref 2, was not large compared with unity. The data for these experiments should be reproduced by the expression

$$\frac{-d(F_2)}{dt} = V = V_0\left[\frac{k_3}{k_4(M)}\frac{(F_2)}{(O_2)} + 1\right]^{1/2}$$

where V_0 is the rate where $(F_2)/(O_2)$ is very small compared with unity. The value of $k_3/k_4(M)$ at 132° and 1 atm is calculated from the value at 15°, using the energies of activation $E_3 = 1.5$ kcal mol^{-1} (see below) and $E_4 = 0$, and is found to be 13.6. The curve obtained in this way is compared in Figure 5 with the experimental data found earlier. The agreement is satisfactory. It is clear that the thermal and photochemical results are mutually consistent.

Two other features of the data require comment. The first relates to the experimental activation energy of the oxygen-inhibited thermal reaction which was reported earlier[1] as 16.7 ± 1 kcal/mol. The mechanism shown above equates this activation energy to $^1/_2$ $[E_{13} + E_2 + E_5 - E_6]$. It seems reasonable to set $E_6 = 0$. If step 13 were the homogeneous dissociation of fluorine, E_{13} would be 37.0 kcal mol^{-1} and, with finite values of E_2 and E_5, the activation energy would exceed 18.5 kcal mol^{-1}. We believe the discrepancy is probably due to a heterogeneous contribution to step 13, which leads to a lower value of the activation energy of this step.

The second feature of the data that deserves mention is the contrast in the importance of step 5 at 15° as compared with 132°. We interpret this to mean that

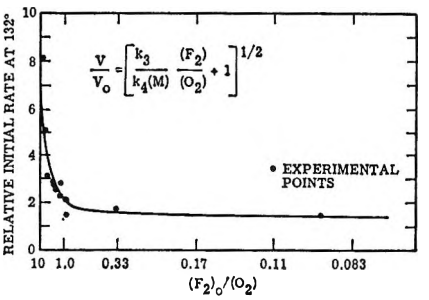

Figure 5. The effect of the fluorine to oxygen ratio on the rate of the hydrogen–fluorine reaction at 132°.[2] Comparison of the experimental data with the predicted curve.

step 5 has an activation energy of 5–6 kcal mol^{-1}. This would result in a 10–15-fold drop in the rate of this reaction as the temperature was lowered from 132 to 15° and this drop would suffice to render the step unimportant at the lower temperature. In view of the relative unreactivity of the HO_2 radical, this magnitude for the activation energy of step 5 seems reasonable.

The Evaluation of the Energy of Activation of Step 3. The value of $k_3/k_4(M)$ found here was 4.6 ± 0.4, corresponding to $k_3/k_4 = 0.193 \pm 0.019$ mol l.$^{-1}$ at a total pressure of 1 atm at 15°. Insertion of a value for k_4 would allow calculation of k_3. Hoare and Walsh[17] cite a value of 8×10^{-31} cc molecule^{-2} sec^{-1} at 20°, corresponding to 2.3×10^{10} l.^{2} mol^{-2} sec^{-1} for M = H_2. Lewis and von Elbe[18] reported the ratio of k_4 for M = H_2 to k_4 for M = N_2 to be 2.5, so that we take $k_4 = 9.2 \times 10^9$ l.^{2} mol^{-2} sec^{-1} for our purposes. This yields $k_3 = 1.8 \times 10^9$ l. mol^{-1} sec^{-1}. It is of interest to derive an activation energy from this figure for comparison with the other hydrogen atom–halogen molecule reactions. Benson[19] has tabulated preexponential factors for the reactions of hydrogen atoms and of deuterium atoms with a number of diatomic molecules. The values of log $(A/T^{1/2})$, where A is the preexponential factor in the simple Arrhenius equation $k = Ae^{-E/RT}$, all fall in the range 8.9–9.8 and yield an average of 9.1, with an average deviation of 0.2. From this quantity, the value of k_3 given above, and $T = 288$°K, the value of E obtained is 1450 cal/mol. The uncertainty listed in the preexponential factor yields an uncertainty of 250 cal in the value of E, and we, therefore, report it as 1.5 ± 0.3 kcal mol^{-1}. This value is compared with those of the other reactions in this series in Table VI. Since all the values are small, there is little that can be said about them. That the value for the H–Cl_2 reaction is clearly higher than the others shows that the strength of the bond being broken is a factor of importance.

(17) D. E. Hoare and A. D. Walsh, *Trans. Faraday Soc.*, **53**, 1102 (1957).

(18) B. Lewis and G. von Elbe, "Combustion, Flames and Explosions in Gases," Academic Press Inc., New York, N. Y., 1961, p 84.

(19) S. W. Benson, "Foundations of Chemical Kinetics," McGraw-Hill Book Co., Inc., New York, N. Y., 1960, p 292.

Table VI: Comparison of E_{act} with the Enthalpy Change for Hydrogen Atom–Halogen Molecule Reactions

Reaction	Activation energy,[a] kcal/mol	ΔH (exothermic), kcal/mol
$H + I_2 = HI + I$	0	36
$H + Br_2 = HBr + Br$	0.9	41
$H + Cl_2 = HCl + Cl$	2–4	45
$H + F_2 = HF + F$	0–0.5	98

[a] S. W. Benson, "Foundations of Chemical Kinetics," McGraw-Hill Book Co., Inc., New York, N. Y., p 34.

Appendix

I. The Analysis of the Photochemical Kinetics. From the steady-state treatments for fluorine atom, hydrogen atom, and the HO_2 radical in steps 1–6 in the text the following equations are found

$$(F)_{ss} \quad 2I_a - k_2(F)(H_2) + k_3(H)(F_2) + k_5(HO_2)(F_2) - k_6(F)(HO_2) = 0 \quad (a)$$

$$(H)_{ss} \quad k_2(F)(H_2) - k_3(H)(F_2) - k_4(H)(O_2)(M) = 0 \quad (b)$$

$$(HO_2)_{ss} \quad k_4(H)(O_2)(M) - k_5(HO_2)(F_2) - k_6(F)(HO_2) = 0 \quad (c)$$

The sum of these is

$$I_a = k_6(F)(HO_2) \quad (d)$$

The rate of the reaction is

$$\frac{-d(F_2)}{dt} = \tfrac{1}{2}[k_2(F)(H_2) + k_3(H)(F_2) + k_5(HO_2)(F_2) + k_6(F)(HO_2)] \quad (e)$$

which simplifies to

$$\frac{-d(F_2)}{dt} = k_2(F)(H_2) \quad (f)$$

(A) Treatment with the assumed inequality

$$k_5(F_2)(HO_2) \gg k_6(F)(HO_2) \quad (g)$$

If the inequality g is combined with eq c, we find that

$$(H) = \frac{k_5(HO_2)(F_2)}{k_4(O_2)(M)} \quad (h)$$

Combining eq h with eq b and h yields

$$(F) = \frac{k_5(HO_2)(F_2)[k_3(F_2) + k_4(O_2)(M)]}{k_2k_4(H_2)(O_2)(M)} \quad (i)$$

or

$$\frac{1}{(HO_2)} = \frac{k_5(F_2)[k_3(F_2) + k_4(O_2)(M)]}{k_2k_4(H_2)(O_2)(M)(F)} \quad (j)$$

Inserting eq j into eq d

$$(F)^2 = \frac{I_a(F_2)[k_3(F_2) + k_4(O_2)(M)]}{k_6k_2k_4(H_2)(O_2)(M)} \quad (k)$$

The rate expression f now becomes

$$\frac{-d(F_2)}{dt} = \left(\frac{k_2}{k_6}\right)^{1/2}(I_a)^{1/2}(H_2)^{1/2}(F_2)^{1/2}\left[1 + \frac{k_3(F_2)}{k_4(O_2)(M)}\right]^{1/2} \quad (l)$$

When $k_3(F_2) \gg k_4(O_2)(M)$, *i.e.*, long chains, the above reduces to

$$\frac{-d(F_2)}{dt} = \left(\frac{k_2k_3}{k_4k_6}\frac{I_a(H_2)}{(O_2)(M)}\right)^{1/2}(F_2) \quad (m)$$

(B) Treatment with the assumed inequality

$$k_6(F)(HO_2) \gg k_5(F_2)(HO_2) \quad (n)$$

If expression n is combined with eq c and d, we find that

$$(H) = \frac{I_a}{k_4(O_2)(M)} \quad (o)$$

From eq b and f

$$\frac{-d(F_2)}{dt} = k_3(H)(F_2) + k_4(O_2)(M)$$

$$\frac{-d(F_2)}{dt} = I_a\left(1 + \frac{k_3(F_2)}{k_4(O_2)(M)}\right) \quad (p)$$

II. The Analysis of the Thermal Reaction Kinetics. In the mechanism for the thermal reaction, the first step of the photochemical reaction, *i.e.*, the photolytic dissociation of fluorine, is replaced by a first-order dissociation of fluorine, *i.e.*

$$F_2 + M \xrightarrow{k_1} 2F + M \quad (q)$$

Combination of this step with steps 2–6 of the photochemical mechanism yields for the steady-state equation for fluorine atom

$$(F)_{ss} = 2k_1(F_2)(M) - k_2(F)(H_2) + k_3(H)(F_2) + k_5(HO_2)(F_2) - k_6(F)(HO_2) = 0 \quad (r)$$

Expressions b and c above for $(H)_{ss}$ and $(HO_2)_{ss}$ are unchanged and the sum of b, c, and r yields

$$k_1(F_2)(M) = k_6(F)(HO_2) \quad (s)$$

Since the rate of the thermal reaction does not go to zero for high oxygen to fluorine ratios, it is necessary to assume inequality g, *i.e.*

$$k_5(F_2)(HO_2) \gg k_6(F)(HO_2)$$

Just as with the photochemical kinetics, this assumption leads to eq h. The combination of h with s yields

$$(H) = \frac{k_1k_5(F_2)^3}{k_6k_4(F)(O_2)} \quad (t)$$

From eq b

$$(H) = \frac{k_2(F)(H_2)}{k_3(F_2) + k_4(O_2)(M)} \quad (u)$$

A solution for (F) can be obtained by equating eq t and u, *i.e.*

$$(F) = \frac{(F_2)}{(H_2)^{1/2}}\left(\frac{k_1k_5(M)}{k_2k_6}\right)^{1/2}\left[\frac{k_3(F_2)}{k_4(O_2)(M)} + 1\right]^{1/2} \quad (v)$$

Since, as before, the velocity of the reaction is expressible by eq f

$$\frac{-d(F_2)}{dt} = k_2(F)(H_2) = \left(\frac{k_2k_1k_5(M)}{k_6}\right)^{1/2}(F_2)(H_2)^{1/2}\left[\frac{k_3(F_2)}{k_4(O_2)(M)} + 1\right]^{1/2} \quad (w)$$

Ultrasonic Absorption and the Kinetics of Conformational Change in Poly-L-lysine

by R. C. Parker, L. J. Slutsky, and K. R. Applegate

Department of Chemistry, University of Washington, Seattle, Washington 98105
(Received February 14, 1968)

The velocity and attenuation of ultrasonic waves in aqueous solutions of poly-L-lysine have been measured as a function of frequency, temperature, and pH. No evidence of dispersion is found, but excess acoustic absorption, characteristic of a single process with relaxation time (2–4) $\times 10^{-8}$ sec, is observed. Arguments are offered in favor of the hypothesis that the observed relaxation is connected with a change in the chain conformation, perhaps with the helix–coil transition.

I. Introduction

An understanding of the kinetics and thermodynamics of conformational change in uniform polypeptides is a useful preliminary to the understanding of the kinetics and thermodynamics of protein denaturation and enzyme-substrate binding. The elementary steps of the helix–coil transition and of changes in the coil conformation, breaking of an intramolecular hydrogen bond and rotation about a C–C single bond, are presumably extremely fast processes, with rates in a range inaccessible to classical kinetic methods. The rates of the changes in solvation and the degree of ionization concomitant with conformational change are also expected to be very high. Studies of the frequency dependence of the velocity and the attenuation of ultrasonic waves can, in favorable cases, provide information about the rates and volume and enthalpy changes of processes with relaxation times less than 10^{-7} sec[1] and thus offer a possible means of determining the rates of the fast processes associated with conformational change in polypeptide solutions.

Poly-L-lysine is a water-soluble uniform polypeptide, the R group being $(CH_2)_4NH_2$. Doty and Applequist[2] have shown that, in the neighborhood of room temperature and at a pH less than 8, when the NH_2 groups are almost completely protonated, the polymer in aqueous solution exists in the random-coil form. As the pH is increased, there is a gradual transition proceeding, presumably through a series of states involving alternating helical and coil segments along a single chain, until at pH 12, when the NH_2 groups are virtually uncharged, the transition from the coil to the helix is essentially complete.

We have determined the velocity and attenuation of 3–100-Mc ultrasonic waves in aqueous solutions of polylysine of weight-average molecular weight 86,300 (corresponding to about 675 residues/chain) as a function of temperature, frequency, pH, and ionic strength. No significant dispersion is observed. For example at 35.6° and pH 9.22, the velocity of sound in 0.156 *M* polylysine in 0.6 *M* NaCl is 1560.6 m/sec at 3 Mc,

(1) K. F. Herzfeld and T. A. Litovitz, "Absorption and Dispersion of Ultrasonic Waves," Academic Press Inc., New York, N. Y., 1959.

(2) J. Applequist and P. Doty, "Polyamino Acids, Polypeptides, and Proteins," M. A. Stahmann, Ed., University of Wisconsin Press, Madison, Wis., 1962.

1561.0 m/sec at 11.5 Mc, and 1561.2 m/sec at 50 Mc. The frequency dependence of the observed excess acoustic absorption can be adequately described in terms of a single relaxation time. The dependence of the adsorption on pH is consistent with the assignment of perturbation of the helix–coil equilibrium as the process responsible. However, perturbation of the proton-transfer equilibrium $-(CH_2)_4NH_3^+ + OH^- = -(CH_2)_4-NH_2 + H_2O$ or equilibria involving the interaction of water with the helical regions of the molecule remain reasonable rival explanations. It will be argued in subsequent sections that it is relatively less probable that viscous relaxation or redistribution of the ion atmosphere contribute significantly to the acoustic absorption.

II. Experimental Section

The polylysine used in this work was obtained from Pilot Chemicals (Lot L-23). A weight-average molecular weight of 86,300 was deduced from light-scattering measurements in 1 *M* NaCl. A viscosity-average molecular weight of 63,000 was estimated by the suppliers, and we obtained a number-average molecular weight of 62,000 from determinations of the osmotic pressure (in 1 *M* NaCl) as a function of the concentration.

The measurements of ultrasonic velocity and attenuation were made using an Arenberg Laboratories pulsed oscillator in an apparatus in many respects similar to that described by Yun, Beyer, and Dill. Data were obtained at the odd harmonics of 1- and 2-Mc ceramic transducers (1 in. in diameter) and 5-Mc quartz transducers (0.4 in. in diameter). The absorption was determined by measuring the amount of attenuation which had to be inserted or removed in the receiver circuit in order to restore a received signal to a preset height as the transmitting crystal was moved with respect to a receiving transducer. Velocities were calculated from the change in delay of a given cycle of a given received pulse when the distance between the transmitting and receiving crystals was changed by a known amount (determined by a Starret precision dial gauge).

In assessing the role that perturbation of the proton-transfer equilibrium plays in determining the excess acoustic absorption, it is necessary to have some estimate of the fraction of the $-(CH_2)_4NH_3^+$ present in the protonated *vs.* the dissociated NH_2 form. This quantity, as determined from the titration curves of the polymer solution, is plotted, for a typical set of conditions, in Figure 1. The "pH" represented in all figures is the uncorrected indication of a pH meter with a standard glass electrode. Since the pH of the solutions used to determine the optical rotation, viscosity, and ultrasonic attenuation was determined with the same electrode at the same temperature and ionic strength, the various curves may be meaningfully inter-

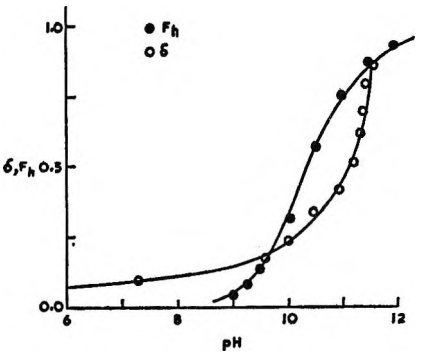

Figure 1. The degree of dissociation (δ) and the fraction of the polymer present in the helical form (F_h) for poly-L-lysine in 0.6 *M* NaCl at 25°.

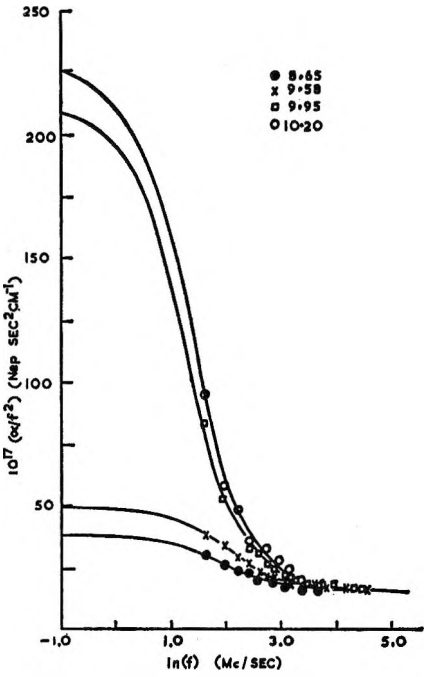

Figure 2. α/f^2 *vs.* ln f for 0.115 *M* poly-L-lysine in 0.6 *M* aqueous NaCl at various values of pH. Not all the points obtained at high frequency are plotted. The temperature is 24.9°.

compared, although at the higher temperatures, ionic strengths, and values of the pH there is a significant sodium ion correction. However, in the discussion of the effects of the proton-transfer reaction, where the hydroxide concentration enters explicitly, the pH has been corrected for "sodium ion error."

III. Results

In Figure 2 the result of a series of determinations of the ultrasonic attenuation (α) as a function of the frequency (f) at several values of the pH at 24.9° is displayed in the form of plots of α/f^2 *vs.* ln f. Values of α/f^2 as a function of the frequency at various temperatures, pH values, concentrations of the polymer, and concentrations of the supporting electrolyte are listed in Table I.

The fraction of the polymer present in helical form (F_h) at a given temperature, pH, and ionic strength was estimated from the dependence of the optical rotation (at 3000 Å) upon the pH at the temperature and the ionic strength in question. A typical result of such a study is given in Figure 3, in which the variation of the specific viscosity (η_{sp}) with pH is also displayed.

In the absence of significant dispersion, the frequency dependence of the ultrasonic attenuation in a medium with a single process with relaxation time τ may be expressed[1]

$$\frac{\alpha}{f^2} = A + \frac{C\tau}{1 + (2\pi\tau f)^2} \tag{1}$$

where A represents the attenuation associated with the viscosity and the thermal conductivity of the medium, as well as that due to any very rapid chemical or structural relaxations. In dilute aqueous solutions, where C_p and C_v are very nearly equal and the temperature fluctuation associated with the passage of an ultrasonic wave has a neglible effect on the equilibrium of a reaction with a moderate ΔH[1,3]

$$C = 2\pi^2\rho c\phi(\Delta V)^2/\bar{V}RT \tag{2}$$

where ρ is the density of the solution, c is the velocity of sound, ΔV is the volume change (per mole) for the process in question, and $\bar{V}$ is the volume per mole of the solvent. For the general equilibrium $\Sigma_i g_i A_i = 0$, ϕ is defined by

$$\phi^{-1} = \sum_i (g_i^2/X_i) - (\sum_i g_i)^2 \tag{3a}$$

where X_i is the mole fraction of the ith species. For the simple two-state equilibrium $H = C$

$$\phi = X_H X_C/(X_H + X_C) \tag{3b}$$

The solid curves in Figure 2 and the values of A, C, and τ in Table II represent the result of a computational least-squares adjustment of the parameters of eq 1 to give the best fit to the data in Table I. Starting from estimated initial values A, C, and τ were successively varied until a minimum value of the sum of the squares of the residuals was obtained, the process being repeated until the parameters do not change in successive cycles of "refinement."

When instead of a single relaxation a Davidson–Cole[4] distribution of relaxation times is introduced, the single parameter τ is replaced by two adjustable parameters, an average relaxation time $\bar{\tau}$ and a quantity (γ) characterizing the width of the distribution.

However, the introduction of an extra adjustable parameter does not substantially improve the fit. The optimum values of the parameters C, A, and $\bar{\tau}$ are only slightly altered from the results obtained from eq 1 and the optimum value of γ is very close to the value (1)

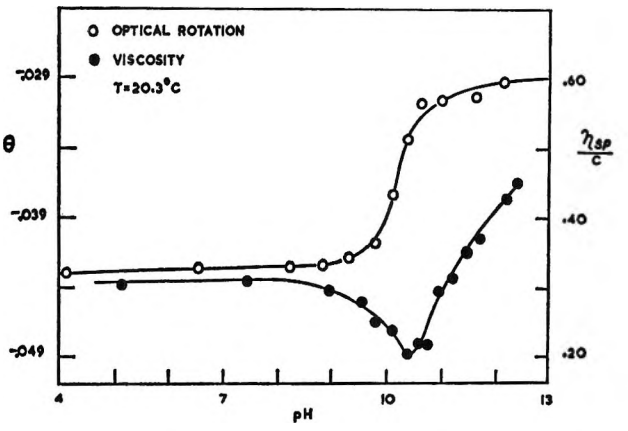

Figure 3. Optical rotation and specific viscosity of aqueous poly-L-lysine in 0.6 M NaCl as a function of pH.

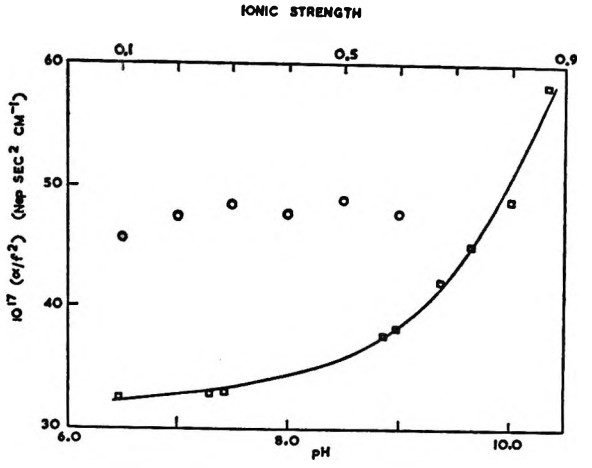

Figure 4. Ultrasonic absorption at 11.6 Mc in 0.156 M poly-L-lysine in 0.6 M NaCl *vs.* pH (□). Ultrasonic absorption in 0.156 M polylysine at 11.6 Mc and pH 10.2 *vs.* the concentration of NaCl (O).

characteristic of a single relaxation time. Thus the indication is that the excess ultrasonic attenuation in aqueous polylysine can be adequately described by a single relaxation with a relaxation frequency ($f_r = 1/(2\pi\tau)$ lying usually within, but at the extreme low end of, the range of frequencies accessible to us.

In Figure 4 the absorption at pH 10.2 at a constant frequency of 11.6 Mcps is plotted as a function of [NaCl], and the dependence of the absorption on pH at 11.6 Mcps and [NaCl] = 0.6 M is displayed. The appearance of excess absorption as the pH is increased is concomitant with the changes in the viscosity and optical rotation associated with the helix–coil transition. However, there are a number of processes, not all

(3) T. A. Litovitz and C. M. Davis, "Physical Acoustics," Vol. IIA, W. P. Mason, Ed., Academic Press Inc., New York, N. Y., 1965.
(4) D. W. Davidson and R. H. Cole, *J. Chem. Phys.*, **19**, 1484 (1951).

Table I: Ultrasonic Attenuation in Aqueous Poly-L-lysine as a Function of Frequency, Temperature, and pH[a]

pH 8.65		pH 9.58		pH 9.95		pH 10.2	
f	α/f^2	f	α/f^2	f	α/f^2	f	α/f^2
A. 0.115 *M* Polylysine in 0.6 *M* NaCl at 24.9°. The Velocity of Sound Is 1545 m/sec							
5.19	39.5	5.14	49.9	5.18	109.	5.18	124.0
7.24	34.7	7.28	44.8	7.27	69.7	7.24	76.6
9.34	30.0	9.40	38.0	9.43	62.0	9.41	63.1
11.43	30.3	11.44	34.5	11.41	43.1	11.49	46.4
13.51	27.3	13.56	29.5	13.42	40.3		
15.62	26.8	15.60	27.8	15.66	33.9	15.50	42.2
17.73	24.6	17.66	27.6	17.71	31.3		
		19.80	27.5	19.80	28.7	19.76	35.6
21.93	23.7	21.91	24.9	21.86	29.0		
		23.92	23.5	23.84	26.5	23.89	31.0
25.77	21.0	25.97	23.6	25.48	25.0		
				27.97	24.5	28.02	26.4
30.03	21.0	30.21	23.9	30.21	23.0		
				32.15	23.8	32.23	26.1
		34.95	21.8	36.04	23.9		
38.30	21.6	38.17	23.4	38.46	23.0		
		40.32	23.3	40.32	22.6	40.16	23.0
		42.44	23.0	42.19	23.5	42.4	23.4
		44.85	21.7	45.25	23.2		
55.00	21.3	55.16	22.8	55.29	23.2	55.00	22.2
		65.13	21.4	65.38	22.0		
		75.34	21.3	75.41	22.2		
		85.41	20.8	85.31	21.2		
		95.62	21.0	95.05	21.5		
H_2O	22.8		22.8		22.8		22.8

pH 5.10		pH 7.20		pH 9.22		pH 9.60	
f	α/f^2	f	α/f^2	f	α/f^2	f	α/f^2
B. 0.156 *M* Polylysine in 0.6 *M* NaCl at 35.8°. The Velocity of Sound Is 1560 m/sec							
5.25	36.4	5.36	44.5	5.23	124.3	5.20	154.
7.33	22.4	7.32	29.3	7.27	79.3	7.23	95.1
9.50	21.8	9.58	30.8	9.43	67.9	9.36	80.3
11.66	17.9	11.63	23.8	11.56	49.0	11.54	56.0
13.75	16.8	13.68	20.2	13.60	42.3	13.64	45.4
15.83	16.5	15.80	19.7	15.70	36.2	15.67	40.4
		17.89	18.9	17.67	33.6	17.60	36.8
		19.88	17.9	19.88	29.4	19.67	33.7
		21.98	17.9	21.93	26.7	21.57	31.3
		24.19	17.4	23.90	25.3	24.00	29.0
25.65	16.5	25.60	16.9	25.65	24.5	25.53	28.0
		28.41	16.8	28.30	23.3	28.06	26.5
30.35	16.6	30.44	16.5	30.30	23.2	29.85	25.6
		32.57		32.57	22.5	31.87	25.3
34.82	16.4	34.56	16.0	35.13	20.0	35.03	20.8
		36.70	16.4				
		38.76	16.1	38.56	22.3	38.17	23.8
		40.69	16.0	40.78	20.6		
45.25	16.3	45.00	16.2	45.05	19.9	44.92	20.0
55.25	17.0	55.55	17.0	55.02	20.8	55.10	19.8
		65.33	16.9	64.58	18.2	64.89	18.7
75.52	16.9	75.55	16.3	74.68	17.3	74.21	18.0
H_2O	16.9		16.9		16.9		16.9

directly connected with the transition, which might reasonably be supposed to be the source of the absorption. In the next section we wish to consider the possible contributions of four processes: proton-transfer reactions of the side chains, solvation, viscous relaxation, and conformational change to the ultrasonic attenuation.

IV. Discussion

For the proton-transfer equilibrium

pH 9.48, [NaCl] = 0.6 M		pH 9.65, [NaCl] = 0 M		pH 9.98, [NaCl] = 0 M	
f	α/f^2	f	α/f^2	f	α/f^2
		C. 0.156 M Polylysine at 20.3°			
5.22	80.4	5.14	76.9	5.21	103.
7.31	65.1	7.31	59.0	7.24	78.4
9.49	59.9	9.49	47.7	9.51	49.2
11.56	47.4	11.64	44.0	11.56	43.0
13.64	43.0	13.71	37.0	13.70	42.2
15.76	38.6	15.82	36.9	15.77	37.0
17.76	37.5	17.86	34.8	17.83	38.2
19.93	37.4	19.92	33.0	19.87	36.0
22.03	33.7	21.92	34.4	22.00	32.8
24.00	31.3	24.04	32.7	24.93	32.5
26.12	29.8	25.59	32.3	26.00	31.9
28.41	29.0	28.20	31.8		
30.18	30.0				
32.21	28.9				
35.10	30.0	34.95	31.4	35.34	31.0
		36.26	31.4	36.6	34.0
38.49	29.0			38.61	30.1
40.65	29.7				
45.29	29.4	45.45	30.9		
55.35	28.2	55.55	30.2	55.56	29.6
65.73	26.2	64.85	29.2	65.57	30.9
75.08	25.8	75.30	28.0	74.70	28.4
H_2O	25.1		25.1		25.1

[a] Frequency is expressed in Mcps, α/f^2 is in units of 10^{-17} neper sec^2/cm. The value of α/f^2 for water given at the end of each column is from J. M. M. Pinkerton, *Nature*, **160**, 128 (1947), and J. M. M. Pinkerton, *Proc. Roy. Soc.*, **B62**, 286 (1949). The last digit of α/f^2 should not be regarded as significant.

Table II: Ultrasonic Absorption Parameters for Aqueous Polylysine

Temp, °C	Concn, M	[NaCl,] M	pH	$10^{17}A$, nepers sec^2/cm	10^8C, nepers sec/cm	$10^8\tau$, sec	F_h
35.8	0.156	0.6	9.60	16.1	88.1	3.4	0.15
35.8	0.156	0.6	9.22	16.1	68.9	3.2	0.06
35.8	0.156	0.6	7.0	16.1	22.7	...	0.03
24.9	0.115	0.6	10.2	20.8	68.2	4.1	0.42
24.9	0.115	0.6	9.95	20.8	60.6	4.3	0.30
24.9	0.115	0.6	9.83	20.8	36.1	2.0	0.25
24.9	0.115	0.6	9.58	20.8	20.7	2.1	0.19
24.9	0.115	0.6	8.65	20.8	12.2	2.4	0.03
20.3	0.156	0	9.98	25.0	54.7	4.2	0.27
20.3	0.156	0	9.65	25.0	33.1	2.4	0.13
20.3	0.156	0.6	9.48	25.0	38.6	2.1	0.10

$$-RNH_3^+ + OH^- \underset{k_b}{\overset{k_f}{\rightleftharpoons}} -RNH_2 + H_2O \qquad (4)$$

A B C D

$$\phi = \left[\frac{1}{X_A} + \frac{1}{X_B} + \frac{1}{X_C} + \frac{1}{X_D}\right]^{-1} \qquad (5)$$

Introducing the degree of ionization, δ, and representing the mole fraction of lysyl residues by X_0, $X_A = X_0(1 - \delta)$, $X_C = X_0\delta$, and

$$\phi = \left[\frac{1}{X_0\delta(1 - \delta)} + \frac{1}{X_B} + \frac{1}{X_D}\right]^{-1} \qquad (6)$$

The value of δ at any pH must be obtained from the titration curve (Figure 1).

However, for the highest pH attained in the acoustic measurements (10.2), the first and third terms in eq 6 have magnitudes of 35 and 1, which are small compared with the value of 6300 of the second term. Thus over the range of pH covered by the ultrasonic measurements, $\phi = X_B$ and the parameter C is given by

$$C = 2\pi^2\rho c X_B(\Delta V)^2/\bar{V}RT \qquad (7)$$

C is thus a linear function of X_B and, therefore, an exponential function of pH in the region covered by the

measurements. Since X_H, and thus C, for the simple two-state equilibrium is also a rapidly increasing function of pH below the midpoint of the transition, it is not practical, within the limited accuracy of our data, to distinguish between the two cases on the basis of the dependence of C on pH.

The relaxation time for the equilibrium represented by eq 4 in the range of pH covered by the experiments is

$$\tau = X_B/k_b\delta X_0 \quad (8)$$

and thus is proportional to X_B. It will be shown in succeeding sections that below the midpoint of the transition there is reason to expect that the relaxation time for the helix–coil transition also increases with increasing X_B. Thus it is not possible to distinguish between the alternatives on the basis of the qualitative dependence of τ on the pH.

A more promising approach is to consider the magnitude of the rate constants and volume changes required to explain the observed ultrasonic attenuation on the basis of perturbation of the ionization equilibrium.[5] Although ϕ is an exponentially increasing function of pH between pH 7 and 10.2, it remains very small in this range, reaching a maximum value of 3×10^{-6} at pH 10.2. Thus the proton-transfer reaction would have to have an extremely large ΔV (60–200 ml/mol of monomer unit) in order to account for the observed absorption. Typical volume changes for analogous proton-transfer reactions are 12 ml/mol for $HCN + OH^- = CN^- + H_2O$,[6a] 28 ml/mol for $NH_4^+ + OH^- = NH_4OH$,[6b] 27.0 ml/mol for $CH_3NH_3^+ + OH^- = CH_3NH_2 + H_2O$,[7] and 21.0 ml/mol for $H^+ + OH^- = H_2O$.[8]

If it is assumed that perturbation of the equilibrium represented by eq 4 is the process responsible for the excess absorption, then, using eq 8, it is possible to estimate the unimolecular rate constant k_b from the observed relaxation times. The values of k_b so calculated range from 0.8×10^5 to 1.5×10^5 sec^{-1}. Eigen and Schwarz[6b] have found k_b for the protonation of methylamine to be 1.6×10^7 sec^{-1}. If it were possible to assume a similar value for the protonation of the lysyl residue in polylysine, one could immediately discount the proton-transfer process as the direct source of the acoustic absorption. However, the rate of proton transfer by a protonated amine RNH_3^+ does depend on the nature of R, and it is necessary to rationalize this dependence before one can estimate a conveniently high value of k_b in polylysine.

We have, therefore, measured the rate constants for the neutralization of a number of amino acids and simple peptides. Our results, as well as those obtained by Eigen and Schwarz for methylamine, are listed in Table III. These data can be explained in terms of a mechanism of the form

$$RNH_3^+ + OH^- \underset{k_{21}}{\overset{k_{12}}{\rightleftharpoons}} RNH_3^-\text{-}OH \underset{k_{32}}{\overset{k_{23}}{\rightleftharpoons}} RNH_2 + H_2O$$

the first step involving the diffusional encounter of the amine and hydroxide ion to form a hydrogen-bonded ion pair and the second step involving the extremely rapid transfer of a proton. The effective over-all rate constants for the forward and back reactions are $k_f = k_{12}$ and $k_b = k_{21}(k_{32}/[k_{32} + k_{23}])$; the rate of the back reaction being the diffusional rate diminished by an "equilibrium constant," expressing, at least qualitatively, the basicity of the amine relative to that of hydroxide ion. One would expect k_{21}, the constant specifying the rate of diffusional separation of RNH_3^+ and OH^-, to be roughly the same for any R[6] and hence the variation in rate from amine to amine to be determined largely by k_{32}/k_{23} and thus by the pK_a of the amine. The results in Table III are in good accord with such an interpretation.

Table III: Rate Constants and pK_a's for the Proton-Transfer Reaction of RNH_3^+

R	$10^{-10}k_f$, M^{-1} sec^{-1}	$10^{-6}k_b$, sec^{-1}	pK_a	
HCH_2	3.7	16	10.63	*a*
$^-OOCCH_2CH_2CH_2$	1.5	3.9	10.40	*b*
$^-OOCCH_2CH_2$	1.3	2.1	10.19	*b*
$^-OOCCH_2$	1.9	0.8	9.60	*b*
$^-OOCCH_2CONHCH_2$	1.6	0.03	8.25	*b*
$^-OOCCH_2CONHCH_2CONHCH_2$	2.1	0.02	7.91	*b*

[a] See M. Eigen and L. De Maeyer, "Technique of Organic Chemistry," Vol. VIII, Part II, A. Weissberger, S. L. Friess, and E. S. Lewis, Ed., John Wiley and Sons, Inc., New York, N. Y., 1961. [b] K. R. Applegate, R. C. Parker, and L. J. Slutsky, to be submitted for publication.

Since the pK_a of the lysyl residue in proteins and polypeptides ranges from 9.5–10.8, reference to Table III would suggest that $(0.1–1.0) \times 10^7$ sec^{-1} is a reasonable assignment of the rate constant k_b and thus that the relaxation of the proton-transfer equilibrium is a considerably faster process than that observed in these experiments.

The standard volume change for the ionization of a protonated amine is quite large compared with the ΔV commonly associated with conformational changes. Doty and Applequist[2] find that they can give a satisfactory description of the titration curves of aqueous polylysine if it is assumed that the helical regions are

(5) E. J. Cohn and J. T. Edsall, "Proteins, Amino Acids and Peptides," Reinhold Publishing Corp., New York, N. Y., 1943.

(6) (a) J. Stuehr, E. Yeager, T. Sachs, and F. Hvorka, *J. Chem. Phys.*, **38**, 587 (1963); (b) M. Eigen and L. De Maeyer, "Technique of Organic Chemistry," Vol. VIII, Part II, A. Weissberger, S. L. Friess, and E. S. Lewis, Ed., John Wiley and Sons, Inc., New York, N. Y., 1961.

(7) H. H. Weber, *Biochem. Z.*, **218**, 1 (1930).

(8) P. Drude and W. Nernst, *Z. Phys. Chim.* ((Leipzig), **15**, 79 (1894).

completely uncharged. Thus at any given pH there is a significant difference in the degrees of ionization of helical and coil segments. In the foregoing we have argued that the equilibration of the dissociation reaction is rapid compared to the relaxation time for conformational change. Thus it may very well be that the volume change associated with perturbation of the conformational equilibrium is largely that due to the concomitant change in the degree of dissociation. The large excess absorption found here relative to the results obtained by Burke, Hammes, and Lewis in solutions of polyglutamic acid[9] may then be a reflection of the large volume change associated with proton transfer by a RNH_3^+ group relative to that of a COOH group.

In summary, we believe that the absorption in polylysine occurs at too low a frequency and is too strong at low values of the pH to be the result of perturbation of the proton-transfer equilibrium.

At frequencies where there is no significant dispersion, the absorption due to viscous processes is[3]

$$\frac{\alpha}{f^2} = \frac{2\pi^2}{\rho c^3}\left(\frac{4}{3}\eta_s + \eta_v\right) \qquad (9)$$

where η_s and η_v are, respectively, the shear and the volume viscosities. The shear viscosity as a function of pH at each of the temperatures at which attenuation data were collected is plotted in Figure 5. With the exception of the run at pH 10.2 at 25°, all the ultrasonic data were taken in a region where the shear viscosity decreases slightly with increasing pH. Even at 10.2 the shear viscosity is less than that determined at low pH where there is no significant excess acoustic absorption. The large pH-dependent attenuation observed in these solutions is not connected with any variation in the shear viscosity. The presence of a substantial pH-dependent bulk viscosity, if not reflected in the behavior of the shear viscosity, would nonetheless be observed as an effect on the high-frequency limiting value of α/f^2 in accordance with eq 9. However, reference to Figure 2 and Tables I and II will indicate that, at any given temperature, at all values of the pH the absorption at high frequencies approaches a common limit which is very close to the value obtained by Pinkerton[10] for pure water. The result is not consistent with the assumption that there is a large pH-dependent volume viscosity in these solutions, and for this reason we believe that viscous relaxation is not the source of the observed absorption.

Burke, Hammes, and Lewis[9] attribute the acoustic absorption in solutions of poly-L-glutamic acid in water–dioxane mixtures to perturbation of a solvation equilibrium. We cannot conclusively rule out a similar interpretation of our results, but by comparison with measurements in solutions of di- and tripeptides, some restrictions can be arrived at.

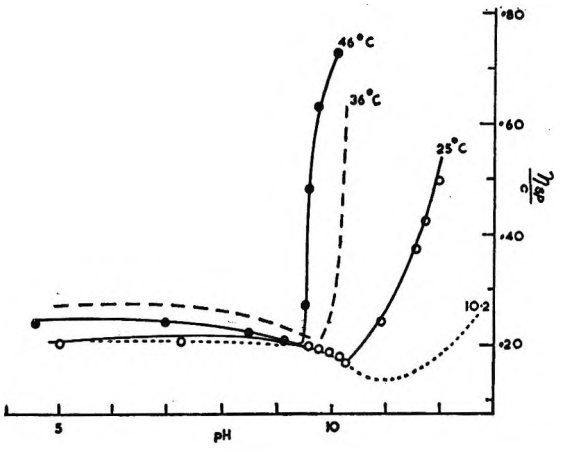

Figure 5. Specific viscosity of aqueous poly-L-lysine as a function of pH and temperature. All measurements were taken in 0.6 *M* NaCl.

Solutions of flexible polyelectrolyte chains are sufficiently complex so that it is difficult to arrive at a clear picture of the change in the physical situation involved in the reversible solvation of a molecule already in solution, although there is extensive, interesting, and somewhat speculative literature on alterations of the water structure possibly induced by solute species. In this literature polypeptides have received some consideration.[11,12]

Presumably solvation can be represented schematically as B = B′, where B′ may represent a structure in which a well-defined bond exists between a water molecule and a section of the polypeptide molecule or simply a mode of packing of water resulting from the local presence of the polymer. If it is assumed that it is perturbation of a solvation equilibrium which is responsible for the acoustic absorption in polylysine solutions, then the strong dependence of α on the pH suggests that the B′ form requires the presence either of unprotonated side chains or of helical sections.

The ultrasonic attenuation at 7.82 Mcps in a 1 *M* solution of diglycine is plotted *vs.* pH in Figure 6. The broken curve represents the form of the attenuation due to the proton-transfer process as predicted from the rate constants and equilibrium constants in Table III. At pH 13 the observed attenuation has returned almost to the value characteristic of water. There is no evidence of large acoustic absorption due to the interaction of water with individual NH_2 groups or peptide linkages, even though the diglycine solution contains a far higher concentration of peptide linkages and, at pH 13, NH_2 groups than any of the polymer solutions. Simi-

(9) J. Burke, G. Hammes, and T. Lewis, *J. Chem. Phys.*, **42**, 3520 (1965).

(10) J. M. M. Pinkerton, *Nature*, **160**, 128 (1947); *Proc. Roy. Soc.*, **B62**, 286 (1949).

(11) *I.e.*, D. T. Warner, *Nature*, **190**, 120 (1961); *J. Theor. Biol.*, **1**, 1279 (1961).

(12) H. J. C. Berendsen, *J. Chem. Phys.*, **36**, 3297 (1962).

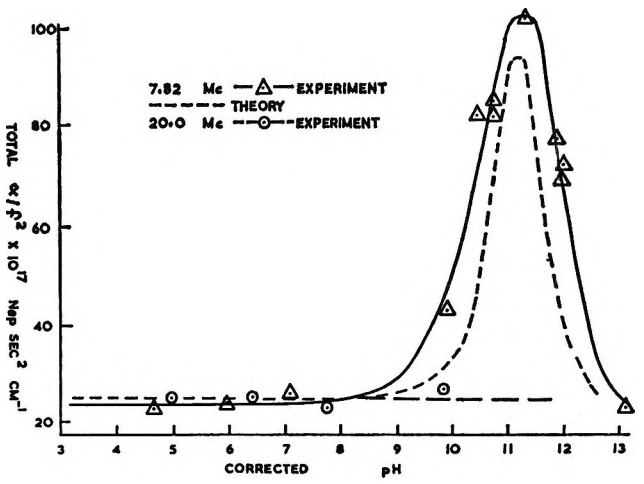

Figure 6. Ultrasonic attenuation in aqueous diglycine (1 M) as a function of pH. The broken line represents the predicted attenuation due to the perturbation of the proton-transfer equilibrium. The pH has been corrected for sodium ion error.

lar results are obtained in aqueous solutions of triglycine. Thus it would appear that if the absorption in solutions of polylysine is to be attributed to solvation, then either the interaction of water with the helical backbone or a cooperative effect requiring the simultaneous proximity of a number of neutral side chains must be involved.

The conclusions of Doty and Applequist[2] would imply that at any pH where there is appreciable helical content there are long sequences of adjacent $-(CH_2)_4NH_2$ groups. A cooperative effect on the structure of water, perhaps similar to the epitaxial stabilization of chain structures or the ice structure as discussed by Berendsen[12] and Jacobson,[13] cannot be ruled out. There is no doubt that with the assumption of a suitably large ΔV the absorption observed here could be consistently explained as the result of the perturbation of an equilibrium involving the interaction of water with the helical portions of the molecule. A minimum volume change can be estimated by assuming that the equilibrium constant for B = B′ is 1. In dilute solution the quantity $\phi/\bar{V}$, which appears in eq 2, then becomes $MF_h/4$ (M is the molar concentration of the polymer). The requisite volume changes range from 5.7 to 7.5 ml/mol of monomer and are thus approximately a factor of 2 greater than the range of 2.9–3.3 ml/mol estimated by Burke, Hammes, and Lewis[9] for the solvation of polyglutamic acid in water–dioxane solution and a factor of 5 greater than the over-all volume change (1–1.5 ml/mol) for the helix–coil transition in polylysine as determined by Noguchi.[14] In the next section it will be argued that Noguchi's result correctly predicts the magnitude of the acoustic absorption if it is assumed that perturbation of the helix–coil equilibrium is the process responsible. Thus, while our results can be interpreted in terms of a solvation equilibrium with a minimum volume change of 5.7–7.5 ml/mol, which is present in the polymer solution but not in solutions containing equivalent amounts of alkyl NH_2 groups or NH_3^+ groups or peptide linkages, we believe that the attribution of the observed acoustic absorption to the perturbation of a conformational equilibrium constitutes a somewhat more satisfactory explanation of the limited amount of data available.

In the next section we will attempt to rationalize our results on this basis after briefly considering the predicted dependence of the relaxation time and the absorption parameter (C) for the helix–coil transition on the fraction of the polymer present in the helical form.

V. The Helix–Coil Transition

In the usual notation of the Zimm–Bragg model, each helical segment which is preceded by a helical segment makes a contribution, s, to the configurational partition function. The first helical segment in a sequence makes a contribution σs. In the subsequent discussion we will use the value of $\sigma = 5 \times 10^{-3}$, determined by Rifkind and Applequist[15] for polyglutamic acid. Representative calculations will also be carried out for $\sigma = 2 \times 10^{-4}$, as determined by Zimm, Doty, and Iso[16] and as used by Applequist[17] for poly(γ-benzyl-L-glutamate).

Schwarz[18] has simplified the Zimm–Bragg model by considering bonding between nearest rather than third nearest neighbors. He obtains an expression for the average relaxation time of the helix–coil equilibrium in terms of s, σ, and k_f', the first-order rate constant for the addition of a helical unit to a sequence of preexisting helical units. His result for long chains and small deviations from equilibrium is

$$(1/\tau) = k_f'[(s-1)^2 + 4\sigma]$$

$$C = \frac{4\pi^2 \rho c M (\Delta V)^2}{RT} s(\partial F_h/\partial s) \qquad (10)$$

$$s(\partial F_h/\partial s) = \sigma(1+s)s/[(s-1)^2 + 4\sigma s]^{1/2}$$

where C is the absorption parameter appearing in eq 1. The value of s can be deduced from F_h as

$$F_h = {}^1/_2\{1 + (s-1)/[(s-1)^2 + 4\sigma s]^{1/2}\}$$

Thus below the midpoint of the transition both C and τ are expected to increase with increasing pH, reaching their maximum values at $F_h = 0.5$. For example, with reference to the data collected at 24.9°, eq 10 predicts $C/C_{max} = 0.48$ and $\tau/\tau_{max} = 0.62$ at $F_h = 0.19$ (pH 9.58) and $C/C_{max} = 0.95$ and $\tau/\tau_{max} = 0.97$ at $F_h =$

(13) B. Jacobson, *Nature*, **172**, 666 (1935).

(14) H. Noguchi, *Biopolymers*, **4**, 1105 (1966).

(15) J. Rifkind and J. Applequist, *J. Amer. Chem. Soc.*, **86**, 4207 (1964).

(16) B. H. Zimm, P. Doty, and K. Iso, *Proc. Natl. Acad. Sci. U. S.*, **45**, 1601 (1959).

(17) J. Applequist, *J. Chem. Phys.*, **38**, 934 (1963).

(18) G. Schwarz, *J. Mol. Biol.*, **11**, 64 (1965).

0.42 (pH 10.2). The results of eq 10 are compared with the experiment in Table IV, using values of C_{max} (71.8×10^{-9} neper sec/cm) and τ_{max} (4.2×10^{-8} sec) derived from measurements at the highest value of F_h attained (0.42). Disagreement between the "theoretical" and the experimental results in Table IV will reflect not only the inaccuracies in the parameters and the inadequacies of the model but also any error in the estimation of F_h from the optical rotation. At low values of F_h, s is very sensitive to the choice of F_h and thus not too much importance should be attached to the comparatively large disagreement between the theory and the experiment at $F_h = 0.03$.

Table IV: Comparison of the Predictions of Eq 10 and 3b with the Experimental Values of C and τ at 24.9°

	F_h				
	0.42	0.30	0.25	0.19	~0.03
C/C_{max} (eq 3b)	0.97	0.84	0.75	0.62	~0.12
C/C_{max} (eq 10)	0.95	0.78	0.65	0.49	~0.05
C/C_{max} (exptl)	0.95	0.84	0.50	0.29	0.17
τ/τ_{max} (eq 10)	0.97	0.86	0.77	0.62	~0.13
τ/τ_{max} (exptl)	0.97	1.0	0.48	0.50	0.57

The data are in crude qualitative agreement with eq 10. However, from the *form* of the dependence of the absorption on pH it does not appear possible to arrive at an evaluation of Schwarz's model or of the more sophisticated theoretical treatment of Polland and Scheraga.[19] Even the most naive model (eq 3b), which would assign a single rate constant and equilibrium constant for the formation of a helical segment regardless of the number of preexisting helical segments (*i.e.*, $\sigma = 1$), would give a consistent description of the data. For purposes of comparison, values of C/C_{max} calculated from eq 3b are given in Table IV.

If one could extend these measurements past the midpoint of the transition, it would be possible to distinguish the absorption associated with the solvation of the helical regions of the molecule, which would presumably continue to increase with increasing F_h, from the absorption due to perturbation of the conformational equilibrium. However, at high pH both the ultrasonic attenuation and the shear viscosities of these solutions become time dependent, indicating the onset of aggregation. Hence our preferential attribution of the observed excess absorption to perturbation of a conformational equilibrium rests primarily on the indirect arguments of the preceding section, with some support from the fact that the data in Table II do indicate that the relaxation time in the neighborhood of the midpoint of the transition is somewhat greater than at very low values of F_h, as would be expected for a conformational transition.

A detailed interpretation of the relaxation times in terms of the kinetics of the elementary steps is difficult, owing to both the limitations of the data and the limitations of the theoretical models. At the higher values of pH, where the absorption is large, it is not possible to carry out measurements at frequencies below the relaxation frequency ($f_r = 1/(2\pi\tau)$), as is necessary if τ is to be determined accurately. At the lower values of pH, where the relaxation times are shorter and the relaxation frequencies conveniently high, the absorption is small. Hence the relaxation times and C's in Table II are reliable to no more than one significant figure. (These remarks do not apply to the results for the amino acids, diglycine, and triglycine, where large samples are available and data were collected at frequencies well below the relaxation frequency in all cases.)

The rate constants calculated from eq 10 with $\sigma = 5 \times 10^{-3}$ are $k_f' = 0.9 \times 10^9$ sec^{-1}, 1.2×10^9 sec^{-1}, and 0.8×10^9 sec^{-1} at 20.3, 24.9, and 35.3°, respectively. If $\sigma = 2 \times 10^{-4}$ is used, the corresponding results for k_f' are 2.3×10^{10}, 3.0×10^{10}, and 2.0×10^{10} sec^{-1}.

The ΔV necessary to explain the observed absorption will depend on the value of σ as well as on the process nominated as the source of absorption. In sufficiently dilute aqueous solution, the quantity $\phi/\bar{V}$ appearing in eq 2 and 3b may be rewritten as $MF_h(1 - F_h)$. Thus $\phi/\bar{V}$ reaches a maximum value of $M/4$ at $F_h = 0.5$. The analogous quantity in Schwarz's model, $Ms(\partial F_h/\partial s)$, has a maximum value of $M/4\sigma^{1/2}$ at the midpoint of the transition. The values of ΔV obtained from Schwarz's equations are between 0.9 and 1.3 ml/mol if σ is taken to be 5×10^{-3} and are between 0.4 and 0.6 ml/mol if $\sigma = 2 \times 10^{-4}$ is used. The volume changes at 24.9° calculated from eq 3b, or equivalently eq 10 with $\sigma = 1$, are between 3.2 and 4.5 ml/mol of monomer. It is thus possible to explain our results using the volume change determined by Noguchi for the helix–coil transition.

If we are indeed observing a conformational relaxation, then these results suggest that change of conformation in a uniform polypeptide is an extremely fast process. While it would be of interest to extend this work to proteins and other nonuniform polypeptides, and it is of course easier to obtain the requisite large samples of many proteins than of synthetic uniform polypeptides, the presence of a variety of ionizable groups will spread the absorption due to proton-transfer reactions over a relatively wide range of pH. In these circumstances the identification of ultrasonic attenuation due to conformational change, at best equivocal in the rather favorable case considered here, may prove to be impossible in more complex systems. It would seem likely, for example, that the very broad relaxation

(19) H. Scheraga and D. Polland, *J. Chem. Phys.*, **45**, 2071 (1966).

spectrum obtained by Carstenson[20] and his coworkers for hemoglobin at neutral pH contains contributions from the proton-transfer reactions of a variety of ionizable groups and that this state of affairs will prove to be common in protein solutions.

Acknowledgment. This work was supported by the National Institutes of Health. The authors also gratefully acknowledge support in the form of fellowships from the Woodrow Wilson (K. R. A.) and A. P. Sloan (L. J. S.) foundations.

(20) E. L. Carstenson and H. P. Schwan, *J. Acoust. Soc. Amer.*, **31**, 305 (1959).

Electron Spin Resonance Studies of Carbon Dispersed on Alumina

by Pierre A. Berger and James F. Roth

Central Research Department, Monsanto Company, St. Louis, Missouri 63166 *(Received February 15, 1968)*

Electron spin resonance studies have been made of carbon dispersed on an acidic alumina. Samples were prepared by pyrolysis of butene-1 and *n*-butane on the alumina surface. Some compositions were doped with Dy^{3+} to provide a magnetic probe. Data have been obtained on the variation with carbon content of line shapes, line widths, spin-lattice relaxation times, spin densities in air and *in vacuo*, and on paramagnetic Curie temperatures. Two different types of carbon phases have been detected. The phase deposited initially exhibits antiferromagnetic coupling possibly due to an interaction of the carbon phase with the support. Subsequently, a new phase of larger domain size is formed that is devoid of magnetic ordering. Crystallographic ordering appears to improve with increasing carbon content. This leads to increased accessibility to oxygen of spin centers contained within the carbon phase. It is concluded that data on spin concentrations *in vacuo* and in air of carbons deposited on various supports provide a measurement of crystallographic particle size.

I. Introduction

A large amount of literature is available on the physical properties of the various forms of bulk carbon, but rather little[1-8] is known about the nature of carbonaceous deposits dispersed on the surface of porous supports and catalysts. Undoubtedly, one reason is that such materials have been most frequently encountered as coke deposits that deactivate catalysts, and as such they have not motivated much study. However, recent results in our laboratories (to be reported at a later date) have shown that carbon dispersed on various supports can exhibit positive catalytic properties, and this has prompted us to investigate the nature of carbon dispersed on alumina.

The turbostratic[9] nature of at least 50% of a carbonaceous deposit formed at 482° on a silica–alumina catalyst has been established by Haldeman and Botty.[4] Poole, *et al.*,[7] have made quantitative esr intensity measurements both in air and *in vacuo* of carbon deposits formed at 500° on a silica–alumina catalyst. Assuming that only the spins located in the surface carbon layer interact with oxygen sufficiently to be broadened beyond detection, their results confirmed the particle size obtained from X-ray diffraction measurements.[4] We have carried out two kinds of esr investigations. First, we have applied the technique of Poole, *et al.*,[7] to the study of carbonaceous deposits formed by the pyrolysis of butene-1 at 540° on a series of supports varying in acidity. It is well known that aluminas exhibit an intrinsic acidity that is related to their catalytic activity.[10] Our aim was to assess the influence of the acidity of the supports on the ratio of surface spins to bulk spins, or in the interpretation of Poole, *et al.*,[7] on the particle sizes of the carbon. A large ratio thereby implies a small particle size. As a comparison of the

(1) M. A. Tanatarov, G. M. Panchenkov, and M. E. Levinter, *Russ. J. Phys. Chem.*, **40**, 850 (1966).

(2) P. E. Eberly, Jr., C. N. Kimberlin, Jr., W. H. Miller, and H. V. Drushel, *Ind. Eng. Chem., Process Des. Develop.*, **5**, 193 (1966).

(3) M. N. Shendrik, G. K. Boreskov, and L. V. Kirilyuk, *Kinetika i Kataliz*, **6**, 313 (1965).

(4) R. G. Haldeman and M. C. Botty, *J. Phys. Chem.*, **63**, 489 (1959).

(5) J. W. Hall and H. F. Rase, *Ind. Eng. Chem., Process Des. Develop.*, **2**, 25 (1963).

(6) M. S. Goldstein, *ibid.*, **5**, 189 (1966).

(7) C. P. Poole, Jr., E. N. Dicarlo, C. S. Noble, J. F. Itzel, Jr., and H. H. Tobin, *J. Catalysis*, **4**, 518 (1965).

(8) F. E. Massoth, *Ind. Eng. Chem., Process Des. Develop.*, **6**, 200 (1967).

(9) J. Biscoe and B. E. Warren, *J. Appl. Phys.*, **13**, 364 (1942).

(10) H. Pines and W. O. Haag, *J. Amer. Chem. Soc.*, **82**, 2471 (1960).

last two columns in Table I shows, the carbon particle size is a pronounced function of the acidity of the support, high acidity supports favoring formation of large particles (ratio of surface to bulk spins of the order of unity), and low acidity supports favoring formation of very small particles (ratio of the order of hundreds).

Table I: Spin Concentrations of Cokes Deposited by Pyrolysis of Butene-1 at 540°

Support	%C	$N_{vac} \times 10^{-18}$ [a]	$N_{air} \times 10^{-18}$ [a]
Low-Acidity Supports			
Al-0104 γ-alumina	4.5	92	
2% Na on Al-0104	5.6	93	0.064
KA-101 γ-alumina	18.0	39	0.235
6% Na on KA-101	10.2	108	0.242
High-Acidity Supports			
Rd-Al acidic alumina	26.72	106	34.9
S-65 silica alumina	29.6	80	31.6

[a] N_{vac} = number of spins detected *in vacuo* per gram of carbon deposited; N_{air} = number of spins detected in air per gram of carbon deposited.

Second, a detailed esr study was devoted to carbon deposited in varying amounts on one specific acidic alumina. The study involved line shape and line width analyses, intensity, and saturation measurements. The description and interpretation of those results are the main subjects of discussion of the present paper.

In order to try to produce interactions with the spins in the carbon, and to establish the possible effect of supported impurities, some of our cokes were deposited on an alumina containing dysprosium. Dy^{3+} was chosen because of its high electronic magnetic moment (Dy_2O_3, 10.5 μ_B)[11] and the absence of an esr signal in the usual working region of magnetic field. Furthermore, Dy^{2+} that might be produced by reduction with carbon has almost the same theoretical magnetic moment as Dy^{3+}.

II. Experimental Section

Preparation of the Samples. The carbonaceous deposits were formed on a high surface area (445 m^2 g^{-1}) acidic alumina, Rd-Al, obtained from Engelhard Industries, Inc. Its acidity factor was determined according to a procedure described by Moore and Roth[12] and found to be 6.9. This implies a high acidity as evidenced by relatively high activity for cracking and skeletal isomerization of *n*-paraffins. The impurity content of this particular alumina was determined by emission analysis (Table II). Particularly noteworthy is the iron content, which is equivalent to $\sim 10^{18}$ Fe atoms/g of Al_2O_3. This corresponds to a value of the order of magnitude of the number of free spins per gram of carbonized sample.

Table II: Impurities in Rd-Al Acidic Alumina (ppm)

Si	Fe	Mg	Cu	Cr	Pt	Ca	Mn, Ni
200	100	100	10	3	<10	~1	<1

A series of cokes was needed on alumina impregnated with dysprosium (Rd-Al-Dy); 120 g of Rd-Al alumina was impregnated with 105 ml (a slight excess over the 0.84 ml/g of water uptake capacity of Rd-Al) of a solution containing 7.2 g of $Dy(NO_3)_3$ (99.9% purity, Research Inorganic Chemical Co.). After 24 hr standing, the catalyst was dried at 120° and then calcined at 540° for 24 hr in air. The nominal dysprosium content was 28 mg of Dy/g of Al_2O_3. With a specific surface area of 445 m^2 g^{-1} for Rd-Al, one Dy^{3+} would fall on a 430 $Å^2 \approx 21 \times 21$ Å square if randomly distributed.

The carbonizations were carried out at 540° in a Vycor reactor that accommodated 13.2 ml of catalyst (in the form of 1/16-in. cylindrical extrudates). The total gas flow was 250 ml min^{-1}, with a 3:1 volume ratio of nitrogen to butene-1 or *n*-butane. The butene-1 (Phillips, 99% pure) contained 0.35% *n*-butane and 0.17% butadiene, the *n*-butane (Matheson, CP grade) 0.16% isobutane and 0.07% *trans*-butene-2.

The carbon contents were determined by combustion. For butene-1 cokes they range from 3 to 22% (g of carbon/g of sample); *i.e.*, the highest carbon content corresponds to about one ideal monolayer of carbon (calculated as graphite layer) on the alumina. The carbons prepared on Rd-Al-Dy were formed much more slowly than on the undoped Rd-Al.

The carbonized samples were ground in air to particle sizes between 105 and 207 μ (65 and 150 mesh), then filled to a height exceeding the effective esr cavity length into capillaries (weight of substance about 30 mg). They were centered in standard quartz esr sample tubes by means of quartz wool. These quartz tubes were themselves sealed to Vycor ground joints for attachment to a conventional glass vacuum manifold where all the operations could be carried out. Standard evacuation and heat treatment were performed at less than 10^{-5} mm pressure and 400°.

In the following, we shall use the following abbreviations when referring to the main three types of samples: A, coke from butene-1 on Rd-Al; B, coke from *n*-butane on Rd-Al; C, coke from butene-1 on Rd-Al-Dy.

Esr Experiments. The esr measurements were performed on a conventional Varian V-4502 spectrometer in a Te_{104} dual cavity operating at a nominal frequency of 9.5 GHz. The apparatus was equipped with a 12-in. magnet, the Varian Fieldial calibrated sweep system,

(11) G. Foëx, C. J. Gorter, and L. J. Smits, "Constantes sélectionnées; diamagnétisme; paramagnétisme," Masson, Paris, 1957.

(12) R. N. Moore and J. F. Roth, U. S. Patent 3,274,287 (1966).

and a dual-channel Moseley 2 FR-AM X–Y recorder. A Hewlett-Packard X-530 A frequency meter was attached to the 20-db coupler provided in the microwave bridge. Diphenylpicrylhydrazyl (DPPH) and potassium peroxylamine disulfonate served for field and sweep calibration purposes, and a single crystal of $CuSO_4 \cdot 5H_2O$ embedded in paraffin as intensity standard. The conventional Varian quartz insert in conjunction with the V-4540 temperature controller permitted measurements to be made from about −180 to 300°. The accuracy of the temperature scale was checked with DPPH and was assumed to follow a Curie law below room temperature.

Particular care was applied in getting reliable quantitative data. In order to monitor changes in the cavity Q a standard was used in one side of the double cavity. For the saturation experiments a Hewlett-Packard 431-B power meter was attached over a 20-db coupler to the cavity wave guide. The sample size was kept small (capillary tubes) to avoid power losses. The Varian bridge was operated in the low power mode. Whenever possible, 400-Hz modulation was used.

Generally the first experimental moment of the recorded derivative was used as intensity measure.[13] Undermodulation conditions were usually applied.

III. Results and Discussion

1. Spin Densities. The first experimental moments (intensities) were determined for types A and B samples in air and *in vacuo* and were corrected for the values of the paramagnetic Curie temperature. A fairly linear relationship seems to exist between the intensities and the carbon content (Figure 1); *i.e.*, the spin densities (in number of spins per gram of carbon) for the individual types of carbons are constant over the range of carbon contents studied. Spin concentrations are given in Table III. We observe that a much larger fraction of spins is destroyed by oxygen in the butane than in the butene-1 coke. This points to a higher accessibility of the spins to oxygen in the case of cokes from *n*-butane than from butene-1 and might be due to differences in porosity, particle size, or ordering of the structure of the respective carbonaceous deposits.

Table III: Spin Concentrations

	Spins/g of carbon	
	In vacuo	In air
Type A[a]	1.04×10^{20}	3.88×10^{19}
Type B[b]	8.12×10^{19}	6.17×10^{18}

[a] Carbon deposit from butene-1. [b] Carbon deposit from *n*-butane.

2. Line Shapes. The method of Tikhomirova and Voevodskii[14] was applied to determine the Gaussian and Lorentzian contributions to the line shapes. Samples A, B, and those of C with low carbon content ($\leq 8.3\%$) had line shapes that were Lorentzian up to a distance of about 3 peak to peak widths (ΔH_{pp}) from the center and Gaussian beyond. Such results are typical for exchange-narrowed lines,[14,15] although other origins cannot be excluded.[15] Samples C with high carbon content had neither Gaussian nor Lorentzian line shapes. The integrated experimental line shapes had maxima ending in a cusp. It has been suggested[16] that this type of line shape may be caused by large sample inhomogeneities. The strong perturbation introduced by the high magnetic moment of Dy^{3+} is expected to be the cause of significant inhomogeneities in our samples. Since we have observed this particular line shape (cusp) only in samples of high carbon content, we conclude that carbon is initially deposited far away from the Dy^{3+} centers. The line shape behavior of type C samples was also observed with type A samples that had been impregnated with a dysprosium nitrate solution after coke deposition.

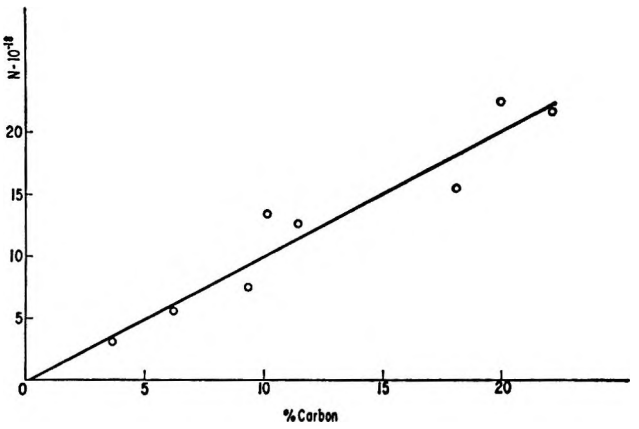

Figure 1. Number of spins per gram of sample measured *in vacuo vs.* amount of carbon deposited on Rd-Al (type A sample).

The discussed line shapes were observed both in evacuated samples (after a standard heat treatment) and in samples exposed to air.

3. Line Widths. The line widths of A, B, and C are summarized in Table IV and Figure 2. We start by considering only A and B and observe the following trends: first, the line width *in vacuo* [ΔH_{pp}(vac)] decreases with increasing carbon content, most drastically in B. Second, the line width in air [ΔH_{pp}(air)] also decreases in this direction, but ΔH_{pp}(air) − ΔH_{pp}(vac) increases. From the spin concentration *in vacuo* (Table

(13) K. Halbach, *Phys. Rev.*, **119**, 1230 (1960).

(14) N. N. Tikhomirova and V. V. Voevodskii, *Opt. Spectry.*, **7**, 486 (1959).

(15) A. Abragam, "The Principles of Nuclear Magnetism," Oxford University Press, New York, N. Y., 1961.

(16) L. S. Singer, "Proceedings of the Fifth Conference on Carbon, Vol. II, The Macmillan Co., New York, N. Y., 1963, p 37.

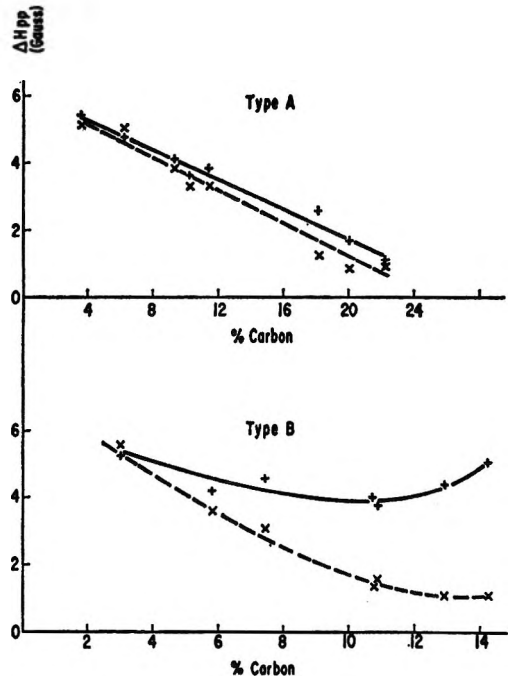

Figure 2. Dependence of the line widths (G) ΔH_{pp}(air) (+, —) and ΔH_{pp}(vac) (×, —) on the amount of carbon deposited on Rd-Al for type A and type B samples.

Table IV: Line Widths[a] of Carbonaceous Deposits

	Type A		Type B		Type C	
% C	ΔH_{pp} (air)	ΔH_{pp} (vac)	ΔH_{pp} (air)	ΔH_{pp} (vac)	ΔH_{pp} (air)	ΔH_{pp} (vac)
3.0			5.22	5.53		
3.56	5.45	5.17				
3.9					5.1	5.9
5.8			4.20	3.60		
6.17	4.79	5.05				
6.5					4.8	5.07
7.42			4.52	3.04		
8.3					4.6	
9.29	4.10	3.84				
10.1	3.65	3.30				
10.8			3.93	1.39		
10.9			3.76	1.55		
11.16				1.39		
11.37	3.85	3.31				
12.6					6.9	4.46
12.94			4.34	1.11		
14.34			5.08	1.11		
16.0					7.42	3.79
18.1	2.55	1.245				
18.5					9.20	3.58
20.0	1.68	0.885				
21.5					8.10	3.51
22.2	1.11	0.915				
Estimated dipolar width		9.44		7.36		

[a] [ΔH] = G.

III) one may estimate the dipolar line width of the magnetically diluted system according to[15]

$$\delta = 5.3(f\gamma\hbar/d^3) = \Delta H_{pp} \times \frac{\sqrt{3}}{2} \quad (1)$$

where f is the fraction of lattice sites occupied by an atom with $S = {}^1/_2$, $\gamma = 17.6 \times 10^6$ G^{-1} sec^{-1}, and d is the spacing between lattice atoms (the formula is derived for a simple cubic lattice). We chose $d = 2.9$ Å for the average C–C distance. The estimated linewidth values shown at the bottom of Table III are too large to account for the experimental results, and, furthermore, independent of the amount of carbon deposited. We therefore conclude that the lines are exchange narrowed with an exchange frequency that increases with carbon content according to the formula[17]

$$\Delta H_{pp} = \frac{\pi}{\sqrt{3}} \frac{\gamma M_2}{J\hbar^{-1}} \quad (2)$$

where M_2 is the second moment of the absorption line and $J\hbar$ is the exchange frequency. The latter varies from about 30 to 300 MHz for type A and B samples. Pastor and Turkevich[18] have shown that a relationship exists between the extent of delocalization and the amount of exchange.

A plausible explanation for the oxygen effect on the line width is the following. When first adsorbed, oxygen depletes an accessible surface layer of its spin but leaves the bulk spin density intact. The contribution of the oxygen to the line width is then ΔH_{pp}(air) − ΔH_{pp}(vac). It is shown to be small (<1 G) and increasing by a factor of about 3 when going from 3.56 to 22.2% carbon of type A, but significantly larger (up to 4 G) and increasing by a factor of about 12 when going from 3.0 to 14.34% carbon of type B. This means a higher accessibility of the spins to oxygen in the case of cokes from *n*-butane than from butene-1. This is consistent with the results of section III.1.

The results obtained with type C samples are more difficult to interpret. In the first place, the line shape results described in section III.2. exclude an interpretation in terms of exchange narrowing except for the three lowest carbon contents, where the line widths are practically identical with the ones of A in the corresponding carbon range.

An A sample with 3.9% C that had been treated with a dysprosium nitrate solution and then calcined in air had ΔH_{pp}(vac) = 7.18 G and ΔH_{pp}(air) = 4.85 G. Obviously, the oxygen blocked the surface spins formerly interacting with the adsorbed Dy^{3+}, thus removing the line broadening. A similar effect was observed with a sample of high carbon content. This demonstrates nicely the sensitivity, specifically, of surface spins to paramagnetic species. It also shows

(17) G. E. Pake, "Paramagnetic Resonance," W. A. Benjamin, Inc., New York, N. Y., 1962.

(18) R. C. Pastor and J. Turkevich, *J. Chem. Phys.*, 23, 1731 (1955).

that oxygen interacts principally with spin centers located in the surface layer.

4. Spin Lattice Relaxation. Power-dependent measurements were carried out with A and C. The microwave power available (120 mW) was insufficient for the observation of saturation effects in C, and in all the cases in the presence of air. This means that oxygen, and even dysprosium on the support surface, are in good thermal contact with the spin system. The saturation data for several samples of type A at room temperature are presented in Figure 3. Since we measure the magnetization rather than the magnetic susceptibility with our spectrometer, we plot $(1/H_1)\cdot(\partial\chi''/\partial H)_{max}$ *vs.* log H_1 to get the family of curves

$$\frac{1}{H_1}\left(\frac{\partial\chi''}{\partial H}\right)_{max} \propto (1 + T_1T_2H_1^2)^{-3/2} \qquad (3)$$

In evaluating absolute values of T_1 (Table V) from these curves we have taken $T_2 = 4.62 \times 10^{-7}$ sec as calculated from eq 1. T_1T_2 is determined by measuring the distance from a specific curve in Figure 2 to a standard curve of known magnitude T_1T_2. To translate microwave power (watts) into the magnetic field amplitude (gauss) at the place of the sample, we made use of the rule of thumb, 1 W $\approx$ 1 G^2, that applies to the Varian cavity.[19]

Table V: Spin-Lattice Relaxation Time (T_1, sec) of Type A Carbons

% carbon content	Room temp	213°K	113°K
3.56	1.1×10^{-4}	1.1×10^{-4}	1.1×10^{-4}
6.17	2.9×10^{-5}		
9.29	7.2×10^{-6}		
18.1	2.5×10^{-6}		
20.0	2.5×10^{-6}		
22.2	2.5×10^{-6}	5.9×10^{-6}	7.2×10^{-6}

We observe that the relaxation time T_1 decreases with increasing carbon content, *i.e.*, with increasing exchange frequency. This effect is in accord with expectation.[20]

The temperature dependence of T_1 was studied for two samples (Table V). From room temperature down to 113°K, T_1 was constant for the sample of low carbon content (3.6%) but changed markedly for the sample of high carbon content (22.2%), increasing with decreasing temperature. The temperature dependence of the latter sample conforms with other work,[20,21] but the lack of temperature dependence of the former is contrary to the theoretical prediction and experimental findings of Goldsborough, *et al.*[20] According to this work, T_1 for the sample with the lower exchange frequency (low carbon sample) should be the more temperature-sensitive one. We conclude from this that

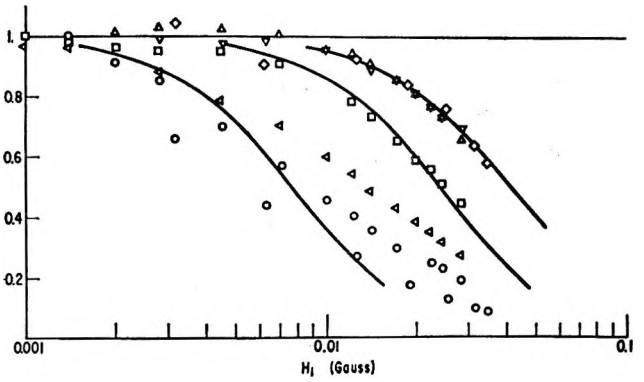

Figure 3. Saturation behavior (eq 3) at room temperature of samples with various carbon contents (% carbon): ◇, 22.2; ▽, 20.0; △, 18.1; □, 9.29; △, 6.17; ○, 3.56. Abscissa: estimated microwave field amplitude H_1. Ordinate: $H_1^{-1} \times$ derivative amplitude, normalized to the value in the absence of saturation.

the result cannot be interpreted in terms of just one species of carbon, but that there are two kinds of carbons, differing in nature, that are deposited consecutively. Furthermore, it is seen in Figure 3 that the saturation curves of the samples with low carbon content do not fit very well to the ideal curve (solid lines). In this case the simple relaxation mechanism underlying eq 3 seems not to be fully justified, or the represented curves are the results of a superposition of relaxation mechanisms from two kinds of carbon. The estimated T_1 values for those samples should be considered with appropriate reservation.

5. Paramagnetic Curie Temperature. The temperature dependence of the intensity of type A samples was measured from 103 to 298°K. Plots of the reciprocal intensity *vs.* temperature gave straight lines. This is characteristic of magnetic systems obeying a Curie–Weiss law. The dependence of the paramagnetic Curie temperature θ_p determined from these plots on the amount of carbon deposited is illustrated in Figure 4. There is a strong antiferromagnetic coupling present at low carbon contents, which monotonically declines in strength with increasing amount of carbon deposited ($\theta_p \approx 0$ at about one-half theoretical monolayer coverage). We propose to interpret this curve to arise in the following way. At low carbon content most of the carbon is in a single specific phase with $\theta_p = \theta_1$ (θ_1 might be obtained by extrapolation to 0% carbon). At higher carbon contents, the phase with $\theta_p = \theta_2 = 0$ predominates. Then, at intermediate carbon contents

$$I^{-1} = \tau - \kappa\theta_1' - \mathfrak{R} \qquad (4)$$

(19) J. S. Hyde, "Experimental Techniques in EPR," Varian Associates, Palo Alto, Calif., 1963, p 17.

(20) J. P. Goldsborough, M. Mandel, and G. E. Pake, *Phys. Rev. Letters*, **4**, 13 (1960).

(21) R. C. Pastor and R. H. Hoskins, *J. Chem. Phys.*, **32**, 264 (1961).

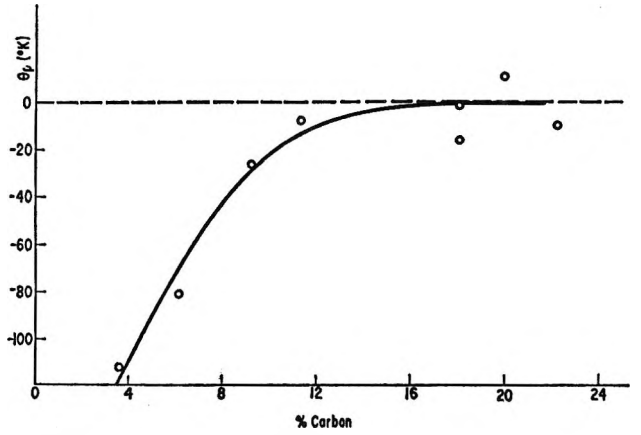

Figure 4. Paramagnetic Curie temperature *vs.* amount of carbon deposited on Rd-Al for type A samples *in vacuo*.

where I is the esr intensity $\propto \chi$, τ is a reduced temperature, θ_1' is a reduced θ_p, κ is the fraction of the species with $\theta_p = \theta_1$, and $\mathfrak{R}$ is equal to a cumbersome algebraic function of θ_1 and θ_2. We can show numerically that $\mathfrak{R}$ is negligible for most ranges of κ in our temperature range. We then obtain the simple result

$$\kappa \cong \frac{\theta'}{\theta_1'} \tag{5}$$

where θ' is the actually measured reduced paramagnetic Curie temperature corresponding to κ. In other words, the curve θ_p (% C) in Figure 4 gives directly the approximate degree of distribution of the two phases present. Finally, a special comment needs to be made about the possible origin of the antiferromagnetic coupling. Campbell, *et al.*,[22] have observed strongly negative θ_p's in carbonized (unsupported) polymers of various origins. The origin of this antiferromagnetic coupling is not established. Paramagnetic surface impurities such as Dy^{3+} have a strong influence on the magnitude of θ_p but also affect carbonization rate and possibly other parameters. Hence, the relation between the observed antiferromagnetism and surface impurities is uncertain. Another more attractive possibility is the existence of two-dimensional antiferromagnetic ordering[23] in the first carbon layer deposited, stabilized by the alumina surface.

IV. Conclusions

The main results of the previous section are summarized in the following four observations.

1. The measured line widths of the esr lines due to the carbonaceous deposits are significantly narrower than the ones calculated from the spin concentrations for dipolar broadening. Furthermore, the line shapes point to the effect of an exchange narrowing mechanism. The calculated exchange frequencies $J/\hbar$ are dependent on the type (A, B) of the carbon, and increase with carbon content. This behavior is ascribed to a growing of the domain sizes of delocalization with augmenting carbonization.

2. The variation of T_1 with varying exchange frequency (and therefore carbon content) is in agreement with theoretical prediction.

3. The accessibility of the spins to oxygen increases with increasing carbon content.

4. Carbon deposited in the first stages of carbonization is of a different physical nature than the one subsequently formed. This is evident from the unexpected temperature dependence of T_1 at low carbon content, and particularly from the measured paramagnetic Curie temperature variation with varying carbon content. Only the primary carbon phase exhibits antiferromagnetic coupling. This is tentatively attributed to a surface stabilized phase (possibly a two-dimensional Ising model) with special magnetic properties.

Observations 1 to 3 are consistent with the concept of expanding domain sizes and crystallographic ordering (*e.g.*, less cross linking between turbostratically oriented domains) with increasing amounts of carbon deposited.

The question of accessibility of spins to oxygen is basic to the concept of using relative spin intensities *in vacuo* and air to estimate particle sizes.[7] Since all of the above results indicate that domain size increases with carbon content, it is at first somewhat surprising to find that the ratio of spin intensities *in vacuo* to those in air is relatively independent of carbon content. However, this apparent anomaly is probably due to a compensation effect caused by the fact that increasing carbon content is accompanied by approximately corresponding increases in both domain size and crystallographic ordering. Growth in domain size would be expected to decrease relative accessibility of spins to oxygen whereas the formation of turbostratic structure should increase spin accessibility.

As may be seen in Table I, relative spin intensity data obtained with various supports can vary by several orders of magnitude, whereas they can vary by several-fold as carbon content is altered. We conclude, therefore, that relative spin intensities *in vacuo* and in air properly reflect a measure of domain size, but that there is a superposition of a second-order effect due to increasing crystallinity. According to this interpretation, the technique of Poole, *et al.*,[7] provides a measure of average "crystallographic" particle size.

Finally, it is instructive to compare the dependence of the measured parameters on carbon content with the dependence of the same parameters on high-temperature treatments (HTT) of bulk low temperature carbons,[16,24-26] and also with carbon content in coals.[27]

(22) D. Campbell, C. Jackson, H. Marsh, and Lord Wynne-Jones, *Carbon*, **4**, 159 (1966).

(23) A. S. Edelstein, *J. Chem. Phys.*, **40**, 488 (1964); **42**, 2879 (1965).

(24) L. S. Singer, W. J. Spry, and W. H. Smith, Proceedings of the Third Conference on Carbon, Buffalo, N. Y., Pergamon Press, New York, N. Y., 1959.

Let us consider carbons heat treated at a temperature below the one at which an inflection occurs in temperature dependent properties (minimum line width, maximum spin density, etc.). There, with increasing HTT, the following parameters decrease: ΔH (*in vacuo*),[16,22,24,25] T_1,[25] $\hbar/J$,[14] $|\theta_p|$,[22] (surface area)$^{-1}$. Exactly the same trend is observed in our case if we substitute the amount of carbon deposited for HTT. (A similar correlation holds with the carbon content of coals.[27]) All the well-known arguments advanced so far toward the explanation of the nature of low-temperature bulk carbons may therefore have analogous implications for supported carbons.

(25) R. C. Pastor and R. H. Hoskins, *J. Chem. Phys.*, **32**, 264 (1961).

(26) H. Marsh and W. F. K. Wynne-Jones, *Carbon*, **1**, 269 (1964).

(27) D. E. G. Austen, D. J. E. Ingram, and J. G. Tapley, *Trans. Faraday Soc.*, **54**, 400 (1958)

Proton-Transfer Complexes. I. Preferential Solvation of *p*-Nitrophenol–Amine Complexes in Nonaqueous-Solvent Mixtures

by Ronald Scott, Dennis De Palma, and Serge Vinogradov[1]

Department of Biochemistry, School of Medicine, Wayne State University, Detroit, Michigan 48207
(Received February 19, 1968)

The ultraviolet and visible absorption spectra of complexes of *p*-nitrophenol with triethylamine or *n*-butylamine were measured in 1-butanol, N,N-dimethylformamide, and dimethyl sulfoxide and in 1-butanol–cyclohexane and N,N-dimethylformamide–benzene mixtures at 25°. It was observed that: (a) the intensity of the absorption band in the 400-mμ region due to the *p*-nitrophenylate anion increased with increase in amine concentration, provided the polarity of the solvent was sufficiently high ($D \geqslant 5$–10); (b) the intensity of the absorption band due to the *p*-nitrophenylate anion in a binary solvent, in the presence of excess amine, increased with solvent polarity; (c) the change in the intensity of the absorption band in the 300-mμ region due to undissociated *p*-nitrophenol followed inversely the change in the intensity of the absorption band in the 400-mμ region; and (d) the stoichiometry of the *p*-nitrophenol–amine proton-transfer complex was approximately 1:1, whether determined from the dissociated or from the undissociated *p*-nitrophenol absorption peaks. The results were interpreted to support the existence of a tautomeric equilibrium between a hydrogen-bonded *p*-nitrophenol–amine complex and a proton-transfer (undissociated ion-pair) complex. It was shown that in binary solvents the tautomeric equilibrium can be shifted only by changing the proportion of the polar- and nonpolar-solvent components.

Introduction

A great deal of interest has been evinced recently in the shape of the potential energy function describing the motion of the connecting proton in hydrogen-bonded complexes.[2,3] The presence of a second minimum in the potential curve of a proton involved in a hydrogen bond has been established by infrared spectroscopic studies of alcohols,[4] phenol–amine and *p*-nitrophenol–amine complexes,[5] and *ortho*-substituted anilines.[6] Barrow has shown that in mixtures of carboxylic acids with pyridine in chloroform there exists a tautomeric equilibrium between hydrogen-bonded and proton-transfer (ion-pair) complexes[7]

$$-O—H—N \rightleftharpoons -O^-—H^+—N \qquad (1)$$

The presence of such tautomeric equilibria in reactions of Brønsted–Lowry acids with Lewis bases in solvents of low dielectric constant has been substantiated further by recent work on the ultraviolet spectra of carboxylic acid–amine complexes in hexane[8] and infrared spectra of mixtures of substituted phenols with *n*-propylamine in benzene and carbon tetrachloride[9] and of fatty acid–pyridine systems in carbon tetrachloride.[10] The ultra-

(1) Author to whom inquiries should be addressed.

(2) G. M. Barrow, *Spectrochim. Acta*, **16**, 799 (1960).

(3) R. L. Somorjai and D. F. Hornig, *J. Chem. Phys.*, **36**, 1980 (1962).

(4) C. L. Bell and G. M. Barrow, *ibid.*, **31**, 300 (1959).

(5) C. L. Bell and G. M. Barrow, *ibid.*, **31**, 1158 (1959).

(6) P. J. Krueger, *Can. J. Chem.*, **42**, 201 (1964).

(7) G. M. Barrow, *J. Amer. Chem. Soc.*, **78**, 5802 (1956).

(8) G. Coppens, C. Gillet, J. Nasielski, and E. Van der Donckt, *Spectrochim. Acta*, **18**, 1441 (1962); J. Nasielski and E. Van der Donckt, *ibid.*, **19**, 1989 (1963).

(9) T. Zeegers-Huyskens, *ibid.*, **21**, 221 (1965).

violet absorption spectra of the *p*-nitrophenol–triethylamine system in dichloroethane were investigated as a function of amine concentration, and the results were interpreted in terms of tautomeric equilibria involving a hydrogen-bonded complex, a proton-transfer complex, and, at high amine concentrations, an amine-solvated proton-transfer complex.[11] Recently, a fluorine nuclear magnetic resonance study of complexes of *p*-fluorophenol with tetrahydrofuran, pyridine, and dimethylformamide in carbon tetrachloride has demonstrated the presence in these systems of 14–20% proton transfer.[12]

The presence of a tautomeric equilibrium between a hydrogen-bonded complex and a proton-transfer complex in a system consisting of a proton-donating acid and an electron-pair-donating base shows that the potential barrier between the two minima must be low. The position of the equilibrium, *i.e.*, the relative heights of the two minima, is sensitive to the relative acid–base strengths of the proton donor and proton acceptor and to the solvent environment. The solvation of the two complexes in equilibrium 1 should be a function of the solvent polarity. It should be possible to shift the equilibrium in a binary mixture of solvents of widely differing polarities only by changing the composition of the solvent mixture. We report below some results obtained with *p*-nitrophenol–amine systems in binary nonaqueous-solvent mixtures which suggest that preferential solvation of one of the two types of complexes is a function of solvent polarity and is probably responsible for shifting the tautomeric equilibrium 1.

Experimental Procedure

The *p*-nitrophenol used was indicator grade (Eastman Kodak Co.) or reagent grade (Aldrich Chem. Co.) recrystallized once from benzene. The triethylamine, *n*-butylamine, isobutylamine, *sec*-butylamine, *t*-butylamine, di-*n*-butylamine, tri-*n*-butylamine, and piperidine used were reagent grade chemicals (Eastman Kodak Co., Aldrich Chemical Co. and Matheson Coleman and Bell Co.). N,N-Dimethylformamide and dimethyl sulfoxide were spectro grade (Matheson Coleman and Bell Co.) or reagent grade (Aldrich Chemical Co.). The benzene and 1-butanol were spectro grade solvents (Matheson Coleman and Bell Co.). The cyclohexane was purified by the method of Vinogradov.[13]

The spectra were obtained with a Cary Model 15 spectrophotometer. Individual solutions were run in a water-jacketed 1-cm quartz cell. Spectrophotometric titrations of *p*-nitrophenol with amine were performed in a thermostated glass apparatus where the solution was circulated continuously through a 2-cm quartz cell placed in the sample compartment of the spectrophotometer. Teflon microburets, 2- and 0.2-ml capacity, were used for the addition of base. The concentration of the amine added was calculated from the volumes of the amine solution added, their concentration, and the volume of the *p*-nitrophenol solution titrated. Solvent mixtures were prepared by volumetric addition of the components at room temperature (25 ± 2°). The concentration of the *p*-nitrophenol varied within the limits (1.5–6.0) × 10^{-5} *M*. In all experiments reagents and solvents from more than one source were used. The temperature was maintained at 25 ± 0.1°, except for experiments with butanol–cyclohexane mixtures when it was kept at 21.5 ± 0.1°.

Results

The spectra of *p*-nitrophenol in cyclohexane and benzene were characteristic of the un-ionized form of the molecule.[14,15] In pure 1-butanol, dimethyl sulfoxide, and N,N-dimethylformamide, an additional absorption band characteristic of the *p*-nitrophenylate anion appeared in the 400-mμ region.[14,15] Addition of triethylamine or *n*-butylamine increased the intensity of this peak, whereas in neither cyclohexane nor benzene was there any evidence of a band in the 400-mμ region, even at very large excesses of amine over *p*-nitrophenol (>10^5:1). In pure 1-butanol, dimethylformamide, and dimethyl sulfoxide, the maximum intensity of the absorption band due to the *p*-nitrophenylate anion was reached at *ca.* 8 vol % of triethylamine. Further additions of the base[16] resulted in a progressive decrease in the intensity of the band in the 400-mμ region until the band disappeared in pure triethylamine. The spectra obtained in the case of dimethylformamide are shown in Figure 1. Using *n*-butylamine, it was found that the adsorption band due to the *p*-nitrophenylate anion persisted even in the pure amine. This prompted us to examine the spectra of *p*-nitrophenol in a number of liquid amines (Figure 2). In triethylamine, tributylamine, and dibutylamine, little or no ionization of *p*-nitrophenol was observed, whereas in primary amines dissociation was prevalent. The behavior of *p*-nitrophenol in piperidine was intermediate between the two extremes.

Beer's-law plots of the absorbances at the peak maxima in the 300- and 400-mμ regions were found to be linear in 1-butanol, dimethyl sulfoxide, and 50% dimethylformamide–50% benzene in the presence of excess triethylamine or 1-butylamine over the concentration range of *p*-nitrophenol used in the present paper. Spectrophotometric titrations of *p*-nitrophenol with

(10) R. S. Roy, *Spectrochim. Acta*, **22**, 1877 (1966).

(11) H. Baba, A. Matsuyama, and H. Kokubun, *J. Chem. Phys.*, **41**, 895 (1964).

(12) D. Gurka, R. W. Taft, L. Joris, and P. von R. Schleyer, *J. Amer. Chem. Soc.*, **89**, 5957 (1967).

(13) S. Vinogradov *Can. J. Chem.*, **40**, 2170 (1962).

(14) L. Doub and J. M. Vandenbelt, *J. Amer. Chem. Soc.*, **69**, 2714 (1947).

(15) A. Burawoy, J. P. Critchley, and A. R. Thompson, *Tetrahedron*, **4**, 403 (1958).

(16) Owing to the lack of solubility of triethylamine, this experiment was not performed in pure dimethyl sulfoxide.

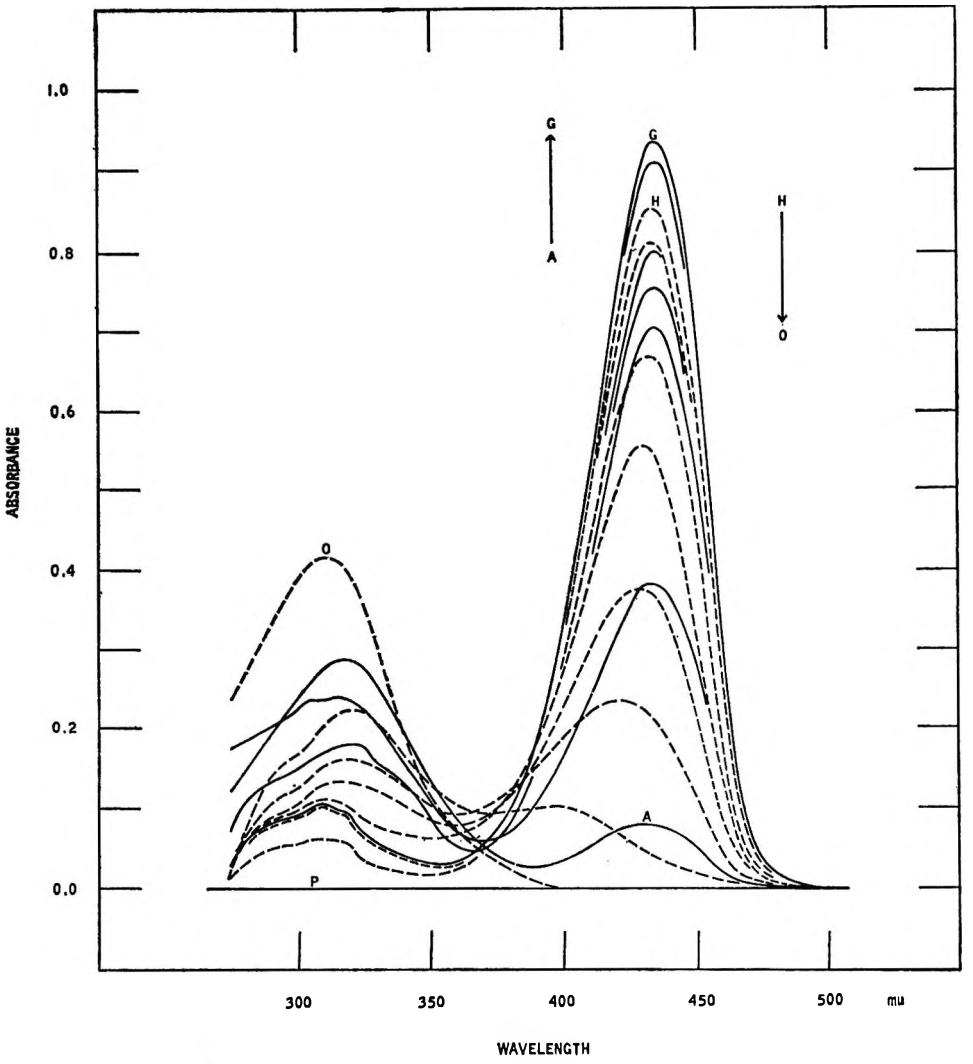

Figure 1. The absorption of 2.5×10^{-5} M p-nitrophenol in mixtures of dimethylformamide + triethylamine (1-cm cell, 25°). The full-line curves are lettered A–G and the broken-line curves are lettered H–O. The volume per cent of triethylamine is: A, 0; B, 0.2; C, 0.5; D, 1.0; E, 2.0; F, 4.0; G, 5.0; H, 10; I, 20; J, 40; K, 50; L, 60; M, 70; N, 80; O, 100. P is the base line.

triethylamine or n-butylamine were performed in 1-butanol, 1-butanol–cyclohexane mixtures, dimethyl sulfoxide, N,N-dimethylformamide, and N,N-dimethylformamide–benzene mixtures. Figure 3 shows some of the curves obtained in a titration in 1-butanol. Progressive addition of amine results in a decrease in the intensity of the peak at 315 mμ due to undissociated p-nitrophenol accompanied by an increase in the intensity of the peak in the 400-mμ region due to the p-nitrophenylate anion with a very clean isosbestic point at ~343 mμ. A plot of the absorbance at the peak maxima *vs.* log amine concentration yields conventional titration curves (Figure 4).

Analogous results were obtained at fixed p-nitrophenol and amine concentrations in butanol–cyclohexane and dimethylformamide–benzene mixtures by varying the proportion of the components. Figure 5 shows some typical results obtained in butanol + cyclohexane mixtures in the presence of a large excess of triethylamine (8 vol %, ≈0.57 M). A plot of the absorbances at the maxima of the dissociated and undissociated p-nitrophenol absorption bands as a function of the volume per cent of 1-butanol is shown in Figure 6.

The spectrophotometric data obtained from titrations at a fixed solvent composition (illustrated in Figures 3 and 4) were treated assuming a simple equilibrium

$$\text{A—H} + n\text{B} \overset{K}{\rightleftharpoons} \text{A}^{-}\text{---H}^{+}\text{—B}_n \qquad (2)$$

where AH is p-nitrophenol and B is the amine. The absorbances measured at the maxima of the dissociated and undissociated p-nitrophenol peaks were plotted as log $[A^-]/[AH]$ *vs.* log [B] (Figure 7). Linear plots were generally obtained with the slope n varying from 0.75 to 1.3. Estimates of log K were obtained from the abscissa intercepts. The results are presented in Table I. Deviations from linearity were observed in

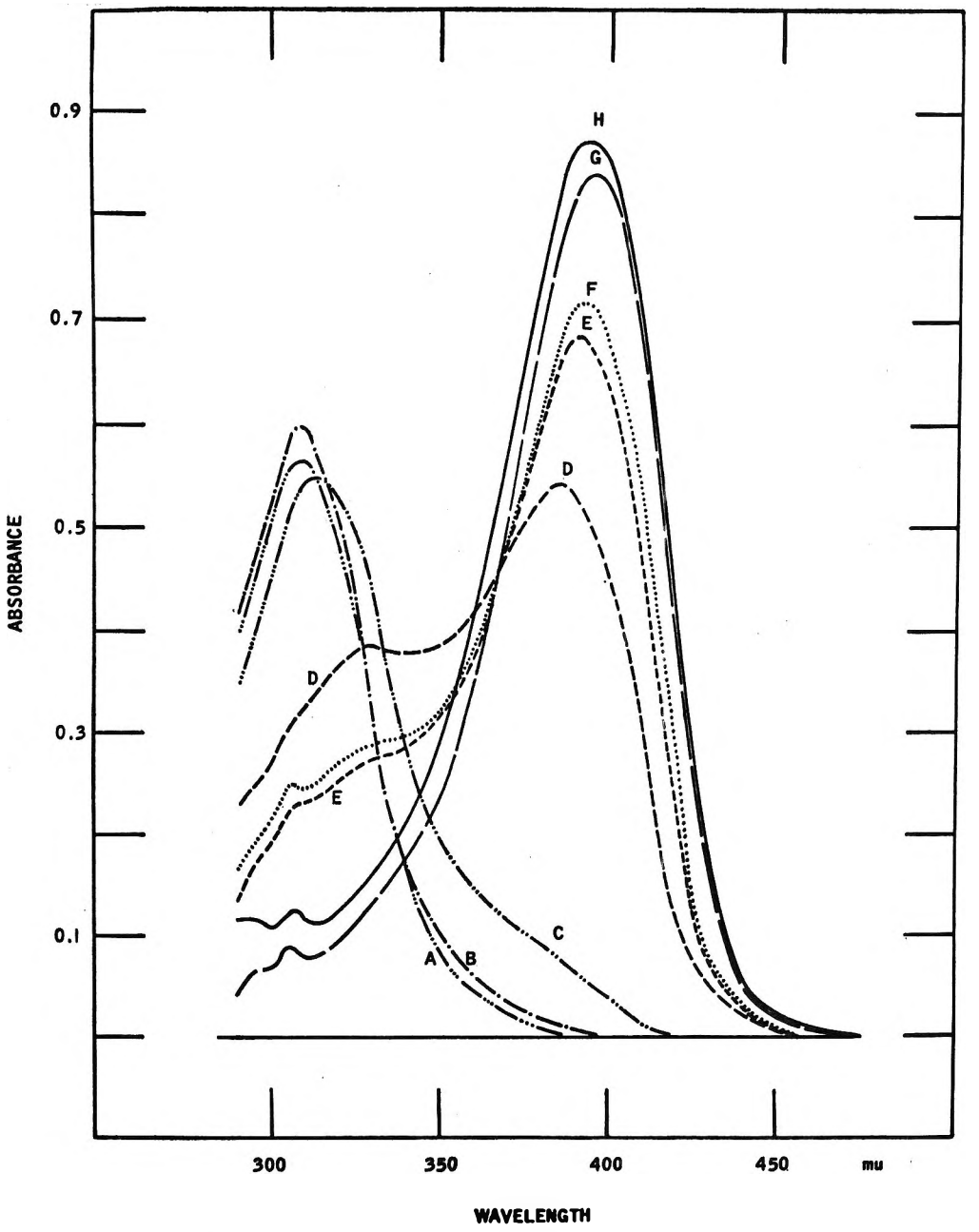

Figure 2. The absorption of 5.0×10^{-5} M p-nitrophenol dissolved in various liquid amines (1-cm cell, 25°): A, triethylamine; B, tributylamine; C, dibutylamine; D, piperidine; E, t-butylamine; F, sec-butylamine; G, n-butylamine; H, isobutylamine.

most titrations at high amine concentrations, particularly in the more polar solvents. In pure 1-butanol, dimethylformamide, and dimethyl sulfoxide, deviations from linearity began at triethylamine concentrations of *ca.* 0.06, 0.015, and 0.01 M, respectively, and at n-butylamine concentrations of *ca.* 0.03, 0.0015, and 0.00015 M, respectively.

Discussion

The formation of a proton-transfer complex results in a high dipole moment, of the order of 10–12 D,[17,18] close to the values observed in known ion pairs, *e.g.*, quaternary ammonium salts.[19] Dipole-moment measurements show that with a given base, *e.g.*, triethylamine, the dipole moment of the phenol–base complex increases with the increasing acidity (decreasing pK_a) of the phenol.[18] Presumably, the dipole moments intermediate between the 2–4 D of the hydrogen-bonded complexes[20] and the 10–12 D of the proton-transfer complexes reflect the coexistence of the two types of complexes in a tautomeric equilibrium eq (1). Because of

(17) J. W. Smith, *J. Chim. Phys.*, **61**, 125 (1964).
(18) H. Ratajczak and L. Sobczyk, *Zh. Strukt. Khim.*, **6**, 262 (1965).
(19) K. Bange and J. W. Smith, *J. Chem. Soc.*, 4244 (1964).
(20) H. Tsubomura, *Bull. Chem. Soc. Jap.*, **31**, 435 (1958).

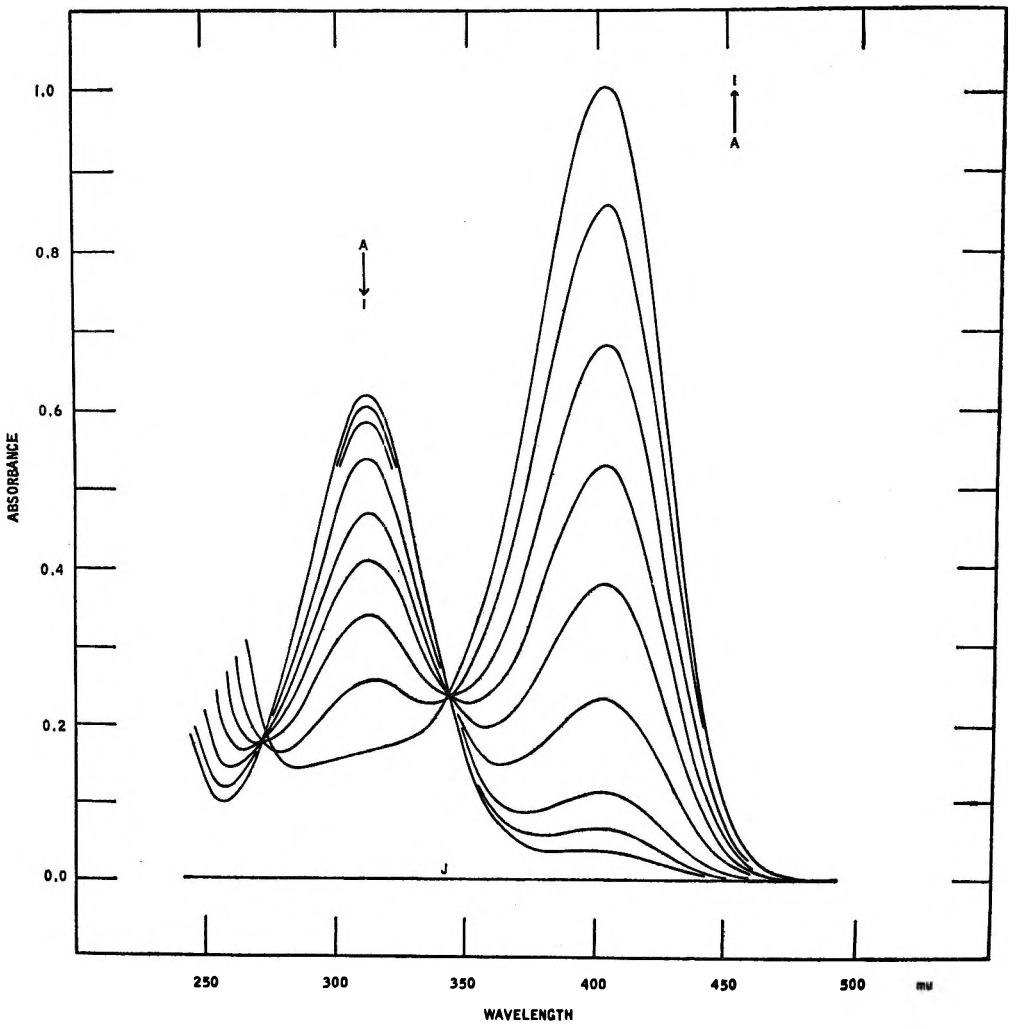

Figure 3. Titration of 3.0×10^{-5} *M* *p*-nitrophenol in 1-butanol with triethylamine (2-cm cell, 25°). Curve, molarity of triethylamine (*M*): A, 0; B, 2.14×10^{-4}; C, 7.14×10^{-4}; D, 2.86×10^{-3}; E, 7.86×10^{-3}; F, 1.64×10^{-2}; G, 3.35×10^{-2}; H, 8.07×10^{-2}; I, 0.348. Curve J is the base line.

Table I: Results of Spectrophotometric Titrations of *p*-Nitrophenol with Triethylamine and 1-Butylamine in Some Nonaqueous Solvents at 25°[a]

Solvent	Base	Concn of *p*-nitrophenol, $\times 10^{-5}$ *M*	Dissociated peak: λ, mμ	Dissociated peak: Intercept (log [B])	Dissociated peak: *n*	Dissociated peak: Log K^b	Undissociated peak: λ, mμ	Undissociated peak: Intercept (log [B])	Undissociated peak: *n*	Undissociated peak: Log K^b
Dimethyl sulfoxide	Triethylamine	1.5	435	−3.00	0.87	2.61	325	−3.00	0.84	2.52
	n-Butylamine	1.5	435	−4.41	1.30	5.73	325	−4.37	1.26	5.51
				−4.50	1.18	5.32		−4.53	1.22	5.53
Dimethylformamide	Triethylamine	1.0	430	−2.08	0.92	1.90	315	−2.12	0.84	1.78
	n-Butylamine	2.0	430	−3.33	0.91	3.03	315	−3.35	0.84	2.81
1-Butanol	Triethylamine	3.0	405	−1.82	0.86	1.57	312	−1.75	0.90	1.58
	n-Butylamine	2.0	405	−2.92	0.84	2.45	310	−2.92	0.80	2.34
80% 1-butanol + 20% cyclohexane	Triethylamine	3.0	405	−1.52	0.87	1.32	310	−1.46	0.91	1.33
	n-Butylamine	2.0	405	−2.03	1.31	2.66	312	−1.98	1.18	2.34
50% dimethylformamide + 50% benzene	Triethylamine	2.5	430	−1.28	0.97	1.24	315	−1.15	0.96	1.10
	n-Butylamine	1.0	430	−2.09	0.75	1.57	315	−2.03	0.76	1.54

[a] Except in the case of butanol–cyclohexane, 21.5°. [b] The values are considered accurate to ±0.15.

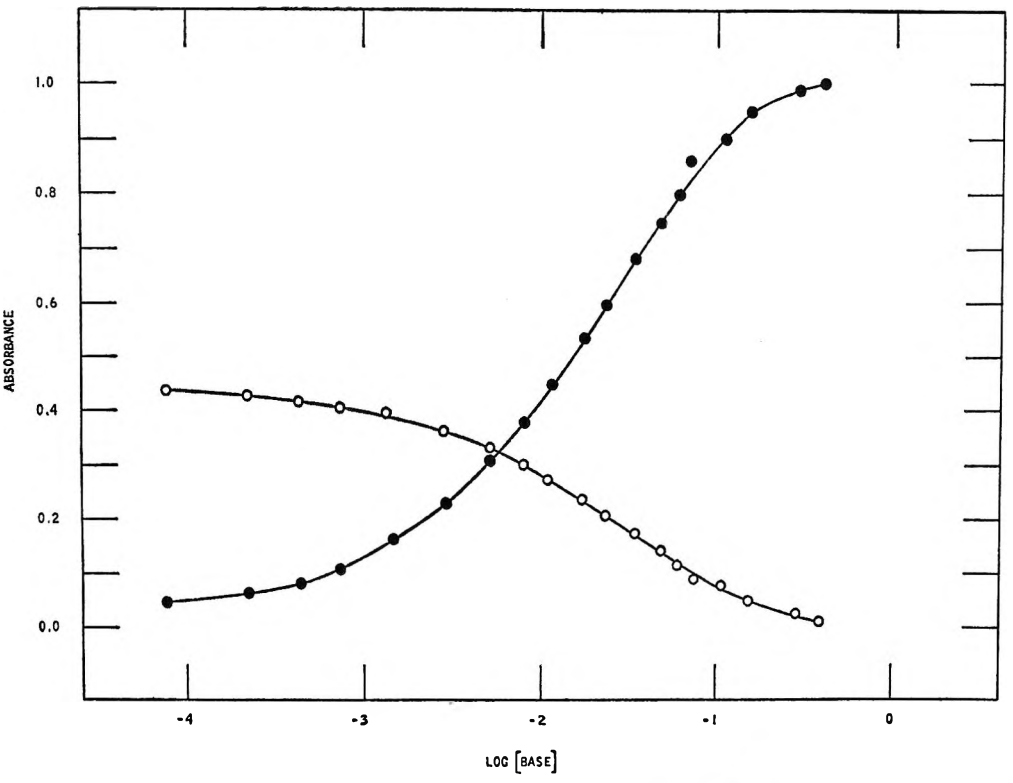

Figure 4. Plots of absorbances at 406 mμ (dissociated *p*-nitrophenol, full circles) and 305 mμ (undissociated *p*-nitrophenol, open circles) as functions of triethylamine concentration (3.0×10^{-5} *M* *p*-nitrophenol in 1-butanol, 2-cm cell, 25°).

the much greater separation of charge in the proton-transfer complexes, their formation should be favored by an increase in the polarity of the solvent. Beyond a certain polarity, however, the complex will dissociate into its constituent ions. *Thus for a given Brønsted–Lowry acid and a Lewis-base system, there should be a range of solvent polarities or dielectric-constant environments which would favor the formation of the proton-transfer complex over either the dissociation of the complex or the formation of hydrogen-bonded complexes.*

The spectra of *p*-nitrophenol in mixtures of dimethylformamide (D = 37.2 at 25°)[21] and triethylamine (D = 2.42 at 25°),[22] shown in Figure 1, and in liquid triethylamine, tri-*n*-butylamine, di-*n*-butylamine[23] (D = 3.20 at 0°),[24] *sec*-butylamine (D = 4.4 at 21°),[22] *t*-butylamine (D = 4.2 at 25°[21] and 4.665 at 5°),[25] isobutylamine (D = 4.4 at 21°),[22] piperidine (D = 5.8 at 22°),[22] and *n*-butylamine (D = 5.3 at 21°[22] and 5.4 at 0°[24]), shown in Figure 2, define the sensitivity of the intensity of the *p*-nitrophenylate anion absorption band at 400–430 mμ to the polarity or dielectric constant of the solvent. Addition of triethylamine to a solution of *p*-nitrophenol in dimethylformamide appears to enhance the ionization of *p*-nitrophenol until the intensity of the peak at 430 mμ reaches a maximum at *ca.* 8 vol % of the amine. Further addition of the amine depresses the ionization of *p*-nitrophenol, apparently by decreasing the polarity of the mixed solvent. The absorption band at 430 mμ disappears at triethylamine concentrations greater than 80 vol % ($D \approx 13$).[26]

The spectra of *p*-nitrophenol in butanol–cyclohexane mixtures in the presence of an excess of triethylamine (Figure 5) show that the increase in the intensity of the *p*-nitrophenylate anion peak at 405 mμ is accompanied by a decrease in the intensity of the undissociated *p*-nitrophenol peak at 310 mμ (Figure 6). The dielectric constants of butanol–cyclohexane mixtures at 21.5° are known.[27] The onset of *p*-nitrophenol ionization occurs at *ca.* 50 vol % of butanol corresponding to a dielectric constant of 7.84.[27] In butanol + triethylamine mixtures, the onset of *p*-nitrophenol ionization occurs also at *ca.* 50 vol % of butanol. Titration of *p*-nitrophenol with triethylamine or *n*-butylamine in a sufficiently polar butanol–cyclohexane mixture; *e.g.*, one containing 80 vol % butanol (D = 13.9),[27] also results in an increase in the *p*-nitrophenylate anion peak intensity and a concomitant decrease

(21) S. J. Bass, W. I. Nathan, R. M. Meighan, and R. H. Cole, *J. Phys. Chem.*, 68, 509 (1964).

(22) National Bureau of Standards Circular 514, U. S. Government Printing Office, Washington, D. C.

(23) Diisobutylamine has D = 2.7 at 22°.[22]

(24) S. K. Garg and P. K. Kadaba, *J. Phys. Chem.*, 68, 737 (1964).

(25) E. Krishnaji and A. Mansingh, *J. Chem. Phys.*, 42, 2503 (1965).

(26) Assuming a linear relationship between the dielectric constant of the mixture and volume per cent of either component.

(27) R. B. McKay and P. J. Hilson, *Trans. Faraday Soc.*, 62, 1459 (1966).

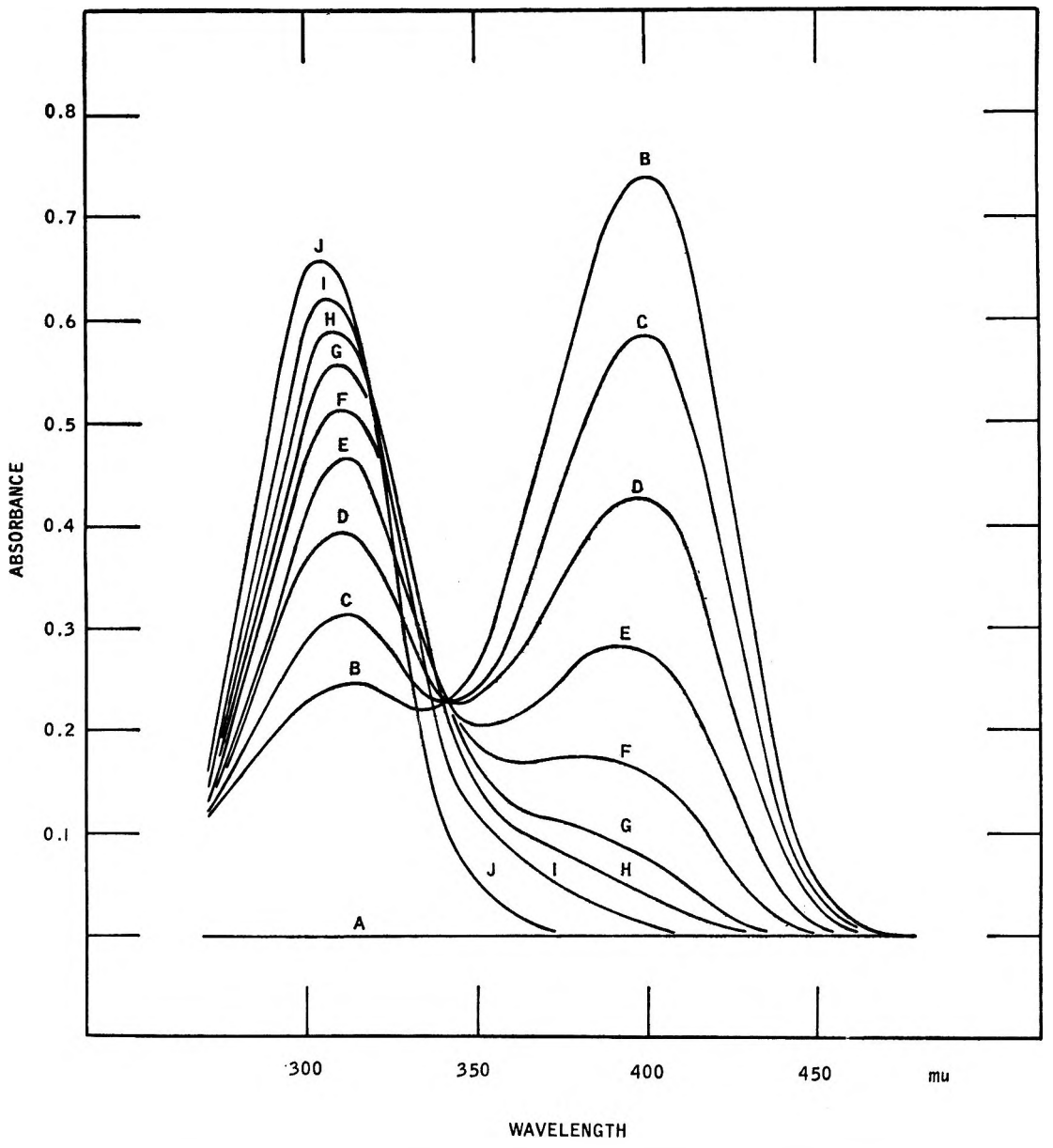

Figure 5. The absorption of 6.0×10^{-5} M p-nitrophenol + 0.57 M triethylamine in 1-butanol + cyclohexane mixtures (1-cm cell, 21.5°). Curve, volume per cent of 1-butanol: B, 100; C, 90; D, 80; E, 70; F, 60; G, 50; H, 40; I, 20; J, 0. Curve A is 0.57 M triethylamine in 1-butanol. Figure 3, curve A, shows the absorption of 3.0×10^{-5} M p-nitrophenol in 1-butanol in a 2-cm cell.

in the intensity of the undissociated peak (Figures 3 and 4). Similar behavior is encountered in mixtures of benzene (D = 2.2726 at 25°)[28] with N,N-dimethylformamide (D = 37.2 at 25°),[21] as well as in pure 1-butanol, dimethylformamide, and dimethyl sulfoxide. The onset of p-nitrophenylate anion absorption in dimethylformamide–benzene mixtures occurs at a benzene content less than 70 vol % ($D \approx 12.8$).[26] The type of results obtained by changing the compositions of the butanol–cyclohexane and dimethylformamide–benzene mixtures at fixed p-nitrophenol and amine concentrations is illustrated by the dimethylformamide–triethylamine system shown in Figure 1. Its behavior can be separated into two distinct phases. Initial addition of triethylamine to a solution of p-nitrophenol in dimethylformamide leads to dissociation of p-nitrophenol as the result of an acid–base reaction. Once the maximum of absorption by the p-nitrophenylate anion is reached, triethylamine begins to behave as a nonpolar-solvent component, in a manner entirely analogous to that of benzene and cyclohexane in the two other solvent mixtures. The result is a progressive decrease in p-nitrophenol ionization, indicative of a reversal of the acid–base reaction. The general conclusion is then that the intensities of the absorption peaks due to the ionized and undissociated p-nitrophenol are directly and in-

(28) J. J. Lindberg, *Acta Chem. Scand.*, **14**, 379 (1960).

versely proportional, respectively, to the polarity of the solvent and the amine concentration. The threshold of polarity for the appearance of proton transfer in the solvents used in the present investigation appears to lie in the region of $D \approx 5$–10.

The foregoing discussion has omitted mention of hydrogen-bonding interactions between *p*-nitrophenol, the amine, and the solvent both as coexistent with and as precursors to proton transfer. It has been amply demonstrated that hydrogen bonding occurs between phenols and amines in inert, nonpolar solvents.[29-32] In ternary solutions with dimethyl sulfoxide and benzene, phenols form –OH---O=S bonds without any appreciable charge displacement.[33] Bell and Crooks found that

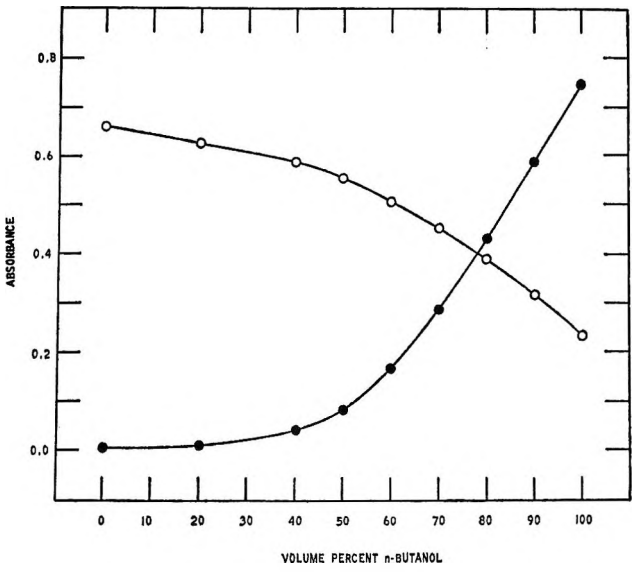

Figure 6. Plots of absorbances at 405 mμ (dissociated *p*-nitrophenol, full circles) and 305 mμ (undissociated *p*-nitrophenol, open circles) as functions of volume per cent of 1-butanol in 1-butanol + cyclohexane mixtures (6.0×10^{-5} *M* *p*-nitrophenol + 0.57 *M* triethylamine, 1-cm cell, 21.5°).

in toluene solution, *m*- and *p*-nitrophenol form only hydrogen-bonded complexes with triethylamine.[34] Dielectric titrations of phenol + amine systems in benzene showed that the compositions of the resultant complexes varied from one acid–base pair to another.[35] Besides the hydrogen-bonding interactions between *p*-nitrophenol and amine, they and their complexes must be involved in complicated interactions with the polar-solvent molecules. It may seem, therefore, that the assumption of a 1:1 hydrogen-bonded phenol–amine complex in equilibrium 1 is an excessive oversimplification. However, proton transfer occurs only in the hydrogen bond between the OH group of a *p*-nitrophenol molecule and the nitrogen atom of an amine molecule. No proton transfer is observed in the solvents used in the present investigation, in the absence of an amine. Furthermore, the presence of more than one type of *p*-nitrophenol–amine hydrogen-bonded complex is more likely to influence the intensity of the peak due to the undissociated *p*-nitrophenol than that of the dissociated *p*-nitrophenol peak. The reasonable agreement between the slopes and abscissa intercepts of the plots of log $[A^-]/[AH]$ *vs.* log [B] for both peaks in different solvents and solvent mixtures (Figure 7 and Table I) indicates that, under the conditions used in the present investigation, the assumption of 1:1 stoichiometry in both the *p*-nitrophenol–amine hydrogen-bonded complex and the proton-transfer complex affords an adequate interpretation of our spectrophotometric data over a range of dielectric constants from pure *n*-butylamine ($D = 5.3$ at 21°)[22] to pure dimethyl sulfoxide ($D = 45.5$ at 25°).[36] It also appears to hold true for *p*-nitrophenol–amine systems in a number of aqueous systems.[37] The presence of only two principal components, the *p*-nitrophenol–amine hydrogen-bonded complex and the proton-transfer complex, is consistent with the occurrence of well-defined isosbestic points in our spectrophotometric titrations.[38,39] The deviations of the plots in Figure 7 from linearity at high relative amine concentrations, generally positive, probably reflect the breakdown of our assumption concerning the 1:1 stoichiometry, in agreement with the known behavior of *p*-nitrophenol complexes with triethylamine in 1,1-dichloroethane.[11]

Our spectrophotometric results are consistent with the general conclusion that formation of a proton-transfer complex from a 1:1 hydrogen-bonded *p*-nitrophenol–amine complex can be induced in a solvent of appropriate polarity by the addition of base and in a binary-solvent mixture in the presence of a sufficient concentration of base by an increase, within limits determined by the solvent system, of the content of the polar-solvent component. The shift in the tautomeric equilibrium 1 toward the proton-transfer complex is probably due to preferential solvation of the latter by the polar-solvent molecules, because of the greater charge separation present in the ion pair relative to the hydrogen-bonded complex. The preferential solvation of the proton-transfer complex by the polar-solvent

(29) J. C. Dearden and W. F. Forbes, *Can. J. Chem.*, **38**, 896 (1960).

(30) H. Baba and S. Suzuki, *J. Chem. Phys.*, **35**, 1118 (1961).

(31) L. Bellon, *Compt. Rend.*, **254**, 3346 (1962).

(32) F. Cruège, P. Pineau, and J. Lascombe, *J. Chim. Phys.*, **64**, 1161 (1967).

(33) J. Lindberg and C. Majani, *Suomem Kemistilehti*, *B*, **38**, 21 (1965).

(34) R. P. Bell and J. E. Crooks, *J. Chem. Soc.*, 3513 (1962).

(35) H. Ratajczak, *Z. Phys. Chem.* (Leipzig), **231**, 33 (1966).

(36) J. J. Lindberg and R. Hakalox, *Finska Kemistsamfundtes Medd.*, **71**, 97 (1962).

(37) R. Scott and S. Vinogradov, submitted for publication in *J. Chem. Soc.*

(38) The presence of an isosbestic point does not limit the number of absorbing species to two.[39]

(39) J. Brynestad and G. P. Smith, *J. Phys. Chem.*, **72**, 296 (1968), and references cited therein.

molecules lowers the second potential minimum of the proton in the $NO_2C_6H_5OH\cdots NR_3$ hydrogen bond sufficiently to make its transfer thermodynamically favorable. The equilibrium constant K in Table I is always higher when n-butylamine is the base, in disagreement with the known basicities of triethylamine and n-butylamine in water (pK_a = 10.65[40] and 10.59,[41] respectively). It is likely that 1-butanol, dimethylformamide, and dimethyl sulfoxide can all solvate the n-butylamine molecules by forming hydrogen-bonded complexes with their NH_2 groups. A substantial enhancement of proton transfer from the p-nitrophenol

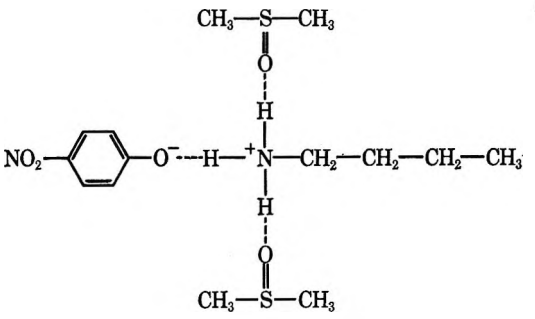

Equilibrium constants for the formation of proton-transfer complexes of p-nitrophenol with bases are not

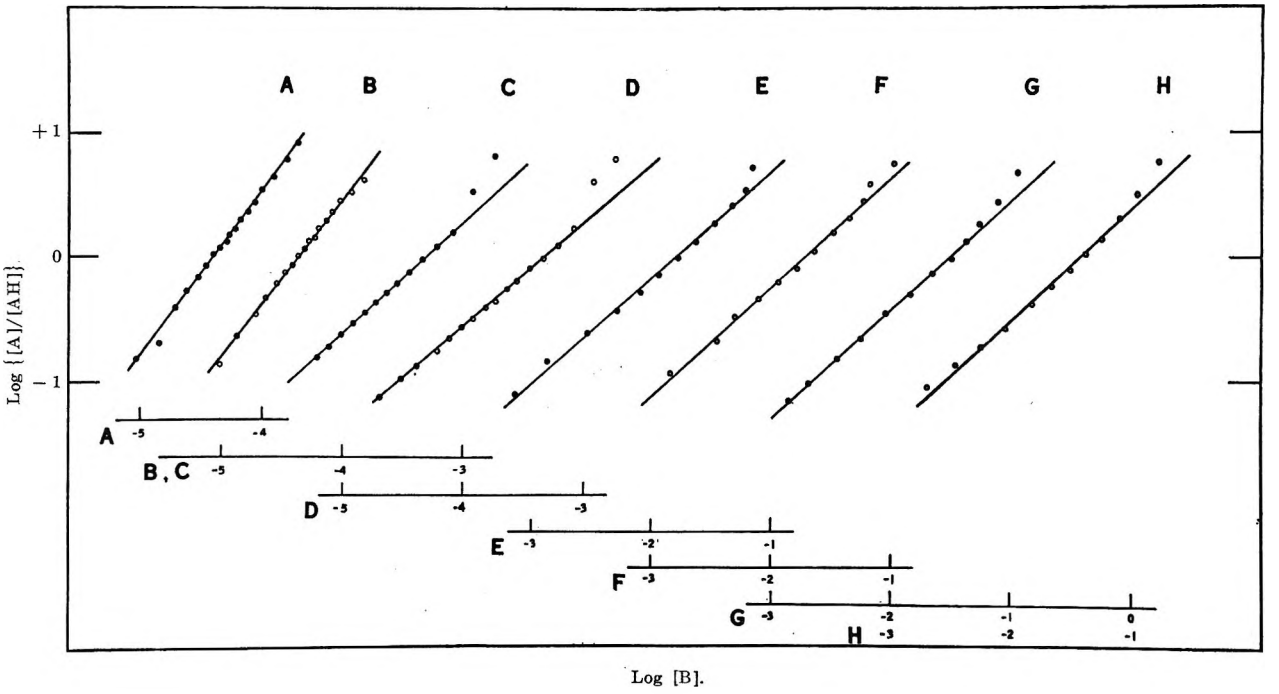

Figure 7. Plots of log $[A^-]/[AH]$ *vs.* log [B] calculated from spectrophotometric absorption data obtained in the 400-mμ region (dissociated p-nitrophenol: A, C, E, G) and the 310-mμ region (undissociated p-nitrophenol: B, D, F, H). The molarity (M) of p-nitrophenol, the solvent, the base used in the titration, the abscissa intercept, and the slope, respectively, are: (A) 1.5×10^{-5}, dimethyl sulfoxide, n-butylamine, 4.41, 1.30; (B) 1.5×10^{-5}, dimethyl sulfoxide, n-butylamine, 4.37, 1.26; (C) 2.0×10^{-5}, dimethylformamide, n-butylamine, 3.33; 0.91; (D) 2.0×10^{-5}, dimethylformamide, n-buyltamine, 3.35, 0.84; (E) 3.0×10^{-5}, 1-butanol, triethylamine, 1.82, 0.86; (F) 3.0×10^{-5}, 1-butanol, triethylamine, 1.75, 0.90; (G) 3.0×10^{-5}, 80 vol % 1-butanol + 20 vol % cyclohexane, triethylamine, 1.52, 0.87; (H) 3.0×10^{-5}, 80 vol % 1-butanol + 20 vol % cyclohexane, triethylamine, 1.46, 0.91. Temperature in all cases 25°, except for 1-butanol + cyclohexane, 21.5°.

oxygen to the n-butylamine nitrogen can occur when the NH_2 groups of the amine are the proton donors in hydrogen-bonded complexes with the hydroxyl group of 1-butanol, the amide nitrogen of dimethylformamide, and the sulfoxide group of dimethyl sulfoxide. Obviously, triethylamine cannot participate as a proton donor in hydrogen-bonded complexes. The greatest difference between the equilibrium constants obtained with the two amines occurs in dimethyl sulfoxide, which probably acts as a strong proton acceptor to form hydrogen-bonded complexes with the NH_2 groups of n-butylamine[42] as shown diagrammatically below

known. The values obtained in the present study (Table I) are in the same range as the equilibrium constants for ion-pair formation in picric acid with amines in nonpolar solvents,[44] in dinitrophenols with

(40) J. Hansen, *Svensk Kem. Tidskr.*, **67**, 256 (1955).

(41) D. H. Everett and B. R. W. Pinsent, *Proc. Roy. Soc.*, **A215**, 426 (1952).

(42) The enthalpy of the hydrogen bond in the pyrrole–dimethyl sulfoxide complex is known to be -3.0 ± 0.5 kcal mol^{-1}.[43]

(43) D. M. Porter and W. S. Brey, Jr., *J. Phys. Chem.*, **72**, 650 (1968).

(44) T. Jasinski and Z. Kokot, *Rocz. Chem.*, **41**, 139 (1967), and references cited therein.

triethylamine in benzene,[45] and in 2,4-dinitrophenol with amines in a variety of nonpolar solvents.[34,46] The spectrophotometric method used in the present study assumes that the spectrum of the proton-transfer complex is the same as that of the *p*-nitrophenylate anion and is incapable of differentiating between an ion pair and a hydrogen-bonded ion pair. We believe it worthwhile to emphasize the difference between the two types of ion pairs[47,48] by calling the latter a proton-transfer complex and pointing out that its formation is the result of a directionally specific interaction. A proton-transfer complex may be distinguished from a non-hydrogen-bonded ion pair by the absence of an isotope effect on the NH stretching frequencies.[49] Dipole-moment measurements would help to establish the presence of ion pairs in *p*-nitrophenol–amine systems. The results of measurements presently in progress, will be reported elsewhere.

Acknowledgment. This work was partly supported by grants from the National Institutes of Health, U. S. Public Health Service, and from the Michigan Heart Association.

(45) M. M. Davis, *J. Amer. Chem. Soc.*, **84**, 3623 (1962).

(46) J. W. Bayles and B. Evans, *J. Chem. Soc.*, 6984 (1965), and earlier references.

(47) Our suggestion is in agreement with the classification of interactions between anions and cations proposed by Griffiths and Symons.[48]

(48) T. R. Griffiths and M. C. R. Symons, *Mol. Phys.*, **3**, 90 (1960).

(49) On this basis, Bell and Crooks have concluded that the ion pairs formed by 2,4-dinitrophenol with pyridine are hydrogen bonded, while those with piperidine or triethylamine are not.[34]

The Sintering of Porous Glass: Benzene Adsorption by Heat-Treated Porous Glasses

by D. A. Cadenhead

Chemistry Department, State University of New York at Buffalo, Buffalo, New York 14214

and D. H. Everett

School of Chemistry, University of Bristol, Bristol, England *(Received March 4, 1968)*

Sintering of porous glass is accompanied by a decrease in the pore volume and surface area but by an increase in the pore size. The data are shown to be consistent with a model of porous glass as a random packing of approximately uniform spheres and a sintering process in which spheres fuse together to form a coarser structure.

Information about the shapes of pores in finely porous substances is not easily derived unambiguously from adsorption data. Frequently such data are analyzed in terms of a more or less arbitrary model. Cylindrical capillaries, slotlike pores, and assemblies of packed spheres are commonly chosen models. In selecting an appropriate model, it is important to take into account structural information from X-ray studies, electron microscope studies, and other sources and to consider the method of preparation of the material. Although some electron microscope studies of porous glass have been made, they give little detailed information about the pore geometry at the 10–50-Å level. The method of preparation by leaching the soluble continuous phase from a two-phase glass suggests that as a first approximation a packed-sphere model is not unreasonable. That the pore spaces are interconnected in a way which leads to interaction between the adsorption processes in neighboring regions is clear from the shape of the hysteresis loop scanning curves.[1] Data for butane adsorption have been presented by Quinn and McIntosh[2] and similar observations were made in the present work on benzene adsorption. More recently, extensive studies of xenon adsorption have been made by Blakeney-Edwards[3] and by Brown,[4] from which a detailed picture

(1) See, *e.g.*, D. H. Everett, "The Solid–Gas Interface," Vol. 2, E. A. Flood, Ed., Marcel Dekker, Inc., New York, N. Y., 1967, Chapter 36; *cf.* also ref 2.

(2) H. W. Quinn and R. McIntosh in *Proc. Int. Congr. Surface Activity, 2nd, London*, **2**, 122 (1957); *Can. J. Chem.*, **35**, 745 (1957).

(3) N. J. Blakeney-Edwards, Ph.D. Thesis, University of Bristol, Bristol, 1964.

(4) A. J. Brown, Ph.D. Thesis, University of Bristol, Bristol, 1963.

Table I: Characteristics of Heat-Treated Porous Glasses from Benzene Adsorption

Sample no.	Treatment	A, $m^2\ g^{-1}$	V_p, $cm^3\ g^{-1}$	$2V_p/A$, Å	$\langle r_k \rangle$, Å	$\langle r_p \rangle$, Å	β_k	β_p
1	None	118	0.196	33.2	18.5	21.5	1.80	1.55
2	12 hr at 600°	99	0.192	38.8	19.2	22.2	2.02	1.75
3	6 hr at 710°	80	0.181	45.3	20.0	23.0	2.26	1.97
4	3 hr at 900°	24	0.151	126	20.6	23.6	6.12	5.35
5	6 hr at 900°	19	0.102	107	23.6	26.6	4.53	4.02
6	6 hr at 915°	0	0.003	...	...	...	...	...

of "pore-blocking" processes has been derived.[1]

In an attempt to obtain further information about the structure of porous glass, a study has been made of the effect of sintering on its adsorptive properties. The benzene adsorption isotherms for a series of glasses treated at increasing temperatures and for progressively longer periods of time are shown in Figure 1. The initial material was a granular porous glass, Corning Code No. 7930, kindly supplied by Dr. M. E. Nordberg; the heat-treatment conditions are summarized in Table I. Heat treatment produces a decrease in the surface area and in the total pore volume and is accompanied by an increase in "pore size," as indicated by the progressive shift of the isotherms toward higher values of relative pressure with increasing severity of the treatment. The "pore-size distribution," as judged by the steepness of the desorption isotherm, broadens as sintering proceeds. However, the lower point of closure of the hysteresis loop remains essentially constant at a relative pressure of 0.20 to 0.21. This is a slightly lower value than that found for the adsorption of benzene by porous carbons, *i.e.*, 0.23–0.25.

These results may be contrasted to those reported by Ries[5] for a series of alumina–silica cracking catalysts sintered *in vacuo* at various temperatures. In this case, studies of N_2 adsorption showed that the decrease in the pore volume and surface area is accompanied by a slight *decrease* in the pore size and by an apparent sharpening of the pore-size distribution.

The sintering process in porous glass can be understood qualitatively if we suppose that the initial material consists of an assembly of substructures which fuse together successively to form larger structural units, the pore spaces between which are correspondingly larger. An approximate quantitative check on this concept may be applied by assuming that the structural units are spheres and by comparing the surface area per gram (A), the pore volume per gram (V_p), and the pore radius (r_p) for each material.

For any given regular pore model, the ratio $2V_p/A$ can be related to a geometrical length parameter characterizing the system.[6] For nonintersecting cylindrical capillaries of uniform size, $2V_p/A$ equals the capillary radius, which (apart from the correction for the adsorbed film) is in turn equal to the Kelvin radius for

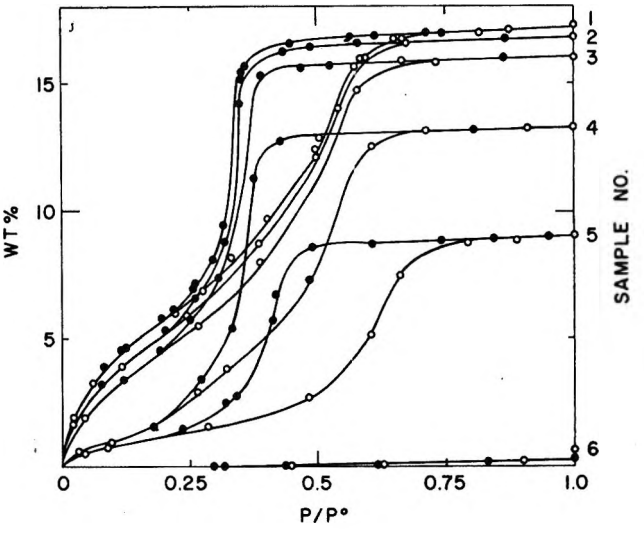

Figure 1. Adsorption and desorption isotherms for benzene on heat-treated porous glass at 25°: ○, adsorption points; ●, desorption points; 1, untreated porous glass, Corning Code No. 7930; 2, heated for 12 hr at 600°; 3, heated for 6 hr at 710°; 4, heated for 3 hr at 900°; 5, heated for 9 hr at 900°; 6, heated for 6.25 hr at 915°. All samples were heated from room temperatures to the maximum temperature in approximately 1 hr, the maximum temperature being approached exponentially. The sintering procedure was carried out in dry air.

desorption from the capillary. Similarly, for parallel-sided slotlike pores, $2V_p/A$ is equal to the width of the slots. For packed spheres of radius r^*, the ratio $\gamma = (2V_p/A)/r^*$ depends on the precise nature of the packing. Values corresponding to simple cubic packing and closest hexagonal packing are given in Table II. Experimentally,[7] it is found that when spheres of uniform size are packed together randomly, it is impossible to achieve a packing density (*i.e.*, the ratio of the sphere volume to the total volume occupied) greater than 0.64; this corresponds to a value of $\gamma = 0.375$.

The Kelvin radius corresponding to the desorption isotherm is related to the size of the largest windows

(5) H. E. Ries, *Advan. Catal.*, **4**, 87 (1952).

(6) D. H. Everett, "Colston Papers," Vol. 10, D. H. Everett and F. S. Stone, Ed., Butterworth and Co. Ltd., London, 1958, p 95.

(7) See, *e.g.*, G. D. Scott, *Nature*, **188**, 908 (1960).

Table II: Characteristics of Some Model Pore Systems[a]

Model	γ	r_c/r^*	r_k/r^*	β
Cylindrical capillaries	...	...	...	1.00
Parallel slots	...	...	...	1.00
Uniform spheres				
Simple cubic packing	0.607	0.414	0.478	1.27
Closest hexagonal packing	0.234	0.155	0.179	1.31
Closest random packing	0.375	0.165	0.190	1.97

[a] See the text for an explanation of the symbols.

giving access to pore spaces. As a plausible approximation, Haines[8] suggested that the critical mean radius of the meniscus which can just penetrate a window is equal to that of the largest sphere which can pass through the window: its radius is equal to that of the inscribed circle of the window. The ratios of the encircled radius (r_c) to the sphere radius for penetration through touching spheres in square and triangular array relevant to simple cubic and closest hexagonal packing, respectively, are given in Table II.

Experiments by Haynes[9] on macroscopic-sphere hexagonal packs show that drainage actually occurs through a triangular window (foramen) when $r_k = 0.179 \pm 0.006)r^*$, a relationship which was confirmed by measuring the maximum pressure needed to blow a bubble of air through an assembly of three equal spheres immersed in water. No similar experiment has been made for the square array, but as an approximation, we may apply the same ratio, r_c/r_k, as that found for the triangular array; this gives $r_k = 0.476r^*$. (Comparison of the capillary rise between three vertical touching rods and four touching rods in square array suggests, in fact, that a different factor may be operative. See ref 9a, pp 80–81.)

For random-sphere packs, the problem is less simple, since in many windows the spheres will not be in contact. A preliminary study by Mason[10] indicates that the probability distribution of "window incircle radii" has a broad maximum at about $0.165r^*$. Assuming that because of the interdependence of domain processes the behavior of the system is determined predominantly by the most common window size and that the same correction factor can be applied to the incircle radius to find the Kelvin radius, we have $r_k = 1.90r^*$.

Finally, we may calculate $\beta = (2V_p/A)/r_k$ for the various models; these values are given in the final column of Table I. When dealing with very small pores, one must additionally allow for the thickness of the adsorbed layer in deducing r_p from r_k.

The data shown in Figure 1 have been analyzed to obtain V_p from the amount adsorbed at the saturation vapor pressure, A both from the BET equation and from the B-point method, and a mean $\langle r_k \rangle$ from the steepest section of the desorption isotherm. The results are shown in Table I. In calculating the pore volume (column 4) and the Kelvin radius (column 6), it was assumed that benzene retains its bulk density (0.88 g cm^{-3}) and bulk surface tension (29 dyn cm^{-1}) in the capillary-condensed state. The molecular area for benzene when the molecule is assumed to lie flat on the surface is 41 Å^2, while that calculated by the conventional formula[11] from the liquid density is 30.7 Å. The surface area of the same batch of porous glass as that used here has been reported as 117,[12] 118,[13] and 115[14] m^2 g^{-1}. The molecular area of benzene required to give this same area from the present measurements is 35.6 Å, which is about the mean of the extreme values quoted above. This suggests that the benzene molecule is not preferentially oriented at the glass surface. To correct the Kelvin radius approximately for the presence of the adsorbed film, we have added 3.0 Å to r_k to obtain the values of r_p in column 7.

The final columns of Table I contain values of β_k and β_p calculated from the experimental value of $2V_p/A$ and either r_k or r_p; these may be compared with the values of β for various models shown in Table II. Within the limitations of the models and the uncertainties associated with the deduction of V_p, A, r_k, and r_p from experimental data, the results of the present analysis are consistent with a packed-sphere model for samples 1–3. That a packed-sphere model is reasonable is confirmed by the fact that the percentage porosity of the untreated material calculated from V_p and the bulk density (1.49 g cm^{-3}) is 29.2%. (The solid matrix then has a density of about 2.08 g cm^{-3} (*cf.* quartz, 2.65 g cm^{-3}; tridymite, 2.30 g cm^{-3}; amorphous SiO_2 (opal), 2.1–2.3 g cm^{-3}).) For closely packed and randomly packed spheres, the values are 26 and 36%, respectively. The observed values of β, which are perhaps significant to ±20%, lie far outside those corresponding to a model either of nonintersecting capillaries or of slotlike pores. The sequence of values of β for the first three samples may well reflect the influence of the early stages of sintering in which spheres begin to coalesce; if the spheres are initially monodisperse, then sintering will lead at first to a bi- or tridisperse system. There are no theoretical calculations nor experimental studies on the random packing of spheres of different

(8) W. B. Haines, *J. Agr. Sci.*, 17, 264 (1927); 20, 97 (1930).

(9) (a) J. M. Haynes, Ph.D. Thesis, University of Bristol, Bristol, 1965; (b) D. H. Everett and J. M. Haynes, *RILEM Bull.*, 27, 31 (1965).

(10) G. Mason, private communication.

(11) P. H. Emmett and S. Brunauer, *J. Amer. Chem. Soc.*, 59, 1553 (1937).

(12) C. H. Amberg and R. McIntosh, *Can. J. Chem.*, 30, 1012 (1952); the molecular area of H_2O equals 10.6 Å^2.

(13) C. H. Amberg, D. H. Everett, L. H. Ruiter, and F. W. Smith, *Proc. Int. Congr. Surface Activity, 2nd, London*, 2, 3 (1957); the molecular area of CO_2 equals 16.5 Å and the molecular area of N_2O equals 16.5 Å.

(14) N. J. Blakeney-Edwards, Ph.D. Thesis, University of Bristol, Bristol, 1964; the molecular area of Xe equals 25 Å^2.

sizes, so that no reliable values of β for this situation are available. However, coalescence will certainly decrease A, and if the structure is sufficiently rigid so that no gross shrinkage occurs, V_p will remain little affected. The observed behavior of A and V_p confirm this. Furthermore, we shall expect a broader distribution of r_k in the heterodisperse system resulting from sintering, again in conformity with the observed behavior. If we accept that $\langle r_k \rangle$ is determined mainly by the commonest window size, then $\langle r_k \rangle$ will vary little in the early stages of sintering and changes in β will arise mainly from changes in A (β will increase). The large values of β found for samples 4 and 5 result from the persistence of relatively small values of r_k even when substantial sintering has occurred. Until most of the small spheres have been eliminated by sintering, the presence of small windows associated with them will tend to depress $\langle r_k \rangle$ and so give an anomalously high value of β.

In the vacuum sintering of aluminosilicate catalysts,[5] nitrogen adsorption shows that the Kelvin radius falls slightly while $2V_p/A$ tends to increase. If the thickness correction to $\langle r_k \rangle$ is made according to the method outlined by Gregg and Sing,[15] then, for the samples studied by Ries, β lies between about 0.8 and 1.2. In view of the tendency for aluminosilicates to form layer structures, $\beta \approx 1$ may be interpreted as indicating the presence of slotlike pores. As Ries has suggested,[5] the sintering process probably consists of the fusion together of platelike units leading to the elimination of both pore volume and surface area but leaving the distance between unfused plates and hence r_p relatively unaffected.

(15) S. J. Gregg and K. S. W. Sing, "Adsorption, Surface Area and Porosity," Academic Press Inc., New York, N. Y., 1967, p 162.

The Thermochemistry of the Gas-Phase Equilibria *trans*-1,2-Diiodoethylene $\rightleftharpoons$ Acetylene + I_2 and *trans*-1,2-Diiodoethylene $\rightleftharpoons$ *cis*-1,2-Diiodoethylene[1]

by Shozo Furuyama, David M. Golden, and Sidney W. Benson

Department of Thermochemistry and Chemical Kinetics, Stanford Research Institute, Menlo Park, California 94205
(Received March 7, 1968)

The equilibrium concentrations of 1,2-diiodoethylene, iodine, and acetylene are determined in the gas phase from 234.5 to 409.4° by spectrophotometric techniques *in situ*. The ratio of *cis*- to *trans*-diiodoethylene is determined from nmr spectra of the separated diiodoethylene. These, when combined with the known entropies, yield the following: for *trans*-1,2-diiodoethylene, $\Delta H_f^\circ_{298} = 49.2 \pm 0.1$ kcal/mol; and for *cis*-1,2-diiodoethylene, $\Delta H_f^\circ_{298} = 49.2 \pm 0.1$ kcal/mol. Values of the contributions to the group C_d–(I)(H) are $\Delta H_f^\circ_{298} = 24.6$ kcal/mol and $S^\circ_{298} = 40.5$ gibbs/mol (*cis* correction, $\Delta H_f^\circ_{298} = 0$ and $S^\circ_{298} = 1.1$ gibbs/mol). Absorption coefficients (OD/M cm) for both *cis*- and *trans*-diiodoethylene as well as the equilibrated mixture have been measured at 239, 252, and 285 mμ and are independent of temperature.

Introduction

trans- and *cis*-diiodoethylene are readily synthesized by the addition of iodine to acetylene in either the gas[2] or liquid phase.[3] However, the only thermochemical study is a statistical calculation of C_p°, S°, $(H^\circ - E^\circ_0)/T$, and $(G^\circ - E^\circ_0)/T$ from spectroscopic data by Puranik and Ramaswamy.[4]

The kinetics and thermochemistry of a number of iodination reactions or organic compounds and pyrolyses of iodo compounds have been studied using uv spectrophotometric techniques.[5] The thermochemical properties not only of stable compounds but also of free radicals have been determined from these studies.

The present paper is one of three papers concerned

(1) Supported in part by Grant No. AP-00353-03 from the Air Pollution Division of the Public Health Service.

(2) C. P. Ellis, *J. Chem. Soc.*, 726 (1934).

(3) H. P. Kaufmann, *Ber. Bunsenges Phys. Chem.*, **55B**, 249 (1922).

(4) P. G. Puranik and L. Ramaswamy, *Proc. Indian Acad. Sci.*, **A52**, 135 (1960).

(5) (a) M. C. Flowers and S. W. Benson, *J. Chem. Phys.*, **38**, 882 (1963); (b) D. M. Golden, R. Walsh, and S. W. Benson, *J. Amer. Chem. Soc.*, **87**, 4053 (1965).

with the reaction CH≡CH + I_2 → CHI=CHI and will report the thermochemistry of the reaction. Studies of the kinetics of the above reaction,[6a] and the *cis–trans* isomerization of diiodoethylene[6b] will be published elsewhere.

Experimental Section

Materials. Reagent grade iodine was resublimed twice before using. Acetylene was purified three times by vacuum distillation at −80°. No contaminant was detected by glpc. *trans*-Diiodoethylene was synthesized by a method similar to that used by Ellis.[2] Approximately equal amounts of acetylene and iodine were introduced into a 200-ml Pyrex bulb and were heated to 100–120° while illuminating with a tungsten lamp for several days. The products were dissolved in M-17 solvent (Furfasol), and the iodine remaining in the products was decomposed with sodium bisulfite. The solution was washed with water and the solvent was removed by a water pump at room temperature. The remaining *trans*-diiodoethylene was recrystallized in methanol twice and resublimed three times *in vacuo*. The melting point was 73.0°, in agreement with the literature.[7] The synthesized *trans*-diiodoethylene had a very strong uv absorption at 236 mμ ($\alpha \approx 8.5 \times 10^3$ OD/M cm) and only one nmr peak at δ 7.05, showing that the material was very pure. Pure *cis*-diiodoethylene was not obtained, but a *cis*-isomer-rich sample was separated from the residual methanol solution as a lower layer during the continuous evacuation of the solution. This lower layer sample had a similar, but less strong (about half), absorption spectrum and two nmr peaks at δ 7.80 and 7.05, the latter corresponding to *trans*-diiodoethylene, as in the above observation. The former absorption was assigned to the *cis* isomer. The ratio of the amount of *cis* to *trans* isomer in the sample was determined to be about 2:1 by simple comparison of these nmr absorption peak heights and areas.

Apparatus. The slightly modified Cary 15 spectrophotometer, adapted for use with a quartz reaction vessel situated in an Al block oven, has been described in detail previously.[5b]

Procedure. Equilibrium in the system CH≡CH + I_2 ⇄ CHI=CHI was approached from both directions, pyrolysis and addition. In most of the experiments, iodine and/or acetylene was added to the diiodoethylene after a suitable amount of the latter was decomposed; this procedure decreased the time necessary to reach equilibrium.

The partial pressures of iodine and diiodoethylene were measured by monitoring the optical densities in the ~18 cm light path vessel at 500 mμ (~6 torr) and 450 mμ (~20 torr) for the former and 239 mμ (0.01–0.4 torr), 252 mμ (0.1–2.0 torr), and 285 mμ (>1.5 torr) for the latter.

The partial pressure of acetylene was determined by subtracting the pressure of iodine and diiodoethylene from the total pressure, with the exception of the cases where the amounts of acetylene and iodine were exactly the same. Pressure was measured by the usual oil manometer–transducer method.

In the determination of equilibrium constants, it was only necessary to know the absorption coefficient of an equilibrated mixture of *cis*- and *trans*-diiodoethylene. In fact, however, the procedure which was used to determine this coefficient leads also to a simple determination of the absorption coefficients of the individual isomers as well. When *trans*-diiodoethylene was introduced into the reaction vessel in the temperature range 270–355°, it was usually observed that the optical density decreased rapidly initially and then decreased rather slowly. The rapid decrease of optical density was due mainly to the isomerization from the *trans* isomer to the *cis* isomer, since the amount of iodine formed during this time was so small that the decrease of optical density at 252 mμ could not be explained by the pyrolysis of diiodoethylene. The slow decrease of optical density was due to the pyrolysis of an equilibrated mixture of both isomers. The absorption coefficient of the *trans*-diodoethylene was determined from the initial (extrapolated) optical density and the initial pressure. The absorption coefficient of the equilibrated *trans*- and *cis*-diiodoethylene mixture was determined from the back extrapolation of the optical density, which was gradually decreasing, and the material balance between the initial amount of diiodoethylene and iodine formed. The absorption coefficient of pure *cis* isomer was calculated from the equation

$$\alpha_c = \alpha_{\text{equil}} + (\alpha_{\text{eq}} - \alpha_t)K_{\text{iso}} \qquad (1)$$

where α_t, α_c, and α_{equil} are absorption coefficients of *trans*-, *cis*-, and equilibrated diiodoethylene, respectively, and K_{iso} is the equilibrium constant between the *trans* isomer and the *cis* isomer (*trans*:*cis*).

The absorption coefficient (at 252 and 285 mμ) of the equilibrated mixture at temperatures higher than 355° and lower than 270° was determined by extrapolation of the linear plot of α *vs.* $1/T$, which was obtained from the data in that temperature range. At temperatures greater than 355°, the pyrolysis becomes too rapid, and at temperatures less than 270° the *cis–trans* isomerization is too slow to use the method outlined above.

The absorption coefficients at 239 mμ were so large that their direct measurement was limited by the difficulty in measuring the necessarily low pressures required to keep the absorption on scale. However, the ratio of OD_{239} and OD_{252} was always constant over the

(6) (a) S. Furuyama, D. M. Golden, and S. W. Benson, submitted for publication; (b) D. M. Golden, S. Furuyama, and S. W. Benson, submitted for publication.

(7) R. M. Noyes, R. G. Dickinson, and V. Schomaker, *J. Amer. Chem. Soc.*, **67**, 1319 (1945); (b) S. T. Miller and R. M. Noyes, *ibid.*, **73**, 2376 (1951).

entire temperature range (3.50 ± 0.07 for *trans*-diiodoethylene and 3.30 ± 0.07 for the equilibrated mixture), so one could precisely obtain α_{238} from α_{252}. The absorption coefficients (OD/M cm) at 239, 252, and 285 mμ thus obtained are listed in Table I.

Table I: Decadic Molar Absorption Coefficients of Diiodoethylene

	Absorption coefficient, $10^{-3}\alpha$, (OD/M cm)		
	239 mμ	252 mμ	285 mμ
trans-Diiodoethylene	7.38	2.11	0.298
Equilibrated diiodoethylene	5.47	1.66	0.291
cis-Diiodoethylene	2.24	0.90	0.279

The composition of *cis* and *trans* isomers in equilibrium was simply determined from the ratios of nmr absorption peaks at δ 7.80 and 7.05 of the products, which were trapped in a Pyrex bulb at liquid nitrogen temperature and were dissolved in carbon tetrachloride. (Iodine remaining in the products was decomposed with sodium bisulfite before the measurements.)

Material Balance. Material balance was satisfactory in all experiments, except for a few cases where iodine addition experiments were done under comparatively high pressures of acetylene (more than 100 torr) at high temperature. In these cases, the estimated amounts of diiodoethylene from absorptions at 239, 252, and 285 mμ differed from each other beyond the limit of the error and exceeded the estimated value from the decrease of iodine. This behavior was especially noted close to equilibrium. In these experiments, the optical densities at 239, 252, and 285 mμ continued to increase even after the decrease of the optical density at 500 mμ (and 450 mμ) ceased. This would indicate the formation of small amounts of by-products having extremely strong absorption (stronger than that of diiodoethylene) at 200–250 mμ. Nmr absorption spectra of the products showed several small absorptions (beside absorptions assigned to *cis*- and *trans*-diiodoethylene), one of which at δ 7.20 seemed to be benzene. Experimental conditions were carefully chosen to minimize the effect of these side reactions.

Results and Discussion

Equilibrium data for the reaction CH≡CH + $I_2 \rightleftarrows$ CHI=CHI (equilibrated mixture) are summarized in Table II.

Equilibrium data for the geometrical isomerization of diiodoethylene are presented in Table III. These data show no real temperature dependence in the range 200–350°. Thus while a second-law treatment yields

$$\log K_{iso} = \log \frac{[trans]}{[cis]} = 0.26 \pm 0.10 - (0.07 \pm 0.24)/\theta \quad (2)$$

the value

$$\log K_{iso} = 0.23 \pm 0.03$$

$$K_{iso} = 1.7 \pm 0.1 \quad (S_t^\circ - S_c^\circ) = 1.1 \text{ gibbs/mol} \quad (3)$$

will be taken as correct over the entire temperature range studied here. (This compares with the value of Noyes, *et al.*,[7] of $\log K_{iso} \approx 0.26$ over the range 129–159° in decalin solution.)

The equilibrium constants for dissociation in Table II (K_{dis}) may be related to the equilibrium constant for the *trans* isomer by

$$\log K_t = \log \left[\left(\frac{1 + K_{iso}}{K_{iso}}\right) K_{dis}\right] = 0.20 + \log K_{dis} \quad (4a)$$

and for the *cis* isomer by

$$\log K_c = \log [(1 + K_{iso})K_{dis}] = 0.43 + \log K_{dis} \quad (4b)$$

The entropy of diiodoethylene is known from group additivity based on vinyl iodide,[8] as well as from the statistical calculations of ref 4. These differ by ~0.6 gibbs/mol, but the group additivity value has been chosen to represent the value for the *trans* isomer, since the spectroscopic assignments for the diiodoethylenes[9a] are less certain at the lowest frequencies than that for vinyl iodide.[9b] Using eq 3, the *cis* isomer is lower by 1.1 gibbs/mol.

Thermochemical quantities used are found in Table IV. Using these data and eq 4a, ΔS°_{600} for the equilibrated mixture is 30.5 gibbs/mol. This leads to a third-law value of $\Delta H^\circ_{600} = 20.1 \pm 0.1$ kcal/mol. Other thermochemical quantities are listed in Table IV. Figure 1 shows the data plotted in van't Hoff form with the line forced to yield the known entropy change and third-law enthalpy change. This line fits the data quite well, as can be seen. Second-law values, determined from a least-squares fit to the data yield $\Delta S^\circ_{600} = 32.2 \pm 0.5$ gibbs/mol and $\Delta H^\circ_{600} = 21.2 \pm 0.2$ kcal/mol. The fact that the second-law entropy differs from the known value by about 3.5 standard deviations provides some warning concerning the usual practice of reliance on the error analysis accompanying least-square line fitting to describe total errors, rather than estimating or acknowledging systematic errors.

From the data obtained here and other available data, one can also estimate the π-bond strength of

(8) (a) S. W. Benson, *et al.*, to be submitted for publication; (b) R. F. Richards, *J. Chem. Soc.*, 1931 (1948).

(9) (a) S. I. Miller, A. Weber, and F. F. Cleveland, *J. Chem. Phys.*, **23**, 44 (1955); (b) P. Torkington and H. W. Thompson, *J. Chem. Soc.*, 303 (1944).

Table II: Equilibrium Data for the Dissociation of 1,2-Diiodoethylene

T(°C)	$\left(\frac{P_{I_2} \times P_{C_2H_2}}{P_{C_2H_2I_2}}\right)_0$ [a]	$\left(\frac{P_{I_2} \times P_{C_2H_2}}{P_{C_2H_2I_2}}\right)_{equilibrium}$ [a]	K (atmospheres)
409.4	0 x 0/5.27	5.25 x 5.25/0.0208	1.743
405.5	0 x 0/10.46	10.38 x 10.38/0.0786	1.780
403.0	0 x 0/6.47	6.44 x 6.44/0.0343	1.594
404.2	0 x 0/4.51	4.49 x 4.49/0.0175	1.512
380.9	0 x 0/9.36	9.26 x 9.26/0.1045	1.079
380.9	0 x 0/6.35	6.28 x 6.28/0.0708	0.829
381.0	0 x 0/6.49	6.44 x 6.44/0.0514	1.062
355.0	4.59 x 18.19/1.78	6.04 x 19.64/0.327	0.477
354.8	0 x 25.81/1.70	1.49 x 27.30/0.123	0.437
354.8	3.72 x 18.18/5.28	8.24 x 22.95/0.510	0.488
355.1	0 x 0/7.16	6.85 x 6.85/0.131	0.473
355.1	15.11 x 6.85/0.131	14.94 x 6.71/0.272	0.485
355.2	14.94 x 55.91/0.272	13.31 x 54.50/1.974	0.490
355.2	18.19 x 0/3.07	21.00 x 2.91/0.161	0.495
331.0	0 x 19.76/5.08	4.40 x 24.33/0.506	0.278
331.4	0.80 x 23.16/3.04	3.17 x 25.77/0.430	0.250
331.4	0 x 0/5.82	5.52 x 5.52/0.164	0.250
331.0	4.90 x 17.47/3.69	7.50 x 20.30/0.750	0.267
331.5	7.09 x 14.56/1.78	8.22 x 15.69/0.650	0.262
331.5	8.22 x 38.18/0.650	7.55 x 37.51/1.460	0.255
332.0	4.63 x 17.13/1.77	5.82 x 18.35/0.550	0.255
331.5	5.98 x 58.0/0	4.67 x 56.70/1.310	0.266
331.6	9.99 x 51.50/0	7.91 x 49.50/2.090	0.247
331.4	4.52 x 10.26/0	4.24 x 9.98/0.240	0.233
332.0	0 x 82.45/1.55	1.08 x 83.60/0.464	0.255
313.3	20.13 x 0/1.65	21.56 x 1.38/0.265	0.148
313.4	0 x 0/7.19	6.74 x 6.74/0.415	0.146
313.4	6.74 x 38.57/0.415	5.32 x 37.43/1.750	0.150
313.3	3.71 x 0/10.68	13.32 x 9.61/1.070	0.157
313.3	13.32 x 78.51/1.07	8.61 x 74.15/5.920	0.142
313.5	1.38 x 20.65/5.73	5.68 x 25.08/1.320	0.140
291.6	4.05 x 21.25/0	2.91 x 20.11/1.140	0.0676
291.6	1.00 x 203.1/0	0.214 x 202.3/0.786	0.0724
291.3	4.44 x 3.90/0.452	4.55 x 4.01/0.342	0.0703
291.3	4.55 x 5.75/0.342	4.39 x 5.51/0.495	0.0649
291.4	4.39 x 19.11/0.495	3.58 x 18.34/1.290	0.0670
290.9	1.66 x 26.94/1.61	2.01 x 27.34/1.210	0.0596
292.9	8.43 x 1.51/1.70	9.96 x 1.51/0.263	0.0752
279.5	0 x 0/1.73	1.56 x 1.56/0.0662	0.0481
272.1	0 x 0/1.87	1.76 x 1.76/0.112	0.0365
270.9	0 x 0/6.43	5.18 x 5.18/0.994	0.0356
245.5	0 x 0/4.00	3.02 x 3.02/0.884	0.0136
242.6	0 x 0/1.62	1.30 x 1.30/0.191	0.0116
234.5	0 x 0/3.93	2.76 x 2.76/1.045	0.00959
224.0 [b]	8.30 x 69.00/0	0.458 x 61.16/7.480	0.00541
199.0 [b]	4.85 x 34.60/0	0.265 x 30.00/4.585	0.00233

[a] The units are given in torr. [b] These points were not included in the determination of thermochemical parameters.

Table III: Equilibrium Data for the Isomerization of *cis*- to *trans*-Diiodoethylene

TEMPERATURE °C	335.2	331.5	331.6	332.0	313.4	291.6	291.1	291.3	245.5	242.6	224.0	199.0	MEAN 550°K
$K = \frac{trans}{cis}$	1.80	1.78	1.70	1.62	1.77	1.67	1.47	1.80	1.54	1.80	1.70	1.73	1.69 ± 0.13

Table IV: Thermochemical Data

	298°K			600°K		
	ΔH° kcal/mole	ΔS° gibbs/mole	ΔC_p gibbs/mole	ΔH° kcal/mole	ΔS° gibbs/mole	ΔC_p gibbs/mole
trans-CHI=CHI(g) $\rightleftharpoons$ CH≡CH(g) + I_2(g)	19.9	30.8	1.87	20.1	31.4	-0.25
cis-CHI=CHI(g) $\rightleftharpoons$ CH≡CH(g) + I_2(g)	19.9	31.9	1.87	20.1	32.5	-0.25
	ΔH_f° kcal/mole	S° gibbs/mole	C_p gibbs/mole	ΔH_f° kcal/mole	S° gibbs/mole	C_p gibbs/mole
CH≡CH(g)[a]	54.190	48.004	10.539	53.961	56.604	13.931
I_2(g)[a]	14.924	62.281	8.814	0	68.511	8.980
I(g)[a]	25.531	43.184	4.968	18.229	46.658	4.968
trans-CHI=CHI(g) obs.	49.2			33.8		
trans-CHI=CHI(g) est.[b]		79.6	17.6		93.9	23.2
trans-CHI=CHI(g) calc.[c]		80.11	17.64		94.39	23.17
cis-CHI=CHI(g) obs.	49.2	78.5		33.8	92.8	
cis-CHI=CHI(g) est.[b]			17.6			23.20
cis-CHI=CHI(g) calc.[c]		79.81	17.75		94.17	23.36
C_d-(I)(H)[b]	24.6[d]	40.5	8.8		47.7	11.60

[a] "JANAF International Tables," D. R. Stull, Ed., The Dow Chemical Co., Midland, Mich., 1963. [b] Reference 8. [c] Reference 4. [d] This work.

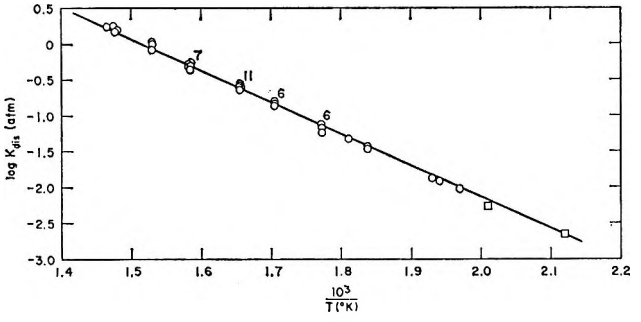

Figure 1. Log K_{dis} (atm) *vs.* $1/T$. The line is the forced third-law fit. The numbers indicate overlapping points. Points marked □ were not used in the analysis.

acetylene, defined as the difference between the bond dissociation energy in diiodoethylene, DH°(CHICH–I), and in the radical, DH°(·CHCH–I), formed by removing the iodine atom from the diiodoethylene. On the assumption that the C–I bond dissociation energy in diiodoethylene is the same as that of phenyl iodide, that is, 65.0 ± 1 kcal/mol,[10] 88.7 ± 1 kcal/mol is the radical heat of formation. The bond dissociation energy in the radical is then −9.0 ± 1 kcal/mol, and the π-bond strength of acetylene is 74.0 kcal/mol. This is in reasonable agreement with the value of ≥70 kcal/mol obtained from a similar calculation, starting with ethylene and using the value ≥108 kcal/mol for the bond dissociation energy, DH°(C_2H_3–H).[11]

The contribution of the group C_d–(I)(H) to $\Delta H_f^\circ{}_{298}$ is 24.6 kcal/mol. We have no concrete evidence by which to identify the unknown side products, which have very strong absorptions at 200–250 mμ. It might be guessed that these are some kind of conjugated iodo compounds like 1,4-diiodobutadienes, because we know that benzyl iodide, which is also a conjugated iodo compound, shows extremely strong absorption at this wavelength.[12] This speculation seems to be supported by the fact that the unknown products were apt to increase with the increase of pressure of acetylene. At high pressures of acetylene, the dimerization (1,4-diiodobutadiene formation) and trimerization (benzene formation) may be the source of these additional products.

Acknowledgment. The authors wish to express their thanks to Dr. A. S. Rodgers for performing several of the preliminary experiments. They also thank Mr. W. Anderson for the nmr measurements.

(10) A. S. Rodgers, D. M. Golden, and S. W. Benson, *J. Amer. Chem. Soc.*, **89**, 4578 (1967).

(11) A. S. Rodgers, D. M. Golden, and S. W. Benson, unpublished work.

(12) R. Walsh, D. M. Golden, and S. W. Benson, *J. Amer. Chem. Soc.*, **88**, 657 (1966).

Relative Viscosity and Apparent Molal Volume of N-Methylpropionamide Solutions at Various Temperatures

by Frank J. Millero

Contribution No. 932, Institute of Marine Sciences, University of Miami, Miami, Florida 33149
(Received March 13, 1968)

The relative viscosities, η_r's, of solutions of benzene, pyridine, and $NaNO_3$ in N-methylpropionamide and apparent molal volumes, ϕ_V's, of benzene, pyridine, benzoic acid, NaCl, KCl, NaBr, KBr, $NaNO_3$, and sodium benzoate in N-methylpropionamide have been determined from 15 to 40°. The results are discussed by comparing the viscosity B coefficients, molal volumes, $\bar{V}^0$'s, and molal expansibilities, $\bar{E}^0$'s, for these solutes in water and N-methylproprionamide.

Introduction

Although there have been many studies of the relative viscosity, η_r, and apparent molal volume, ϕ_V, of solutes in aqueous solutions and in low dielectric solvent systems, few studies have been made of these properties in high dielectric solvent systems.[1-3] The present paper deals with solutions of nonelectrolytes and electrolytes in N-methylpropionamide (NMP). NMP has a high dielectric constant (176 at 25°)[4] and is a highly associated liquid.[4,5] Both electrolytes and nonelectrolytes (polar and nonpolar) are soluble in NMP; thus quite a wide variety of solutes can be studied in this solvent.

Viscosity measurements were made on pure NMP and solutions of benzene, pyridine, and $NaNO_3$ in NMP at 5° intervals from 15 to 40°. Density measurements were also made for these solutions and also for some other solutions (NaCl, KCl, NaBr, KBr, sodium benzoate, and benzoic acid in NMP). The relative viscosities, η_r's, apparent molal volumes, ϕ_V's, and apparent molal expansibilities, ϕ_E's, were calculated for these solution.

Experimental Section

The preparation and purification of NMP has been described elsewhere.[1,6] All the solutes were of reagent grade and were used without further purification. The solutions were all made by weight.

The density measurements were made with a magnetic-float densitometer similar to the one described elsewhere.[7] The apparatus was calibrated with doubly distilled H_2O from 15 to 40° at 5° intervals. The apparatus reproduced the density of water[8] to ±11 ppm over this range. The sensitivity of the densitometer used in this study was less than that obtained recently[7] because of differences in the magnetic interaction constants, f (f = 9.5 g/A for the densitometer used in this study compared with f = 3.5 g/A for the recently described apparatus.)[7]

The viscosity measurements were made with Ostwald-type viscometers calibrated with standard viscosity oil, National Bureau of Standards Oil H, Lot No. 12. No kinetic corrections were made; however, head corrections were made for the thermal expansion of the liquid.

For both calibrations with the National Bureau of Standards Oil H and measurements on pure NMP, correction factors for the viscometer constant, K, were calculated as $1 + (V_s - V)/(\pi R^2 h)$. Here, V_s is the nominal volume of the charge (10 ml) and V is the actual volume based on the weight of the charge and its density at the temperature of the measurement; R is the radius of the lower bulb; and h is the mean difference between the liquid levels during the run. This correction was small and was neglected for the other solutions.

The temperature bath used for the density and viscosity measurements was controlled to ±0.005°. The bath temperature was set to better than ±0.01° with a platinum thermometer and resistance bridge.

Results and Discussion

The viscosity, η^0, of NMP at various temperatures was calculated from the equation

$$\eta^0 = Kd^0\tau^0 \quad (1)$$

where K is a constant, d^0 is the density, and τ^0 is the flow time of pure NMP. K was determined by cali-

(1) (a) T. B. Hoover, *J. Phys. Chem.*, **68**, 876 (1964); (b) T. B. Hoover, *ibid.*, **68**, 3003 (1964).

(2) L. R. Dawson, R. H. Graves, and P. G. Sears, *J. Amer. Chem. Soc.*, **79**, 298 (1957).

(3) D. Feakins and K. G. Lawrence, *J. Chem. Soc., A*, 212 (1966).

(4) S. J. Bass, W. I. Nathan, R. M. Meighan, and R. H. Cole, *J. Phys. Chem.*, **68**, 509 (1964).

(5) R. Lin and W. Dannhauser, *ibid.*, **67**, 1805 (1963).

(6) G. R. Leader and J. F. Gormley, *J. Amer. Chem. Soc.*, **73**, 5731 (1951).

(7) F. J. Millero, *Rev. Sci. Instrum.*, **38**, 1441 (1967).

(8) L. W. Tilton and J. K. Taylor, *J. Res. Nat. Bur. Stand.*, **18**, 205 (1937).

brating the viscometers with Oil H. The average η^0 and d^0 of NMP at various temperatures are given in Table I. The average deviation of η^0 over this range was ±0.001 to ±0.004 cP. The η^0 results agree very well with the values obtained by Hoover[1b] at various temperatures. The density values listed in Table I are those taken from the recent measurements of Malmberg and Hoover.[9] These density values are lower than those reported earlier,[1a] owing to the presence of water in the NMP used in the earlier work.

Table I: Density and Viscosity of N-Methylpropionamide at Various Temperatures

Temp, °C	Density, g/ml	Viscosity, cP
15	0.93855	6.994
20	0.93452	6.016
25	0.93050	5.215
30	0.92650	4.554
35	0.92250	4.001
40	0.91850	3.533

The relative viscosity, η_r, for the various solutions was calculated from the equation

$$\eta_r = \frac{\eta}{\eta^0} = \frac{d\tau}{d^0\tau^0} \qquad (2)$$

where η, d, and τ are the viscosity, density, and flow time for the solution. The η_r's for benzene and pyridine solutions at various concentrations (c is the number of moles per liter of solution) were fit to equations of the form

$$\eta_r = 1 + A'c + B'c^2 + C'c^3 \qquad (3)$$

The constants for the equations at various temperatures are given in Table II. The average deviations between the experimental and the calculated η_r's were 0.005 and 0.002 for the benzene and pyridine NMP solutions, respectively. However, the results from different series of solutions differ by as much as ±0.05. Reproducibility for the benzene solutions at high concentrations and at high temperatures was difficult, owing to the volatility of benzene.

The η_r for the $NaNO_3$ solutions in NMP was fitted to a Jones–Dole-type equation

$$\eta_r = 1 + A\sqrt{c} + Bc \qquad (4)$$

The constants for these equations at various temperatures are given in Table III. The average deviations between the experimental and calculated η_r's were ±0.005 for a given experiment; however, the results from different series of solutions differ by as much as ±0.01. The standard deviations for A were between 0.02 and 0.05 $(l./mol)^{1/2}$ at the various temperatures, and the standard deviations for B were between 0.06 and 0.12 l./mol.[9] A better fit of the data for the $NaNO_3$–NMP solutions was obtained by estimating the theoretical value of A and by adding the Dc^2 term to eq 4. This reduces the B values by about 25% (values in parentheses in Table III) and reduces the standard deviations of the B values to 0.01–0.06 l./mol.[9]

Table II: Constants for the η_r Equation for Benzene and Pyridine in NMP at Various Temperatures[a]

Temp, °C	Benzene (0.14–2.8 M)[b] $-A'$, l./mol	Benzene $10^2B'$, $(l./mol)^2$	Benzene $10^2C'$, $(l./mol)^3$	Pyridine (0.27–4.10 M) $-A'$, l./mol	Pyridine $10^2B'$, $(l./mol)^2$	Pyridine $10^2C'$, $(l./mol)^3$
15	0.2231	8.10	−1.80	0.2404	3.22	0.19
20	0.1485	−0.60	0.44	0.2297	3.14	0.21
25	0.1283	−2.69	0.98	0.2216	3.04	0.22
30	0.3683	−471	0.63	0.2163	2.98	0.22
35	0.3829	−488	0.66	0.2011	2.77	0.18
40	0.3859	−476	0.64	0.1932	2.35	0.17

[a] The constants given in this table were determined from one set of experiments by a least-squares best-fit method with the aid of an IBM 1401 computer. The root-mean-square fit was 0.005 for benzene–NMP and 0.002 for pyridine–NMP solutions. The constants are given to enough significant figures to comply with this precision; however, the constants probably have larger uncertainties (since the η_r from a different series varied by as much as ±0.05).[9] [b] The constants at 30, 35, and 40° are only valid over the concentration range from 0.1 to 0.5 M; thus they should not be used outside this concentration range. It was impossible to work at higher concentrations at these temperatures, owing to the volatility of the benzene–NMP solutions.

Table III: Constants for the η_r Equation for $NaNO_3$ in NMP at Various Temperatures[a]

Temp, °C	$NaNO_3$ (0.05–0.5 M) $-A$, $(l./mol)^{1/2}$	B, l./mol
15	0.021	1.296 (1.085)[b]
20	0.039	1.277 (1.099)
25	0.034	1.243 (1.053)
30	0.049	1.234 (1.034)
35	0.029	1.204 (1.009)
40	0.069	1.182 (0.973)

[a] The A and B constants were determined from one set of experiments by a least-squares best-fit method with the aid of an IBM 1401 computer. Although the root-mean-square deviation of this proposed fit was 0.005, the uncertainties in the A and B constants are larger (±0.02–0.06 $(l./mol)^{1/2}$ for A and ±0.06–0.12 l./mol for B), based on measurements of other salts in NMR. (See ref 9 and J. V. Botscheller and W. G. Bourdiun, National Bureau of Standards unpublished data.) [b] These values of B were calculated by using the estimated theoretical value of A (approximately 0.008 $(l./mol)^{1/2}$) and adding an additional term Dc^2 to eq 4. The theoretical value of A was determined from the Fuoss approximate relation $A = \beta/80\Lambda^0$, where β is the electrophoretic term in the conductance limiting law ($\beta = 82.486/\eta(DT)^{1/2}$): R. M. Fuoss and F. Accascina, "Electrolytic Conductance," Interscience Publisher, New York, N. Y., 1959, p 234.

(9) C. G. Malmberg and T. B. Hoover, personal communication.

Benzene and pyridine both decrease the viscosity of NMP presumably by breaking down the solvent structure. Pyridine has the greater structure-breaking effect, although benzene has a lower absolute viscosity (both solutes have similar molar volumes in the pure state). Pyridine is apparently able to break down the structure of NMP by dilution and also by formation of terminal hydrogen bonds with NMP. The viscosity B coefficients for $NaNO_3$ in NMP and its change with temperature is of the same order of magnitude as KCl in NMP.[1a] Owing to their large uncertainty, the values for A listed in Table III cannot be compared with their estimated theoretical value.[9] A few measurements were made on NaBr solutions in NMP at one concentration and B was estimated by assuming that A was zero. Values of B = 2.19 l./mol at 15° and B = 2.04 l./mol at 25° were calculated for NaBr. These large B coefficients in NMP and NMF (N-methylforamide) have been discussed elsewhere.[3] If one assumes that the B coefficient is proportional to the molal volume, $\bar{V}^0$, one might expect B to increase by the same order of magnitude as $\bar{V}^0$ when comparing NMP with water. $\bar{V}^0$ for $NaNO_3$ increases by 41% when transferred from water to NMP, while B increases by 2900%. This difference cannot be explained by electrostriction, since the electrostriction differences between NMP and water are in the opposite order (*i.e.*, $\bar{V}^0$(elect) in water > $\bar{V}^0$(elect) in NMP). Another possible explanation for the large B coefficients (*i.e.*, structure-forming ability of salts in NMP) may be due to the formation of intimate ion pairs across the linear hydrogen bonds. When one compares the η_r of $NaNO_3$ in NMP with that in water on a mole basis (1 m $NaNO_3$ in NMP is equivalent to 5 m $NaNO_3$ in H_2O), the effect of $NaNO_3$ is not as great. For example, η_r = 1.57 for 5 m $NaNO_3$ in H_2O[10] and η_r = 2.34 for 1 m $NaNO_3$ in NMP (a 49% increase). The change of B and V^0 with increasing temperature are both negative for salts in NMP. This parallelism does not exist in H_2O because of the ability of some ions or salts to have structure-breaking or structure-making effects.

The apparent energy of activation of viscous flow, ΔE, given by the equation

$$\frac{\Delta E}{R} = \frac{\partial \ln \eta}{\partial 1/T} \qquad (5)$$

has been calculated for these solutions, and the results at 25° at various concentrations are shown in Figure 1. Benzene and pyridine both decrease ΔE, while $NaNO_3$ increases ΔE. The effects of these solutes on ΔE conform with the previous discussion.

The densities of the pyridine and benzene NMP solutions at various temperatures were fit to equations of the form

$$d = d^0 + Em + Fm^2 + Gm^3 \qquad (6)$$

where d^0 is the density of pure NMP, m is the molality, and E, F, and G are constants. The density of $NaNO_3$ was fit to similar equations, except for replacing m by $\sqrt{m}$. The constants for these equations are given in Table IV, which also includes the average deviations between the measured and calculated densities.

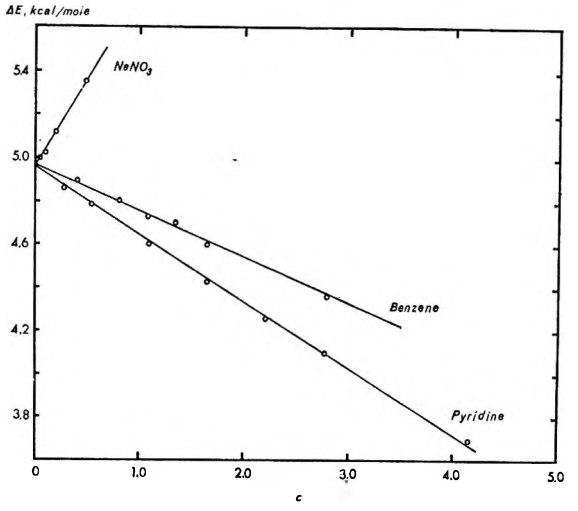

Figure 1. Apparent energy of activation for viscous flow, ΔE, for various solutes in NMP *vs.* molarity, c, at 25°.

Table IV: Constants for the Density Equation for Benzene, Pyridine, and $NaNO_3$ in NMP[a] at Various Temperatures[a]

Temp, °C	10^2E	10^2F	10^3G	Av dev, g/ml
	Pyridine in NMP (0.29–6.65 m)			
15	5.721	−1.279	0.190	±0.0001
20	5.793	−1.423	0.220	±0.0002
25	5.515	−8.857	0.074	±0.0003
30	5.756	−1.515	0.240	±0.0002
35	5.656	−1.488	0.238	±0.0002
40	5.497	−1.122	0.145	±0.0002
	Benzene in NMP (0.14–3.98 m)			
15	−2.992	−0.0735	−0.109	±0.0004
20	−2.732	−0.215	0.455	±0.0005
25	−2.737	−0.248	0.477	±0.0004
	$NaNO_3$ in NMP (0.05–0.5 m)			
15	−1.086	50.60	−5.970	±0.00000
20	−1.221	50.80	−5.748	±0.00001
25	−0.722	49.09	−4.148	±0.00002
30	−1.146	50.73	−5.533	±0.00002
35	−1.021	50.28	−5.107	±0.00003
40	−1.055	50.23	−4.684	±0.00003

[a] Determined by a least-squares best-fit method with the aid of an IBM 1401 computer. The units for the constants E, F, and G are as follows: for the benzene, pyridine, and NMP solutions, the units are, respectively, g/ml(kg of H_2O/mol), g/ml(kg of H_2O/mol)^2, and g/ml(kg of H_2O/mol)^3; for the $NaNO_3$–NMP solutions, the units are, respectively, g/ml(kg of H_2O/mol)$^{1/2}$, g/ml(kg of H_2O/mol), and g/ml(kg of H_2O/mol)$^{3/2}$.

(10) R. H. Stokes and R. Mills, "The International Encyclopedia of Physical Chemistry and Chemical Physics," Vol. 3, Pergamon Press Inc., New York, N. Y., 1965, Topic 16.

The apparent molal volumes, ϕ_V's, were calculated from the density data of the solutes studied in this paper (and also the unpublished data of Botscheller and Borduin[11]) from the equation

$$\phi_V = \frac{1000(d^0 - d)}{d^0 dm} + \frac{M}{d} \quad (7)$$

The infinite dilution values, $\phi_V^0 \equiv \bar{V}^0$, were calculated from the equation

$$\phi_V = \phi_V^0 + S_V c \quad (8)$$

for the nonelectrolytes and c was replaced by $\sqrt{c}$ for the salts. Figures 2 and 3 show ϕ_V *vs.* c or $\sqrt{c}$ for some of the solutes at 25°. Table V gives $\bar{V}^0$ and S_V for pyridine, benzene, and $NaNO_3$ solutions of NMP at various temperatures. Table VI gives $\bar{V}^0$ and the average apparent molal expansibilities at infinite dilution, $\phi_E^0 \equiv \bar{E}^0$, for all the solutes studied at 25°.

Table V: Molal Volume at Infinite Dilution, $\bar{V}^0$, and the Limiting Slope, S_V, for Benzene, Pyridine, and $NaNO_3$ at Various Temperatures[a]

Temp, °C	Benzene $\bar{V}^0$, ml/mol	Benzene S_V	Pyridine $\bar{V}^0$, ml/mol	Pyridine S_V	$NaNO_3$ $\bar{V}^0$, ml/mol	$NaNO_3$ S_V
15	87.4	~0	29.0	1.7	40.6	−2.7
20	87.7	~0	30.9	3.5	40.3	−3.0
25	88.1	~0	31.3	3.6	39.6	−2.0
30	89.2	~0	32.1	3.0	40.1	−3.2
35	88.9	~0	33.2	3.5	39.9	−2.7
40	90.3	~0	34.3	3.2	39.7	−3.4

[a] The average deviations of $\bar{V}^0$ for benzene, pyridine, and $NaNO_3$ are ±0.7, ±0.5, and ±0.3 ml/mol, respectively.

Table VI: Molal Volume, $\bar{V}^0$, and Molal Expansibility, $\bar{E}^0$, at Infinite Dilution for Various Solutes in NMP at 25°

Solute	$\bar{V}^0$, ml/mol	$\bar{E}^0$, ml/mol deg
Benzene	88.1	0.09
Pyridine	31.3	0.18
$NaNO_3$	39.6	−0.04
NaCl	30.7	−0.06
KCl	35.5	−0.07
NaBr	35.8	−0.05
KBr	40.9	−0.04
NaOBz	103.6	...
HOBz	100.2	...
	Av dev ±0.3–0.8	Av dev ±0.01–0.04

The limiting slope for the salts in NMP, S_V, cannot be compared with the theoretical Debye–Hückel limiting slope, because the change of the dielectric constant with pressure and the compressibility of NMP are not known. The limiting slope[12] is equal to $S_V = kw^{1/2}$, where $w = {}^1/_2 \Sigma (\nu_i Z_i^2)$ and $k = 2N^2 e^3 (2\pi/1000RT)^{1/2} \epsilon^{-3/2}(\mathrm{d} \ln \epsilon/\mathrm{d}p - \beta/3,)$ where N is Avogadro's number; ϵ and β are the dielectric constant and the compressibility of the solvent, respectively; and the other terms have their usual meaning. If one compares the S_V values in methanol (15.77 at 25°)[13] and water (1.86 at 25°)[12] as a function of ϵ, it is not surprizing that the value is negative in NMP solutions.

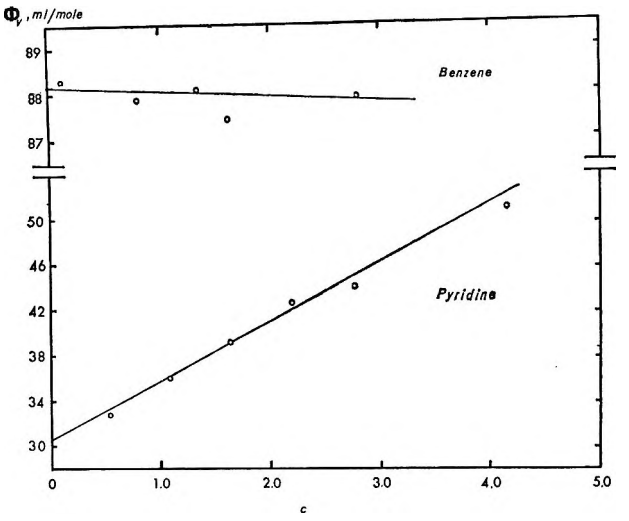

Figure 2. Apparent molal volumes, ϕ_V, of benzene and pyridine in NMP in various concentrations, c, (molar units) at 25°.

The ϕ_V and ϕ_E of benzene in NMP are independent of concentration and are approximately equal to the values of pure benzene (88.8 ml/mol and 0.100 ml/mol deg, respectively, at 25°).[14] These results indicate that there is little or no solute–solvent interaction between benzene and NMP. The $\bar{V}^0$ of pyridine in NMP is smaller than the molar volume of pure pyridine (80.5 ml/mol at 25°)[14] and also smaller than $\bar{V}^0$ of pyridine in H_2O (78.0 ml/mol at 25°.)[15] These results indicate that the solute–solvent interactions between pyridine and NMP are very large and not electrostatic in nature. These facts support the earlier postulation that pyridine breaks down the structure of NMP by forming terminal hydrogen bonds which decrease the volume. S_V is positive, since the effect of pyridine in decreasing the volume of NMP (or breaking down the linear hydrogen bonds) is less important as more is added. The ϕ_E is positive, since at higher temperatures there is less structure in NMP to break down.

The additivity of $\bar{V}^0$ for salts in NMP can be shown by comparing the differences between the salt pairs, $\bar{V}^0$(KCl) − $\bar{V}^0$(NaCl), $\bar{V}^0$(KBr) − $\bar{V}^0$(NaBr), $\bar{V}^0$(NaBr) −

(11) J. V. Botscheller and W. G. Borduin, National Bureau of Standards, unpublished data.

(12) O. Redlich, *J. Phys. Chem.*, **67**, 469 (1963).

(13) J. Padova and I. Abrahamer, *ibid.*, **71**, 2112 (1967).

(14) "Handbook of Chemistry and Physics," 35th ed, Chemical Rubber Publishing Co., Cleveland, Ohio, 1957.

(15) Calculated from the density data of V. S. Griffiths, *J. Chem. Soc.*, 1326 (1952).

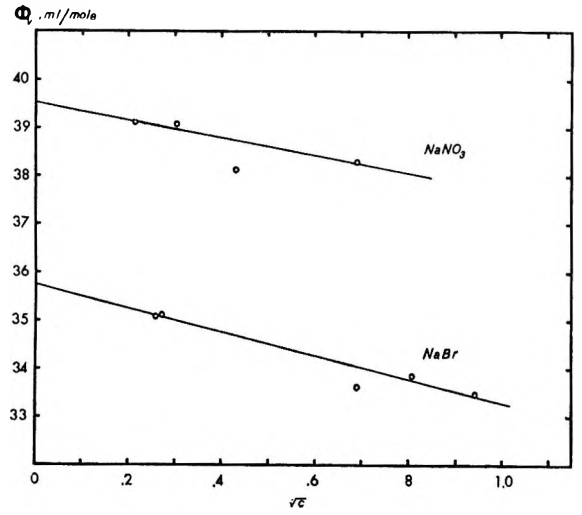

Figure 3. Apparent molal volumes, ϕv, of $NaNO_3$ and NaBr in NMP *vs.* $\sqrt{c}$ at 25°.

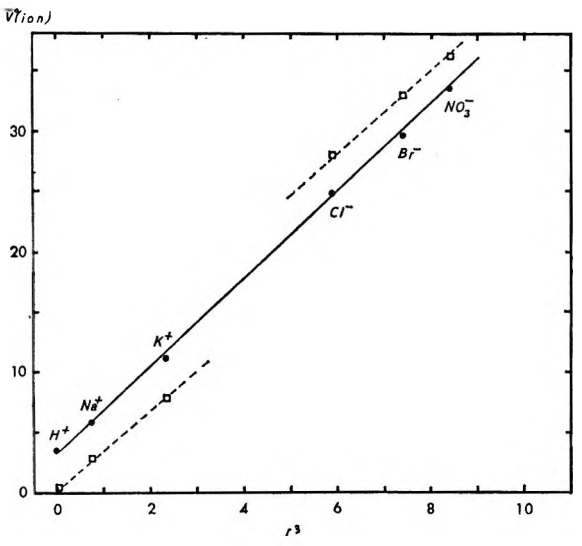

Figure 4. Ionic molal volume, $\bar{V}^0$ (ion) for various ions in NMP *vs.* r^3 at 25° for two different values of H^+: dotted lines, $\bar{V}^0$ (H^+) = 0; solid line, $\bar{V}^0$ (H^+) = 3.4 ml/mol.

$\bar{V}^0$(NaCl), and $\bar{V}^0$(KBr) − $\bar{V}^0$(KCl). From these differences one obtains, $\bar{V}^0$(K–Na) = 4.8, 5.1 ml/mol and $\bar{V}^0$(Br–Cl) = 5.1, 5.4 ml/mol. The division of $\bar{V}^0$(salt) in NMP into its ionic components can be made by the method for calculating $\bar{V}^0$(ion) in H_2O used by Mukerjee.[16] As a first approximation, $\bar{V}^0(H^+)$ was equated to zero (or $\bar{V}^0$(HOBz) = $\bar{V}^0(OBz^-)$; the values of $\bar{V}^0$ (ion) based on this division were then plotted *vs.* r^3 (the crystal radius).[16] $\bar{V}^0(H^+)$ was then adjusted until the best fit for both cations and anions was obtained. Table VII gives $\bar{V}^0$(ion) based on a value of $\bar{V}^0(H^+)$ = 3.4 ml/mol and $\bar{V}^0$(ion) in H_2O.[16,17] Figure 4 shows the plot of $\bar{V}^0$(ion), from Table VII, *vs.* r^3, from which $\bar{V}^0$(ion) of other monovalent ions in NMP can be estimated, $\bar{V}^0$(ion) = $4.28r^3$ + 3.4 ml/mol. The slope of $\bar{V}^0$(ion) *vs.* r^3 is larger than the theoretical values of

Table VII: Molal Volume of Ions, $\bar{V}^0$(ion), in NMP and H_2O and $\Delta\bar{V}^0$(trans) from H_2O to NMP at 25°

Ion	Crystal radius,[16,17] Å	$\bar{V}^0$(ion), ml/mol NMP	$\bar{V}^0$(ion), ml/mol H_2O[16,17]	$\Delta\bar{V}^0$(trans) (H_2O–NMP), ml/mol
H^+	...	3.4	−4.5	7.9
Na^+	0.95	6.0	−5.7	11.9
K^+	1.33	11.1	4.5	6.6
Cl^-	1.81	24.7	22.3	2.4
BR^-	1.95	29.8	29.2	0.6
NO_3^-	2.03	33.6	33.6	0
OBz^-	...	97.7	...	...

2.52, and $\bar{V}^0(H^+)$ is positive, apparently due to the radius of an ion in solution being larger than the crystal radius (since void space effects in NMP should be smaller than those in H_2O).[18,19] Further work must be done on other salts to prove this postulation.

The volume of transfer of an ion from water to NMP, $\Delta\bar{V}^0$(trans), Table VII, can be attributed to the differences in electrostriction or solute–solvent interactions, since the intrinsic volume of an ion in NMP and H_2O should be nearly equal. The electrostriction volume, $\bar{V}^0$(elect), is generally taken to be proportional to Z^2/r, where Z is the charge.[16–20] Thus $\Delta\bar{V}^0$(trans) from H_2O to NMP would be expected to be proportional to $Z^2/r(A'' - B'')$, where A'' and B'' are constants related to ϵ and d ln ϵ/dP of H_2O and NMP, respectively. Figure 5 shows a plot of $\Delta\bar{V}^0$(trans) *vs.* $1/r$ taken from Table VII. This plot indicates that if $r > 2.22$ Å $\Delta\bar{V}^0$(trans) is very small (~0) or the electrostriction for monovalent ions with $r > 2.22$ Å is very small in H_2O. If one assumes the electrostriction, $\bar{V}^0$(elect), in NMP is small, the maximum value for the constant A'' for H_2O in the equation $\bar{V}^0$(elect) = $A''Z^2/r$ is 11, compared with a theoretical value of 6 obtained by Benson and Copeland[21] and an empirical value of 8 obtained by Mukerjee.[16] The value for the constant B'' in NMP (3–5) could be used to estimate (d ln ϵ/dP in NMP; however, until more work is done for divalent and trivalent salts in NMP this estimation may be meaningless.

The molal expansibilities, ϕ_E's, of the various solutes in NMP were calculated from $d\phi_V/d_T$, and the average infinite dilution values, $\phi_E^0 \equiv \bar{E}^0$, are given in Table VI. The $\bar{E}^0$ of salts in NMP is negative (similar to other solvents, *e.g.*, MeOH),[22] while values in H_2O are posi-

(16) P. Mukerjee, *J. Phys. Chem.*, **65**, 740 (1961).

(17) L. A. Dunn, *Trans. Faraday Soc.*, **62**, 2348 (1966).

(18) L. G. Hepler, *J. Phys. Chem.*, **61**, 1426 (1957).

(19) B. E. Conway, R. E. Verrall, and J. E. Desnoyers, *Z. Phys. Chem.* (Leipzig), **230**, 157 (1965).

(20) E. Glueckauf, *Trans. Faraday Soc.*, **61**, 914 (1965).

(21) S. W. Benson and C. S. Copeland, *J. Phys. Chem.*, **67**, 1194 (1963).

(22) R. W. Gurney, "Ionic Process in Solution," McGraw-Hill Book Co., Inc., New York, N. Y., 1953.

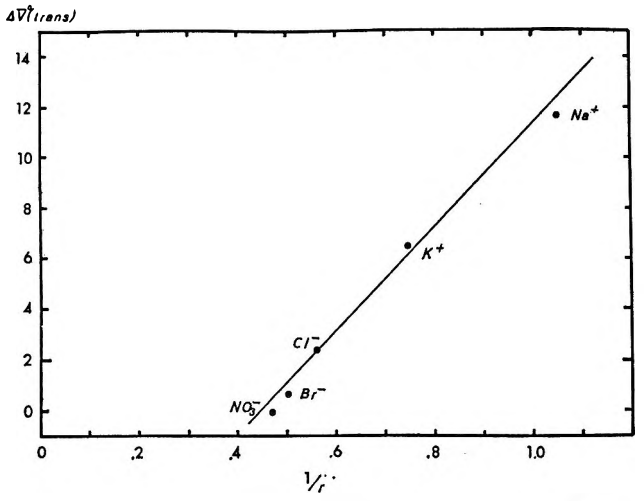

Figure 5. The change in volume in transfer of an ion, $\Delta\bar{V}^0$ (trans), from H_2O to NMP *vs.* $1/r$ at 25°.

tive.[22,23] These results indicate that the positive values of $\bar{E}^0$(salt) in H_2O are related to the ability of the salt to change the structure of water over and above normal electrostriction.

A few measurements[11] were made on the density of mixed pairs of salts in NMP at 25°. (See Table VIII).

Table VIII: The Mean Apparent Molal Volume, Φ, of Salt Mixtures in NMP

Mixture	Φ, ml/mol Measd	Φ, ml/mol Calcd	% error
0.0956 *m* NaOBz + 0.0950 *m* NaCl	65.3	67.3	3.1
0.0274 *m* KCl + 0.0275 *m* NaBr	38.8	35.7	7.9
0.0153 *m* KCl + 0.0150 *m* NaBr	41.9	35.7	14.7

The mean apparent molal volume, Φ, of such a mixture can be calculated from the equation

$$\Phi = \frac{V - 11.48\bar{V}^0(\text{NMP})}{m_1 + m_2} \quad (9)$$

where V is the volume of solution containing 1000 g of NMP, $\bar{V}^0$(NMP) is the molar volume of pure NMP, and m_1 and m_2 are the molalities of the two electrolytes. This equation can be rewritten as

$$\Phi = \frac{1}{m_1 + m_2}\left(\frac{1000 + m_1M_1 + m_2M_2}{d} - \frac{1000}{d^0}\right) \quad (10)$$

where M_1 and M_2 are the molecular weights of the two electrolytes, d is the density of the solution, and d^0 is the density of NMP. Young and Smith[24] have shown that their mixture rule

$$\Phi = \frac{m_1\phi_1 + m_2\phi_2}{m_1 + m_2} \quad (11)$$

accurately represents the data of Wirth for KCl–NaCl,[25] KBr–NaCl,[25] and $NaClO_4$–$HClO_4$[26] mixtures in aqueous solutions. ϕ_1 and ϕ_2 are the molal volumes for the salts in pure NMP at ionic strength corresponding to $m_1 + m_2$. The results of this comparison for the different pairs is shown in Table VIII. The per cent error is larger than the results in H_2O; however, this may be due to the uncertainties in the density data.

In conclusion, this preliminary study of solutes in NMP has shown how the η_r and $\bar{V}^0$ can be used to obtain a better understanding of solute–solvent interactions in a high dielectric solvent system.

Acknowledgment. The author wishes to thank Dr. W. G. Borduin, who directed the experimental part of this research, and Dr. T. B. Hoover for his helpful comments and suggestions. The author also wishes to thank the Office of Saline Water for support of part of this research.

(23) F. J. Millero and W. Drost-Hansen, presented at the 154th National Meeting of the American Chemical Society, Chicago, Ill., Sept 1967.

(24) T. F. Young and M. B. Smith, *J. Phys. Chem.*, **58**, 716 (1954).

(25) H. E. Wirth, *J. Amer. Chem. Soc.*, **59**, 2549 (1937).

(26) H. E. Wirth and F. N. Collier, Jr., *ibid.*, **72**, 5292 (1950).

Paramagnetic Resonance Study of the Triplet States of Various Aromatic Nitrogen Heterocycles, Biphenyl, and Acenaphthene

by Yasuhiko Gondo and August H. Maki

Department of Chemistry, University of California, Riverside, California 92502 *(Received March 14, 1968)*

Electron paramagnetic resonance spectra have been observed on the phosphorescent $^3(\pi,\pi^*)$ states of 5,6:7,8-dibenzoquinoxaline, 1,2:3,4-dibenzophenazine, 1,10-phenanthroline, 5,6-benzoquinoline, 7,8-benzoquinoline, biphenyl, 2,2′-bipyridyl, 4,4′-bipyridyl, and acenaphthene. Magnetophotoselection measurements have also been made on some of these compounds in order to aid in the assignments of the principal axes of the zero-field splitting tensors. Among the determined zero-field splitting parameters, the $|D|$ and $|E|$ values of 0.1068 and 0.000 cm^{-1}, respectively, of the dibenzoquinoxaline are interesting ($|D| = 0.134$ cm^{-1} for triphenylene). Polarization directions of the electronic absorption bands are discussed. Lifetimes of the triplet states and their temperature dependences were observed.

Introduction

Paramagnetic resonance has proven a powerful method for the investigation of phosphorescent triplet states of organic molecules since the initial observation by Hutchison and Mangum[1] of electron paramagnetic resonance signals from triplet naphthalene in a durene single crystal. In addition, it has been shown that observation of triplet-state epr is possible even in glasses,[2-4] and this has led to a variety of applications for these systems. Among them, the technique of magnetophoselection[5-7] has proven especially useful in relating the principal axis system of the zero-field splitting tensor to the optical-polarization axes of a molecule.[7-9]

In this paper, the phosphorescent triplet states of various aromatic nitrogen heterocyclic molecules, biphenyl, and acenaphthene have been investigated by epr spectroscopy in rigid glasses of ethanol and of diethyl ether. Magnetophotoselection studies have been carried out on many of these molecules whose triplet states produce sufficiently intense $\Delta m = 1$ spectra. Phosphorescence lifetimes have been measured. Replacement of an aromatic CH group by a nitrogen atom in a molecule frequently results in an enhancement of the phosphorescence intensity.[10] Although the phosphorescence intensity is not necessarily related to the ease of observing the $\Delta m = 1$ transitions, most of the nitrogen heterocyclic compounds investigated in this paper have produced remarkably intense spectra, thus facilitating the magnetophotoselection studies. The compounds which we have investigated are given in Figure 1.

Experimental Section

Epr spectra were measured using a Varian X-band epr spectrometer (V-4502) having a modulation frequency of 100 kHz. Spectra were recorded with the radiofrequency magnetic field perpendicular to the static field. The static magnetic field was calibrated by means of a proton resonance gauss meter, the frequency of which was monitored by a Hewlett-Packard 5245L electronic counter. The microwave frequency was measured using a Hewlett-Packard 2590A transfer oscillator, 5253B frequency converter, and the same electronic counter.

The sample solutions were sealed in quartz tubes of 4 mm o.d. after degassing on a vacuum line. The sample was irradiated in a slotted-face Varian V-4531 cavity. Light from a 200-W (PEK or Osram) superpressure mercury arc lamp was focused through a quartz optical system. The sample was cooled by a flow of cold nitrogen gas, which was passed through a heat-exchange coil submerged in liquid nitrogen.

The technique of magnetophotoselection was used to aid in the assignment of $\Delta m = 1$ epr transitions and electronic absorption spectra.[7,11] The polarized light was obtained using either a polarizing Polaroid sheet or a glan prism located on a quasi-cylindrical part of the light beam. Either a water sample having 3-cm path or an aqueous solution of nickel sulfate having a 2-cm path was used as an infrared filter. A monochromator was not used. Both flattened and cylindrical quartz

(1) C. A. Hutchison, Jr., and B. W. Mangum, *J. Chem. Phys.*, **29**, 952 (1958); **34**, 908 (1961).

(2) J. H. van der Waals and M. S. de Groot, *Mol. Phys.*, **2**, 333 (1959).

(3) M. S. de Groot and J. H. van der Waals, *ibid.*, **3**, 190 (1960).

(4) W. A. Yager, E. Wasserman, and R. M. R. Cramer, *J. Chem. Phys.*, **37**, 1148 (1962).

(5) Ph. Kottis and R. Lefebvre, *ibid.*, **41**, 3660 (1964).

(6) J. M. Lohste, A. Haug, and M. Ptak, *ibid.*, **44**, 648, 654 (1966).

(7) M. A. El-Sayed and S. Siegel, *ibid.*, **44**, 1416 (1966).

(8) S. Siegel and L. Goldstein, *ibid.*, **43**, 3354 (1965).

(9) G. P. Rabold and L. H. Piette, *Photochem. Photobiol.*, **5**, 733 (1966).

(10) M. A. El-Sayed, *J. Chem. Phys.*, **38**, 2834 (1963).

(11) S. Siegel and H. S. Judeikis, *J. Phys. Chem.*, **70**, 2205 (1966).

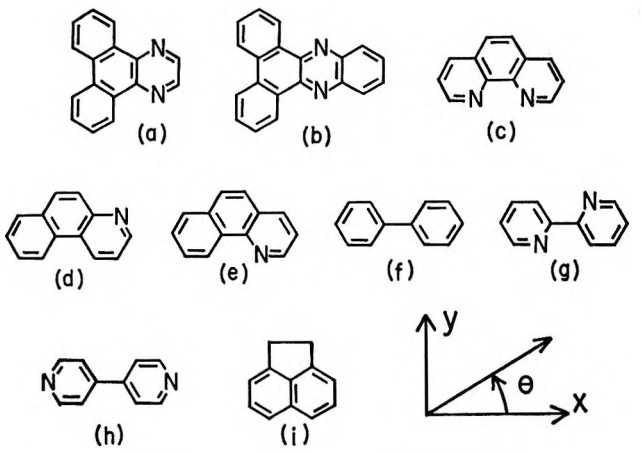

Figure 1. The compounds studied in this work, with coordinate axes: (a) 5,6:7,8-dibenzoquinoxaline, (b) 1,2:3,4-dibenzophenazine, (c) 1,10-phenanthroline, (d) 5,6-benzoquinoline, (e) 7,8-benzoquinoline, (f) biphenyl, (g) 2,2′-bipyridyl, (h) 4,4′-bipyridyl, (i) acenaphthene. A right-handed coordinate system is adopted.

tubes (4 mm o.d.) were used, although a flattened tube was used by El-Sayed and Siegel.[7] Our results were not noticeably affected by flattening the tube. The arrangement of the optical system was essentially the same as that described by Rabold and Piette.[9]

Phosphorescence and its excitation spectrum were measured using a conventional phosphoroscope by exciting the samples with light, from a 450-W xenon arc lamp, which was monochromatized by passing through a Bausch and Lomb monochromator as described previously.[12] The samples, in quartz tubes (7 mm o.d.), were immersed in liquid nitrogen.

Decay constants of phosphorescence were measured by setting the monochromator at an appropriate wavelength and then photographically recording the phosphorescence decay subsequent to excitation by a short pulse of light. The output of a photomultiplier was coupled directly to an oscilloscope.

Decay constants of $\Delta m = 2$ epr transition were measured by setting the static magnetic field at a fixed value which gave a maximum of first-derivative signal and by recording the decay of the maximum after mechanical cessation of excitation.

1,10-Phenanthroline and biphenyl were obtained from Matheson Coleman and Bell. All the other aromatic compounds used in this work were obtained from Aldrich Chemical Co. 5,6:7,8-Dibenzoquinoxaline and 1,2:3,4-dibenzophenazine were recrystallized three and two times from benzene, respectively. 1,10-Phenanthroline monohydrate was recrystallized twice from water and then was dried by heating over phosphorus pentoxide under vacuum. The anhydrous phenanthroline obtained was sublimed under vacuum. 5,6-Benzoquinoline was treated with sulfuric acid in ethanol, and the precipitate obtained was treated with sodium hydroxide in water. This process was repeated three times. The final purification step was vacuum sublimation. The same procedure was applied for 7,8-benzoquinoline. Biphenyl and 2,2′-bipyridyl were recrystallized three times from ethanol. 4,4′-Bipyridyl dihydrochloride was treated with sodium hydroxide in water, and the 4,4′-bipyridyl precipitated was recrystallized twice from hot water. The product 4,4′-bipyridyl dihydrate was dried over phosphorus pentoxide under vacuum. Acenaphthene was recrystallized three times from ethanol. The following solvents were used without further purification: ethanol (U. S. Industries Chemical Co., reagent grade) and diethyl ether (Mallinckrodt, analytical reagent).

Triplet Decay Constants

Phosphorescence and its excitation spectra were measured for every compound studied in this work and compared with published data.[13-17] These spectra confirmed that the observed phosphorescent triplet states were all genuine.

The observed decay constants of the $\Delta m = 2$ epr transition and the phosphorescence are given in Table I. All the decays were exponential within experimental error. Table II shows the temperature effects on the decay constants of phosphorescence observed for 5,6-benzoquinoline, biphenyl, and acenaphthene. Since appreciable differences were not found between the decay constants of the $\Delta m = 2$ epr transition and those of the phosphorescence, the measurements of temperature effects on the decay constants were not carried out for the other compounds. If the fluctuations in the decay constants of the $\Delta m = 2$ epr transition are compared with the temperature dependences of phosphorescence decay constants of these three compounds, it is concluded that the temperature was controlled, as expected, at $-175°$ within a fluctuation of $\pm 5°$ in the epr experiments. For all the compounds studied, we find a good correspondence between the decay constants of the epr transition and those of phosphorescence. This is another confirmation that the genuine phosphorescent states of these molecules were observed in the epr experiments. Incidentally, similar temperature effects have been observed in isopropyl alcohol for the phosphorescences of several aromatic compounds, such as naphthalene, phenanthrene, and biphenyl.[18] The

(12) D. R. Kearns and W. A. Case, *J. Amer. Chem. Soc.*, **88**, 5087 (1966).

(13) For 5,6:7,8-dibenzoquinoxaline and 1,2:3,4-dibenzophenazine, see F. Dörr and H. Gropper, *Ber. Bunsenges. Phys. Chem.*, **67**, 193 (1963).

(14) For azaphenanthrenes, see: Y. Kanda and R. Shimada, *Spectrochim. Acta*, **15**, 211 (1959); H. Gropper and F. Dörr, *Ber. Bunsenges. Phys. Chem.*, **67**, 46 (1963).

(15) For biphenyl, see Y. Kanda, R. Shimada, and Y. Sakai, *Spectrochim. Acta*, **17**, 1 (1961).

(16) For bipyridyls, see Y. Gondo and Y. Kanda, *Bull. Chem. Soc. Jap.*, **38**, 1187 (1965).

(17) For acenaphthene, see A. P. Marchetti and D. R. Kearns, *J. Amer. Chem. Soc.*, **89**, 768 (1967).

(18) G. v. Foerster, *Z. Naturforsch., A*, **18**, 620 (1963).

Table I: The Decay Constants of the Lowest Excited Triplet States[a]

Compd	Concn, $\times 10^{-2}$ mol./l.	Methods: Epr $\Delta m = 2$ transition at $-175 \pm 5°$, sec	Methods: Phosphorescence at $-196°$, sec
5,6:7,8-dibenzoquinoxaline	0.472	0.94	0.95
1,2:3,4-Dibenzophenazine	0.0286	0.27	0.27
1,10-Phenanthroline	0.900	1.36	1.46
5,6-Benzoquinoline	0.743	2.28–2.57[b]	2.97
7,8-Benzoquinoline	0.919	1.95	2.02
2,2′-Bipyridyl	1.40	0.89	0.95
4,4′-Bipyridyl	0.500	0.50	0.53
Biphenyl	0.942	2.61–3.29[b]	4.21
Acenaphthene	1.37	1.69–1.83[b]	2.64

[a] The solvent was diethyl ether for 4,4′-dipyridyl. Ethanol was used for all the other compounds. [b] These variations were due to temperature fluctuations. No appreciable fluctuations were observed in the decay constants of the epr signals for any compounds other than these three.

Table II: Temperature Effect on the Lifetimes of the Phosphorescence of 5,6-Benzoquinoline, Biphenyl, and Acenaphthene in Ethanol[a]

Compd	Temp, °C	Lifetime, sec
5,6-Benzoquinoline	−196	2.97
	−184	2.85
	−177.5	2.45
	−174	1.63
	−170	1.39
	−166	0.082
Biphenyl	−196	4.21
	−185	3.83
	−176	2.98
	−172	3.19
	−171	2.69
Acenaphthene	−196	2.64
	−187	2.64
	−183	2.64
	−176.5	2.28
	−172	1.01
	−171	0.58
	−167	0.14

[a] The concentrations are the same as given in Table I. For these variable-temperature measurements, the sample tube was attached to a large slowly warming copper block whose temperature was monitored by a thermocouple.

cause is a softening of the glass and the onset of diffusion. This effect will be noticeable first in long-lived triplet states. It may be noted that the decay constants of phosphorescence of the aromatic nitrogen heterocyclic compounds all are shorter than those of the parent hydrocarbons. For comparison, decay constants of 16, 3.8, and 4.2 sec were reported for triphenylene, phenanthrene, and biphenyl, respectively,[19] in EPA at 77°K. This shortening may be ascribed to increased spin–orbit coupling caused by nitrogen substitution.[10]

Epr Spectra

The epr spectra observed of triplet molecules in frozen glassy solvents can be classified roughly as $\Delta m = 2$ and $\Delta m = 1$ transitions, where m is the strong-field quantum number of the electron spin. This classification is not rigorous, since at X-band microwave frequencies and for $^3(\pi,\pi^*)$ states of aromatics which have zero-field splittings of ~ 0.1 cm^{-1}, the strong-field spin states are mixed together. In glasses, the $\Delta m = 2$ transitions, or "half-field" transition, is found to occur at about half the magnetic field of the free electron resonance. The $\Delta m = 1$ transitions, which are allowed only in perpendicular polarization (the static magnetic field perpendicular to the microwave magnetic field) occur as rather sharp peaks, roughly symmetrically distributed about the normal $g = 2$ field. The fields at which the sharp peaks are observed are usually called the stationary resonance fields (srf) and occur for those triplets whose principal x, y, and z axes are closely aligned with the static magnetic field. Each orientation gives rise to a pair of transitions, so that six of these transitions may be observed in all. In triplets whose zero-field splitting tensor[20–22] has axial symmetry, the x and y fields are the same, and only four $\Delta m = 1$ transitions are observed. A numerical analysis of the line shape of the $\Delta m = 2$ transition and its relationship to the zero-field splitting tensor has been given by Kottis and Lefebvre.[23] The $\Delta m = 1$ transitions have been analyzed by Wasserman, Snyder, and Yager[24] and by Kottis and Lefebvre.[25] Our discussion of the epr spectra refers to these treatments.

The degeneracy of the triplet state is lifted even in zero magnetic field as a result of dipolar spin–spin interactions between unpaired electrons and, to some extent, by spin–orbit coupling. Spin–orbit contributions are expected to be relatively more important in aromatic nitrogen heterocyclic molecules than in their parent hydrocarbons. The spin Hamiltonian for the zero-field interaction may be expressed as

$$\mathcal{H} = DS_z^2 + E(S_x^2 - S_y^2) \qquad (1)$$

(19) R. E. Kellogg and R. P. Schwenker, *J. Chem. Phys.*, **41**, 2860 (1964).

(20) M. Gouterman and W. Moffitt, *ibid.*, **30**, 1107 (1959).

(21) R. McWeeny and Y. Mizuno, *Proc. Roy. Soc.*, **A259**, 554 (1961).

(22) A. D. McLachlan, *Mol. Phys.*, **6**, 441 (1963).

(23) Ph. Kottis and R. Lefebvre, *J. Chem. Phys.*, **39**, 393 (1963).

(24) E. Wasserman, L. Snyder, and W. A. Yager, *ibid.*, **41**, 1763 (1964).

(25) Ph. Kottis and R. Lefebvre, *ibid.*, **41**, 379 (1964).

or by

$$\mathcal{H} = -(XS_x^2 + YS_y^2 + ZS_z^2) \quad (2)$$

The parameters in these expressions are related by $D = -{}^3/_2 Z$ and $E = {}^1/_2(Y - X)$. X, Y, and Z are the principal values of the zero-field splitting tensor,[20-22] and S_x, S_y, and S_z are the spin angular-momentum operators for the triplet state.

The quantity $D^* = (D^2 + 3E^2)^{1/2}$ may be obtained from the position of the $\Delta m = 2$ transition by the relation

$$D^* = \sqrt{3}[{}^1/_4(h\nu)^2 - (g\beta H_{min})^2]^{1/2} \quad (3)$$

in which ν is the microwave frequency, g is the spectroscopic splitting constant of the triplet state (assumed isotropic in this work), and β is the Bohr magneton. H_{min} is the minimum field for the $\Delta m = 2$ transitions of the polycrystalline sample, where the "piling up" of intensity occurs, leading to the observed epr peak.[2,3] H_{min} was originally thought to coincide with H_0, the low-field derivative maximum of the transition, but the detailed analysis of the line shape[23] has yielded a relationship which can be expressed as

$$H_{min} = H_0 + 0.45\Delta H_0 \quad (4)$$

where ΔH_0 is the distance between the low-field derivative maximum and the first zero.

The srf of the $\Delta m = 1$ spectra were used to obtain absolute values of the zero-field splitting parameters by means of the relation[24-26]

$$|X| = (g\beta)^2(H_{x_2}^2 - H_{x_1}^2)/6h\nu \quad (5)$$

and the similar expressions for $|Y|$ and $|Z|$. H_{x_2} and H_{x_1} are the magnetic fields of the high- and low-field x-axis peaks, respectively, and g is assumed to be isotropic and equal to the free-electron value. The root-mean-square zero-field splitting parameter, D^*, is given by

$$D^* = [{}^3/_2(X^2 + Y^2 + Z^2)]^{1/2} \quad (6)$$

In order to establish the validity of eq 4, we have calculated D^* for the triplet states studied: (a) using eq 3 with H_0 in place of H_{min}, (b) using eq 3 with H_{min} calculated from eq 4, and (c) using values of X, Y, and Z obtained from the $\Delta m = 1$ spectra in eq 6. The results are presented in Table III. Except for the triplet state of 5,6:7,8-dibenzoquinoxaline, H_{min} is seen to give superior agreement with the $\Delta m = 1$ spectra than is H_0.

The zero-field splitting parameters which were obtained from the $\Delta m = 1$ transitions are presented in Table IV. Values of about 0.1 cm^{-1} were obtained for D in all cases, which is consistent with $^3(\pi,\pi^*)$ phosphorescent states.[27,28] Relative signs of the zero-field splitting parameters were obtained from the requirement that the trace of the tensor should vanish, *i.e.*

$$X + Y + Z = 0$$

Table III: Root-Mean-Square Zero-Field Splitting Parameters, D^* (cm^{-1})[a]

Compd	$\Delta m = 2$ transition[b] H_0	$\Delta m = 2$ transition[b] H_{min}	$\Delta m = 1$ transitions
5,6:7,8-Dibenzoquinoxaline	0.1064	0.1049	0.1068
1,2:3,4-Dibenzophenazine	0.0930	0.0909	0.0905
1,10-Phenanthroline	0.1344	0.1331	0.1334
5,6-Benzoquinoline	0.1323	0.1311	0.1316
7,8-Benzoquinoline	0.1310	0.1293	0.1296
Biphenyl	0.1113	0.1092	0.1096
2,2′-Bipyridyl	0.1129	0.1115	0.1118
4,4′-Bipyridyl	0.1222	0.1202	0.1199
Acenaphthene	0.1012	0.0988	0.0995

[a] Solvents and concentrations are given in Table I. An isotropic g value of 2.0023 was assumed. See also Table IV. [b] For definitions of H_0 and H_{min}, see the text and eq 4.

Absolute signs were assigned in some cases by comparison with the hydrocarbon analogs for which they are known.

The fundamental epr data are shown in Table V. Quantitative results of magnetophotoselection measurements are given in Table VI for those triplets which gave sufficiently intense $\Delta m = 1$ spectra for quantitative study. The results of magnetophotoselection studies and details of the assignment of zero-field splitting parameters are given in the following sections, in which we discuss the individual triplet states.

Detailed Results and Discussion

A. 5,6:7,8-Dibenzoquinoxaline. The phosphorescence of 5,6:7,8-dibenzoquinoxaline is extraordinarily intense,[13] and it was also easy to observe the $\Delta m = 1$ spectrum, which is shown in Figure 2. The strong resonance at $g = 2$ from free-radical photodecomposition products can be observed in Figure 2. Photodecomposition was extensive, so two separate samples had to be used to obtain accurate field measurements. The spectrum is quite similar to that of the parent hydrocarbon, triphenylene, although its $|D|$ value of 0.1068 cm^{-1} is quite a bit less than the value of 0.134 cm^{-1} reported[3,26] for triphenylene. Replacement of a CH group by a nitrogen atom is not expected to affect seriously the zero-field splitting parameters, as can be seen from a comparison of quinoxaline,[29] quinoline, and isoquinoline[30,31] with naphthalene.[1] The molecular symmetry of 5,6:7,8-dibenzoquinoxaline does not re-

(26) J. B. Farmer, C. L. Gardner, and C. A. McDowell, *J. Phys. Chem.*, 69, 953 (1965).
(27) H. Sternlicht, *J. Chem. Phys.*, 38, 2316 (1963).
(28) J. Higuchi, *ibid.*, 39, 1847 (1963).
(29) J. S. Vincent and A. H. Maki, *ibid.*, 39, 3088 (1963).
(30) J. S. Vincent and A. H. Maki, *ibid.*, 42, 865 (1965).
(31) B. Smaller, *ibid.*, 37, 1578 (1962).

Table IV: Zero-Field Splitting Parameters (cm^{-1}) from $\Delta m = 1$ Transitions[a]

Compd	X	Y	Z	$D (= -\frac{3}{2}Z)$	$E (= \frac{1}{2}(Y - X))$
5,6:7,8-Dibenzoquinoxaline	±0.0361[b]	$Y = X$	∓0.0712	±0.1068	0.000
1,2:3,4-Dibenzophenazine	±0.0447	±0.0126	∓0.0574	±0.0862	∓0.0161
1,10-Phenanthroline	0.0829	−0.0140	−0.0692	0.1038	−0.0485
5,6-Benzoquinoline[c]	0.0819	−0.0136	−0.0682	0.1023	−0.0477
7,8-Benzoquinoline[c]	0.0805	−0.0131	−0.0674	0.1011	−0.0468
Biphenyl	±0.0400	±0.0329	∓0.0729[d]	±0.1094	∓0.0036
2,2′-Bipyridyl[c]	±0.0488	±0.0243	∓0.0733	±0.1099	∓0.0122
4,4′-Bipyridyl	±0.0439	±0.0359	∓0.0798[d]	±0.1197	∓0.0040
Acenaphthene	0.0462	0.0181	−0.0644	0.0966	−0.0140

[a] Solvents and concentrations are given in Table I. Coordinate system is given in Figure 1. An isotropic g value of 2.0023 is assumed. Absolute signs for the zero-field splitting parameters of the three azaphenanthrenes and acenaphthene were obtained from a comparison with those of the parent hydrocarbons. [b] Obtained with eq 4. See the text. [c] The principal axes of the zero-field splitting tensors should be different from the coordinate axes defined in Figure 1. For convenience, the zero-field splitting parameters are listed under the column headings of X, Y, and Z. [d] The z-axis peaks were not observed. These Z's were obtained from X and Y by using the relation $X + Y + Z = 0$.

Table V: Srf and Klystron Frequencies for Triplet State Epr Lines[a]

Triplet	$\Delta m = 2$			$\Delta m = 1$						
	H_0[b]	H_{min}[b]	ν[c]	H_{z_1}[b]	H_{x_2}[b]	H_{y_1}[b]	H_{y_2}[b]	H_{z_1}[b]	H_{z_2}[b]	ν[c]
5,6:7,8-Dibenzoquinoxaline[d]	1483.4	1487.5	9093.8	2606	3782	2606	3782	2102	4387	9095.3[e]
1,2:3,4-Dibenzophenazine	1519.5	1524.4	9105.1	2500	3946	2997	3407	2322	4168	9106.5
1,10-Phenanthroline	1393.7	1398.2	9091.7	1893	4567	2909	3373	2075	4326	9096.0
5,6-Benzoquinoline[f]	1402.7	1406.9	9099.4	1911	4550	2920	3369	2091	4311	9096
7,8-Benzoquinoline[f]	1407.8	1413.7	9101.6	1934	4529	2932	3367	2108	4300	9099.4
Biphenyl	1469.8	1475.8	9095.4	2542	3847	2650	3725	*g*	*g*	9095.4
2,2′-Bipyridyl[f]	1464.8	1468.8	9093.4	2405	3992	2782	3580	2066	4419	9093[h]
4,4′-Bipyridyl[i]	1436.2	1442.6	9094.0	2465	3902	2583	3761	*g*	*g*	9094.8[j]
Acenaphthene[k]	1499.2	1505.3	9104.2	2465	3961	2895	3485	2210	4277	9093.5

[a] In ethanol glass at −175 ± 5°, unless otherwise specified. The concentrations are given in Table I. Assignment of principal axes from magnetophotoselection, unless otherwise indicated. [b] The magnetic field is expressed in gauss. [c] The klystron frequency is expressed in megacycles per second. [d] The zero-field splitting tensor has axial symmetry. Equation 4 was used to obtain H_{x,y_1} and H_{x,y_2}. The principal axes were assigned by comparison with the parent hydrocarbon. [e] The frequency quoted is for the X and Y transitions. The frequency for the Z transitions was 9092.6 MHz. [f] See footnote *c* to Table IV. [g] The z-axis peaks were too weak to observe. [h] The value quoted is for X and Z transitions. The frequency of Y transitions was 9107 MHz. [i] Run in diethyl ether glass. The principal axes were assigned by comparison with biphenyl triplet. [j] The value quoted is for X transitions. The frequency of Y transitions was 9095.5 MHz. [k] Assignment of principal axes by comparison with naphthalene triplet state.

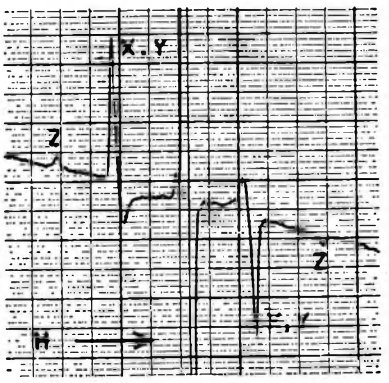

Figure 2. Epr $\Delta m = 1$ spectrum of the phosphorescent triplet state of 5,6:7,8-dibenzoquinoxaline in ethanol glass. See Table V.

quire an axially symmetric zero-field splitting tensor, so the result $E = 0.000$ cm^{-1} is surprising, as is the departure of D from its value in the triphenylene triplet. These discrepancies may arise partly from enhanced spin–orbit coupling effects in the aza aromatic molecule.[32]

B. 1,2:3,4-Dibenzophenazine. The phosphorescence of 1,2:3,4-dibenzophenazine is very intense, as reported in the literature,[13] and it was not difficult to observe the $\Delta m = 1$ transitions in ethanol glass at concentrations as low as 10^{-4} mol/l. The $\Delta m = 1$ spectrum is shown in Figure 3. A concentration higher than 3×10^{-4} mol/l. could not be obtained because of limited solubility in ethanol. The assignment of the peaks was aided by a magnetophotoselection experiment on the low-field half of the spectrum. From the electronic absorption spectrum reported by Dörr and Gropper[13] and the phosphorescence excitation spectrum

(32) J. W. McIver, Jr., and H. F. Hameka, *J. Chem. Phys.*, 45, 767 (1966).

Table VI: Magnetophotoselection Studies. Relative Intensities of X, Y, and Z Transitions[a]

Triplet	Srf (assignment), Gauss	Excitation: First absorption band[b] Isotropic[d]	E ‖ H	E ⊥ H	Excitation: λ ≥250 mμ[c] Isotropic[d]	E ‖ H	E ⊥ H
1,2:3,4-Dibenzophenazine	2322 (Z)	0.14	0.07	0.19	...	...	...
	2500 (X)	0.33	0.56	0.12	...	...	...
	2977 (Y)	0.53	0.37	0.69	...	...	...
1,10-Phenanthroline	1893 (X)	...	...	...	0.23	0.39	0.12
	2075 (Z)	...	...	...	0.29	0.13	0.35
	2909 (Y)	...	...	...	0.48	0.49	0.53
5,6-Benzoquinoline[e]	1911 (X)	0.23	0.45	<0.1	0.24	0.48	0.06
	2091 (Z)	0.25	0.19	0.34	0.26	0.14	0.33
	2920 (Y)	0.52	0.36	0.66	0.50	0.39	0.61
7,8-Benzoquinoline[e]	1934 (X)	0.21	0.37	<0.1	0.22	0.44	0.07
	2108 (Z)	0.22	0.20	0.38	0.23	0.13	0.28
	2932 (Y)	0.57	0.43	0.62	0.56	0.44	0.66

[a] Magnetophotoselection measurements were made on biphenyl and 2,2′-bipyridyl as well, but the results are of only qualitative significance because of the poor signal-to-noise ratio. Measurements in ethanol glass were made at $-175 \pm 5°$. Concentrations are given in Table I. **E** and **H** stand for the electric vector of the exciting light and the static magnetic field, respectively. [b] The ultraviolet polarizing Polaroid sheet was used, so only the longest wavelength transition was excited. [c] The glan prism was used. Effective exciting wavelengths were longer than 250 mμ. [d] Isotropic exciting light. No polarizer was used. [e] See footnote c to Table IV.

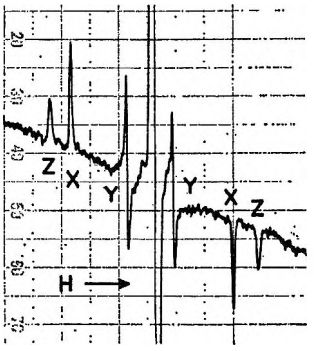

Figure 3. Epr $\Delta m = 1$ spectrum of the phosphorescent triplet state of 1,2:3,4-dibenzophenazine in ethanol glass. See Table V.

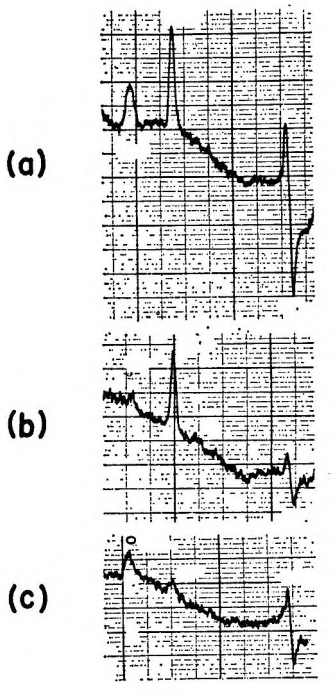

Figure 4. Magnetophotoselection measurement on the epr $\Delta m = 1$ spectrum of 1,2:3,4-dibenzophenazine: (a) isotropic excitation, (b) polarized excitation with the electric vector **E** of the exciting light parallel to the static magnetic field **H**, (c) polarized excitation with **E** perpendicular to **H**. See Table VI and the text. Only half of the $\Delta m = 1$ spectrum is shown. Excitation was into the longest wavelength absorption band.

obtained in this work, it is apparent that the polarized excitation light is absorbed principally in the longest wavelength absorption band of the molecule, which is assumed to be the long-axis (x axis of Figure 1) polarized ^1L_b band, since the polarizing Polaroid sheet used in this work transmits 50% of the incident light at 400 mμ, 20% at 340 mμ, and 0% at 338 mμ. A water filter described in the Experimental Section was used as an infrared filter. The spectra obtained in the magnetophotoselection experiments are shown in Figure 4. The quantitative relative peak heights are given in Table VI. It is evident that the 2500-G peak of Figure 3 can be assigned to an X transition, since only this peak was enhanced with the **E** ‖ **H** excitation, **E** and **H** being the electric vector of the exciting light and the static magnetic field, respectively. The peaks at 2322 and 2997 G are shown to correspond from Figure 4 and Table VI to the molecular axes perpendicular to the polarization of the ^1L_b absorption band. The assignment of these peaks is not unambiguous. If we assume that the absolute value of D exceeds that of E, which is the case for all the aromatic $^3(\pi,\pi^*)$ states thus far investigated in single crystals, then the 2322-G peak must be assigned as the Z transition and the 2997-G peak

must be assigned as the Y transition. This assignment leads to the zero-field splitting parameters, which are given in Table IV with their relative signs. If the longest wavelength transition should turn out to be actually short-axis polarized, then the assignment of the X and Y peaks is interchanged, leading to a reversal of the relative signs of D and E, given in Table IV.

C. 1,10-Phenanthroline, 5,6-Benzoquinoline, and 7,8-Benzoquinoline. The three azaphenanthrenes gave fairly intense phosphorescence, in agreement with those observed previously.[14] The epr spectra were sufficiently intense that magnetophotoselection measurements were possible on the $\Delta m = 1$ transitions. The zero-field splitting parameters are given in Tables III and IV, and the results of magnetophotoselection experiments are presented in Table VI. The epr absorption of the lowest triplet state of phenanthrene has been studied in a biphenyl-host single crystal[33] and that of phenanthrene-d_{10} has been measured[34] in a low-temperature glass. The assignment of the $\Delta m = 1$ peaks of the azaphenanthrenes studied in this work was made by comparison with the single-crystal measurements, assuming that a nitrogen atom substitution does not affect seriously the zero-field splitting tensor of the low-lying $^3(\pi,\pi^*)$ state.[29-31] The magnitude of D is somewhat larger for each of the azaphenanthrenes studied than for phenanthrene.[33] The principal axes of the zero-field splitting tensors of the benzoquinolines are not expected to coincide with the coordinate system defined in Figure 1, although the deviations may be small. For convenience, however, the expressions X peaks, etc., are used even for the benzoquinolines. The magnetophotoselection experiments were done under two conditions of excitation. (a) The polarizing Polaroid sheet was used, with the same infrared filter as in the dibenzophenazine experiment. The excitation was thus limited to the longest wavelength electronic absorption band which corresponds to the ^1L_b band of phenanthrene. (b) A glan prism and the same filter were used so that the excitation was into bands of wavelengths longer than 250 mμ, *i.e.*, into absorption bands corresponding to both the ^1L_a and ^1L_b bands of phenanthrene. The effective limit of 250 mμ was obtained from the phosphorescence excitation spectra. As can be seen from Table VI, the longest wavelength transition of each of the azaphenanthrenes is polarized at least roughly along the x direction of the zero-field splitting tensor, since the X peaks are the only ones enhanced with the $\mathbf{E} \parallel \mathbf{H}$ excitation. Because of the weakness of the ^1L_b band of 1,10-phenanthroline relative to the benzoquinolines, the intensity of the epr spectrum obtained under conditions a did not allow the quantitative measurement of the intensities. It was obvious, however, that the X peak was relatively enhanced with $\mathbf{E}\|\mathbf{H}$. With excitation into both bands, under conditions b, the same polarization tendencies are found for the epr transitions of the azaphenanthrenes, as can be seen from Table VI. This shows that the second longest wavelength transitions of the azaphenanthrenes are polarized roughly along the long axis of the molecules. The numerical data given in Table VI show that the X peaks of both benzoquinolines are relatively more enhanced under $\mathbf{E}\|\mathbf{H}$ excitation under conditions b than under conditions a. This is evidence for a smaller deviation of the zero-field x axis from the polarization direction of the second longest wavelength transition than that of the longest wavelength transition. Gropper and Dörr[14] have measured the polarization spectra of absorption with respect to fluorescence for 1,10-phenanthroline and 7,8-benzoquinoline. The polarization directions of the two longest wavelength absorptions were found to be nearly parallel, which is additional evidence supporting our conclusions from the magnetophotoselection measurements.

D. Biphenyl, 2,2′-Bipyridyl, and 4,4′-Bipyridyl. The epr data for biphenyl and its two nitrogen-substituted analogs are given in Tables IV and V. The solvent was ethanol, except for 4,4′-bipyridyl for which diethyl ether was used because of rapid and extensive photodecomposition in the former solvent. Even in ether, only the X and Y peaks of the $\Delta m = 1$ spectrum could be observed. From the phosphorescence excitation spectra, it was found that the excitation maxima occurred at 286.5, 303.5, and 303.5 mμ, respectively, for biphenyl, 2,2′-bipyridyl, and 4,4′-bipyridyl. Magnetophotoselection measurements were made only for biphenyl and 2,2′-bipyridyl using the glan prism as outlined in the previous section and an aqueous solution of nickel sulfate described in the Experimental Section as an infrared filter. A magnetophotoselection experiment has also been carried out by Siegel and Judeikis[11] for biphenyl and some related compounds.

We will discuss the results for 2,2′-bipyridyl first, since there is no problem of vibronic interaction in the electronic absorption bands responsible for the population of the triplet state in this molecule. The absorption bands have maxima at 280 and 233 mμ,[35] and both are polarized essentially along the x axis, as shown in Table VII. The values of θ, the deviation of the transition moment from the x axis, as well as the assignment of the transitions are theoretical.[36] Another theoretical calculation[37] has also revealed the essential features of the two absorption bands. Because of the low symmetry of the molecule (a *trans* conformation is assumed[37]), the principal axes of the zero-field splitting tensor are not expected to coincide with the axis sys-

(33) R. W. Brandon, R. E. Gerkin, and C. A. Hutchison, Jr., *J. Chem. Phys.*, **37**, 447 (1962); **41**, 3717 (1964).

(34) M. S. de Groot and J. H. van der Waals, *Physica*, **29**, 1128 (1963).

(35) P. Krumholz, *J. Amer. Chem. Soc.*, **73**, 3487 (1951).

(36) Y. Gondo, unpublished results.

(37) Y. Gondo, *J. Chem. Phys.*, **41**, 3928 (1964).

tem defined in Figure 1. For convenience, however, the expressions x axis, etc., will be used for this molecule. The epr absorptions at 2405 and 3992 G (Table V) are assigned to X peaks, since they persist with $\mathbf{E} \parallel \mathbf{H}$ but disappear with $\mathbf{E} \perp \mathbf{H}$. Since the Z peak was too weak to be observed using polarized excitation, the remaining peaks were assigned on the basis that the value of $|D|$ is found to be larger than $|E|$ in all aromatic $^3(\pi,\pi^*)$ states thus far investigated. From the similarity of the epr spectra of biphenyl and 4,4′-bipyridyl to that of 2,2′-bipyridyl, a similar assignment of D and E values was obtained by analogy. They are given in Table IV. The values obtained for biphenyl are in good agreement with those obtained by Siegel and Judeikis.[12]

Table VII: Electronic Excitation Energies and Intensities Associated with Transitions from the Ground State in Biphenyl and 2,2′-Bipyridyl

Obsd excitation energy (f or ϵ),[b] eV	Calcd[a] Excitation energy, eV	Calcd[a] Polarization[c] (θ)	Calcd[a] f[b]	Calcd[a] Symmetry[d]
	(1) Biphenyl			
5.02[e] (0.44)	4.95	0°	0.797	$^1B_{2u}$
	4.70		0.000	$^1B_{1g}$
4.18[f]	4.66		0.000	$^1B_{3u}$
4.16[g]				
	(2) 2,2′-Bipyridyl			
5.32[h] (10,200)	5.15	−8° 55′	0.408	^1B_u
	4.64		0.000	^1A_g
4.43[h] (13,300)	4.34	6° 40′	0.422	^1B_u

[a] Reference 36. The *trans* conformation was assumed. [b] f, oscillator strength; ϵ, molar extinction coefficient. [c] θ is defined in Figure 1. [d] Character tables are given in, for example, H. Eyring, J. Walter, and G. E. Kimball, "Quantum Chemistry," John Wiley and Sons, Inc., New York, N. Y., 1944. [e] Solution, absorption maximum. See Y. Gondo, ref 37. [f] Crystal, absorption onset. See ref 37. [g] Solution, see ref 37. [h] Solution, see ref 35 and 37.

Magnetophotoselection measurements on biphenyl produced a result similar to that described above on 2,2′-bipyridyl. Again, the Z peaks were too weak to be observed. The result obtained shows that the excitation was predominantly into the absorption band polarized along the long molecular axis. In the electronic absorption spectrum of biphenyl, there is a problem of vibronic interaction. In other words, the longest wavelength absorption, the onset of which occurs around 300 mμ, is due to a forbidden transition. The assignment of the longest wavelength transitions is given in Table VII. The maximum of the phosphorescence excitation spectrum is found at 286.5 mμ, as mentioned above. Thus it seems controversial to assign the absorption band responsible for populating the triplet state only to the 250-mμ band in biphenyl.[12] There is no positive reason to neglect the role of the forbidden transition in the excitation of the triplet state in biphenyl. Incidentally, molecular orbital calculations[36,37] suggest the presence of two forbidden transitions at wavelengths longer than 250 mμ, as shown in Table VII. These forbidden transitions may become allowed by vibronic mixing with the long-axis polarized intense transitions. Because of these problems, the magnetophotoselection study of the triplet state in 2,2′-bipyridyl provides a more secure basis for the assignment of the $\Delta m = 1$ peaks of biphenyl and the bipyridyls than does the corresponding study on biphenyl.

From a theoretical point of view it would be interesting to carry out a magnetophotoselection study on the triplet state of 4,4′-bipyridyl, since it has been found that the longest wavelength absorption band of this molecule corresponds to an allowed transition polarized along the short axis of the molecule.[36] The photodecomposition of this compound prevented us from doing this experiment.

E. Acenaphthene. The epr spectrum of the triplet state of acenaphthene is quite similar to that of naphthalene[38] and naphthalene-d_8.[24] Our assignment of the zero-field splitting tensor is made by analogy with the single-crystal study of naphthalene by Hutchison, *et al.*,[1] with the absolute signs as determined by Hornig and Hyde.[39]

Acknowledgments. This work was supported by the National Institutes of Health, Public Health Service, by means of Grant GM 12327, for which we are deeply grateful. We wish to thank Professor David R. Kearns for the use of his facilities for the optical measurements.

(38) M. S. de Groot and J. H. van der Waals, *Mol. Phys.*, **6**, 545 (1963).

(39) A. W. Hornig and J. S. Hyde, *ibid.*, **6**, 33 (1963).

The Hydration of Pyridine in Organic Solvents

by James R. Johnson, Paul J. Kilpatrick, Sherril D. Christian, and Harold E. Affsprung[1]

Department of Chemistry, University of Oklahoma, Norman, Oklahoma 73069 *(Received March 18, 1968)*

Measurements have been made of the solubility of water at various water activities in solutions of pyridine in the solvents cyclohexane, CCl_4, toluene, benzene, and 1,2-dichloroethane at 25°. Hydration constants for formation of the pyridine monomer monohydrate and dimer monohydrate have been inferred for each system. In addition, the analysis of data indicates that the trihydrate or dihydrate of monomeric pyridine is present at the higher water activities in all the solvents except cyclohexane. A method for predicting the effect of solvation on molecular complex formation reactions is developed and used in correlating the hydration data for pyridine.

Introduction

Although there have been several reports of the molecular interaction of water and pyridine, relatively little quantitative information is available about molecular complexes of the two compounds. This study is concerned with the hydrogen bonding of pyridine and water at low concentrations in a number of organic solvents of varying reactivity. Techniques reported earlier have been used to determine the stoichiometry and equilibrium constants for the hydrated species.[2-4]

We recently reported a method for predicting the effects of solvation on molecular complex formation equilibria and applied the method to correlate Gibbs free energy data for the formation of pyridine monohydrate.[5] The technique is given a more general development in this article and is utilized in treating the solvation of other hydrates of pyridine.

Experimental Section and Results

Partition measurements were obtained at 25.0 ± 0.1°, using techniques similar to those reported previously.[3,4] The materials were purified by distillation through a 30-plate Oldershaw column.

Solutions were analyzed for total pyridine spectrophotometrically, using the peak at 251 mμ. Aqueous solutions of pyridine were found to obey Beer's law at this wavelength over the concentration range 4×10^{-6} to 6×10^{-5} *M*. Aqueous solutions were analyzed for pyridine after diluting an aliquot with water to a concentration in the range 4×10^{-6} to 6×10^{-5} *M*. Pyridine in organic solutions was first extracted into a known large quantity of water and then the aqueous extract was analyzed. Since a minute trace of benzene or toluene absorbs strongly at 251 mμ, the analytical technique had to be modified for these systems. Pyridine in a known quantity of organic solution (1 ml) was first extracted into 100 ml of water at 25°. An aliquot of the aqueous extract (usually 10 ml) was then added to a small, known quantity of carbon tetrachloride (usually 1 ml) and further diluted with water until the aqueous concentration of pyridine was in the range 4×10^{-6} to 6×10^{-5} *M*. The CCl_4 served to remove most of the benzene or toluene which had been present in the aqueous extract of the aromatic pyridine solution. The absorbance of the final aqueous extract was determined and was compared with the absorbance of a standard sample prepared similarly.

Measurements of the solubility of water in organic pyridine solutions at several water activities were obtained using the solute isopiestic method described earlier.[2] Organic solutions were equilibrated by vapor-phase contact with aqueous solutions of calcium chloride of known water activity. After approximately 2 days, samples of the organic solutions were withdrawn and titrated by the Karl Fischer method. The Karl Fischer reagent was standardized alternatively by titrating weighed amounts of sodium tartrate dihydrate or by titrating a 25° water-saturated benzene solution. (It was assumed that the solubility of water in benzene at 25° was 0.0350 *M* at unit water activity.[6])

Table I gives partition data for pyridine distributed between water and the organic solvents cyclohexane, carbon tetrachloride, toluene, benzene, and 1,2-dichloroethane at 25°. The ratio of the concentration of pyridine in the organic phase, f_P°, to the concentration of pyridine in the water phase, c_P^W, appears to be constant to within experimental uncertainty, over the concentration range investigated. The approximate constancy of this ratio indicates that the concentration of species having more than one pyridine molecule per aggregate is small. The following distribution constants, c_P°/c_P^W, for monomeric pyridine distributed

(1) Deceased August 5, 1967.

(2) S. D. Christian, H. E. Affsprung, J. R. Johnson, and J. D. Worley, *J. Chem. Educ.*, **66**, 1629 (1962).

(3) J. R. Johnson, S. D. Christian, and H. E. Affsprung, *J. Chem. Soc.*, 1 (1965).

(4) J. R. Johnson, S. D. Christian, and H. E. Affsprung, *ibid.*, 764 (1967).

(5) S. D. Christian, J. R. Johnson, H. E. Affsprung, and P. J. Kilpatrick, *J. Phys. Chem.*, **70**, 3376 (1966).

(6) J. R. Johnson, S. D. Christian, and H. E. Affsprung, *J. Chem. Soc.*, 77 (1966).

Table I: Partition Data for Pyridine at 25°

f_P°, mol/l.	C_P^W, mol/l.	f_P°, mol/l.	C_P^W, mol/l.
Pyridine–Water–1,2-Dichloroethane		Pyridine–Water–Carbon Tetrachloride	
0.0602	0.0117	0.0511	0.0282
0.1120	0.0211	0.1049	0.0525
0.1587	0.0334	0.1464	0.0808
0.1981	0.0401	0.2074	0.1041
0.2614	0.0584	0.2348	0.1363
0.3198	0.0684	0.3032	0.1773
0.3907	0.0809	0.3434	0.1938
0.4100	0.0865	0.3747	0.2183
0.4809	0.1015	0.4359	0.2453
0.5147	0.1152	0.4664	0.2646
Pyridine–Water–Benzene		Pyridine–Water–Cyclohexane	
0.0611	0.0107	0.0412	0.0762
0.0895	0.0193	0.0820	0.1512
0.1308	0.0350	0.1198	0.2139
0.1871	0.0563	0.1532	0.2875
0.2376	0.0692	0.1898	0.3667
0.2568	0.0740	0.2252	0.4415
0.2943	0.0909	0.2477	0.5010
0.3492	0.1094	0.2750	0.5862
0.4155	0.1351	0.3289	0.6514
0.4540	0.1495	0.3571	0.7439
Pyridine–Water–Toluene			
0.0535	0.0235		
0.1056	0.0487		
0.1542	0.0716		
0.2111	0.0965		
0.2592	0.1238		
0.3024	0.1407		
0.3348	0.1705		
0.4006	0.1922		
0.4271	0.2051		
0.4713	0.2413		

between the organic solvents and water were determined: 0.49, 1, 71, 1.95, 3.00, and 4.11 for the organic solvents cyclohexane, carbon tetrachloride, toluene, benzene, and 1,2-dichloroethane, respectively.

Table II gives water solubility data expressed in formal concentrations, f_W°, for the pyridine solutions in organic solvent at various fixed water activities, a_W, at 25°. Figure 1 shows a typical plot of Δf_W°, the increase in water solubility in the organic phase owing to the presence of pyridine, *vs.* f_P° for the benzene system.

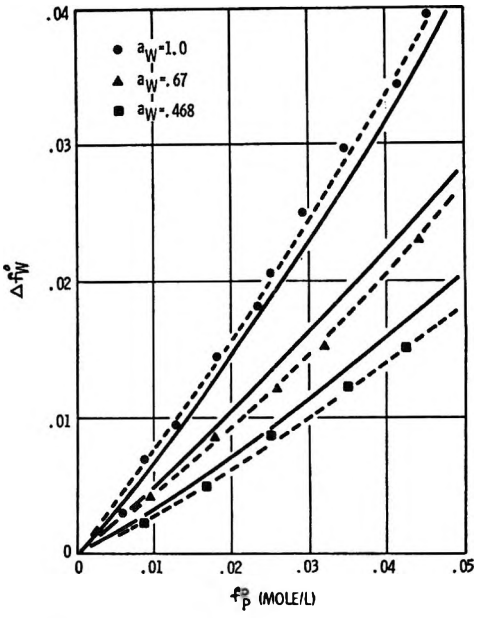

Figure 1. A plot of Δf_W° *vs.* f_P° for the pyridine–water–benzene system.

Discussion

A. Equilibrium Constants. Thompson[7] and Saumagne and Josien[8] have measured infrared spectra of mixtures of pyridine and water in carbon tetrachloride, from which they conclude that pyridine forms a 1:1 hydrate. Sidorov[9] has postulated the existence of both the 1:1 hydrate and a 2:1 hydrate in which the hydrogen atoms of a water molecule bridge two pyridine molecules. In considering dilute solutions of water in pure pyridine, he postulated a complex having more than one water molecule per aggregate; however, he concluded that the solubility of water was too small in carbon tetrachloride to allow a study to be made of complexes having more than one water molecule per aggregrate.

Mohr, Wilk, and Barrow[10] have studied the hydration of various organic bases in CCl_4. From their studies they conclude that at low base concentration a 1:1 hydrate is present, but that at higher concentrations there is evidence for a 2:1 hydrate. Li and coworkers[11,12] have reported pmr data for mixtures of water and several bases in cyclohexane, from which they infer that 1:1 and 2:1 hydrates are present. More recently, Gregory, Christian, and Affsprung[13] have investigated the hydration of cyclohexylamine and its methyl derivatives in benzene and of triethylamine in several organic solvents. They conclude that the 1:1 hydrate is the important molecular complex in these systems and that the dimer hydrate is not present in significant amounts at amine concentrations up to about 0.5 *M*.

Initially, attempts were made to analyze the water solubility data obtained here by assuming the presence of only two hydrated species

(7) W. K. Thompson, *J. Chem. Soc.*, 4028 (1964).

(8) P. Saumagne and M. L. Josien, *Bull. Soc. Chim. Fr.*, **6**, 813 (1958).

(9) A. N. Sidorov, *Opt. Spectry.* (USSR), **8**, 24 (1960).

(10) S. C. Mohr, W. D. Wilk, and G. M. Barrow, *J. Amer. Chem. Soc.*, **87**, 3048 (1965).

(11) F. Takahashi and N. C. Li, *ibid.*, **88**, 1117 (1966).

(12) S. F. Ting, S. M. Wang, and N. C. Li, *Can. J. Chem.*, **45**, 425 (1967).

(13) M. D. Gregory, S. D. Christian, and H. E. Affsprung, *J. Phys. Chem.*, **71**, 2283 (1967).

Table II: Water Solubility Data for Pyridine at 25°

$f_P°$, mol/l.	a_W	$f_W°$, mol/l.	$\Delta f_W°$	$\Delta f_W°$(calcd), mol/l.
		1,2-Dichloroethane		
0.0	0.437	0.0501	...	...
0.1310	0.437	0.0597	0.0096	0.0076
0.2283	0.437	0.0655	0.0154	0.0140
0.3385	0.437	0.0725	0.0224	0.0220
0.4439	0.437	0.0800	0.0299	0.0304
0.5002	0.437	0.0842	0.0341	0.0351
0.0	1.000	0.1262	...	...
0.0602	1.000	0.1344	0.0082	0.0084
0.1120	1.000	0.1421	0.0159	0.0160
0.1587	1.000	0.1463	0.0201	0.0231
0.1994	1.000	0.1566	0.0304	0.0294
0.2619	1.000	0.1653	0.0391	0.0395
0.3198	1.000	0.1755	0.0493	0.0491
0.3907	1.000	0.1899	0.0637	0.0613
0.4809	1.000	0.2019	0.0757	0.0775
0.5146	1.000	0.2109	0.0847	0.0837
0.4100	1.000	0.1947	0.0685	0.0674
		Benzene		
0.0	0.468	0.0158	...	...
0.0904	0.468	0.0184	0.0026	0.0026
0.1769	0.468	0.0212	0.0054	0.0053
0.2558	0.468	0.0248	0.0090	0.0081
0.3492	0.468	0.0280	0.0122	0.0118
0.4338	0.468	0.0310	0.0152	0.0154
0.0	0.670	0.0231	...	...
0.0967	0.670	0.0272	0.0041	0.0042
0.1799	0.670	0.0315	0.0084	0.0082
0.2606	0.670	0.0350	0.0119	0.0124
0.3222	0.670	0.0385	0.0154	0.0159
0.4367	0.670	0.0458	0.0227	0.0229
0.0	1.000	0.0349	...	...
0.0611	1.000	0.0380	0.0031	0.0044
0.0895	1.000	0.0411	0.0062	0.0065
0.1308	1.000	0.0443	0.0094	0.0097
0.1871	1.000	0.0493	0.0144	0.0143
0.2376	1.000	0.0531	0.0182	0.0186
0.2568	1.000	0.0555	0.0206	0.0203
0.2943	1.000	0.0597	0.0248	0.0236
0.3492	1.000	0.0643	0.0294	0.0287
0.4155	1.000	0.0690	0.0341	0.0351
0.4540	1.000	0.0742	0.0393	0.0399
		Toluene		
0.0	0.455	0.0111	...	...
0.0986	0.455	0.0150	0.0039	0.0024
0.1954	0.455	0.0160	0.0049	0.0051
0.2886	0.455	0.0189	0.0078	0.0080
0.3701	0.455	0.0227	0.0116	0.0108
0.6132	0.455	0.0304	0.0193	0.0203
0.0	0.710	0.0186	...	...
0.1040	0.710	0.0229	0.0043	0.0042
0.1954	0.710	0.0271	0.0085	0.0084
0.2729	0.710	0.0314	0.0128	0.0122
0.3712	0.710	0.0363	0.0177	0.0175
0.0	1.000	Toluene 0.0270	...	...
0.0545	1.000	0.0301	0.0031	0.0033
0.1085	1.000	0.0337	0.0067	0.0068
0.1551	1.000	0.0366	0.0096	0.0099
0.2052	1.000	0.0402	0.0132	0.0135
0.2592	1.000	0.0444	0.0174	0.0175
0.3093	1.000	0.0473	0.0203	0.0213
0.3485	1.000	0.0510	0.0240	0.0244
		Carbon Tetrachloride		
0.0	0.468	0.0040	...	...
0.0997	0.468	0.0055	0.0015	0.0013
0.2211	0.468	0.0070	0.0030	0.0031
0.0	0.670	0.0058	...	...
0.0977	0.670	0.0079	0.0021	0.0019
0.1858	0.670	0.0097	0.0039	0.0038
0.2749	0.670	0.0120	0.0062	0.0059
0.4656	0.670	0.0170	0.0112	0.0126
0.3763	0.670	0.0142	0.0084	0.0086
0.0	1.000	0.0087	...	...
0.0522	1.000	0.0102	0.0015	0.0015
0.0981	1.000	0.0126	0.0039	0.0029
0.1439	1.000	0.0129	0.0042	0.0044
0.1978	1.000	0.0145	0.0058	0.0063
0.2316	1.000	0.0165	0.0075	0.0075
0.2967	1.000	0.0188	0.0101	0.0100
0.3490	1.000	0.0211	0.0124	0.0122
0.3796	1.000	0.0223	0.0136	0.0135
0.4503	1.000	0.0254	0.0167	0.0160
0.4688	1.000	0.0260	0.0173	0.0175
		Cyclohexane		
0.0	0.885	0.0028	...	...
0.1154	0.885	0.0046	0.0018	0.0018
0.2046	0.885	0.0065	0.0037	0.0034
0.3128	0.885	0.0089	0.0061	0.0058
0.4238	0.885	0.0116	0.0088	0.0086
0.5428	0.885	0.0150	0.0122	0.0120
0.0	0.670	0.0021	...	...
0.1121	0.670	0.0035	0.0014	0.0013
0.2247	0.670	0.0052	0.0031	0.0029
0.3349	0.670	0.0070	0.0049	0.0048
0.4471	0.670	0.0090	0.0069	0.0070
0.5235	0.670	0.0106	0.0085	0.0087
0.0	1.000	0.0029	...	...
0.0396	1.000	0.0034	0.0005	0.0006
0.0784	1.000	0.0043	0.0014	0.0013
0.1174	1.000	0.0050	0.0021	0.0020
0.1511	1.000	0.0057	0.0028	0.0027
0.1962	1.000	0.0062	0.0033	0.0037
0.2163	1.000	0.0071	0.0042	0.0041
0.2476	1.000	0.0077	0.0048	0.0049
0.2694	1.000	0.0083	0.0054	0.0054
0.2975	1.000	0.0089	0.0060	0.0061
0.3353	1.000	0.0099	0.0070	0.0071

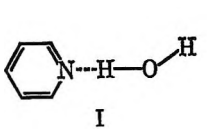

I

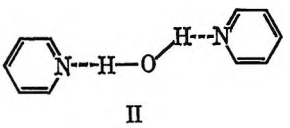

II

However, for all the systems except the cyclohexane system, a significant improvement in the fit of data results if the presence of a complex having more than one water molecule per pyridine molecule is assumed—

Table III: Formation Constants for the Pyridine Hydrates at 25°

Solvent	K_{PW}, l./mol	K_{P_2W}, (l./mol)^2	K_{PW_2}, (l./mol)^2	K_{PW_3}, (l. mol)^3	Root-mean-square dev
Cyclohexane	5.32 ± 0.11	6.80 ± 0.31	...	...	0.00019
Carbon tetrachloride	3.21 ± 0.14	2.77 ± 0.39	...	...	0.00030
	2.87 ± 0.09	2.73 ± 0.19	...	1690 ± 420	0.00023
	2.63 ± 0.10	3.03 ± 0.20	18.3 ± 4.5	...	0.00023
Toluene	2.43 ± 0.12	0.98 ± 0.36	...	...	0.00148
	1.78 ± 0.09	1.58 ± 0.17	...	236 ± 27	0.00066
	1.48 ± 0.10	1.63 ± 0.17	7.25 ± 0.83	...	0.00065
Benzene	2.11 ± 0.26	1.18 ± 0.88	...	...	0.00140
	1.53 ± 0.06	1.47 ± 0.15	...	156 ± 12	0.00062
	1.21 ± 0.07	1.47 ± 0.15	6.32 ± 0.48	...	0.00065
1,2-Dichloroethane	1.64 ± 0.19	0.29 ± 0.66	...	...	0.00290
	1.13 ± 0.08	0.96 ± 0.19	...	8.45 ± 1.22	0.00189
	0.99 ± 0.08	0.96 ± 0.19	1.00 ± 0.15	...	0.00189

viz., the pyridine monomer dihydrate or trihydrate. If the following species are assumed to be present: W, W_3, P, PW, P_2W, and PW_n (n = 2 or 3), where W and P represent the monomeric units of water and pyridine, respectively, the equations

$$f_P^\circ = c_P^\circ + K_{PW}c_W^\circ c_P^\circ + K_{PW_n}c_W^{\circ n}c_P^\circ + 2K_{P_2W}c_W^\circ c_P^{\circ 2} \quad (1)$$

and

$$\Delta f_W^\circ = f_W^\circ - (c_W^\circ + 3K_{W_3}c_W^{\circ 3}) = K_{PW}c_W^\circ c_P^\circ + K_{P_2W}c_P^{\circ 2}c_W^\circ + nK_{PW_n}c_P^\circ c_W^{\circ n} \quad (2)$$

can be derived. c_W° and c_P° represent the molar concentrations of monomeric water and pyridine in the organic solution; K_{W_3}, K_{PW}, K_{PW_n}, and K_{P_2W} are the formation constants of the species W_3, PW, PW_n, and P_2W, respectively; and it is assumed that each solute species individually obeys Henry's law. The self-association constant for water in 1,2-dichloroethane, K_{W_3}, has been determined previously[6] and it has been shown that the concentrations of self-associated aggregates of water are small compared with c_W° in the other four solvents.[14] Henry's law constants for the water monomer have been reported for each of the solvents;[6] these constants permit calculation of c_W° from measured values of a_W, the water activity. There remain, then, only three unknown equilibrium constants (K_{PW}, K_{P_2W}, and K_{PW_n}) to be inferred from an analysis of sets of f_P°, Δf_W°, and a_W data.

A method of least-squares analysis similar to techniques described previously[4,15] was utilized in all computations. Initial trial values of the constants K_{PW}, K_{P_2W}, and either K_{PW_2} or K_{PW_3} were used in calculating values of c_P° from eq 1 for each experimental f_P°. Improved values of the three equilibrium constants were then inferred by fitting Δf_W° data in the form of eq 2, using $c_P^\circ c_W^\circ$, $c_P^{\circ 2}c_W^\circ$, and $c_P^\circ c_W^{\circ n}$ as explicit dependent variables and assuming that all the experimental errors reside in the measured values of Δf_W°. The new values of the K's were used to compute improved values of c_P° from the set of measured f_P° values, and the Δf_W° values were refitted. The iteration process was repeated until no further changes resulted in the derived values of the hydration equilibrium constants. Table III lists the calculated least squares of the parameters, with their standard errors, and the values of the root-mean-square deviation in Δf_W° corresponding to the best fit of data.

The solid lines in Figure 1 are calculated curves corresponding to the best two-parameter fit of data, assuming only the presence of the hydrates PW and P_2W. The dashed lines correspond to the three-parameter least-squares fit of data, assuming that the hydrate species PW, P_2W, and PW_3 are present; virtually the same calculated curves are obtained if the species PW, P_2W, and PW_2 are assumed to be present. It is obvious that the incorporation of terms corresponding to the monomer dihydrate or trihydrate significantly improve the fit of data for the benzene system. The extent of the improvement for the aromatic and halogenated solvent systems is indicated by the root-mean-square deviation values in Table III. Values of Δf_W°-(calcd) in Table II have been computed by using the constants reported in Table III for the assumed species PW, P_2W, and PW_3 in all the solvents except cyclohexane. In cyclohexane, the limiting solubility of water is less than 0.003 M, and it is only necessary to assume the presence of PW and P_2W in fitting the data.

The equilibrium constant for the formation of the 1:1 hydrate is similar in magnitude to values reported for the 1:1 interaction of methanol and pyridine[16] and

(14) J. R. Johnson, Ph.D. Dissertation, University of Oklahoma, Norman, Okla., 1966.

(15) S. D. Christian, *J. Chem. Educ.*, 42, 604 (1965).

pyrrole and pyridine[17] in CCl_4 (3.1 and 3.0 l./mol, respectively). The values of K_{P_2W} are somewhat larger than would be expected if the two hydrogen bonds in P_2W exert no influence on each other. A statistical argument can be advanced to predict that K_{P_2W} should equal $K_{PW}^2/4$, if it can be assumed that the formation energies of the two hydrogen bonds are equal and that the stepwise formation entropies differ only owing to symmetry number effects.[18] Formation of a hydrogen bond between pyridine and one water proton should, by an inductive effect, weaken the acid strength of the second proton;[19] therefore, some other effect must be operative to enhance the formation of the complex P_2W. The ratio $K_{P_2W}:K_{PW}^2/4$, which should equal unity in the noninteracting sites model, varies from nearly 1 in cyclohexane to approximately 3 in 1,2-dichloroethane, increasing as the reactivity and polarizability or polarity of the solvent increases. It may be reasonable to attribute the relative stabilization of the more polar complex, P_2W, to solvent–solute interactions of the dipole–dipole and dipole–induced-dipole types.

The root-mean-square deviation values in Table III do not make it possible to distinguish between the possible species PW_2 and PW_3. However, as a result of previous investigations of the molecular complexity of water, we concluded that water dissolved in organic solvents possessing a single basic group tends to associate to form the trimer in preference to the dimer.[20] By analogy, we believe the hydrated species

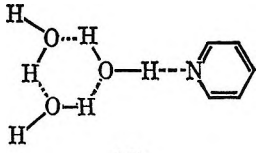

III

should be more stable than any form of PW_2. The formation constant for the monomer trihydrate, K_{PW_3}, respresents the equilibrium constant for the reaction of $P + 3W \rightarrow PW_3$. Using the known values of K_{PW_3} and K_{W_3}, it can be calculated that the equilibrium constant for the reaction $P + W_3 \rightarrow PW_3$ is equal to 2.0 l./mol in 1,2-dichloroethane, whereas the equilibrium constant for the reaction $P + W \rightarrow PW$ is 1.13 l./mol in that solvent. If it were true that each unbonded proton in the water trimer is as capable of forming a hydrogen bond with pyridine as is a proton in monomeric water, the equilibrium constant for the reaction $P + W_3 \rightarrow PW_3$ should equal $3K_{PW}/2$ or 1.7 l./mol in 1,2-dichloroethane, in reasonable agreement with the observed value, 2.0 l./mol.

B. Solvation Theory. The effect of solvation on the energies and free energies of molecular complex formation reactions can be directly related to the changes in thermodynamic functions for the unreacted monomers and the complex which occur when these species are transferred from the gas phase to a given solvent. When solvation effects are discussed, it is convenient to consider that a typical donor–acceptor interaction ($A + D \rightarrow AD$) occurs in both the vapor phase (v) and in a solvent (s). Then the following equilibria and mass action constants may be formulated, for a sufficiently dilute concentration range in both phases

$$A(v) + D(v) \longrightarrow AD(v) \qquad (K_{AD}^{v} = [AD(v)]/[A(v)][D(v)]) \quad (3)$$

$$A(s) + D(s) \longrightarrow AD(s) \qquad (K_{AD}^{s} = [AD(s)]/[A(s)][D(s)]) \quad (4)$$

$$A(v) \longrightarrow A(s) \qquad (K_{D,A} = [A(s)]/[A(v)]) \quad (5)$$

$$D(v) \longrightarrow D(s) \qquad (K_{D,D} = [D(s)]/[D(v)]) \quad (6)$$

$$AD(v) \longrightarrow AD(s) \qquad (K_{D,AD} = [AD(s)]/[AD(v)]) \quad (7)$$

The equilibrium constants are not all independent—it is readily shown that

$$K_{AD}^{s}/K_{AD}^{v} = K_{D,AD}/K_{D,A}K_{D,D} \quad (8)$$

The essence of the solvation theory previously communicated[5] is the assumption that the thermodynamic constants for reaction 7 are simply related to those for reactions 5 and 6 under quite general conditions. Consider the physical processes represented by the three reactions. Processes 5 and 6 represent the solvation of the individual donor and acceptor molecules, whereas reaction 7 represents solvation of the complex. The magnitude of the internal energy change for reaction 7, at least for relatively weak donor–acceptor interaction, might be expected to be less than the sum of the magnitudes of the internal energy changes for reactions 5 and 6, because a portion of the solvating surfaces of molecules A and D is unable directly to contact the solvent after the molecule AD is formed. The fraction of the solvation energy of the donor and acceptor that is retained by the complex may be expressed as

$$\alpha = \frac{\Delta E_{AD}^{v\rightarrow s}}{\Delta E_{A}^{v\rightarrow s} + \Delta E_{D}^{v\rightarrow s}} \approx \frac{\Delta H_{AD}^{v\rightarrow s}}{\Delta H_{A}^{v\rightarrow s} + \Delta H_{D}^{v\rightarrow s}} \quad (9)$$

in which the ratio of the enthalpies is nearly equal to that of the internal energies, provided both the numerators and the denominators are large compared with RT. The designation $v \rightarrow s$ indicates transfer of 1 mol of a given species from the ideal vapor phase to the infinitely dilute solution in solvent s. If α is strictly

(16) G. Coppen, J. Nasielski, and N. Sprecher, *Bull. Soc. Chim. Belges*, **72**, 626 (1963).

(17) R. H. Linnel, *J. Chem. Phys.*, **21**, 179 (1953).

(18) S. D. Christian, H. E. Affsprung, and C. Lin, *J. Chem. Soc.*, 437, 2378 (1965).

(19) H. S. Frank and W.-Y. Wen, *Discussion Faraday Soc.*, **24**, 133 (1957).

(20) J. R. Johnson, S. D. Christian, and H. E. Affsprung, *J. Chem. Soc.*, 1924 (1967).

independent of temperature (from 0°K to the temperature at which the formation constant is determined), it can be shown that analogous relations obtain among the Gibbs free energy and entropy changes for reactions 5–7

$$\alpha = \frac{\Delta G^\circ_{AD}{}^{v\to s}}{\Delta G^\circ_{A}{}^{v\to s} + \Delta G^\circ_{D}{}^{v\to s}} = \frac{\Delta S^\circ_{AD}{}^{v\to s}}{\Delta S^\circ_{A}{}^{v\to s} + \Delta S^\circ_{D}{}^{v\to s}} \tag{10}$$

where α is the same constant as that defined by eq 9, and standard states of 1 mol/l., ideal dilute solution, are chosen for each of the species in both phases. (The convenience of choosing concentration-based standard states for all phases is that if this convention is used the vapor phase is treated no different from any other phase, and the irrelevant pV terms which must be considered in relation to ΔH and K_p values are avoided. The equilibrium constants for reactions 5–7 are dimensionless, and the equilibrium constants for reactions 3 and 4 have the same dimensions.

Proof that relation 9 implies relation 10 if α is strictly constant may be developed

$$\Delta S^\circ_{AD}{}^{v\to s} = \int_0^T \frac{1}{T}\frac{d\Delta H_{AD}{}^{v\to s}}{dT}dT$$

$$= \alpha\int_0^T \frac{1}{T}\frac{d(\Delta H_A{}^{v\to s} + \Delta H_D{}^{v\to s})}{dT}dT$$

$$= \alpha(\Delta S^\circ_A{}^{v\to s} + \Delta S^\circ_D{}^{v\to s})$$

and since $\Delta H_{AD}{}^{v\to s} = \alpha(\Delta H_A{}^{v\to s} + \Delta H_D{}^{v\to s})$, it is also necessary that $\Delta G^\circ_{AD}{}^{v\to s} = \alpha(\Delta G^\circ_A{}^{v\to s} + \Delta G^\circ_D{}^{v\to s})$.

Note that if eq 9 and 10 are simultaneously valid, with a single value of the constant α, the task of predicting solvent effects is greatly simplified. To illustrate this, suppose that α has been determined for an association reaction from free energy data, using eq 10. It is then possible to use eq 9 to predict the energy change $\Delta E_{AD}{}^{v\to s}$ from measured values of the internal energy changes for the unreacted components ($\Delta E_A{}^{v\to s}$ and $\Delta E_D{}^{v\to s}$). Consequently, the difference between the ΔE for complex formation for reactions 3 and 4 may be computed. Alternately, if α can be predicted in advance from some theory of solution (see below), the change induced by the solvent in both ΔE and ΔG° for the association reaction can be predicted. The ultimate goal of the solvation theory outlined here is to predict values of K_{AD} and ΔE for the formation reaction in any solvent from values determined for only one phase and thermodynamic properties of the individual donor and acceptor molecules in the various media.

Recently, Stevens[21] has attempted to predict values of the parameter α by employing a lattice model of the liquid state similar to that proposed by Barker[22,23] and other investigators.[24-26] To illustrate his application of the lattice theories, consider the estimation of ΔE for transfer of 1 mol of pyridine from the ideal dilute solution in benzene to the vapor phase. If the theory of Goates, *et al.*,[24,25] is followed, it is assumed that a molecule of benzene possesses 12 lattice sites, and we denote the interaction energy of a site on one molecule with an adjacent benzene molecule by ϵ_{BB}. By analogy, we assume that the pyridine molecule dissolved in benzene experiences 11 such interactions, each of energy ϵ_{BB}, with neighboring benzene molecules, plus a unique twelfth interaction of energy ϵ_{NB} between the pyridine nitrogen atom and a neighboring benzene site. The energy required to vaporize a pyridine molecule from an infinitely dilute solution in benzene, leaving a cavity the size of the pyridine molecule, is therefore $11\epsilon_{BB} + \epsilon_{NB}$. Collapse of the cavity leads to the release of energy corresponding to formation of six interactions ($12/2 = 6$), each of energy ϵ_{BB}. The net energy of vaporization of pyridine is thus equal to $5\epsilon_{BB} + \epsilon_{NB}$.

Similar formulations may be made for the water monomer and the complex dissolved in dilute solution in benzene. The water molecule is assumed to have four sites interacting with benzene, and the complex, PW, is assigned 14 sites (11 from pyridine and 3 from water), with one site each having been lost from the water and pyridine molecules upon formation of the N···H hydrogen bond.

Stevens has examined available heat of mixing and heat of vaporization data for polar molecules and solvents of interest in hydrogen-bonding studies, and from these data he has compiled a table of reasonably consistent values of site interaction energies of various types. Using the tabulated ϵ values, he predicts values of α in the range 0.7–0.8 for the reaction P + W → PW in solvents of the type utilized in this investigation.

A test of the solvation theory and of the conclusion that α depends little on the choice of solvent can be made by using relations 9 and 10 in combination with thermodynamic data for reactions 3–7. If α is independent of both temperature and the choice of solvent, it may be shown that

$$K_{AD}{}^s/K_{AD}{}^v = K_{D,AD}/(K_{D,A}K_{D,D}) = (K_{D,A}K_{D,D})^{\alpha-1}$$

or

$$K_{AD}{}^{s'}/K_{AD}{}^{s''} = \left(\frac{K_{D,A}{}^{s'}K_{D,D}{}^{s'}}{K_{D,A}{}^{s''}K_{D,D}{}^{s''}}\right)^{\alpha-1} \tag{11}$$

where $K_{AD}{}^{s'}$ and $K_{AD}{}^{s''}$ are formation constants for the association reaction in solvents s′ and s″, respectively,

(21) T. S. Stevens, Ph.D. dissertation in preparation, University of Oklahoma, Norman, Okla.

(22) J. A. Barker, *J. Chem. Phys.*, **20**, 1526 (1952).

(23) J. A. Barker and F. Smith, *ibid.*, **22**, 375 (1954).

(24) B. Dacre and G. C. Benson, *Can. J. Chem.*, **41**, 278 (1963).

(25) J. R. Goates, R. L. Snow, and J. B. Ott, *J. Phys. Chem.*, **66**, 1301 (1962).

(26) O. Redlick, E. L. Derr, and G. J. Pierotti, *J. Amer. Chem. Soc.*, **81**, 2283 (1959).

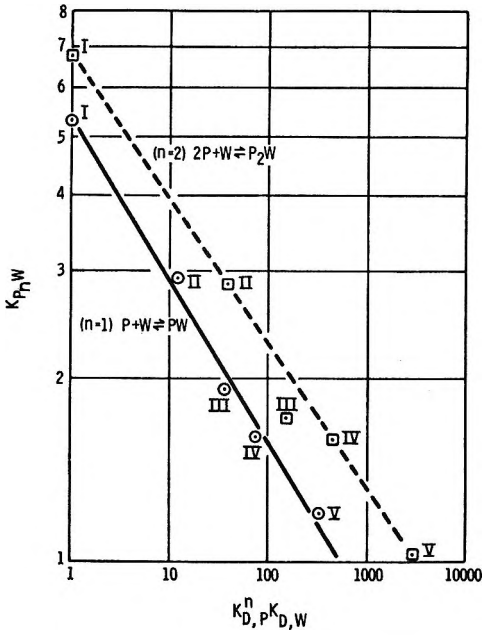

Figure 2. Correlation of association and distribution constants: I, cyclohexane; II, carbon tetrachloride; III, toluene; IV, benzene; V, 1,2-dichloroethane.

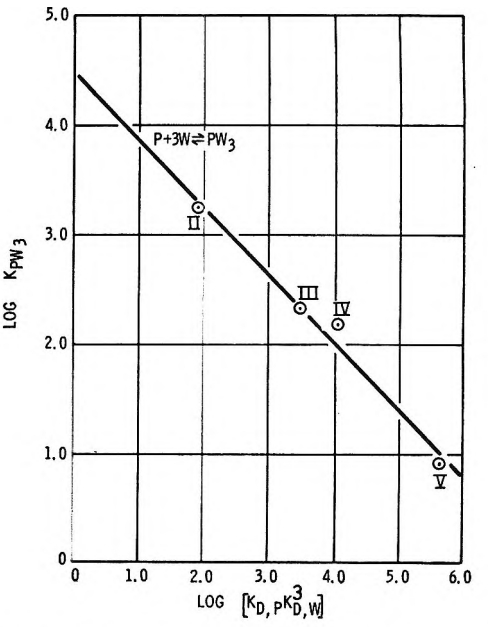

Figure 3. Correlation of association and distribution constants for the reaction P + 3W ⇄ PW_3 at 25°: II, carbon tetrachloride; III, toluene; IV, benzene; V, 1,2-dichloroethane.

and $K_D^{s'}$ and $K_D^{s''}$ represent distribution constants for the designated species between v and s′ and v and s″, respectively. Therefore, a plot of log K_{AD} *vs.* log $(K_{D,A}K_{D,D})$ should be linear, with a slope of $\alpha - 1$. Similarly, for an association reaction $A_2 + D \rightarrow A_2D$, a plot of log K_{A_2D} *vs.* log $(K_{D,A}{}^2K_{D,D})$ should be linear with a slope equal to $\alpha - 1$ for that reaction.

Figures 2 and 3 show plots of association and distribution data in the logarithmic form convenient for testing eq 11 and the analogous expressions for the other association equilibria established in the pyridine–water systems. The distribution constants, $K_{D,P}$ and $K_{D,W}$, used in calculating the abscissas are all defined relative to cyclohexane; *i.e.*, each is assigned a value of unity in that solvent. The slope of the plot of log K_{PW} *vs.* log $(K_{D,P}K_{D,W})$ is −0.29, yielding a value of $\alpha = 0.71$, in good agreement with the values calculated by Stevens from the lattice theory. Similarly, a value of 0.75 is obtained for α for the reaction $2P + W \rightarrow P_2W$ and a value $\alpha = 0.38$ is calculated for the reaction $P + 3W = PW_3$.

The value $\alpha = 0.75$ for formation of P_2W agrees reasonably well with values calculated from the lattice theory (0.69 in benzene and 0.73 in CCl_4). However, lattice calculations of α for the formation of PW_3 are somewhat greater than the calculated value of 0.38 obtained from Figure 3 (values near 0.5 are predicted from the lattice theory).

The results obtained to date with the solvation theory described here have been encouraging, and we are in the process of testing the method further with data for hydrogen bonding,[21] charge transfer,[27] and other types of complex-formation reactions.

Acknowledgment. We wish to acknowledge the support of the United States Department of the Interior, Office of Saline Water.

(27) J. Grundnes and S. D. Christian, *J. Amer. Chem. Soc.*, in press.

Spectroscopic Characterization of a New Polymorph of Metal-Free Phthalocyanine

by James H. Sharp and Marcel Lardon

Xerox Research Laboratories, Rochester, New York *(Received March 21, 1968)*

The infrared, visible, and near-infrared absorption spectra of thin films of a new polymorph of metal-free phthalocyanine (H_2Pc), designated as x-H_2Pc, have been compared with those of the well-known α and β-H_2Pc polymorphs. Distinct differences among the three polymorphs in the 700–800-cm^{-1} infrared region and in the visible and near-infrared electronic spectra (10,000–20,000 cm^{-1}) were observed. The electronic spectrum of x-H_2Pc can be interpreted as that of a dimer. In accordance with this assumption, the correct number of electronic energy levels, their relative oscillator strengths, the resonance splittings, and the relative orientation of the molecules of the dimer have been obtained from an analysis of the electronic spectra. A parallel plane model for the dimer is considered and the intermolecular separation is computed from the exciton dipole–dipole approximation. A comparison of the proposed structure for x-H_2Pc with that of β-H_2Pc, where the crystal structure is known, accounts satisfactorily for observed differences in the NH stretching frequencies.

I. Introduction

Metal-free phthalocyanine (H_2Pc) has been reported to exist in at least three polymorphic forms. The β form is the most stable polymorph and single crystals can be prepared by sublimation at 550°. The detailed structure of the β crystal has been reported by Robertson,[1] who found that it is a monoclinic crystal belonging to the $P2_1/a$ space group and that there are two phthalocyanine molecules per unit cell.

The X-ray powder diffraction pattern for another polymorph of phthalocyanine, designated as the α form, has been reported by several workers.[2-6] Assour[7] and Sidorov and Kotlyar[8] have found that the α form is completely converted to the β phase when heat-treated above 300°. A third crystalline modification of phthalocyanine, called the γ form, has been reported by Eastes.[9] Assour,[7] however, has presented experimental evidence that the α and γ forms differ only in particle size. Since it has not been possible to grow single crystals of the α and γ polymorphs, no detailed X-ray analyses have been reported. Infrared spectroscopy has been effectively employed to distinguish between the α and β forms,[4,8,10] but no infrared spectra of the γ polymorph have been reported.

Another crystal form of phthalocyanine, designated x-phthalocyanine (x-H_2Pc) because of its unique X-ray diffraction pattern, has recently been reported.[11]

The purpose of this work is to characterize x-H_2Pc with respect to its infrared, visible, and near-infrared absorption spectra. For comparison purposes, similar spectra for the well-known α and β polymorphs are also presented.

II. Experimental Section and Results

1. Sample Preparation. Metal-free phthalocyanine is commercially available and was purified by repeated solvent extraction techniques. Thin films of α-H_2Pc were prepared by vacuum evaporation (10^{-6} torr) of the purified material onto rectangular KBr flats and Pyrex cover glass slides held at ambient temperatures. The evaporations were carried out in a Bendix Balzers Model BA-3 evaporator. Thin films of β-H_2Pc were obtained by heat treating the evaporated α films for several hours at 300°. A kinetic study of the $\alpha \rightarrow \beta$ thermal conversion has been reported.[12]

The new x polymorph can be prepared by neat milling α-H_2Pc for approximately 1 week.[11] Thin films of the resulting x material were prepared by depositing a suspension of x-H_2Pc in heptane onto KBr or Pyrex windows and allowing the heptane to evaporate. The films were then gently heated at 80° in an oven for several hours. Several samples for spectroscopic analyses were also prepared using the Nujol mull technique in which a suspension of the x polymorph in Nujol was pressed between KBr or Pyrex plates. For spectroscopic characterization in the visible and near-infrared absorption regions, a thin film of x-H_2Pc in an epoxy–phenolic copolymer (1 part x-H_2Pc:12 parts,

(1) J. M. Robertson, *J. Chem. Soc.*, 615 (1935); 1195 (1936); 219 (1937).

(2) G. Susich, *Anal. Chem.*, **22**, 425 (1950).

(3) F. R. Tarantino, D. H. Stubbs, T. F. Cooke, and L. A. Melsheimer, *Am. Ink Maker*, **29**, 35, 425 (1950).

(4) A. A. Ebert, Jr., and H. B. Gottlieb, *J. Amer. Chem. Soc.*, **74**, 2806 (1952).

(5) F. W. Karasek and J. C. Decius, *ibid.*, **74**, 4716 (1952).

(6) M. Shigemitsu, *Bull. Chem. Soc. Jap.*, **32**, 607 (1959).

(7) J. M. Assour, *J. Phys. Chem.*, **69**, 2295 (1965).

(8) A. N. Sidorov and I. P. Kotlyar, *Opt. Spectry.*, **11**, 92 (1961).

(9) J. W. Eastes, U. S. Patent 2,770,620 (1956).

(10) D. N. Kendall, *Anal. Chem.*, **25**, 382 (1953).

(11) J. F. Byrne and P. F. Kurz, U. S. Patent 3,357,989 (1967).

(12) J. H. Sharp and R. L. Miller. *J. Phys. Chem.*, to be published.

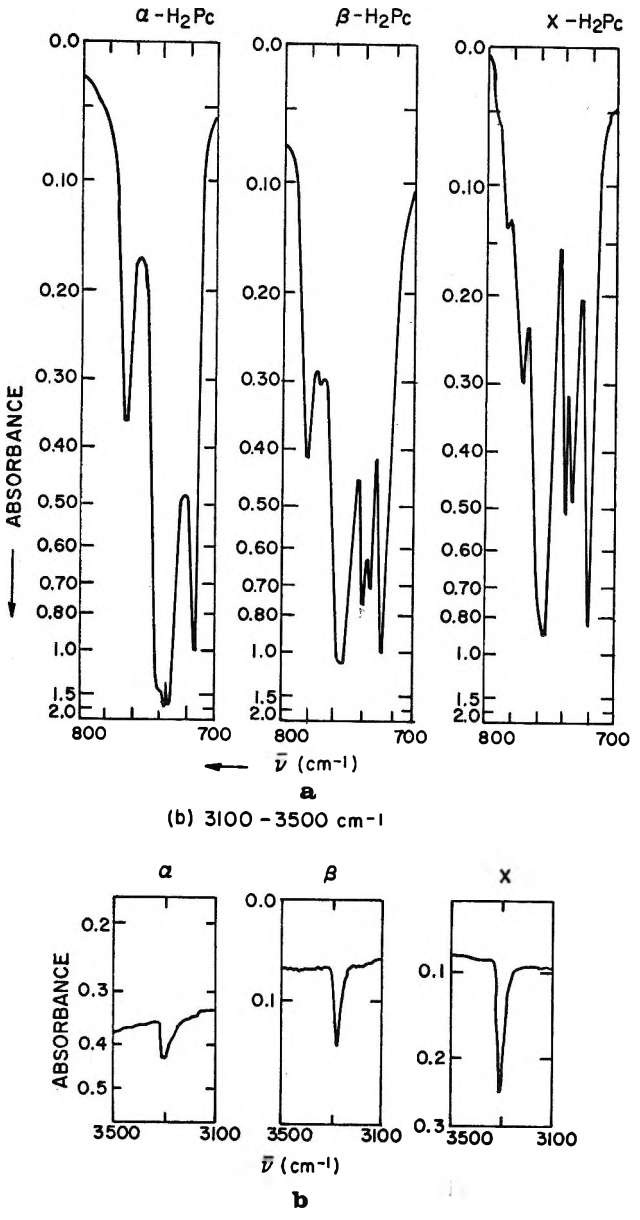

Figure 1. (a) Infrared spectra of the α-, β-, and x-H_2Pc polymorphic films in the 700–800-cm^{-1} region. (b) Infrared spectra of the α-, β-, and x-H_2Pc polymorphic films near 3300 cm^{-1}.

by weight, of resin) cast on a Pyrex substrate was also prepared.

2. Spectroscopy. The infrared absorption spectra of α-, β-, or x-H_2Pc on KBr substrates were recorded at room temperature with either a Perkin-Elmer Model 337 spectrometer or a Beckman Model IR-10 spectrometer. The resulting spectra in the 700–800-cm^{-1} region, where the most significant differences among the three polymorphs are observed, are shown in Figure 1a. Differences near 3300 cm^{-1} were also noted and these are shown in Figure 1b. A summary of the main absorption frequencies for the three polymorphs in these two regions is given in Table I.

The visible and near-infrared absorption spectra of

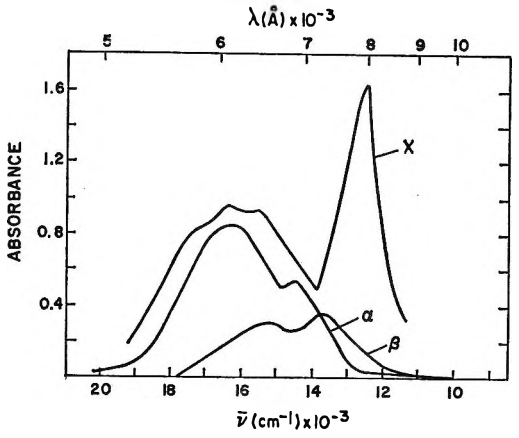

Figure 2. Visible and near-infrared electronic spectra of thin films of α-, β-, and x-H_2Pc at 77°K.

Table I: Absorption Frequencies[a] in the 700–800- and 3300-cm^{-1} Infrared Regions for the α-, β-, and x-H_2Pc Polymorphs

α-H_2Pc	β-H_2Pc	x-H_2Pc
714 (s-m)		720 (s)
	724 (s)	
733 (s)	733 (s-m)	734 (s-m)
738 (s)	739 (s-m)	739 (s-m)
743_{sh} (m)		
	755 (s)	755 (s)
767 (w-m)	772 (s)	772 (m-w)
	782 (m)	784 (w)
3302 (w)	3284 (m)	3302 (w-m)

[a] Intensities of the absorption are qualitatively described as weak (w), medium (m), or strong (s). A subscript sh indicates a shoulder.

the three polymorphic films were recorded on a Cary Model 14R automatic spectrophotometer. All spectra were recorded at 77°K and a comparison of the α-, β-, and x-H_2Pc films is given in Figure 2. The absorption spectra of the x-H_2Pc films were essentially identical regardless of the method of preparation of the film.

III. Discussion

1. Infrared Spectra. The infrared absorption spectra of the three polymorphic H_2Pc films, shown in Figure 1, show subtle yet distinct differences in both intensity and frequency of the vibrational modes. We have found that the 700–800-cm^{-1} region is particularly sensitive for differentiating between the three polymorphs. The out-of-plane CH deformation frequencies of the four adjacent hydrogen atoms of *ortho*-disubstituted aromatics[13] and the NH deformation frequencies[8,10,14,15] both occur in this region. Since phthalocyanine is a

(13) L. J. Bellamy, "The Infrared Spectra of Complex Molecules," John Wiley and Sons, Inc., New York, N. Y., 1959, p 77.

(14) H. F. Shurvell and L. Pinzuti, *Can. J. Chem.*, **44**, 125 (1966).

(15) S. F. Mason, *J. Chem. Soc.*, 976 (1958).

planar molecule, these bending modes will be influenced by the orientation of adjacent molecules, which also determines the polymorphic phase. Other authors[14] have assigned the 720-cm^{-1} absorption occurring in the α and β polymorphs to an out-of-plane NH deformation in analogy to a band observed at 719 cm^{-1} in porphins[15] whose ring structures are similar to that of phthalocyanine. However, since several metal phthalocyanine derivatives, where NH absorptions are absent, also show an absorption band at 720 cm^{-1}, this absorption frequency is probably a CH deformation mode.

In the NH stretching absorption region ($\simeq$3300 cm^{-1}), the α and x polymorphs show absorption at 3302 cm^{-1} whereas the absorption in the β polymorph is red-shifted by 18 cm^{-1} to 3284 cm^{-1}. In order to account for the observed NH stretching frequencies of the three polymorphs it is necessary to consider both intra- and intermolecular hydrogen bonding. In pyrrole,[15] for example, where intramolecular hydrogen bonding is negligible, the red shift of 97 cm^{-1} in going from solution to the solid is attributed to intermolecular hydrogen bonding. However, for the porphins, where considerable intramolecular hydrogen bonding is present,[15] the NH stretching frequency in solution is appreciably red-shifted ($\simeq$200 cm^{-1}) from that of pyrrole in solution. An additional red shift of only 4 cm^{-1} is found in going from solution to solid.

In recent work, Chen[16] has proposed a "shared hydrogen" model for phthalocyanine where each imino hydrogen is shared by two neighboring nitrogen atoms as shown in Figure 3. Since the intramolecular hydrogen bonding is appreciable in each of the three phthalocyanine polymorphs, a substantial but identical red shift from the the "free" NH stretching frequency ($\simeq$3497 cm^{-1}) is predicted. The α and x polymorphs have the same NH stretching frequency but the additional red shift of 18 cm^{-1} observed for the β polymorph indicates a weakening of the H–N–H bonding due to intermolecular bonding. This is in accord with the crystal structure[1] of β-phthalocyanine where the molecules are arranged in parallel stacks as shown in Figure 4.

2. Visible and Near-Infrared Spectra. The phthalocyanine molecule has D_{2h} symmetry and this is evident from solution absorption spectra. For example, the lowest observed electronic transition of copper phthalocyanine, which has D_{4h} symmetry, is at 6780 Å.[17] In a solution of metal-free phthalocyanine, however, the 6780 Å transition is split into two peaks which are located at 6990 Å (14,306 cm^{-1}) and 6650 Å (15,038 cm^{-1}) as shown in Figure 5. The polarized absorption spectra of single crystals of β-H_2Pc, reported by Lyons, *et al.*,[18] also clearly show the splitting of the lowest electronic transition.

The absorption spectra of thin films of α and β-H_2Pc, shown in Figure 2, also reflect the splitting of the lowest electronic transition. In the case of α-H_2Pc the two resulting electronic transitions are located at 14,430 and

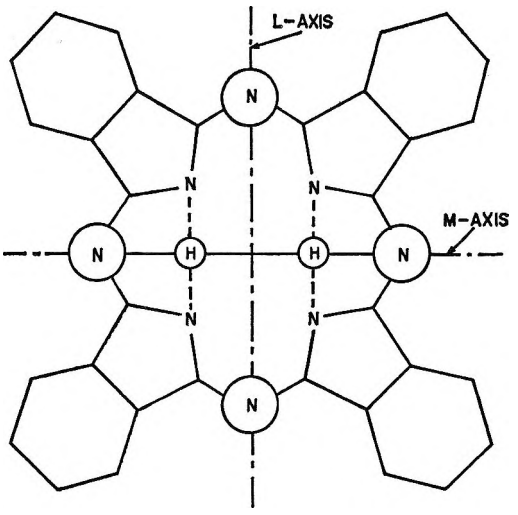

Figure 3. The "shared hydrogen" model for the phthalocyanine molecule.[16]

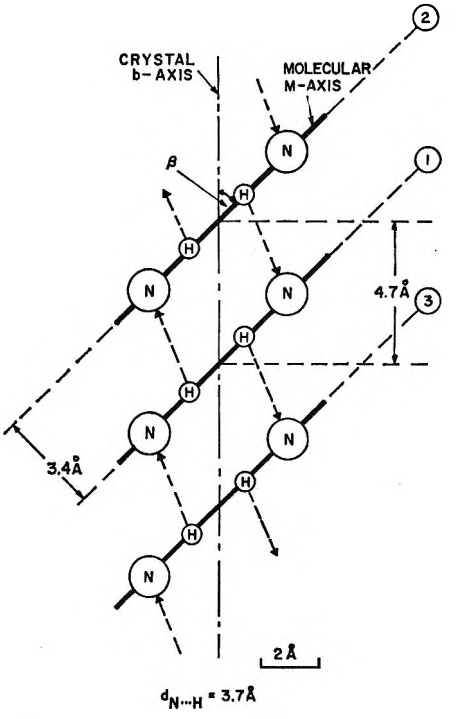

Figure 4. Intermolecular hydrogen bonding in β-H_2Pc, β = 45.9°.

16,320 cm^{-1}, whereas the film of β-H_2Pc shows electronic transitions at 13,500 and 15,400 cm^{-1}. In contrast to the electronic spectra of the α- and β-H_2Pc films, the x-H_2Pc film shows four electronic transitions located at 12,500, 15,490, 16,380, and 17,150 cm^{-1}. The transition located at 12,500 cm^{-1} (8000 Å) in the x-H_2Pc film

(16) I. Chen, *J. Mol. Spectrosc.*, **23**, 131 (1967).

(17) J. M. Assour and S. E. Harrison, *J. Amer. Chem. Soc.*, **87**, 651 (1965).

(18) L. E. Lyons, J. R. Walsh, and J. W. White, *J. Chem. Soc.*, 167 (1960).

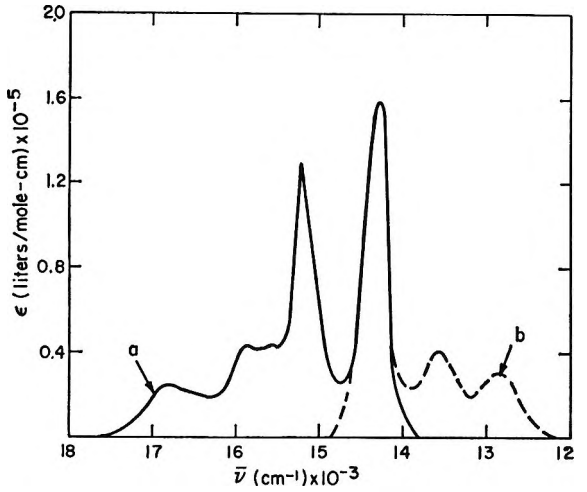

Figure 5. (a) Absorption spectrum of metal-free phthalocyanine in 1-chloronaphthalene. (b) Normalized fluorescence spectrum of metal-free phthalocyanine in 1-chloronaphthalene at 77°K (Assour and Harrison[17]).

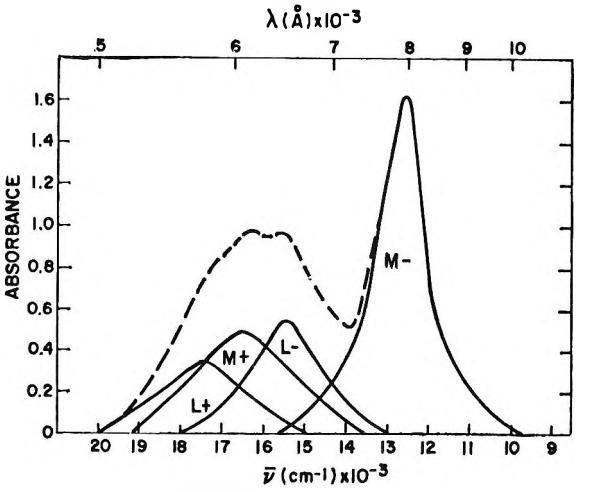

Figure 6. The quantitatively resolved spectrum of x-H_2Pc in the 9000–20,000-cm^{-1} absorption region.

spectrum is particularly unique for identification purposes.

The additional peaks in the x-H_2Pc film spectrum can be qualitatively accounted for by assuming that the x-H_2Pc modification has a dimeric structure. In an attempt to develop a model for x-H_2Pc, the absorption spectrum of the x-H_2Pc film has been compared to that of the α-H_2Pc film. Since α-H_2Pc is a metastable and less ordered polymorph,[12] its absorption spectrum should more closely approximate that of a monomer (solution spectrum). The lowest electronic transition observed in the α film shows only a small red shift ($\simeq$124 cm^{-1}) from that observed in solution. The observed absorption frequencies of the monomer (α-H_2Pc) and the dimer (x-H_2Pc) and the assigned resonance splittings, $\Delta\epsilon(0)$, are given in Table II. An estimate of the relative orientation of the molecules of a dimer can be made from the intensities and frequencies of the observed electronic transitions. Figure 6 shows the absorption spectrum of the x-H_2Pc film which has been quantitatively resolved into the four observed electronic transitions. The relative oscillator strengths and the assigned electronic transitions are given in Table III.

Table II: Observed Absorptions and Assigned Resonance Splittings

Phthalocyanine form	Absorption frequency, cm^{-1} −	0	+	Av observed resonance splittings, $\Delta\epsilon(0)$, cm^{-1}
α (monomer)		14,430		
x (dimer)	12,500		16,380	±1940
α (monomer)		16,320		
x (dimer)	15,490		17,150	±830

Table III: Relative Oscillator Strengths of the Assigned Electronic Transitions of x-H_2Pc

Assigned electronic transition, cm^{-1}	Relative oscillator strength
M^- (12,500)	55
M^+ (16,380)	28
L^- (15,490)	29
L^+ (17,150)	14

3. The Parallel Plane Dimer. The simplest dimer model to account for the above oscillator strengths is one in which the planes of the two phthalocyanine molecules are parallel to one another. This situation is depicted in Figure 7 where the electric dipole vectors along the M axes of the two molecules form an angle θ with the x axis of the planar coordinate system. Vectorial addition gives two components, M^+ and M^-, whose squares are proportional to their respective oscillator strengths (see Table III) as expressed in

$$|M^+|^2 = |2M \cos\theta|^2 \propto 28 \quad (1)$$

$$|M^-|^2 = |2M \sin\theta|^2 \propto 55 \quad (2)$$

From the above equations, θ is found to be 55°. Similarly, the electric dipole moments along the L axes of the two molecules each form an angle ϕ with the x axis of the planar coordinate system and the resulting L^+ and L^- components are related to their respective oscillator strengths by

$$|L^+|^2 = |2L \sin\phi|^2 \propto 14 \quad (3)$$

$$|L^-|^2 = |2L \cos\phi|^2 \propto 29 \quad (4)$$

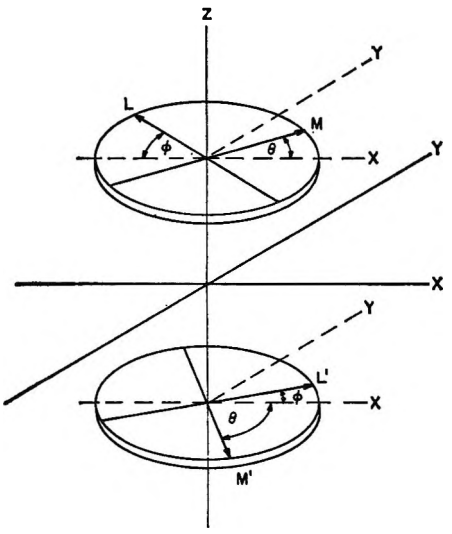

Figure 7. Pictorial representation of the parallel plane dimer model of x-H_2Pc.

Equations 3 and 4 give a value of 35° for ϕ. Since L and M are orthogonal to one another, θ plus ϕ must be 90°.

It is interesting to note that this model is in agreement with the apparent lack of intermolecular hydrogen bonding found in the infrared spectrum of the x-H_2Pc polymorph. Since the two molecules of the dimer form an angle of 110° (2θ or $180 - 2\phi$) with respect to each other in the molecular plane, intermolecular hydrogen bonding is reduced as shown in Figures 8a and 8b. For example, if the distance between the molecular planes in x-H_2Pc is the same as in β-H_2Pc, *i.e.*, 3.4 Å, then the distance between the bridge nitrogen and the imino hydrogen is increased from 3.7 Å in β-H_2Pc to 3.9 Å in x-H_2Pc.

4. The Exciton Dipole–Dipole Approximation. A physical picture of the exciton dipole–dipole splitting arising from the interaction of two molecules of a dimer can be made through the dipole–dipole approximation.[19] This approximation, derived from a classical point-multiple expansion, considers only the dipole–dipole term and is valid only when the intermolecular separation, R, is significantly larger than the distance, r_i, associated with the dipole strength, D_{mn}, of the molecule defined by

$$D_{mn} = \langle m \rangle^2 = \left(\int \Psi_m M \Psi_n d\tau\right)^2 \qquad (5)$$

M is the dipole moment operator, $\Sigma_i e r_i$, where r_i is the distance of the ith electron from the center of positive charge of the molecule, and m is the transition moment integral. Although this approximation is questionable in the case of the phthalocyanine molecule, a semiquantitative description of the observed resonance splittings and the intermolecular separation can be obtained.

The dipole–dipole exciton splitting, $\Delta\epsilon(0)$, is given by[20] the equation

$$\Delta\epsilon(0) = -D_{m,n} \sum_g \left(\frac{3 \cos \alpha_{1z} \cos \alpha_{gz} - \cos \alpha_{1g}}{R_{1g}^3}\right) \qquad (6)$$

where D_{mn} is the dipole strength and R_{1g} is the intermolecular separation. The z axis is the line joining the centers of the molecules and α_{1g} is the angle between the direction of the transition dipoles along the L, M, or N axes of molecule 1 and molecule g. In the case of a parallel plane dimer, eq 6 reduces to

$$\Delta\epsilon(0) = \frac{D_{m,n}}{R_{12}^3} \cos \alpha_{12} \qquad (7)$$

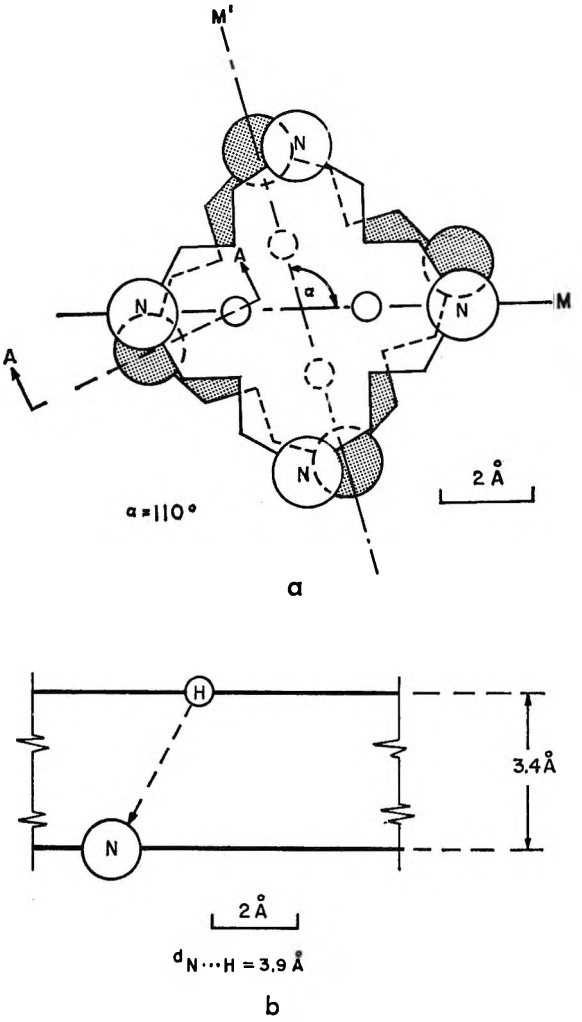

Figure 8. (a) Normal projection of the dimer of x-H_2Pc with an angle, α, of 110° between the M and M' axes of the two molecules. (b) Cross section A–A through the dimer, showing the intermolecular hydrogen bonding between the imino (shared) hydrogen of the upper and the bridge nitrogen of the lower molecule. The interplanar distance is assumed to be 3.4 Å as in β-H_2Pc.

(19) See, for example, E. S. Emerson, M. A. Conlin, A. E. Rosenoff, K. S. Norland, H. Rodriguez, D. Chin, and G. R. Bird, *J. Phys. Chem.*, **71**, 2396 (1967).

(20) R. M. Hochstrasser, "Molecular Aspects of Symmetry," W. A. Benjamin, Inc., New York, N. Y., 1966, p 311.

since α_{1z} and α_{2z} are 90°. The dipole strength is related to the oscillator strength, $f_{m,n}$, of an electronic transition by

$$D_{m,n} = \frac{3he^2}{8\pi^2 m_e c g_n \nu_{mn}} f_{mn} \text{ erg cm}^3 \quad (8)$$

where h is Planck's constant, e is the electronic charge, c is the velocity of light, m_e is the mass of the electron, g_n is the degeneracy of the excited state, and ν_{mn} is the frequency of the transition in cm^{-1}.

The oscillator strengths for M and L electronic transitions of metal-free phthalocyanine can be computed from the solution absorption spectrum and the normalized fluorescence spectrum,[17] which are shown in Figure 5. The oscillator strength of an electronic transition is given by

$$f_{mn} = 4.32 \times 10^{-9} \int_{\nu_1}^{\nu_2} \epsilon d\nu \text{ erg cm} \quad (9)$$

where ϵ is the molar extinction coefficient in l./mol cm and ν is the frequency in cm^{-1}. Hence, $f_{mn}{}^M$ and $f_{mn}{}^L$ are found to be 0.44 and 0.23 erg cm, respectively. The ratio of these oscillator strengths, $f_{mn}{}^M/f_{mn}{}^L$, is 1.9, which is identical with the ratio of the relative oscillator strengths of the dimer given in Table III. Using eq 8 the dipole strengths, $D_{mn}{}^M$ and $D_{mn}{}^L$ are computed to be 6.5×10^{-35} and 3.2×10^{-35} erg cm^3, respectively.

The separation distance between molecules of x-H_2Pc, $R_{12}{}^x$, is found from eq 7 by using the observed resonance splitting of 1940 cm^{-1} for the M transition, the corresponding dipole strength, $D_{mn}{}^M$, and a value of 110° (2θ) for α_{12}. Similarly, $R_{12}{}^x$ can be determined using the splitting of 830 cm^{-1} for the L transition, the corresponding dipole strength, $D_{mn}{}^L$, and the value of 110° ($180 - 2\phi$) for α_{12}. In the former case, $R_{12}{}^x$ is computed to be 3.9 Å, whereas the latter case gives a value of 4.1 Å. In Figure 9 the stacking of H_2Pc molecules along the z axis in the proposed dimer model is compared to that along the b-crystal axis in β-H_2Pc.

It should be emphasized that the above model is necessarily a simple one and the close agreement between the model and the spectroscopic data may be somewhat fortuitous. The validity of the dipole–dipole approximation, in the case of the phthalocyanine molecule, is certainly open to question, the interaction between the M^+ and L^- and the M^- and L^+ electric dipole vectors has been neglected, and other nonparallel plane models may also be envisioned. In conclusion, however, the proposed model for x-H_2Pc accounts satisfactorily for the observed electronic spectrum and for the reduced intermolecular hydrogen bonding observed in the infrared spectrum. In the case of the dimer model, where the molecules are 4.0 Å apart, the distance between the bridge nitrogen and the imino hydrogen is 4.5 Å compared to 3.7 Å in β-H_2Pc.

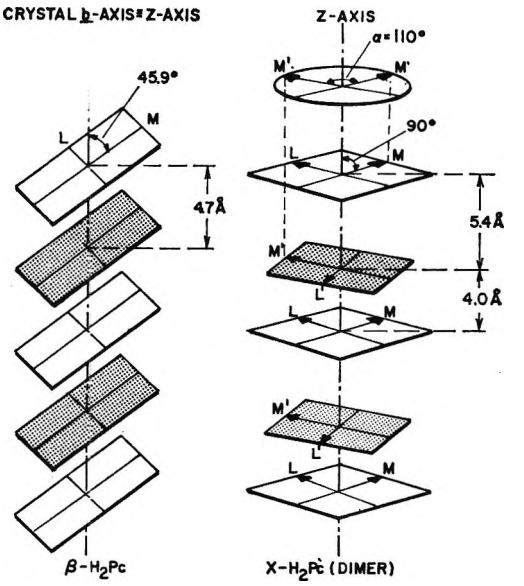

Figure 9. Stacking of H_2Pc molecules along the b-crystal axis in β-H_2Pc and along the z axis in the proposed model of x-H_2Pc.

Acknowledgment. We wish to thank Mr. R. L. Miller and Mr. H. Six for their assistance in sample preparation and spectroscopic characterization. We are particularly indebted to Drs. D. L. Stockman, G. E. Johnson, P. K. Watson, and J. W. Weigl for stimulating discussions.

The Sorption of Orthophosphate on Crystalline Metal Oxides[1]

by D. R. Vissers[2]

Oak Ridge National Laboratory, Oak Ridge, Tennessee 37830 *(Received March 21, 1968)*

Isotherms for the sorption of orthophosphate from aqueous solutions onto crystalline metal oxide surfaces such as thoria or zirconia contain plateau regions which remain unchanged over wide ranges of concentration of the sorbing species and which change abruptly from one plateau to another when they do change. The amount of orthophosphate sorbed per unit area of surface appears to be independent of the sintering temperature of the oxide. The plateau regions present in the experimentally determined sorption isotherms appear to be related to monolayer coverages predictable from geometric considerations of the orthophosphate molecule and the metal oxide surfaces presumed to be present. This interpretation of the results indicates that for sorption of orthophosphate from an aqueous medium onto a crystalline metal oxide surface a fixed stoichiometry exists between the sorbed phosphate molecules and the metal oxide sites present on the surface for a fairly wide range of conditions.

Introduction

The chemisorption of gaseous molecules onto heterogeneous metal and metal oxide surfaces has long been known to occur in monolayers.[3,4] The amount of chemisorbed material in a monolayer is thought to be related to the geometry of the ion, atom, or molecule being chemisorbed and to the properties of the reactive sites on the adsorbent.[5-7] The latter properties are determined by the chemical nature of the surface as well as by the arrangement of the reactive sites which make up the surface. The geometric arrangement of reactive sites on crystalline materials is of course determined by the crystal faces present. Monolayer adsorption of polar organic compounds, in particular, long-chain organic acids,[8,9] and quaternary ammonium halides[10] tagged with tritium or carbon-14, have been used to determine the surface areas of various materials.

Kraus and coworkers[11] studied the effect of firing temperature of hydrous zirconium oxide on chromate uptake and showed that as the firing temperature is increased the uptake of chromate per unit weight of hydrous zirconium oxide usually is decreased. The loss in capacity was attributed to an increase in crystallite size, which caused a decrease in the effective surface area per unit weight of hydrous oxide. Crystallite growth was independently confirmed by an increase in the sharpness of the lines observed in the X-ray diffraction patterns. No surface area measurements were made on the material, and consequently, no exact relationship could be drawn between the amount of chromate absorbed and the (apparent) surface area present for sorption.

In this study the uptake of phosphate on the fired oxides of zirconium, thorium, and cerium(IV) was investigated in an effort to correlate the phosphate sorption with the nitrogen-determined BET surface area of the sorbent, a postulated geometric array of reactive sites present in the surface, and an assumed geometry of the orthophosphate molecule.

Methods

The hydrous oxides of hafnium, zirconium, and cerium(IV) were prepared by precipitation from a 0.5 *F* metal ion solution with concentrated ammonium hydroxide. The precipitate was filtered and washed several times with distilled water on a 4-in. sintered glass filter. The hydrous oxide was then air-dried and fired to the desired temperature. Hydrous thorium oxide was prepared by steam denitration of solid $Th(NO_3)_4 \cdot 4H_2O$. This material was then fired at 800°. The 100-mesh zirconium metal powder used in these studies was obtained from the WahChang Corp. The fired hydrous oxides used in these studies ranged from 40 to 100 mesh in size.

The sorption of orthophosphate on the hydrous metal oxides and zirconium metal powder was determined through the use of radiotagged phosphorus-32. Two scintillation-type detectors were used in the investigations. A 2π scintillation detector was used to carry out sorption-rate studies, and a well-type detector was used to determine the values of phosphate sorption in the batch-type studies.

(1) Research jointly sponsored by The Office of Saline Water, U. S. Department of the Interior, and the U. S. Atomic Energy Commission under contract with the Union Carbide Corp.

(2) Chemical Engineering Division, Argonne National Laboratory, Argonne, Ill. 60439.

(3) I. Langmuir, *J. Amer. Chem. Soc.*, **38**, 2221 (1916).

(4) J. J. F. Scholten and A. Van Montfoort, *J. Catal.*, **1**, 85 (1962).

(5) J. H. de Boer, J. M. H. Fortuin, B. C. Lippens, and W. H. Meijs, *ibid.*, **2**, 1 (1963).

(6) J. H. de Boer, G. M. M. Houben, B. C. Lippens, W. H. Meijs, and W. K. A. Walrave, *ibid.*, **1**, 1 (1962).

(7) J. K. Roberts, *Proc. Roy. Soc.*, **A152**, 445 (1935).

(8) H. A. Smith and T. Fort, Jr., *J. Phys. Chem.*, **62**, 519 (1958).

(9) H. A. Smith and R. M. McGill, *ibid.*, **61**, 1025 (1957).

(10) J. Kivel, F. C. Albers, D. A. Olsen, and R. E. Johnson, *ibid.*, **67**, 1235 (1963).

(11) K. A. Kraus, H. O. Phillips, T. A. Carlson, and J. S. Johnson, "Progress in Nuclear Energy," Series IV, Vol. 2, "Technology, Engineering and Safety," Pergamon Press Ltd., London, 1960.

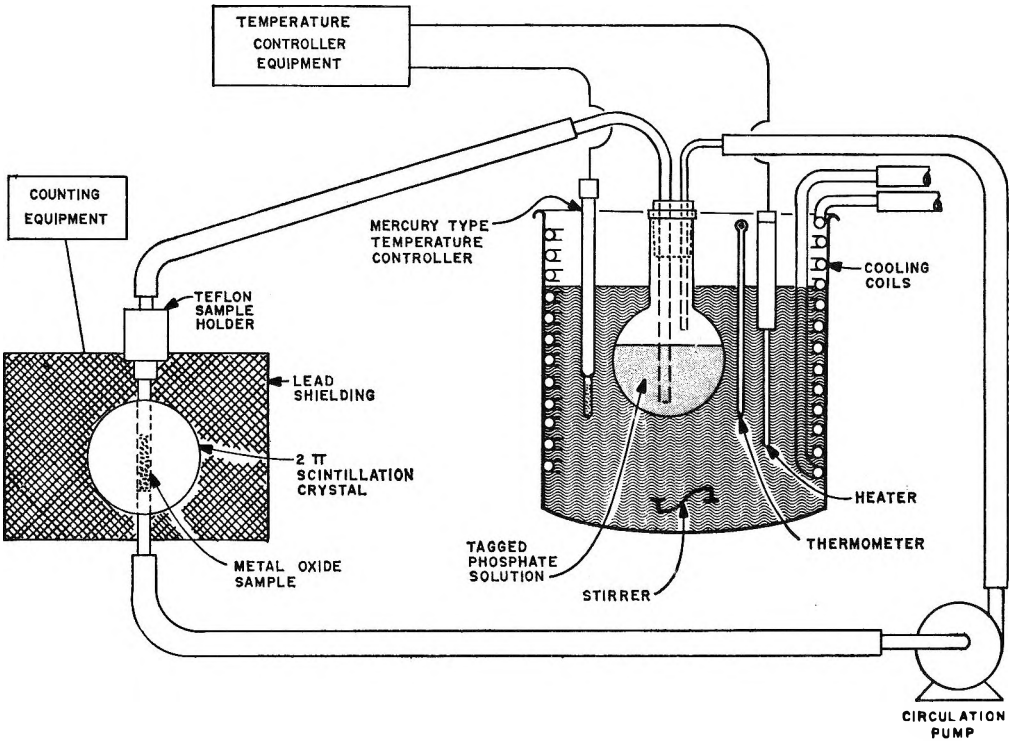

Figure 1. Sorption rate study apparatus.

The phosphate solutions used in all the studies were prepared from a standard solution of phosphoric acid. The pH's of the solution were adjusted with either perchloric acid or potassium hydroxide solutions. The phosphorus-32 tracer was treated to remove heavy metals and hydrolyze any pyrophosphates present.

The surface areas of the metal oxide powders were determined by the standard BET surface area method using nitrogen. The much smaller specific surface area of the zirconium metal was determined by the BET method using krypton. The molecular surface areas of nitrogen and krypton in these studies were assumed to be 16.2 and 19.5 $Å^2$, respectively.

Three different batch sorption techniques were used to obtain the phosphate sorption data. In a batch technique employed with zirconium oxide, an excess of radioactively tagged phosphate of a known specific activity was passed through a column containing a weighed quantity of sorbent. The column was then rinsed with distilled water, and the sorbed phosphate was eluted batchwise with 1-ml quantities of 1 *F* sodium hydroxide solution followed by 1 *F* hydrofluoric acid solution. The total activity of the sorbed phosphate was determined by counting each aliquot of the eluted phosphate in a well-type scintillation counter. The number of moles of phosphate eluted was computed from the total eluted activity. This technique was used to determine the phosphate sorption data on the zirconium oxide as a function of pH.

The second technique employed involved placing a weighed quantity of sorbent in a solution of tagged phosphate. The size of the sample was selected so that less than 5% of the phosphate present in the original solution of known specific activity was sorbed. After equilibration, the sample was transferred to a column, and the amount of phosphate sorbed was again determined as described earlier. This technique was used to obtain all the phosphate sorption data reported on zirconium metal. It was also used to obtain the phosphate sorption data on the zirconium oxide at pH 3 as a function of phosphate concentration. The technique was not used in the phosphate sorption studies on the thorium and cerium(IV) oxides, since the sorbed phosphate could not be desorbed by nondestructive means from these oxides.

A third technique was used in carrying out phosphate-sorption studies on cerium(IV) and thorium oxides. The technique involves placing a weighed quantity of powdered metal oxide into 2 ml of solution of radioactively tagged phosphate of known specific activity. The amount of metal oxide used was such that it sorbed about 10% of the phosphate present. The quantity of phosphate sorbed after equilibration was determined by noting the change in the activity of the tagged phosphate solution. The activity of the solution after equilibration was determined by centrifuging the solutions which contained the metal oxide and pipetting and counting 1 ml of the final solution. The amount of phosphate sorbed was determined by comparing the activity of the solution after equilibration with its activity before equilibration. This technique was found to be rapidly and easily adapted to any of the sub-

stances studied. However, large deviations did occur at low phosphate concentrations, where a large weighing error was present. The automatic balance used for these studies was assumed to have a weighing error of approximately 0.0005 g. The exact value of the weighing error was not determined, since the balance was routinely maintained and was adjusted from time to time.

The phosphate-sorption rate studies were carried out in the apparatus shown schematically in Figure 1. The system consisted of a thermostated closed loop which contained a circulation pump, a 2π scintillation detector, a solution reservoir, and a Teflon column containing the powdered metal or metal oxide being studied. The inner diameter of the column was 0.250 in.; the wall thickness of the column was approximately 20 mils. The rate study was carried out by circulating approximately 100 ml of the tagged-phosphate solution of known specific activity through the packed column of powdered metal oxide, which possessed approximately 12 m^2 of surface area, for a selected time. The column was then emptied by suction, and duplicate 10-sec counts were made of the packed bed in the column; the operation was repeated. A continuous time sequence was used to handle the sorption-rate data; that is, the 10-sec counting time was included in the recorded lapsed time. This procedure does introduce a slight error in the rate measurement. It is also apparent that not all of the tagged-phosphate solution can be removed by the suctioning technique; however, at the end of the rate study the column was suctioned and counted, then was rinsed with distilled water, and was recounted. The amount of phosphate rinsed from the column ranged from 0 to 3% of the total phosphate sorbed, which showed the suctioning technique to be satisfactory.

The crystallographic lattice parameters for the hydrous metal oxides were obtained from Wyckoff's book.[12] The size of the phosphate molecule was obtained from the work of Durrant and Durrant[13] and of Smith[14] on the structure of crystalline phosphoric acid.

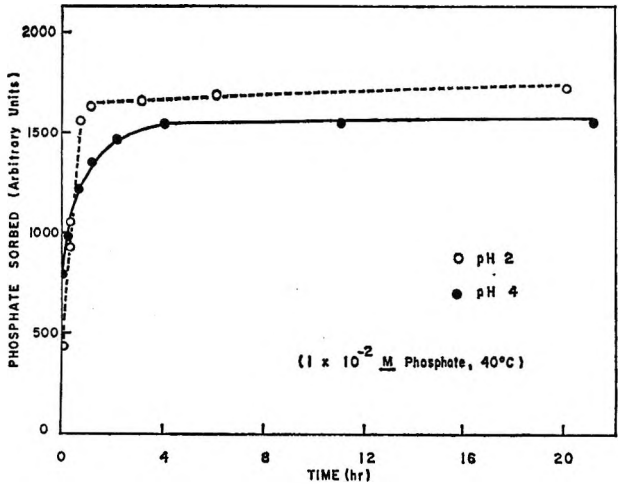

Figure 2. Sorption rate of phosphate on 800°-fired thorium oxide.

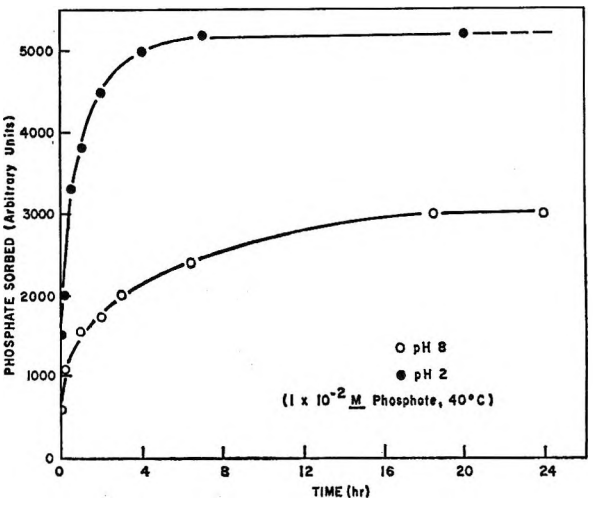

Figure 3. Sorption rate of phosphate on 400°-fired zirconium oxide.

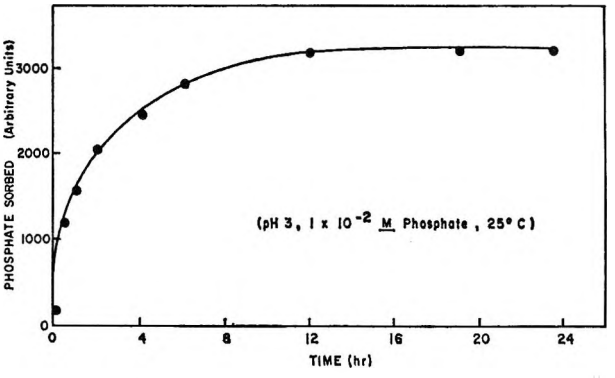

Figure 4. Sorption rate of phosphate on 400°-fired ceric oxide.

Results

Phosphate Sorption. Preliminary phosphate sorption rate studies were carried out on fired oxides of thorium, zirconium, and cerium(IV), as well as on powdered zirconium metal, to determine the time required to approach equilibrium. The results of these studies are presented in Figures 2–5 and reveal that the time required to approach equilibrium is pH dependent. At the lower pH's, the apparent equilibration times vary from 4 to 12 hr. In Figures 2–5 the ordinates have been normalized so that a unit represents the same amount of phosphate sorbed.

(12) R. W. Wyckoff in "Crystal Structures," Vol. 1, 2d ed, Interscience Publishers, New York, N. Y., 1963.

(13) P. J. Durrant and B. Durrant, "Introduction to Advanced Inorganic Chemistry," Longman's Publishing Co., London, 1962.

(14) J. P. Smith, W. E. Brown, and J. R. Lehr, *J. Amer. Chem. Soc.*, 77, 2728 (1955).

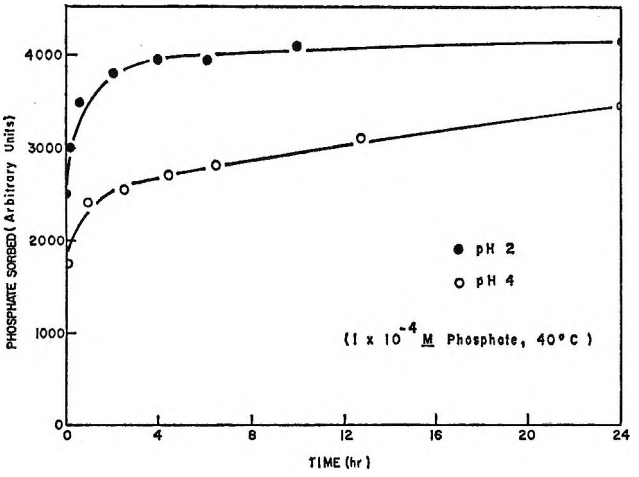

Figure 5. Sorption rate of phosphate on 100-mesh zirconium metal powder.

The effect of pH on the uptake of phosphate by the metal oxides and zirconium metal was investigated to obtain some knowledge about the phosphate sorption step. The batch-sorption pH studies were carried out in 10^{-2} *M* phosphate on the metal oxides and in 10^{-4} *M* phosphate on the zirconium metal. Equilibration time was approximately 20 hr. The effect of pH on the phosphate uptake is shown in Figures 6 and 7. The standard deviation is shown on each point for the metal oxides and takes into consideration the statistical counting errors and the assumed weighing error of 0.5 mg. The deviation shown on each point for the zirconium metal is only meant to indicate the experimental scatter present in the duplicate or triplicate determinations. Calculated concentrations of the phosphate species present at the various pH's are shown as a reference in these figures. The amount of phosphate sorbed is expressed in moles per square meter of surface as determined by the BET surface area determination. The phosphate uptake on these surfaces may also be expressed as the area occupied by a sorbed phosphate molecule. The phosphate sorption data at the higher pH's may not be equilibrium data, since at the higher pH's the kinetic studies indicate equilibrium is probably not established in 20 hr.

These studies indicate that the metal oxide surfaces, which include the powdered zirconium metal, are more receptive to the phosphate molecule at the lower pH's. In the cases of metal oxide powders the amount of phosphate sorbed per unit area tends to become constant, and the plots exhibit plateau regions at pH 3 and below. No plateau was present in the plot made in connection with the zirconium metal powder study. The explanation for this is probably the fact that the perchlorate ion at pH 2 and below begins competing successfully for the surface sites, as was shown by batch-phosphate sorption studies carried out at pH 3 in the presence of 1 *F* lithium perchlorate where the amount of phosphate sorbed was greatly reduced.

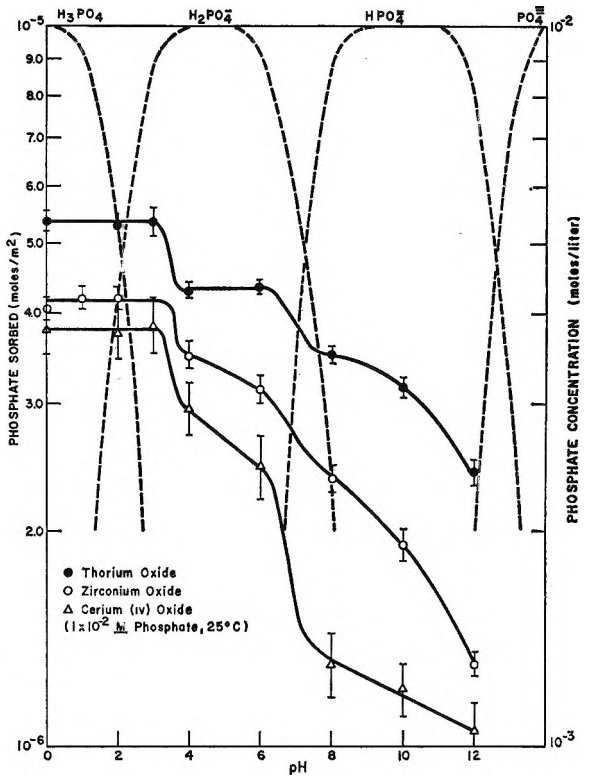

Figure 6. Phosphate sorption on the fired oxides of thorium, zirconium, and cerium(IV).

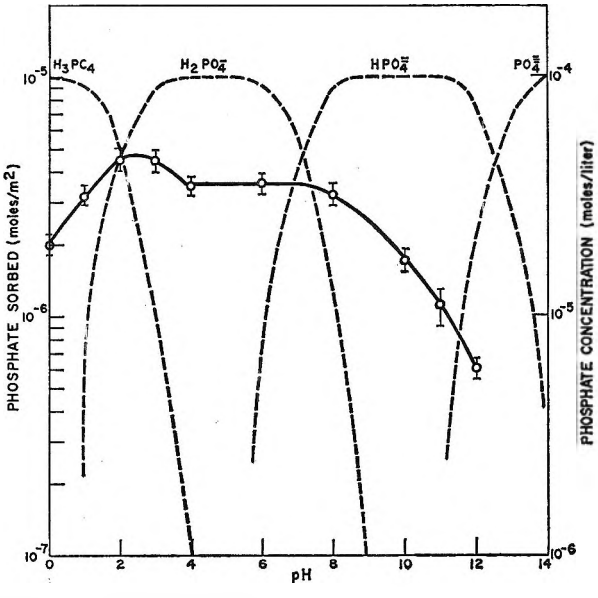

Figure 7. Phosphate sorption on 100-mesh zirconium metal powder.

Since no experimental information is available on the chemical nature of the surface and the change brought about by changes in pH, it is not possible to draw any conclusions about the surfaces.

Sorption Isotherms. Phosphate sorption isotherms were obtained on all of the materials at room temperature. These studies were carried out at pH 3 in

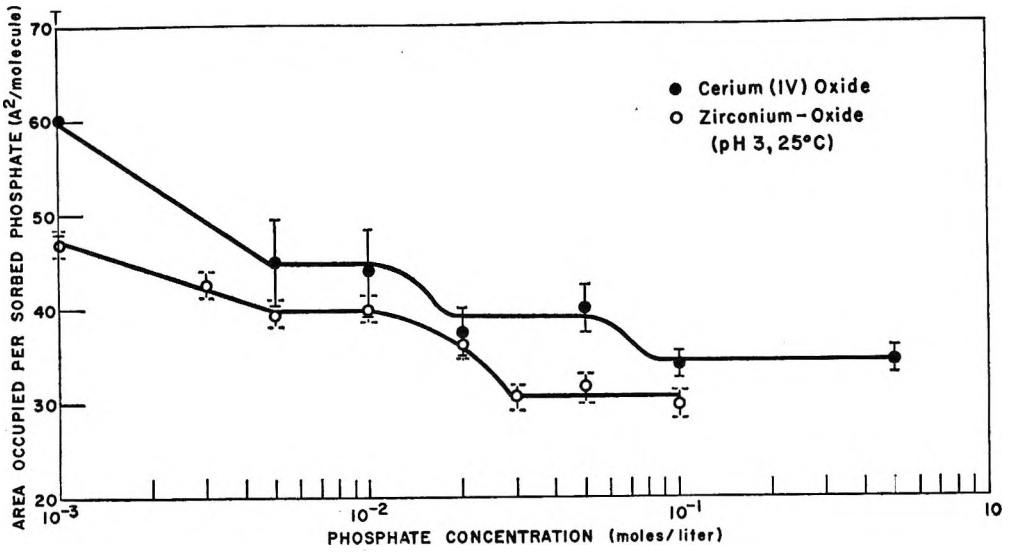

Figure 8. Phosphate sorption on fired zirconium and ceric oxides

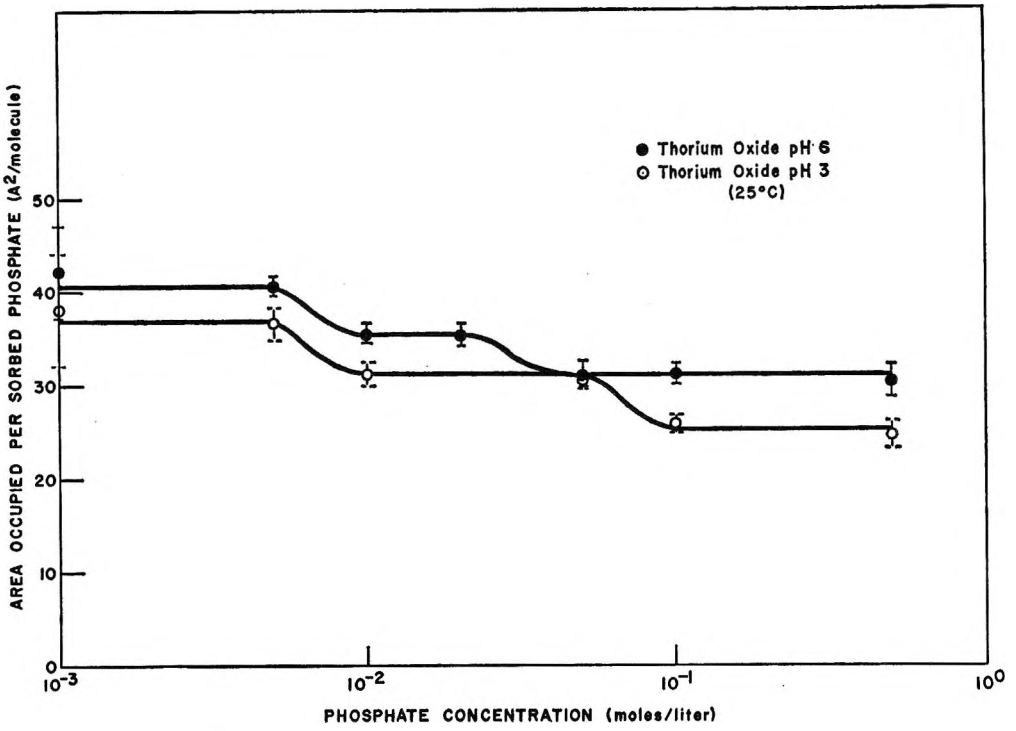

Figure 9. Phosphate sorption on fired thorium oxide.

10^{-3} to 5×10^{-1} M phosphate over a period of approximately 20 hr, unless stated otherwise. The phosphate sorption isotherms for the respective metal oxides are presented in Figures 8 and 9. The standard deviation is shown on each point as before.

On the high-surface-area cerium(IV) and thorium oxides, relatively large weighing errors were present at the low phosphate concentrations because of the small metal oxide samples used, 0.0010–0.0025 g. These errors disappeared as the sample size was increased in the studies at the higher phosphate concentrations. The principal source of error at the higher phosphate concentrations was the counting error.

The phosphate sorption isotherms for 700°-fired zirconium oxide and 400°-fired ceric oxide are shown in Figure 8. The zirconium oxide sorption isotherm shows the presence of two plateaus, at 39.5 ± 1.0 and at 30.7 ± 1.0 Å²/sorbed phosphate molecule, respectively, where the amount of phosphate sorbed is independent of changes in the concentration of phosphate. Plateau-like regions at 44 ± 4, 39 ± 2.5, and 34.2 ± 1.5 Å²/sorbed phosphate molecule, respectively, may also be

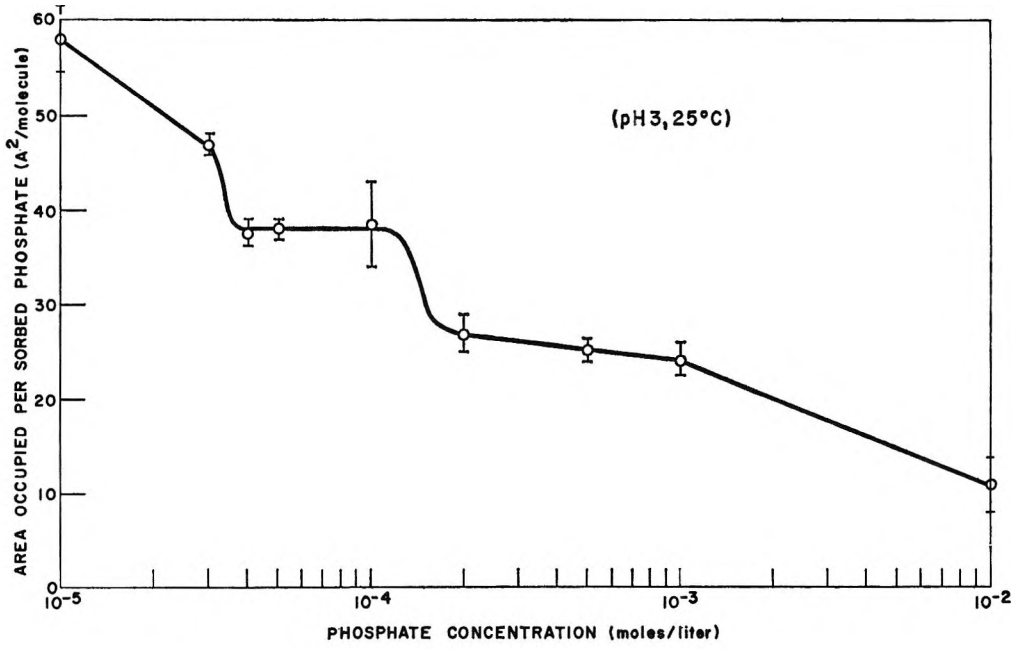

Figure 10. Phosphate sorption on 100-mesh zirconium metal powder.

present in the ceric oxide–phosphate sorption isotherm. Phosphate sorption isotherms were also obtained on the thorium oxide at both pH 3 and 6 as shown in Figure 9. The plateaus in the phosphate sorption isotherm on the thorium oxide at pH 3 occur at 31.0 ± 1.2 and 25.1 ± 1.5 Å²/sorbed phosphate molecule, respectively. At pH 6 the thorium oxide–phosphate sorption isotherm shows plateaus at 35.4 ± 0.5 and 30.5 ± 0.5 Å²/sorbed phosphate molecule, respectively. The phosphate sorption isotherm at pH 3 for powdered zirconium metal is shown in Figure 10 and shows a possible plateau at about 37.8 ± 0.5 Å²/sorbed phosphate molecule. The deviation shown on each point for the zirconium metal is due to the experimental scatter present in the duplicate or triplicate determinations.

The phosphate sorption isotherm shown in Figure 11 was obtained on hafnium oxide fired at 400°. The results of this study show that the isotherm for hafnium oxide does not contain a sorption plateau. Preliminary studies carried out on the fired oxides of titanium(IV) and yttrium indicate that the uptake of phosphate on these materials greatly exceeds monolayer coverages. These high levels of phosphate uptake on titania and yttria, ~7 Å²/sorbed phosphate molecule, indicated that these oxides are probably being converted to the phosphates in bulk.

Firing Temperature. The effect of firing temperature on phosphate sorption by zirconium oxide was also studied. The firing temperature was varied between 400 and 1100°. The studies were carried out at pH 2 in a 10^{-2} *M* phosphate solution. The results of this study, as shown in Table I, reveal that the amount of phosphate sorbed per unit area is essentially independent of firing temperature. Lauric acid adsorption on fired aluminum oxides,[6] on the other hand, was found to be quite sensitive to firing temperature. The latter phenomenon was thought to be related to the pore-size variations with firing temperature; this same explanation may apply to the ZrO_2 fired at 1100°, where the surface area as determined by the nitrogen BET method may not be entirely available to the larger phosphate molecule for sorption.

Table I: Phosphate Sorption on Zirconium Oxides Fired at Temperatures Ranging from 400 to 1100°

Material firing temp, °C	BET surface area, m²/g	Phosphate sorbed, × 10⁶ mol/m²	Area occupied by phosphate, Å²/molecule
ZrO_2 (400)	129.8	4.2 ± 0.1	40 ± 1.0
ZrO_2 (600)	26.6	4.2 ± 0.1	40 ± 1.0
ZrO_2 (700)	18.9	4.2 ± 0.1	40 ± 1.0
ZrO_2 (800)	7.9	4.4 ± 0.2	38 ± 2.0
ZrO_2 (1100)	2.8	3.9 ± 0.1	43 ± 1.0

Discussion

Geometrical Considerations. Hydrous metal oxides when fired at high temperatures are thought to be completely dehydrated. The resulting surfaces are reactive and when exposed to water vapor may form a hydroxylated surface. In the discussion that follows, a simple hydroxylated metal oxide surface is assumed. The arguments which follow might also have been made for a surface of reactive metal ion sites, since two hydroxyl sites are equivalent to one metal ion site. From a consideration of the fluorite crystal structure of the metal oxides used in this study, it seems reasonable to assume

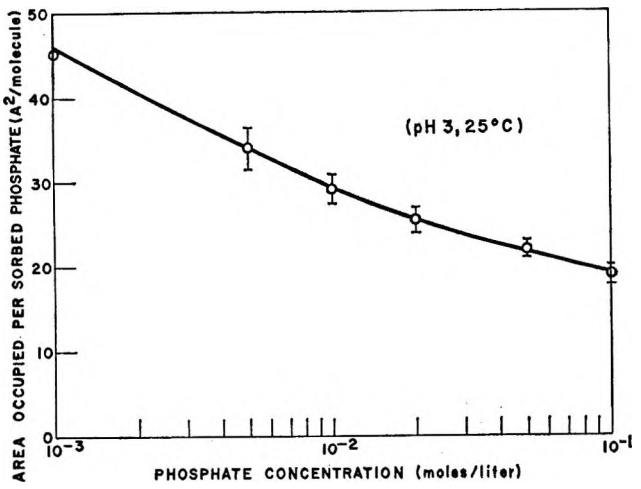

Figure 11. Phosphate sorption on fired hafnium oxide.

as an approximation that the oxygen ions of the surface would be positioned the same as those in the bulk. This leads to a strain-free, highly symmetrical configuration involving a geminal hydroxyl site for each metal site on the surface. Wadsworth[15] in studying the thorium oxide surface by means of infrared absorption spectrometry has attributed the intense band he found at 3650 cm^{-1} to this geminal structure. Similar studies have not been carried out on the fired oxides of cerium(IV) or zirconium; however, it is assumed that the geminal-type structure is present on these surfaces as well.

The effect of pH on the rate and extent of phosphate sorption by the crystalline metal oxides and powdered zirconium metal indicates that the more highly protonated forms of the orthophosphate are probably preferred for sorption. The strong effects of pH on phosphate sorption on powdered zirconium metal indicate that its surface, which is certainly oxidized, differs from the fired metal oxide surface. The amphoteric nature of the metal oxides will also affect the uptake of phosphate by them. The surface hydroxyl sites on the fired metal oxides are certainly affected by the solution hydroxyl ion concentration. At high hydroxyl ion concentrations, there is a keen competition for the site between the phosphate and hydroxyl ions. Until more definitive studies, such as infrared studies of the sorbed phosphate molecules, are carried out on these surfaces, one can only speculate as to the extent of the competition or the form of the sorbed phosphate molecule. One might assume the sorbed phosphate molecule is ionic in nature, with the potassium ion as a counterion in the solvent, close to the surface, as is the case in colloidal solutions.

The presence of plateaus in the phosphate sorption isotherms on the metal oxides and on the powdered zirconium metal are believed to result from chemisorbed monolayers. The sorption of phosphate species is thought to be related in a stoichiometric manner to the geminal hydroxyl groups (or metal ion sites). To establish this stoichiometry, it is necessary to know the density of geminal hydroxyls on the metal oxide surfaces. In the past, the density of reactive sites on heterogeneous surfaces was usually assumed to be equal to the average density in the 100, 101, and 111 crystallographic planes. This assumption certainly is reasonable and could be used in the absence of further information on the subject. However, in 1927–1928, Kossel[16] and Stranski[17] independently developed a theory of crystal growth which enables one to predict the external form of a crystal from the structure of the lattice. The theory is based on the assumption that the probability of continuation of growth on a crystal plane is larger on points where the energy gained by the addition of a new atom or ion is the largest; thus the 100 and 111 faces would predominate. However, since this is an argument based on thermodynamics and ignores kinetic factors, its universal validity might be questioned.

Ryshkewitch[18] states, "Thoria crystallizes in the cubic system in the form of cuboctahedrons. Apparently, it has no other crystal forms." The analysis of the phosphate sorption data as presented in this discussion is based on the assumption that metal oxide crystal surfaces are composed of equal amounts of the 100 and 111 crystallographic planes.

The sorbed phosphate molecule was assumed to be tetrahedral and to have an oxygen-to-oxygen distance of 2.54 Å, a value found by Smith[14] and coworkers as the average distance between oxygens in crystalline phosphoric acid. This value is in agreement with the value predicted by Durrant and Durrant[13] for oxygen atoms of 75% ionic character in the phosphate radical. The calculated area occupied by a freely rotating phosphate molecule is thus 23.50 $Å^2$ and has a diameter of 5.47 Å.

Scale models of the 100 and 111 planes of the respective metal oxides and of the phosphate molecule were prepared. Zirconium oxide is essentially monoclinic, with the following cell dimensions: a_0 = 5.1454 Å, b_0 = 5.2075 Å, c_0 = 5.3107 Å, and B = 99°, 14′. Monoclinic zirconium oxide has a slightly distorted cubic fluorite structure. To make possible a simple geometric analysis of the zirconium oxide structure, the system was assumed to be pseudocubic with a_0 equal to 5.22 Å, an arithmetic average of c_0, b_0, and c_0. The

(15) M. E. Wadsworth and F. A. Olson, Progress Report for the Period Feb 1, 1964 to Jan 31, 1965, Subcontract 2176, Chemical Technology Division, Oak Ridge National Laboratory, Oak Ridge, Tenn.

(16) W. Kossel, *Nachr. Akad. Wiss. Göettingen Math.-Physik. Kl.*, IIA, 135 (1927).

(17) I. N. Stranski, *Z. Phys. Chem.* (Frankfurt am Main), **136**, 259 (1928); *Discussions Faraday Soc.*, **5**, 13 (1949).

(18) E. Ryshkewitch, in "Oxide Ceramics," Academic Press Inc., New York, N. Y., 1960, p 408.

100 and 111 crystallographic planes were again assumed to be predominant.

In preparing a model of the sorption of phosphate on the respective metal oxide surface planes, the following assumptions were made: a stoichiometry exists between the chemisorbed phosphate molecules and the geminal hydroxyl groups or metal ion sites on the metal oxides surface and the sorbed phosphate molecules are symmetrically arranged and are sorbed in such a manner as to either permit or prevent free rotation of the sorbed species depending on their separation. The average surface area occupied by a geminal hydroxyl group is equivalent to the average surface area occupied by a metal ion site for the respective oxide as presented in Table II.

Table II: The Area Occupied by a Geminal Hydroxyl Group on the 100 and 111 Crystallographic Planes of Three Metal Oxides

Metal oxide	Surface area per geminal hydroxyl group, Å²/group — 100 plane	111 plane
Zirconium oxide	13.62	11.42
Thorium oxide	15.63	13.53
Cerium(IV) oxide	14.63	12.64

Models of the phosphate sorption on the 100 and 111 planes of the respective metal oxides were prepared. These models consist of schematics of the respective planes and of the sorbed phosphate molecules properly oriented and drawn to the same scale.

The phosphate sorption models for the fired oxides indicate the phosphate species are sorbed with a stoichiometry of either two or three geminal hydroxyl groups per sorbed phosphate molecule, irrespective of the plane it is being sorbed on. This stoichiometry does not mean that a sorbed phosphate molecule reacts with two or three geminal hydroxyl groups but means that the average surface area the sorbed molecule occupies is equivalent to that occupied by two or three geminal groups or metal ion sites. The stoichiometry is thus an indication of how closely the sorbed phosphates are packed and whether or not they are far enough apart to rotate freely. Where the stoichiometry is three geminal hydroxyl groups to one phosphate molecule, the sorbed molecules are free to rotate; where the stoichiometry is 2:1, the molecules are not free to rotate, except on the thorium oxide surface where $a_0 =$ 5.59 Å as compared with 5.41 and 5.22 Å for the cerium(IV) and zirconium oxide systems. Consequently, it is possible to have a third type of stoichiometry on the 100 plane of the thorium oxide, which is three geminal hydroxyl groups to two sorbed phosphate molecules. Models of the different types of stoichiometry for the respective planes of thorium oxide are presented in Figure 12. Table III contains all of the arrangements which are probable for the metal oxide systems. The chemisorbed phosphate monolayers predicted by these arrangements are compared with the experimentally observed plateaus of the phosphate sorption isotherm.

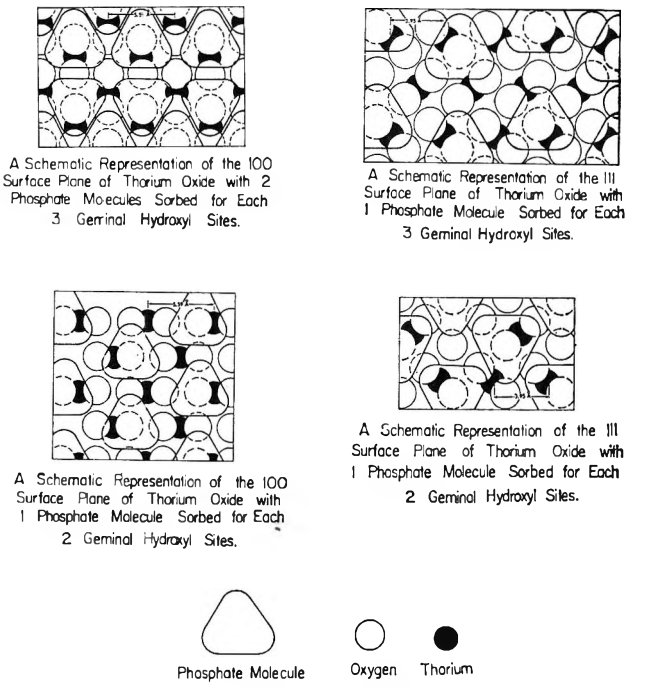

Figure 12. Schematic representations of surface planes of thorium oxide with phosphate molecules adsorbed: solid lines, surface plane; dashed lines, below surface.

Table III: Monolayer Areas Calculated from Proposed Phosphate Sorption Stoichiometries on the Metal Oxides and Experimentally Determined Areas

Metal oxide	Stoichiometry[a] — 100 plane	111 plane	Predicted areas, Å²/sorbed phosphate molecule	Experimentally determined areas, Å²/sorbed phosphate molecule
Zirconium oxide	3:1	3:1	37.53	39.5 ± 1.0
	3:1	2:1	31.82	30.7 ± 1.0
	2:1	3:1	30.75	37.8 ± 0.5[b]
Ceric oxide	3:1	3:1	40.9	34.2 ± 1.5
	3:1	2:1	34.58	39.0 ± 2.5
	2:1	3:1	33.59[c]	44.0 ± 4.0
	2:1	2:1	27.27	
	4:1, 3:1	3:1	44.0[d]	
Thorium oxide	2:1	3:1	35.92	35.4 ± 0.5
	2:1	2:1	29.16	30.5 ± 0.5
	3:2	3:1	32.15[c]	31.0 ± 1.2
	3:2	2:1	25.25	25.1 ± 1.5

[a] Ratio of geminal hydroxyl groups to sorbed phosphate molecules. [b] Zirconium metal substrate. [c] Not very probable. [d] Equal amounts of 4:1 and 3:1 stoichiometries on the 100 plane.

The agreement between the observed and predicted monolayer coverages is satisfactory in all cases except for the value of 44 Å²/sorbed phosphate molecule on the cerium(IV) oxide. To predict monolayer coverage at 44 Å², it is necessary to assume that an equal amount of 4:1 and 3:1 stoichiometries is present on the 100 plane. The existence of such a stoichiometry is questionable; however, it is possible.

The scatter on the points for the experimentally determined sorption plateaus for the zirconium metal and cerium(IV) oxide is large, and the presence of these plateaus is questionable. However, the scatter on the points for the experimentally determined plateaus for the zirconium and thorium oxides is very small, and these plateaus certainly appear to be present. The agreement between the experimentally observed monolayers and those predicted by the proposed model certainly indicates that the model is a workable one.

Low-energy electron diffraction studies on the fired metal oxides under the proper conditions might provide support for this model if they could establish which crystallographic planes predominate in the fired metal oxide surfaces.

Acknowledgments. The author wishes to personally thank Dr. R. G. Wymer of the Oak Ridge National Laboratory for the many hours spent with him in discussions on this work. Thanks are also expressed to Dr. K. H. McCorkle and to F. Nelson for their many helpful ideas and to Arnold Lyle for making the sorption measurements. The author also wishes to thank the many other people at Oak Ridge National Laboratory who assisted him in this work. The supporting analytical services of W. R. Laing and members of his group at Oak Ridge National Laboratory are also gratefully acknowledged.

Nuclear Magnetic Resonance Studies of Weak Intermolecular Forces: Medium Effects in Saturated Heterocyclic Rings[1]

by Harold Finegold

U. S. Department of Agriculture, Agriculture Research Service, Human Nutrition Research Division, Beltsville, Maryland 20705 *(Received March 22, 1968)*

Vicinal coupling anomalies similar to those noted in acyclic and cyclic amino acid systems can be explained by reference to enhanced medium effects that develop in more appropriate nmr model systems. These incorporate an ethanic fragment directly into a five-membered ring. A gradation of values in *gauche*-vicinal coupling constants spanning a 14% range can be achieved despite the fact that the systems are rotationally invariant. This range of coupling, effected by weak intermolecular forces other than H bonding, corresponds to as much as 35% of the free energies typically associated with corresponding ethanic flexible systems. It is concluded that rotational energies of acyclic systems that are calculated from relations using medium effects on spin-coupling constants may contain an unspecified contribution from solute–solvent intermolecular forces. Detailed nmr parameters are determined for all systems using field-swept spin decoupling, computer calculations, second-moment analyses, and explicit analytical solutions.

Introduction

The internal rotational energies of a large number of liquid ethanic systems have been treated by nmr spectroscopy using both the variable-temperature approach for certain of the weakly coupled ones[2] and the variable-medium effect for the more strongly coupled, including asymmetric ethanes.[3-5] The reliability of both methods depends on the maintaining of a simple exponential relation between the rotationally averaged nmr parameters and the rotational energies of the n conformers of the form $\langle J_{vic} \rangle = \sum_n^n J \exp(-k^n E)$. It is usually assumed in the defined chemical systems, particularly when the vicinal spin-coupling constant rather than the chemical shift is the nmr parameter of choice,

(1) H. Finegold, Abstracts, 153rd National Meeting of the American Chemical Society, Miami Beach, Fla., April 1967, No. O75.

(2) H. S. Gutowsky, G. G. Belford, and P. E. McMahon, *J. Chem. Phys.*, **36**, 3353 (1962).

(3) R. J. Abraham, L. Cavalli, and K. G. R. Pachler, *Mol. Phys.*, **11**, 471 (1967).

(4) H. Finegold, *J. Chem. Phys.*, **41**, 1808 (1964).

(5) H. Finegold, *Abstr. Symp. Mol. Spectrosc. Ohio State Univ.*, **18**, 55 (1963).

that no serious deviation from adherence to this simple relation can affect the applicability of the nmr data. It is the purpose of this paper to examine how reliable this assumption is under chemical conditions that cannot be considered exceptional. The examination must be experimental, since any *a priori* determination is precluded by the absence of comprehensive details on the weak intermolecular forces affecting spin couplings.

An indication that coupling constant sensitivity to weak intermolecular forces other than hydrogen bonding might be much greater than expected first appeared sometime ago in the complex A_3BCD analyses of the geminal coupling in certain asymmetric ethanes. It was experimentally shown, contrary to all existing theoretical considerations, that this coupling could significantly change value when the molecule was rotated, although the angular coordinate remained invariant between the specific coupled protons under consideration.[4,6] Recently a number of workers have rediscovered, corroborated, and commented on the same effect between geminal protons in similar systems.[7,8] The broader significance of the weak interactions responsible for geminal coupling anomalies lies particularly in their possible pervasiveness to the diagnostically very important vicinal couplings used to determine rotational energies, dielectric constants, dihedral angles, conformations, and other molecular properties. There have been only scattered literature reports of vicinal-coupling anomalies due to medium effects, and the deviations observed have been much too ambiguous. Undoubtedly, the real difficulty in unambiguously identifying the weaker interactions in important systems can be traced to their being so effectively masked in these systems by the more dominant forces, such as internal rotation. During a study of the rotational energies of several (acyclic) amino acid systems of biomolecular significance along with a comparison of the nmr properties of the cyclized homologs, cycloserine and homocysteine thiolactone, small vicinal-coupling anomalies noted in the latter were considered to have a possible relationship to unsatisfactory energies calculated for the former. A more suitable nmr model system to elucidate the pervasive possibilities of anomalous vicinal coupling effects in this and similar systems is here considered.

The model used in this paper incorporates an ethanic fragment directly into a medium-sized ring. Medium-sized rings are chosen because larger rings that are not substantially substituted or bridged may have low barriers to inversion, and small rings, while having distinct advantages from the point of view of spectral analysis, are so highly strained that the hybridization of the ring carbons can no longer be considered as sp^3. Five-membered rings represent an intermediate case between flexible and strained rings, where the tetrahedral character is still sufficiently strong to ensure valid comparisons with the structural features of acyclic hydrocarbons, and the thermodynamic barrier to ring inversion is relatively high (of the order of 15 kcal/M).

Dioxolanes ($OCH_2CH_2OCH_2$) and related structures, such as dioxolones (OCH_2CH_2OCO), thia-oxolanes ($OCH_2CH_2SCH_2$), and thiadioxolones (OCH_2CH_2OSO), where an alkyl group or other substituent may replace any of the hydrogens, have been previously investigated[9-12] by nmr and other techniques for various purposes unrelated to the present work. Ethylene-2,1,3-thiadioxolone-2 is the chief compound examined in this work and is diagrammatically represented in Figure 1a, with X = S. The quasi-axial double bond makes an angle of approximately 115° with the plane of the ring. The strong π-d character associated with the heteroatom bonding orbitals insures that the potential barrier for this ring will be well above the high values normally associated with hydrocarbon five-membered rings. For the dual purposes of comparing effects on spectral parameters and for determining the assignments of chemical shifts to positions *trans* (*anti*) and *cis* (*syn*) to the double bond, the *anti*- and *syn*-methyl-substituted isomers are also examined (propylene-2,1,3-thiadioxolone-2, Figure 1b and c, X = S). The ethanic configuration is always expected to be staggered, as correctly shown in the projection diagrams, owing to the localized pyramidal configuration in the vicinity of the heteroatom and the potential interactions involving the methyl group. Finally, the analogous methyl-substituted compound with X = C (propylene-1,3-dioxolone-2, Figure 1d) is examined for the purpose of comparing the preceding nmr parameters with the situation where the X atom is trigonal, so that the molecule is not capable of existing in stereoisomeric forms.

Experimental Section

Research grade dioxolones and thiadioxolones (which can be formally considered as derivatives of carbonic and sulfurous acids, respectively) were obtained commercially. They were scanned by infrared and nmr spectroscopy in order to determine their purity and conformity to structure. Solvents, including the per-deuterated materials where required, were of the highest purity and were vacuum distilled prior to use. Spectra

(6) H. Finegold, *Proc. Chem. Soc.*, 213 (1962).

(7) S. L. Smith and R. H. Cox, *J. Chem. Phys.*, **45**, 2848 (1966).

(8) E. I. Snyder, *J. Amer. Chem. Soc.*, **88**, 1155 (1966); **85**, 2624 (1963).

(9) R. Fraser, R. W. Lemieux, and J. D. Stevens, *J. Amer. Chem. Soc.*, **83**, 3901 (1961).

(10) M. Anteunis and F. Alderweireldt, *Bull. Soc. Chim. Belges*, **73**, 889, 903 (1964).

(11) J. G. Pritchard and P. C. Lauterbur, *J. Amer. Chem. Soc.*, **83**, 2105 (1961).

(12) R. J. Abraham and K. A. McLauchlan, *Mol. Phys.*, **5**, 513 (1962); R. J. Abraham, *J. Chem. Soc.*, 256 (1965).

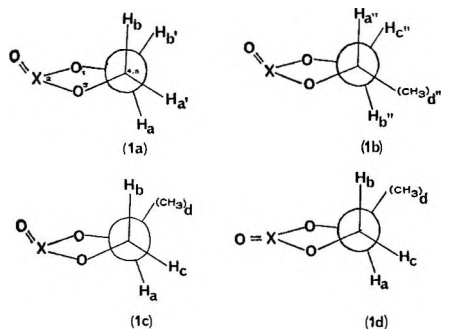

Figure 1. Newman projection formulas for dioxolone-type compounds, where X = S in 1a–c and X = C in 1d. The conformation is *anti* in 1b and *syn* in 1c.

were obtained on a Varian Associates high-resolution spectrometer operated with external field-frequency lock at 60.005 MHz in the field-swept mode. Spin-decoupled spectra were also obtained by field sweeping during the double irradiation. Computer calculations were performed at the Department of Commerce, National Bureau of Standards, Computer Services Division, and at the Department of Agriculture, ARS, Biometrical Services Unit. Prepared solutions were examined at 37° with small quantities of tetramethylsilane (TMS) admixed for internal referencing of the line frequencies, $-\Delta\nu$ (in hertz), where $\Delta\nu = \nu_{sample} - \nu_{TMS}$. Lines were measured by audiomodulation of the radiofrequency in conjunction with the repetitive application of digital sweeps of the magnetic field from a triggering 0.5-V signal for the most optimized calibration stability.

Some of the compounds cited in this work, have been previously examined by nmr spectroscopy, as noted above, but only first-order estimates of parameters or estimates based on interpolations from spectral tabulations (such as those by Wiberg and Nist[13]) have been made. The investigation described here required fully detailed and accurate treatments of all spectra.

In the spectral analyses, a perturbation treatment of the A_2B_2 spectra[14] was found to be inadequate, because the medium effects in several cases generated J to δ ratios associated with appreciable mixing of basis functions. In general, use of the explicit expressions derived by Dischler and Englert[15] was found to give the most satisfactory results, as subsequently verified by matching the experimental frequencies and intensities with a computer diagonalization[16,17] of the trial spin Hamiltonians. Chemical shifts were initially calculated by second-moment analyses. This information in conjunction with Dischler and Englert's observations was used to locate the lines that determined the values of N ($=J_{ab} + J_{ab'}$), L ($=J_{ab} - J_{ab'}$), and M ($=J_{aa'} - J_{bb'}$). Most of the difficulty in the analyses was encountered in determining K ($=J_{aa'} + J_{bb'}$). This required the resolution and accurate identification of six lines in each half-spectrum in addition to the lines that determine N, if a sufficiently accurate estimate of this parameter, crucial for determining medium effects on vicinal coupling, were to be obtained. An additional difficulty, peculiar to the wide range of chemical shifts and the magnitudes of the constantly varying coupling constants, was the fact that the spectral lines connecting with the $3S_0$ states[18] actually crossed over in several spectra to emerge in the opposite halves among transitions of the nuclear sets with differing chemical shifts. Confusion and mislabeling of transitions were avoided in this regard by calculating sets of parameters in the neighborhood of the crossover point.

The analyses of the six-spin $ABCD_3$ spectra were performed as discussed earlier,[14,19] using an initial $ABMX_3$ model. Again, extensive use was made of the principles of subspectral analysis with the A and B transitions being treated as a composite of eight subspectra, and ν_A and ν_B in the compilation of transition

Table I: Ethylene-2,1,3-thiadioxolone-2 ($OCH_aH_a'CH_bH_b'OSO$).

Chemical-Shift Assignments of *syn* (ν_a) and *anti* (ν_b) Hydrogens for 5 % (v/v) Solutions of Varying Dielectric Value (60 MHz)

ϵ (solvent)	Solvent	$\nu_0\delta$ ($=\nu_a - \nu_b$), Hz	ν_a, Hz	ν_b, Hz
	Nonaromatic			
2.0	$CH_2CH_2CH_2CH_2CH_2CH_2$[a]	24.12	275.92	251.80
2.2	CCl_4	21.84	288.63	244.96
2.2	$OCH_2CH_2OCH_2CH_2$	19.16	286.16	247.84
4.8	$CDCl_3$	20.96	290.77	248.85
20.7	$(CD_3)_2CO$	15.26	280.3	265.1
22.4	OCH_2CH_2OSO[b]	16.72	275.46	258.74
37.5	CH_3CN	16.86	277.65	260.79
	Aromatic			
2.3	CHCHCHCHCHCH	32.64	244.9	212.3
12.3	NCHCHCHCHCH	20.50	275.95	255.45
34.8	O_2NCHCHCHCHCHCH	19.16	292.16	253.84

[a] Contains $CDCl_3$ (10%) to aid miscibility. [b] Neat liquid.

(13) K. B. Wiberg and B. J. Nist, "Interpretation of NMR Spectra," W. A. Benjamin Co., New York, N. Y., 1962.

(14) H. G. Hecht, *Theor. Chim. Acta*, **3**, 202 (1965).

(15) V. B. Dischler and G. Englert, *Z. Naturforsch.*, **16a**, 1180 (1961).

(16) A. A. Bothner-By and C. Naar-Colin, *J. Amer. Chem. Soc.*, **83**, 231 (1961).

(17) R. L. Kornegay and L. C. Snyder, Bell Telephone Laboratories Technical Memorandum, Jan 1963.

(18) Designated according to J. A. Pople, W. G. Schneider, and H. J. Bernstein, "High-resolution Nuclear Magnetic Resonance," McGraw-Hill Book Co., Inc., New York, N. Y., 1959.

(19) D. D. Elleman, S. L. Manatt, and C. D. Pearce, *J. Chem. Phys.*, **42**, 650 (1965).

Table II: Geminal and *trans*-Vicinal Coupling Constants for $OCH_aH_{a'}CH_bH_{b'}OSO$ in Various Solvents (60 MHz)

Solvent	% Solute (v/v)	$J_{a'b}$ (= $J_{ab'}$), Hz	J_{ab} (= $J_{a'b'}$), Hz	N, Hz	L, Hz
$CH_2CH_2CH_2CH_2CH_2CH_2$[a]	5	−8.10	6.48	−1.62	14.58
	8	−8.29	6.59	−1.70	14.87
CCl_4	5	−8.15	6.58	−1.57	14.73
	40	−8.30	6.62	−1.68	14.91
$OCH_2CH_2OCH_2CH_2$	5	−8.31	6.60	−1.71	14.90
	40	−8.45	6.56	−1.89	15.00
$CDCl_3$	5	−8.42	6.70	−1.72	15.12
	40	−8.36	6.59	−1.77	14.95
$(CD_3)_2CO$	5	−8.29	6.51	−1.78	14.79
	40	−8.40	6.46	−1.94	14.86
OCH_2CH_2OSO[b]	...	−8.41	6.56	−1.85	14.97
CH_3CN	5	−8.42	6.58	−1.84	15.00
	40	−8.36	6.52	−1.84	14.88
CHCHCHCHCHCH	5	−8.25	6.56	−1.69	14.80
	40	−8.38	6.55	−1.78	14.97
NCHCHCHCHCH	5	−8.31	6.52	−1.79	14.83
	40	−8.27	6.49	−1.78	14.76
$O_2NCHCHCHCHCHCH$	5	−8.42	6.54	−1.89	14.96
	40	−8.31	6.57	−1.74	14.88

[a] Contains $CDCl_3$ to aid miscibility. [b] Neat liquid.

energies for the two spin AB-type system being replaced by $\{\nu_{A'} + F_z^1/_2(J_{AM}) + F_z^3/_2(J_{AX})\}$ and $\{\nu_{B'} + F_z^1/_2(J_{BM}) + F_z^3/_2(J_{BX})\}$, respectively. Spin decoupling was required to obtain preliminary estimates of certain chemical shifts. Coupling constants could not be obtained for *syn*-propylenethiadioxolone, which requires a superconducting solenoid for optimal measurements. Nevertheless, it was possible to obtain satisfactory estimates of the chemical shifts for binary systems of this compound using approximation methods.

Results

1. Ethylene-2,1,3-thiadioxolone-2. This compound was examined in varying concentrations in ten systems representing a range of solvent dielectric constants. The assignments of the calculated chemical shifts to specific protons *syn* and *anti* to the double bond was established as outlined later in the discussion of the propylenethiadioxolone systems and are given in Table I. Geminal and *trans*-vicinal couplings in systems covering the same range of solvent dielectrics and including very dilute and more concentrated solution data are included in Table II, along with the calculations of the N and L parameters from which the couplings were obtained ($M \leqslant 0.5$ Hz for all systems). Table III includes data on the *gauche*-vicinal couplings for the same binary systems but taken over a wider concentration range for those systems in which this constant appeared to show more sensitivity to concentration effects.

The geminal couplings show notable variation with both solvent dielectric and concentration within any particular solvent. The range is from −8.15 Hz in 5% CCl_4 to −8.45 Hz in 40% dioxane. Concentration variations approximating 0.2 Hz were found for the

Table III: *Gauche*-Vicinal Coupling Constants for $OCH_aH_{a'}CH_bH_{b'}OSO$ at Several Concentrations in Various Solvents (60 MHz)

Solvent	ϵ (solvent)	% solute, (v/v)	$J_{aa'}$ (= $J_{bb'}$), Hz	K, Hz
$CH_2CH_2CH_2CH_2CH_2CH_2$[a]	2.0	5	7.00	13.99
		8	6.90	13.79
CCl_4	2.2	2.5	6.99	13.97
		5	7.00	14.00
		10	6.85	13.70
		40	6.74	13.48
$OCH_2CH_2OCH_2CH_2$	2.2	5	6.83	13.65
		20	6.92	13.83
		40	6.86	13.72
CHCHCHCHCHCH	2.3	5	7.46	14.92
		10	7.56	15.11
		20	7.10	14.19
		40	6.84	13.67
$CDCl_3$	4.8	5	6.88	13.75
		40	6.63	13.25
NCHCHCHCHCH	12.3	5	6.74	13.47
		40	6.61	13.22
$(CD_3)_2CO$	20.7	5	6.77	13.53
		40	6.62	13.24
OCH_2CH_2OSO[b]	22.4	...	6.70	13.39
$O_2NCHCHCHCHCHCH$	34.8	5	6.76	13.51
		40	6.69	13.37
CD_3CN	37.5	5	6.70	13.39
		40	6.60	13.19

[a] Contains $CDCl_3$ to aid miscibility. [b] Neat liquid.

two solvents with low dielectric values, CCl_4 and $OCH_2CH_2OCH_2CH_2$. The *trans*-vicinal couplings (*trans* referring to proton positions on opposite sides of the ring) show little variation with solvent and average 6.56 Hz in dilute solution: the low is 6.48 Hz and the high is 6.70 Hz, corresponding to a 3% variation. By contrast as well as by all other standards, the most significant variations occur for the *gauche*-vicinal couplings, which range from a low of 6.61 Hz to a high of 7.56 Hz; *i.e.*, they show a change of about 14%.

The chemical-shift differences, $(\nu_0\delta)_{b-a}$, show more than a twofold variation over the solvent dielectric range with a low of 15.26 Hz in 5% acetone-d_6 and a high of 32.64 Hz in benzene. The shift difference in CCl_4 is 21.84 Hz but even here concentration effects are notable: in a 10% concentration in CCl_4 solution, the shift decreases to 20.08 Hz and continues decreasing as the concentration in CCl_4 increases (though no difference detectable within experimental error was found between a 5 and 1% concentration in CCl_4).

2. dl-Propylene-2,1,3-thiadioxolone-2. In order to determine the chemical-shift assignments (*syn* or *anti* to the quasi-axial double bond) of the ethylenethiadioxolone indicated in Table I and to determine if the *gauche*-vicinal effect could be found to persist in a slightly more substituted system, the two geometric isomers of *dl*-propylene-2,1,3-thiadioxolone-2 were examined. The results of the $ABCD_3$ analyses on the chemical shifts of the *anti* isomer are indicated in Table IV. Table V gives the coupling constants for the same isomer. The chemical shifts of the *syn* isomer, determined by field-swept homonuclear spin decoupling and second-moment analyses of each of the ABC bands, are listed in Table VI. Because of the high value of J/δ, spin-coupling parameters could not be accurately determined, except for J_{ad}, but the spectral features could be approximately reproduced using J's similar to those of the *anti* isomer.

Table IV: Calculated Chemical Shifts and Proton Position Assignments in *anti-dl*-Propylene-2,1,3-thiadioxolone-2 Binary Systems (60 MHz)

Solvent	$\nu_{a''}$, Hz	$\nu_{b''}$, Hz	$\nu_{c''}$, Hz	$\nu_{d''}$, Hz
CCl_4	302.2	277.8	229.8	83.7
$CDCl_3$	306.1	280.1	231.3	84.8
$(CD_3)_2CO$	306.6	281.4	237.3	83.4
CD_3CN	305.3	279.4	233.4	81.8
CDCDCDCDCDCD	285.6	258.2	207.3	62.0
NCDCDCDCDCD	304.4	279.4	230.0	74.2
O_2NCDCDCDCDCDCD	308.1	282.5	233.5	82.9

The *gauche*-vicinal couplings, J_{ac}, of the *anti* isomer, calculated by computer methods, show a notably significant variation though the magnitude of the variation is not as great as for the comparable coupling in ethylenethiadioxolone. The variations found for the geminal couplings, J_{bc}, and also J_{ad} (the methyl-to-methine hydrogen coupling), were less significant. The *trans*-vicinal coupling, J_{ab}, also showed little variation. The negative long-range coupling, J_{cd}, never deviated to a positive nor did it decrease to significantly more negative values.

Of the chemical shifts ν_b, ν_c, $\nu_{b''}$, and $\nu_{c''}$ in both propylenethiadioxolone isomers (Figure 1b and 1c), it can be shown that the difference between one pair of chemical shifts, $\nu_{c''} - \nu_c$, selected from among the four possible pairs of differences containing one value from each isomer, should be approximately equal to the chemical-shift difference, $(\nu_0\delta)_e$, in ethylenethiadioxolone (Figure 1a). From Figure 1a

$$\nu_b = (\Delta\sigma_{SO})_m + \sum_l \Delta\sigma_l$$

$$\nu_a = (\Delta\sigma_{SO})_n + \sum_o \Delta\sigma_o$$

where $(\Delta\sigma_{SO})_m$ and $(\Delta\sigma_{SO})_n$ are specific contributions to the average value of the screening tensors at b and a, respectively. These specific contributions are due to the diamagnetic anisotropy of the S=O bond susceptibility. $\sum_l \Delta\sigma_l$ and $\sum_o \Delta\sigma_o$ are the summation of the several remaining average screening tensors that affect ν_b and ν_a, respectively. Since it is readily shown that $\sum_l \Delta\sigma_l = \sum_o \Delta\sigma_o$, then

$$\nu_b - \nu_a = (\Delta\sigma_{SO})_m - (\Delta\sigma_{SO})_n$$

From Figure 1b and c

$$\nu_{c''} = (\Delta\sigma_{SO})_{n'} + (\Delta\sigma_{CC})_p + \sum_q \Delta\sigma_q$$

$$\nu_c = (\Delta\sigma_{SO})_{m'} + (\Delta\sigma_{CC})_r + \sum_s \Delta\sigma_s$$

where $\Delta\sigma_{CC}$ refers to the screening-tensor contribution of the methyl–carbon bond anisotropy. Since $(\Delta\sigma_{CC})_p = (\Delta\sigma_{CC})_r$ and $\sum_q \Delta\sigma_q = \sum_s \Delta\sigma_s$, then

$$\nu_{c''} - \nu_c = (\Delta\sigma_{SO})_{n'} - (\Delta\sigma_{SO})_{m'}$$

Because of the near equality in the value of their corresponding dihedral angles, $(\Delta\sigma_{SO})_{n'} \approx (\Delta\sigma_{SO})_n$ and $(\Delta\sigma_{SO})_{m'} \approx (\Delta\sigma_{SO})_m$, so that

$$\nu_{c''} - \nu_c \approx (\nu_0\delta)_e \approx (\nu_b - \nu_a)$$

Thus the chemical-shift difference, $(\nu_0\delta)_e$, in ethylenethiadioxolone approximately equals the difference between the chemical shifts of the hydrogens *trans* to the methyl groups in *anti*- and *syn*-propylenethiadioxolone.

Experimentally, the existence of such a pair of chemical shifts in the propylenethiadioxolone isomers

Table V: Calculated Coupling Constants in *anti-dl*-Propylene-2,1,3-thiadioxolone-2 Binary Systems

Solvent	J_{ad}, Hz	J_{bc}, Hz	J_{ab}, Hz	J_{ac}, Hz	J_{cd}, Hz	J_{bd}, Hz
CCl_4	6.35	−8.22	6.82	6.10	−0.15	0
$OCH_2CH_2OCH_2CH_2$	6.35	−8.29	6.74	5.95	−0.15	0
CD_3CN	6.40	−8.39	6.80	5.80	−0.15	0
NCDCDCDCDCD	6.35	−8.26	6.73	5.89	−0.15	0
CDCDCDCDCDCD	6.35	−8.30	6.70	5.96	−0.15	0

Table VI: Chemical Shifts and Proton Position Assignments in *syn-dl*-Propylene-2,1,3-thiadioxolone-2 Binary Systems (60 MHz)

Solvent	ν_a, Hz	ν_b, Hz	ν_c, Hz	ν_d, Hz
CCl_4	270.8	262.5	249.9	94.0
$CDCl_3$	271.0	264.9	252.8	95.1
$(CD_3)_2CO$	283.3	266.2	253.1	93.0
CD_3CN	276.1	265.5	251.0	91.6
CDCDCDCDCDCD	257.8	241.4	231.9	75.2
NCDCDCDCDCD	273.7	264.2	252.5	86.2
O_2NCDCDCDCDCDCD	281.9	268.1	255.6	93.9

can be verified, and the stereochemical identity of the c and c″ protons can be established by examining all four possible pairs to find the one pair, $\nu_k - \nu_l$, satisfying for each of the corresponding ethylene and propylene isomer solution systems the relation $[(\nu_0\delta)_e]_i \approx (\nu_k - \nu_l)_i$. Table VII lists the values of the protons selected to correspond to c and c″ in the isomers, their differences, $\nu_{c''} - \nu_c$, and the corresponding $\nu_0\delta$ value of the ethylenethiadioxolone solutions.

Table VII: Chemical Shift Assignments in Thiadioxolones: Medium Effects on a Shift Difference Between the Propylenethiadioxolone Isomers ($\nu_c - \nu_{c''}$) Corresponding to the Ethylenethiadioxolone Shift Difference ($\nu_0\delta$) at 60 MHz

Solvent	ν_c, Hz	$\nu_{c''}$, Hz	$\nu_c - \nu_{c''}$, Hz	$\nu_0\delta$ [$=(\nu_a - \nu_b)$], Hz
CCl_4	249.9	229.8	20.1	21.8
$CDCl_3$	252.8	231.3	21.5	21.0
$(CD_3)_2CO$	253.1	237.3	15.8	15.3
CD_3CN	251.0	233.4	18.6	16.9

The above considerations taken together with the assignments of the *trans* and *gauche* configurations which follow immediately from the A_2B_2 analysis of ethylenethiadioxolone establish the position geometries with respect to S=O of ν_a and ν_b for this compound, as in Table I. When taken in conjunction with the experimentally observed sensitivity to medium effects of *gauche* couplings, these considerations also establish the position geometries of ν_b and ν_c with respect to ν_a and ν_d (and, hence, S=O) for each of the propylene isomers, as in Table IV and VI.

3. Propylene-1,3-dioxolone-2. Both the chemical shifts and the vicinal and geminal couplings (see Table VIII) show considerably less variation in the nonaromatic binary systems of this compound than in the corresponding thiadioxolone systems. Even in the case of the aromatic solvents, there is negligible variation in the coupling constants, though there are somewhat more pronounced effects on the chemical shifts. The skeletal framework of this compound is expected to be planar, with the double bond in the plane of the ring.

Discussion

Since the plan of the early work on the determination of rotational energies by medium effects emphasized the role of solution dielectric constants[4,5] and since the early observations of anomalous geminal coupling effects also related to this physical property, it was clear from the first that the measurements in this study should focus on a broad and diverse range of solution dielectrics. This, of course, did not mean that other weak intermolecular forces such as H bonding and specific medium associations were not implicated in the variability of couplings. However, these other factors have never been shown to exert a strong effect on the geminal couplings, and the interest here is in isolating the possible effect on vicinal couplings of the forces responsible for geminal coupling changes.

From Table II it is clear that the geminal couplings are not constant in the ethylenethiadioxolone systems and that there is a trend for the values of the geminal coupling in dilute solution to decrease as the solution dielectric increases. A similar trend is not detectable in the measurements of the *trans*-vicinal couplings in the same table. However, the *gauche*-vicinal couplings in Table III show a clear trend, except for the benzene system, to correlate in the dilute solution systems with solution dielectric just as do the geminal couplings, and both the direction and the magnitude of the changes are

Table VIII: Calculated Chemical Shifts and Coupling Constants in 1,3-Propylenedioxolone-2 Binary Systems at 60 MHz

Solvent	ν_d, Hz	ν_a, Hz	ν_b, Hz	ν_c, Hz	J_{ab}, Hz	J_{ac}, Hz	J_{ad}, Hz	J_{bc}, Hz	J_{bd}, Hz	J_{cd}, Hz
CHCHCHCHCH	58.50	257.10	237.83	207.80	7.61	7.09	6.30	−8.28	0	0
$CDCl_3$	87.5	292.5	273.9	241.9	7.55	7.02	6.26	−8.30	0	0
O_2NCHCHCHCHCH	89.90	297.74	279.70	247.20	7.61	7.16	6.05	−8.33	0	0
CD_3CN	84.73	290.75	271.80	240.50	7.60	7.16	6.49	−8.33	0	0
$(CD_3)_2CO$	86.0	294.2	275.7	243.8	7.61	7.14	6.26	−8.34	0	0
NCHCHCHCH	78.4	289.50	271.45	239.45	7.60	7.06	6.37	−8.22	0	0

the same. The *gauche*-vicinal coupling decreases from 7.00 to 6.70 Hz as the solvent dielectric goes from 2.0 to 37.5. Under the same conditions, the geminal coupling goes from −8.10 to −8.42 Hz. The benzene system deviates to a marked degree in the trend, the coupling going from 7.00 Hz in CCl_4 (ϵ 2.2) to 7.46 Hz in benzene (ϵ 2.3) and back down to 6.88 Hz in chloroform (ϵ 4.8). No similar excursion is found for the geminal couplings: the coupling decreases from −8.15 Hz in CCl_4 to −8.25 Hz in benzene and continues to −8.42 Hz in chloroform. Interestingly, the chemical-shift parameter, $\nu_0\delta$, which is perhaps the most sensitive to electron distribution in the molecule (but also the least selective compared with the various coupling parameters) shows the features just noted for the *gauche*-vicinal couplings. The $\nu_0\delta$ values show a regularity of decrease from 24.12 Hz in cyclohexane to 16.86 Hz in acetonitrile, except for an excursion to 32.64 Hz for the benzene system.

If the propylenethiadioxolones are considered, the same features can be noted regarding the *gauche*-vicinal constants for the *anti* isomer. In Table V the value of J_{ac} decreases from 6.10 Hz in CCl_4 to 5.80 Hz in acetonitrile. There is also a sharp change in the benzene system, and the direction of change in geminal coupling is the same, though the magnitude is quite small. None of these trends can be established in the case of the propylenedioxolone systems, not necessarily because the available data is very restricted owing to the immiscibility of this compound in solvents of low dielectric constant.

There are at least three hypotheses that might account for the trends noted. The first is that of inversion of the thiadioxolone molecules due to the unoccupied bonding orbital of the sulfur. On this hypothesis a tunneling frequency analogous to but lower than the frequency in the ammonia molecule would obtain, with perhaps a rather different residence time in each of the inverting states, owing to differences in configurational stability. On this basis, the differences in solution dielectric would be expected to affect the configurational stability just as they do in acyclic ethanes,[4] with concomitant changes in time-averaged vicinal couplings and chemical shifts. The difficulty with this hypothesis is that there is no evidence for inversion for this type of molecule in the corresponding acyclic configuration, as nmr studies[20,21] and earlier theoretical treatments have shown. There would be even less likelihood for it in the tied-down ring configuration.

A second hypothesis is that the ring conformation exists as an equilibrium mixture of "envelope" and of pseudorotating "puckered" conformations, the latter with C_2 symmetry. However, the rather strong π character associated with three of the bonds in all of the molecules considered here might be expected to stabilize the configuration. In the case of the thiadioxolones, the tendency would be for stability of the "envelope" conformation; in the case of the dioxolones, there would be planar ring stability.

On the third hypothesis, reaction-field effects of varying solution dielectrics[22,23] similar to those postulated earlier to account for rotational properties of acyclic ethanes[4] would continue to play an important role in determining the vicinal couplings of configurationally stable as well as rotating molecules. On this basis, the valency electron polarizability of the ring or chain substituents could play the significant role in determining the changes in vicinal and geminal couplings. For the specific molecules considered in this paper, we have three oxygen substituents per molecule, with the semipolar bond of the thiadioxolone the more highly polarizable of the two types. In addition we have the highly polarizable sulfur orbitals. The precise geometric orientation of the polarizable orbitals to the reaction-field tensor of the medium would be expected to be a significantly determining feature and could account qualitatively for the differences noted between thiadioxolones and dioxolones and among the several binary systems. As the experimental results here bear out, the magnitude of this effect can be quite large in certain aromatic systems and makes some contribution in most other solutions. It is clear, therefore, that adjustment factors taking these phenomena into account will be required in equations involving the use of nmr vicinal couplings in the calculation of other physical properties of molecules.

(20) J. S. Waugh and F. A. Cotton, *J. Phys. Chem.*, **65**, 562 (1961).
(21) H. Finegold, *Proc. Chem. Soc.*, 283 (1960).
(22) P. Laszlo and J. I. Musher, *J. Chem. Phys.*, **41**, 3906 (1964).
(23) A. D. Buckingham, T. Schaefer, and W. G. Schneider, *ibid.*, **32**, 1227 (1960).

Fluorescence Yields of Aromatic Compounds

by William R. Dawson and Maurice W. Windsor

Chemical Sciences Department, TRW Systems, Redondo Beach, California 90278 *(Received March 28, 1968)*

Values of fluorescence yields for 18 compounds in solution at 23° are reported and they are compared with previous literature values. Modifications of the technique of Weber and Teale for measurement of fluorescence yields are described. Fluorescein in 0.1 *N* NaOH and anthracene in ethanol are the best fluorescence standards on the basis of agreement of fluorescence yields with other work. The use of quinine as a fluorescence standard is complicated by variation of its fluorescence yield with H_2SO_4 concentration and the excitation wavelength. Several other compounds, including chrysene, show no variation of fluorescence yield with a change of excitation wavelength. Radiative lifetimes estimated from integrated absorption spectra are found to be consistently shorter than the radiative lifetimes estimated from fluorescence yields and lifetimes. The fluorescence yields of pyrene-d_{10} and anthracene-d_{10} in ethanol are significantly lower than those of corresponding solutions of pyrene-h_{10} and anthracene-h_{10}, respectively. No significant effect of compound deuteration upon the fluorescence yields of seven other compounds is found.

I. Introduction

An accurate knowledge of the quantum yield of fluorescence (fluorescence yield, Φ_F) of a compound is important for many reasons. It enables one to assess the importance of nonradiative processes which compete with fluorescence to deactivate the first excited singlet state, S_1.[1] Comparison of Φ_F for perprotonated and perdeuterated compounds allows the estimation of the size of any deuterium effect on the rate of radiationless deactivation of S_1[1] analogous to that observed for the deactivation of the lowest triplet level T_1.[2] Measurements of Φ_F as a function of the excitation wavelength indicate whether or not the intersystem crossing to the triplet manifold occurs from singlet levels above that responsible for fluorescence. Finally, together with the fluorescence lifetime, the fluorescence yield enables the radiative lifetime of the fluorescence state to be calculated. The values so obtained provide a check on the validity of the theoretical relations used to derive the radiative lifetime from the area under the corresponding absorption curve.[3]

There is a large amount of data on fluorescence yields in the literature. Absolute values[4-7] comprise only a small fraction of this body of data. The majority of measurements[8-12] have been made by reference to one of a few fluorescence standards for which absolute yields had been measured previously. It is, therefore, important that the accuracy of the fluorescence yields of these standards be verified by independent measurements from several laboratories. Accordingly, we have remeasured fluorescence yields of some compounds which have been used as fluorescence standards, since, aside from solutions of fluorescein and anthracene, there is a near absence of overlap in the data from different laboratories. Melhuish[7,13] proposed that dilute quinine in 1.0 *N* H_2SO_4 having a fluorescence yield of 0.546 be used as a fluorescence standard. This value has been used in employing quinine in both 1.0[8] and 0.1 *N*[10,12] H_2SO_4 as a fluorescence standard. However, the use of quinine as a fluorescence standard is complicated by reports that the fluorescence yield of quinine varies with solvent acidity[14] and the excitation wavelength.[15] Accordingly, we have remeasured the fluorescence yield of quinine in 0.1, 1.0, and 3.6 *N* H_2SO_4 by the technique originally developed by Weber and Teale[6] (WT) and measured the fluorescence yield of quinine in 1.0 *N* H_2SO_4 using different excitation wavelengths.

The WT method has the advantage that errors resulting from self-absorption and quenching of fluorescence can be readily eliminated by extrapolating measurements to zero concentration. We use a modified version of the WT technique using an improved method for the extrapolation. A statistical method was used to estimate the reproducibility of the fluorescence yields.

We have also made a study of the effects of compound deuteration and the change of excitation wavelength upon the fluorescence yields of several compounds.

(1) M. W. Windsor and W. R. Dawson, *Mol. Cryst.*, **3**, 165 (1967).
(2) C. A. Hutchison and B. W Mangum, *J. Chem. Phys.*, **32**, 1261 (1960).
(3) S. J. Strickler and S. A. Berg, *ibid.*, **37**, 814 (1962).
(4) S. J. Vavilov, *Z. Physik.*, **22**, 266 (1924).
(5) E. J. Bowen, *Proc. Roy. Soc.*, **A154**, 349 (1936).
(6) G. Weber and F. W. J. Teale, *Trans. Faraday Soc.*, **53**, 646 (1957).
(7) W. H. Melhuish, *J. Phys. Chem.*, **65**, 229 (1961).
(8) J. B. Birks and D. J. Dyson, *Proc. Roy. Soc.*, **A275**, 35 (1963).
(9) E. J. Bowen and J. Sahu, *J. Phys. Chem.*, **63**, 4 (1959).
(10) C. A. Parker and W. T. Rees, *Analyst*, **85**, 587 (1960).
(11) C. A. Parker, *Anal. Chem.*, **34**, 50 (1962).
(12) A. N. Fletcher, *J. Mol. Spectrosc.*, **23**, 221 (1967).
(13) W. H. Melhuish, *J. Phys. Chem.*, **64**, 762 (1962).
(14) J. Eisenbrand, *Z. Anal. Chem.*, **179**, 170 (1961).
(15) R. F. Chen, *Anal. Biochem.*, **19**, 374 (1967).

Altogether, fluorescence yields of solutions of nine aromatic hydrocarbons, their perdeuterated analogs, and nine other compounds are reported.

II. Experimental Section

A. Materials. Anthanthrene was obtained from Professor E. Clar. Other fluorescent compounds were obtained from commercial suppliers. Purity of the compounds was established on the basis of melting points, absorption spectra, or insensitivity of the fluorescence yield to recrystallization of the compound. It was necessary to purify fluorescein chromatographically by Lindquist's method[16] and to purify the ordinary and perdeuterated forms of both chrysene and pyrene by elution from a silica gel column with benzene. Ordinary and perdeuterated coronene were purified by elution with benzene from a column filled with Woelm basic alumina. Deuterated chemicals were obtained from Merck Sharp and Dohme of Canada Ltd. Their isotopic purity exceeded 95% and their absorption spectra were very similar to the spectra of the protonated analogs. This indicates either high purity or the presence of the same impurities in the protonated as in the deuterated forms of the compound.

Solvents for the fluorescent compounds include distilled water, benzene-free absolute ethanol, and spectroscopic grade benzene or hexane which were dried over sodium. Oxygen was removed from all the fluorescent solutions, except those of fluorescein and quinine which do not show significant oxygen quenching of fluorescence, by bubbling solvent-saturated helium through the solution until the fluorescence intensity became constant.

B. Method for Measuring Fluorescence Yields. Fluorescence yields, Φ_F, are determined in the WT method[6] by the comparison of the intensities of fluorescence with the intensities of excitation light scattered from nonabsorbing, colloidal reference solutions. The signals F and S, due, respectively, to light from the fluorescent and light-scattering reference solutions, emitted perpendicular to the excitation beam, were related to Φ_F by the equation[6]

$$\Phi_F = 0.76\frac{(dF/dE_F)_{E_F\to 0}}{(dS/dE_S)_{E_S\to 0}}\frac{f_{\lambda_0}}{\langle f_\lambda\rangle_{av}} \qquad (1)$$

where E_F and E_S are the absorbances per centimeter of the fluorescent solution and the scattering solution, respectively, at the wavelength λ_0 of the excitation light. f_{λ_0} and $\langle f_\lambda\rangle_{av}$ are proportional, respectively, to the detector signals per incident photon of the excitation and fluorescent light, averaged over the wavelength range of fluorescence, and 0.76 is the correction factor for the difference in spatial distribution of light emitted from the fluorescent and light-scattering solutions. Light is emitted nearly isotropically from the fluorescent solutions studied, while the emission from the light-scattering solutions is more intense in the direction of the excitation beam than it is perpendicular to the excitation beam.

Estimates of $(dF/dE_F)_{E_F\to 0}$ and $(dS/dE_S)_{E_S\to 0}$ in eq 1 were obtained by Weber and Teale as limiting slopes at the origins of plots of F and S against E_F and E_S, respectively. Owing to the variation with the concentration of the attenuation of excitation light across the portion of the fluorescence cell in view of the fluorescence detector, these slopes decrease with increasing concentration. This downward curvature, together with the scatter of data near the origin, make an accurate estimation of the limiting slopes difficult. Graphical determination of these slopes may be avoided by using l'Hospital's rule to replace the differentials in eq 1 by the corresponding nondifferential ratios in eq 2.[17] A term containing the indices of refraction, n_F and n_S, of the fluorescent and scattering solutions taken at the wavelengths of the fluorescent and scattered light,[18] respectively, is also introduced to correct for different refractive dispersions of the fluorescent and scattered light in passing nearly normally through a planar cell window into air and toward the detector.[7]

$$\Phi_F = 0.76\frac{(F/E_F)_{E_F\to 0}}{(S/E_S)_{E_S\to 0}}\frac{f_{\lambda_0}}{\langle f_\lambda\rangle_{av}}\left(\frac{n_F}{n_S}\right)^2 \qquad (2)$$

Equation 2 is a useful modification of eq 1, because F/E_F and S/E_S can be graphically extrapolated to zero concentration more accurately than the zero concentration limits of dF/dE_F and dS/dE_S can be estimated.

The precision of the extrapolation to zero concentration of F/E_F and S/E_S can be further improved by noting that a slope of -1.0 is indicated by eq 3 and 4 for plots of F/E_F and S/E_S against E_F and E_S, respectively

$$\log (F/E_F)_{E_F\to 0} = \log (F/E_F) + E_F \qquad (3)$$

$$\log (S/E_S)_{E_S\to 0} = \log (S/E_S) + E_S \qquad (4)$$

Derivations of eq 3 and 4 are given in the Appendix. Plots of log (F/E_F) against E_F for several fluorescent compounds and of log (S/E_S) against E_S for the light-scattering solution are given in Figure 1. A line of slope -1.0 can be drawn through all but one of the families of points in Figure 1, so the data can be fitted to eq 3 and 4. The single exception is anthanthrene excited with 3655-Å light, where a larger negative slope is indicated. This is due to neglect, in derivation of eq 3 and 4, of secondary absorption processes which for most compounds does not lead to significant errors. However, anthanthrene absorbs the shorter wavelength portion of its own fluorescence much more strongly

(16) L. Lindquist, *Ark. Kemi.*, **16**, 79 (1960).

(17) W. R. Dawson and J. L. Kropp, *J. Opt. Soc. Amer.*, **55**, 822 (1965).

(18) Because the solutions used were dilute, indices of refraction of pure solvents were used in eq 2. Indices of refraction of solvents from 2500 to 6000 Å were obtained from the International Critical Tables, McGraw-Hill Book Co., Inc., New York, N.Y., 1926.

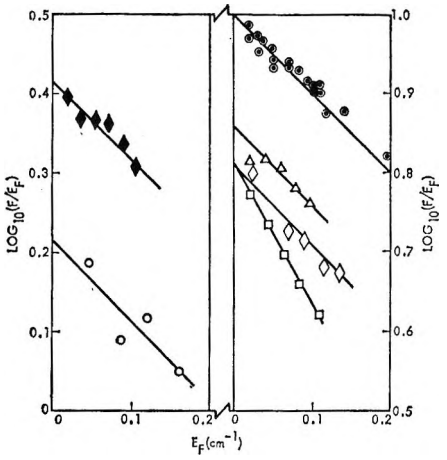

Figure 1. Extrapolation of log (F/E_F) to $E_F = 0$: ○, phenanthrene in ethanol, 3131-Å excitation; ◆, picene in benzene, 3131-Å excitation; △, quinine in 1.0 N H_2SO_4, 3655-Å excitation; □, anthanthrene in benzene, 3655-Å excitation; ◇, anthanthrene in benzene, 4358-Å excitation. ⊙, Ludox light-scattering solutions: 3131-, 4358-, and 3655-Å excitation. (Ordinate and abscissa are log (F/E_S) and E_S, respectively, for the scattering solutions.)

than it absorbs the 3655-Å excitation light. This results in larger attenuation of fluorescence in the more concentrated solutions that were measured. Conversely, it is not surprising that the usual slope of −1.0 is obtained in Figure 1, for anthanthrene excited with 4358-Å light, since the extinction coefficient of anthanthrene is about 20 times larger at 4358 than at 3655 Å. This permits use of much less concentrated solutions with the 4358-Å excitation, which give less self-absorption of fluorescence.

When a good fit of a line of slope −1.0 to the plot of log (F/E_F) against E_F can be made, reliable values of log $(F/E_F)_{E_F\to 0}$ or log $(S/E_S)_{E_S\to 0}$ can be calculated using eq 3 and 4 for each solution measured, even for values of E_F or E_S as large as 0.2. Then by using the corresponding values of $(F/E_F)_{E_F\to 0}$ and $(S/E_S)_{E_S\to 0}$ in eq 2, a separate value of fluorescence yield can be obtained from the measurements made on each pair of one light-scattering solution and one fluorescent solution. Several estimates of Φ_F are thereby obtained which permit a statistical calculation of the reproducibility of the average value of Φ_F.

Data for fluorescent and scattering solutions are each positioned in order of increasing solution concentration and the data for each fluorescent solution and scattering solution having the same position are arbitrarily paired for calculating the values of fluorescence yield. The number of estimates of fluorescence yield of a compound is accordingly equal to n, the number of pairs of fluorescence and scattering solutions measured. Averages of these estimates of fluorescence yield, together with 90% confidence limits, are calculated from eq 5[19] to give the final results.

$$\Phi_F = \frac{1}{n}\sum_{i=1}^{n}\Phi_{F\,i} \pm A\sqrt{\frac{\sum_{i=1}^{n}\left[\Phi_{F,i}^2 - \frac{1}{n}\left(\sum_{i=1}^{n}\Phi_{F,i}\right)^2\right]}{n(n-1)}} \qquad (5)$$

In this equation, A is 6.31, 2.92, 2.35, 2.13, or 2.02 when n is, respectively, 2, 3, 4, 5, or 6. There should be a probability of 0.90 that the fluorescence yield does not fall outside the limits from eq 5 as a result of random errors. However, systematic errors due to instrumental bias are not included in this estimate.

C. Apparatus for Measuring Fluorescence Yields. Figure 2 is a diagram of the apparatus for the measurement of fluorescence yields. Light from a low-pressure mercury arc lamp (Spectroline Hg-3), E, is collimated with a quartz lens, L, and passed through a filter, F_1, and a shutter, S, into the square end (1 × 1 cm) of a 4 cm long quartz fluorescence cell, C. This cell slides reproducibly into a blackened light baffle having an 0.8 cm in diameter aperture, A, which permits detection of fluorescence or scattered light. The distance between the end of the cell and the aperture center is 1.0 cm. The baffle, B, defines a cone with a half angle of 10°. Fluorescence or scattered light from the cell passing this aperture falls on the quantum-counter cell, Q. This quartz cell contains a 5×10^{-3} M solution of rhodamine B in glycerol, which converts the incident light into an orange fluorescence. After passing through a Corning 3-66 filter, F_2, this fluorescence is detected with an RCA 6217 photomultiplier tube, P, placed to one side of cells C and Q. The relative response per photon of the detector at various wavelengths was determined by comparison with thermopile readings and is plotted against the wavelength in Figure 3, together with the fluorescence spectrum of fluorescein. The former curve indicates that the detector response per photon is constant within a few per cent at wavelengths below 6000 Å.[20] Therefore, except for fluorescein, $f_{\lambda_0}/\langle f_\lambda\rangle_{av}$ in eq 2 is 1.0 for the solutions tested, since they emit no appreciable fluorescence beyond 6000 Å. In the case of fluorescein in 0.1 N NaOH,

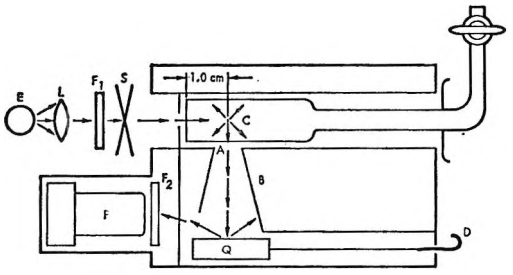

Figure 2. Apparatus for measurement of fluorescence yields.

(19) W. J. Youden, "Statistical Methods for Chemists," John Wiley and Sons, Inc., New York, N. Y., 1951, pp 18, 19.

(20) W. H. Melhuish, *J. Opt. Soc. Amer.*, **52**, 1256 (1962).

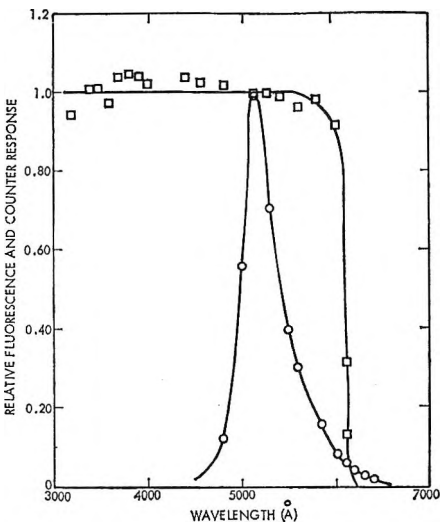

Figure 3. Fluorescence spectrum of fluorescein in 0.1 N NaOH, O. Output per incident photon of the rhodamine B quantum counter, □.

the fluorescence yield must be corrected to take account of the red fluorescence that is not absorbed by the rhodamine B quantum counter, Q. From a detailed analysis of the curves in Figure 3, $f_{\lambda_0}/\langle f_\lambda \rangle_{av}$ is 1.03 for fluorescein in 0.1 N NaOH.

A black baffle, B, between C and Q eliminates reflection of fluorescence light from C to P. Error due to direct detection of this primary fluorescence from cell C is thereby made negligible. The baffles are particularly necessary in the case of solutions, such as fluorescein in 0.1 N NaOH, having an orange-red component of fluorescence which is not absorbed by F_2. Absence of scattered fluorescence light at P is checked for each solution by making sure that the photocurrent from P falls to zero when Q is taken out of the fluorescence beam from C by pulling handle D.

Individual lines, or closely spaced groups of Hg lines, are isolated by F_1. The 4358-Å line and the 3655-Å line group were isolated by the Corning filters for these lines. The 3341-Å line was separated using the filters described by Kasha.[21] A 3-cm path of $NiSO_4$ and $CoSO_4$, each at a concentration of 1.0 M, plus 1 cm of 0.025 M potassium biphthalate and 1 cm of 1.0×10^{-3} M K_2CrO_4, were used to isolate the 3131-Å line group;[21,22] 3 cm of the $NiSO_4$ and $CoSO_4$ solutions plus 10 cm of Cl_2 at atmospheric pressure were used to isolate the 2537-Å line group. Over 98% of the photons transmitted by the filter combinations for isolation of the 4358-, 3655-, or 3131-Å line groups were in their respective line group. However, 12% of the photons transmitted by the filter combination for isolating the 2537-Å radiation was in the 2653-Å line group. The method of accounting for this lack of monochromaticity is given in section II-D.

D. Procedure for Measuring Fluorescent Yields. All measurements were made at 23°. Values of F are taken as the difference of the detector signals obtained on opening shutter, S, (Figure 2) with the fluorescence cell filled first with the fluorescent solution and then with pure solvent. Values of S are measured under the same excitation conditions but using aqueous solutions of submicron silica particles[23] (Ludox LS, E. I. du Pont de Nemours and Co.) to give the necessary Rayleigh scattering of light. Individual measurements of E_S or E_F for each solution (placed in a 2-cm quartz absorption cell) were made with a Cary 14 spectrophotometer. The wavelength, λ_0, at which E_S and E_F were measured was the average wavelength of photons in the Hg line group used for excitation. An accurate estimate of the exact value of λ_0 was obtained by recording the emission spectrum of the excitation lamp L with a Cary 14 spectrophotometer. Values of E_F and E_S were usually chosen to lie in the range 0.01–0.15 cm^{-1}. The corresponding over-all concentration range of the fluorescent solutions was approximately 10^{-3} to 10^{-6} M. However, for each compound, at least one measurement was made at a concentration of 10^{-4} M or lower, where self-quenching and self-absorption of fluorescence are small.

With the 2537-Å excitation light, the experimental method had to be modified for two reasons. First, as shown by deviations of the scattering from the inverse fourth power of the wavelength, Ludox solutions absorb as well as scatter light at wavelengths below 3000 Å. Therefore, with the 2537-Å excitation it was necessary to replace Ludox solutions by perylene[24] in ethanol. Second, with nominally 2537-Å excitation, 12% of the excitation photons were actually in the 2653-Å Hg line group. For the 2537-Å measurements, consequently, fluorescence yields were calculated using eq 6 rather than eq 2

$$\Phi_F = 0.94 \frac{(F_u/\bar{E}_u)_{\bar{E}_u \to 0}}{(F_P/\bar{E}_P)_{\bar{E}_P \to 0}} \left(\frac{n_u}{n_P}\right)^2 \qquad (6)$$

where 0.94 is the fluorescence yield of the dilute perylene solutions. The parameters are related to the test and perylene solutions, respectively, by the subscripts u and P and

$$\bar{E} = 0.12E_F(2653 \text{ Å}) + 0.88E_F(2537 \text{ Å})$$

E. Measurement of Spectra. Fluorescence and absorption spectra are required for the calculation of radiative lifetimes[3] from the integrated absorption spectra. Absorption spectra, expressed as molar extinction coefficients, were measured using a Cary 14 spectropho-

(21) M. Kasha, *J. Opt. Soc. Amer.*, 38, 929 (1948).

(22) E. J. Bowen, "The Chemical Aspects of Light," 2nd ed, Clarenden Press, Oxford, 1946.

(23) D. M. Hercules and H. Frankel, *Science*, 131, 1611 (1960).

(24) Perylene in ethanol was used as a fluorescent standard because close agreement was obtained for the fluorescence yield using a 3131-, 3655-, and 4358-Å excitation (Table III), so it is probable that the same value is obtained using a 2537-Å excitation.

Table I: Comparison of Fluorescence Yields at Room Temperature with Previous Determinations

Compd	Solvent	Present values of Φ_F (with 90% confidence limits)	Excitation wavelength, Å	Other values of Φ_F
Quinine	1.0 *N* H_2SO_4	0.54 ± 0.02	3655	0.546[a]
Quinine	0.1 *N* H_2SO_4	0.50 ± 0.02	3655	0.58[b]
Perylene	Ethanol	0.94[c]	*c*	0.89[a]
Perylene	Benzene	0.99 ± 0.03	3655	0.89[a]
Acridone	Ethanol	0.72 ± 0.02	3655	0.825[a]
Anthracene	Ethanol	0.27 ± 0.01	3655	0.27,[a] 0.30,[d-f] 0.28[g] 0.295,[h] 0.306[h]
Anthracene	Benzene	0.27 ± 0.01	3655	0.256,[a] 0.29[d]
Fluorene	Ethanol	0.68 ± 0.04	2537	0.53[d]
Naphthalene	Ethanol	0.205 ± 0.014	2537	0.12,[d] 0.21,[e] 0.19[i]
Phenanthrene	Ethanol	0.125[c]	*c*	0.10,[d] 0.13[e]
Aminoacridine	Water	0.81 ± 0.02	*c*	0.99[d]
Fluorescein	0.1 *N* NaOH	0.87[c]	*c*	0.93,[d] 0.85,[g] 0.84,[j] 0.79[k]
Triphenylene	Ethanol	0.065 ± 0.006	2537	0.09[e]
Chrysene	Ethanol	0.17[c]	c	0.17[e]
Pyrene	Ethanol	0.53 ± 0.02	3131	0.72[e]
Pyrene	Benzene	0.60 ± 0.03	3131	0.80[l]
Pyrene	Cyclohexane	0.58 ± 0.01	3131	0.32,[m] 0.68[l]
Benzene	Hexane	0.053 ± 0.008	2537	0.04,[c] 0.07,[m] 0.05,[n] 0.11[o]
9,10-Dichloro-anthracene	Benzene	0.71 ± 0.04	3655	0.65[p]

[a] Reference 7. [b] J. W. Eastman, *Photochem. Photobiol.*, **6**, 55 (1967). [c] Average of values from Table II, measured with different excitation wavelengths. [d] Reference 6. [e] Reference 25. [f] T. Medinger and F. Wilkinson, *Trans. Faraday Soc.*, **61**, 620 (1965). [g] Reference 10. [h] Reference 12. [i] Reference 11. [j] Reference 4. [k] L. S. Forster and R. S. Livingston, *J. Chem. Phys.*, **20**, 1315 (1952). [l] Reference 26. [m] Reference 27 (cyclohexane solutions). [n] J. B. Birks, M. D. Lum, and D. A. Weyl in "Progress in Reaction Kinetics," Vol. 4, G. Porter, Ed., Pergamon Press Ltd., London, p 281. [o] E. J. Bowen and A. H. Williams, *Trans. Faraday Soc.*, **35**, 44 (1939). [p] E. J. Bowen, *ibid.*, **50**, 17 (1954).

tometer. Fluorescence spectra were measured by detecting the fluorescence emitted perpendicular to the excitation beam with a monochromator (Bausch and Lomb 250 mm) and photomultiplier (RCA 6217). The variation with wavelength of the response of the monochromator–photomultiplier detector was determined by directing monochromatic light alternately onto the monochromator and a rhodamine B quantum counter and noting the ratio of the responses as a function of wavelength. The resulting instrumental-response spectrum was used to correct the fluorescence spectra. The fluorescence spectra were also corrected for self-absorption of fluorescence by measuring the spectra at several concentrations and extrapolating to the fluorescence spectra at zero concentration.

III. Results and Discussion

A. Comparison of Results to Previous Literature Values. Fluorescence yields from this work are listed in Table I, together with comparable literature values. A comparison of present values of fluorescence yield with values obtained by several other workers can be made for only one or two compounds. With such a limited basis of comparison, close agreement may either indicate accurate measurements or be fortuitous. However, for six or more compounds, our values of Φ_F may be compared with those of Melhuish,[7] Weber and Teale[6] (WT), or Parker[10,11,25] and coworkers. Our values of fluorescence yields agree to within 13% with corresponding values reported by Melhuish, and the average absolute deviation of our values from the corresponding values of Melhuish was only 6% of Melhuish's value. Close agreement of present values of fluorescence yields with the results of WT[6] are not obtained, despite the use of their basic method. There seems to be a systematic difference between our values and values of WT that is dependent on the excitation wavelength used in the measurements. Present values are 6–18% lower than comparable values of WT for fluorescein, anthracene, and 9-aminoacridine, which WT measured using 3655 or 3131-Å excitation, but present values are 25–60% higher than the values of WT for phenanthrene, naphthalene, and fluorene which were obtained using a 2537-Å excitation. With the exception of the value for benzene in hexane, our fluorescence yields agree to within 7% with corresponding values reported by Parker[11] and by Parker and Rees.[10] The larger disagreement in the values for benzene is probably attributable to the unusually large error in determining the fraction of the excitation light absorbed by benzene that results from the unusually sharp ab-

(25) C. A. Parker and T. Joyce, *Trans. Faraday Soc.*, **62**, 2785 (1966).

sorption peaks of benzene. Present values of fluorescence yields are also in very close agreement with values reported by Parker and Joyce[25] for all compounds except pyrene and triphenylene. The disagreement in these values for pyrene leads to large differences in the estimate of the quantum yield $\Phi_{F'}$ of radiationless deactivation of the lowest excited singlet state directly to the ground level from the relation $\Phi_{F'} = [1 - (\Phi_F + \Phi_T)]$. Inserting 0.28[25] for the triplet yield Φ_T gives either 0.00 if the value of Φ_F from Parker and Joyce is used or 0.19 if our value of Φ_F is used. Other literature values of fluorescence yields are for pyrene in solvents other than ethanol. Fluorescence yields of pyrene in benzene and cyclohexane reported by Birks[26] are appreciably higher than our values, while the fluorescence yield of pyrene in cyclohexane from Berlman[27] is much lower than Birks' value or ours.

B. Dependence of Fluorescence Yield Upon Excitation Wavelength. Weber and Teale[28] have established that fluorescence yields of several compounds are constant over a wide range of excitation wavelength. Our measurements, given in Table II, support this conclusion. Values of fluorescence yield for each compound, determined using different excitation wavelengths, agree to within their respective limits of error with the exception of quinine in 1.0 N H_2SO_4, for which the fluorescence yield obtained using a 3131-Å excitation was lower than was obtained with other excitation wavelengths. These results are evidence that the measurements are free of any serious variation of systematic error upon change of the excitation wavelength.

Constancy of fluorescence yield with excitation wavelength indicates that the probability of reaching the fluorescent level from higher levels initially populated upon absorption is 100%. This leads to the conclusion that intersystem crossing to the triplet manifold does not occur from higher singlet levels but takes place exclusively from the emitting level S_1, the lowest excited singlet state. On the basis of an increased phosphorescence to fluorescence ratio obtained on exciting progressively higher singlet states of chrysene at −196°, O'Dwyer, El Bayoumi, and Strickler (OES)[29] proposed that intersystem crossing to the triplet manifold from higher singlet levels occurs. Lim, Laposa, and Yu[30] have suggested that the results of OES are due to concentration effects and impurities rather than to intersystem crossing from higher excited singlet states. Our results in Table II indicate that such intersystem crossing from singlet states above S_1 must be very small for chrysene in ethanol at 23°. The fluorescence yields upon exciting to the same three levels that OES studied, using 2537-, 3131-, and 3655-Å excitation, are 0.16, 0.175, and 0.17, respectively. Since with 3655-Å excitation the emitting level is populated directly, the probability P of populating the emitting level upon absorption of a photon of 2537- or 3131-Å light is the ratio of the fluorescence yields with a 2537- or 3131-Å excitation to that with a 3655-Å excitation. The values of P obtained are 0.94 with 2537-Å excitation and 1.03 with 3131-Å excitation. These small variations of P from unity may be due to experimental error. Therefore, no significant intersystem crossing is shown to occur from upper, excited singlet levels of chrysene in ethanol at 23°.

The pyrene-h_{10} and pyrene-d_{10} solutions used in the fluorescence-yield measurements ranged in concentration between 10^{-5} and 10^{-6} for the 3131-Å measurements and from 4×10^{-5} to 16×10^{-5} M for the 3655-Å measurements. Results of Medinger and Wilkinson[31] indicate that dimer fluorescence is negligible for the 3131-Å measurements but is a small fraction of the total fluorescence in the 3655-Å measurements. The total yield of the excimer and ordinary fluorescence of pyrene in ethanol at concentrations below 3×10^{-4} M was shown by Medinger and Wilkinson[31] to fall within 10% of the fluorescence yield of pyrene at infinite dilution. The fluorescence yield of pyrene in Table II that was obtained using a 3655-Å excitation includes the contributions of both ordinary and excimer fluorescence; however, in view of the above results, the value given closely approximates the fluorescence yield of infinitely dilute pyrene.

C. Standard Solutions for Fluorescence Yield Measurements. A survey of Table I to specify reliable standards for fluorescence yield measurement reveals that anthracene in ethanol and fluorescein in 0.1 N NaOH are the only solutions whose fluorescence yields have been determined with good over-all agreement by several laboratories. These two solutions are, therefore, probably the best fluorescence standards for measurements on dilute solutions where the self-absorption of fluorescence by anthracene or fluorescein is not significant.

Since there is little overlap in the fluorescence and absorption spectra of quinine,[7,13] concentrated quinine solutions may be used as a fluorescence standard without significant errors occurring as a result of self-absorption of fluorescence. There have not been as many fluorescence-yield determinations for quinine as for anthracene or fluorescein. Our value of the fluorescence yield of quinine in 1.0 N H_2SO_4 agrees closely with Melhuish's value. However, our value of the fluorescence yield of quinine in 0.1 N H_2SO_4 is 14% lower than

(26) J. B. Birks and I. H. Munro in "Progress in Reaction Kinetics," Vol. 4, G. Porter, Ed., Pergamon Press, Ltd., London, 1967, p 284.

(27) I. B. Berlman, "Handbook of Fluorescence Spectra of Aromatic Molecules," Academic Press Inc., New York, N. Y., 1965.

(28) G. Weber and F. W. J. Teale, *Trans. Faraday Soc.*, **54**, 640 (1958).

(29) M. F. O'Dwyer, M. A. El Bayoumi, and S. J. Strickler, *J. Chem. Phys.*, **36**, 1395 (1962).

(30) E. C. Lim, J. D. Laposa, and J. H. Yu, *J. Mol. Spectrosc.*, **19**, 412 (1966).

(31) T. Medinger and F. Wilkinson, *Trans. Faraday Soc.*, **62**, 1785 (1966).

Table II: Dependence of Fluorescence Yields Upon Excitation Wavelength

Compd	Solvent	Excitation wavelength, Å				
		2537	3131	3341	3655	4358
Perylene	Ethanol	0.94[a]	0.96[b]	...	0.93 ± 0.03	0.92 ± 0.06
Phenanthrene	Ethanol	0.12 ± 0.005	0.13 ± 0.005	...	...	...
Chrysene	Ethanol	0.16 ± 0.006	0.175 ± 0.014	...	0.17 ± 0.018	...
Quinine	1.0 *N* H_2SO_4	0.55 ± 0.02	0.48 ± 0.02	0.56 ± 0.04	0.54 ± 0.02	
Pyrene-h_{10}	Ethanol	...	0.53 ± 0.02	...	0.54 ± 0.03	...
Pyrene-d_{10}	Ethanol	...	0.44 ± 0.02	...	0.47 ± 0.01	...
Fluorescein	0.1 *N* NaOH	...	0.86[b]	...	0.84[b]	0.92 ± 0.04
Anthanthrene	Benzene	...	...	...	0.62[b]	0.63 ± 0.03

[a] The average value of Φ_F obtained using a 3131-, 3655-, and 4358-Å excitation is 0.94, which is assumed to be the fluorescence yield of perylene in ethanol using a 2537-Å excitation. [b] No 90% confidence limits are given, because self-absorption of fluorescence necessitated making a graphical extrapolation of fluorescence data to zero concentration of the fluorescent compound.

Eastman's value.[32] Furthermore, we find that the fluorescence yield of quinine increases with the sulfuric acid concentration from 0.50 in 0.1 *N* H_2SO_4 to 0.54 in 1.0 *N* H_2SO_4 and to 0.60 in 3.6 *N* H_2SO_4. Similar dependence of the fluorescence yield of quinine with the sulfuric acid concentration was noted by Eisenbrand,[14] who found no variation in Φ_F for quinine between 0.01 and 0.2 *N* H_2SO_4 but observed that the fluorescence yield of quinine in 1.0 and 3.6 *N* H_2SO_4 is, respectively, 6 and 13% higher than the fluorescence yield of quinine in 0.1 *N* H_2SO_4. This variation of fluorescence yield is noteworthy, because quinine in 0.1 *N* H_2SO_4 has often been used as a fluorescent standard,[10,12] along with the same value of Φ_F that Melhuish reported for quinine in 1.0 *N* H_2SO_4. Accordingly, the value of Φ_F assigned to quinine in 0.1 *N* H_2SO_4 appears to be incorrect and results in estimates of fluorescence yield that are 6 to 8% too high.

The fluorescence yield of quinine (Table II) also varies with excitation wavelength; the fluorescence yield is 0.48 with a 3131-Å excitation and 0.54 to 0.56 with the other wavelengths used. Previous workers have disagreed about the dependence of the fluorescence yield of quinine upon the wavelength of the excitation. Rosen and Edelman[33] and Drobnik and Yeargers[34] found no variation of the fluorescence yield with the excitation wavelength. Eastman[32] obtained a fluorescence yield of 0.58 for quinine in 0.1 *N* H_2SO_4 with both 2538- and 3650-Å excitation, and Fletcher[12] obtained the same relative fluorescence yield using 3170- and 3650-Å excitation. However, Borresen[35] found that the fluorescence yield with a 3450-Å excitation is 1.47 times larger than with a 2500-Å excitation. Chen[15] found that the fluorescence yield of quinine in 0.1 *N* H_2SO_4 was constant with the variation of the excitation wavelengths below 3400-Å but that the ratio of the fluorescence yield obtained with the 3655-Å excitation to the fluorescence yield obtained with the 3131-Å excitation is 1.09. This ratio, calculated from data in Table II, is 1.12. However, a difference of fluorescence yields obtained by changing excitation wavelength from 3131 to 2537Å is indicated in Table II, which is in disagreement with results by Chen. We obtained no change in the fluorescence yield or the absorption spectrum of quinine that was purified either by recrystallization from ethanol or by elution from a silica gel column with 1.0 *N* H_2SO_4. Therefore, the variation of fluorescence yield of quinine with excitation wavelength is unlikely to be due to fluorescence of an impurity. On the basis of the variations Chen[15] found both in the fluorescence polarization with the fluorescence wavelength and in the fluorescence spectrum with the excitation wavelength, he suggests the anomalous fluorescence yield of quinine is due to the presence of more than one level from which fluorescence originates. In view of the anomalous behavior of quinine fluorescence with variations in excitation wavelength and acid concentration, caution should be used in applying quinine as a fluorescence standard.

D. Radiative Lifetime and Absorption Intensity. Strickler and Berg (SB)[3] developed an equation relating the radiative lifetime for a vibronic transition to the extinction coefficients over the corresponding absorption band. This equation was modified slightly by Birks and Dyson.[8] Two sets of values for the radiative lifetime of fluorescence, τ_0, are given in Table III. Values in the column headed τ_0 (emission) are obtained by dividing lifetimes measured by Ware and Baldwin[36] (WB) by our values of fluorescence yield. Values in the column headed τ_0(absorption) have been calculated from the SB equation using our measurements of the absorption and corrected fluorescence spectra. The values of τ_0(absorption) agree closely with corresponding values by SB, WB, and BD for all the compounds except fluorescein and quinine. The maximum

(32) J. W. Eastman, *Photochem. Photobiol.*, **6**, 55 (1967).

(33) P. Rosen and G. M. Edelman, *Rev. Sci. Instrum.*, **36**, 809 (1965).

(34) J. Drobnik and E. Yeargers, *J. Mol. Spectrosc.*, **19**, 454 (1966).

(35) H. C. Borresen, *Acta Chem. Scand.*, **19**, 2089 (1965).

(36) W. R. Ware and B. A. Baldwin, *J. Chem. Phys.*, **40**, 1703 (1964).

Table III: Comparison of Radiative Lifetimes of Fluorescence from Emission and Absorption Measurements

Compd	Solvent	τ, nsec[a]	Φ_F	τ_0(emission), nsec[b]	τ_0(absorption), nsec	τ_0(absorption)/ τ_0(emission)
Anthracene	Benzene	4.26	0.27	15.8	12.9	0.81
Perylene	Benzene	5.02	0.99	5.07	4.76	0.94
9,10-Dichloro-anthracene	Benzene	9.98	0.71	14.1	10.7	0.76
Acridone	Ethanol	13.0	0.72	18.0	14.5	0.81
9-Aminoacri-dine	Ethanol	15.15	0.81	18.7	14.6	0.78
Fluorescein	0.1 *N* NaOH	4.62	0.87	5.31	4.15	0.78
Quinine	1.0 *N* H_2SO_4	19.4	0.54	36.0	17.3	0.48

[a] Reference 36. [b] Equal to τ/Φ_F.

extinction coefficient of absorption for fluorescein, measured by us and by Lindquist,[16] is larger than the value reported by SB, so that our value of τ_0(absorption) is proportionally smaller than that of SB. The origin of the larger difference between our values of τ_0(absorption) for quinine and those of BD is not clear, since our calculations were based upon an absorption spectrum for quinine that was in close agreement with that reported by BD.

Equality of corresponding values of τ_0(absorption) and τ_0(emission) would establish the validity of the SB equation. However, for six of seven compounds in Table III, values in the τ_0(absorption) column are 6–25% smaller than the corresponding values of τ_0(emission), and for quinine, the remaining compound, τ_0(absorption) was 52% lower than τ_0(emission). A similar trend was obtained by BD, but WB, using values of Φ_F from three different laboratories, observed no consistent tendency for either τ_0(emission) or τ_0(absorption) to be larger than the other. The unusually low value of τ_0(absorption) relative to τ_0(emission) for quinine is probably associated with the inclusion of two unresolved vibronic transitions in the longest wavelength absorption band. The presence of these two transitions is shown by the large deviation from mirror-image symmetry between the spectra of the fluorescence and of the last absorption band[8] and by the change with excitation wavelength over the last absorption band of the fluorescence polarization.[15]

There is a good approximation to mirror symmetry between the spectra of the fluorescence and the longest wavelength absorption band for compounds in Table III, other than quinine. Therefore, in these compounds the longest wavelength absorption band is largely associated with the transition between the same two electronic states as in the fluorescence and there is no large contribution to the longest wavelength absorption band from a second electronic transition. However, if such a second transition constituted only a small fraction of the last absorption band, there would still be approximately mirror symmetry between fluorescence and absorption, but the estimate of τ_0(absorption) would be lower than τ_0(emission). The consistently lower values in Table III of τ_0(absorption) than of τ_0(emission) are probably partly associated with our inability in the calculation of τ_0(absorption) to discard contributions of secondary, weak transitions, which are known to be present in the last absorption band of many aromatic compounds.

Aromatic compounds and their derivatives have characteristic transitions from the ground level to the ^1L_b state, giving extinction coefficients which are typically 2–10%[37] of the extinction coefficients for the transition from the ground state to ^1L_a state. For anthracene, 9,10-dichloroanthracene and perylene, the fluorescence is associated with the ^1L_a transition, which occurs at slightly longer wavelengths than the ^1L_b transition. From Pariser's[38] theoretical results, the ^1L_b level of anthracene lies 530 cm^{-1} above the ^1L_a level, so that the spectra for absorption to the levels overlap. Estimates for these three compounds of τ_0(absorption), therefore, would be expected to be from 2 to 10% lower than τ_0(emission) and are actually found to be 6–25% lower. The compounds in Table III containing nitrogen and oxygen also may have weak, unresolved absorption bands that similarly result in the underestimation of τ_0(absorption). The presence of such weak bands might be detected by making sensitive studies of variation of fluorescence polarization with excitation wavelength.

E. Effect of Compound Deuteration on Fluorescence Yields. Replacement of hydrogen by deuterium in aromatic compounds results in increased phosphorescence lifetime, owing to a decreased rate for radiationless deactivation of the lowest triplet state.[2] Analogous effects of deuteration on radiationless or radiative rates for deactivation of the lowest excited singlet state S_1 would result in changes of the fluorescence lifetime and of fluorescence and triplet yields. Change in these parameters caused by deuteration[1] has been found to be small for most compounds studied. Ermo-

(37) H. B. Klevens and J. R. Platt, *J. Chem. Phys.*, **17**, 470 (1949).
(38) R. Pariser, *ibid.*, **24**, 250 (1956).

Table IV: Effect of Compound Deuteration Upon Fluorescence Yields

Compound	Excitation wavelength, Å	Solvent	Φ_{FH}[a]	Φ_{FD}[a]	Φ_{FD}/Φ_{FH} Present data	Φ_{FD}/Φ_{FH} From Berlman[b]
Pyrene	3131	Ethanol	0.53 ± 0.02	0.44 ± 0.02	0.83 ± 0.07	...
	3655	Ethanol	0.54 ± 0.03	0.47 ± 0.01	0.87 ± 0.07	...
Anthracene	3655	Ethanol	0.27 ± 0.01	0.24 ± 0.009	0.89 ± 0.07	0.89[c]
		Benzene	0.27 ± 0.01	0.23 ± 0.011	0.85 ± 0.08	0.89[c]
1,2:5,6-Dibenz-anthracene	3131	Ethanol	0.115 ± 0.005	0.10 ± 0.01	0.87 ± 0.13	...
1,12-Benzperylene	3655	Ethanol	0.255 ± 0.013	0.245 ± 0.011	0.96 ± 0.09	...
Chrysene	3131	Ethanol	0.175 ± 0.013	0.19 ± 0.011	1.09 ± 0.13	...
	3131	Benzene	0.23 ± 0.02	0.24 ± 0.011	1.04 ± 0.13	...
Triphenylene	2537	Ethanol	0.065 ± 0.004	0.068 ± 0.002	1.05 ± 0.09	1.38[c]
1,2-Benzanthracene	3131	Ethanol	0.20 ± 0.008	0.21 ± 0.010	1.05 ± 0.10	...
Coronene	3131	Ethanol	0.21 ± 0.017	0.22 ± 0.016	1.05 ± 0.15	...
Naphthalene	3131	Ethanol	0.205 ± 0.008	0.22 ± 0.011	1.07 ± 0.09	1.17[c]

[a] With 90% confidence limits. [b] Reference 27. [c] Fluorescence yields are for cyclohexane solutions.

laev[39] found no significant change upon partial deuteration in the fluorescence yields of naphthalene and biphenyl, and Lim and Laposa[40] found no effect of deuteration on the fluorescence yields of naphthalene, phenanthrene, and triphenylene in EPA at 77°K. The triplet yield[41] and rate of triplet formation[42] of naphthalene-h_8 and naphthalene-d_8 have been found to be equal. Laposa, Lim, and Kellogg[43] reported that there is no significant difference in the fluorescence lifetimes of ordinary and deuterated analogs of anthracene, phenanthrene, 1,2-benzanthracene, and chrysene in EPA solution at 77°K. However, different values of fluorescence yields and lifetimes for hydrogenated and deuterated forms of several compounds in cyclohexane at 25° have been reported by Berlman.[27] Brinen, Hodgson, and Orloff[42] reported a faster rate of triplet formation in phenanthrene-h_{10} than in phenanthrene-d_{10} under similar conditions of excitation. Poole[44] measured the fluorescence yields at low pressure of gaseous benzene-h_6 and benzene-d_6 and found a larger value for benzene-d_6, which he attributed to a higher triplet yield for benzene-h_6 than for benzene-d_6.

The fluorescence yields Φ_{FH} and Φ_{FD} of ordinary and deuterated forms, respectively, of nine compounds in deoxygenated solutions at 23° are given in Table IV together with the ratio of Φ_{FD} to Φ_{FH}. The ratio Φ_{FD}/Φ_{FH} is greater than unity for five compounds and less than unity for four compounds. Values from Berlman's results of Φ_{FD}/Φ_{FH} for naphthalene, triphenylene, and anthracene are also given in Table IV. Although there is good quantitative agreement only for anthracene, Berlman's data[27] are in agreement with the present results that upon deuteration the fluorescence yields of naphthalene and triphenylene increase while the fluorescence yield of anthracene decreases. Limits of Φ_{FD}/Φ_{FH} were obtained by dividing upper and lower limits of Φ_{FD}, respectively, by the lower and upper limits of Φ_{FH}. Considering these limits, anthracene and pyrene are the only compounds in Table IV for which reliable differences of Φ_{FD}/Φ_{FH} from unity are established. Furthermore, values of Φ_{FD}/Φ_{FH} are not changed greatly by changing the solvent for anthracene from ethanol to benzene or by changing the excitation wavelength with pyrene from 3131 to 3655 Å. These results indicate that the deuteration effect upon fluorescence yield is not solvent dependent in the case of anthracene and is unlikely to be an anomalous effect resulting from impurities in pyrene. An impurity would have to have the same absorption spectrum as pyrene in order to produce the same fluorescence yield using different excitation wavelengths.

The decrease of fluorescence yield resulting from deuteration of anthracene and pyrene is a result of increased rates of radiationless deactivation of S_1 (to ground state S_0 or the lowest triplet state T_1) and/or to a decreased rate of radiative deactivation of S_1. Determination of which rate constants change with deuteration must await determinations of fluorescence lifetimes and triplet yields. However, the absorption spectra of anthracene-h_{10} and anthracene-d_{10} are closely similar, and the radiative rate constant of the two from integrated absorption spectra differ by no more than 5%. Accordingly, the lowered fluorescence yield of deuterated anthracene is probably a result of the increased rates of radiationless deactivation of S_1. Kellogg[45] found an upper triplet level, T_2, in anthracene only 650 cm^{-1} above S_1. The variation in this small

(39) V. R. Ermolaev, *Usp. Fiz. Nauk*, **80**, 349 (1963).

(40) E. C. Lim and J. D. Laposa, *J. Chem. Phys.*, **41**, 3257 (1964).

(41) A. A. Lamola and G. S. Hammond, *ibid.*, **43**, 2129 (1965).

(42) J. S. Brinen, W. G. Hodgson, and M. K. Orloff, *J. Mol. Spectrosc.*, **23**, 112 (1967).

(43) J. D. Laposa, E. C. Lim, and R. E. Kellogg, *J. Chem. Phys.*, **42**, 3025 (1965).

(44) J. A. Poole, *J. Phys. Chem.*, **69**, 1343 (1965).

(45) R. E. Kellogg, *J. Chem. Phys.*, **44**, 411 (1966).

gap, resulting from the substitution of deuterium for hydrogen, might result in a large change in the rate of intersystem crossing to T_2.

The effect of deuteration upon intersystem crossing in pyrene may also be important. By triplet–triplet absorption studies in the infrared, Windsor and Novak[46] located a higher triplet, T_2, for pyrene in epoxy plastic which lies approximately 1300 cm^{-1} above S_1. Stevens, Thomaz, and Jones[47] found that the fluorescence lifetime of pyrene in ethanol varies with temperature and obtained an activation energy of 800 cm^{-1} for the intersystem-crossing process. These two results led Windsor and Novak[46] to conclude that, in the vicinity of room temperature, intersystem crossing from S_1 to the triplet manifold in pyrene occurs predominantly *via* thermal excitation and crossover to T_2. A small decrease of the S_1–T_2 energy gap in deuterated pyrene could, therefore, lead to an increased rate of intersystem crossing and lead to the observed decrease in the fluorescence yield of deuterated pyrene. For instance at 23° a decrease of the S_1–T_2 gap by only 140 cm^{-1} would double the Boltzmann population of T_2 and should give a corresponding increase in the rate of intersystem crossing. Such a frequency shift of 140 cm^{-1} on deuteration seems possible, in view of comparable observed shifts of the energy gap between S_1 and the ground state S_0 that are obtained by deuteration of many aromatic compounds. This argument is also consistent with our recent observation that the fluorescence yield of perdeuterated pyrene in polymethylmethacrylate increases more rapidly as the temperature is lowered than does that of ordinary pyrene.

The fluorescence lifetimes of 16×10^{-4} M solutions of pyrene-h_{10} and pyrene-d_{10} in ethanol at 23° are 356 and 330 nsec,[48] respectively. The fluorescence lifetime, therefore, decreases 7% upon deuteration, which compares with a corresponding 13 or 17% decrease of fluorescence yield. Values of the radiative lifetime of fluorescence, τ_0, obtained by dividing the fluorescence lifetime by the average of the fluorescence yields in Table IV with a 3131- and 3656-Å excitation, are 665 nsec for pyrene-h_{10} and 725 nsec for pyrene-d_{10}. However, the difference between these values is comparable with the uncertainty in the values, so that an effect of compound deuteration upon the radiative lifetime of fluorescence has not been established. Indeed, values of the radiative lifetimes in polymethylmethacrylate of pyrene-d_{10} and pyrene-h_{10} are equal to within a few per cent.[49]

Acknowledgments. This work was supported in part by the Office of Naval Research Contract N00014-67-C 0327. We are grateful to Dr. J. L. Kropp for useful discussions.

Appendix

A derivation of eq 3 and 4 is given in this section. Suppose that the excitation light penetrates, respectively, a and b cm into the solution before coming adjacent to the front and back edges of the square aperture shown in Figure 2, between the cell and the detector. Then F is proportional to the excitation absorbed across the aperture

$$F = K(10^{-aE_F} - 10^{-bE_F}) \quad \text{(A1)}$$

If the exponential terms are expanded in a series, terms of like power in E_F are collected, and both sides are divided by $2.3(b - a)E_F$, the relation becomes

$$F/E_F = K\left(1 - 2.3\frac{a + b}{2}E_F + (2.3)^2\frac{(a^2 + ab + b^2)E^2_F}{6} + \ldots\right) \quad \text{(A2)}$$

The first two terms in the above series and in the series expansion of $10^{-(a+b)E_F/2}$ are the same. Therefore, for small values of E_F the relation $F/E_F = K10^{-(a+b)E_F/2}$ is an accurate approximation. Taking the logarithms of both sides of the foregoing expression and introducing the boundary value at $E_F \to 0$ gives

$$\log (F/E_F) = \log (F/E_F)_{E_F \to 0} - {}^1/_2(a + b)E_F \quad \text{(A3)}$$

A similar relation may be developed by parallel arguments for the light-scattering measurements so that

$$\log (S/E_S) = \log (S/E_S)_{E_S \to 0} - {}^1/_2(a + b)E_S \quad \text{(A4)}$$

Equations A3 and A4 indicate that the plots in Figure 2 of $\log [F/E(F, \lambda_0)]$ and $\log [S/E(S, \lambda_0)]$ against $E(F, \lambda_0)$ and $E(S, \lambda_0)$, respectively, should have slopes of $-(a + b)/2$, which is shown in Figure 2 to be -1.0, since the center of the aperture is 1.0 cm from the end of the cell. Therefore, eq A3 and A4 become, in turn

$$\log (F/E_F)_{E_F \to 0} = \log (F/E_F) + E_F \quad \text{(A5)}$$

and

$$\log (S/E_S)_{E_S \to 0} = \log (S/E_S) + E_S \quad \text{(A6)}$$

which are identical with eq 3 and 4, respectively.

(46) M. W. Windsor and J. R. Novak in "The Triplet State," A. B. Zahlan, Ed., Cambridge University Press, London, 1967, p 229.

(47) B. Stevens, F. Thomaz, and J. Jones, *J. Chem. Phys.*, **46**, 405 (1967).

(48) Fluorescence lifetimes were measured by J. L. Kropp of our laboratories.

(49) Unpublished results obtained in our laboratory.

The Krypton-Radiosensitized Reaction of Deuterium Atoms with Ethylene[1]

by A. Tewarson and F. W. Lampe

Department of Chemistry, The Pennsylvania State University, University Park, Pennsylvania
(Received March 28, 1968)

The radiation-induced reaction of deuterium with ethylene, sensitized by krypton, is shown to proceed by the addition of deuterium atoms to ethylene, followed by the reaction of thermalyzed ethyl radicals. Substantial yields of C_4H_{10} and of C_2H_3D show that unimolecular decomposition of initially formed $C_2H_4D^*$ is an important process. The variation of the relative yields of butane-d_0, -d_1, and -d_2 with D_2 pressure show that stabilization of $C_2H_4D^*$ relative to its decomposition is considerably smaller than is observed, when thermal D atoms are added to C_2H_4. It is thus suggested that the D atoms formed in the radiosensitized process are kinetically "hot." Yields of ethane in excess of that formed by disproportionation of ethyl radicals are best explained by the reaction of D atoms with ethyl radicals.

Introduction

It has been known for some time that hydrogen atom reactions with a substrate can be sensitized by subjecting mixtures of substrate, hydrogen, and a rare gas to ionizing radiation.[2,3] The technique is based upon the use of high concentrations of sensitizer and hydrogen relative to the substrate. In this way, nearly all the energy absorbed by the system is used in the ionization and excitation of the sensitizer and hydrogen. The initial ionization is followed rapidly by the ion–molecule reactions 1 and 2 which produce atomic hydrogen. In addition, if X is Kr or Xe, reaction 3 can occur,[4] with the result that all ionization events lead to XH^+ and H. Excited molecular hydrogen may

$$X^+ + H_2 \longrightarrow XH^+ + H \quad (1)$$

$$H_2^+ + H_2 \longrightarrow H_3^+ + H \quad (2)$$

$$H_3^+ + X(\text{Kr or Xe}) \longrightarrow XH^+ + H_2 \quad (3)$$

dissociate and excited sensitizer may induce decomposition of molecular hydrogen. Upon neutralization of XH^+, more hydrogen atoms are produced, so that the technique effectively channels nearly all the absorbed energy into hydrogen atom formation. By virtue of its relatively low concentration, the substrate does not absorb a significant fraction of the radiation energy and hence its chemical conversion is induced primarily by hydrogen atom attack. Using this technique, Lampe[2] studied the effect of various sensitizers on the radiation-induced reaction of hydrogen atoms with ethylene, while Maschke and Lampe[3] used the technique to study the deuterium–methane exchange. This paper describes a study of the krypton radiosensitized reaction of deuterium atoms with ethylene, a system in which exchange also occurs.[5]

Experimental Section

Radiation Source. The electron beam from the van de Graaff electrostatic accelerator at Gulf Research and Development Co., Pittsburgh, Pa., was used for all irradiations. The voltage was maintained at 2.5 mV and the electron-beam current at approximately 10 μA.

Reaction Vessels. In all experiments spherical 1-l. vessels of Pyrex glass were used. These vessels had freeze-out fingers and were painted externally with conducting silver paint to provide a path to ground for any electrons stopped by the glass. Each vessel was fitted with a break-seal, so as to eliminate the contact of gases with stopcock grease during irradiations and subsequent storage. All vessels were evacuated to about 10^{-6} torr, from one to several hours, before filling with samples to be irradiated.

Materials. Research grade ethylene (99.9 mol %) and propylene (99.99 mol %) were obtained from Phillips Petroleum Co. Deuterium was obtained from Isomet Corp., and krypton was obtained from Air Reduction Rare Gas Purifying Division. All of these were used as received, with the exception that the ethylene, propylene, and krypton were pumped for several hours while immersed in liquid nitrogen.

Analyses. Analyses of the irradiated samples were carried out by a combination of gas chromatography and mass spectrometry. The general composition of the irradiated samples was determined gas chromato-

(1) This paper is based on a thesis submitted to the Pennsylvania State University by A. Tewarson in partial fulfillment of the requirements for the degree of Master of Science, 1965.

(2) F. W. Lampe, *J. Amer. Chem. Soc.*, **82**, 1551 (1960).

(3) A. Maschke and F. W. Lampe, *ibid.*, **86**, 569 (1964).

(4) O. A. Schaefer and S. O. Thompson, *Radiat. Res.*, **10**, 671 (1959).

(5) A. H. Turner and R. J. Cvetanovic, *Can. J. Chem.*, **37**, 1075 (1959).

graphically using a 6-ft high-activity silica gel column at 90° and a 6-ft hexadecane column at 45°. The silica gel column was used to separate krypton, ethane, ethylene, and acetylene, while the hexadecane column was employed in the propane, butene, and butane determinations.

Isotopic compositions of a given chemical component were determined on a Bendix 14-101 time-of-flight mass spectrometer using parent peaks and statistical fragmentation corrections based on the known butane spectrum.

Dosimetry. Propylene was used as a gas-phase dosimeter. It has been reported[6] that hydrogen is formed in the radiolysis of propylene with $G(H_2) = 1.1$ and that the yield of H_2 is directly proportional to dose over a range of propylene conversion greater than that used in our dosimetry runs. Using the above $G(H_2)$ and standard electron energy-loss data,[7] the dose rate to 300 torr of krypton for 2.5-MeV electrons at a current of 10 μA was determined to be 4.58×10^{15} eV cm^{-3} sec^{-1}, with an uncertainty of about 5%. Standard energy-loss data[7] were used to compute energy-absorption rates by deuterium and ethylene.

Irradiations Procedure. All irradiations were carried out at room temperature or slightly above, owing to some heating of the vessel walls at the entrance and exit areas of the electron beam. All irradiations were conducted with 300 torr of krypton and 30 torr of ethylene, but with varying pressures of deuterium.

Results and Discussion

When mixtures consisting of 30 torr of C_2H_4, 300 torr of Kr, and 300 torr of D_2 were irradiated, the only significant chemical products observed were acetylene, ethane, propane, and butane. Small amounts of C_4H_8 were observed in the higher dose irradiations. The G values for these products, obtained by extrapolation of concentration–dose data to zero dose are shown in Table I, where they are compared with the 100-eV yields reported by Meisels[8] in a study of the radiolysis of pure ethylene. These systems differ, of course, in that in our study, as indicated by the dosimetry calculations, only ~5% of the radiation dose is absorbed by ethylene. Earlier work on rare gas-sensitized hydrogen atom reactions[2] has shown the initial rate of acetylene formation in C_2H_4–H_2–rare gas mixtures to be independent of the pressure of the rare gas, while the sum of the initial rates of formation of ethane, propane, and butane increases linearly with the rare gas pressure. This indicates that in these systems acetylene arises solely from energy absorption by ethylene. The observed (Table I) reduction of $G(C_2H_2)$ to 7% of the value formed in pure ethylene[8] is thus consistent with the earlier conclusion[2] and our dosimetry calculations.

Table I: Yields (100 eV) of Products in the Radiolysis of Pure C_2H_4 and C_2H_4–D_2–Kr Mixtures

Molecule	G(mixture),[a] molecules/100 eV	G(pure C_2H_4),[b] molecules/100 eV
C_2H_4	−16	−20
H_2	~0	1.2
HD	~0	...
C_2H_3D	2	...
C_2H_6	0.41	0.85
C_2H_5D	0.14	...
C_2H_2	0.24	3.5
Propanes	0.15	0.56
C_4H_{10}	0.90	2.3
C_4H_9D	0.90	...
$C_4H_8D_2$	0.40	...

[a] C_2H_4 (30 torr), Kr (300 torr), D_2 (300 torr). [b] Reference 7.

A material balance on the Kr-sensitized system (Table I) shows that the products account for only ~35% of the ethylene consumed. This is in contrast to the Ar-sensitized hydrogenation, in which the same products accounted for 70–80% of the ethylene reacted.[9] Thus the principal mode of reaction of ethylene in the experiments reported herewith must be polymerization to higher molecular weight products not detectable by our analytical technique. The increase in the fraction of ethylene going to polymer that we observe in Kr sensitization, as contrasted with Ar sensitization,[9] is not unexpected. Thus the specific reaction rate of (1) is 3.5 times slower for Kr^+ than for Ar^+,[10,11] and charge exchange with C_2H_4 (the process competing with (1)) produces $C_2H_4^+$ in the case of Kr^+ but not in the case of Ar^+.[12] Charge exchange of Ar^+ with C_2H_4 produces only $C_2H_3^+$ and $C_2H_2^+$.[12] Further, the $C_2H_4^+$ is known to initiate ionic polymerization in C_2H_4.[13] Less polymerization is, therefore, expected in Ar sensitization, with the result that more nearly complete material balances are obtained for the low molecular weight products.

In the radiolysis of pure C_2H_4, the alkanes are formed only by free-radical reactions[8,14] and these free radicals, in turn, are formed by ion–molecule reactions and molecular and ionic decomposition reactions that are characteristic of direct energy absorption by C_2H_4. In the present study, direct energy absorption by C_2H_4 is not an important process, as judged by the H_2 and C_2H_2 yields. Hence, we assume that the radicals arising from ion–molecule reactions initiated by energy absorption in C_2H_4 do not make a significant contribution to

(6) K. Yang and P. L. Gant, *J. Phys. Chem.*, **65**, 1861 (1961).
(7) National Bureau of Standards Circular 577 and Supplement, U. S. Department of Commerce, Washington, D. C., 1958.
(8) G. G. Meisels, *J. Amer. Chem. Soc.*, **87**, 950 (1965).
(9) F. W. Lampe, *Radiat. Res.*, **10**, 691 (1959).
(10) D. P. Stevenson and D. O. Schissler, *J. Chem. Phys.*, **23**, 1353 (1955).
(11) D. O. Schissler and D. P. Stevenson, *ibid.*, **24**, 926 (1956).
(12) J. L. Franklin and F. H. Field, *J. Amer. Chem. Soc.*, **83**, 3555 (1961).
(13) F. H. Field, *ibid.*, **83**, 1523 (1961).
(14) M. C. Sauer and L. M. Dorfman, *J. Phys. Chem.*, **66**, 322 (1962).

the formation of the alkanes shown in Table I. The persistence of the ethane, propane, and butane yields as ethylene is diluted with krypton and deuterium and the value of the ratio G(ethane)/G(butane) suggest that these products arise from the attack of D atoms on ethylene. This suggestion is strengthened by Meisel's observation[8] that, even in the pure ethylene radiolysis, the principal radical, C_2H_5, is formed solely by the addition of H atoms to ethylene. Therefore, in the following discussion we assume that the sensitized radiolysis produces D atoms at a rate determined principally by the Kr and D_2 partial pressures and that the reaction sequence leading to the paraffinic products, ethane, propane, and butane, begins with the addition of D to C_2H_4, *viz.*

$$D + C_2H_4 \longrightarrow C_2H_4D^* \qquad (4)$$

where the $C_2H_4D^*$ indicates an ethyl-d_1 radical that contains excess vibrational energy. The formation of the alkanes shown in Table I is then determined by the subsequent reactions of $C_2H_4D^*$.

Disproportionation–Combination of Monodeuterioethyl Radicals. In ethyl radical reactions it is usually assumed that the ethane-to-butane ratio of the products constitutes a measure of the ratio of the rate constants for disproportionation to combination. The observed increase of this ratio with decreasing pressure was originally attributed[5,15,16] to an enhanced disproportionation rate constant for vibrationally excited ethyl radicals relative to that for thermal radicals. This interpretation was largely based on the very large absolute rate constants for H atom addition to ethylene found by Melville and Robb,[17] the consequence being very low steady-state concentrations of H atoms. Later measurements of the relative rates of H atom addition to olefins[18–21] have cast doubt on the original absolute values and the assumption of a negligibly small steady-state H atom concentration may no longer be applicable. Thus a quite different explanation for the enhanced ethane-to-butane ratios in such systems, which involves the reaction of H atoms with thermal ethyl radicals and which has already been advanced,[2,22–24] has come to be more widely accepted.

The G(ethane)/G(butane) ratios found in this study are shown plotted *vs.* D_2 pressure in Figure 1. The value of this ratio is higher than the accepted value for thermal radicals of ~0.1[5] and, moreover, increases slightly as the D_2 pressure is increased. It is to be noted that as the D_2 pressure is increased in these experiments the rate of D atom formation and hence the steady-state concentration of D atoms are also increased. Since the ratio increases with increasing pressure, there can be no question of the deactivation of hot radicals. Since the D atom stationary concentration also increases, the excess ethane produced is most logically attributed to a reaction of D atoms with ethyl radicals that ultimately produces some ethane,

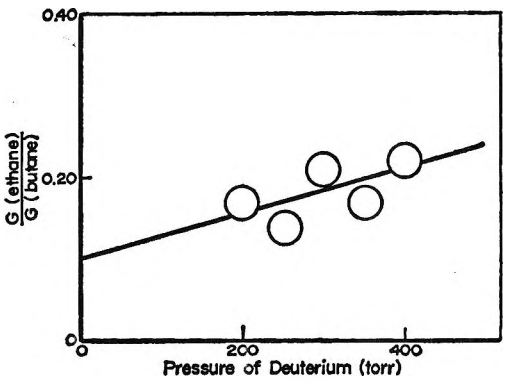

Figure 1. Dependence of the ethane-to-butane ratio on the deuterium partial pressure.

in accordance with the mechanism recently advanced.[2,22,24] As shown in Figure 1, the value of G(ethane/G(butane) extrapolated (by a least-squares fit) to zero pressure of D_2 is 0.1 ± 0.03.

It is to be noted in Table I that considerable quantities of C_4H_{10} are formed, pointing to the presence of C_2H_5 radicals in appreciable concentrations. Further, the yield of C_2H_3D (G = 2) is too large, even taking into account the rather large uncertainty of perhaps ±30%, to attribute this product to formation *via* the disproportionation of C_2H_4D radicals. These facts are consistent, however, with the reaction sequence.[5,22–24]

$$C_2H_4D^* \longrightarrow C_2H_3D + H \qquad (5)$$

$$C_2H_4D^* + M \longrightarrow C_2H_4D + M \qquad (6)$$

$$H + C_2H_4 \longrightarrow C_2H_5^* \xrightarrow{M} C_2H_5 \qquad (7)$$

Decomposition of $C_2H_5^*$ need not be considered further, since the H atoms released must eventually result in a thermalized ethyl radical; the negligible yields of HD indicate that exchange *via* the H + D_2 reaction is insignificant. The remainder of the alkane products are then most easily ascribed to the further reaction of C_2H_5 and C_2H_4D radicals as discussed below.

(15) J. N. Bradley, H. W. Melville, and S. C. Robb, *Proc. Roy. Soc.* **A236**, 318 (1956).

(16) P. J. Boddy and J. C. Robb, *ibid.*, **A249**, 518 (1959).

(17) H. W. Melville and J. C. Robb, *ibid.*, **A202**, 181 (1950).

(18) B. de B. Darwent and R. Roberts, *Discussions Faraday Soc.*, **14**, 55 (1953).

(19) J. N. Bradley, H. W. Melville, aud J. C. Robb, *Proc. Roy. Soc.*, **A236**, 454 (1956).

(20) K. R. Jennings and R. J. Cvetanovic, *J. Chem. Phys.*, **35**, 1233 (1961).

(21) K. Yang, *J. Amer. Chem. Soc.*, **84**, 719 (1962).

(22) M. J. Smith, P. M. Beatty, J. A. Pinder, and D. J. LeRoy, *Can. J. Chem.*, **33**, 821 (1955).

(23) B. S. Rabinovitch, D. H. Dills, W. H. McLain, and J. H. Current, *J. Chem. Phys.*, **32**, 493 (1960).

(24) C. A. Heller and A. S. Gordon. *ibid.*, **36**, 2648 (1962).

Butane Formation. In pure C_2H_4 radiolysis, Meisels[8] found that the principal mode of butane formation was the combination of ethyl radicals. In our sensitized system, in which energy absorption by ethylene is very small, this is most probably the only mode of butane formation. Thus, we have

$$C_2H_5 + C_2H_5 \longrightarrow C_4H_{10} \quad (8)$$

$$C_2H_5 + C_2H_4D \longrightarrow C_4H_9D \quad (9)$$

$$C_2H_4D + C_2H_4D \longrightarrow C_4H_8D_2 \quad (10)$$

From statistical considerations of the relative rates of butane formation, it is easily shown that

$$\frac{G(C_4H_9D)}{[G(C_4H_{10})G(C_4H_8D_2)]^{1/2}} = 2$$

The experimental ratio from Table I, which represents an extrapolation to zero conversion, is 1.5. It is not likely that this deviation from the statistical value is due to different absolute radical combination rates nor is it likely due to analytical errors inherent in using purely statistical mass spectral breakdown corrections to calculate the yields of C_4H_9D and C_4H_{10}. We believe that the presence of deuterated butenes, which have been observed at high conversions, results in a high value for the yield of C_4H_{10}. This explanation receives support from the observation that the ratio decreases to 1.30 as the D_2 pressure is raised to 400 torr and increases to 1.8 as the D_2 pressure is decreased to 200 torr. The absence of significant amounts of $C_4H_7D_3$ indicates the virtual absence of $C_2H_3D_2$ radicals.

The variation of the relative yields of butanes with D_2 concentration yields some information on the magnitudes of k_5 and k_6, the specific reaction rates for decomposition and deactivation, respectively. Assuming a steady state for free radicals and equal combination rate constants for C_2H_5 and C_2H_4D, it is easily shown from the reaction mechanism that

$$\frac{\dfrac{d[C_4H_8D_2]}{dt}}{\dfrac{d[C_4H_9D]}{dt}} = \frac{G(C_4H_8D_2)}{G(C_4H_9D)} = {}^1/_2\frac{k_6[M]}{k_5} \quad (11)$$

Actually, any pair of the three deuterated butanes may be taken to yield a relation similar to eq 11, but we have chosen $C_4H_8D_2$ and C_4H_9D because the mass spectral determinations of these two involve the fewest fragmentation corrections.

Different gases have different efficiencies as third bodies in eq 11, so that $k_6[M]/k_5$ in our system is actually

$$\frac{k_6[M]}{k_5} = \frac{1}{k_5}\{k_6^{C_2H_4}[C_2H_4] + k_6^{Kr}[Kr] + k_6^{D_2}[D_2]\} \quad (12)$$

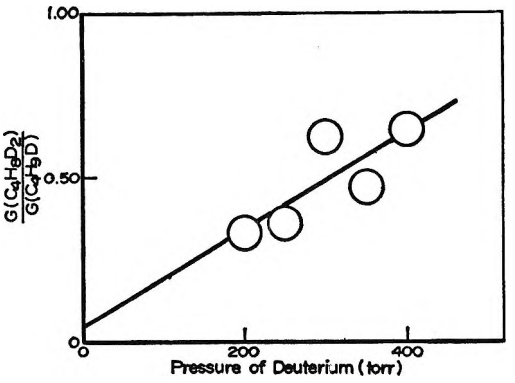

Figure 2. Dependence of deuterium substitution in the butane product on the deuterium partial pressure.

A plot of the left-hand side of eq 11 *vs.* D_2 pressure is shown in Figure 2. The slope of the line gives

$$\frac{k_6^{D_2}}{k_5} = 9.2 \times 10^{-20}\ \text{cm}^3/\text{molecule}$$

Provided the rate of formation of H atoms *via* the direct absorption of energy by ethylene is negligible, compared with the rate of formation of D atoms in all our experiments (which appears within ~10% error to be true), the extrapolation to zero $[D_2]$ can be made. Since in all cases $[Kr]/[C_2H_4] = 10$, this extrapolation yields the value

$$\frac{k_6^{C_2H_4} + 10k_6^{Kr}}{k_5} = 4.5 \times 10^{-20}\ \text{cm}^3/\text{molecule}$$

Our values for the stabilization-to-decomposition ratio of $C_2H_4D^*$ radicals, namely the quantity $k_6[M]/k_5$, are one to two orders of magnitude smaller (the actual value depending upon the pressure) than is to be expected on the basis of the work of Current, Rabinovitch, Heller, and Gordon.[25] The reason for this discrepancy is most likely to be found in the drastically different methods used to produce the D atoms and in the sensitivity of k_5 to the amount of vibrational excitation in $C_2H_4D^*$. Thus, the experimental work of Heller and Gordon[24] and Current and Rabinovitch,[26] upon which the conclusions concerning the magnitude of $k_6[M]/k_5$ are based,[25] utilized methods that produced D atoms with close to thermal kinetic energy. In our study most of the D atoms are produced by neutralization processes, *viz.*

$$KrD^+ + e \longrightarrow Kr + D \quad (13)$$

$$D_3^+ + e \longrightarrow 3D \quad (14)$$

in which we must expect the D atoms to have excess kinetic energy. Thus the $C_2H_4D^*$ formed in our studies most likely has more vibrational energy than

(25) J. H. Current, B. S. Rabinovitch, C. A. Heller, and A. S. Gordon, *J. Chem. Phys.*, 39, 3535 (1963).

(26) J. H. Current and B. S. Rabinovitch, *ibid.*, 38, 1967 (1963).

is the case in previous investigations,[24,26] with the result that k_5, the unimolecular decomposition rate constant, is much larger in our system than previously measured.[24,26] As shown by Rabinovitch and Setser,[27] k_5 is very sensitive to the excess energy in $C_2H_4D^*$. From the calculations of Rabinovitch and Setser,[27] we conclude that an excess kinetic energy in our D atoms of about 10–15 kcal/mol would account for our low value of the stabilization:decomposition ratio. Since processes 13 and 14 must release of the order of 300 kcal/mol, this is not an unlikely value for the average kinetic energy of our D atoms, even though a large excess of Kr is used. The results of this study thus strongly suggest that the rare gas radiosensitization technique produces hydrogen atoms that are kinetically "hot."

Ethane and Propane Formation. As already discussed, the magnitude of the ratio G(ethane)/G(butane) and its dependence on D_2 pressure lead us to conclude that there is an excess of ethane that is formed in reactions not involving excited radicals but rather in reactions involving thermal radicals and deuterium atoms. Thus we postulate in agreement with previous workers[2,22-24]

$$C_2H_5 + C_2H_5 \longrightarrow C_2H_6 + C_2H_4 \quad (15)$$

$$C_2H_5 + C_2H_4D \longrightarrow C_2H_4 + C_2H_5D \quad (16)$$

$$C_2H_4D + C_2H_4D \longrightarrow C_2H_3D + C_2H_5D \quad (17)$$

$$C_2H_5 + D \longrightarrow C_2H_5D^* \quad (18)$$

$$C_2H_5D^* \longrightarrow CH_3 + CH_2D \quad (19)$$

$$C_2H_5D^* + M \longrightarrow C_2H_5D + M \quad (20)$$

$$CH_3 + C_2H_4D \longrightarrow C_3H_7D \quad (21)$$

etc.

In accord with this mechanism we have found C_2H_5D (G = 0.14), traces of $C_2H_4D_2$, and deuterated propanes among the products. Quantitative analysis of the deuterated propanes was, however, not possible, owing to the large mass spectral corrections necessary for the breakdown of the much more abundant butanes.

Acknowledgment. This work was supported by Contract No. AF33(615)-1307 of the Office of Aerospace Research. We also wish to thank the National Science Foundation for providing funds to aid in the purchase of the mass spectrometer. We are indebted to Dr. T. Hardwick of the Gulf Research and Development Company for providing us with irradiation time and facilities.

(27) B. S. Rabinovitch and D. W. Setser, *Advan. Photochem.*, 1, 1 (1963).

Tautomerism and Geometric Isomerism in Arylazophenols and Naphthols. IV. Spectra and Reversible Photoreactions of *m*- and *p*-Hydroxyazobenzene

by Gavriella Gabor, Yael F. Frei, and Ernst Fischer[1]

Department of Chemistry, The Weizmann Institute of Science, Rehovoth, Israel (*Received March 29, 1968*)

Both *m*- and *p*-hydroxyazobenzene undergo reversible *cis* ⇄ *trans* photoisomerization, but the photoreactions, as well as the thermal reversion to the *trans* isomer, are complicated in both compounds by the formation of dimers or aggregates through intermolecular hydrogen bonds, and in the *para* compound also by tautomerization through hydrogen transfer along these H bonds. In *p*-hydroxyazobenzene the thermal reversion *cis*⇄*trans* is strongly solvent and concentration dependent. Its rate in aliphatic hydrocarbon solvents changes with the temperature in an unusual way, having a maximum at about −20°. The reversion may involve the formation of hydrogen-bonded dimers, in which reversible tautomerization to the respective phenylhydrazone takes place. Such a mechanism may give rise to the observed temperature dependence. In *m*-hydroxyazobenzene the kinetics of the *cis*→*trans* thermal reaction are regular. At temperatures below about −50° aggregates, probably dimers, of the *cis* isomer form spontaneously. The *trans* isomer dimerizes at still lower temperatures. Irradiation of the *cis* dimer forms the mixed *cis–trans* dimer, which separates into its components only at −25°. Activation energies are needed for the spontaneous formation and decomposition of dimers. The observed complex photochemical behavior may result from the superposition of photoisomerization (both in the monomer and in the dimer) and of the subsequent thermal formation or decomposition of the various dimers. This is one of the few examples of aggregates being involved in organic reactions.

In previous publications[2,3] we have described the reversible photochemistry of *o*-hydroxyazobenzene and related compounds. In these compounds the behavior is dominated by the intramolecular hydrogen bonds and the possible tautomerization to the corresponding phenylhydrazones.

The present paper deals with *m*- and *p*-hydroxyazobenzene. Both these derivatives can undergo dimerization or, more generally, aggregation by intermolecular hydrogen bonding. The *para* derivatives can also undergo tautomerization *via* intermolecular hydrogen transfer. Their thermal and photochemical behavior seems to be determined by these two processes, because the respective methoxy derivatives, like azobenzene itself, show a normal photoisomerization behavior; *i.e.*, at any temperature, irradiation at a specific wavelength leads to the same photostationary isomeric mixture, irrespective of the isomeric composition of the mixture before irradiation. We shall describe each of these compounds separately.

p-Hydroxyazobenzene

The reversible *cis*⇄*trans* photoisomerization and the thermal *cis*→*trans* isomerization of this compound at and above room temperature have been described.[4-6] Schulte-Frohlinde[6] observed that the thermal isomerization is autocatalytic; *i.e.*, its rate increases at higher concentrations of this compound.

We have investigated this compound in a wide temperature range, with methylcyclohexane (MCH), toluene, or ethanol serving as solvents. Both the spectroscopic and the kinetic behavior strongly depend on the solvent.

(*a*) *Absorption Spectra.* Figure 1A shows that at room temperature the solvent dependence is slight. Cooling had little effect on solutions in ethanol–methanol mixtures down to −140° and in toluene down to −80°. In MCH the change with temperature is profound, as shown in Figures 1B and C. On gradual cooling of such solutions, the spectrum at −80° resembles that in alcohol at 25°. Below −100° the peak shifts to longer wavelengths, and a new absorption region rises beyond 400 nm. When the same solution is now gradually heated, the main peak is sharply reduced, while the absorption beyond 400 nm increases. These changes are most marked at −60° and gradually disappear at higher temperatures. At −60° and below, some solute "disappears" by precipitation, as evidenced by a lowering of the absorbance all along. The solutions are clearly supersaturated under these conditions. Beer's law was found to hold in benzene solutions up to 5×10^{-4} *M* at 25°. In MCH the limited solubility did not allow similar measurements.

(*b*) *Photoisomerization.* This took place in all

(1) To whom correspondence should be addressed.

(2) Part II: G. Gabor and E. Fischer, *J. Phys. Chem.*, 66, 2478 (1962).

(3) Part III: G. Gabor, Y. Frei, D. Gegiou, M. Kaganowitch, and E. Fischer, *Israel J. Chem.*, 5, 193 (1967).

(4) G. S. Hartley, *J. Chem. Soc.*, 633 (1938).

(5) W. R. Brode, J. H. Gould, and G. M. Wyman, *J. Amer. Chem. Soc.*, 74, 4641 (1952).

(6) D. Schulte-Frohlinde, *Ann. Chem.*, 612, 138 (1958).

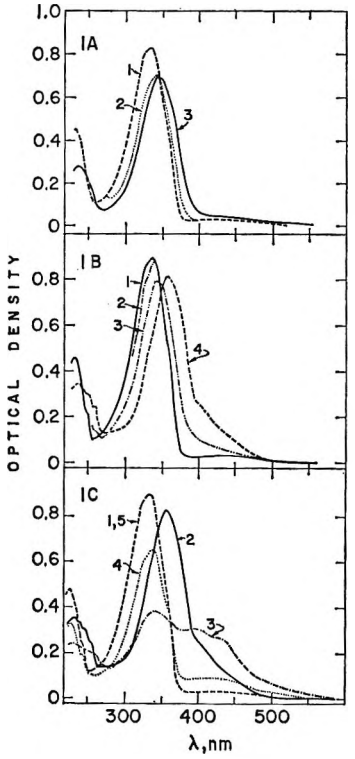

Figure 1. *trans*-*p*-Hydroxyazobenzene, 2.5 × 10^{-5} *M*: (A) in various solvents: (1) methylcyclohexane, (2) benzene, (3) ethanol; (B) in methylcyclohexane–isohexane, the effect of progressive cooling: (1) at 25°, (2) at −60°, (3) at −80°, (4) at −110°; (C) in methylcyclohexane–isohexane, the effect of progressive heating after rapid cooling to −110°: (1) at 25°, (2) at −110°, (3) warmed to −60°, (4) warmed to −40°, (5) warmed to 25°.

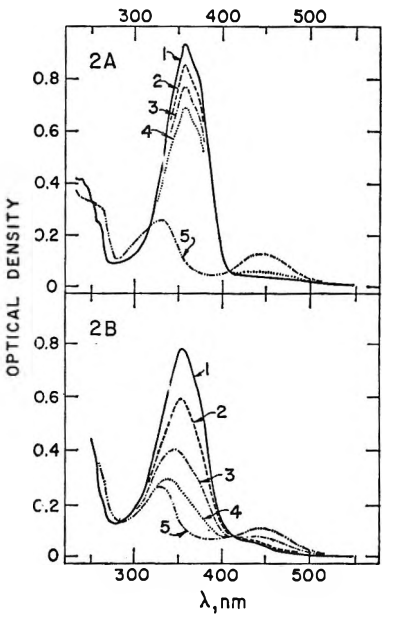

Figure 2. *trans*-*p*-Hydroxyazobenzene, about 2.6 × 10^{-5} *M*: (A) in ethanol–methanol at −140°: (1) before irradiation, (2) photostationary state attained by irradiation at 436 nm, (3) photostationary state attained by irradiation at 546 nm, (4) photostationary state attained by irradiation at 313 nm, (5) photostationary state attained by irradiation at 365 nm (solution 5 is practically the pure *cis* isomer); (B) in methylcyclohexane at −100°: (1) before irradiation, (2) photostationary state attained by irradiation at 436 nm, (3) photostationary state attained by irradiation at 405 nm, (4) photostationary state attained by irradiation at 365 nm, (5) extrapolated for the pure *cis* isomer.

solvents. However the reverse, *cis*→*trans*, thermal reaction, *cf.* (c) below, was too fast in toluene even at −80°, so that no accurate spectral measurements of the irradiation product could be made in this solvent. The results of irradiation in MCH at −100° and in ethanol–methanol at −140° are shown in Figure 2. It seems that in the latter solvent (2A), irradiation at 365 nm causes practically complete conversion into the *cis* isomer. The spectral changes observed are similar to those described earlier for azobenzene and its derivatives[7,8] and may be assigned to a *trans*→*cis* conversion. Irradiation of solutions in MCH below −100° (presumably containing aggregates) gave complex results, which are as yet difficult to interpret.

(*c*) *Kinetics of the Thermal Reversion.* The spontaneous reversion to the *trans* isomer, following 365-nm irradiation, is roughly a first-order reaction in alcoholic solutions. It was studied in the temperature region −70 to −100°. The Arrhenius parameters were $A = 10^{6.8}$ sec^{-1} and E_a = 8.5 kcal/mol (the corresponding values for azobenzene are 10^{11} sec^{-1} and 23 kcal/mol). In benzene, toluene, and MCH, the reversion kinetics are rather unusual. In benzene we confirmed Schulte-Frohlinde's results regarding the concentration dependence of the reaction rate. The reaction did not

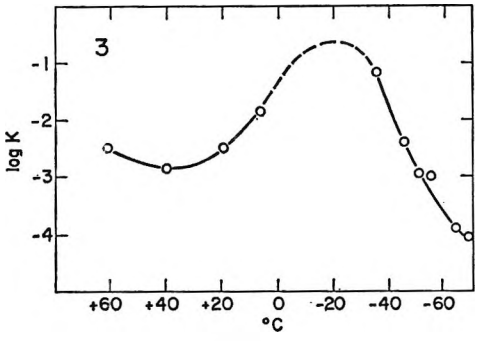

Figure 3. Temperature dependence of the rate of thermal reversion in a 2.5 × 10^{-5} *M* solution of *p*-hydroxyazobenzene in methylcyclohexane, following 365-nm irradiation at the temperature indicated. In the temperature region covered by the dashed part of the curve, the reversion was too fast to be measurable.

follow first-order kinetics. The half-life at 5 × 10^{-4} *M* was about one-tenth of that at 3 × 10^{-5} *M*. In further experiments we used toluene instead of benzene because of its wider temperature range of fluidity. The

(7) G. Zimmerman, L. Chow, and U. Paik, *J. Amer. Chem. Soc.*, **80**, 3528 (1958).

(8) E. Fischer, M. Frankel, and R. Wolovsky, *J. Chem. Phys.*, **23**, 1367 (1955).

kinetics of reversion in 3×10^{-5} M solutions in toluene were studied between -80 and 40°. The half-life of the reversion was about 0.5 min at all temperatures between 37 and $-40°$, increased to 3 min at $-80°$, and decreased to about 0.2 min at 60°. The reversion kinetics are even more unusual in MCH. A plot of log (concentration) against time is S shaped, with slow initial and final parts and a faster middle part. If the rate constant in the middle part is plotted against the temperature, a curve with a maximum at around $-20°$ is obtained, as shown in Figure 3. The rates at intermediate temperatures were too fast to be measured with "slow" methods.

(*d*) *Discussion.* As mentioned in the introduction, *p*-hydroxyazobenzene may undergo two reactions not possible in the corresponding methoxy derivatives: (a) formation of dimers or polymers, by virtue of intermolecular hydrogen bonds involving the hydroxy group and the azo nitrogen; (b) tautomerization, to form the corresponding phenylhydrazone; and (c) combinations of the two processes.

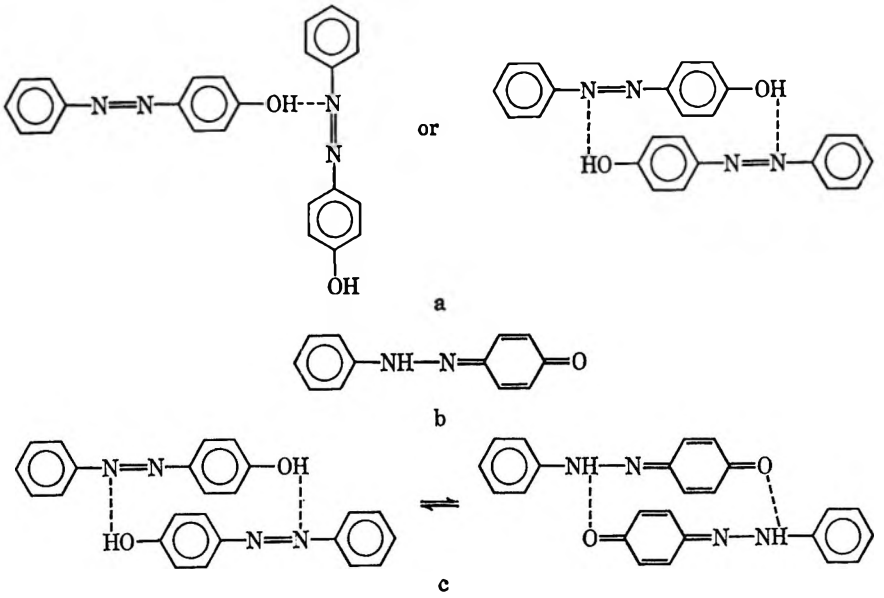

Unlike the situation in the analogous naphthalene derivative,[9] 1-phenylazo-4-hydroxynaphthalene, there is no spectroscopic evidence for the existence of the tautomer in appreciable amounts. However, it may still serve as an intermediate.[3,9] Tautomerization in this case has to be an intermolecular process, with the hydrogen being transferred either *via* the solvent, in the case of alcoholic solutions, or *via* a second solute molecule, along the hydrogen bonds indicated in (a), in hydrocarbon solvents. This may provide at least a qualitative explanation for the low Arrhenius parameters observed in alcoholic solutions and for the dependence of the isomerization kinetics on the concentration and the temperature observed in hydrocarbon solvents. Both the concentration and the temperature will, of course, affect the formation of dimers, which are intermediates in the isomerization mechanism envisaged, *cis*→hydrazone→*trans*. The spectral changes during cooling and, in particular, the new absorption band beyond 400 nm are probably due to dimerization, or rather aggregation, to be followed eventually by precipitation. In toluene and alcohol where solvent–solute interaction and, thereby, the solubility are much stronger, no such aggregation occurs. A peculiarity which we have also observed in other cases of aggregate formation is the necessity of a precooling stage, *viz.* the absorption curves at $-60°$ in Figures 1B and C.

The involvement of tautomerization and aggregation in the thermal reversion *cis*→*trans* might also be responsible for the complex temperature dependence of this reaction in methylcyclohexane, which seems to result from the interplay of several processes and equilibria whose change with the temperature affects the isomerization rate in opposite ways.

We do not feel justified to attempt a more detailed description on the basis of the results at hand.

m-Hydroxyazobenzene

The reversible *cis*⇄*trans* photoisomerization and the thermal *cis*→*trans* isomerization of this compound down to $-25°$ is similar to that of azobenzene proper.[3] At lower temperatures the absorption spectra, the photoconversion, and the spontaneous (thermal) reversion behave in a somewhat peculiar way, which will be described here.

(*a*) *Absorption Spectra.* The spectra of the pure *trans* isomer and that of a mixture rich in the *cis* isomer, in aliphatic hydrocarbon mixtures as solvents, change significantly on cooling. (See Figures 4–7.) In the *trans* case this manifests itself in a shift to longer

(9) E. Fischer and Y. F. Frei, *J. Chem. Soc.*, 3159 (1959).

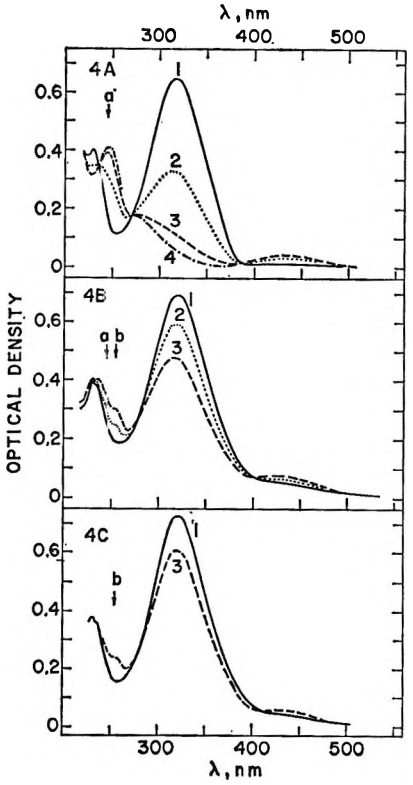

Figure 4. *trans-m*-Hydroxyazobenzene in methylcyclohexane–isohexane, 5×10^{-5} *M*. Results of irradiation at 365 nm, at various temperatures: curves 1, before irradiation; curves 2, after partial photoisomerization; curves 3, after establishment of the photostationary state; (A) at −25°, (B) at −120°, (C) at −140°. The *trans*-isomer content of these photostationary mixtures is 11% at −25°, 64% at −120°, and 86% at −140°. Curve 4 in A is extrapolated assuming solution 3 to contain 11% *trans* isomer.

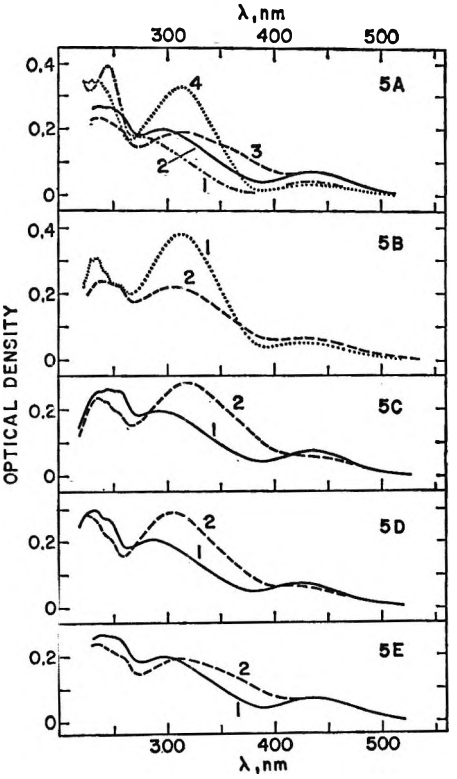

Figure 5. *trans-m*-Hydroxyazobenzene in methylcyclohexane–isohexane, 5×10^{-5} *M*. Thermal and photoinduced changes under various conditions: (A) the solution was irradiated to completion at 365 nm, at −25°, (curve 1), then cooled to −75° (curve 2), further irradiated with 365-nm light (curve 3), and heated to −25° (curve 4) (the *cis* content of solution 1 is 89% and of solution 4 is 50%); (B) curve 1, a 1:1 mixture of the *cis* and *trans* isomer obtained at −25° and cooled to −75°; curve 2, the solution described by curve 1, following 365-nm irradiation at −75° (when solution 2 is heated to −25°, the resulting absorption curve is identical with that of a mixture of isomers at −25° containing 55% *cis* isomer); (C) curve 1, the solution containing 89% *cis* isomer cooled from −25 to −140°; curve 2, the solution described by curve 1, after 365-nm irradiation at −140°; (D): curve 1, solution containing 89% *cis* isomer cooled from −25 to −120°; curve 2, the solution described by curve 1, after 365-nm irradiation at −120°; (E): curve 1, the solution containing 89% *cis* isomer cooled from −25 to −75°; the solution described by curve 1, after 365-nm irradiation at −75°. The *cis* content of the solutions described by curves 2 is 45% at −140°, 47% at −120°, and 50% at −75°.

wavelengths, from 315 nm at 25° to 326 nm at −180°, in an increased absorbance at around 380 nm, and in a decreased absorbance at the peak. In the *cis* case the minimum is shifted from 380 to 400 nm, the absorbance at 310 nm is increased, and the peak at 245 nm is sharply reduced on cooling from −25 to −75°. The extent of the decrease at 245 nm indicates that a considerable fraction of the *cis* isomer undergoes the reaction responsible for this change. No further change occurs at lower temperatures, showing that the reaction is either virtually complete at around −75° or else that below about −75° the thermal equilibria concerned are no longer established. The spectral changes between −75 and −25° (curves 1 and 2 in Figure 5A) are reversible. No similar changes were observed in alcoholic solutions. At temperatures above 0°, *cis*→*trans* isomerization sets in, leading eventually to the pure *trans* isomer.

(*b*) *Photoinduced Spectral Changes.* At −25° photoisomerization proceeds in the usual way, with photostationary states being established which are determined only by the wavelength of the light used for irradiation and not by the starting isomeric composition (Figure 4A). At −120° and lower temperatures, irradiation of the *trans* isomer results in spectral changes similar to those encountered at −25°, complete with isosbestic points, except that the *cis* peak at 245 nm is replaced by the plateau around 255 nm. The extent of the *trans*→*cis* phototransformation decreases sharply with decreasing temperature (see Figure 4), as already observed in other azo compounds and also in *m*-methoxyazobenzene. At each temperature the reaction may be largely reversed by irradiation in the visible region, *e.g.*, at 436 nm, while irradiation at 365 nm, following that at 436 nm, results in the same absorption. The isomeric composition of the photostationary states obtained in

Table I: Per Cent *trans* Isomer in the Photostationary State Attained at Various Temperatures and Wavelengths of Irradiating Light, in 5 × 10^{-5} *M* Solutions of the *trans* Isomer

	Wavelength, nm								
	−25°			−120°		−140°			−180°
	313	365	436	365	436	313	365	436	365
m-Hydroxyazobenzene	..	12	87	64	97	86.5	86	100	100
m-Methoxyazobenzene	28	17	83	31	94	71	40	100	80

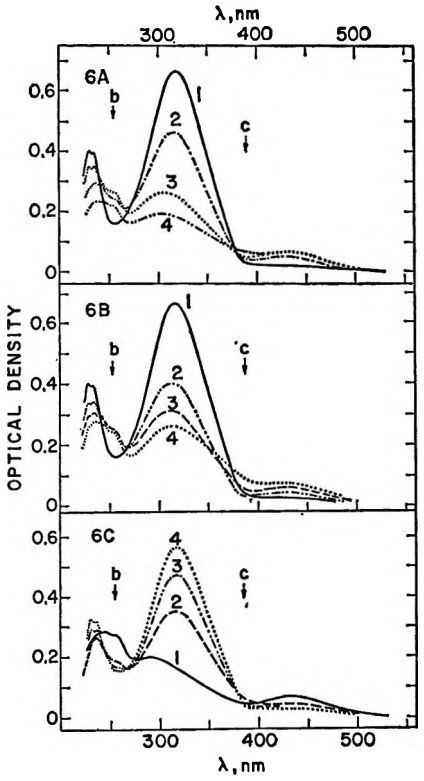

Figure 6. *trans-m*-Hydroxyazobenzene in methylcyclohexane–isohexane, 5 × 10^{-5} *M*. Photoinduced changes at −75°: curves 1, before irradiation, except in C, where the solution was first irradiated at 365 nm at −25° and then cooled to −75°; curves 2–4, results of progressive irradiation: (A) irradiation at 365 nm, (B) at 313 nm, (C) at 436 nm. In curves 4 in A and B, some precipitation is already noticeable. These solutions contain 50% and 54% *trans* isomer, respectively. In C the absorption rises continuously at 320 nm, falls continuously at b, but passes through an optimum at c, during irradiation.

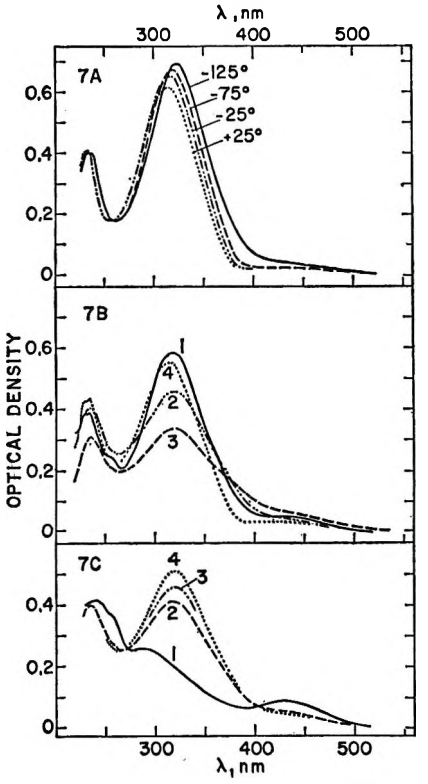

Figure 7. *trans-m*-Hydroxyazobenzene in methylcyclohexane–isohexane, 5 × 10^{-5} *M*: (A) at various temperatures; (B) at −120°: curve 1, after irradiation of *trans* at 365 nm; curve 2, after irradiation of 90% *cis* isomer at 436 nm; curve 3, after irradiation of 50% *cis* isomer at 436 nm; curve 4, all above, heated to −25°; (C) at −120°: curve 1, solution of 89% *cis* isomer cooled from −25 to −120°, curve 2, after 1 min of irradiation at 436 nm; curve 3, after 4 min of irradiation at 436 nm (contains 86% *trans* isomer), curve 4, after 30 min of irradiation at 436 nm (contains 93% *trans* isomer). The main change in isomeric composition thus takes place during 1 → 2.

this way at various temperatures was determined by taking the spectra at −25° (see below) and is listed in Table I. However, when the solutions are first converted largely into the *cis* isomer by 365-nm irradiation at −25°, then cooled to −120° or below, and further irradiated at 365 nm, very different results are obtained, as seen in Figures 5C and D. Curves 2 in these figures yield, on heating to −25°, curves similar to curve 2 in Figure 4A, indicating that these solutions contain about 50% of each isomer. On recooling these solutions, their spectra behave as expected from a mixture of the isomers, the spectrum of each of which changes as described above. Curves 2 in Figures 5C and D thus represent unstable irradiation products which "decompose" irreversibly at −25° to form a mixture of the *cis* and *trans* isomers. This fact makes it possible to determine the isomeric composition of the irradiation products obtained at lower temperatures by heating them to −25°.

Similar results are obtained by 365-nm irradiation at −75° (Figure 5E). The sequence of events at this temperature is summarized in Figure 5A, where curve 1 → 2 and curve 3 → 4 are spontaneous reactions, while

curve 2 → 3 is a radiative one. Finally, if the 1:1 mixture of isomers is cooled from −25 to −75° and then irradiated at 365 nm, a pronounced spectral change is again observed (curves 1 → 2 in Figure 5B). When solution 2 is heated to −25°, it is found to contain 45% *trans* isomer, *i.e.*, not much less than before this irradiation. This shows that the pronounced spectral change curve 1 → 2 (in 5B) is *not* due to an isomerization. Qualitatively similar results were obtained at −100, −120, and −140°, except that the absorbance at the peak was somewhat higher.

When the *trans* isomer is irradiated at −75° with 365- or 313-nm light, Figures 6A and B, the initial spectral changes represent a regular *trans*→*cis* photoisomerization, similar to the one obtained at −25°, with an isosbestic point at about 390 nm. However, when the fraction of *cis* isomer approaches about one-half, the change already described in Figure 5B takes place; *i.e.*, the further spectral changes are no longer due to isomerization. It is remarkable that the absorbance at b changes only in the initial stages, while that at c changes mostly in the later stages (Figure 6B).

Prolonged irradiation causes precipitation (this is in line with many related observations of precipitation being aided by irradiation) which manifests itself in a general reduction of the absorbance at shorter wavelengths, while the absorbance around 390 nm (region c) increases continuously.

When a 90% *cis* solution (obtained by 365-nm irradiation at −25°) is irradiated at −75° with light at 436 nm, Figure 6C, the absorbance at the peak increases continuously, that at b decreases to its final value already in the early stages, while that at c passes through an optimum (curve 2). Just as in the reverse reaction, the major part of the change at b (255 nm) occurs during the initial stage. The solution described by curve 2 in Figure 6C, despite the low absorbance at the peak, actually contains already 86% *trans* isomer, as shown by subsequent analysis at −25°.

The result of 436-nm irradiation of a 90% *cis* solution at −120° is described in Figure 7C. Finally, when the solution described by curve 2 in Figure 5E is cooled to −120° and irradiated at 436 nm, curve 3 in Figure 7B results. Subsequent analysis at −25° showed the *trans* content to be about 85%. Thus solutions of identical isomeric composition can have widely different absorption spectra at −120°. Figure 7B summarizes these results. Curves 1–3 all yield the same curve 4 when heated to −25° (*ca.* 86% *trans* isomer) and also when recooled to −120°.

Experiments with 5×10^{-4} *M* solutions of *m*-hydroxy azobenzene showed that at 0° the photoisomerization is normal. The *trans* isomer precipitates at −40°, while the *cis* isomer does so already below −15°. Irradiation of a solution of the *trans* form at −25° gives results rather similar to those obtained at −75° with a 5×10^{-5} *M* solution. The tendency toward precipitation is thus more pronounced in solutions of the *cis* isomer, as already observed at low concentrations and temperatures.

(*c*) *Discussion.* The spectral and photochemical phenomena described above are characterized by the complete thermal reversibility of the system (both at −25° where a clean *cis–trans* mixture is always obtained and at 90° where rapid and probably complete reversion to the *trans* isomer occurs) and by the virtual absence of a clear connection between the absorption spectra and the isomeric composition, at temperatures below about −50°.

It is suggested that all the unusual phenomena described are due to the formation of hydrogen-bonded aggregates at temperatures below about −50°, either spontaneously on cooling or by irradiation. As a working hypothesis we shall consider these aggregates to be dimers, either pure *cis*, pure *trans*, or mixed ones: [*c–c*], [*t–t*], or [*c–t*]. All three dimers are characterized by increased absorption in the region 390–420 nm and, for [*c–t*] and [*t–t*], by low absorption at the main peak

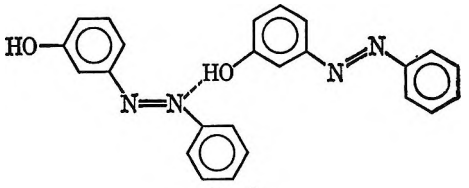

[*t–t*]

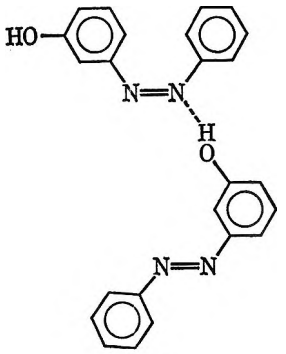

[*c–t*]

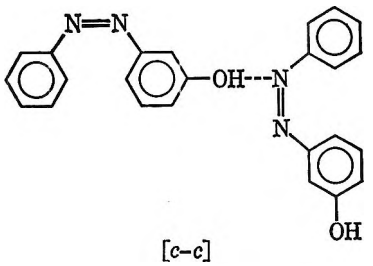

[*c–c*]

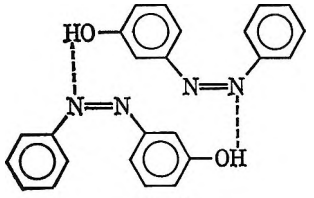

[*c–c*]

around 320 nm. In the *cis* isomer dimerization results in a plateau around 255 nm, replacing the peak at 245 nm. Spontaneous dimerization on cooling is extensive, possibly even complete, in solutions of the *cis* isomer at −75° but not in solutions of the *trans* isomer. There is no evidence for spontaneous formation of [*c*–*t*]. Some activation energy is needed to form the dimers, since the extent of their formation depends somewhat on the rate of cooling. An activation energy is also necessary for the thermal decomposition of [*c*–*t*] and [*t*–*t*] formed radiatively at low temperatures. [*t*–*t*] decomposes above about −120°, while [*c*–*t*] falls apart somewhere between −75 and −25°. The much stronger tendency of the *cis* isomer to dimerize and eventually to precipitate is probably due to the fact that in this isomer the nitrogen atoms are more exposed and, therefore, are more prone to participate in H bonding with another molecule, possibly involving even two H bonds.

All the photoinduced changes observed are actually the result of the superposition of photoisomerization (both in the monomer and in the dimer) and thermal formation or decomposition of these dimers. The rates of the thermal reactions vary with the temperature to different extents and, therefore, the contribution of these reactions varies at different temperatures. The photoreactions are controlled in the usual way[7,8] by the quantum yields and the relative absorption at the wavelength of the light used for irradiation. The quantum yield *trans*→*cis* declines sharply on cooling, again as observed in other azo compounds.[10]

The following cycle or parts thereof may explain most of the results, as shown by the examples below.

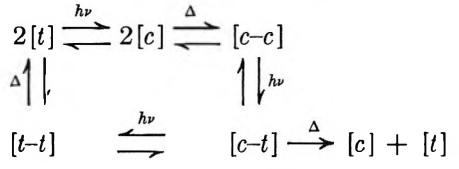

At temperatures down to −25°, regular reversible photoisomerization takes place. At −120° and lower, the *trans* exists as a mixture of much [*t*] and some [*t*–*t*]. A 365-nm irradiation causes [*t*] → [*c*] and [*t*–*t*] → [*t*–*c*], while the reverse process takes place by 436-nm irradiation. The product of 365-nm irradiation (curve 3 in Figure 4B) is not in thermal equilibrium, as evidenced by the fact that on heating to −25° and recooling to −120° a curve different from curve 3 results. However, the *cis* isomer produced by radiative [*t*] → [*c*] is spectrally different from the monomeric *cis* isomer, which has a peak at 245 nm. This peak is replaced by the plateau at 255 nm, which characterizes [*c*–*c*]. Since the radiative behavior of this product is different from that of [*c*–*c*] formed at higher temperatures (*cf.* below), it must be a more loosely bound "dimer," which is decomposed by 436-nm irradiation into [*c*] + [*t*].

When a *cis*-rich solution is cooled to −120° or below, it exists mainly as [*c*–*c*]. A 365-nm irradiation causes [*c*–*c*] → [*c*–*t*] and possibly some [*c*–*t*] → [*t*–*t*] and [*c*] → [*t*], curves 1 → 2 in Figures 5C–E. The main constituent of solutions 2 is thus [*c*–*t*]. Heating to −25° causes decomposition into [*c*] + [*t*], which on recooling to −120° form a mixture of [*c*–*c*] and some [*t*–*t*], similar to curve 1 in Figure 5B. A 436-nm irradiation of [*c*–*c*] forms [*c*–*t*] and [*t*–*t*]. The latter decomposes above −120°, and, therefore, the main product of such an irradiation at −120° and below is [*t*–*t*], while at −75° it is the monomeric *trans* isomer. The three curves 1–3 in Figure 7B were all obtained with a mixture of about 14% *cis* and 86% *trans* isomers, with the latter existing either largely in the monomeric form (curve 1) or as a mixture of [*t*] + [*c*–*t*] + [*t*–*t*] in various proportions (curve 2 and 3).

The transformation described by curve 1 → 2 in Figure 5B could be due to "[*c*]" + [*t*] $\xrightarrow{h\nu}$ [*c*–*t*], where "[*c*]" denotes electronically excited *cis* isomer. However, the alternative combined pathway given above, 2[*t*] $\xrightarrow{h\nu}$ 2[*c*], 2[*c*] $\xrightarrow{\Delta}$ [*c*–*c*], and [*c*–*c*] $\xrightarrow{h\nu}$ [*c*–*t*], appears more plausible, since there is no need to postulate bimolecular reactions involving excited (*i.e.*, short-lived) molecules.

The observed concentration dependence of the photoinduced changes and of the tendency to precipitate is in line with the basic assumption of dimerization or aggregation.

In conclusion, it appears that the experimental evidence for photoisomerization within dimers is conclusive, while for photodimerization it is ambiguous.

Experimental Section

m- and *p*-Hydroxyazobenzene and the respective methoxy derivatives were synthesized according to the literature and had the following corrected melting points: *m*-hydroxyazobenzene, 114–115°; *m*-methoxyazobenzene, 33°; *p*-hydroxyazobenzene, 157.5–159.5°; *p*-methoxyazobenzene, 55–56°.

The apparatus used for photochemical and spectroscopical work in the temperature range 100 to −180° was essentially as described in earlier publications from this laboratory.[11]

Acknowledgment. The authors are grateful to Mr. M. Kaganowitch for synthesizing the compounds and to Mrs. Nelly Castel and Mr. Y. Shabtai for technical assistance.

(10) (a) E. Fischer, *J. Amer. Chem. Soc.*, **82**, 3249 (1960); (b) S. Malkin and E. Fischer, *J. Phys. Chem.*, **66**, 2482 (1962).

(11) Y. Hirshberg and E. Fischer, *Rev. Sci. Instrum.*, **30**, 197 (1959).

Dielectric Study of Intermolecular Association in Sterically Hindered Octanol Isomers[1]

by Gyan P. Johari and Walter Dannhauser

Department of Chemistry, State University of New York at Buffalo, Buffalo, New York 14214 *(Received April 3, 1968)*

The equilibrium dielectric constant of 2-methyl- and 3-methyl-4-heptanol and also 2,5-dimethyl-, 2,4-dimethyl-, 2,2-dimethyl-, and 3,4-dimethyl-3-hexanol has been measured over a wide range of temperature. All isomers have closely similar dielectric behavior quantitatively as well as qualitatively. The Kirkwood correlation factor is less than unity at all temperatures in each case. The results suggest the existence of a monomer–dimer (ring) association and equilibrium constants for ring–dimer formation are deduced. $\Delta H°$ for H-bond formation in rings is estimated as −4.5 kcal/mol; $\Delta S°$ per mole of H-bond formation varies from −12 to −16 eu.

Introduction

The entropy of a dielectric is given[2] by the expression

$$S = S_0 + \frac{E^2}{8\pi}\frac{\partial \epsilon}{\partial T} \qquad (1)$$

where S_0 is the entropy in the absence of an applied electric field, E. Most polar liquids have a negative temperature coefficient of the dielectric constant, and the field thus decreases the entropy by partially aligning the dipoles. If $\partial\epsilon/\partial T > 0$, the field increases the entropy, implying a randomization superimposed on the alignment due to the field, and this in turn implies that the zero-field "structure" must be highly ordered in a very specific manner. (For this reason, $\partial\epsilon/\partial T$ of crystals may be positive.)

In a previous paper[3a] of this series, we presented dielectric data pertaining to some isomeric octyl alcohols that exhibited both types of behavior mentioned above. Also, for some of the compounds of that study, $\partial\epsilon/\partial T$ changes sign as a function of temperature, implying a temperature-dependent fundamental change in the liquid structure. The alcohols exhibiting this behavior are all characterized by a sterically hindered environment around the –OH group; *i.e.*, they all have an alkyl group(s) on the same or the carbon atom neighboring that to which the –OH is attached. We concluded that such alcohols associate intermolecularly to form essentially planar, nonpolar ring-dimers at high temperatures and that these species were transformed to linear chain n-mers as the temperature decreased.

As part of our continuing study of liquid structure by dielectric methods, we wanted to examine several more examples of compounds which might show this interesting and rather unusual behavior. We have continued to use isomeric octanols as test samples in order to compare their behavior with those compounds studied previously. In this paper, we report dielectric data for six isomeric octanols and demonstrate that intermolecular association into nonpolar ring species is common to them all and is easily predictable for other species.

Experimental Section

Materials. 3-Methyl-4-heptanol (3;4), 2-methyl-4-heptanol (2;4), and 2,5-dimethyl-3-hexanol (2;5;3) were obtained from Chemical Samples Co., Ohio. These samples have a quoted purity of better than 98%. 3,4-Dimethyl-3- (3;4;3), 2,4-dimethyl-3- (2;4;3), and 2,2-dimethyl-3-hexanol (2;3;2) were "Baker" grade. All samples were refluxed over CaH_2 and fractionally distilled at 50:1 reflux ratio. The samples were identified by their boiling point, density, and refractive index. See Table I.

Bridges and Cells. A General Radio Type 1615 A bridge was used for the capacitance measurements. Readings of capacitance were taken at several frequencies to ensure that the calculated dielectric constants are free from dispersion or polarization errors. A three-terminal, guarded, parallel-plate cell, which has been described earlier,[3b] was used. Because of the very small dielectric constant of these liquids, the cell with a nominal geometric capacitance of 15 pF was used. The cell constant was determined before each run. Corrections were applied for the small stray capacitance, which was determined by calibration with cyclohexane and CCl_4, and the temperature coefficient of the cell constant. Temperatures were measured with a calibrated thermocouple inside the cell.

Densities were measured at 25° with a pycnometer. These values are summarized in Table I. Densities at

(1) Supported by the Office of Saline Water, U. S. Department of the Interior, *via* Grant 14-01-0001-604.

(2) H. Fröhlich, "Theory of Dielectrics," 1st ed, Oxford University Press, New York, N. Y., 1949.

(3) (a) W. Dannhauser, *J. Chem. Phys.*, **48**, 1911 (1968); (b) W. Dannhauser and A. F. Flueckinger, *ibid.*, **38**, 69 (1963).

Table I: Physical Properties of Octanol Isomers

Properties	2;2;3	2;4;3	3;4;3	2;5;3	2;4	3;4
Density (25°), g/ml	0.8213	0.8311	0.8409	0.8132	0.8103	0.8331
Boiling point, °C	154.5	159	159.5	157.5	165	166.5
$n^{25}D$	1.4250	1.4285	1.4325	1.4212	1.4328	1.4223

other temperatures were calculated by the equation $\rho_t = \rho_0 - \alpha t$. The value $\alpha = 7 \times 10^{-4}$, determined dilatometrically for 3;4, was taken to be the same for all isomers.

Results

Equilibrium dielectric constants for 3;4, 2;4, 2;2;3, 2;4;3, 3;4;3, and 2;5;3 were measured from about 140 to −80°, or until the sample froze. The measured equilibrium dielectric constants were plotted against temperature on a large scale. Interpolated values at integral temperatures for all the six isomer are summarized in Table II.

Table II: Dielectric Constant of Octanol Isomers as a Function of Temperature

t, °C	2;4	3;4	2;2;3	2;4;3	2;5;3	3;4;3
−80	4.350	...	...	...	2.475	2.486
−70	3.982	2.600	...	2.480	2.425	2.500
−60	3.712	2.598	...	2.448	2.396	2.519
−50	3.522	2.601	...	2.443	2.384	2.541
−40	3.388	2.618	...	2.480	2.384	2.564
−20	3.301	2.702	2.653	2.613	2.520	2.664
0	3.344	2.878	2.779	2.816	2.715	2.852
20	3.476	3.123	3.005	3.125	2.965	3.115
40	3.661	3.376	3.284	3.461	3.240	3.355
60	3.754	3.550	3.487	3.624	3.445	3.497
80	3.759	3.618	3.563	3.655	3.534	3.528
100	3.678	3.541	3.524	3.572	3.540	3.467
120	3.539	3.386	3.376	3.435	3.414	3.336
140	3.336	3.280	3.251	3.321	3.271	3.236

Figure 1 shows the temperature dependence of the equilibrium dielectric constants of these isomers. Literature data,[4] available for 2;4 and 3;4, are also plotted for comparison. We note that our data for 2;4 are uniformly higher and have a qualitatively different temperature dependence than those of Smyth and Stoops;[4] for 3;4, their data are so different, qualitatively as well as quantitively, that we suspect there was a mistake in the identity of their sample.

Discussion

We reported in an earlier paper[3a] that, according to their dielectric behavior, pure liquid octanol isomers can be grouped roughly into two categories: (1) isomers which show the "conventional" dielectric behavior typical of most polar liquids (*i.e.*, the dielectric constant increases monotonically with decreasing temperature);

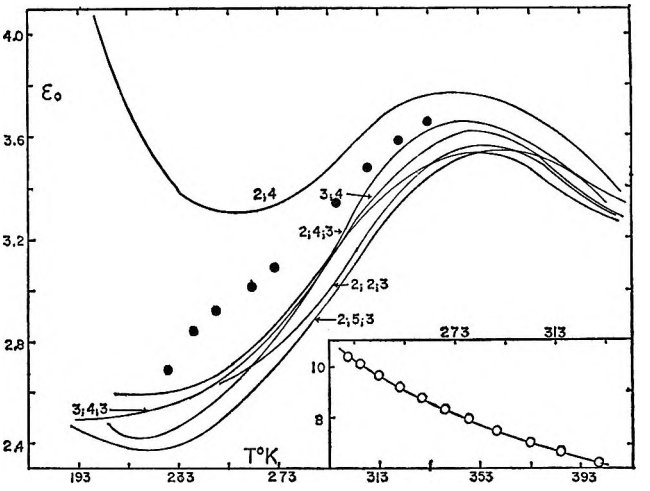

Figure 1. Equilibrium dielectric constant of isomeric octanols as a function of temperature. Filled circles and inset are data of Smyth and Stoops[4] for 2;4 and 3;4, respectively.

these are the isomers in which the –OH group is relatively less sterically hindered; and (2) isomers in which the dielectric constant goes through a maximum with decreasing temperature; these are the isomers in which the –OH group is more sterically hindered because of the presence of an alkyl group close to it (within the chain). As seen in Figure 1, the six isomers under discussion all follow the behavior of the second category. Starting at the highest temperature, the dielectric constant increases with decreasing temperature, there is a reversal near 70°, and the dielectric constant then decreases with decreasing temperature. In 2;4, 2;5;3, and 2;4;3, there is another reversal of the temperature dependence of dielectric constant at very low temperatures and the dielectric constant then increases rapidly with decreasing temperature. From the profile of the ϵ_0–T plots of 3;4, 2;2;3, and 3;4;3, it appears that in these isomers the reversal in the temperature dependence of ϵ_0 would occur at temperatures below −80°.

As in earlier papers,[3a] we discuss the equilibrium dielectric polarization in terms of Kirkwood's theory[2,5] which permits a specific representation of near-neighbor interactions. According to the Kirkwood–Fröhlich theory, a correlation factor, g, is defined as

(4) C. P. Smyth and W. N. Stoops, *J. Amer. Chem. Soc.*, **51**, 3339 (1929).

(5) J. G. Kirkwood, *J. Chem. Phys.*, **7**, 911 (1939).

$$\epsilon_0 = \epsilon_\infty + \frac{3\epsilon_0}{2\epsilon_0 + \epsilon_\infty}\left(\frac{\epsilon_\infty + 2}{3}\right)^2 \frac{4\pi N\rho\mu_0^2}{3MkT}\, g \qquad (2)$$

Here, ϵ_0 is the equilibrium dielectric constant, M is the molecular weight, N is the Avogadro number, k is the Boltzmann constant, ρ is the density of the liquid, and μ_0 is the molecular dipole moment *in vacuo*, which we have taken as 1.68 D for all the isomers. The limiting high-frequency dielectric constant characteristic of induced polarization, ϵ_∞, has been taken as 1.05 n^2D, evaluated at each temperature by assuming the validity of the Clausius–Mossoti relation.[6] The correlation factor, g, is a measure of short-range intermolecular forces, such as hydrogen bonding, which give rise to specific dipole–dipole orientation. The magnitude of g depends on both the geometry and extent of association. A correlation factor greater than unity is interpreted as being due to predominantly parallel alignment of near-neighbor dipoles, less than unity to an antiparallel alignment.

Values of the correlation factor calculated from eq 2 are plotted against temperature in Figure 2. For all isomers except 2;4, the correlation factor is less than unity and decreases with decreasing temperature. This decrease is relatively very small above 100°. At low temperatures the correlation factor goes through a shallow minimum near −60° for 2;4;3 and 2;5;3 and at −40° for 2;4. The correlation factor of 3;4;3 and 3;4 drops to less than 0.05 at very low temperatures and becomes relatively insensitive to changes in temperature. In terms of the Kirkwood–Fröhlich theory, the positive temperature coefficient of g indicates an increase in the predominantly antiparallel association with decreasing temperature in these liquids. We suggest that the extraordinarily small correlation factor of these compounds is due to intermolecular association into small rings where, as in carboxylic acid dimers, the molecular dipoles largely cancel each other. The upsweep in the g's of 2;4, 2;4;3, and 2;5;3 indicate the existence of a ring–chain equilibrium[3a] and that chain formation is favored at low temperatures.

Using the same specific molecular model as earlier,[3a] we attempt to make the foregoing conclusions quantitative. For all isomers, at temperatures where the correlation factor is less than unity, we consider monomers in equilibrium with ring dimers of zero dipole moment.[7] For the monomer–ring dimer equilibrium

$$A_1 + A_1 \rightleftarrows A_2 \qquad (3)$$

where A_1 refers to a monomer and A_2 to a ring dimer, the equilibrium constant (using volume fraction units) is related to the correlation factor as[3a]

$$K = \frac{1}{g}\left(\frac{1}{g} - 1\right) \qquad (4)$$

Equilibrium constants calculated from eq 4 are plotted logarithmically against reciprocal temperature in Figure 3. $\Delta H°$, $\Delta S°$, and $\Delta G°$ for ring-dimer association in the pure liquid were estimated from these plots and are listed in Table III. We have also included our

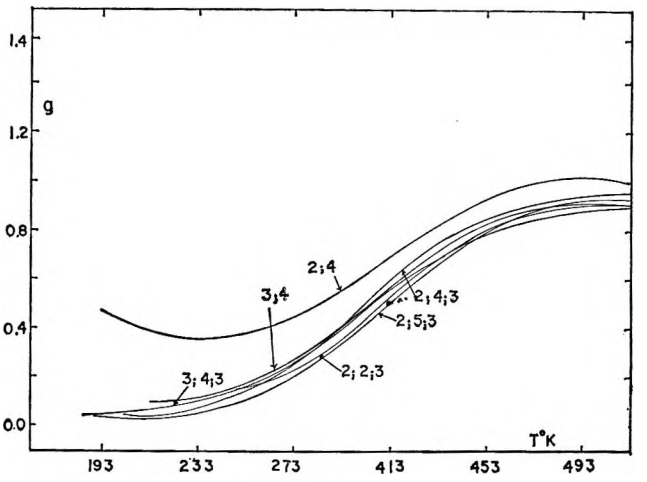

Figure 2. Kirkwood correlation factor as a function of temperature.

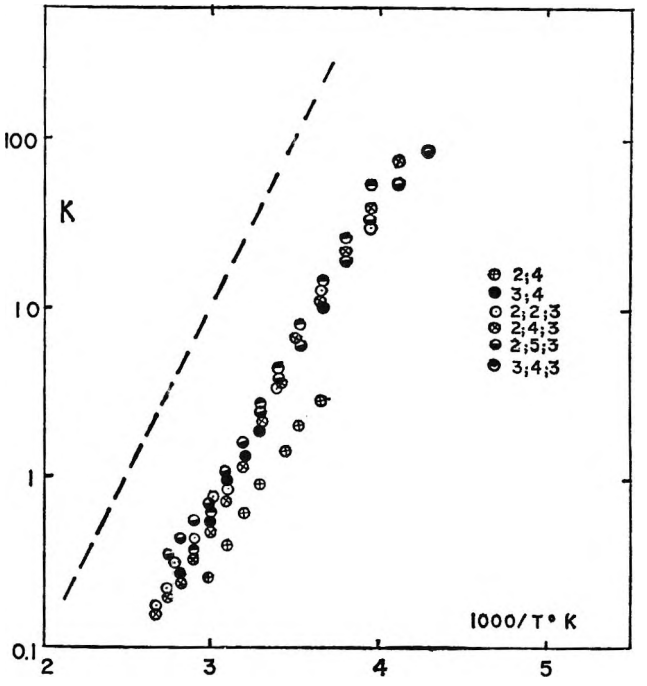

Figure 3. Equilibrium constant for ring-dimer formation (volume fraction units) plotted logarithmically against reciprocal absolute temperature. Dashed line corresponds to a slope of $9.0 \times 10^3/2.3R$.

(6) The choice of ϵ_∞ is quite critical for liquids whose ϵ_0 is very close to ϵ_∞. We have chosen $\epsilon_\infty = 1.05$ n^2D as a reasonable compromise between 1.1 n^2D, which was found to be too large from our relaxation measurements, and 1.0 n^2D, which does not include atomic polarization. However, calculations of g based on $\epsilon_\infty = 1.1$ n^2D do not affect our conclusions.

(7) We do not claim that dimers are the only ring species. In order to keep the model relatively simple, we have chosen dimers. It might be noted further that very large rings cannot account for the very low values of g. Because of the flexibility of H bond, the near-neighbor correlation in very large rings is not essentially different from that in long chains.

Table III: Thermodynamic Parameter for Ring-Dimer Formation in Pure Liquid Octanol Isomers, Based on Volume Fraction Units

Liquid	$-\Delta H°$, kcal/mol	$-\Delta G°_{298}$, kcal/mol	$-\Delta S°_{298}$, eu/mol
2-Methyl-4-heptanol	8.7	0.103	28.9
3-Methyl-4-heptanol	8.8	0.636	27.3
2;2-Dimethyl-3-hexanol	9.6	0.774	29.5
2;4-Dimethyl-3-hexanol	9.7	0.610	30.7
2;5-Dimethyl-3-hexanol	9.6	0.780	29.7
3;4-Dimethyl-3-hexanol	8.8	0.694	27.3
2-Methyl-3-heptanol[a]	8.6	0.41	27.2
3-Methyl-3-heptanol[a]	7.7	0.78	23.2
4-Methyl-3-heptanol[a]	9.0	0.24	29.4
5-Methyl-3-heptanol[a]	10.5	−0.35	36.6

[a] Taken from ref 3a.

values[3a] of these parameters for 2;3, 3;3, 4;3, and 5;3 for comparison.

The enthalpy per mole of H-bond formation in ring dimers ranges from 4.3 to 4.8 kcal in these isomers. These values are so closely similar that they can be approximated (within the experimental error) by a singly value of $\Delta H° \approx 4.5$ kcal/mol. This is in contrast to the molar enthalpy of H-bond formation in chain species[3a] which is quite characteristic of the isomers and ranges from 6 to 9 kcal. The apparent identity of $\Delta H°$ values in all the isomers of this investigation confirms that association into rings is much less specific than association into chains. Furthermore, the $\Delta H°$ of ring formation is significantly less than that of chain formation. Evidently, the H bonds in rings are weak in comparison to those in chains.

The molar entropy of H-bond formation in these sterically hindered isomers range from −13.7 to −15.4 eu. However, we do not see any correlation between the entropy of H-bond formation in rings and the amount of steric hindrance about the –OH group. It appears that the presence of a methyl group on the same or on a neighboring carbon atom makes the –OH group so sterically hindered that causing further changes in the immediate structural environment by introducing more methyl groups does not significantly affect the dielectric properties. In this respect, it is interesting to note the extreme sensitivity of the intermolecular association to the position of the –OH group, as can be seen for example by comparing 2;2;3 and 2;2;1 (*neo*-octanol):[8] the former appears to associate exclusively into rings in the temperature range accessible to us; the latter, while possibly favoring rings at higher temperatures (the correlation factor is slightly less than 1), definitely favors linear chain species at lower temperatures.

We conclude that octanol isomers in which the environment about the –OH group is sterically hindered by an alkyl group on the same or on the next carbon atom tend to associate into ring dimers, while those isomers whose –OH group is less severely hindered associate into linear chains. The relative population of ring and chain species is strongly temperature and pressure dependent so the octanols provide an ideal system with which to explore the subtleties of intermolecular association. With our experience so far as a guide, it is easy to predict other classes of compounds[9] which might show similar behavior. Dielectric behavior of the type discussed in this paper is probably less exceptional than is usually supposed.

(8) W. Dannhauser, L. W. Bahe, R. Y. Lin, and A. F. Flueckinger, *J. Chem. Phys.*, **43**, 257 (1965).

(9) R. Perrin and P. Issartel, *Bull. Soc. Chim. France*, 1083 (1967), have determined dielectric constants of some methyl- and dimethyl phenols. They discuss their results in terms of a temperature-dependent "Onsager moment" which, in our notation, means a temperature dependent correlation factor. For highly hindered species, *i.e.*, 2,6-dimethyl phenol, g is close to unity and almost independent of temperature. Their experiments are restricted to relatively high temperatures though, and so they find no evidence for antiparallel association. $d\epsilon/dT < 0$ in all cases, but it is close to zero for the hindered species. Carboxylic acids (with formic acid a notable exception) have long been suspected of associating in antiparallel ring dimers. A. E. Lutskii and S. A. Mikhailenko, *Zh. Strukt. Khim.*, **4**, 14 (1963), have shown that $d\epsilon/dT > 0$ for acetic–valeric acid. However, they suggest that disruption of the ring dimer is only one aspect of the behavior and believe that a major change of the dipole moment upon formation of an H bond is the most important factor.

Spatial Distribution of Trapped Radicals in γ-Irradiated Ethylene Glycol Dimethacrylate Polymers

by John Zimbrick, Frank Hoecker, and Larry Kevan

Departments of Chemistry and Radiation Biophysics, University of Kansas, Lawrence, Kansas 66044
(Received April 3, 1968)

Trapped radicals are produced in γ-irradiated ethylene glycol dimethacrylate gels. A nine-line epr spectrum is observed which is identical with the spectrum seen in irradiated methyl methacrylate gels. Paramagnetic-relaxation times as a function of radiation dose from 0.5–2 Mrads were measured by power-saturation methods. The spin–spin relaxation time is constant with dose and indicates that the radicals are trapped inhomogeneously in radiation-produced spurs in which the local radical molarity is several times greater than the average radical molarity.

I. Introduction

Radiation energy is deposited by γ rays in condensed systems inhomogeneously and produces an initial inhomogeneous distribution of energetic ionized and excited species. For very fast chemical reactions, the initial spatial inhomogeneity of the species involved must be taken into account. In liquid water radiolysis such reasoning has led to the development of the "spur" model and the consequent successful application of diffusion kinetics.[1] Likewise, in condensed systems such as polymers and frozen solutions, it is of considerable interest to determine if trapped species exhibit an inhomogeneous spatial distribution.

Recently we showed how paramagnetic-relaxation experiments can give new insights into the spatial distributions of trapped electrons and hydrogen atoms in frozen aqueous systems.[2–5] Trapped electrons in irradiated alkaline ices at 77°K show no change in their relaxation time over a range of γ dose from 0.2 to 3 Mrads, even though the electron concentration increases linearly in this range; this implies that the average spin–spin interaction and the local concentration of electrons remains constant in this dose range. The results are explained by an inhomogeneous distribution of electrons trapped in spurs in which only intraspur spin–spin interactions are important.[2,3] At higher doses the spurs overlap, interspur spin–spin interactions become important, and the relaxation time decreases with dose. In contrast, trapped hydrogen atoms in irradiated acidic ices at 77°K exhibit a decreasing relaxation time and a linearly increasing concentration over a radiation dose range of 0.3–5 Mrads.[4,5] This is the behavior expected for a homogeneous distribution. The trapped hydrogen atoms are trapped only near oxyanion molecules and are expected to have a uniform spatial distribution. The relaxation results confirm this.

In the present work we have extended our paramagnetic-relaxation method to trapped organic free radicals. This method depends on microwave-power saturation and can be applied only to organic radicals that saturate within the range of available microwave power (typically 200 mW). We have found that radicals trapped in irradiated ethylene glycol dimethacrylate (EDMA) gels at room temperature fulfill this requirement. The EDMA monomers have the structure

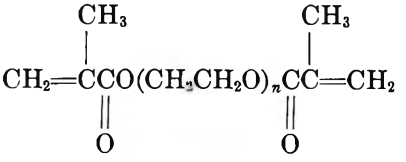

and structures with n = 1–4 have been studied. Irradiation produces a rigid cross-linked polymer. Trapped radicals in irradiated poly(methyl methacrylate) which is not cross-linked are also saturable and have been studied recently with similar aims by Bullock, *et al.*[6,7] The identity of the EDMA radicals and the effect of radiation dose and temperature on their relaxation time are reported. In addition, the local radical concentration and the sample-average radical concentration have been measured and compared. The results indicate that the radicals in EDMA gels are of the methacrylate type and are trapped with an inhomogeneous spatial distribution within radiation-produced spurs.

(1) A. Kuppermann in "Chemical and Biological Actions of Radiations," Vol. V, M. Haissinsky, Ed., Academic Press Inc., New York, N. Y., 1961, p 85.

(2) J. Zimbrick and L. Kevan, *J. Amer. Chem. Soc.*, **88**, 3678 (1966).

(3) J. Zimbrick and L. Kevan, *J. Chem. Phys.*, **47**, 2364 (1967).

(4) J. Zimbrick and L. Kevan, *Nature*, **214**, 693 (1967).

(5) J. Zimbrick and L. Kevan, *J. Chem. Phys.*, **47**, 5000 (1967).

(6) A. T. Bullock and L. H. Sutcliffe, *Trans. Faraday Soc.*, **60**, 2112 (1964).

(7) A. T. Bullock, W. G. Griffiths, and L. H. Sutcliffe, *ibid.*, **63**, 1846 (1967).

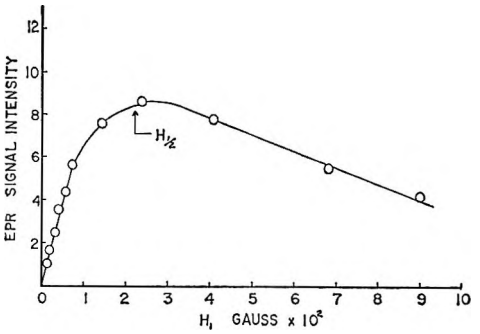

Figure 1. The slow-passage progressive-saturation curve of the central line in the epr spectrum of γ-irradiated tri-EDMAX. The dose is 0.55 Mrad.

II. Theory

Portis[8] has classified the types of paramagnetic line broadening as homogeneous or inhomogeneous. An epr line is homogeneously broadened by interactions which allow the spin system to remain in thermal equilibrium during resonance absorption. Inhomogeneous line-broadening interactions with nuclear spins cause different sets of electron spins to see different net local magnetic fields. Each such set of electron spins forms a "spin packet" and the observed spectrum of the total spin system is an envelope of the superimposed spin packets. The shape of the envelope depends on the intensity distribution of local magnetic fields seen by the electron spins and the ratio of the spin-packet width to the envelope width. If the spin-packet width is much less than the envelope width, as is often observed, and if the spin packets do not interact magnetically, then the envelope shape is dependent only on the intensity distribution of local magnetic fields and is Gaussian.

An electron-spin system saturates when the population ratio between the upper and lower spin energy states deviates from its thermal equilibrium value. Power saturation is most readily studied by obtaining saturation curves which are plots of epr signal intensity *vs.* microwave magnetic field, H_1. A study of saturation behavior allows one to determine the product T_1T_2 or sometimes T_1 alone; T_1 is the spin–lattice relaxation time and T_2 is the spin–spin relaxation time. The relevant theory for obtaining relaxation times from saturation curves under slow-passage conditions has been summarized in a previous paper.[3]

A typical saturation curve for the central epr line of free radicals in triethylene glycol dimethacrylate gel is shown in Figure 1. An ideal inhomogeneously broadened line would have resulted in a saturation curve which had a slope of 0 at high values of H_1, whereas an ideal homogeneous line would have yielded a curve which bends down at high H_1 values even more sharply than the free-radical curve.[3] If homogeneous saturation behavior is assumed, T_1T_2 can be calculated from

$$T_1T_2 = 1/\gamma^2H_{1/2}^2 \quad (1)$$

where γ is the gyromagnetic ratio of the electron and is equal to $1.76 \times 10^7\ G^{-1}\ \text{sec}^{-1}$ and $H_{1/2}$ is the value of H_1 at which the epr signal intensity is one-half of what it would have been in the absence of saturation. If ideal inhomgeneous saturation behavior is assumed, T_1T_2 is calculated by

$$T_1T_2 = 3/\gamma^2H_{1/2}^2 \quad (2)$$

For an intermediate case such as that shown in Figure 1, Castner's analysis[9] may be applied using curve-fitting procedures to correct $H_{1/2}$ and then using eq 1 to obtain T_1T_2. This method also allows the calculation of T_2 separately from

$$T_2 = \frac{1.70}{a\gamma\Delta H_{\text{ms}}^{\text{G}}} \quad (3)$$

where $\Delta H_{\text{ms}}^{\text{G}}$ is the measured line width at the maximum slope of the observed Gaussian line and a is a measure of the ratio of the Lorentzian spin-packet width to the observed Gaussian line width; a is determined from the saturation curve.[9]

III. Experimental Section

Mono-, di-, tri-, and tetraethylene glycol dimethacrylate monomers (abbreviated mono-, di-, tri-, and tetra-EDMAX, where the X indicates that inhibitor has been removed) were obtained from Sartomer Resin Co. and contained 60 ppm of hydroquinone as an inhibitor of thermal polymerization. The hydroquinone was removed by forming its sodium salt in 1.5 *M* NaOH and extracting with water. The monomer was then dried over $MgSO_4$ and was stored in a refrigerator.

Samples were prepared by pipetting about 2 ml of each monomer into a 3 mm o.d. $\times$ 5 cm Spectrosil quartz tubes. These were irradiated at about 35° in a ^{60}Co γ irradiator at a dose rate of 0.54 Mrad/hr as determined by ferrous sulfate dosimetry. Polymerization occurred[10,11] and radicals were trapped in the monomer gels which appeared to be stable for at least several days after irradiation.

The epr measurements were made at room temperature by placing the irradiated samples in a quartz epr dewar. After a sample had been measured at room temperature, it could be measured at 77°K by simply filling the dewar with liquid nitrogen. All epr measurements were made on a Varian 4500 spectrometer equipped with a V-4500-41A low–high power microwave bridge, an audio modulation system, and a Varian dual cavity with dewar inserts. The bridge was operated in low-power mode, which allowed a microwave power

(8) A. M. Portis, *Phys. Rev.*, **91**, 1071 (1953).

(9) T. G. Castner, *ibid.*, **115**, 1506 (1959).

(10) F. E. Hoecker and I. W. Watkins, *Int. J. Appl. Radiat. Isotopes*, **3**, 31 (1958).

(11) F. E. Hoecker, *Health Phys.*, **8**, 381 (1962).

variation over a 40-db range. Slow-passage conditions were achieved by operating with a field-modulation frequency of 40 cps and a typical modulation amplitude of 0.3 G. The slow-passage progressive-saturation measurements were made as described previously.[3]

IV. Results

A typical epr spectrum of radicals trapped in irradiated tri-EDMAX is show in Figure 2. This is a direct recorder trace from the present work and shows the first-derivative absorption signal obtained with fast-passage (100 kc) operating conditions. Spectra from mono-, di-, and tetra-EDMAX are not shown because they are identical with that of Figure 2.

The relaxation time $(T_1T_2)^{1/2}$ of free radicals trapped in tri-EDMAX was measured as a function of radiation dose and temperature under slow-passage conditions. The central line of the epr spectrum was used for the measurements. From saturation curves such as the one shown in Figure 1 the value of $H_{1/2}$ was measured and $(T_1T_2)^{1/2}$ was calculated from eq 2 assuming ideal inhomogeneous conditions. Castner's[9] method was also used to calculate $(T_1T_2)^{1/2}$ (eq 1) and T_2 (eq 3). These data are presented in Table I.

Table II contains measurements of the line width between derivative maxima, ΔH_{ms}, of the central epr line *vs.* H_1 for trapped free radicals in tri-EDMAX at room temperature.

Table I: Relaxation Time *vs.* Radiation Dose and Temperature for Free Radicals Trapped in Tri-EDMAX Gels

a (Castner)	$10^6(T_1T_2)^{1/2}$ (Castner),[a] sec	10^6T_2 (Castner),[b] sec	10^4T_1, sec	$10^6(T_1T_2)^{1/2}$ (Portis),[c] sec	γ dose, Mrads	Temp, °K
0.5	3.1	3.6	2.7	4.4	0.55	298
0.5	3.1	3.6	2.7	4.5	1.04	298
0.5	3.3	3.7	3.0	4.7	2.09	298
0.3	3.6	5.9	2.6	4.9	2.09	73

[a] Equation 1. [b] Equation 3. [c] Equation 2.

Table II: Epr Line Width in Free Radicals in Tri-EDMAX *vs.* the Microwave Magnetic Field[a]

ΔH_{ms}, G	H_1, G
5.2	0.00354
5.2	0.0121
5.2	0.0238
5.2	0.0900

[a] Measured on the central line of the epr spectrum.

V. Discussion

A. Radical Identification. The nine-line epr spectrum of Figure 2 for radicals trapped in tri-EDMAX is similar to those for radicals in mono-, di-, and tetra-

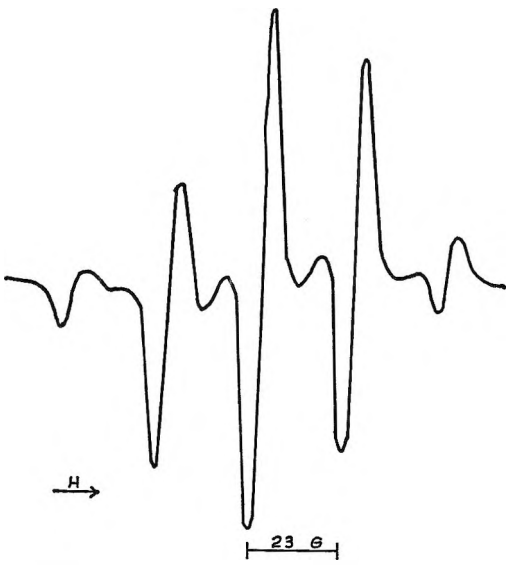

Figure 2. Epr spectrum of γ-irradiated tri-EDMAX at room temperature and at a 0.55-Mrad dose.

EDMAX. The only observable difference among them is that the trapped-radical yield increases in the direction mono → di → tri → tetra-EDMAX. Relative yield ratios for the mono–tetra-EDMAX monomers are 1.0:1.3:2.5:2.6. The increase in radical yield correlates with the increase in the length of the monomer molecule and the density of monomer solution. It is concluded that the radical species is the same in all four monomer gels.

Irradiated poly(methyl methacrylate) (PMMA) produces a radical with an epr spectrum identical with that in the EDMAX gels.[12] This spectrum has received a great deal of study and there has been considerable argument as to whether the nine-line spectrum is due to one or two radicals.[13] However, the model suggested by Symons[14] and supported by the high-resolution experiments of Fischer[15] and the deuteration experiments of Kourim and Vacek[16] lead us to assign the spectrum in Figure 2 to the single radical

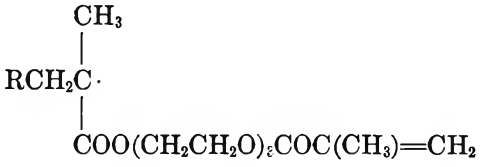

where R is the polymer chain. The quartet from the CH_3 group (a^{CH_3} = 23 G) is split by the two nearly equivalent methylene protons (a^{CH_2} = 11 and 14 G)[15]

(12) E. E. Schneider, M. J. Day, and G. Stein, *Nature*, **168**, 645 (1951).

(13) R. E. Michel, F. W. Chapman, and T. J. Mao, *J. Chem. Phys.*, **45**, 4604 (1966); see earlier references therein.

(14) M. C. R. Symons, *J. Chem. Soc.*, 1186 (1963).

(15) H. Fischer, *J. Polym. Sci.*, **82**, 529 (1964).

(16) P. Kourim and K. Vacek, *Trans. Faraday Soc.*, **61**, 415 (1965).

to give the observed nine-line spectrum; resolution of the even-numbered spectral lines is not achieved.

B. Line Shape and Broadening Mechanism. Table II shows that the central line of the monomer radical epr spectrum does not widen appreciably at the highest microwave powers available from the klystron. The average line-shape factor for this line was measured and found to be 2.3; 2.2 is the theoretical value for a pure Gaussian line.[17] These two results imply that the epr line is broadened mainly by inhomogeneous mechanisms. The broadening is principally due to unresolved hyperfine interaction and to the nuclear-spin state of the β protons.[15] Analysis of progressive-saturation curves (Figure 1) by Castner's method results in a value of approximately 0.5 for his a parameter (eq 3). Although Castner's method involves considerable uncertainty when a is as large as 0.5, it does indicate that the spin-packet width is not negligible in comparison to the total line width.

C. Dose and Temperature Effects on Spatial Distributions of Radicals. Table I summarizes relaxation time as a function of radiation dose and of temperature for radicals trapped in tri-EDMAX gels. $(T_1T_2)^{1/2}$ has been determined by Portis' method, as well as by Castner's method. Castner's method has also been applied to the epr central line widths to calculate T_2 (eq 3) separately. The data show that (a) $(T_1T_2)^{1/2}$ and T_2 do not change significantly when the radiation dose is increased to 2 Mrads; and (b) T_2 appears to increase upon going from 298 to 77°K, whereas T_1 does not change significantly.

Bullock and Sutcliffe[6] have made similar measurements on methyl methacrylate radicals and it is interesting to compare the results obtained in this work for tri-EDMAX radicals, which have a similar structure, with their results for radicals trapped in photopolymerized pure methyl methacrylate. They obtain a value of 2.9×10^{-6} sec at 299°K for $(T_1T_2)^{1/2}$ by Castner's method, which compares favorably with the value 3.1×10^{-6} sec obtained in the present work. Their values of 5.7×10^{-8} sec for T_2 and 2.5×10^{-4} sec for T_1 are in fair agreement with $T_2 = 3.6 \times 10^{-8}$ sec and $T_1 = 2.7 \times 10^{-4}$ sec obtained here. Their value of Castner's a parameter is approximately equal to 0.30 and, considering the precision of the method, is comparable with the value $a \simeq 0.5$ measured in this work. It is clear from these comparisons that the relaxation characteristics of trapped methyl methacrylate radicals are very similar to those for the trapped radicals in tri-EDMAX gels. The EDMAX gels are cross-linked while PMMA is not, and the mobility of segments is lower in the EDMAX gels. These structural features apparently do not affect the relaxation characteristics.

From 0.5 to 2.0 Mrads, T_2 remains constant, although the concentration of radicals is increasing linearly in this dose range. In analogy to our previous interpretations,[2-5] this indicates that the radicals are trapped in spurs and that the local radical concentration is higher than the average radical concentration. These organic radicals exhibit the same relaxation behavior as do trapped electrons in alkaline ices. At higher doses the value of T_2 should decrease, owing to the overlap of spurs.

The value of Castner's a allows one to calculate the dipolar spin-packet line width, $\Delta H_{ms}{}^{L}$, from

$$\Delta H_{ms}{}^{L} = \frac{a\Delta H_{ms}{}^{G}}{1.47} \tag{4}$$

Wyard[18] has modified Kittel and Abrahams'[19] treatment of dipolar line width to apply to nonequivalent magnetic centers in glassy and polycrystalline samples and obtained $\Delta H_{ms}{}^{L} = 32\ M$, where M is a local molarity of trapped spins contributing to the dipolar line width. The radicals in EDMAX gels may be equivalent, in which case $\Delta H_{ms}{}^{L} = 48\ M$; we shall use the value of 48 M to calculate the local spin molarity. The calculated local spin molarity is 0.037 M and is constant from 0.5 to 2 Mrads. Assuming that G(radical) = 4, the average spin concentration at 2 Mrads is only 0.0084 M, which is a factor of 5 less than the local spin molarity. A similar analysis on trapped radicals in poly(methyl methacrylate) also shows a ratio of local to average radical concentration greater than 1.[7] The actual ratio of local to average spin molarity at a given dose depends on the quantitative validity of $\Delta H_{ms}{}^{L} = 48\ M$ and on the precision of a, but it is certainly greater than 1 at doses up to 2 Mrads. This is completely consistent with the spur concept deduced from radiation dose effects. The local spin molarity and, consequently, T_2 are expected to change with radiation of different linear energy transfer; such experiments are in progress.

The temperature data indicate that T_2 increases by 60% as the temperature is lowered from 299 to 73°K. This curious temperature dependence also is found for radicals in irradiated poly(methyl methacrylate).[6] The increase in T_2 indicates that the local radical concentration is decreased at lower temperatures. This could be related to contraction of adjacent polymer chains, but the magnitude of the effect is similar in linear poly(methyl methacrylate) and in cross-linked EDMA gels. The effect of a wider temperature range on T_2 needs to be studied before more speculation on the cause of the temperature dependence is warranted.

Acknowledgment. This research was supported by the Air Force Rocket Propulsion Laboratory and the U. S. Atomic Energy Commission. This is U. S. Atomic Energy Commission Document No. COO-1528-23. J. Z. is grateful to the U. S. Atomic Energy Commission for an Advanced Health-Physics Fellowship.

(17) G. E. Pake and E. M. Purcell, *Phys. Rev.*, **74**, 1184 (1948).
(18) S. J. Wyard, *Proc. Phys. Soc.*, **86**, 587 (1965).
(19) C. Kittel and E. Abrahams, *Phys. Rev.*, **90**, 238 (1953).

Transport Processes in Hydrogen-Bonding Solvents. I. The Conductance of Tetraalkylammonium Salts in Ethanol and Propanol at 25°

by D. Fennell Evans[1] and Philip Gardam

Department of Chemistry, Case Western Reserve University, Cleveland, Ohio 44106 *(Received April 8, 1968)*

Conductance measurements are reported for Me_4NCl, Bu_4NCl, Me_4NBr, Et_4NBr, Pr_4NBr, Bu_4NBr, Et_4NI, Pr_4NI, Bu_4NI, i-Am_3BuNI, and $Hept_4NI$ in ethanol and propanol and Bu_4NClO_4 in propanol at 25°. Analysis of the data by the Fuoss–Onsager equation gave an average value of $\mathring{a}$ of 4.2 ± 0.2 Å in ethanol and 5.0 ± 0.5 Å in propanol, while analysis by the Fuoss–Hsia equation gave equally small, but constant, values of $\mathring{a}$ which appeared to be independent of dielectric constant. All of the salts were found to be associated, and the extent of ionic association increased with increasing size of the anion for any given cation. This unusual association pattern is discussed in terms of the normal behavior observed in acetone, a solvent which is isodielectric with propanol.

Introduction

Contrary to the predictions of electrostatic theory, the association of electrolytes in solvents containing hydroxy groups appears to increase with ionic size.[2] However, the data which suggest such an idea do not permit unambiguous conclusions. This is due to the presence of factors which complicate the interpretation of systems that have been studied in detail and to the fragmentary information available in systems which lack complicating features.

The two most thoroughly studied hydroxy solvents are methanol and water. Analysis of the concentration dependence of conductance in methanol solutions gives association constants for the alkali metal and tetraalkylammonium halides which increase as the size of the ion increases.[2] For example, constants of 0, 4, and 18 have been obtained for tetrabutylammonium chloride, bromide, and iodide, respectively. However, all of the constants in methanol are small, less than 20, and must be interpreted with reservation, since it has been shown that association constants as large as 40 may be artifacts arising from errors in the theory used to evaluate the data.[3]

The behavior of electrolytes in aqueous solution has been discussed in terms of a similar association pattern.[4,5] In this case, the extent to which the peculiar concentration dependence reflects structural effects, arising from the unique three-dimensional structure of water, and the extent to which it reflects ionic association remains an open question. The association constants that have been recorded are small, *ca.* 5, as would be expected in a high dielectric medium and are often obtained only by arbitrary assumptions in the analysis of the data.[5]

When the higher alcohols are chosen as the solvent system, the pattern of ionic association of hydroxy solvents may be investigated without such complications as three-dimensional structural effects or small association constants. This homologous series also allows investigation over wide variations of dielectric constant, viscosity, and temperature. In this paper, which is the first of a series, we report the conductance behavior of the tetraalkylammonium halides and perchlorates in ethanol and propanol at 25°.

Experimental Section

Materials. Conductivity grade ethanol was prepared by distilling absolute ethanol (Rossville Gold Seal) in 4-l. batches from 20 g of magnesium ethoxide and 10 g of magnesium metal.[6] All distillations were carried out in a 1.3-m Stedman column under nitrogen and only the middle fraction was retained. The magnesium metal was dried at room temperature over phosphorus pentoxide in a vacuum desiccator. Magnesium ethoxide was prepared by mixing magnesium metal with absolute ethanol, the reaction being catalyzed by a drop of bromoethane.

Conductivity grade 1-propanol was prepared by drying the Fisher reagent grade alcohol over calcium oxide for several days and then distilling the alcohol from a fresh batch of calcium oxide.[7] Tests for unsaturated impurities with bromine water were negative.

The densities of these alcohols at 25° were determined in single-neck pycnometers to be 0.78511 and 0.79960

(1) To whom all correspondence should be directed.

(2) R. L. Kay, C. Zawoyski, and D. F. Evans, *J. Phys. Chem.*, **69**, 4208 (1965).

(3) R. L. Kay and J. L. Dye, *Proc. Nat. Acad. Sci.*, **49**, 5 (1963).

(4) R. M. Diamond, *J. Phys. Chem.*, **67**, 2513 (1963).

(5) (a) B. J. Levien *Aust. J. Chem.*, **18**, 1161 (1965); (b) H. E. Wirth, *J. Phys. Chem.*, **71**, 2922 (1967).

(6) J. R. Graham, C. S. Kell, and A. R. Gordon, *J. Amer. Chem. Soc.*, **79**, 2352 (1957).

(7) W. C. Vosburgh, L. C. Connel, and J. A. V. Butler, *J. Chem. Soc.*, 933 (1933).

Table I: Equivalent Conductances in Ethanol at 25°

10^4C, mol/l.	Λ	10^4C, mol/l.	Λ	10^4C, mol/l.	Λ	10^4C, mol/l.	Λ
Me_4NCl (A = 0.03)		Et_4NBr (A = 0.09)		Et_4NI (A = 0.10)		He_4NI (A = 0.13)	
3.304	47.093	3.912	48.368	3.844	50.976	3.350	37.846
6.595	44.898	7.880	46.003	7.969	48.124	6.764	35.795
10.076	43.077	12.603	43.974	12.206	46.010	10.301	34.235
13.775	41.532	17.434	42.366	17.003	44.135	14.144	32.890
18.281	39.986	21.926	41.131	21.901	42.578	17.768	31.839
24.437	38.385	27.432	39.859	27.571	41.092	21.955	30.800
30.602	36.911	33.016	38.762	33.711	39.741	26.392	29.857
43.106	34.790	39.399	37.681	39.957	38.569	31.117	28.985
56.299	33.085						
Bu_4NCl (A = 0.05)		Pr_4NBr (A = 0.09)		Pr_4NI (A = 0.11)		i-Am_3BuNI (A = 0.13)	
2.062	39.140	4.317	42.455	4.843	44.422	4.017	40.556
4.529	37.747	9.207	40.138	10.002	41.617	8.037	38.239
7.845	36.548	14.001	38.529	15.808	39.395	12.296	36.444
11.423	35.503	19.080	37.173	22.020	37.589	16.631	35.000
15.141	34.607	24.075	36.070	28.438	36.094	21.323	33.717
23.382	33.135	29.887	34.990	34.950	34.839	26.733	32.480
28.548	32.371	35.719	34.063	41.434	33.774	32.047	31.453
34.911	31.554	40.239	33.423	48.080	32.827	37.923	30.470
42.393	30.744						
Me_4NBr (A = 0.07)		Bu_4NBr (A = 0.08)		Bu_4NI (A = 0.11)			
5.316	47.017	4.768	39.128	4.601	41.492		
11.066	43.654	10.210	36.841	9.303	38.956		
16.664	41.374	16.013	35.157	14.751	36.869		
22.626	39.499	21.380	33.952	20.074	35.296		
28.645	37.910	27.445	32.825	25.533	33.991		
35.940	36.379	33.429	31.897	31.306	32.829		
		39.465	31.084	37.366	31.769		
		45.982	30.312	43.718	30.829		

g/cm³, for ethanol and propanol, respectively. These figures are slightly higher than the lowest recorded densities for these alcohols, 0.78506 for EtOH[6] and 0.79950 for PrOH.[8]

The viscosities of these alcohols at 25° were determined in two Cannon Ubbelohde viscometers and found to be 0.01084 P for ethanol and 0.01952 P for propanol. The value for ethanol agrees with those previously reported,[9] while that for propanol disagrees by 1%.[10]

Because of the large number of values reported for the dielectric constant of these solvents, this property has been redetermined using the all-glass platinum cells described by Kay and Vidulich.[11] The value of ϵ 24.33 found for ethanol agrees best with that given by Wyman[12] and that for propanol, ϵ 20.45, agrees with that reported by Dannhauser.[13] The specific conductances of these alcohols as measured in the conductance cells before beginning runs had a range of (2–10) × 10^{-9} ohm^{-1} cm^{-1} for ethanol and (2–9) × 10^{-9} ohm^{-1} cm^{-1} for propanol.

The tetraalkylammonium salts were purified by recrystallization. For all the salts employed, except tetraheptylammonium iodide, the method of purification has been described in detail previously.[2,14] Tetraheptylammonium iodide (Eastman Kodak) was dissolved in acetone, filtered through a fritted-glass funnel, precipitated by the addition of ether, recrystallized similarly a second time, and dried in a vacuum oven overnight at 56°. We would like to thank Professor J. Coetzee of the University of Pittsburgh, who provided us with a sample of the tetrabutylammonium perchlorate.

Equipment and Techniques. The electrical equipment, conductance cells, and techniques were similar to those previously reported.[2,14,15] The measurements

(8) C. B. Kretschmer, *J. Phys. Colloid Chem.*, **55**, 1351 (1951).

(9) O. L. Hughes and H. Hartley, *Phil. Mag.*, **15**, 610 (1933).

(10) T. A. Gover and P. G. Sears, *J. Phys. Chem.*, **60**, 330 (1956).

(11) G. A. Vidulich and R. L. Kay, *Rev. Sci. Instrum.*, **37**, 1662 (1966).

(12) J. Wyman, *J. Amer. Chem. Soc.*, **53**, 3292 (1931).

(13) W. Dannhauser and L. W. Bahe, *J. Chem. Phys.*, **40**, 3058 (1964).

(14) D. F. Evans, C. Zawoyski, and R. L. Kay, *J. Phys. Chem.*, **69**, 3878 (1965).

Table II: Equivalent Conductances in Propanol at 25°

10^4C, mol/l.	Λ	10^4C, mol/l.	Λ	10^4C, mol/l.	Λ	10^4C, mol/l.	Λ
Me_4NCl (A = 0.02)		Et_4NBr (A = 0.07)		Et_4NI (A = 0.09)		He_4NI (A = 0.10)	
5.811	19.483	4.301	22.604	3.305	24.477	2.819	18.909
10.703	17.542	8.630	20.537	7.370	21.935	5.760	17.276
15.736	16.181	13.780	18.925	11.092	20.431	9.655	15.860
21.720	15.011	18.027	17.950	15.863	19.034	13.372	14.886
27.704	14.126	23.136	17.023	21.403	17.834	17.440	14.064
33.629	13.425	29.151	16.166	26.591	16.961	22.102	13.316
43.393	12.528	34.013	15.594	33.062	16.083	27.009	12.679
		39.952	14.999	39.672	15.366	31.983	12.142
Bu_4NCl (A = 0.05)		Pr_4NBr (A = 0.05)		Pr_4NI (A = 0.09)		i-Am_3BuNI (A = 0.10)	
2.338	19.167	5.844	19.976	5.259	21.004	2.907	20.402
7.141	17.433	12.246	17.926	10.255	18.914	6.442	18.368
12.025	16.334	17.928	16.738	17.035	17.139	9.724	17.120
16.953	15.526	24.713	15.696	24.587	15.803	14.616	15.788
22.932	14.772	31.259	14.921	30.529	15.012	19.499	14.812
31.391	13.944	37.775	14.297	36.624	14.350	24.836	13.982
40.306	13.275	45.381	13.692	43.462	13.734	30.197	13.313
44.879	12.991	54.150	13.119	50.529	13.199	35.516	12.763
Me_4NBr (A = 0.05)		Bu_4NBr (A = 0.07)		Bu_4NI (A = 0.09)		Bu_4NClO_4 (A = 0.07)	
1.991	23.295	4.253	19.406	4.550	20.028	3.848	21.151
5.003	20.755	9.014	17.652	9.492	17.894	8.979	18.028
7.637	19.312	13.910	16.463	14.109	16.596	14.748	16.034
10.382	18.189	18.885	15.565	18.790	15.619	20.649	14.665
13.422	17.218	23.939	14.846	24.055	14.762	26.794	13.618
17.774	16.134	29.506	14.203	29.984	13.998	33.609	12.737
22.015	15.311	34.926	13.680	36.303	13.337	40.770	12.003
27.390	14.500	41.946	13.113	43.119	12.750	50.361	11.227

were carried out in Kraus type conductance cells[16] and the precision, speed, and convenience of the measurements were all enhanced by the use of the Hawes–Kay cup-dropping device.[17] The use of this device generally allows several complete conductance runs to be carried out in 1 day by one worker.

The cells, which had cell constants of approximately 0.8, were calibrated with reagent grade potassium chloride.[16,18] The usual small frequency correction was applied to a resistance measurement. The temperature of the conductance bath was controlled to ±0.005° and was set at 25° with a calibrated platinum resistance thermometer.

Results

The measured equivalent conductances and the corresponding electrolyte concentrations in moles per liter are shown in Table I for ethanol and Table II for 1-propanol. Also given is A, the density increment used to calculate the volume concentration. These increments were obtained by density measurements on the most concentrated solutions used in the conductance measurements and were assumed to follow the relationship $d = d_0 + A\bar{m}$, where $\bar{m}$ represents the moles of salt per kilogram of solution.

The data were analyzed with the Fuoss–Onsager equation in the form[19]

$$\Lambda = \Lambda_0 - S(c\gamma)^{1/2} + Ec\gamma \ln (c\gamma) + (J - B\Lambda_0)c\gamma - K_a f^2 c\gamma\Lambda \quad (1)$$

The value of B, which corrects for the effect of the added electrolyte on the viscosity of the solvent, was set equal to zero. The value of B does not affect the limiting conductance or the association constant. In all nonaqueous solvents, where the B correction has been determined, the value of $\mathring{a}$ was increased by the constant amount of 0.2 ångstroms for all of the tetraalkylammonium halides.

Shown in Table III are the parameters obtained from the Fuoss–Onsager equation by a least-squares computer program. Included are the standard deviations

(15) C. G. Swain and D. F. Evans, *J. Amer. Chem. Soc.*, **88**, 383 (1966).

(16) H. M. Daggett, E. J. Blair, and C. A. Kraus, *ibid.*, **73**, 799 (1951).

(17) J. L. Hawes and R. L. Kay, *J. Phys. Chem.*, **69**, 2420 (1965).

(18) J. E. Lind, J. J. Zwolenik, and R. M. Fuoss, *J. Amer. Chem. Soc.*, **81**, 1557 (1959).

(19) R. M. Fuoss and F. Accascina, "Electrolytic Conductance," Interscience Publishers, New York, N. Y., 1959.

Table III: Conductance Parameters in Ethanol and Propanol at 25°

Salt	Λ_0	d, Å	K_a	$\sigma\Lambda$
		EtOH		
Me_4NCl	51.67 ± 0.07	4.2 ± 0.2	122 ± 4	0.05
Bu_4NCl	41.54 ± 0.05	4.4 ± 0.3	39 ± 5	0.04
Me_4NBr	53.56 ± 0.09	4.1 ± 0.3	146 ± 6	0.03
Et_4NBr	53.15 ± 0.03	4.5 ± 0.1	99 ± 2	0.02
Pr_4NBr	46.86 ± 0.03	4.3 ± 0.1	78 ± 3	0.02
Bu_4NBr	43.51 ± 0.05	4.3 ± 0.2	75 ± 4	0.03
Et_4NI	56.34 ± 0.03	4.6 ± 0.1	133 ± 2	0.02
Pr_4NI	49.94 ± 0.04	4.1 ± 0.1	120 ± 2	0.02
Bu_4NI	46.65 ± 0.04	4.0 ± 0.1	123 ± 3	0.02
i-Am_3BuNI	45.31 ± 0.02	4.0 ± 0.1	130 ± 2	0.01
He_4NI	41.93 ± 0.02	4.3 ± 0.1	139 ± 3	0.01
		PrOH		
Me_4NCl	25.05 ± 0.02	4.2 ± 0.1	456 ± 3	0.01
Bu_4NCl	21.16 ± 0.03	4.4 ± 0.1	149 ± 5	0.02
Me_4NBr	26.91 ± 0.02	6.4 ± 0.2	638 ± 5	0.01
Et_4NBr	27.19 ± 0.02	5.0 ± 0.1	373 ± 4	0.01
Pr_4NBr	24.42 ± 0.05	4.4 ± 0.1	270 ± 7	0.02
Bu_4NBr	22.92 ± 0.03	4.6 ± 0.1	266 ± 6	0.01
Et_4NI	29.01 ± 0.05	5.5 ± 0.2	466 ± 8	0.02
Pr_4NI	26.08 ± 0.05	4.5 ± 0.1	391 ± 7	0.02
Bu_4NI	24.60 ± 0.04	4.7 ± 0.1	415 ± 6	0.01
i-Am_3BuNI	24.02 ± 0.03	4.9 ± 0.2	462 ± 6	0.01
He_4NI	22.18 ± 0.03	4.8 ± 0.2	442 ± 6	0.01
Bu_4NClO_4	27.13 ± 0.03	4.2 ± 0.1	769 ± 6	0.01

in each parameter and the standard deviation, $\sigma\Lambda$, of the individual points.

Discussion

Limiting Ionic Conductance. Some indication of the internal consistency of the data (Table III) can be obtained from the values of $\Lambda_0(R_4NI) - \Lambda_0(R_4NBr)$ and $\Lambda_0(R_4NBr) - \Lambda_0(R_4NCl)$ for the Me_4N^+, Et_4N^+, Pr_4N^+, and Bu_4N^+ salts. The iodide–bromide differences are 3.14 ± 0.04 and 1.70 ± 0.06 in ethanol and propanol, respectively, while the analogous bromide–chloride differences are 2.01 ± 0.03 and 1.81 ± 0.05.

Meaningful comparison of our results with those of other workers can be made only where the data in the literature are of a high enough precision and over a wide enough concentration range to be analyzed by modern theories. Such data have been analyzed by eq 1 and the resulting conductance parameters published elsewhere.[20] Hartley, *et al.*, investigated the tetramethylammonium and tetraethylammonium halides in ethanol and from their data the following values of limiting conductances in ethanol have been calculated: $\Lambda_0(Me_4NCl)$ = 51.87 ± 0.04, $\Lambda_0(Me_4NBr)$ = 54.03 ± 0.02, $\Lambda_0(Et_4NBr)$ = 53.54 ± 0.03, and $\Lambda_0(Et_4NI)$ = 56.5 ± 0.6. A similar analysis of the Whorton and Amis data from their studies of the corresponding picrates furnished the following values for Λ_0: $\Lambda_0(Me_4NPi)$ = 55.03 ± 0.05 and $\Lambda_0(Et_4NPi)$ = 54.2 ± 0.1.

The single-ion conductances, λ_0, in ethanol given in Table IV were obtained from the Λ_0 values in Table III and Gordon's limiting chloride conductance, $\lambda_0(Cl^-)$ = 21.87, by use of the following procedure. From $\Lambda_0(Me_4NCl)$ and $\Lambda_0(Bu_4NCl)$ the values of $\Lambda_0(Me_4N^+)$ and $\Lambda_0(Bu_4N^+)$ were obtained; these latter results together with $\Lambda_0(Bu_4NBr)$ and $\Lambda_0(Me_4NBr)$ gave an average value of $\lambda_0(Br^-)$ = 23.88 ± 0.03, which, when combined with $\Lambda_0(Et_4NBr)$ and $\Lambda_0(Pr_4NBr)$, gave values for $\lambda_0(Et_4N^+)$ and $\lambda_0(Pr_4N^+)$. Having $\lambda_0(Et_4N^+)$, $\lambda_0(Pr_4N^+)$, and $\lambda_0(Bu_4N^+)$, an average value of $\lambda_0(I^-)$ = 27.00 ± 0.04 was obtained by subtraction from the Λ_0 values for the corresponding iodides in Table III. It should be noted that the ethanol values given in Table IV differ from the previously tabulated values[21] by as much as 3% in extreme cases. However, owing to the internal consistency of our data and the absence of such consistency in the previously published data, our results should be given considerably more weight.

Table IV: Values for Limiting Single-Ion Conductances

Ion	λ_0 In EtOH	λ_0 In PrOH
Me_4N^+	29.65	14.40
Et_4N^+	29.27	15.05
Pr_4N^+	22.98	12.19
Bu_4N^+	19.67	10.71
i-Am_3BuN^+	18.31	10.17
$Hept_4N^+$	14.93	8.29
Cl^-	(21.87)	10.45
Br^-	23.88	12.22
I^-	27.00	13.81
ClO_4^-		16.42

Gover and Sears studied the tetramethylammonium and tetrapropylammonium halides in 1-propanol. The Λ_0 values obtained from a recalculation by the Fuoss–Onsager equation agree with those given in Table III in the case of the bromides, but there is a discrepancy of 1 to 2% for the iodides. Because of the high density of the propanol used by Gover and Sears, ρ = 0.8008 as compared with a density of ρ = 0.7996 reported here, and because of the internal consistency of our data, we believe that our values are to be preferred.

The Λ_0 values in propanol given in Table III cannot be unambiguously split into single-ion conductances because of the lack of the necessary transference numbers. As a tentative approach to this problem, the

(20) See ref 2 for conductance parameters recalculated by the Fuoss–Onsager equation from data of Hartley, *et al.*, Whorton and Amis, and Gover and Sears.

(21) R. L. Kay and D. F. Evans, *J. Phys. Chem.*, **70**, 2325 (1966).

limiting ionic conductances for the ions i-Am_3BuN^+ and $Hept_4N^+$ in ethanol were calculated from the corresponding values in methanol[22] using the appropriate Walden product ratio. The resulting ethanol figures agreed with those given in Table IV to within 0.5–1.5%. This suggested that the same procedure could be used to obtain values for the limiting ionic conductances in propanol. The propanol values given in Table IV were calculated from the ratio of the viscosities in ethanol and propanol and the limiting ionic conductances for i-Am_3BuN^+ and $Hept_4N^+$ ions in ethanol (see Table IV). An average value for $\lambda_0(I^-)$ of 13.87 ± 0.08 in propanol was obtained and used to calculate the other limiting ionic conductances in propanol shown in Table IV.

A further discussion of the variation of the limiting ionic conductance–viscosity product with solvent will not be presented here, because similar data from butanol and pentanol will permit a more detailed discussion.

Ion-Size Parameter. The Fuoss–Onsager ion-size parameter $\hat{a}$ was found to be constant for all of the salts investigated and equal to 4.2 ± 0.2 Å for ethanol and 5.0 ± 0.5 Å for propanol. A slightly smaller but constant value of $\hat{a}$ = 3.5 ± 0.2 Å has been obtained for the same salts in methanol, acetonitrile, and nitromethane,[2,14,23] suggesting a small but real dependence of $\hat{a}$ on dielectric constant.

The data shown in Tables I and II were also analyzed by the Fuoss–Hsia equation.[24] In this equation, the terms in $c^{3/2}$ have been explicitly integrated and retained. This results in a complex expression which is most conveniently evaluated with the aid of a computer. The following examples are typical of the parameters resulting from this analysis: for Me_4NBr in propanol, Λ_0 = 26.90 ± 0.01, $\hat{a}$ = 4.4 ± 0.1 Å, and K_a = 626 ± 4; for Bu_4NI in propanol, Λ_0 = 24.67 ± 0.02, $\hat{a}$ = 3.7 ± 0.1 Å and K_a = 423 ± 4. Comparison of all the results obtained from the Fuoss–Hsia equation with those in Table III showed that the two sets of parameters were almost identical within the least-squares-determined precision of the parameters. The one exception was the $\hat{a}$ parameter, which was found to be equal to 3.9 ± 0.3 Å in both solvents. This result confirms the observation by Fuoss and Hsia that this new equation gives $\hat{a}$ parameters which are more independent of dielectric constants. However, the fact remains that the value of $\hat{a}$ obtained in the alcohols from either analysis is unrealistically small and does not follow the trend in ionic crystallographic sizes.

Ionic Association. Inspection of Table III shows that the pattern of ionic association in ethanol and propanol solutions does not exhibit the simple dependence upon ionic size predicted by electrostatic theory. This can be seen more clearly in Figure 1, where log K_A for salts in propanol is plotted against the reciprocal of the sum of the estimated crystallographic radii. The discussion given below is equally applicable to ethanol;

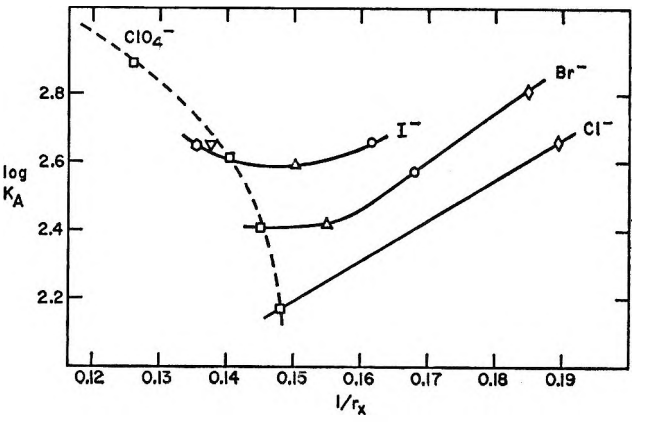

Figure 1. Association constants for the tetraalkylammonium halides and perchlorates as a function of ionic size in propanol: ◇, Me_4N^+; ○, Et_4N; △, Pr_4N; □, Bu_4N; ▽, i-Am_3BuN^+; ○, n-$Hept_4N^+$.

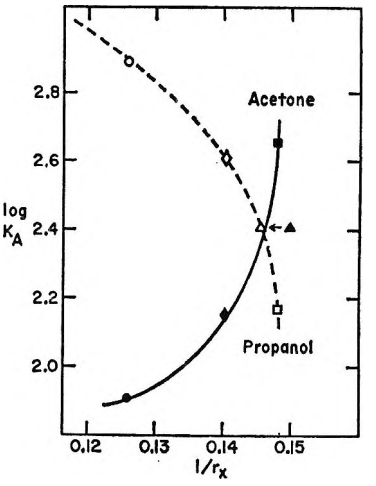

Figure 2. Association constants for tetrabutylammonium salts in the isodielectric solvents acetone and propanol: □, Cl; △, Br; ◇, I; ○, ClO_4.

however, the values of K_A are smaller and hence subject to more uncertainty.[8] Each solid line in Figure 1 connects the points of salts of a common anion. The association constants for the chlorides and bromides change in the manner predicted by the relative size of the cations, while K_A for the iodides appears to be almost constant. The most interesting feature is the fact that the association constant increases with increasing size of the anion. This is illustrated most vividly in Figure 1, where the points for K_A for the tetrabutylammonium salts in propanol are connected by the dashed curve. The association constant for the

(22) The conductance parameters for $(n\text{-}C_7H_{15})_4NI$ in MeOH at 25° are Λ_0 = 92.08 ± 0.08, a = 4.1 ± 0.6 Å, and K_A = 20 ± 3.

(23) R. L. Kay, S. L. Blum, and H. I. Schiff, *J. Phys. Chem.*, 67, 1223 (1963).

(24) R. M. Fuoss and K.-L. Hsia, *Proc. Nat. Acad. Sci.*, 57, 1550 (1967). We would like to thank Professor Fuoss for a copy of the computer program.

perchlorate is greater than that for the chloride by a factor of 5. This is the type of behavior that would be predicted if solvation were the predominant factor in controlling the extent of ion pairing. The observed peculiarities can be accounted for by the assumption that solvation of the anion increases in the order $Cl > Br > I > ClO_4$ and that solvation of the cations is relatively independent of size. It should be noted that in the cases where solvation is the predominant factor the extent of ion pairing will always be diminished. The value of K_A obtained in such a situation will be less than that which would be obtained in the absence of solvation.

Shown in Figure 2 are the association constants for tetrabutylammonium salts in propanol as compared with those in acetone.[25] The dielectric constant for acetone is 20.47 at 25°. Thus acetone and propanol are isodielectric.[26] In contrast to propanol, acetone is a normal solvent, in the sense that the association constants for electrolytes increase with decreasing ionic size. As the size of cation and anion increases, it is reasonable to anticipate that specific interaction with the solvent will become less important and that the ionic association should be only a function of the dielectric constant. Therefore, as $1/r_x$ approaches zero, the association constants for salts in isodielectric solvents should approach one another asymptotically. As can be seen in Figure 2, the lines diverge as $1/r_x$ becomes small, so that the association constant for the Bu_4ClO_4 in propanol is greater than that in acetone by one order of magnitude. This would seem to rule out simple solvation as the major factor controlling ionic association in propanol. The alcohols appear to constitute a separate class of solvents, distinct in behavior from many other nonaqueous solvents but similar in some respects to water. The implications of this will be discussed in forthcoming papers.

Acknowledgment. This work was supported by Contract No. 14-01-0001-1281 with the Office of Saline Water, U. S. Department of the Interior.

(25) M. B. Reynolds and C. A. Kraus, *J. Amer. Chem. Soc.*, **70**, 1709 (1948); M. J. McDowell and C. A. Kraus, *ibid.*, **73**, 3293 (1951).

(26) In their study of isodielectric solvents, J. T. Denison and J. B. Ramsey, *J. Amer. Chem. Soc.*, **77**, 2615 (1955), found that K_A was smaller by a factor of 7–10 for a number of electrolytes in ethylene chloride (ϵ_{25} 10.23) than in ethylidene chloride (ϵ_{25} 10.00). They attributed this decrease in K_A to preferential solvation of the ions by the more polar *gauche* form of ethylene chloride and were able to obtain agreement between the experimental and calculated values of K_A by assuming an effective dielectric constant of 11.8. Although this points out the shortcomings of using a bulk property of a liquid in interpreting short-range interactions, it should be noted that no such adjustment of ϵ will account for the opposite trends in K_A in propanol and acetone.

Transient Convective Diffusion in Capillaries

by Allen R. Overman

Agronomy Department, University of Illinois, Urbana, Illinois *(Received April 8, 1968)*

A transient solution has been obtained of the one-dimensional continuity equation for convective diffusion in a capillary. The resulting equation has been compared with data in the literature for the system D_2O–H_2O, and an agreement of 2% was found in the transient domain for a Peclet number of 3.88. A simple physical concept of solute transport in this system accrues from the analysis.

In a recent paper a simplified treatment of convective diffusion in capillaries was presented.[1] An expression for solute distribution within the capillary was obtained as a function of the Peclet number and the boundary conditions for the steady state. The expression for the average solute concentration was used to test the theory for the system D_2O–H_2O at a Peclet number of 3.88 and an agreement of 2% was found. This paper presents an extension of the analysis to the transient state.

Theory

First consider the continuity equation for convective diffusion (*cf.* Taylor[2])

$$D\left[\frac{\partial^2 C}{\partial X^2} + \frac{1}{r}\frac{\partial}{\partial r}\left(r\frac{\partial C}{\partial r}\right)\right] - V_0\left[1 - \frac{r^2}{a^2}\right]\frac{\partial C}{\partial X} - \frac{\partial C}{\partial t} = 0 \quad (1)$$

where C is the solute concentration; r, X, and t are the

Table I: Transient Behavior of Average Concentration

	t, days							
	0	1	2	4	6	10	14	16
$(\bar{C} - C_l)/(C_0 - C_l)$ (theory)	1.000	0.867	0.832	0.797	0.781	0.768	0.765	0.764
$(\bar{C} - C_l)/(C_0 - C_l)$ (exptl)	1.000	0.885	0.848	0.789	0.780	0.766	0.775	0.771
% error	...	2.03	1.89	−1.01	−0.13	−0.26	1.29	0.91

radial, longitudinal, and time variables, respectively; a is the radius of the capillary; D is the molecular diffusion coefficient; and V_0 is the streaming velocity at the center of the tube. At this point two approximations are made: the radial variation in C is neglected and the coefficient of $\partial C/\partial X$ is replaced by the average velocity, $\bar{V}$, in the tube. The approximate continuity equation is

$$\frac{\partial^2 C}{\partial X^2} - \frac{\bar{V}}{D}\frac{\partial C}{\partial X} - \frac{1}{D}\frac{\partial C}{\partial t} = 0 \qquad (2)$$

for the domain $0 < X < l$, where l is the length of the capillary. The concentration $C(X, t)$ is subject to the initial and boundary conditions $C(X, 0) = C_0$, $C(0, t) = C_0$, and $C(l, t) = C_l$. In the sequel $\bar{V}$ and D are treated as constants.

Equation 2 is most easily solved by the method of Laplace transforms.[3] For further examples on the solution of boundary-value problems by this technique, the reader is referred to a standard treatise on heat transfer.[4] The format is as follows. Transform the partial differential equation and boundary conditions. Integrate the resulting total differential equation and evaluate the two arbitrary constants. Obtain the inverse transform through the inversion integral by the use of the residue theory. The result is

$$\frac{C - C_l}{C_0 - C_l} = 1 - \frac{e^{\theta X/l} - 1}{e^{\theta} - 1} - 2e^{-\frac{\theta}{2}\left(1-\frac{X}{l}\right)} \sum_{n=1}^{\infty} \times \frac{n\pi \cos n\pi}{\frac{\theta^2}{4} + n^2\pi^2} e^{-\left(\frac{\theta^2}{4}+n^2\pi^2\right)\frac{Dt}{l^2}} \sin n\pi \frac{X}{l} \qquad (3)$$

where $\theta = l\bar{V}/D$ is the Peclet number. For $\theta = 0$, eq 3 reduces to the solution given for the diffusive system.[4] In the limit of $t \to \infty$, eq 3 reduces to the steady-state component

$$\frac{C - C_l}{C_0 - C_l} = 1 - \frac{e^{\theta X/l} - 1}{e^{\theta} - 1} \qquad (4)$$

as obtained and shown graphically in the previous paper.[1] An expression for the average concentration follows

$$\frac{\bar{C} - C_l}{C_0 - C_l} = \frac{1}{l}\int_0^l \frac{C - C_l}{C_0 - C_l} dX = \frac{1}{2}\left[1 + \zeta\left(\frac{\theta}{2}\right)\right] + 2\sum_{n=1}^{\infty}\left(\frac{n\pi}{\frac{\theta^2}{4} + n^2\pi^2}\right)^2\left(1 - e^{-\frac{\theta}{2}}\cos n\pi\right)e^{-\left(\frac{\theta^2}{4}+n^2\pi^2\right)\frac{Dt}{l^2}} \qquad (5)$$

where $\zeta(Z) \equiv (\coth Z) - Z^{-1}$ is the Langevin function. Again in the limit of $t \to \infty$, the steady-state result

$$\frac{\bar{C} - C_l}{C_0 - C_l} = \frac{1}{2}\left[1 + \zeta\left(\frac{\theta}{2}\right)\right] \qquad (6)$$

obtains as before, which also was shown graphically.[1]

Analysis

Data already reported[1] were compared with eq 5. In that experiment, $\theta = 3.88$, $C_0 = 4.00\%$ D_2O, $C_l \approx 0.00\%$, $D = 2.37$ cm²/day, and $l = 10$ cm. The results are shown in tabular and graphical form below. The transient curve for diffusion ($\theta = 0$) has been included for comparison. Per cent difference between calculated and observed $(\bar{C} - C_l)/(C_0 - C_l)$ is within 2% for all time values measured. (See Table I and Figure 1.)

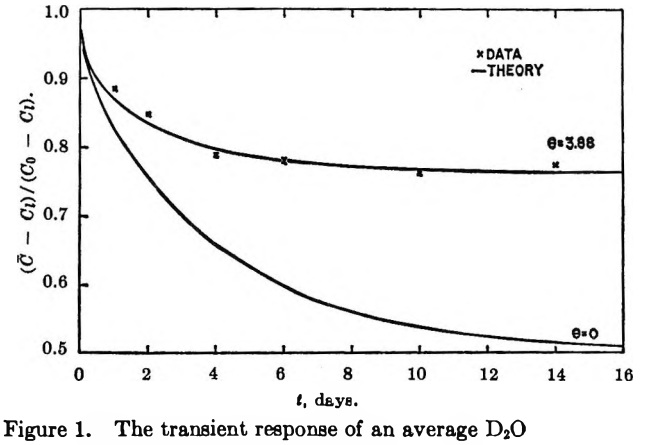

Figure 1. The transient response of an average D_2O concentration in a capillary: ×, data; ——, theory.

(1) A. R. Overman and R. J. Miller, *J. Phys. Chem.*, **72**, 155 (1968).
(2) G. I. Taylor, *Proc. Roy. Soc.*, A219, 186 (1953).
(3) E. J. Scott, "Transform Calculus with an Introduction to Complex Variables," Harper and Row, New York, N. Y., 1955.
(4) H. S. Carslaw and J. C. Jaegar, "Conduction of Heat in Solids," 2nd ed, Oxford University Press, London, 1959.

Conclusions

When eq 5 was derived, the radial term of eq 1 was neglected and the Poiseuille velocity distribution was replaced by the average streaming velocity. These two assumptions seem to be related, in that for low Peclet numbers and $a/l \ll 1$ the radial concentration profiles are essentially flat in the transient domain $t > 1$ day. It is the author's intention to show this by a more exact solution of eq 1 in which the radial component is retained. In systems of the type considered here, a steady state is reached in which the net transport of solute is composed of the simple sum of that by diffusion and by convection along the longitudinal axis, *i.e.*, diffusion occurs relative to a moving frame of reference. This simplifies the mathematical analysis.

For very high Peclet numbers, the system may be treated by neglecting $\partial^2 C/\partial X^2$ as has been done by Taylor[2] and by Aris.[5] No attempt has been made in the present work to determine the range of applicability of eq 5.

At present the work is being extended to porous systems in an effort to obtain a better description of convective diffusion in membrane systems. This should provide a better understanding of the flow processes through soils as well as through artificial and biological membranes.

Acknowledgment. The work upon which this publication is based was supported in part by funds provided by the United States Department of Interior as authorized under the Water Resources Act of 1964, Public Law 88-379.

(5) R. Aris, *Proc. Roy. Soc.*, **A235**, 67 (1956).

Solubility and Complex Formation Equilibria of Silver Chloride in Anhydrous Dimethylformamide

by James N. Butler

Tyco Laboratories, Inc., Waltham, Massachusetts 02154 *(Received April 25, 1968)*

The equilibria of silver chloride in dimethylformamide solutions containing excess chloride have been studied potentiometrically in a constant ionic medium (0.1 *M* tetraethylammonium perchlorate) at 25°. Equilibrium constants were fitted by a nonlinear least-squares pit-mapping technique. Only mononuclear complexes AgCl and $AgCl_2^-$ were found. The over-all formation constants for these complexes are: $\log \beta_1 = 12.11 \pm 0.085$ and $\log \beta_2 = 16.295 \pm 0.015$. The complex $AgCl_3^{2-}$ is negligible under the conditions of these experiments, and $\log \beta_3$ is less than 17.7. The solubility product of silver chloride is $\log K_{s0} = 14.49 \pm 0.01$ (errors are standard deviations). Estimates of the constants at zero ionic strength are made, and the results are discussed in terms of ionic solvation.

Introduction

Dimethylformamide (DMF) is a solvent of considerable interest for studies of electrochemical reactions and coordination chemistry. The silver–silver chloride reference electrode is in common use, and the solubility and complex-formation equilibria of silver chloride are important both for an understanding of this reference electrode and for their relevance to solvation phenomena in this solvent.

Previous publications from this laboratory[1,2] have reported detailed studies of the equilibria of silver chloride in propylene carbonate. This paper presents the results of a brief potentiometric study in dimethylformamide. While this work was in progress, results on the same system were published by Alexander, Ko, Mac, and Parker,[3] but their experiments were preliminary in character, not all the equilibrium constants were evaluated, and no statistical limits of error were established for the constants they reported.

By analogy with water and propylene carbonate,[1,2] the following equilibria are expected

$$AgCl(s) \rightleftharpoons Ag^+ + Cl^- \quad (K_{s0})$$

(1) J. N. Butler, *Anal. Chem.*, **39**, 1799 (1967).

(2) J. N. Butler, D. R. Cogley, and W. Zurosky, *J. Electrochem. Soc.*, **115**, 445 (1968).

(3) R. Alexander, E. C. F. Ko, Y. C. Mac, and A. J. Parker, *J. Amer. Chem. Soc.*, 89, 3703 (1967).

$$Ag^+ + Cl^- \rightleftharpoons AgCl(soln) \quad (\beta_1)$$

$$Ag^+ + 2Cl^- \rightleftharpoons AgCl_2^- \quad (\beta_2)$$

$$Ag^+ + 3Cl^- \rightleftharpoons AgCl_3^{2-} \quad (\beta_3)$$

(The IUPAC notation for equilibrium constants[4] is used.) These equilibria have been verified by our experiments, and the complex $AgCl_3^{2-}$ has been shown to be negligible.

Experimental Section

The method was the same as described previously.[1] The potential of a concentration cell consisting of two silver electrodes separated by a salt bridge was measured with a high-impedance differential voltmeter. The reference compartment contained 0.1 *M* Et_4NCl saturated with AgCl, the salt bridge contained 0.1 *M* Et_4NClO_4, and the titration compartment contained 0.1 *M* Et_4NClO_4, to which additions of 0.1 *M* Et_4NCl and 0.1 *M* $AgClO_4$ were made from micrometer burets.

DMF (Fisher Certified) was dried with a 5A molecular sieve and contained less than 0.005% water and less than 0.003% volatile organic impurities, as analyzed by gas chromatography. The solutions of Et_4NCl and Et_4NClO_4 (Eastman, dried over $CaSO_4$) also contained less than 0.005% water, but the $AgClO_4$ solution (Chemical Procurement) contained 0.016% water.

Solutions of $AgClO_4$ in DMF were colorless and clear when first prepared, but within 7 days they became crimson and turbid, even though they were not exposed to light for more than about 1 hr during that period. The AgCl precipitate also was white when first formed but turned brownish over the course of 1 day.

In freshly prepared solutions, the silver–silver ion electrode in 0.1 *M* Et_4NClO_4 obeyed the Nernst equation to within ±0.2 mV in the unsaturated region and to within ±1 mV in the saturated region and in the region where excess silver ion was present. To minimize possible decomposition of the reference electrode solution, we used a silver chloride-saturated chloride solution for the reference electrode. The potential of this electrode is approximately 0.4 V more negative than the fixed concentration of $AgClO_4$ which we used in our previous work.

Solution preparation, storage, and all experiments were carried out in a dry-nitrogen atmosphere in a glove box. The cell was jacketed, and (except for one preliminary experiment) the temperature was maintained at 25.0 ± 0.05° by means of a Haake circulating thermostat.

Results

Typical titration curves are shown in Figure 1. Table I lists the detailed numerical data for the portion of the titration curve before the end point in four titrations which we considered to be accurate and on which the calculations were performed. Although the concentrations are given to four decimal places, this is merely a computational convenience to avoid round-off errors and does not reflect the true accuracy of the concentration values, which is approximately ±0.01 m*M*. As can be seen from Figure 1, the saturation limit is clearly defined by a discontinuity in slope, and the points in Table I are labeled "saturated" or "unsaturated," according to whether they fell above or below the saturation limit. The potentiometrically determined saturation limit was verified by visual observation of precipitate formation in the titration cell.

Table I: Titration Data[a]

C_{Ag}	C_{Cl}	E
Set No. 1[b] (T = 25.0°, E^0 = 0.6585 V)		
Unsatd		
0.0574	4.8273	−0.1819
0.1721	4.8227	−0.1750
0.2866	4.8181	−0.1685
0.5718	4.8067	−0.1600
1.1382	4.7840	−0.1406
1.6993	4.7615	−0.1204
2.2551	4.7392	−0.0269
Satd		
2.5310	4.7282	0.0639
2.8057	4.7171	0.0701
3.3513	4.6953	0.0800
3.8918	4.6736	0.0942
4.1601	4.6629	0.1050
4.2672	4.6586	0.1119
4.3206	4.6564	0.1162
4.4273	4.6522	0.1277
4.5338	4.6479	0.1469
Set No. 3[d] (T = 25.0°, E^0 = 0.6265 V)		
Unsatd		
0.0517	1.2944	−0.2543
0.2581	1.2922	−0.1781
0.5152	1.2894	−0.1202
Satd		
0.7200	1.2872	0.0542
0.8222	1.2861	0.0660
0.9242	1.2850	0.0743
1.0260	1.2840	0.0843
1.1276	1.2829	0.0963
1.2291	1.2818	0.1306

C_{Ag}	C_{Cl}	E
Set No. 2[c] (T = 25.0°, E^0 = 0.585 V)		
Unsatd		
0.0598	0.6918	−0.1616
0.1196	0.6915	−0.1530
0.1793	0.6911	−0.1325
0.2389	0.6908	−0.0900
Satd		
0.2985	0.6904	0.0330
0.3580	0.6901	0.0400
0.4175	0.6898	0.0450
0.4769	0.6894	0.0533
0.5362	0.6891	0.0617
0.5955	0.6887	0.0716
0.6548	0.6884	0.0965
0.6844	0.6882	0.1502
Set No. 4[e] (T = 25.0°, E^0 = 0.637 V)		
Unsatd		
0.0001	1.5369	−0.1616
0.0586	1.5362	−0.1614
0.2924	1.5332	−0.1437
0.5833	1.5294	−0.1040
Satd		
0.8729	1.5257	0.0829
1.0171	1.5238	0.0924
1.1610	1.5220	0.1024
1.2184	1.5212	0.1079
1.2758	1.5205	0.1150
1.3332	1.5197	0.1217
1.3905	1.5190	0.1319
1.4477	1.5182	0.1506
1.5049	1.5175	0.2010

[a] The approximate precision of C_{Ag} and C_{Cl} is 0.01 m*M*. *E* is in volts and concentrations are millimolar. [b] The residual AgCl is 1.2 m*M*. [c] The residual AgCl is 0.37 m*M*. [d] The residual AgCl is 0.075 m*M*. [e] The residual AgCl is 0.5 m*M*.

From the data for unsaturated solutions in Table I, we selected a single set of data to obtain the equilibrium constants for complex formation. The preliminary

(4) L. G. Sillen and A. E. Martell, "Stability Constants," Special Publication No. 17, The Chemical Society, London, 1964.

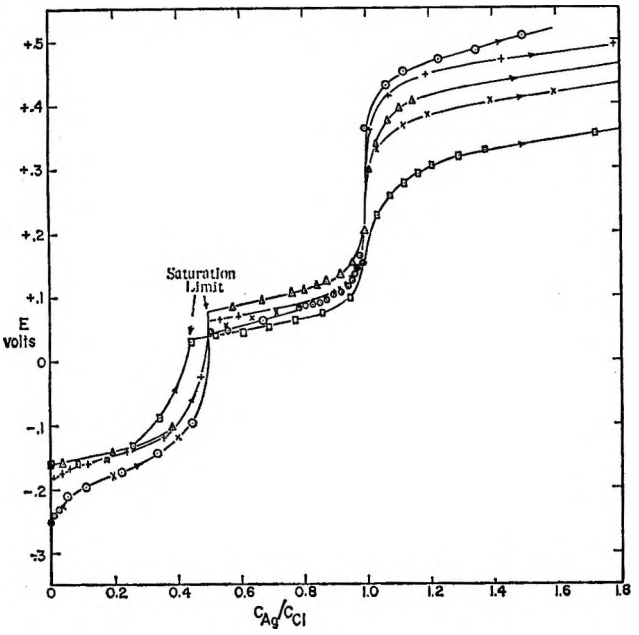

Figure 1. Potentiometric titration curves: ⊙, 30°, 0.005 *M*; +, 25°, 0.005 *M* (set 1); ⊡, 25°, 0.0005 *M* (set 2); △, 25°, 0.0013 *M* (set 3); ×, 25°, 0.0015 *M* (set 4). The concentration given is C_{Cl}. All titrations were carried out in 0.1 *M* Et_4NClO_4 supporting electrolyte.

measurements (at 29.8°) were discarded because the solutions appeared somewhat unstable. Set 1 showed small systematic deviations from the theoretical form of the titration curve which appeared to be due to excess AgCl (approximately 1.2 m*M*) being present in the titration cell before the titration was begun. Thus from set 1 we used only the unsaturated point of highest C_{Ag}/C_{Cl} ratio (point 7), and this was corrected for the estimated amount of AgCl present. We included points 2–4 from set 2 and points 1–3 of set 3. To each of these sets was also applied a small correction for residual AgCl: 0.37 m*M* for set 2 and 0.075 m*M* for set 3. These residual corrections were estimated from the potential at the beginning of the titration curve; if there were no residual AgCl, the potential at this point should be infinitely negative, and its value gives a sensitive measure of the traces of Ag^+ present in the solution. Set 4 was not included in this group of most reliable data because the solutions appeared slightly discolored.

The combined set of selected unsaturated data was used in our least-squares valley-search program[1] to obtain the optimum values of the equilibrium constants β_1, β_2, and β_3 for the formation of complexes with one, two, and three chloride ions, respectively, on silver. Figure 2 shows the map of the valley in β_2–β_3-space, with log β_1 fixed at 12.00. There is no pit as such; the value of β_2 is quite well defined in the region near 16.30, but the minimum value of U (defined by eq 8 in ref 1) is obtained with $\beta_3 = 0$. Cross sections in β_3-space and β_1-space show well-defined quadratic valleys, from which standard deviations can be calculated. The best values of the constants, with their standard deviations, are

$$\log \beta_1 = 12.11 \pm 0.085$$

$$\log \beta_2 = 16.295 \pm 0.015$$

To obtain 90% confidence limits, multiply these deviations by 2.

The cross section in β_3-space, using the optimum values for the other two constants, shows no minimum at all, but there is a clear upper bound for β_3. If we allow for a one-sided statistical error in a manner similar to that used to obtain the standard deviation, we may say (with 90% confidence) that

$$\log \beta_3 < 17.7$$

With somewhat less confidence, we may infer that β_3 is even smaller and that the complex $AgCl_3^{2-}$ is of negligible importance in DMF solutions. Here is the supporting evidence for this statement. The shape of the valley in Figure 2 is such that if an erroneous value is used for β_2 it is possible to obtain a cross section in β_3-space, which indicates a minimum at values of log $\beta_3 = 18$ or higher. This is a mathematical deception, however, because when the full map of the valley is available, it is seen that the minimum value of U lies at $\beta_3 = 0$. One might argue that this comes about because we used data with a relatively high C_{Ag}/C_{Cl} ratio, but Table I shows that we have included points ranging from $C_{Ag}/C_{Cl} = 0.58$–0.086 without *any* evidence of a minimum in β_3-space. This is a marked contrast to our experience with propylene carbonate,

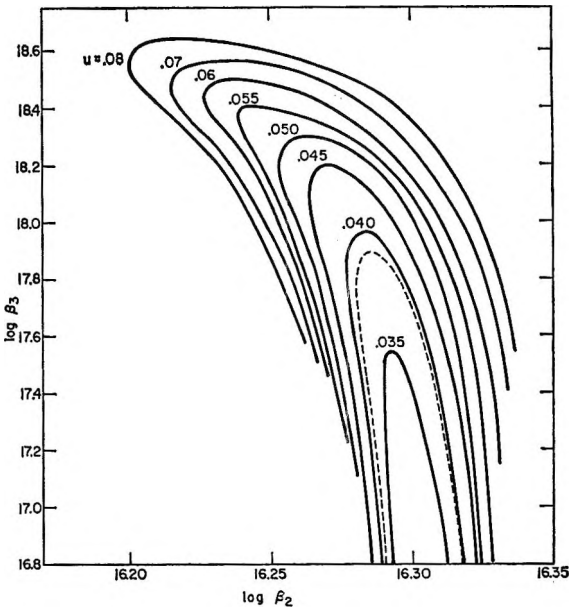

Figure 2. Map of the deviation function U (defined in ref 1) as a function of equilibrium constants β_2 and β_3: – – – –, standard-deviation contour (calculated with log β_1 = 12.00). Note that the minimum occurs at $\beta_3 = 0$.

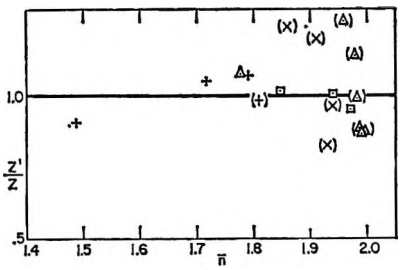

Figure 3. Deviation of experimental points from theoretical curve for unsaturated solutions: △, set 1; +, set 2; ⊡, set 3; ×, set 4. Calculated with $\log \beta_1 = 12.11$, $\log \beta_2 = 16.295$, and $\log \beta_3 = 17.5$. The functions Z and Z' are defined in ref 1. The observation that there is no trend among the various data sets indicates that the complexes are mononuclear.

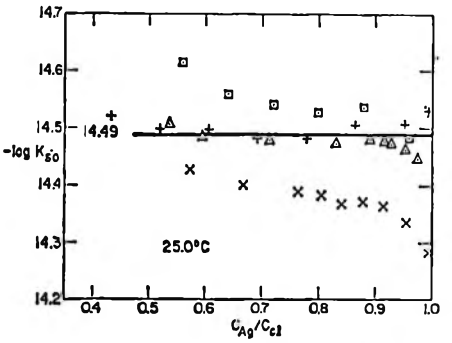

Figure 4. Solubility product values calculated from saturated points on titration curves. Symbols are the same as in Figure 3. Note that set 4 deviates from the others, which may reflect some decomposition of the solutions.

in which the complex $AgCl_3^{2-}$ is significant at C_{Ag}/C_{Cl} ratios as high as 0.4 or 0.5 and the minimum in β_3-space is well defined.[1]

Figure 3 shows the deviation Z'/Z (defined by eq 8–10 of ref 1) of the points from the theoretical curve. In addition to the points used to obtain the constants, we have also plotted the other points (in parentheses) from sets 1–4. Although they scatter more widely than the "best data," there is no systematic deviation which would indicate that we prejudiced our choice of best data. All the points are normally distributed about $Z'/Z = 1$, which lends further confidence to our least-squares procedure and to the constants derived by it. The fact that the assumed equilibria fit the experimental data with no obvious trend, even though C_{Ag} varies by a factor of 40, indicates that only mononuclear complexes are present.

In Figure 4 we have plotted the solubility-product values obtained by the previously described method[1] from all the saturated points of sets 1–4. The data of set 4 appear to be significantly lower than those of the other three sets, as well as exhibiting stronger systematic deviations. This is consistent with the fact that the solutions used in obtaining set 4 were discolored and may have partially decomposed. No systematic error in K_{s0} would result from the presence of AgCl in the solution at the beginning of the titration, since the equation from which K_{s0} is calculated[1] involves only the difference $C_{Ag} - C_{Cl}$ and not the concentrations themselves. Similarly, β_1 does not enter the expression for K_{s0} so errors in this constant are irrelevant for this purpose so long as they do not affect the value of β_2. The best value for the solubility product of AgCl in DMF is found to be

$$\log K_{s0} = -14.49 \pm 0.01$$

where the error is the standard deviation of the best estimate.

The data obtained at 29.8° are consistent with the above constants but show systematic deviations which cannot be explained on the basis of AgCl being present before the start of the titration. Although as much as 0.10 mM AgCl may have been present, the deviations probably resulted from a failure to equilibrate the reference electrode adequately in this early experiment or from decomposition of the solutions because of the higher temperature. The solubility product values also show strong systematic deviations, and two separate sets gave $\log K_{s0} = -14.55 \pm 0.05$ and -14.7 ± 0.1. Thus it does not seem to be profitable to estimate enthalpies and entropies of solvation in this system by measuring temperature coefficients of equilibrium constants at temperatures above room temperature, since decomposition appears to be a problem. It may be possible, however, to obtain accurate data below room temperature, since the freezing point of DMF is around −60°, if sufficient time is allowed for equilibrium to be established.

Discussion

Alexander, Ko, Mac, and Parker[3] obtained values for K_{s0} and β_2 from potentiometric titrations of 0.01 M Et_4NCl with 0.01 M $AgNO_3$ in DMF without supporting electrolyte. Thus the ionic strength varied over the course of the titration. Their cell was open to the atmosphere, but they reported no substantial differences when experiments were performed under dry nitrogen or in the dark. They did not report analyses of their solvent but dried it with 4A molecular sieves and fractionated it twice at reduced pressure under dry nitrogen, so that it probably contained less than 0.02% water. Their constants were $\log \beta_2 = 16.3$ and $\log K_{s0} = -14.5$, which agree remarkably well with our results.

From this excellent agreement, we may infer several conclusions: (1) water has little effect on the equilibrium constants for AgCl, (2) there is little ion pairing in the supporting electrolyte, (3) neither nitrate nor perchlorate form appreciable complexes with Ag^+, and (4) Et_4N^+ does not form appreciable complexes with either Cl^- or $AgCl_2^-$. Thus we may conclude that our constants are reasonably accurate approximations to the values which would be obtained in absolutely an-

hydrous DMF with an ideally noncomplexing supporting electrolyte.

If there is no ion pairing in these solutions, we may use the Debye–Hückel theory to calculate equilibrium constants at zero ionic strength. Using a dielectric constant of 36.71[5] and an ion-size parameter of 3 Å for all monovalent ions, we obtain at zero ionic strength

$$\log \beta_1^0 = 12.80 \pm 0.09$$

$$\log \beta_2^0 = 16.99 \pm 0.03$$

$$\log K^0_{s0} = -15.18 \pm 0.03$$

If ion pairing were important, we would obtain more positive values of $\log \beta_1^0$ and β_2^0 and a more negative value of $\log K^0_{s0}$.

It is of particular interest to examine two other equilibrium constants which may be obtained by combination of the above constants. The equilibrium constant K_{s1}, for the formation of AgCl complexes in solution from solid AgCl, is independent of electrostatic effects and reflects primarily the coordination of the solvent to the silver ion

$$\mathrm{AgCl(s)} \rightleftharpoons \mathrm{AgCl(soln)}$$

For this reaction

$$K_{s1} = K_{s0}\beta_1 = 10^{-2.38\pm0.09}$$

For water,[6,7] this constant is $10^{-6.6\pm0.1}$, and for propylene carbonate,[1] it is $10^{-4.7\pm0.2}$. Thus the coordination of DMF to the silver atom in the AgCl complex is considerably stronger than that of water or propylene carbonate.

The equilibrium constant $K_{s,2}$ for the formation of $AgCl_2^-$ from solid AgCl

$$\mathrm{Cl^-} + \mathrm{AgCl(s)} \rightleftharpoons \mathrm{AgCl_2^-}$$

is also simple to interpret. For this reaction

$$K_{s2} = K_{s0}\beta_2 = 10^{+1.80\pm0.02}$$

This constant reflects the difference in free energy between two monovalent ions. On the basis of size alone, one expects that K_{s2} should be slightly greater than unity, but hydrogen bonding of the solvent to Cl^- may cause it to become smaller, and coordination of the solvent to silver ion may cause it to become larger. Here again, we may compare with water[6,7] ($\log K_{s2} = -4.7 \pm 0.1$) where hydrogen bonding is strong and with propylene carbonate ($\log K_{s2} = 1.00 \pm 0.05$) where both hydrogen bonding with Cl^- and coordination to $AgCl_2^-$ are weak.

Within this framework, we may also examine the equilibrium constant K_{s2} for AgCl in other amides. The hydrogen bonding of the solvent to chloride decreases and the coordination of solvent to silver increases in the following order: formamide,[8] $\log K_{s2} = -2.1$; N-methylformamide,[8] $\log K_{s2} = -1.5$; dimethylformamide, $\log K_{s2} = 1.80 \pm 0.02$; dimethylacetamide,[3] $\log K_{s2} = 2.9$; hexamethylphosphorotriamide,[3] $\log K_{s2} = 4.6$. No information is available on K_{s2} in any of the other amide solvents.

These two equilibrium constants K_{s1} and K_{s2} are particularly useful for theoretical interpretation, because they are almost unaffected by either ionic strength or ion pairing with the supporting electrolyte. Thus even though substantial systematic error due to these sources may exist in K_{s0}, β_1, or β_2, these errors are almost entirely canceled in the combinations K_{s1} and K_{s2}.

One final point may be made concerning the very small value of β_3 that we have obtained, which reflects the low concentration of the complex $AgCl_3^{2-}$. In both water and propylene carbonate, this complex is of considerable importance, and its absence in DMF implies that the coordination sphere of silver is saturated when only two chloride ligands are bound. The other ligands must be solvent. This again reflects the stronger coordination of DMF to the silver ion as compared with other solvents. Nuclear magnetic resonance studies[9] have shown that dimethylformamide complexes with silver salts have a structure similar to those with Lewis acids or protonating acids, implying that coordination takes place through the carbonyl oxygen rather than through the nitrogen.[10]

Acknowledgments. The author thanks Mr. Walter Zurosky, Jr., for his assistance with the experimental work and Mr. David Cogley for assistance with the computer calculations. This research was supported by the Air Force Cambridge Research Laboratories, Office of Aerospace Research, under Contract No. 19(628)-6131 but does not necessarily constitute the opinion of that agency.

(5) G. R. Leader and J. F. Gormley, *J. Amer. Chem. Soc.*, **73**, 5731 (1951).

(6) I. Leden, *Svensk. Kem. Tidskr.*, **64**, 249 (1952).

(7) E. Berne and I. Leden, *ibid.*, **65**, 88 (1953).

(8) Yu. M. Povarov, V. E. Kazarinov, Yu. M. Kessler, and A. I. Gorbanev, *Zh. Neorg. Khim.*, **9**, 1008 (1964).

(9) S. J. Kuhn and J. S. McIntyre, *Can. J. Chem.*, **43**, 995 (1965).

(10) G. Fraenkel and C. Neimann *Proc. Nat. Acad. Sci. U. S.*, **44**, 688 (1958).

The Thermodynamics of the Vanadium Pentoxide (Solid or Liquid)–Water Vapor System

by L. N. Yannopoulos[1a]

U. S. Army Nuclear Defense Laboratory, Edgewood Arsenal, Maryland *(Received December 11, 1967)*

The reaction between V_2O_5(s or l) and H_2O(g) has been investigated between 639.0 and 899.0° by the vapor transfer method. The presence of a volatile vanadium hydroxide, $VO(OH)_3$(g), has been indirectly deduced from isothermal vapor pressure data. These data indicate the existence of the heterogeneous equilibrium, V_2O_5(s or l) + $3H_2O$(g) $\overset{O_2}{\rightleftarrows}$ $2VO(OH)_3$(g), if one vanadium atom is assumed in the gaseous molecule. The determined heat and entropy for the reaction of steam with liquid and solid vanadium pentoxide, within the experimental uncertainty, are 44.0 ± 0.5 kcal/mol and −1.03 ± 0.10 cal/mol deg, respectively.

Introduction

Experimental work on the formation and stability of several gaseous metallic hydroxide compounds at elevated temperatures has been reviewed and critically evaluated.[1b,2] It is of interest to note that experimental information on many of these gaseous compounds, especially when supplied by various experimental methods, may provide a basis for correlating the conditions and chemistry of their formation to their analogous existing gaseous oxyhalides. Glemser and Muller[3] present some vapor pressure data on the system V_2O_5(s)-H_2O(g) in an oxygen atmosphere between 500 and 650°. They report all of their data at a flow rate of 100 cc/min and conclude that the formation of the complex species $V_2O_3(OH)_4$(g) is the product. Neugebauer[4] also makes a brief reference to the increased volatility of liquid vanadium pentoxide in the presence of steam at 900°.

The transpiration study of Glemser and Muller[3] lacked flow rate data demonstrating equilibrium in the V_2O_5(s) + H_2O(g) reaction. Since there was also an absence of quantitative vapor pressure data on the V_2O_5(l)–H_2O(g) system, a study of the V_2O_5 (s or l)–H_2O(g) system was undertaken to ascertain the conditions of formation of any volatile vanadium hydroxides and to determine their thermodynamic properties.

Experimental Section

Quantitative vapor pressure data were obtained by the vapor transfer method. The experimental arrangement consisted of a 10-in. long quartz cell ($^1/_2$-in. bore tube) placed in the hot zone of a furnace. The cell contained a constriction in the thermal gradient zone to minimize thermal diffusion of the gases. Cell volume was minimized to 15 cc by the insertion of $^1/_4$-in. sealed quartz or Vycor tubes. Insertion and removal of the oxide sample, contained in a quartz boat, was facilitated by the use of a quartz taper joint close to the downstream end of the hot zone. The joint was tested to 900° for expansion and gas leakage and was found to function satisfactorily.

The temperature of the Kanthal wire-wound resistance furnace was monitored by a chromel–alumel (C/A) thermocouple positioned next to the reaction cell opposite the quartz sample boat and was controlled to within ±2° by an automatic controller–recorder and a dual powerstat relay-type arrangement. In addition, the temperature was periodically checked by a calibrated C/A thermocouple, positioned next to the control thermocouple, and a potentiometer. A plateau-shaped curve of temperature *vs.* position along the hot zone ensured the absence of any longitudinal thermal gradients.

Oxygen-enriched saturated steam, generated in a small glass vessel by bubbling oxygen through water, was introduced into the reaction cell *via* a $^1/_4$-in. Pyrex tube and Pyrex–quartz graded seal. The glass vessel and its contents were maintained at constant temperature by submerging the vessel in a constantly stirred glycerol bath thermostated to ±0.025°. The steam, passing over the sample in the hot zone, reacted with the solid or liquid vanadium pentoxide (Fisher certified reagent of 100.1% total assay) to form the gaseous product. The product, transported downstream to the cooler part of the $^1/_4$-in. exit tube, decomposed and condensed on the walls of the tube as the oxide, V_2O_5. The steam was then condensed in a 0° trap. The inlet and outlet tubes were maintained a few degrees above 100° by separate heating tapes (extending to the level of the glycerol at the inlet side) to prevent steam condensation. The carrier gas flow rate was checked

(1) (a) Address all correspondence to Westinghouse Electric Corporation, Research and Development Center, Pittsburgh, Pa., 15235; (b) O. Glemser and H. G. Wendlandt, *Advan. Inorg. Chem. Radiochem.*, 5, 215 (1963).

(2) S. A. Jordan, Ph.D. Thesis, University of Pennsylvania, 1965.

(3) O. Glemser and A. Muller, *Z. Anorg. Allg. Chem.*, 325, 220 (1963).

(4) J. Neugebauer, *Acta Chem. Hung.*, 37, 247 (1963).

intermittently at both the inlet and outlet of the cell by a pinchcock buret and continuously monitored by a calibrated flowrator tube at the inlet. The flow rate from the gas cylinder was controlled by a Nupro bellows metering valve.

The microgram quantities of vanadium pentoxide condensate were analyzed for vanadium by utilizing a colorimetric method based on the formation of phosphotungstovanadic acid complex.[5,6] The vanadium pentoxide deposit was clearly defined in the outlet tube and was removed by heating the tube with an electric heat gun while HCl and distilled water were poured through the tube to dissolve the deposit. The solution was directly collected in a 10- or 25-ml volumetric flask. Vanadium concentrations varied from 3.0 to 15.0 μg/ml. Absorbance measurements were read on a Beckman DU-2 Spectrophotometer at 410 mμ using a 1-cm quartz cell.

The total pressure (barometric), the temperature of the carrier gas at its measured position, the gas flow rate, the quantity of water collected, the amount of V_2O_5 deposited on the condensation tube, and the duration of each experiment were recorded and used to calculate the apparent vapor pressure of vanadium pentoxide, the water vapor pressure, and the total gas flow rate at STP. Possible effects on the vapor pressure, such as impurities in the oxygen carrier gas, the reuse of the vanadium pentoxide sample for succeeding runs, the duration of the experiment, the surface area of the powdered vanadium pentoxide and its liquid oxide, and the lowering of oxygen pressure by the introduction of $Ar-O_2$ mixtures were checked.

Results

Measurements were taken under oxidizing conditions in the temperature range of 639.0–899.0°. Preliminary experiments with only oxygen flowing over the V_2O_5(s or l) sample revealed no visible deposits of vanadium pentoxide on the walls of the outlet condensation tube. The introduction of saturated $H_2O(g)-O_2(g)$ mixtures resulted in distinct deposits of V_2O_5, indicative of its increased volatility in the presence of steam. When steam was introduced alone the deposits of V_2O_5 were also observed. The water vapor pressures were in excess of 100 mm because of the low volatility of vanadium pentoxide at lower water vapor pressures.

The apparent vapor pressures of V_2O_5(s or l) were calculated and analyzed as a function of the water vapor pressure, P_{H_2O}. A linear log–log plot of the pressures of the deduced hydroxide species $VO(OH)_3(g)$ as a function of the water vapor pressure, P_{H_2O}, is presented in Figure 1. The slopes of the lines from least-squares analysis are 1.47 ± 0.06, 1.57 ± 0.15, 1.50 ± 0.06, 1.47 ± 0.15, 1.44 ± 0.13, and 1.54 ± 0.17 for 639.0, 718.5, 749.0, 800.5, 850.0, and 899.0°, respectively. These slopes are close to 1.5, which indicates that the heterogeneous vanadium pentoxide–water vapor reaction takes place according to the following chemical equilibrium if one vanadium atom in the gaseous hydroxide molecule is assumed

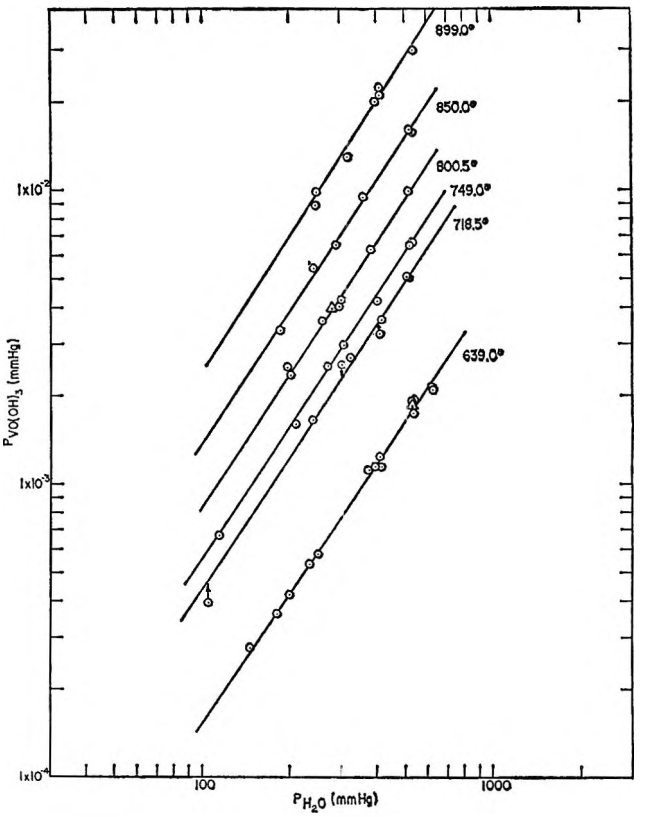

Figure 1. Experimental isotherms for the V_2O_5 (s or l)–$H_2O(g)$ system. Δ refers to equilibrium points with $Ar-O_2$ mixtures.

$$V_2O_5(\text{s or l}) + 3H_2O(g) \overset{O_2}{\rightleftarrows} 2VO(OH)_3(g)$$

The points Δ at 639.0 and 800.5° were obtained with an $Ar-O_2$ mixture as a carrier gas of 6.1 and 25.4% oxygen, respectively, of the total gas in the system. It is expected that any rate of change of the V_2O_5–condensed phase activity is low enough to be insignificant since the volatility of V_2O_5(s or l) with the $Ar-O_2$ mixture did not deviate. In addition, the vapor pressures were unaffected by different purity levels of oxygen (99.5 and 99.99%), changes of the sample surface area, or different reaction times of the experiment. Furthermore, even if a polymer species, such as $V_4O_{10}(g)$, were considered in the vaporization process, it can safely be assumed that, in the absence of steam and in the presence of oxygen carrier gas, there is no contribution of a volatile species of V_2O_5 to the total apparent vapor pressure. Therefore, the interpretation of the data appears to be valid and the vapor pressure of the hydroxide species $VO(OH)_3(g)$ is twice the apparent vapor pressure of

(5) M. D. Cooper and P. K, Winter, *Anal. Chem.*, 12, 605 (1949).
(6) S. Killingbeck, Ph.D. Thesis, University of Kansas, 1964.

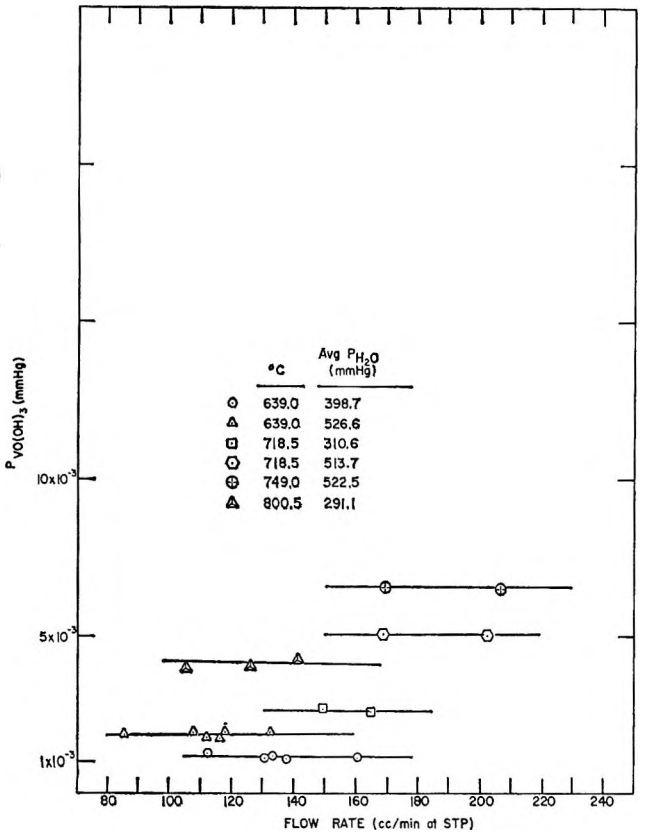

Figure 2. Flow rate dependence of the vandium oxide trihydroxide equilibrium pressures.

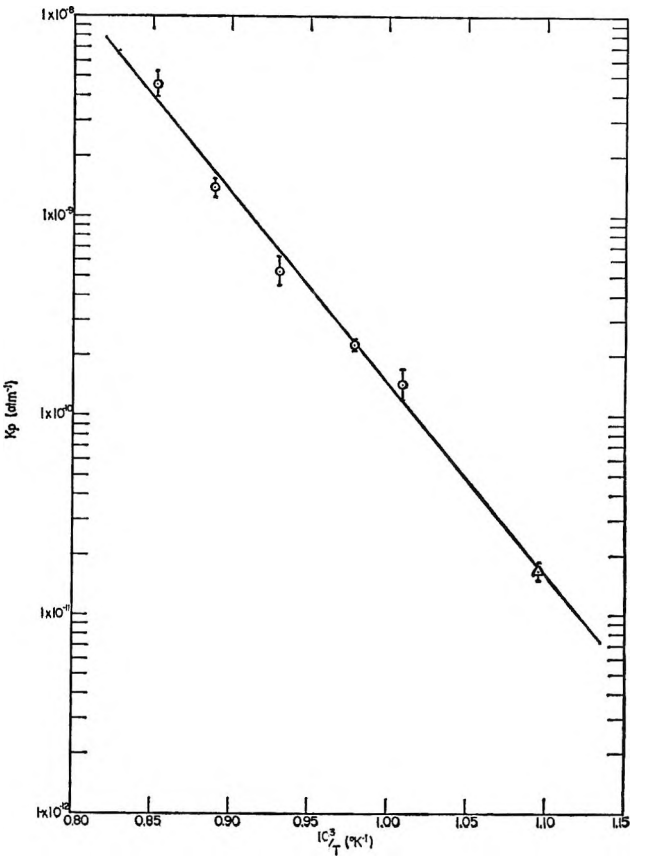

Figure 3. Temperature dependence of the equilibrium constant. Δ refers to the V_2O_5(s)–H_2O(g) system.

V_2O_5(s or l), Figure 1, in accordance with the deduced stoichiometry for the reaction.

Equilibrium attained during the experiments is demonstrated in Figure 2 by the nearly constant vapor pressures of $VO(OH)_3$(g) as a function of the STP flow rates. There is less than 5% deviation of $P_{VO(OH)_3(g)}$ over the water vapor pressure range covered while at each datum point the reproducibility of the total number of moles and of the water vapor pressures is better than 1.0%.

The equilibrium constants were calculated directly from the vapor pressure for each point on the basis of the stoichiometry of the formulated reaction. The mean values, with standard deviations, in reciprocal atmospheres, are $(1.68 \pm 0.17) \times 10^{-11}$, $(1.45 \pm 0.25) \times 10^{-10}$, $(2.24 \pm 0.13) \times 10^{-10}$, $(5.34 \pm 0.92) \times 10^{-10}$, $(1.39 \pm 0.14) \times 10^{-9}$, and $(4.60 \pm 0.63) \times 10^{-9}$ for 639.0, 718.5, 749.0, 800.5, 850.0, and 899.0°, respectively.

Figure 3 is a typical van't Hoff plot of the data. This plot shows that the lower point Δ at 639.0°, which represents the equilibrium constant of the solid vanadium pentoxide reaction with steam, is linear with the other points of the liquid vanadium pentoxide–steam reaction. Within the uncertainty of the measurements, this point is linear because of the proximity of this temperature to the melting point (656°) of V_2O_5(s).

A least-squares analysis of all the points of Figure 3 yields the equation

$$\log K_p = \frac{-9619.1 \pm 116.0}{T} + (-0.225 \pm 0.023)$$

The heat and entropy of the reaction, with their probable errors, are then calculated as 44.0 ± 0.5 kcal/mol and −1.03 ± 0.10 cal/mol deg, respectively. If the data for the V_2O_5(l) + H_2O(g) reaction are considered alone, a similar treatment gives 43.6 ± 1.0 kcal/mol and −1.03 ± 0.13 cal/mol deg for the respective heat and entropy. Therefore, the data in this temperature range can be represented by one equation within the experimental uncertainty and with the assumption that any heat capacity effects are negligible.

Discussion

Examination of the vapor pressure data reveals an agreement with the literature[3,4] with regard to the volatility of the solid or liquid vanadium pentoxide in the presence of steam and oxidizing atmosphere, but a disagreement as to the identity of the gaseous hydroxide species formed.

Taking the value for the heat of sublimation of V_2O_5(s) to $(V_2O_5)_2$(g) and the value for the depolymerization of $(V_2O_5)_2$(g), reported by Berkowitz, Chupka, and

Inghram[7] and also quoted by Glemser and Muller,[3] a value of 91.0 kcal/mol for the change $V_2O_5(s) \rightleftarrows V_2O_5(g)$ is calculated. Combining this value with our value of 44.0 kcal/mol for the heterogeneous reaction yields a heat value of −47.0 kcal/mol for the corresponding homogeneous reaction

$$V_2O_5(g) + 3H_2O(g) \rightleftarrows 2VO(OH)_3(g)$$

With Kelley's[8,9] entropies of formation for $V_2O_5(s)$, $V_2O_5(l)$, and $H_2O(g)$, plus our entropy of reaction, the values for the entropy of formation of the gaseous species, $VO(OH)_3(g)$, at 800 and 1000°K were calculated as 114.1 and 130.4 eu, respectively.

Similarly, from literature data[8,9] and from the free energies of reaction, the free energy function value, $(G^\circ_T - H^\circ_{298.16})/T$, of $VO(OH)_3(g)$ is estimated to be −66.4 and −72.8 cal/mol deg at 800 and 1000°K, respectively. The corresponding calculated[8] values for the analogous gaseous oxyhalide species, $VOCl_3(g)$, are 105.4 and 111.0 eu for their entropy of formation, and −90.5 and −94.5 cal/mol deg for their free energy function at the respective temperatures of 800 and 1000°K. The gaseous species isostructural to $VOCl_3(g)$, *i.e.*, $POCl_3(g)$ and $POF_3(g)$, have values for their entropies of formation[8,9] at 800°K of 100.2 and 88.2 eu, respectively. These values compare reasonably with the value of 105.4 eu for $VOCl_3(g)$ at this temperature.

From the entropy value, −15.0 eu, of Glemser and Muller[3] for their reported reaction $V_2O_5(s) + 2H_2O(g) \overset{O_2}{\rightleftarrows} V_2O_3(OH)_4(g)$, a value of 161.0 eu for the entropy of formation of $V_2O_3(OH)_4(g)$ at 800°K is obtained. There is no information available in the literature on any gaseous oxyhalide compound, $V_2O_3X_4(g)$, analogous to this pyrovanadic-type gaseous oxide hydroxide species. Furthermore, if a least-square analysis of the vapor pressure data tabulated by Glemser and Muller[3] is performed, the values for the slopes of the isothermal plots are 1.65 ± 0.07, 2.11 ± 0.38, 1.96 ± 0.24, and 2.05 ± 0.18 for 500, 550, 600, and 650°, respectively. The authors[3] assumed an average slope of 2.0 to arrive at the stoichiometry of the $V_2O_5(s) + H_2O(g)$ reaction which justifies their conclusion of the existence of a $V_2O_3(OH)_4$ gaseous species. In view of (a) their low value of 1.65 ± 0.07, which corresponds closer to our slope of 1.5, (b) the larger scattering of their data as evidenced by the deviations of the slope values at 550 and 600°, (c) the absence of flow rate data on their part to demonstrate the existence of equilibrium, and (d) the absence of an analogous gaseous oxyhalide, such as $V_2O_3X_4$, the presence of such a complex gaseous hydroxide as a major product of the high temperature $V_2O_5(s \text{ or } l) + H_2O(g)$ reaction is considered doubtful.

The proximity of the values for the entropies of formation of $VO(OH)_3(g)$ and $VOCl_3(g)$ and Wells'[10] slightly distorted tetrahedral structure of the latter molecule derived from electron diffraction data, suggests an isostructural configuration, such as

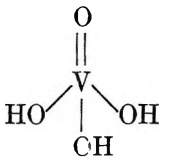

for the gaseous vanadium oxide trihydroxide, $VO(OH)_3$.

Acknowledgment. The author wishes to thank Dr. W. S. Koski of the Johns Hopkins University and Dr. G. R. B. Elliott of the Los Alamos Scientific Laboratory for their encouragement and helpful suggestions. This work was supported in part by the U. S. Atomic Energy Commission.

(7) J. Berkowitz, W. A. Chupka, and M. G. Inghram, *J. Chem. Phys.*, 27, 87 (1957).

(8) K. K. Kelley, "Contributions to the Data on Theoretical Metallurgy," U. S. Bureau of Mines Bulletin 584, U. S. Government Printing Office, Washington, D. C., 1960.

(9) K. K. Kelley, "Contributions to the Data on Theoretical Metallurgy," U. S. Bureau of Mines Bulletin 592, U. S. Government Printing Office, Washington, D. C., 1961.

(10) A. F. Wells, "Structural Inorganic Chemistry," 2nd ed, Oxford University Press, London, 1950.

Intramolecular Hydrogen Bonding in the Lowest Excited Singlet States of Some Substituted Salicylic Acids[1]

by Stephen G. Schulman and Herman Gershon

Boyce Thompson Institute for Plant Research, Yonkers, New York 10701 *(Received March 1, 1968)*

The pH dependences of the absorption spectra of several substituted salicylic acids were determined. The anomalously small shifts in absorption maxima of these compounds have been attributed to intramolecular hydrogen bonding in the lowest excited singlet states of the acidic species of the molecules studied.

Introduction

The unusually high dissociation constant of salicylic acid compared with that of benzoic acid and the *m*- and *p*-hydroxybenzoic acids has been attributed to intramolecular hydrogen bonding between the hydroxyl and carboxyl groups of salicylic acid, which stabilized the anion much more than the undissociated acid.[2] Ingold[3] has suggested that the hydroxylic proton forms a partially covalent bond with the carboxyl group, thereby introducing a partial positive charge into it and facilitating the release of the carboxylic proton. The stabilization of the singly dissociated anion of salicylic acid by hydrogen bonding also seems to affect the dissociation of the phenolic proton since the second dissociation constant of salicylic acid[4] is anomalously low compared with that of the phenolic group of *p*-hydroxybenzoic acid.[5]

In the present work the ultraviolet absorption spectra of a series of substituted salicylic acids were studied. These spectra show abnormally small shifts of the absorption maxima as a function of pH compared with those usually observed for aromatic carboxylic acids and phenols.[6] The shift in the absorption maximum of a particular band, upon change of pH, enables calculation of the difference between equilibrium constants for dissociation equilibria in ground and electronically excited states of the same conjugate acid–base pair from the Förster cycle:[7] $\Delta pK_a = pK_a - pK_a^* = 2.10 \times 10^{-3} (\bar{\nu}_A - \bar{\nu}_B)$, at 25°, where pK_a and pK_a^* are the equilibrium constants of the ground and excited state dissociations and $\bar{\nu}_A$ and $\bar{\nu}_B$ are the frequencies, in cm^{-1}, of the absorption maxima of conjugate acid and base, respectively. The validity of the calculation of ΔpK_a values from absorption spectra is based upon several assumptions. First, it is necessary to assume that the entropy of dissociation in the excited state is the same as that in the ground state. Second, the Förster cycle is derived from the O–O vibronic bands of the electronic transitions observed in the absorption spectra. Due to the population of "hot bands" at room temperature, the position of the O–O band cannot be located exactly. If, however, it is assumed that the spacings between vibronic levels in ground and excited states of both members of the conjugate pair are similar, then the band maxima, at room temperature, of both members of the conjugate pair will be displaced equally from the O–O band. The separation between these two band maxima may then be used to calculate ΔpK_a. These assumptions have been discussed extensively by Jaffé and Jones.[8] Anomalously small differences between $\bar{\nu}_A$ and $\bar{\nu}_B$ translate into unusually high acidities and basicities for the excited states of carboxylic acids and phenols. The present study is an attempt to rationalize the abnormal ΔpK_a values of salicylic acid and its derivatives in terms of intramolecular hydrogen bonding in the excited states of these molecules.

Experimental Section

Salicylic acid, 3-hydroxy-2-naphthoic acid, and 4-bromo-3-hydroxy-2-naphthoic acid were obtained from Pfister Chemical Works, Inc., Ridgefield, N. J. 3,5-Diiodosalicylic acid was purchased from Matheson Coleman and Bell, East Rutherford, N. J. *o*-Methoxybenzoic acid, *p*-hydroxybenzoic acid, *m*-hydroxybenzoic acid, 5-chlorosalicylic acid, 5-bromosalicylic acid, 5-iodosalicylic acid, 5-nitrosalicylic acid, 3-5-dichlorosalicylic acid, and 3,5-dibromosalicylic acid were purchased from City Chemical Corporation, New York, N. Y., and 3-nitro-salicylic acid and 3,5-dinitrosalicylic acid were obtained from Eastman Organic Chemicals, Rochester, N. Y. All of these reagents were purified by triple recrystallization from ethanol. Spectra were taken on a Cary Model 15 recording spectrophotometer

(1) This work was supported in part by the U. S. Public Health Service Grant No. AI-05808.

(2) G. E. K. Branch and D. L. Yabroff, *J. Amer. Chem. Soc.*, **56**, 2568 (1934).

(3) C. K. Ingold, "Structure and Mechanism in Organic Chemistry," Cornell University Press, Ithaca, N. Y., 1953, p 749.

(4) A. Agren, *Svensk Kem. Tidskr.*, **68**, 189 (1956).

(5) E. E. Sager, M. R. Schooley, A. S. Carr, and S. F. Acree, *J. Res. Nat. Bur. Stand.*, **35**, 521 (1945).

(6) A. Weller, *Progr. Reaction Kinetics*, **1**, 387 (1961).

(7) T. Förster, *Z. Elektrochem.*, **54**, 42 (1950).

(8) H. H. Jaffé and H. L. Jones, *J. Org. Chem.*, **30**, 964 (1965).

on 1×10^{-4} M solutions of the salicylic acids in 0.1 M $HClO_4$, in Fisher pH 7 buffer solution, and in 1.0 M NaOH in 1 cm square silica cells.

Results

The frequencies of the band maxima for the lowest singlet–singlet transitions of salicylic acid and its derivatives, under various conditions of acidity, are shown in Table I. Table II shows the values of ΔpK_{a_1} and ΔpK_{a_2}, for dissociation of carboxylic and phenolic groups, respectively, calculated from the Förster cycle and the data of Table I.

Table I: pH Dependences of the Lowest Energy Singlet–Singlet Transitions of Salicylic Acid and Some of Its Derivatives

	$\bar{\nu}_{max}$, cm^{-1}		
	0.1 M $HClO_4$	pH 7 buffer	1.0 M NaOH
Salicylic acid	33,100	33,800	33,760
o-Methoxybenzoic acid	33,770	35,800	35,800
Methyl salicylate	33,100	33,100	30,200
p-Hydroxybenzoic acid	39,000	40,060	35,620
m-Hydroxybenzoic acid	33,800	35,100	32,070
5-Chlorosalicylic acid	31,250	31,950	31,850
5-Bromosalicylic acid	31,580	32,300	32,070
5-Iodosalicylic acid	31,080	31,980	31,780
3,5-Dichlorosalicylic acid	31,210	31,990	31,520
3,5-Dibromosalicylic acid	30,500	31,550	31,390
3,5-Diiodosalicylic acid	30,100	31,100	30,900
3-Hydroxy-2-naphthoic acid	27,700	28,250	28,210
4-Bromo-3-hydroxy-2-naphthoic acid	27,200	27,950	27,500
3-Nitrosalicylic acid	28,610	28,190	23,600
5-Nitrosalicylic acid	31,180	29,920	24,480
3,5-Dinitrosalicylic acid	30,430	29,310	24,520

Table II: ΔpK_{a_1} (Carboxylic Group) and ΔpK_{a_2} (Phenolic Group) for the Lowest Singlet–Singlet Transitions of Salicylic Acid and Some of Its Derivatives, Calculated from the Förster Cycle and the Data of Table I

	ΔpK_{a_1}	ΔpK_{a_2}
Salicylic acid	−1.5	0.1
o-Methoxybenzoic acid	−4.3	...
Methyl salicylate	...	6.1
p-Hydroxybenzoic acid	−2.2	9.3
m-Hydroxybenzoic acid	−2.7	6.4
5-Chlorosalicylic acid	−1.5	0.2
5-Bromosalicylic acid	−1.5	0.5
5-Iodosalicylic acid	−1.9	0.4
3,5-Dichlorosalicylic acid	−1.6	1.0
3,5-Dibromosalicylic acid	−2.2	0.3
3,5-Diiodosalicylic acid	−2.1	0.4
3-Hydroxy-2-naphthoic acid	−1.2	0.1
4-Bromo-3-hydroxy-2-naphthoic acid	−1.6	0.9
3-Nitrosalicylic acid	0.9	9.6
5-Nitrosalicylic acid	2.6	11.4
3,5-Dinitrosalicylic acid	2.4	10.0

Discussion

The data of Table II show that in the lowest excited singlet state of salicylic acid the acid strength of the carboxylic group is diminished by 1.5 log units. Wehry and Rogers[9] have shown that the corresponding difference in benzoic acid is 5.3 log units. This demonstrates that the presence of the hydroxyl group in salicylic acid has the effect of strengthening the acidity of the carboxylic function, in the excited state, relative to the unsubstituted benzoic acid. In order to assess the influence of the hydroxylic proton on the dissociation of the carboxylic group, in the excited state, the ΔpK_a of the methyl ether of salicylic acid was determined. This was found to be 4.3 log units, which is close to the value for benzoic acid. From these data it is reasonable to conclude that, in the lowest excited singlet state of salicylic acid, the hydroxylic proton bonds to the carboxyl group, introduces positive charge into that group, and thereby facilitates the release of the carboxylic proton. Weller[10] studied the fluorescence spectra of salicylic acid and its methyl ester and observed an abnormally large Stokes shift for the emission spectra of these compounds. No such shift was observed for the emission spectra of *o*-methoxybenzoic acid and its methyl ester. This anomaly was attributed to an intramolecular proton shift in the lowest excited singlet state of salicylic acid which resulted in the formation of a zwitterion. Naboikin, *et al.*,[11] observed the appearance of an extra band in the fluorescence of the methyl ester of 3-hydroxy-2-naphthoic acid which was attributed to the formation of an intramolecular hydrogen bond between the phenolic proton and the carbonyl oxygen of the carbomethoxy group. Hirota[12] found similar effects in the absorption and fluorescence spectra of 3-hydroxy-2-naphthoic acid and related the solvent dependence of the spectra shifts to the degree of proton transfer from the hydroxyl to the carboxyl group. Although the present study is concerned with the anomalously small shifts in the absorption spectra of these and related compounds, the preceding studies lend strength to the theory of intramolecular hydrogen bonding in the lowest excited states of these molecules. The ΔpK_{a_1} values for the *meta* and *para* isomers of salicylic acid were found to be 2.7 and 2.2 log unit, respectively. Although the high acidities of these compounds in their lowest excited singlet states cannot be explained by intramolecular hydrogen bonding, as in salicylic acid, it is conceivable that there is extensive intermolecular hydrogen bonding between the hydroxyl and carboxyl groups of these compounds, having essen-

(9) E. I. Wehry and L. B. Rogers, *J. Amer. Chem. Soc.*, **88**, 351 (1956).

(10) A. Weller, *Z. Elektrochem.*, **60**, 1144 (1956).

(11) U. V. Naboikin, B. A. Zadorozhnyi, and E. N. Pavlova, *Opt. Spectry.*, **8**, 347 (1960).

(12) K. Hirota, *Z. Phys. Chem.* (Frankfurt am Main), **35**, 222 (1962).

tially the same effect on ΔpK_{a_1} as the intramolecular case in salicylic acid.

The ΔpK_{a_1} values for all of the halogenated salicylic acids as well as 3-hydroxy-2-naphthoic acid and its 4-bromo derivative are similar to that of salicylic acid. Those of the nitrosalicylic acids, however, are quite different. It has been a rather firmly established rule that in the lowest excited singlet states of aromatic carboxylic acids the carboxyl group becomes more basic than in the ground singlet state.[6] This can be attributed to charge transfer from the aromatic ring to the carboxyl group upon singlet–singlet excitation. The ΔpK_{a_1} values of the nitrosalicylic acids, however, clearly show that upon singlet–singlet excitation the carboxyl group becomes more acidic. This can be attributed to the anomalously high acidity of the excited states of the salicylic acids, due to intramolecular hydrogen bonding coupled with the extremely strong inductive effect of the nitro group in the excited state.[13] These two phenomena compete effectively with charge transfer to the carboxyl group, actually removing charge from it and thereby enhancing its acidity in the excited singlet state.

It may be noted that the enhancement of the acidity of the carboxyl groups of the nitrosalicylic acids is lower in 3-nitrosalicylic acid than in 5-nitrosalicylic acid even though they are both *meta* to the carboxyl group. This is probably due to competition of the nitro group in the 3-position, with the carboxyl group, for the phenolic proton. This effect diminishes the hydrogen bonding between the phenolic and carboxylic groups thereby enhancing the basicity of the carboxyl group in the excited state. Dippy and Hughes[14] observed a failure of ground-state dissociation constants of substituted salicylic acids to adhere to simple additivity of substituent free energy effects. The data of Table II show this to be the case for the excited-state ΔpK_a and pK_a^* values.

The value of ΔpK_{a_2} for salicylic acid is shown in Table II as 0.1 log unit. This is anomalously low for the enhancement of the acidity of a phenolic group upon excitation to the lowest excited singlet state.[6] The methyl ester of salicylic acid, which does not have a dissociable proton on its carbomethoxy group and is therefore not so good a hydrogen bonding molecule as salicylic acid, has a ΔpK_a of 4.3 log units while the ΔpK_{a_2} values of the *meta* and *para* isomers of salicylic acid are 6.1 and 9.3 log units, respectively. Furthermore, with the exception of the nitro-substituted salicylic acids, all of the substituted salicylic acids as well as 3-hydroxy-2-naphthoic acid and its 4-bromo derivative have ΔpK_{a_2} values similar to that of salicylic acid. This situation can also be explained by intramolecular hydrogen bonding in the lowest excited singlet states of the singly ionized anion–doubly ionized anion conjugate. The singly ionized salicylic acid is stabilized by hydrogen bonding of the hydroxylic proton to the carboxylate function. This makes it more difficult to remove than that in methyl salicylate. While intermolecular hydrogen bonding is possible in the cases of the *m*- and *p*-hydroxybenzoic acid anions, the internally hydrogen bonded salicylate anion is more stable because of the lower entropy of the internal hydrogen bond. This makes it more difficult to ionize the singly dissociated salicylic acid anion.

The nitro-substituted salicylic acids again present an anomaly because of the strong electron-withdrawing effect of the nitro group in the excited state. These compounds have quite acidic phenolic protons in spite of the intramolecular hydrogen bonding effect.

From these experiments, it appears that the effects of intramolecular hydrogen bonding upon acidity in the lowest excited singlet states of salicylic acid and its derivatives parallel those in the ground states of these molecules.

Acknowledgment. The authors are grateful to Miss Marilyn Lantz for helpful discussions.

(13) S. Schulman and H. Gershon, unpublished work.

(14) J. F. J. Dippy and S. R. C. Hughes, *Tetrahedron*, 19, 1527 (1963).

Absorption Maxima of the Visible Band of Iodine in Different Groups of Solvents

by E. M. Voigt

Department of Chemistry, Simon Fraser University, Burnaby 2, British Columbia, Canada and Department of Chemistry, University of California, Berkeley, California 94720 *(Received April 13, 1968)*

The wavelength of the maximum of the visible absorption band of iodine was measured in a large number of different solvents. A transition energy increase with respect to the gas-phase value was observed in most of the solvents studied which ranged up to 15 kcal. Relating the band position to the ionization potential of the solvents yielded a striking division of the blue-shifted band into a series of characteristic solvent classes. It was found that the transition energy of iodine was affected most strongly by the electron donor ability of the solvent and less strongly by the ionization potential and steric structure of the solvent molecules. In a number of cases a reversal of the slope of wavelength *vs.* ionization potential was observed, which could be associated in part with a change in molecular shape of the solvents while keeping their donor character constant. Almost all of the observed changes could be explained with reference to two possible interactions: (1) charge-transfer interactions and (2) contact-charge-transfer interactions. Possibly, exchange repulsion of the excited state of iodine with nonbonding electron pairs is a further cause of the blue shifts. These interactions are very specific and, therefore, sensitive to steric conditions. It was found that the over-all molecular shape modifies the specific orbital overlap, thereby influencing the interaction process for various types of systems.

Introduction

The pronounced and unusual dependence of the transition frequency of the iodine visible absorption band upon temperature, pressure, and solvent was first investigated by Ham.[1] More recent data by Walkley, Glew, and Hildebrand[2] on the solvent dependence of the iodine transition showed specific correlations between the position of the band maximum in alkyl halides and aromatics as solvents and their ionization potentials. This is a very interesting correlation, since a fair number of these solvents have been shown to form weak 1:1 charge-transfer complexes with iodine (heats of formation, $\Delta H \gtrsim 2$ kcal/mol). This suggests that the iodine band position relates to charge-transfer interactions between iodine and the nonbonding halogen electrons of the alkyl halides or the π electrons of the aromatics, respectively.

In order to investigate this question further, we have extended the measurements in two ways, *viz.*, by choosing (a) solvents with different, strong donor capacities toward iodine and known ionization potentials and (b) series of solvents in which the donor site was kept constant while the molecular shape was changed.

In the past several different explanations have been proposed to account for the observed behavior of the iodine visible transition, notably by Bayliss,[3] Mulliken,[4] and Nagakura,[5] which will be discussed later in this paper.

Experimental Section

The absorption spectra of the iodine solutions were obtained on a Cary Model 14 spectrophotometer using a pair of matched 1-cm stoppered fused silica cells with the solvent as reference. The cells were thermostated at 25°. The iodine used was Baker Analyzed, resublimed, and dried in a desiccator over phosphorus pentoxide.

A number of solvents of either chromatographic or spectrograde purity, which were available commercially were used directly, unless they might have contained small amounts of water. Accordingly, the esters and alcohols were refluxed over sodium metal or magnesium turnings and then distilled off into dry bottles from which solutions were made up in a drybox. Other liquids were purified using standard methods in the literature. The fluorocarbons and some other alkyl halides were fractionally distilled.

All solutions were prepared directly before measurement. The iodine concentration was kept low, generally 10^{-4} to 10^{-3} M. For each solution several tracings of the iodine spectrum were taken and the results were averaged.

Results

The experimental data obtained in this study are listed in Table I in terms of (a) the iodine absorption maxima measured, in millimicrons, together with addition values selected from literature and (b) ionization potentials of the solvent, I, in electronvolts. These are plotted in Figure 1.

(1) J. Ham, *J. Amer. Chem. Soc.*, **76**, 3875, 3881, 3886 (1954).

(2) J. Walkley, D. N. Glew, and J. H. Hildebrand, *J. Chem. Phys.*, **33**, 621 (1960).

(3) N. C. Bayliss and A. L. G. Rees, *ibid.*, **8**, 377 (1940); N. C. Bayliss, *ibid.*, **18**, 292 (1949).

(4) R. S. Mulliken, *Rec. Trav. Chim.*, **75**, 845 (1956).

(5) S. Nagakura, *J. Amer. Chem. Soc.*, **80**, 520 (1958).

Table I: Maxima of the Visible Absorption Band of Iodine in Solvents of Different Types[a] and Ionization Potentials

	I, eV[b]	λ, mμ
Alkanes		
c-C_6H_{10}	10.53	523
n-C_7H_{16}	10.08	522
c-C_6H_{14}	9.88	523
i-C_8H_{18}	9.86	521
Alkyl halides		
C_7F_{16}	12.08	523
CCl_2FCClF_2	11.99	522
CCl_3F	11.77	519
CCl_4	11.47	517
$CHCl_3$	11.42	512
CH_2Cl_2	11.35	506
CH_2ClCH_2Cl	11.12	497
CH_3CHCl_2	11.07	504
C_2H_5Cl	10.98	494
$(CH_3)_2CHCl$	10.78	495
1-Chlorobutane	10.67	497
1-Chloro-2-methylpropane	10.66	500
1-Chlorohexane	~10.35 (estd)	502
1-Chlorooctane	~10.1 (estd)	504
$CHBr_3$	10.51	503
CH_2Br_2	10.48	500
C_2H_5Br	10.29	490
1-Bromobutane	10.13	491.5
1-Bromopentane	10.10	492.5
$(CH_3)_2CHBr$	10.08	485
2-Bromobutane	9.98	492
2-Bromooctane	~9.58 (estd)	490.5
$(CH_3)_3CBr$	9.89	478
CH_3I	9.54	481
C_2H_5I	9.33	478
n-C_3H_7I	9.26	478.5
n-C_4H_9I	9.21	479
n-$C_6H_{13}I$	~9.07 (estd)	480
Isobutyl iodide	9.18	479–479.5
sec-Butyl iodide	9.09	~472
2-Iodopropane	9.17	~473
Aromatics		
C_6F_6	9.97	520
$C_6H_5CF_3$	9.68	512
C_6H_5F	9.2	507
C_6H_6	9.24	502
C_6H_5Cl	9.07	508
C_6H_5Br	8.98	503
C_4H_4S	8.86	505–508
$C_6H_5CH_3$	8.82	496
C_6H_5I	8.73	493
1,3,5-$C_6H_3(CH_3)_3$	8.40	489
$C_6H_5OCH_3$	8.22	490
β-Methylfuran	8.4	495
Alcohols and ethers		
CH_3OH	10.85	440
C_2H_5OH	10.48	443
n-C_3H_7OH	10.2	445
i-C_3H_7OH	10.16	446–447
n-C_4H_9OH	10.04	448–449
$CH_3OC_2H_4OCH_3$	~9.7	458
$(C_2H_5)_2O$	9.53	466
$(n\text{-}C_3H_7)_2O$	9.27	470
$(i\text{-}C_3H_7)_2O$	9.20	472–473
p-$C_4H_8O_2$ (in *n*-C_6H_{12})	9.13	452
c-$(CH_2)_4O$	8.89	446
Hydrosulfides and sulfides		
CS_2	10.8	520
C_2H_5SH (in *n*-C_6H_{14})	9.29	460
$(CH_3)_2S$ (in *n*-C_6H_{14})	8.69	437
$CH_3SC_2H_5$ (in CCl_4)	8.55	~430
$(C_2H_5)_2S$ (in CCl_4)	8.43	430–435
$(n\text{-}C_3H_7)_2S$ (in CCl_4)	8.30	425
$(n\text{-}C_3H_7)_2S$	8.30	418
Nitrogen compounds[c]		
NH_3 (in *n*-C_7H_{16})	10.15	430
C_5H_5N (in *n*-C_7H_{16})	9.32	422
CH_3NH_2 (in *n*-C_7H_{16})	8.97	418
$C_2H_5NH_2$ (in *n*-C_7H_{16})	8.86	417
n-$C_4H_9NH_2$ (in *n*-C_7H_{16})	8.71	417
$(CH_3)_2NH$ (in *n*-C_7H_{16})	8.24	412
$(C_2H_5)_2NH$ (in *n*-C_7H_{16})	8.01	410
$(CH_3)_3N$ (in *n*-C_7H_{16})	7.82	414
$(C_2H_5)_3N$ (in *n*-C_7H_{16})	7.50	414
Others		
$(CH_3)_2CON(CH_3)_2$ (in *n*-pentane)	8.60	~440

[a] Solvents are pure liquids except as noted. [b] Ionization potentials are photoionization potentials taken from K. Watanabe, T. Nakayama, and T. Mottl, *J. Quant. Spectrosc. Radiat. Transfer*, **2**, 369 (1962), except where estimated. [c] The nitrogen compounds were selected from data of H. Yada, J. Tanaka, and S. Nagakura, *Bull. Chem. Soc. Jap.*, **33**, 1660 (1960).

From this figure it is apparent that most solvents investigated shifted the visible absorption band of iodine toward higher energies than its gas-phase value with a maximum shift of 110 mμ, corresponding to 15 kcal in this wavelength region. The outstanding feature of these data, however, is that there are not only two lines, as found by Walkley, Glew, and Hildebrand,[2] one for solvents containing nonbonding electrons, the other for solvents containing π electrons, but also a whole series of lines, apparently related to the Lewis-base character of the key atoms of a given solvent group. Thus the absorption band is increasingly blue shifted,

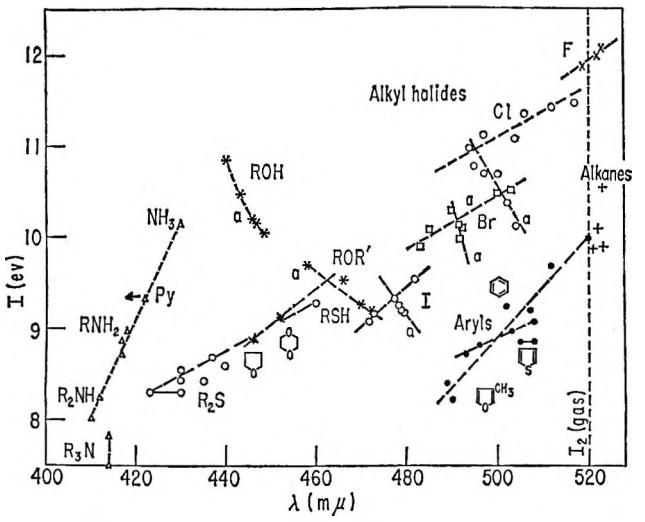

Figure 1. Relations between the wavelengths of the maxima of the visible absorption bands of dissolved iodine, λ_{max} (in millimicrons), and the ionization potentials of the solvents I (in electronvolts); solvent groups: alkanes, alkyl halides, aromatics, oxygen compounds, sulfur compounds, nitrogen compounds. The points may be identified by the descending order of I in each group in Table I.

beginning with aromatics and followed by solvents in the order of the increasing basic character of their key solvent atom: F, Cl, Br, I, O, S, N.

It is revealing to analyze these data in detail on the basis of two distinct situations: (a) blue shifts at constant ionization potential and (b) ionization-potential values for a given transition energy. In regard to condition a, one finds that for a given ionization-potential value the energy of the iodine transition increases by irregular jumps for solvent groups containing characteristic atoms (or atom groups) in the order: aromatics < I < O < S < N. As mentioned above, this is roughly the order of Lewis-base character of the systems. The over-all increase in transition energy between aromatic solvents and N-containing solvents (least and most shifting solvents, respectively) at given I values is found to be 0.52 eV or 12 kcal. Thus compared with an aromatic solvent, iodine interacts with an environment containing basic nitrogen, so that its electronic transition energy is increased by 12 kcal. Evidently, this extraordinary sensitivity of the iodine excitation energy to a specific *atomic* environment arises from some strong chemical interaction predominating in solutions containing the above atoms. Although this interaction can be modified by secondary effects, it nevertheless determines the spectroscopic characteristics of the iodine transition in these solutions. If the data are considered with respect to condition b above, at low transition energies a striking insensitivity of the I_2-band maximum position to the ionization potential is observed. A set of parallel lines can be distinguished comprising aromatic, iodo-bromo-, chloro-, and fluoro- substituted solvents, respectively, for which the iodine transition is barely displaced from its gas-phase value. We are dealing here obviously with a different kind of interaction from that encountered under condition a. It is a specific interaction which does not alter the transition energy by much but which increases in effectiveness in the above solvent groups as follows: aromatics < I- < Br- < Cl-containing alkanes.

In Figure 1 we observe yet another interesting set of lines marked a and which are either vertical or slope in a direction the reverse of the others. These lines refer to straight-chain alkyl halide solvents, as opposed to the branched-chain alkyl halides which show the more common "normal" slopes. We also include here the solvent groups ROR′ (oxygen ethers) and R_3N (tertiary amines). In view of the conclusions reached above, it is logical to separate effects on the iodine transition energy at high values of this energy from effects at low values. For the solvent groups ROR′ and NR_3, there is obviously a strong interaction (of type a) which causes major blue shifts to 460 and 414 mμ, respectively. The main interaction, however, is somewhat weakened by a secondary effect which modifies the major blue-shift values and which leads to zero or negative slope. It is likely that we are dealing with a steric effect of the alkyl groups, since normal slopes are observed for the primary and secondary amines, and it is particularly apparent in the normal slope of the cyclic ethers (Figure 1). Unlike the open-chain alkyl ether solvents, ROR′, the R groups of the cyclic ethers have restricted rotation about the O–C bonds and can, therefore, not interfere with the interaction site of the oxygen atom. For the weakly blue-shifting alkyl halide solvents, we are dealing with an interaction of type b which is responsible for the major part of the increase in transition energy, *i.e.*, to 500 and 480 mμ. Again, a secondary effect becomes apparent, leading to negative slopes. In this case the negative slope occurs for straight-chain alkyl halide solvents as compared with the regular slopes found for the corresponding branched-chain solvents (Table I, Figure 1). Although the secondary effect is obviously related to the nature of the alkyl groups attached to the halogen atoms, it is unlikely that steric factors alone can account for the observed data in this case.

We have not mentioned the group of alcohols, ROH, so far. They show large blue shifts (larger than the ethers which have all lower ionization potentials) and negative slope. The alcohols are an exceptional set of solvents in two respects: first, they are H-bonding solvents and, therefore, have competitive equilibria with chemical interactions similar in strength to the I_2–ROH interactions. Secondly, they are solvents with high dielectric constants. As shown in Figure 1 for pyridine, increasing the dielectric constant of the solution increases the blue shift of the iodine transition (the arrow in Figure 1 indicates the shift when the pyridine con-

centration is increased over the reported value in *n*-heptane). The blue shifts observed in other strongly polar solutions such as dimethyl sulfoxide, the nitriles, ketones, formamide, H_2O, etc. have not been included in the present data partly because the blue shift depends on the dielectric constant of the solutions and partly because most of these solvents interact chemically with iodine. The variation of the energy of the iodine transition with the dielectric constant of the solvent is being further investigated in this laboratory.

Discussion

In this discussion we make the following assumptions. (1) The observed iodine absorption, $^3\Pi_{0^+u} \leftarrow {}^1\Sigma_g^+(B \leftarrow X)$, is essentially the same transition in all solutions but more or less shifted from its gas-phase absorption maximum at 520 mμ. This has been generally accepted until now. We should like to point out, however, that it has never been proven that the transition retains its identity throughout a range of interactions as wide as that present in Figure 1, especially in view of the fact that at least five electronic states are expected to lie within 2000 cm^{-1} of the iodine B state, several of which are known to interact with B in the gas phase.

(2) Liquids which act as simple dielectrics toward iodine, *i.e.*, liquids in which iodine experiences only ordinary physical interactions, such as London and induced-dipole forces, affect the energy of the visible iodine transition as described by McRae's theory of electronic transitions in dielectric media.[6] This theory predicts red shifts of an electronic band by a dielectric whenever the excited state is more polarizable (or more polarized) than the ground state. The iodine transition investigated should show only small red shifts in going from the vapor phase to dilute solutions in nonpolar solvents. (The B←X band of iodine is a singlet–triplet transition. Since the triplet state interacts with its environment largely by exchange interactions, the effect of the medium as a dielectric upon it will be small.) This has indeed been observed for iodine dissolved in a series of nonpolar solvents and will be reported separately.[7]

The overwhelming majority of solvents, however, cause pronounced blue shifts of the visible transition of iodine which can be clearly separated into solvent classes and which depend in part upon the ionization potentials of the solvents. We have shown that the blue shifts can be analyzed in terms of two different specific interactions between solvent molecules and iodine, one being a strong chemical interaction and the other a weaker nonbonding one. We identify the strong interactions as charge-transfer interactions which are highly specific because they depend on orbital overlap and molecular symmetry. They lead to electron donor–acceptor complexes between iodine as the acceptor and the solvent molecule as donor in the sense of Mulliken's charge-transfer theory.[3] The existence of these complexes has been demonstrated repeatedly by thermodynamic and/or spectroscopic methods for at least some solvents of each group studied here, with the exception of the alkyl halides. This point, therefore, need not be elaborated further. The nature of the weak interactions is not as certain. Further experimental information is needed to identify them fully. However, it is probable that they are mainly contact-charge-transfer interactions between iodine and the nonbonding electrons of the halogen atoms. Exchange repulsion of the excited state of iodine with the nonbonding electrons of the halogens may contribute as well. This will be discussed in greater detail below.

The actual mechanism of the blue shift of the iodine transition energy through interaction with other molecules is not well understood. Several qualitative explanations have been suggested for the blue shift occurring in complexing solvents, notably by Mulliken[4] and Nagakura;[5] none, however, have been suggested for noncomplexing solvents. Both explanations rest on the fact that charge transfer to the iodine molecule involves the same antibonding σ_u^* orbital as the electronic excitation of iodine to the B state. Mulliken[4] suggested, therefore, that the major contribution to the blue shift of the visible iodine transition in complexes derives from strong repulsive exchange interactions between donor and iodine, the electronic interaction radius of which is greatly increased by excitation. These interactions raise the energy of the excited state of iodine in proportion to the strength of the charge-transfer interaction. The energy depends as well on the electron-density distribution of the donor orbital. Nagakura[5] offers a similar but somewhat simpler explanation of the blue shift in terms of an LCMO approximation. Upon mixing the interacting donor orbital and the iodine σ_u^* orbital, the energy of the latter increases while that of the former decreases. Assuming that the iodine π_g orbital energy is not affected by complex formation, again an increase of the iodine transition energy is expected which is proportional to the amount of charge transfer and dependent upon the type of donor orbital which interacts. These interpretations of the blue shift of the I_2 absorption imply that the shift is fairly independent of the physical state in which the system exists, particularly when strong donor–acceptor interactions are present.

These explanations have been substantiated to some degree by comparison of the blue shift in various solutions with the heats of formation of I_2 complexes found for the same solutions.[9] The blue shift has also been

(6) E. G. McRae, *J. Phys. Chem.*, **61**, 562 (1957).

(7) E. M. Voigt, *ibid.*, to be published.

(8) R. S. Mulliken, *J. Amer. Chem. Soc.*, **72**, 600 (1950); **74**, 811 (1952), and related papers.

(9) R. P. Lang, *ibid.*, **83**, 1185 (1962).

correlated to the bond length of I_2, which increases on complex formation.[10] However, recent results on iodine charge-transfer complexes in the gas phase[11] have thrown doubt on the validity of the interpretations of the blue shift. Tamres[11b] and Kroll[11d] observed that the position of the I_2 visible band remained apparently unaffected by charge-transfer complexing, even in the case of the very strong diethyl sulfide–I_2 and dimethyl sulfide–I_2 complexes and even though charge transfer in the gas phase and in solution were comparable in strength. However, some decrease in the intensity of the iodine band upon addition of donor was observed in the gas phase.[11d] In order to interpret the results, Tamres suggested an unspecified "cage effect" operative in solution but absent in the gas phase. Kroll, on the other hand, proposed that the structure of the ground state of the charge-transfer complex in solution differs from that in the gas phase and that this difference affects the excited state of iodine sufficiently to remove the blue shift in the gas phase. A simpler, more satisfactory explanation of the reported data is obtained if one assumes that *charge-transfer complexes with electronically excited I_2 cannot be observed in the gas phase.* Charge-transfer interactions mix repulsive states into the B state of I_2, which will almost certainly lead to dissociation of I_2 into $I(^2P_{3/2})$ and $I(^2P_{1/2})$ atoms in the gas phase, since this has been observed even for uncomplexed I_2. Furthermore, this is a highly temperature-sensitive process, a fact which is important since the experiments are carried out at elevated temperatures. In solution the same dissociative process occurs; however, it is well known that the rate of recombination of atoms in solution is about 1000 times greater than in the gas phase at atmospheric pressure where third-body collisions are rate determining. The observed I_2 absorption, unaffected in the band's maximum position but of decreased intensity, can thus be attributed to the remaining undissociated and uncomplexed iodine in the gas phase. If our explanation of the gas-phase data is correct, Mulliken's interpretation of the blue shift remains a possible mechanism.

Accepting then Mulliken's interpretation, slightly modified as proposed in the preceding paragraph, our data suggest that the relation to the ionization potential of the charge-transfer complexes with the solvents studied should correlate with their blue shift of the I_2 band, as far as solutions with strong interactions are concerned. Certainly no known charge-transfer property varies in an identical manner with respect to the ionization potential as do the blue shifts reported here. However, in a study of I_2–amine complexes,[12] it has been shown that the charge-transfer energy and ionization potential relation for these strong complexes differs remarkably from the same relation for weaker I_2 complexes. This leads one to expect that there exist a whole series of charge-transfer energy ionization potential curves, with parameters jumping in values proportionally to those obtained here for the blue shifts from solvent class to solvent class. In connection with this point, it will be interesting to compare the results for the intensities, band half-widths, and oscillator strengths of the I_2 band in the solvents studied here. These measurements are presently being obtained in our laboratory.

In the wavelength region of small blue shifts, a set of lines were observed comprising the solvent classes RBr, RCl, and mixed fluorocarbons, which we attributed to weak nonbonding, yet specific, interactions of these solvents with iodine. As mentioned earlier, these may tentatively be ascribed to contact-charge-transfer interactions. They perturb the excited state of iodine in the same way as the bonding-charge-transfer interactions. Evidence for this is the appearance of strong new absorption bands in the near-uv region when iodine is added to bromoalkane–heptane solutions.[13] Such additional absorptions have not been observed as yet for solutions of iodine in RCl or in perfluorocarbon solvents. These molecules have very high ionization potentials, and it is therefore likely that they interact with iodine without contact charge transfer. Conceivably, exchange repulsion of the excited state of iodine with a nonbonding electron pair on the halogen atoms can lead to the observed blue shifts for these solvents. The ionization potential now indicates the tightness of binding of the outer electron octet of the halogens which is in the order F > Cl > Br. Their p-orbital electron densities follow the same order. The overlap volume with the σ_u^* orbital of I_2, however, is greatest with Br, followed by Cl, and is very small for F. The balance of these effects accounts very well for the observed order of blue shifts in these solvents (Figure 1).

The specific nature of the interactions which lead to blue shifts of the iodine transition were seen to result from orbital overlap between the excited iodine molecule and the various donor molecules. Any factor which reduces this overlap can decrease the blue shift as well. Molecular geometry, therefore, which can sterically hinder the key atom of its solvent series, may reduce the blue shift of iodine relative to unhindered members of the series. If the solvent molecule is a strong base toward iodine but has a small interacting orbital, as is the case for the amines and ethers, normal and branched alkyl chains can lower the iodine transition energy relative to molecules having unobstructed O or N atoms. The effect observed for the normal- and branched-chain halides is particularly interesting.

(10) E. K. Plyler and R. S. Mulliken, *J. Amer. Chem. Soc.*, **81**, 823 (1959).

(11) (a) F. T. Lang and R. L. Strong, *ibid.*, **87**, 2345 (1965); (b) M. Tamres and J. M. Goodenow, *J. Phys. Chem.*, **71**, 1982 (1967); (c) E. I. Ginns and R. L. Strong, *ibid.*, **71**, 3059 (1967); (d) M. Kroll, *J. Amer. Chem. Soc.*, **90**, 1097 (1968).

(12) H. Yada, J. Tanaka, and S. Nagakura, *Bull. Chem. Soc. Jap.*, **33**, 1660 (1960).

(13) R. M. Keefer and L. J. Andrews, *J. Amer. Chem. Soc.*, **74**, 1891 (1952).

Long, freely rotating alkyl chains were shown to decrease the blue shift of the iodine transition distinctly as compared with the compact, branched members of the same solvent classes. Since, however, the alkyl halides have interaction radii varying considerably in size from the chlorides to the iodides, it is difficult to explain how the steric effect of a normal chain can be similar in magnitude in the various halide solvents, as is observed (Figure 1). It is possible that in the regions of weak interactions contact charge transfer of iodine with the alkyl groups occurs superimposed on the interactions with the halogen atoms. There is spectroscopic[14] and thermodynamic[15] evidence that such interactions between iodine and saturated hydrocarbons exist. This problem is being studied in greater detail at present.[7]

Acknowledgments. This work was carried out in the laboratory of the Department of Chemistry of the University of California at Berkeley, and is supported by the National Science Foundation under a contract administered by Professor J. H. Hildebrand. The author wishes to thank Professor Hildebrand for his continued interest and encouragement throughout the course of these studies.

(14) (a) D. F. Evans, *J. Chem. Phys.*, **23**, 1424, 1426, 1429 (1955); (b) H. S. Hastings, *et al.*, *J. Amer. Chem. Soc.*, **75**, 2900 (1953).

(15) J. H. Hildebrand and J. Dymond, *Proc. Nat. Acad. Sci.*, **54**, 1001 (1965).

Reactions of Hydrocarbons with Mixtures of Active Nitrogen and Hydrogen Atoms. II. "Anomalous" Reactions: the Reactions of Cyanogen, Hydrogen Cyanide, and Acetylene

by David R. Safrany[1] and Walter Jaster

Atomic Energy of Canada Limited, Whiteshell Nuclear Research Establishment, Pinawa, Manitoba, Canada
(Received February 6, 1968)

The reactions of cyanogen, acetylene, and hydrogen cyanide with mixtures of active nitrogen and H atoms have been studied in a very fast flow, low-pressure (50 m/sec linear velocity and 0.2 mm of pressure) Wood-Bonhoeffer apparatus. The reaction of $(CN)_2$ with active nitrogen is explained by a branching chain reaction involving C_2N radicals and C atoms: $CN + N \rightarrow N_2 + C$; $C + (CN)_2 \rightarrow C_2N + CN$; $C_2N + N \rightarrow 2CN$. The reactions of C_2H_2 and HCN with active nitrogen also proceed by this mechanism, except that in these systems (1) $(CN)_2$ is first produced by the initial reactions of C_2H_2 and HCN and (2) the $(CN)_2$ chain reaction is perturbed by the presence of C_2H_2 or HCN, respectively. Upon addition of H atoms to the $(CN)_2 + N$ system, all the N atoms present, as measured by NO titration, form HCN owing to the occurrence of the reaction $H + C_2N \rightarrow HCN + C$. The addition of H atoms to the $C_2H_2 + N$ system has less effect upon HCN formation, even though the $(CN)_2$ chain reaction predominates in this system, because C_2H_2 competes strongly with C_2N for H atoms. The reaction of $(CN)_2$ was found to be strongly inhibited by hydrocarbons, because CN radicals abstract and replace H atoms. Because of this inhibition, any $(CN)_2$ that may be produced in reactions of hydrocarbons with active nitrogen merely remains an inert constituent of the mixture, even though the reaction of $(CN)_2$ *alone* is extremely fast.

Introduction

Recently we reported a study of the reactions of alkenes and alkanes with mixtures of active nitrogen and H atoms.[2] We proposed that both NH radicals and HCN are produced in these systems by the parallel alkyl radical reactions

$$C_nH_{2n+1} + N \longrightarrow NH + C_nH_{2n} \quad (1)$$

$$C_nH_{2n+1} + N \longrightarrow HCN + C_{n-1}H_{2n-1} + H \quad (2)$$

In the absence of large concentrations of H atoms, NH radicals disproportionate to form N_2 by the reaction

$$NH + NH \longrightarrow N_2 + 2H \quad (3)$$

Owing to the occurrence of reaction 3, only a fraction, about one-half, of the N atoms present, as measured by

(1) To whom correspondence should be sent.

(2) D. R. Safrany and W. Jaster, *J. Phys. Chem.*, **72**, 518 (1968).

titration with NO,[3,4] are converted to HCN. Reaction 3 can be suppressed by adding H atoms, however, and the HCN formation can be increased to agree with the N atom concentration determined by the NO titration, because NH radicals are consumed by the reaction

$$H + NH \longrightarrow H_2 + N \qquad (4)$$

The N atoms that would form N_2, in the absence of H atoms, by reactions 1 and 3 are regenerated by reaction 4 and are recycled until they all eventually form HCN.

We have denoted reactions of hydrocarbons with active nitrogen in which N_2 is produced by disproportionation of NH radicals "normal" reactions.[2] From studies of five alkenes and alkanes, we concluded that the reactions of most alkenes and alkanes with active nitrogen can be explained by our mechanism.[2]

In contrast to alkene and alkane reactions, we found that addition of H atoms to the reaction of acetylene with active nitrogen did not give quantitative conversion of N atoms to HCN. This anomalous behavior could be explained if species other than NH radicals are the N_2 precursor(s) in this system; if NH radicals are not produced, reaction 4 could not regenerate N atoms.

This other N_2 precursor could be the CN radical, which is known to be a minor species in hydrocarbon-active nitrogen systems[5,6] but which might be a major intermediate in reactions of substances containing less hydrogen than alkenes and alkanes. Alkenes and alkanes, which are rich in hydrogen, might be anticipated to preferentially form NH radicals, while substances containing less hydrogen might be expected to form CN radicals.

To further elucidate, therefore, the nature of the N_2 precursor in hydrocarbon-active nitrogen systems, we studied the reactions of active nitrogen with $(CN)_2$, a substance containing no hydrogen, and with HCN and C_2H_2, substances containing little hydrogen. As will become apparent, CN radicals are indeed the N_2 precursor in these systems. Furthermore, the basically different behavior of the over-all reactions of these substances with active nitrogen, compared with the reactions of alkenes and alkanes,[5] also owes itself to reactions of CN radicals. We denote, therefore, the reactions of active nitrogen with $(CN)_2$, HCN, and C_2H_2 "anomalous" reactions.

Experimental Section

The preparation of gases used in this investigation as well as the apparatus and experimental technique are given in part I of this series of papers.[2]

Results

1. Visual Behavior of Reaction Flames. Our key observation is the striking similarity of the $(CN)_2$, C_2H_2, and HCN reactions under certain conditions. Although a flame could be produced in all three reactions, the N_2 afterglow was never completely quenched, even when the reactant was added in large excess. In contrast to the reactions of alkenes and alkanes, in which the reactions go to complete consumption of the reactive species,[2,5] reactive species survived downstream from the reaction flame. This survival of reactive species has never been reported by others, or observed by us for any substances other than $(CN)_2$, C_2H_2, and HCN, and provides strong evidence for our conclusion that the basic reactions in these systems are the same.

a. Cyanogen Experiments. The addition of small quantities of $(CN)_2$ to active nitrogen led to formation of the short, intense red-violet reaction flame observed by others.[6] As mentioned above, however, complete quenching of the nitrogen afterglow was never observed. Instead, a diffuse pink-white light emission, which was easily discerned but which had not been reported by previous investigators, could be seen downstream from the reaction flame. This pink-white afterglow extended beyond the cold trap into the vacuum pump, a distance of about 10 m, and corresponded to a reaction time of several seconds for the reactions responsible for the afterglow. Examination of the afterglow with a hand spectroscope showed a series of narrow bands covering the entire visible region of the spectrum, which presumably were the CN red and violet band systems. Weakly superimposed on this spectrum were the red, yellow, and green components of the N_2 first positive band system normally observed in the Lewis–Rayleigh afterglow, showing that a small concentration of N atoms remained.

H atoms for our mixed-atom experiments were produced by subjecting molecular H_2 to an electrical discharge. When H_2 was added to the $(CN)_2$ + N reaction but before the H atom discharge was activated, the reaction *flame* was substantially quenched while the pink-white afterglow *downstream* increased in intensity. In addition, the weak nitrogen afterglow superimposed on the pink afterglow also increased in intensity to the extent that it could now be discerned with the unaided eye, showing that fewer N atoms were consumed when molecular H_2 was present.

When atomic H was present (produced by activating the discharge tube through which H_2 flowed), the reaction rate increased so that the *flame* reappeared, while the pink-white afterflow decreased to about the same intensity as in the absence of H_2, showing that

(3) G. B. Kistiakowsky and G. G. Volpi, *J. Chem. Phys.*, **27**, 1141 (1957).

(4) P. Harteck, R. R. Reeves, and G. Mannella, *ibid.*, **29**, 608 (1958).

(5) H. G. Evans, G. R. Freeman, and C. A. Winkler, *Can. J. Chem.*, **34**, 1271 (1956).

(6) C. Haggart and C. A. Winkler, *ibid.*, **38**, 329 (1960).

N atoms were again almost, but not completely, consumed.

To determine the concentration of N atoms surviving downstream from the reaction flame, we attempted to titrate the pink-white afterglow with NO. Instead of the usual decrease in afterglow intensity when small quantities of NO are added to active nitrogen,[3,4] we observed an intense red chemiluminescence. Examination of the chemiluminescence with a hand spectroscope again showed the presence of CN bands. Addition of NO in excess of that required to cause emission of CN radiation gave a sharp transition from the CN chemiluminescence to an intense green-white air afterglow, showing that the N atoms present were consumed, that O atoms were produced, and that the O atoms produced did not react with $(CN)_2$.[7] Owing to interference, by the enhanced emission of CN radiation, with the visual endpoint of the NO titration, no further attempt was made to measure the concentration of N atoms.

Occasionally, at some apparently critical concentration of $(CN)_2$, low-pressure explosions (which appeared as flame fronts, with bright emission of CN radiation and which would diffuse upstream against the flowing gases or propagate rapidly into the "dead spaces" of the apparatus) were observed in the 30 cm in diameter cold trap. Since the pressures in the system were typically 0.1–0.2 mm, this suggests that branching chain reactions occurred under these conditions.

Large quantities of the brown-black polymer observed by earlier workers[6] and which rapidly dirtied the reaction vessel were produced at all flow rates of $(CN)_2$. Most of the polymer was produced in the region of the reaction flame (about 5–50 cm downstream from the $(CN)_2$ inlet), but smaller quantities were also produced downstream. In agreement with earlier workers, polymer formation was inhibited by the molecular H_2 necessarily present in our mixed-atom experiments.[6]

b. Acetylene Experiments. Addition of small quantities of C_2H_2 to active nitrogen ($[N] \approx 100\ [C_2H_2]$) did not produce a flame but gave a slow reaction; the weak CN radiation from this reaction extended downstream into the vacuum pump and appeared similar to the pink-white light emission observed downstream from the reaction flame of the $(CN)_2$ reaction. In contrast to the $(CN)_2$ reaction, very little polymer was produced at these low C_2H_2 flow rates.

When slightly more C_2H_2 was added ($[N] \approx 20\text{-}[C_2H_2]$), the reaction shortened to about 10 cm in length and a *flame*, corresponding to a fast reaction of 2–3 msec in duration, with a bright emission of CN radiation formed at the C_2H_2 inlet. At this concentration of C_2H_2, the nitrogen afterglow was again, as with the $(CN)_2$ reaction, almost but not completely quenched; the pink-white light emission observed when smaller amounts of C_2H_2 were added could still be weakly seen downstream. At this concentration of C_2H_2, the reaction appeared very similar to the $(CN)_2$ reaction. Large quantities of brown-black polymer were also formed and rapidly dirtied the walls of the reaction vessel, also in a manner analogous to the $(CN)_2$ reaction. Under these conditions, the reaction displayed the behavior discribed by earlier workers.[8]

When more C_2H_2 was added ($[C_2H_2] \geq [N]$), the reaction flame itself was quenched by the additional C_2H_2, and the pink-white afterglow, observed when smaller quantities of C_2H_2 were added, increased in intensity and could once again be easily seen downstream.

Polymer formation was also inhibited when these large concentrations of C_2H_2 were present.

c. HCN Experiments. Owing to the toxicity of HCN and the large gas flows required in our apparatus, the reaction of HCN with active nitrogen was only studied semiquantitatively. Even our rather limited observations concerning this reaction, however, provide important information concerning the mechanism and clearly show the relation of this system to the $(CN)_2$ and C_2H_2 systems.

The reaction of HCN with active nitrogen appeared similar to the C_2H_2 reaction; *viz.*, addition of small quantities of HCN ($[N] > [HCN]$) led to a slow reaction, while addition of larger quantities ($[HCN] > [N]$) gave the bright red-violet reaction flame typical of the $(CN)_2$ or C_2H_2 reactions.[5,6,8] When $[HCN] > [N]$, moreover, N atoms were rapidly consumed, although, as with the $(CN)_2$ and C_2H_2 reactions, the N_2 afterglow was never completely quenched and the "typical" pink-white afterglow could be seen downstream. The only products were a small quantity of $(CN)_2$ (about 5% of the N atom concentration) and H_2, in stoichiometric quantities corresponding to the HCN consumed.

Addition of H_2 for the mixed-atom experiments quenched the flame and the slow reaction, peculiar to the $(CN)_2$ and C_2H_2 reactions, was again observed. Activation of the H atom discharge increased the reaction rate somewhat (as shown by formation of a weak flame), but the pink-white afterglow was quenched only to a slightly greater extent than in the absence of atomic H.

2. Analysis of Polymers. Since the polymers in the C_2H_2 + N and $(CN)_2$ + N systems appeared similar, both visually (brown-black) and in the manner in which they appeared to be formed on the walls of the reaction vessel (5–50 cm downstream from the reactant

(7) N atoms are consumed and an equivalent number of O atoms are produced by the very fast reaction[3,4] $N + NO \rightarrow N_2 + O$. The green-white chemiluminescence is owed to the very slow reaction of the O atoms produced with the NO added in excess of that required to consume the N atoms present, according to $NO + O \rightarrow NO_2 + h\nu$. Survival of the air afterglow in the presence of large concentrations of $(CN)_2$ moreover, shows that the reaction of O atoms with $(CN)_2$ was negligibly slow under our conditions.

(8) J. Versteeg and C. A. Winkler, *Can. J. Chem.*, 31, 129 (1953).

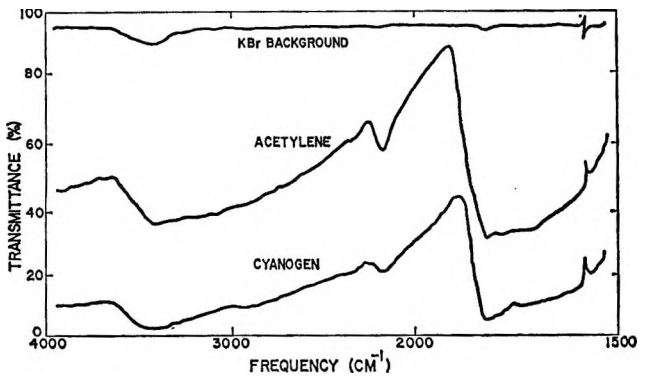

Figure 1. Infrared absorption spectra of polymers produced in the $(CN)_2$ + N and C_2H_2 + N reactions.

inlet), carbon–hydrogen–nitrogen, and infrared–absorption analyses were obtained to determine their properties. Table I gives the results of the C–H–N analyses. The mean nitrogen content of 32.7 wt % for the polymer produced in our C_2H_2 + N systems agrees well with the 32% found by earlier workers for this substance.[8] Figure 1 compares the infrared spectra of the polymers, which, as can be seen, are similar. The interpretation of these data is discussed in section 3 of the Discussion.

Table I: Composition of Polymers Produced in the C_2H_2 + N and $(CN)_2$ + N Reactions

Reaction	Wt % Carbon	Hydrogen	Nitrogen	Empirical formula
C_2H_2 + N	63.3	4.70	32.6	$C_{2.26}H_{2.02}N$
C_2H_2 + N	63.2	4.51	32.8	$C_{2.26}H_{1.94}N$
$(CN)_2$ + N	51.8	...	48.2	$C_{1.25}N$
$(CN)_2$ + N	52.2	...	48.0	$C_{1.27}N$

3. Formation of C_2HCN in the C_2H_2 + N and $(CN)_2$ + N Systems. The similar behavior of the C_2H_2 and $(CN)_2$ *flame* reactions suggested that $(CN)_2$ is produced in early stages of the C_2H_2 reaction and that, once an optimum rate of $(CN)_2$ formation has been attained, the extremely rapid reaction of $(CN)_2$ with N atoms occurs. As will be seen in the Discussion, we propose branching chain reactions of CN radicals for the basic mechanism of the $(CN)_2$ reaction. Since C_2HCN has, moreover, been observed mass spectrometrically to be a product of the C_2H_2 + N reaction,[9] the self-inhibition of the over-all reaction, therefore, when large concentrations of C_2H_2 are added, might be ascribed to the consumption of CN radicals by the reaction proposed by Herron[9]

$$CN + C_2H_2 \longrightarrow C_2HCN + H \qquad (5)$$

To elucidate further the role of C_2HCN in the C_2H_2 + N system, we looked for this substance and found that its concentration first increased, then decreased, and then increased again upon addition of C_2H_2 to active nitrogen. Interestingly, the formation of C_2HCN paralleled, approximately, the formation of $(CN)_2$, which had previously been found to follow this behavior.[8] These results are shown in Figure 2.

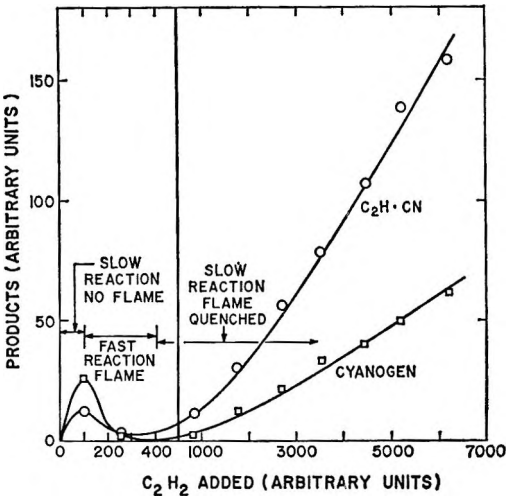

Figure 2. Formation of $(CN)_2$ and C_2HCN in the reaction of acetylene with active nitrogen.

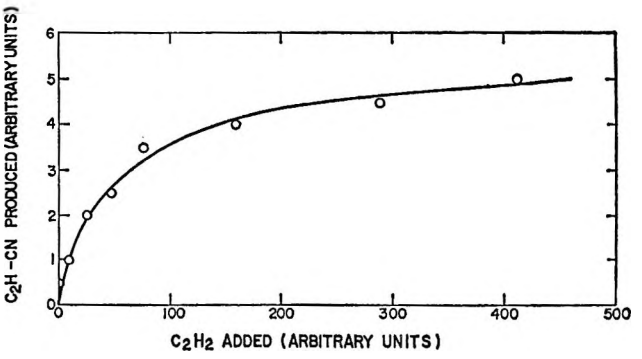

Figure 3. Formation of C_2HCN when C_2H_2 is added to the reaction of cyanogen with active nitrogen.

If C_2HCN is indeed produced in the C_2H_2 + N system by reaction of CN radicals according to reaction 5, this substance should also be produced if C_2H_2 is added to a $(CN)_2$ + N system, since CN radicals are certainly present in the latter system.[6] The results of adding C_2H_2 to the latter system are shown by Figure 3. The increase to a maximum is qualitatively the behavior to be expected for a simple competition for CN by C_2H_2.

C_2HCN was not available for calibration of the mass spectrometer and was, therefore, only identified by the peaks observed at mass-to-charge ratios of 51 and 50. Consequently, the concentrations in Figures 2 and 3 are given in arbitrary units.

4. Addition of H Atoms to the $(CN)_2$ + N System—

(9) J. T. Herron, J. L. Franklin, and P. Bradt, *Can. J. Chem.*, **37**, 579 (1959).

Table II: Formation of HCN in the Reaction of $(CN)_2$ with Active Nitrogen, Hydrogen Atoms, and with Mixtures of Hydrogen Atoms and Active Nitrogen, Effect of H_2 and NH_3

	Expt	Products, μ						
		H_2	N_2	$(CN)_2$	HCN	NH_3	NO	HCN:NO
(1)	(a) $N_2 + (CN)_2$	...	115	15.1	...	...	...	...
	(b) $N + (CN)_2$	...	125	9.4	...	...	...	...
	(c) NO titration	...	...	...	...	...	17.1	...
(2)	(a) $N_2 + H_2 + (CN)_2$	99.3	24.5	6.38	...	...	...	...
	(b) $N + H_2 + (CN)_2$	95.5	24.7	4.79	2.26	...	...	0.36
	(c) $H + N_2 + (CN)_2$	104	24.5	5.92	1.03	...	...	0.16
	(d) $H + N + (CN)_2$	90.1	24.8	3.02	7.40	...	...	1.17
	(e) NO titration	...	...	...	...	...	6.35	...
(3)	(a) $N_2 + (CN)_2 + NH_3$	...	107	23.4	...	47.5	...	...
	(b) $N + (CN)_2 + NH_3$	...	104	21.4	3.40	45.5	...	0.20
	(c) NO titration	...	...	...	...	...	17.1	...

Formation of HCN. CN *radicals* are known to react with H-containing substances. H_2[6] and NH_3[10] form HCN, while CH_4 forms both HCN and CH_3CN.[6] *Molecular* $(CN)_2$ reacts with H atoms, also forming HCN.[11,12] It was not surprising, therefore, to find that HCN was produced in our mixed-atom experiments even when only one discharge at a time, *viz.*, either N or H, was activated, since CN radicals and H atoms were produced in these experiments.

Table II experiment 2a gives the composition of the gas mixture prior to the activation of the discharge. Experiment 2b gives the formation of HCN with the *N atom* discharge alone activated; the 2.26 μ of HCN produced under these conditions is the HCN produced by the reaction of CN radicals formed in the $(CN)_2$ + N reaction with H_2[6]

$$CN + H_2 \longrightarrow HCN + H \qquad (6)$$

Experiment 2c gives the formation of HCN with the H atom discharge alone activated; the 1.03 μ of HCN produced in this experiment is the HCN produced by the reaction of H atoms with $(CN)_2$[11,12]

$$H + (CN)_2 \longrightarrow HCN + CN \qquad (7)$$

With *both* discharges activated, the HCN produced was strikingly increased over that produced when either the N or H atom discharge alone was activated. Experiment 2d, moreover, shows that the HCN produced under these conditions was not merely the sum of that produced in experiments 2b and c but was more than double this amount, *viz.*, 7.40 μ compared with 2.26 + 1.03 = 3.29 μ. The additional HCN produced in the mixed-atom experiments, therefore, corresponds to the reaction of H atoms with an intermediate produced in the $(CN)_2$ + N reaction.

It can be seen that the total HCN produced in experiment 2d *exceeded* the NO titration value for the N atom concentration, 6.35 μ, shown by experiment 2e. Furthermore, the increase in HCN, upon activation of the N atom discharge, over that produced by activation of the H atom discharge alone (the difference between experiment 2d and 2c) equalled the N atom concentration, showing that all the N atoms present formed HCN.

As in our previous paper,[2] H atom concentrations were not measured for these experiments but, again, probably approximated N atom concentrations.[11]

Experiments 3a–c show the formation of HCN when NH_3 was added to the reaction of $(CN)_2$ with N atoms and confirm the general ability of CN radicals to abstract H from H-containing substances.

The blank experiments 1a–c ensured that HCN was not formed in the absence of H-containing substances.

5. Addition of H Atoms to the C_2H_2 + N System. As will be discussed later, we conclude that the similarity of the C_2H_2 and $(CN)_2$ reactions is owed to the formation of large concentrations of $(CN)_2$ in the former system, with the result that the observed reaction is, in reality, that of $(CN)_2$ with N atoms but perturbed by the presence of C_2H_2. It might be anticipated, therefore, that, analogous to the $(CN)_2$ reaction, N atoms would also be quantitatively converted to HCN upon addition of H atoms to the C_2H_2 + N system.

Table III, however, shows that this is not the case. Experiment 4b shows that 1.02 μ of HCN was produced in the reaction of C_2H_2 with N atoms alone. In contrast to the $(CN)_2$ system, the addition of H atoms, experiment 4c, increased the HCN to only 2.13 μ, well below the N atom concentration measured by the NO titration, 3.93 μ, shown in experiment 4d.

We suspected, therefore, that even though $(CN)_2$ was indeed produced in early stages of the C_2H_2 reaction, the C_2H_2 necessarily present was preventing HCN for-

(10) I. M. Campbell and B. A. Thrush, *Proc. Chem. Soc.*, 410 (1964).
(11) K. H. Geib and P. Harteck, *Ber. Deut. Chem. Ges.*, **B66**, 1815 (1933).
(12) C. Haggart and C. A. Winkler, *Can. J. Chem.*, **37**, 1791 (1959).

Table III: Formation of HCN upon Addition of Hydrogen Atoms to the Reaction of C_2H_2 with Active Nitrogen

	Expt	Products, μ					
		N_2	H_2	C_2H_2	HCN	NO	HCN:N
(4)	(a) $N_2 + H_2 + C_2H_2$	120	45.6	42.0	...	...	...
	(b) $N + H_2 + C_2H_2$	120	45.5	40.6	1.02	...	0.26
	(c) $N + H + C_2H_2$	120	45.5	39.8	2.13	...	0.54
	(d) NO titration	...	...	...	...	3.93	...

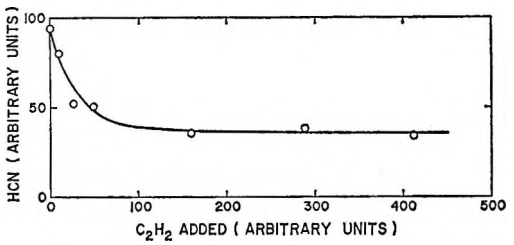

Figure 4. Effect of C_2H_2 upon the formation of HCN in the $(CN)_2 + N + H$ System.

mation by rapidly combining H atoms by the reactions[13]

$$C_2H_2 + H \longrightarrow C_2H_3 \quad (8)$$

$$C_2H_3 + H \longrightarrow C_2H_2 + H_2 \quad (9)$$

before H atoms could react with the HCN precursors produced in the concurrent $(CN)_2$ reaction.

If this is indeed the case, addition of C_2H_2 to a $(CN)_2 + N + H$ system (in which N atoms are quantitatively converted to HCN by reactions of H atoms with reaction intermediates, experiment 2d Table II) should also reduce HCN formation because of competition of reactions 8 and 9 with the reactions that form HCN. Figure 4 shows the effect of adding C_2H_2 to a $(CN)_2 + N + H$ system and illustrates the striking extent to which HCN formation is suppressed.

6. Mass Spectra of Polymers and Condensation Products Observed in the $(CN)_2 + N$ and $C_2H_2 + N$ Systems. To obtain an insight into the mechanisms of the over-all $(CN)_2 + N$ and $C_2H_2 + N$ reactions, we looked for stable dimers and higher polymers of radicals likely to be present in these systems. For these experiments, the mass spectra of the $(CN)_2 + N$ and $C_2H_2 + N$ systems were monitored on an oscilloscope, while the concentration of $(CN)_2$ or C_2H_2 was varied until the polymer peaks of interest attained their maximum amplitudes. The mass spectra were then recorded at these maxima.

These experiments showed a peak at mass-to-charge ratio of 76 in the $(CN)_2 + N$ system, which corresponds to dicyanoacetylene, $C_2(CN)_2$, the dimer of C_2N. In contrast to the latter system, the mass spectrum of the $C_2H_2 + N$ system showed peaks at mass-to-charge ratios of both 76 *and* 75, corresponding to condensation products composed of combinations of C$_2$H and CN radicals and, surprisingly, C atoms. No attempt was made to unequivocally characterize the peaks at *m/e* 76 and 75, but these correspond to species such as

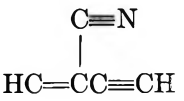

and

respectively, in addition to contributions from $C_2(CN)_2$. The kinetic origins of these substances are discussed in detail later.

The maximum concentrations of volatile condensation products were estimated from these spectra to be about 0.01% of the N atom concentration. Since these peaks probably correspond to the more stable, partially polymerized products, these concentrations are significant, because they clearly represent only a small fraction of the total polymer produced. Most of the high molecular weight products of the reactions are formed as nonvolatile solids at the walls of the reaction vessel and are, therefore, not detectable mass spectrometrically.

7. Mixtures of $(CN)_2$ with Hydrocarbons. The $(CN)_2 + N$ chain reaction could be inhibited by adding H_2, NH_3, or C_2H_2. To determine whether this apparently general inhibiting effect of hydrogen-containing substances included all hydrocarbons, we added arbitrarily chosen hydrocarbons, *viz.*, propylene, isobutylene, and methylacetylene, to $(CN)_2 + N$ systems.

The concentration of $(CN)_2$ given in Table IV, column 6, shows the lack of reaction under these conditions, while column 7 shows the formation of HCN. The lack of appreciable consumption of $(CN)_2$ under these conditions should be compared with the large consumption when hydrocarbons are absent. See Table II, experiments 1a–c.

These experiments show that, in all cases, despite the fact that $(CN)_2$ *alone* reacts extremely rapidly with active nitrogen, the consumption of $(CN)_2$ by N atoms is completely inhibited when hydrocarbons are present. Furthermore, the rate of the *hydrocarbon* + N reaction

(13) E. W. R. Steacie, "Atomic and Free Radical Reactions," Reinhold Publishing Corp., New York, N. Y., 1954.

Table IV: Consumption of $(CN)_2$ When Added to the Reactions of C_3H_6, i-C_4H_8, and CH_3C_2H with Active Nitrogen

			Products, μ							
		Expt	H_2	N_2	C_3H_6	i-C_4H_8	CH_3C_2H	$(CN)_2$	HCN	NO	HCN:N
(5)	(a)	$N_2 + H_2 + C_3H_6 + (CN)_2$	81.2	31.0	11.1	...	...	6.92	...	...	...
	(b)	$N_2 + H + C_3H_6 + (CN)_2$	74.6	28.6	7.0	...	...	6.85	0.20	...	0.014
	(c)	$N + H_2 + C_3H_6 + (CN)_2$	96.6	29.9	6.8	...	...	7.08	10.3	...	0.71
	(d)	$N + H + C_3H_6 + (CN)_2$	86.9	31.1	2.01	...	...	6.60	14.0	...	1.0
	(e)	NO titration	...	...	...	...	...	...	...	14.0	...
(6)	(a)	$N_2 + H_2 + i$-$C_4H_8 + (CN)_2$	80.9	34	...	7.91	...	7.39	...	...	...
	(b)	$N_2 + H + i$-$C_4H_8 + (CN)_2$	81	33.7	...	7.05	...	7.28	0.68	...	0.051
	(c)	$N + H_2 + i$-$C_4H_8 + (CN)_2$	95.5	31.8	...	6.18	...	7.20	7.54	...	0.57
	(d)	$N + H + i$-$C_4H_8 + (CN)_2$	97.3	28.6	...	4.50	...	6.80	12.8	...	0.96
	(e)	NO titration	...	...	...	...	...	...	...	13.3	...
(7)	(a)	$N_2 + H_2 + CH_3C_2H + (CN)_2$	74.2	28.5	...	...	19.5	8.0	...	...	...
	(b)	$N_2 + H + CH_3C_2H + (CN)_2$	65.6	31.4	...	...	15.2	7.79	0.68	...	0.05
	(c)	$N + H_2 + CH_3C_2H + (CN)_2$	83.9	25.8	...	...	12.1	7.97	7.59	...	0.56
	(d)	$N + H + CH_3C_2H + (CN)_2$	76.9	26.4	...	...	7.85	7.57	12.8	...	0.95
	(e)	NO titration	...	...	...	...	...	...	...	13.5	...

is completely unaffected by the presence of $(CN)_2$, the $(CN)_2$ behaving merely as an inert constituent of the mixture. Moreover, in the experiments with N atoms alone, HCN formation was the same as was produced in the absence of $(CN)_2$, *viz.*, about one-half of the NO titration value for N atoms, $[N]_{NO}$; *i.e.*, in experiment 6c HCN equals 7.54 μ and in experiment 6e $[N]_{NO}$ equals 13.3 μ. Similar results are shown by experiments 5c and e and 7c and e.

$(CN)_2$ behaves nearly as an inert gas even when H atoms are added to the hydrocarbon + N + $(CN)_2$ mixture; although some $(CN)_2$ is consumed by reaction 7, the only major effect is to increase HCN formation so that agreement with NO titration values for [N] is obtained. In the case of C_3H_6, for example, addition of H atoms, experiment 5d, increased HCN formation to 14.0 μ, compared with 10.3 μ for the N atom reaction without H atoms, experiment 5c. As discussed in the Introduction, this is the same behavior that is observed when hydrocarbons are added to active nitrogen in the absence of $(CN)_2$. The inert behavior of $(CN)_2$ under a variety of conditions, therefore, clearly shows (1) that the reactions of $(CN)_2$ with active nitrogen are minor when hydrocarbons are present and (2) that the reaction of the hydrocarbon in hydrocarbon + $(CN)_2$ + N systems proceeds independently of the reaction of $(CN)_2$.

Discussion

Standard heats of formation of substances referred to in this paper are presented in Table V. For the sake of convenience, $\Delta H_f°$, both from the elements, column 1, and from the gaseous atoms, column 2, are tabulated.

1. The Reaction of Cyanogen. Winkler[6] concluded that the reaction of $(CN)_2$ with active nitrogen proceeds by a *nonchain* mechanism in which CN and CN_2 radicals are the reactive intermediates. Other investigators[14,15] have proposed that the reaction proceeds *via* a *chain* mechanism involving, again, CN_2. According to Winkler,[6] CN_2 could be produced by the addition–decomposition reaction

$$(CN)_2 + N \longrightarrow [(CN)_2N] \longrightarrow CN + CN_2 \quad (10)$$

Bayes[14] proposed the two-body association reaction

$$CN + N \longrightarrow CN_2 \quad (11)$$

while Campbell and Thrush[10] proposed the three-body combination reaction

$$CN + N + M \longrightarrow CN_2 + M \quad (12)$$

In all these mechanisms, the CN_2 radical was postulated to react rapidly with N atoms by the reaction

$$CN_2 + N \longrightarrow N_2 + CN \quad (13)$$

Since reaction 13 regenerates CN radicals, this reaction, together with either reaction 11 or 12, constitutes a mechanism whose over-all effect is to catalytically combine N atoms.

Our proposed mechanism for the $(CN)_2$ + N reaction differs from those summarized above, in that we conclude that CN_2 radicals are only a minor species and that the important reactive intermediates, in addition to CN, are C_2N radicals and carbon atoms.

Since the length of the reaction flames corresponded to reaction times of only 1–3 msec even under our conditions of 0.1–0.2 mm of pressure and since we occasionally observed low-pressure explosions, we also propose that the reaction occurs by a chain mechanism. We further postulate, however, that the reaction proceeds by a *branching* mechanism involving CN radicals as the chain-branching species.

(14) K. D. Bayes, *Can. J. Chem.*, 39, 1074 (1961).
(15) N. H. Kiess and H. P. Broida, *Symp. Combust., 7th*, 207 (1959).

Table V: Standard Heats of Formation, $\Delta H_f°$, of Substances at 25° in the Gas Phase[a]

Substance	$\Delta H_f°$, kcal/mol: From the element	From the gaseous atoms
H	52	0
H_2	0	−104
N	113	0
N_2	0	−225
O	60	0
O_2	0	−120
C(g)	171	0
C(graphite)	0	−171
CN	97	−187
$(CN)_2$	74	−493
C_2N	133 (± 30)	−322
CN_2	140	−256
NCN	103	−293
HCN	30	−306
$C_2(CN)_2$	126	−783
$C_2(CN)$	137	−489
N≡CCC≡N	150	−588
N≡C=C=C=N	158	−580
N≡CC=C=N	154	−584
C_2H_2	58	−388
CHCN	114	−393
C_2HCN	89	−589
$(C_2H)_2CN$	155	−917
N≡CCC≡CH	176	−673
N=C=C=C=CH	169	−680
C_2H	116	−278
CH_2	85	−190
C_2H_3	59	−439
NH	79	−86
NH_2	43	−174
NH_3	−9	−278
NO	23	−150
CO	−25	−256

[a] A negative ΔH refers to the enthalpy change for an exothermic process.

The source of trace concentrations of CN radicals for chain initiation is unimportant to explain a chain branching reaction sequence, but we have evidence which suggests that the initial reaction is the reaction

$$(CN)_2 + N_2^* \longrightarrow N_2 + 2CN \qquad (14)$$

where N_2^* denotes an electronically excited molecule.[16-18] Once a few CN radicals have been produced, the following sequence of reactions can explain our observations. CN radicals can react according to reaction 15, which is followed by the C-atom reaction 16, to give C_2N. C_2N can then react with N atoms to give two CN radicals by the chain-branching step, reaction 17

$$CN + N \longrightarrow N_2 + C \qquad (15)$$

$$(CN)_2 + C \longrightarrow C_2N + CN \qquad (16)$$

$$C_2N + N \longrightarrow 2CN \qquad (17)$$

The extremely fast rate of the over-all reaction is readily explained if reactions 15–17 are fast.

ΔH for reaction 15 is −38 kcal/mol. The heat of formation of C_2N is not very well known but, in order that reaction 16 occur readily under our experimental conditions, must be of the order of 149 kcal/mol. This value is well within the value of 133 ±30 kcal/mol reported by Merer and Travis.[19] Furthermore, a value of 144 kcal/mol can be calculated by assuming that the ratio of the heat of atomization (ΔH_a) of Si_2N to that of $C_2N(g)$ is equal to the ratio of the dissociation energies of SiN(g) and CN(g). $\Delta H_f°$ for HCN and $(CN)_2$ have been calculated using calorimetric data, given in Lewis and von Elbe,[20] for the heats of combustion of HCN and $(CN)_2$. These yield values for $\Delta H_f°$ of 30 kcal/mol for HCN and 74 kcal/mol for $(CN)_2$. The value of $\Delta H_f°$ for CN, 97 kcal/mol, corresponding to $D_{CN} = -187$ kcal/mol, has been taken from Gaydon.[21] For further discussion of these values, see the Appendix.

After N atoms are consumed, C atoms can again attack $(CN)_2$ *via* reaction 16, but, *in the absence of N atoms,* C_2N and CN radicals diffuse to the walls of the reaction vessel and polymerize

$$C_2N \xrightarrow{\text{walls}} \text{polymer} \qquad (18)$$

$$CN \xrightarrow{\text{walls}} \text{polymer} \qquad (19)$$

The effects of additives are explained by reactions of the additives with radicals produced in the system. Clearly, the over-all reaction is inhibited by H_2, NH_3, and C_2H_2, because CN radicals are consumed by reactions such as reactions 5, 6, and 20

$$CN + NH_3 \longrightarrow HCN + NH_2 \qquad (20)$$

Since CN radicals are a major chain carrier, the over-all reaction is inhibited.

The large increase in HCN formation upon addition of H atoms can be explained by reaction of H atoms with C_2N radicals by the reaction

(16) Briefly, we have found that addition of CO to the reaction of $(CN)_2$ with active nitrogen completely inhibits the over-all reaction. CO has the strongest binding energy of any diatomic molecule ($D_{CO} \equiv 256$ kcal/mol[17]) and cannot, therefore, be attacked in a two-body reaction by any species at room temperature. We attribute the inhibition by CO, therefore, to the energy-transfer reaction $N_2^* + CO \rightarrow N_2 + CO^*$, where CO* does not dissociate $(CN)_2$. This conclusion is discussed in detail in the following article.

(17) J. L. Cottrell, "The Strengths of Chemical Bonds," Butterworth and Co. Ltd., London, 1958.

(18) Neither the concentration nor the identity of the N_2^* need be considered here, since only a small concentration would be required for chain initiation. By itself, the fact that the nitrogen afterglow emits radiation from the N_2 first positive band system ($N_2B^3\pi g \rightarrow N_2A^3\Sigma_u^+$), shows that at least a small concentration of N_2^*, with enough energy to dissociate $(CN)_2$, must be present.

(19) A. J. Merer and D. N. Travis, *Can. J. Phys.*, **44**, 353 (1966).

(20) B. Lewis and G. von Elbe, "Combustion, Flames and Explosions of Gases," Academic Press Inc., New York, N. Y., 1951.

(21) A. G. Gaydon, "Dissociation Energies and Spectra of Diatomic Molecules," Chapman and Hall, Ltd., London, 1953.

$$H + C_2N \longrightarrow HCN + C \quad (21)$$

Consideration of the possible mechanisms for this increased HCN formation provides further insight into the nature of the reactive intermediates. If two-body addition of N to $(CN)_2$, which is discussed later, and three-body reactions are eliminated, the only other reasonable intermediate is CN_2. HCN could be produced from this species, upon addition of H atoms, by the reaction

$$H + CN_2 \longrightarrow HCN + N \quad (22)$$

We, however, exclude CN_2 as the major reactive intermediate for the following reasons.

(1) Reaction 22 regenerates N atoms. If CN_2 were the reactive intermediate and if reaction 22 were indeed the reaction responsible for increased HCN upon addition of H atoms, the formation of HCN would be independent of [N] and would equal the concentration of added *H atoms*, rather than that of *N atoms*, a requirement in conflict with our observations.

(2) The empirical formula of the polymer, $(C_{1.26}N)_x$, shows that the polymer is not merely a polymer of cyanogen, $[(CN)_2]_x$, or of CN radicals, $(CN)_x$, but contains more carbon than nitrogen. Again, if CN and/or CN_2 were the only reactive intermediates, the polymer would be expected to contain a greater atom ratio of nitrogen, since reactive intermediates are the polymer precursors.

(3) Dicyanoacetylene, $C_2(CN)_2$, the dimer of C_2N radicals, is observed as a product of the reaction while no compounds of nitrogen-rich species, *viz.*, of CN or CN_2, are observed.

These observations, therefore, provide evidence for our conclusions that the important intermediate in the $(CN)_2$ + N system is the C_2N radical and that increased HCN formation upon addition of H atoms owes itself to the occurrence of reaction 21 rather than reaction 22.

Evidence for the occurrence of reaction 15 is also given by items 2 and 3 above. Since, however, the polymers and condensation products of the C_2H_2 + N system are similar to those produced in the $(CN)_2$ + N system, details of polymer formation are presented after the discussion of the C_2H_2 + N system.

HCN formation *greater* than [N] determined by NO titration is also readily explained. Clearly, a fraction of the additional HCN will be produced by the competitive fast reaction of H atoms with $(CN)_2$, reaction 7.[11,12]

The chemiluminescence observed upon addition of NO downstream from the reaction flame is explained by reactions such as

$$C + NO \longrightarrow CN^* + O \quad (23)$$

$$N + NO \longrightarrow N_2 + O \quad (24)$$

followed by

$$C_2N + O \longrightarrow CN^{**} + CO \quad (25)$$

Reaction 23 is sufficiently exothermic ($\Delta H = -39$ kcal/mol) to excite CN to the $A^2\pi$ state, the principal CN-red emitting state, while reaction 25 can excite both the $A^2\pi$ and $B^2\Sigma^+$ electronic states[22] ($\Delta H \approx -100$ to -130 kcal/mol). The reaction

$$(CN)_2 + O \longrightarrow \text{products} + CN^* \quad (26)$$

can be eliminated because it is too slow to account for the observed light emission.[23]

We can only speculate about the reactions responsible for the long-lived pink-white afterglow that survives downstream from the reaction flame. Since, however, this afterglow emits both the N_2 first positive band system and the CN-red band system, N atoms and CN radicals must be present. The survival of N atoms in the presence of CN radicals is surprising, in view of the rather strong evidence which we have obtained for the occurrence of reaction 15 and which is presented in section 4 of the Discussion.

In spite of the occurrence of reaction 15, a certain N atom concentration is maintained by some mechanism as a consequence of the *kinetic* equilibrium among reactive species. If, as we suggest, C_2N radicals are also present in the reaction zone of the $(CN)_2$ reaction, the kinetic equilibrium might be maintained by a reaction such as the reaction

$$C_2N + CN \longrightarrow C_2(CN) + N \quad (\Delta H \sim 5 \text{ kcal/mol}) \quad (27)$$

which can regenerate N atoms. This reaction, of course, is also highly speculative and only illustrates the type of reaction that might be expected to occur.

CN radiation from the afterglow is more amenable to explanation. Downstream from the reaction flame, the surviving intermediates will be undergoing reactions leading to attainment of *thermodynamic* equilibrium. Since the chemiluminescent reactions persist downstream for reaction times of several seconds, a slow reaction is responsible for the CN radiation. It seems likely, therefore, that in the afterglow CN radicals are directly excited in three-body processes such as the reaction

$$C + N + M \longrightarrow CN^* + M \quad (28)$$

One point should be noted here. According to our mechanism, elemental carbon can never be a major product as long as $(CN)_2$ is present (the normal condition), since C atoms produced by reaction 15 will always react according to reaction 16. Furthermore, CN radicals are simultaneously regenerated by reaction 16. Our mechanism, therefore, explains the seemingly ambiguous requirements that reaction 15

(22) G. Herzberg, "Spectra of Diatomic Molecules," 2nd ed, D. Van Nostrand Co., Inc., Princeton, N. J., 1950.

(23) P. Harteck and U. Kopsch, *Z. Physik. Chem.*, B12, 327 (1931).

occur rapidly, that elemental carbon not be the major solid product and, yet, as shown by the inhibiting effect of hydrogen-containing substances, that CN radicals be an important intermediate.

We exclude as the initial reaction a two-body addition of N to $(CN)_2$, with subsequent unimolecular decomposition of the energy-rich adduct, according to reaction 10, because the reaction was found to be efficiently inhibited by substances which react with the postulated chain carriers, CN radicals and C atoms, but which do not react with either $(CN)_2$ or N atoms. This behavior could not be the case if the only role of additives was to compete with N atoms for the initial reaction with $(CN)_2$ (or with $(CN)_2$ for reaction with N atoms). That the additives indeed react with chain carriers, in particular with CN radicals and not with the addition complex itself, is shown by the formation of HCN as a product when H_2 or hydrocarbons are added.

We only mention briefly here the effects of additives upon the $(CN)_2$ + N system. Complete description of the associated phenomena requires lengthy discussion and is, therefore, presented in detail in the next article.

2. The Reactions of C_2H_2 and HCN. When hydrocarbons react with active nitrogen, only small amounts of $(CN)_2$ (~0.1% of [N]) are produced.[5] The reaction of C_2H_2 is anomalous, since much larger quantities (~1–5% of [N]) are produced.[8,24]

HCN gave only a very slow reaction with active nitrogen when [N] > [HCN]. Under conditions such that flames are formed, however ([HCN] > [N]), the products are $(CN)_2$ and H_2.

These observations, the similar behavior of the $(CN)_2$, C_2H_2, and HCN reactions, and thermochemical considerations suggest that the $(CN)_2$ chain reaction plays an important role in the reactions of both C_2H_2 and HCN with active nitrogen. The over-all mechanisms of the latter reactions, however, are complicated by the presence of C_2H_2 or HCN, respectively.

a. The Reaction of C_2H_2. As described under Results, section 1b, the most striking feature of the C_2H_2 reaction is the strong dependence of the over-all reaction rate upon the concentration of C_2H_2. This behavior can be explained in terms of initial relatively slow reactions of C_2H_2 with N atoms which produce $(CN)_2$, followed at some critical concentration of C_2H_2 by (1) the extremely fast chain reaction of $(CN)_2$ discussed in the last section and (2) self-inhibition of the $(CN)_2$ reaction when further concentrations of C_2H_2 are added.

Our mechanism is

$$C_2H_2 + N \xrightarrow{k_{29}} CHCN + H \qquad (\Delta H = -6 \text{ kcal/mol}) \quad (29)$$

$$CHCN + N \xrightarrow{k_{30}} (CN)_2 + H \qquad (\Delta H = -99 \text{ kcal/mol}) \quad (30)$$

$$CHCN + N \xrightarrow{k_{31}} HCN + CN \quad (31)$$

$$CN + C_2H_2 \xrightarrow{k_5} C_2HCN + H \quad (5)$$

$$CN + C_2H_2 \xrightarrow{k_{32}} HCN + C_2H \quad (32)$$

$$[(CN)_2 + N] \xrightarrow{k_{33,\text{over-all}}} \text{products} \quad (33)$$

$$C_2H \xrightarrow{\text{walls}} \text{polymer} \quad (34)$$

$$C_2N, CN \xrightarrow{\text{walls}} \text{polymer} \qquad \text{(from concurrent } (CN)_2 \text{ reaction)} \quad (35)$$

The specific rate for the initial attack of C_2H_2 by N atoms has been reported by Avramenko and Krasnen'kov[25] to be ~3.2×10^{-16} cm³/molecule sec at 300°K, although these authors postulated that the initial attack of C_2H_2 is by the reaction

$$N + C_2H_2 \xrightarrow{k_{36}} CN - CH_2 \quad (36)$$

Both the initial reaction, however, and especially the specific rate given by these authors appear questionable, since the specific rate for $(CN)_2$ formation, $k_{\Delta(CN)_2}$, must be at least large enough to account for the large amounts of $(CN)_2$ produced in the C_2H_2 + N reaction.

Neglecting consumption of $(CN)_2$ by reactions subsequent to the initial reactions 29 and 30, we calculate, from the lengths of the reaction flames under our conditions, a lower limit for the specific rate for $(CN)_2$ formation of $k_{\Delta(CN)_2} \approx 6 \times 10^{-15}$ cm³/molecule sec. If, furthermore, the specific rates k_{30} and k_{31} are taken as typical of two-body reactions of radicals, *viz.*, ~10^{-12} cm³/molecule sec, the rate $k_{\Delta(CN)_2}$ will be rate limiting for $(CN)_2$ formation and the value of k_{29} can be taken as that of $k_{\Delta(CN)_2}$.

The rates k_5 and k_{32} are estimated to be ~10^{-15} cm³/molecule sec from the data of Robertson and Pease,[26] who found $\Delta H_a \approx 7$ kcal/mol for the analogous reaction of CN radicals with H_2, reaction 6. This moderate specific rate for CN radical reactions is in accord with the relatively large quantities of H_2 or C_2H_2 that we found necessary to inhibit the $(CN)_2$ + N reaction. The rate $k_{33,\text{over-all}}$ denoted by the bracketed reaction 33 corresponds to the over-all $(CN)_2$ chain reaction discussed in the last section and is extremely fast, $k_{33,\text{over-all}} \sim 10^{-11}$ cm³/molecule sec.

Qualitative support for our mechanism is given by the variation of $(CN)_2$ and C_2HCN with $[C_2H_2]$.

(24) D. R. Safrany, Ph.D. Thesis, Rensselaer Polytechnic Institute, Troy, N. Y., 1964.

(25) L. I. Avramenko and V. M. Krasnen'kov, *Izv. Akad. Nauk SSSR, Ser. Khim.*, **5**, 822 (1964).

(26) N. C. Robertson and R. N. Pease, *J. Chem. Phys.*, **10**, 490 (1942).

Refer to Figure 2. The initial increase in both $(CN)_2$ and C_2HCN during the *first* slow stage of the reaction (up to ~100 units of C_2H_2) is ascribed to the reaction sequence 29–32. The reaction is slow at this concentration of C_2H_2 because (1) the concentrations of reactants are low and (2) the relatively slow reaction 29 is rate limiting. At this concentration of C_2H_2, $(CN)_2$ formation is insufficient to initiate the secondary chain consumption of $(CN)_2$ by reaction 33, and $(CN)_2$ increases.

At some critical concentration of C_2H_2 (~200–400 units of C_2H_2), an optimum concentration of $(CN)_2$ is produced and the fast $(CN)_2$ chain reaction replaces reactions 29–32 as the predominant reactions. Also at this concentration of C_2H_2, the apparent over-all rate becomes extremely fast and the main features of the $(CN)_2$ + N reaction are observed, *viz.*, formation of a flame, polymer formation, etc. C_2HCN also decreases to very low concentrations under these conditions, because the over-all $(CN)_2$ reaction 33 consumes CN radicals much faster than they react to form C_2HCN by reaction 5.

The over-all reaction assumes a *second* slow stage upon addition of further concentrations of C_2H_2, because the $(CN)_2$ chain reaction is inhibited by the additional C_2H_2. Reactions 29–32 still occur, but in the absence of reaction 33, the over-all rate again assumes that of the slower reaction 29. Since $(CN)_2$ is no longer consumed, $(CN)_2$ increases while the increase in C_2HCN under these conditions simply represents the competition between CN radicals and N atoms for C_2H_2 by reactions 5, 29, and 32.

Our postulated initial attack of C_2H_2, reactions 29 and 30, deserves comment. One of the major difficulties in explaining the reactions of hydrocarbons with active nitrogen has been that direct attack of alkenes and alkanes by N atoms is either too endothermic to proceed at room temperatures or requires considerable molecular rearrangement. See, for example, reference 5. C_2H_2 seems to be unique, however, since its molecular structure is such that direct attack by N atoms is possible if N atoms replace H atoms according to our postulated reactions. Reactions 29 and 30 are energetically possible because of the large carbon–nitrogen bond strength in molecules, $D_{C\equiv N}$ = 210 kcal/mol when bound in molecules,[17] while $D_{C\equiv N}$ = 187 kcal/mol for the free molecule.[21]

HCN can be produced in the C_2H_2 + N system: (1) by reactions 31 and 32; (2) by reactions of the H atoms produced by reactions 5, 29, and 30, with C_2N radicals produced in the reaction sequence 33, as described in the last section; and (3) by reaction of H atoms with $(CN)_2$, reaction 7.

In addition to inhibiting the $(CN)_2$ reaction sequence, eq 33, the C_2H_2 necessarily present also perturbs the maximum amount of HCN that can be produced upon addition of even large concentrations of H atoms.

As described in the Results, section 4, addition of H atoms to the $(CN)_2$ + N system produces large amounts of HCN. As shown in Figure 4, however, this large concentration of HCN is dramatically reduced when C_2H_2 is added. We attribute this inhibition to rapid combination of H atoms by reactions 8 and 9, since the over-all rate for the latter reactions is moderately fast, $k_{8+9,\text{over-all}} \approx 10^{-14}$ cm^3/molecule sec.[27] H atoms are, therefore, consumed in competition with the reactions that form HCN. In view of this finding, it becomes clear that conditions are similar in the C_2H_2 + N system and that the anomalously low conversion of N atoms to HCN in this system upon addition of H atoms is owed to the rapid combination of H atoms by the C_2H_2 necessarily present.

Evidence for the occurrence of reactions 5 and 32 is argued as follows. There is no doubt that the C_2HCN formed upon addition of C_2H_2 to a $(CN)_2$ + N system is produced by reaction of CN radicals with C_2H_2, reaction 5. See Figure 3 and the Results, section 3. Extrapolating this finding to the C_2H_2 + N system, conditions are again similar to those of the former system, and it appears likely that C_2HCN is also produced in the C_2H_2 reaction by reaction 5.

Figure 4 shows that HCN formation is never completely suppressed, even under conditions when H atoms should be rapidly combined by the presence of large concentrations of C_2H_2. This finding suggests, therefore, that HCN is formed under these conditions by reactions not involving H atoms. The obvious reaction is the abstraction reaction 32.

Polymer formation in the C_2H_2 + N system is discussed after the reaction of HCN.

b. The Reaction of HCN. Although our quantitative data concerning the HCN + N system are very limited, the general features of this system are so similar to those of the $(CN)_2$ + N and C_2H_2 + N systems that we have little doubt that the major reaction is also the $(CN)_2$ chain reaction.

We must speculate about the initial formation of $(CN)_2$. Small concentrations of $(CN)_2$ might be formed by reactions such as reaction 37 followed by reaction 38

$$N_2^* + HCN \longrightarrow N_2 + H + CN \qquad (37)$$

$$CN + HCN \longrightarrow (CN)_2 + H \qquad (38)$$

Once a critical concentration of $(CN)_2$ has been formed, the reactions discussed in the last two sections can be extended to the HCN + N system.

The HCN system is less complicated than the C_2H_2 system because the possible perturbations of the $(CN)_2$ chain reaction are fewer than in the C_2H_2 system. The only reactions that would be expected to occur are reactions 7 and 21, which, however, merely regenerate HCN and radicals necessary to propagate the $(CN)_2$

(27) E. L. Tollefson and D. J. LeRoy, *J. Chem. Phys.*, **16**, 1057 (1948).

reaction. The secondary $(CN)_2$ reaction, therefore will be less affected by the presence of HCN than it is by the presence of C_2H_2. Indeed, in contrast to the C_2H_2 reaction, no self-inhibition occurs when concentrations of HCN are added in excess of the minimum required to sustain the $(CN)_2$ reaction.

3. Kinetic Origins of Large Molecular Weight Products. According to our mechanism for the $(CN)_2$ chain reaction, the polymer is formed because reactions 15 and 17 cannot occur after N atoms are consumed. Instead, C_2N and CN diffuse to the walls of the reaction vessel and polymerize, reactions 18 and 19.

We have proposed that C_2H radicals are produced in the C_2H_2 + N system by the abstraction reaction 32. In addition, C_2N and CN radicals are produced in the concurrent $(CN)_2$ reaction. Since C_2H radicals are an important species in the photochemical polymerization of C_2H_2,[13] they might also be expected to polymerize readily in C_2H_2 + N systems, reaction 34, together with C_2N and CN radicals, reaction 35, and, hence, account for the hydrogen content of the polymer. That reaction 34 can contribute to the composition of the polymer becomes even more apparent when it is considered that C_2H and CN radicals are isoelectronic and might, therefore, be expected to copolymerize readily.

The compositions of the high molecular weight products of both the $(CN)_2$ + N and C_2H_2 + N systems support these conclusions. The important observation is that these products are composed of combinations of CN, C_2N, C_2H, and C, thereby providing strong support for our postulate that these species are, indeed, the important radicals in these systems.

Since the purpose of this investigation was not to look for previously unidentified polymeric products of these systems but, rather, to obtain from these products an insight into the over-all reaction mechanisms, infrared absorption spectra of the $(CN)_2$ + N and C_2H_2 + N polymers are presented only to show that the spectra are consistent with the mass spectral data concerning the composition of the polymers.

Both polymers give absorptions at approximately 1610 and 2180 cm^{-1}, corresponding to the C=N and C≡N stretching vibrations, respectively.[28] The frequency shifts to slightly lower values than with simple nitriles suggest that the vibrations are perturbed owing to conjugation. Both polymers also display a broad unidentified band in the vicinity of 3250 cm^{-1}. Clearly, the similarities between the infrared spectra of the polymers support our conclusion that structurally similar radicals are involved in their formation.[29]

4. Evidence for the Reaction CN + N → N_2 + C. Experimental evidence for the occurrence of reaction 15 is given by the empirical formula of the $(CN)_2$ + N polymer, *viz.*, $(C_{1.28}N)$, and the observation that $C_2(CN)_2$, the dimer of C_2N, is a product of the $(CN)_2$ + N system.

In the C_2H_2 + N system, there can be little doubt that $C_2(CN)_2$ is produced by successive replacements of H in C_2H_2 by CN, by reaction 5 followed by the reaction

$$CN + C_2HCN \longrightarrow C_2(CN)_2 + H \qquad (39)$$

In the $(CN)_2$ + N system, however, replacement reactions cannot occur (the replacement of N in $(CN)_2$ by CN is highly endothermic) unless C_2N radicals are postulated to be one of the species, as in reaction 27.[31] C_2N radicals, however, can only be produced if carbon atoms are present, while carbon atoms, in turn, can only be produced if a C≡N bond is broken at some stage of the over-all reaction. The most likely reaction is reaction 15.

The mass spectrometric observation of $C_2(CN)_2$ as a product of the $(CN)_2$ reaction, therefore, provides strong evidence for the occurrence of reaction 15. The large carbon-to-nitrogen ratio of the $(CN)_2$ + N polymer also supports these views.[32]

5. The Role of $(CN)_2$, HCN, and CN Radicals in Hydrocarbon-Active Nitrogen Systems. Since $(CN)_2$ *alone* reacts extremely rapidly with active nitrogen, it has long been the consensus of opinion that consumption of N atoms in hydrocarbon-active nitrogen systems (to form N_2) probably occurs by parallel reactions of the small quantities of $(CN)_2$ that are products of these systems. Our experiments with mixtures of $(CN)_2$ and hydrocarbons, however, show conclusively that hydrocarbon-active nitrogen reactions cannot proceed by a mechanism that proposes parallel reactions of $(CN)_2$, since the $(CN)_2$ chain reaction is inhibited by all hydrocarbons.

It is clear that, in general, inhibition occurs because CN radicals react rapidly with hydrocarbons by abstraction

$$CN + RH \longrightarrow HCN + R \qquad (40)$$

(28) L. J. Bellamy, "The Infrared Spectra of Complex Molecules," J. Wiley and Sons, Inc., New York, N. Y., 1962.

(29) It has been brought to our attention that polymer is formed in the HCN + N system under certain conditions.[30] This behavior is not surprising, in light of our proposed reaction mechanism for this system. Data giving the composition of the polymer are unavailable, but it appears reasonable to predict, in view of the similarities between the $(CN)_2$ + N, C_2H_2 + N, and HCN + N systems, that the polymer would be produced by reactions 18 and 19, again after the $(CN)_2$ chain reaction has consumed N atoms.

(30) J. W. S. Jamieson, private communication.

(31) Replacement of N in $(CN)_2$ by CN radicals according to CN + NCCN → NCCCN + N is highly endothermic, $\Delta H_a \sim 92$ kcal/mol, because two carbon–carbon single bonds are formed.[17] Even if N=C=C=C=N were produced, the reaction would still be endothermic, $\Delta H_a \sim 100$ kcal/mol. In contrast, reaction 27, discussed in the $(CN)_2$ reaction, is much less endothermic because of the possibility for triple-bond conjugation in $C_2(CN)$ (eq 27).

(32) We have, since the writing of this paper, further investigated the $(CN)_2$ + N system and have obtained additional evidence that C atoms are indeed produced. The results of these experiments are presented in the following article.

and by substitution

$$CN + RH \longrightarrow RCN + H \qquad (41)$$

These findings, therefore, strongly support mechanisms such as those given by Herron[33] and us[2] which propose that NH radicals are the nitrogen-containing radicals. These findings also show that the reactions that produce $(CN)_2$ in hydrocarbon-active nitrogen systems, including subsequent reactions of $(CN)_2$, are only side reactions and do not contribute significantly to the over-all kinetics. The only system in which $(CN)_2$ plays an important role is the C_2H_2 + N system.[34]

These findings can also be extrapolated to exclude as kinetically important subsequent reactions of HCN, the major product of the reactions of hydrocarbons with active nitrogen, that might be expected to lead to the formation of N_2 (by the fast $(CN)_2$ stage of the reaction), since this reaction will also be inhibited by hydrocarbons.

Conclusions

We propose that the reaction of $(CN)_2$ with active nitrogen proceeds by a branching chain reaction involving C_2N radicals, CN radicals, and C atoms. N atoms are consumed by reaction 15. The reaction is inhibited by hydrogen-containing substances, because CN radicals are consumed competitively. It is this general inhibition that prevents consumption of N atoms in hydrocarbon-active nitrogen systems, either by parallel reactions of $(CN)_2$ or HCN. When H atoms are added to the $(CN)_2$ + N reaction, the N atoms present are quantitatively converted to HCN by reaction 21.

The reaction of C_2H_2 is related to the $(CN)_2$ reaction, since $(CN)_2$ is produced by the initial reactions of C_2H_2. If C_2H_2 is added beyond an optimum concentration, however, the fast $(CN)_2$ chain reaction is inhibited, since CN radicals react rapidly with C_2H_2. Addition of H atoms to the C_2H_2 reaction has less effect upon HCN formation than upon the $(CN)_2$ reaction, because H atoms are rapidly combined by the C_2H_2 that is necessarily present.

The reaction of HCN also appears to proceed *via* the initial formation of $(CN)_2$.

Appendix

One of the reviewers of this article has suggested that some of the values for thermochemical data used in this paper might perhaps not be the best available. It was, furthermore, suggested that the data given in the JANAF tables[36] be used. As a matter of interest we have indeed used data given by the JANAF tables, except when these data were not listed or when it was felt that better values were available.

Owing to the present interest in the reactions of hydrocarbons with active nitrogen, two points deserve some mention here.

(1) Concerning the use of the JANAF tables, many species of interest are not listed in the tables. In particular, the well-known C_2H_3 and C_2H_5 radicals and, quite surprisingly, even the stable C_2H_6 molecule are not listed in the JANAF tables. Heats of formation for several of the stable species in Table V, therefore, have been calculated from heats of combustion using long-accepted values from various sources[37] upon which, in fact, are based many of the JANAF tables values. Where heats of formation or combustion were not available, heats of formation have been estimated using generally accepted bond dissociation energy values given in Table VI.[17]

Table VI

Bond	Dissociation energy, kcal/mol
C–C	84
C=C	145
C≡C	195
C=N	~145
C≡N (bound in a molecule)	210
C–H	~100

In any event, with the exception of D_{CN}, which is discussed next, the discrepant values do not affect the reactions of interest in this paper to the extent that the direction of a reaction might change.

(2) The high value for the dissociation energy of CN, D_{CN} = 187 kcal/mol,[21] has been deliberately used in this paper. It was not our intent to get involved in a discussion concerning the long-controversial value of D_{CN}. It is our opinion, however, that the low value of 175 kcal/mol used by the JANAF tables is incorrect. In spite of the volume of literature that has been published regarding this problem, the following arguments, two of which are based upon chemical kinetic measurements and which we strongly favor, have generally been neglected.

(a) It had been pointed out by Robertson and Pease[26] that only a value for D_{CN-CN} of about 120–130 kcal/mol, which corresponds to a D_{CN} of 183–187 kcal/mol, was consistent with their kinetic interpretation of the results of their study of the thermal reaction of $(CN)_2$ with H_2. Except for the possibly large experimental errors involved, their arguments appear valid.

(33) J. T. Herron, *J. Phys. Chem.*, 69, 2736 (1965).

(34) It might be anticipated that $(CN)_2$ might play a role in the reactions of higher alkynes with active nitrogen. We have investigated the reaction of methylacetylene with active nitrogen, however, and found that $(CN)_2$ does not play an important role in this system.[35]

(35) D. R. Safrany and W. Jaster, *J. Phys. Chem.*, 72, 3323 (1968).

(36) "JANAF Thermochemical Tables," Dow Chemical Co., Midland, Mich., 1960; appended to Aug. 1967.

(37) See, for example, many of the publications of the National Bureau of Standards by F. D. Rossini.

(b) Our primary argument for the high value for D_{CN} is the experimental observation that $(CN)_2$ reacts very rapidly with H atoms even at the low 0.2-mm pressures and short reaction times of our experiments. If HCN is indeed produced by the generally accepted reaction 7,[11,12] D_{CN} must have the high value in order that the reaction be even thermally neutral, since the values $\Delta H_f((CN)_2) = 74$ kcal/mol, $\Delta H_f(H) = 52$ kcal/mol, and $\Delta H_f(HCN) = 30$ kcal/mol are well known. If the JANAF tables value for D_{CN} is accepted, reaction 7 would be 12 kcal/mol (endothermic) and, clearly, could not occur under our experimental conditions.

(c) A determination of D_{CN}, which has generally been overlooked and which to us appears impeccable as regards the method used, is that by Long.[38] The arguments presented by Long are based solely on Hess' law calculations, using well-established thermochemical or spectroscopic data. The only unknown parameters necessary for Long's determination were the C–C bond dissociation energies for CH_3CN and HCN, and D_{I-CN}. These were determined by relatively simple experiments in which the long-wavelength limits for photodissociation of these substances were determined.

Measurement of dissociation energies from long-wavelength limits suffers from the disadvantage that the energy states of the products must be known. Adequate arguments seem to us, however, to have been presented in Long's paper to ensure that the states of the dissociation products were indeed known. Furthermore, since nearly the same values of D_{CN} were obtained by using three independent measurements upon three different systems, average $\Delta H_f^\circ = 92.5$ kcal/mol, equivalent to $D_{CN} = 191$ kcal/mol, it appears unrealistic to consider the possibility that drastically incorrect results would be obtained for all three determinations of the corresponding bond energies.

(38) L. H. Long, *Proc. Roy. Soc.*, A198, 63 (1949).

The Effect of Additives upon the Reaction of Cyanogen with Active Nitrogen: Reactions of Carbon Atoms, CN Radicals, and the Chemiluminescent Reaction of C_2N Radicals with Atomic Oxygen

by David R. Safrany[1] and Walter Jaster

Atomic Energy of Canada, Limited, Whiteshell Nuclear Research Establishment, Pinawa, Manitoba, Canada *(Received February 6, 1968)*

The reaction of cyanogen with active nitrogen was found to be inhibited by additives with decreasing efficiency as follows: $O_2 \gg CH_4 > N_2O > CO \gg CO_2 > SF_6$. In contrast to the very efficient inhibition by *molecular* O_2, addition of *atomic* O in the *absence* of O_2 enhanced the reaction and produced intense CN chemiluminescence. The observations can be explained in terms of reactions of the additives with reaction intermediates.

Introduction

We have just reported the results of a study of the reaction of $(CN)_2$ with active nitrogen.[2] The behavior of the $(CN)_2 + N$ system could be explained by the following mechanism: chain initiation

$$(CN)_2 + N_2^* \longrightarrow N_2 + 2CN \qquad (1)$$

where N_2^* denotes an excited N_2 molecule, and chain propagation

$$CN + N \longrightarrow N_2 + C \qquad (2)$$

$$C + (CN)_2 \longrightarrow C_2N + CN \qquad (3)$$

$$C_2N + N \longrightarrow 2CN \qquad (4)$$

In that study we found that, although a flame was formed, the reaction did not go to complete consumption of reactive species; a weak long-lived pink-white afterglow remained downstream from the reaction flame. Addition of NO to this pink-white afterglow gave a bright red chemiluminescence which consisted of the CN red and violet band systems. We attrib-

(1) To whom correspondence should be sent.

(2) D. R. Safrany and W. Jaster, *J. Phys. Chem.*, 72, 3305 (1968).

uted this effect primarily to the reaction of C_2N radicals with atomic oxygen

$$C_2N + O \longrightarrow CN^* + CO \qquad (5)$$

although we could not eliminate other reactions.

The reactive species we proposed to be important in the $(CN)_2$ + N system, *viz.*, excited N_2 molecules, CN radicals, and carbon atoms, are of interest to the understanding of certain combustion and planetary-atmospheric phenomena. We, therefore, attempted: (1) to confirm the presence of these reactive species by experiments with additives and (2) further to elucidate the reactions of these species. We report here the results of these experiments.

Experimental Section

The apparatus used for this investigation consisted of a very fast flow, low-pressure (50 m/sec linear velocity, 0.2 mm of pressure) Wood-Bonhoeffer system. The general experimental technique and materials used have already been described in detail elsewhere.[3]

For these experiments, $(CN)_2$ was added to active nitrogen under conditions such that $[(CN)_2] \approx [N]$. Under these conditions, a flame was formed and N atoms were rapidly although, as described in our previous paper, not completely consumed.[2] Additives were then added either: (1) admixed with the $(CN)_2$ or (2) upstream from the reaction flame.

a. Quenching Experiments. The visual behavior of the reaction flames upon addition of a quenchant gas was classified into one of three categories, according to the extent to which CN radiation was quenched and the extent to which the over-all reaction was inhibited.

Group I. CN radiation from the reaction flame was completely quenched by the additive in the time available for reaction (~20 msec), and the over-all reaction was also completely inhibited. Neither $(CN)_2$ nor N atoms were consumed after the addition of the quenchant, and the mixture of $(CN)_2$ and active nitrogen reverted to the original intensity of the N_2 afterglow before the addition of $(CN)_2$ alone. Molecular O_2 was the only quenchant in this group.

Group II. CN radiation from the reaction flame was partially quenched in the time available for reaction (again ~20 msec), and the over-all reaction was only partially inhibited. Under these conditions, the length of the reaction flame increased over the length in the absence of additive, owing to the decrease in the over-all reaction rate. After addition of quenchants in this group, the N_2 afterglow downstream from the reaction flame only reverted to a fraction of its original intensity before the addition of $(CN)_2$ alone, since a considerable concentration of N atoms was consumed. CH_4, N_2O, and CO were categorized in this group.

Group III. CN radiation from the reaction flame and the over-all reaction were unaffected by the presence of additive. Addition of quenchants in this group merely increased the length of the reaction flame slightly, owing to dilution, and the reaction appeared identical with the reaction without additive. CO_2 and SF_6 were classified in this group.

Quenching efficiencies of additives were determined quantitatively by adding quenchant until the reaction was inhibited to some predetermined extent, which was the same for all additives. At this concentration of additive, the discharge was turned off and the mass spectrum of the gas mixture was obtained. The predetermined extent of inhibition was measured by eye, and the quenching efficiencies, therefore, may be subject to considerable error. The values given, however, are certainly correct to considerably better than order-of-magnitude accuracies.

b. Addition of NO Upstream from the Reaction Flame. In our first study of the $(CN)_2$ + N system, we did not determine whether the chemiluminescence we observed upon addition of NO *downstream* from the reaction flame was owed to a direction reaction of NO with a radical present in the reaction zone or whether oxygen atoms were first produced by the very fast reaction[4,5]

$$N + NO \longrightarrow N_2 + O \qquad (6)$$

and then reacted with the intermediate to give the chemiluminescence, by reaction 5.

To elucidate, therefore, the role of O atoms, we added NO upstream from the $(CN)_2$ inlet so that NO would be completely consumed and O atoms would be produced by reaction 6 before the flowing gas reached the $(CN)_2$ inlet.

The effect of adding NO was quite spectacular. The chemiluminescence observed when NO was added downstream from the $(CN)_2$ inlet was also observed when NO was added upstream. The intensity, however, was much greater when NO was added upstream and could easily be seen with the room lights on. Clearly, the radicals responsible for the chemiluminescent reaction with O atoms were present in much higher concentration in the reaction flame than in the long-lived afterglow downstream. Although no intensity measurements were made, to account for the observed intensity, the visible radiation emitted from the reaction flame must have corresponded to several watts of radiated power (compared with milliwatts for the reaction of $(CN)_2$ with active nitrogen in the absence of NO).

The intensity of the CN chemiluminescence was a function of NO concentration and reached a maximum just before N atoms were completely replaced by O atoms by reaction 6, *viz.*, at a O:N ratio of about 10:1.

(3) D. R. Safrany and W. Jaster, *J. Phys. Chem.*, 72, 518 (1968).

(4) G. B. Kistiakowsky and G. G. Volpi, *J. Chem. Phys.*, 27, 1141 (1957).

(5) P. Harteck, R. R. Reeves, and G. Mannella, *ibid.*, 29, 608 (1958).

When the NO added exceeded the concentration of N atoms (so that all the N atoms were consumed by reaction 6 and only NO and O atoms were the remaining active species), the CN chemiluminescence was extinguished. The green-white air afterglow[6] could then be observed to extend well downstream into the vacuum pump, with no reduction in intensity due to the presence of $(CN)_2$, showing that, in the absence of N atoms, the reaction of $(CN)_2$ with O atoms was negligibly slow.

c. Detection of Carbon Atoms. It has been reported that C atoms add readily to C_2H_4 to produce allene[7]

$$C + C_2H_4 \longrightarrow C_3H_4 \qquad (7)$$

Addition of C_2H_4 to the $(CN)_2$ + N system, therefore, might be expected to lead to formation of allene if C atoms were present. CN radicals, however, react rapidly with all hydrocarbons;[2] the addition of hydrocarbons to the $(CN)_2$ + N reaction, therefore, strongly inhibits the over-all chain reaction, because CN radicals are a major chain carrier and are consumed.[2] Addition of C_2H_4, therefore, could not be used to detect C atoms in this system.

To circumvent this difficulty, we added O_2 and N_2O instead, although O_2 reacts rapidly with CN radicals,[8] since these substances react only very slowly with atomic N,[4] do not react with C_2H_4, and might be expected to react with C atoms.

Both O_2 and N_2O were found to inhibit the over-all reaction. In the case of N_2O, we attempted further to elucidate the nature of this inhibition by adding a constant flow rate of N_2O, designated $[N_2O]_0$, varying the concentration of $(CN)_2$, and measuring the concentration of N_2O, designated $[N_2O]$. Figure 1 shows that consumption of N_2O, $\Delta[N_2O] = [N_2O]_0 - [N_2O]$, was small when small concentrations of $(CN)_2$ were added, reached a maximum value, and then decreased as further concentrations of $(CN)_2$ were added.

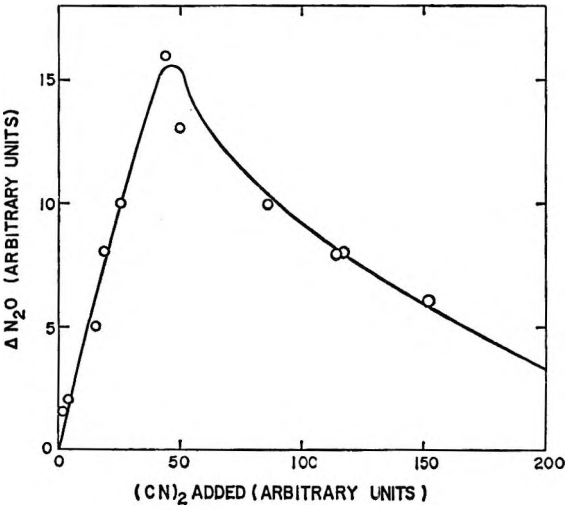

Figure 1. N_2O consumption, ΔN_2O, upon addition of N_2O to the $(CN)_2$ + N reaction as a function of added $(CN)_2$. The N_2O added initially was kept constant at 158 arbitrary units.

Table I: Relative Quenching Efficiencies of Additives upon the $(CN)_2$ + N Reaction: Microns of Additive Required to Quench the CN Radiation

Additive	Group	N_2	$(CN)_2$	Partial quenching, μ	Complete quenching, μ	No quenching
O_2	I	183	13.8	3.5	6.8	...
CH_4	II	183	13.8	13.7	39	...
N_2O	II	183	13.8	41	79	...
CO	II	183	13.8	72	82	...
CO_2	III	183	13.8	272	...	...
SF_6	III	183	13.8	...	...	>390

Results of Quenching Experiments

Table I gives the relative quenching efficiencies of various additives. The most striking observations are the anomalously high quenching efficiency of molecular O_2 and the relatively efficient quenching by CO. Inhibition of the over-all reaction by CO is particularly surprising, since, as will be discussed later, the reactions by which inhibition can occur are limited with this substance. The 6.8 μ of O_2 (column 6) required to completely inhibit the reaction is more than ten times less than the concentrations of N_2O and CO required, *viz.*, 79 and 82 μ, respectively. The quenching efficiency of CH_4 is intermediate between these values; 39 μ completely inhibited the reaction. CO_2 exhibited only partial quenching when 272 μ were added, while SF_6 showed no inhibition even when more than 390 μ were added.

Since molecular O_2 is such an efficient inhibitor of the reaction, it might be anticipated that the chemiluminescent phenomenon would not be observed if O atoms were produced by subjecting molecular O_2 to an electrical discharge, rather than by adding NO, since, in the former method, complete dissociation is not attained and molecular O_2 would remain to inhibit the reaction. In accord with this consideration, the reaction was completely inhibited; neither the chemiluminescence nor any detectable consumption of either $(CN)_2$ or N atoms was observed when O atoms were produced by discharging molecular O_2. As soon as the flow of molecular O_2 was shut off, however, the reaction again reverted to the fast rate typical of the uninhibited $(CN)_2$ + N reaction.

Discussion

1. Inhibition of the Over-all Reaction by Additives. The inhibition of the over-all reaction by additives can

(6) The green-white air afterglow is owed to the slow reaction $NO + O \rightarrow NO_2 + h\nu$.

(7) M. Marshall, C. MacKay, and R. Wolfgang, *J. Amer. Chem. Soc.*, 86, 4741 (1964).

(8) N. Basco, *Proc. Roy. Soc.*, A283, 302 (1965).

be explained by reactions of the quenchants with reactive intermediates.

Inhibition by CH_4 is owed to the scavenging of CN radicals by the abstraction and substitution reactions

$$CN + CH_4 \longrightarrow HCN + CH_3 \quad (8)$$

$$CN + CH_4 \longrightarrow CH_3CN + H \quad (9)$$

This conclusion is supported by the findings that: (1) the products of adding CH_4 to the $(CN)_2$ + N reaction are HCN and CH_3CN;[9] (2) C_2HCN and HCN are produced when C_2H_2 is added,[10] and (3) H-containing substances, in general,[2] *viz.*, H_2,[9] NH_3,[11] CH_3C_2H, C_3H_6, and i-C_4H_8, are efficient inhibitors of the over-all reaction. These findings clearly illustrate the reactivity of CN radicals toward H-containing substances in the $(CN)_2$ + N system and need not be further discussed.

CN radicals are known to react rapidly with O_2

$$CN + O_2 \longrightarrow CNO + O \quad (10)$$

and may also react with N_2O

$$CN + N_2O \longrightarrow CNO + N_2 \quad (11)$$

Reaction 10 has been reported to occur by Morrow and McGrath,[12] and the specific rate has been given as $k \approx 8 \times 10^{-12}$ cm³/molecule sec by Basco.[8] Earlier work by Paul and Dalby[13] gave rates for formation of CNO, from unspecified reactions of CN radicals with O_2 and H_2O, of $k \approx 9 \times 10^{-12}$ cm³/molecule sec and $k \approx 5 \times 10^{-13}$ cm³/molecule sec, respectively. Basco and Norrish,[14] furthermore, gave a specific rate of $k \approx 3 \times 10^{-12}$ cm³/molecule sec for the reaction of CN with NO, one possible path of which is the reaction

$$CN + NO \longrightarrow CO + N_2 \quad (12)$$

Clearly, the reactions of CN radicals with O_2 and NO are about one order of magnitude faster than the reaction with H_2O.

The specific rate of the reaction of CN radicals with N_2O, reaction 11, might be expected to have a value somewhere between those of the reactions with H_2O and with O_2, *viz.*, $k_{11} \approx 2 \times 10^{-12}$ cm³/molecule sec. The difference of a factor of 10 in the quenching efficiencies of O_2 and N_2O, therefore, might be explained as simply being due to a difference in the specific rates of reactions 10 and 11.

This rationalization, however, cannot explain the variation of N_2O consumption with $(CN)_2$ concentration shown in Figure 1. If the only effect of adding N_2O is to provide a simple competition for CN radicals by reaction 11, N_2O consumption would decrease exponentially to zero instead of going through a maximum.

The behavior depicted in Figure 1 is explained, however, if C atoms are postulated as a second reactive species. In addition to reacting with CN radicals, reaction 11, N_2O might also react with C atoms

$$C + N_2O \longrightarrow CN + NO \quad (13)$$

a reaction which has been postulated to occur when ^{11}C atoms are produced by nuclear transformations.[15] The reaction

$$^3C + {}^1N_2O \longrightarrow {}^1CO + {}^1N_2 \quad (14)$$

would not be expected to occur, since it is spin disallowed. At small concentrations of $(CN)_2$ (when $[N] > [(CN)_2]$), the over-all reaction will be slow and only small steady-state concentrations of reactive intermediates, including C atoms, will be produced. As more $(CN)_2$ is added, the reaction rate increases to some optimum value, at which the concentrations of reactive intermediates attain their maximum values. Since N_2O consumption will be proportional to the concentration of reactive intermediates, N_2O consumption also increases under these conditions. Addition of further concentrations of $(CN)_2$ beyond this optimum value, however, will lead to a decrease in N_2O consumption, because $(CN)_2$ will compete with N_2O for C atoms, by reaction 3, when the concentration of $(CN)_2$ becomes large.

The extremely efficient quenching by molecular O_2 also suggests that C atoms are a second reactive species. Molecular O_2 is about six times more efficient in quenching the over-all $(CN)_2$ + N reaction than even CH_4, which in itself is an efficient inhibitor. It appears unlikely that a reaction involving abstraction of an O atom by CN from O_2 reaction 10, could be much faster than a reaction involving abstraction of an H atom, reaction 8. This consideration suggests, therefore, that, as with N_2O, the anomalously efficient inhibition by O_2 is also, at least owed in part to a parallel reaction of C atoms. The most likely reaction is

$$C + O_2 \longrightarrow CO + O \quad (15)$$

This reaction has also been observed with ^{11}C atoms in the work cited previously.[15] The agreement between the conclusions of the present work and those of the ^{11}C work is rather remarkable, when the widely different experimental methods used are considered.

CO and N_2O show approximately the same quenching efficiency. In the case of N_2O, chemical reactions which can scavenge radicals and thereby inhibit the over-all reaction are possible, since the O atom is weakly bound, D_{N_2-O} = 40 kcal/mol.[16] CO, however,

(9) C. Haggart and C. A. Winkler, *Can. J. Chem.*, **38**, 329 (1960).
(10) J. T. Herron, J. L. Franklin, and P. Bradt, *ibid.*, **37**, 579 (1959).
(11) I. M. Campbell and B. A. Thrush, *Proc. Chem. Soc.*, 410 (1964).
(12) T. Morrow and W. D. McGrath, *Trans. Faraday Soc.*, **62**, 642 (1966).
(13) D. E. Paul and F. W. Dalby, *J. Chem. Phys.*, **37**, 592 (1962).
(14) N. Basco and R. G. W. Norrish, *Proc. Roy. Soc.*, **A283**, 291 (1965).
(15) J. Dubrin, C. MacKay, M. L. Pandow, and R. Wolfgang, *J. Inorg. Nucl. Chem.*, **26**, 2113 (1964).
(16) J. L. Cottrell, "The Strength of Chemical Bonds," Butterworth and Co. Ltd., London, 1958.

has the greatest bond strength of any diatomic molecule, D_{CO} = 256 kcal/mol.[16] Hence two-body chemical reactions of CO will be too endothermic to occur at room temperatures.[17] Inhibition of the over-all reaction by CO, therefore, can only be attributed to inhibition of the initial chain-initiating step, reaction 1, by an energy-transfer mechanism.

If the excited molecule depicted in eq 1 is the long-lived $N_2(A^3\Sigma_u^+)$ molecule, the relatively efficient inhibition of the $(CN)_2$ + N reaction by chemically inert CO can be understood, since the CO molecule has a triplet energy level ($a^3\pi$) only 518 cm^{-1} lower than the $N_2(A^3\Sigma_u^+)$ level,[18] and an efficient resonant energy transfer from $N_2(A^3\Sigma_u^+)$ to ground state CO ($X^1\Sigma^+$) might be expected to occur

$$N_2(A^3\Sigma_u^+) + CO(X^1\Sigma^+) \longrightarrow N_2(X^1\Sigma_g^+) + CO(a^3\pi) \quad (16)$$

Deactivation of $N_2(A^3\Sigma_u^+)$ molecules by reaction 16 could inhibit the initial formation of CN radicals by reaction 1 if $CO(a^3\pi)$ did not transfer energy to $(CN)_2$, even though $CO(a^3\pi)$ possesses enough electronic excitation energy to dissociate $(CN)_2$.[18]

CO_2 and SF_6 are much less efficient inhibitors than CO. With these additives, the high bond strength of CO_2[16] and the known, generally inert behavior of SF_6 again preclude chemical reactions with reactive intermediates. These substances did not quench the over-all reaction to any significant extent. We can only conclude, therefore, either that: (1) energy transfer from N_2* to CO_2 and SF_6 is very slow or (2) that energy is indeed transferred to give CO_2* and SF_6* but that these species then dissociate $(CN)_2$ rapidly. Since it is not the purpose of this paper to speculate regarding the reactions of excited molecules, no further discussion is warranted.

2. CN Chemiluminescence Observed upon Addition of NO. The CN chemiluminescence observed upon addition of NO upstream from the reaction flame is explained by the reaction of O atoms with C_2N radicals according to reaction 5.

Earlier workers proposed that the reactive intermediate in the $(CN)_2$ + N reaction is not C_2N but is the CN_2 radical.[9,11,19] An alternate reaction that might, therefore, be postulated to explain the CN chemiluminescence is

$$CN_2 + O \longrightarrow CN^* + NO \quad (17)$$

Reaction 17, however, would be followed by the very fast reaction 6. O atoms would be rapidly regenerated and a chain mechanism for formation of CN* would result. If this were indeed the case, a small concentration of added NO would suffice to give the chemiluminescence, a consideration which conflicts with our observations. We conclude, therefore, that the CN chemiluminescence is owed to the reaction of O atoms with C_2N radicals by reaction 5.

The results of this investigation also provide an alternate explanation for the increase in CN radiation upon addition of NO to C_2H_2 + N systems which was observed by Fontijn.[20] Fontijn concluded that since the enhanced CN radiation went through a maximum as NO was added, this was indicative that O atoms were more efficient in producing CN precursors in their reactions with C_2H_2 than the N atoms they replaced (by reaction 6).

In our previous paper, however, we studied the reaction of C_2H_2 with N atoms as well as the reaction of $(CN)_2$.[2] We found that large concentrations of $(CN)_2$ were formed by the initial reactions of C_2H_2 and that subsequent reactions were those of $(CN)_2$ with active nitrogen, reactions 2–4. In view of these findings, there can be little doubt that the enhanced CN radiation upon addition of NO to the C_2H_2 + N reaction is due to the reaction of O atoms with C_2N radicals that are produced in the subsequent reactions of $(CN)_2$ with N atoms rather than to any preferential reactions of O atoms with C_2H_2.

(17) Three-body reactions are negligible under our conditions of fast flow and low pressure.

(18) G. Herzberg, "The Spectra of Diatomic Molecules," 2nd ed, D. Van Nostrand Co., Inc., New York, N. Y., 1950.

(19) K. D. Bayes, *Can. J. Chem.*, 39, 1074 (1961).

(20) A. Fontijn, *J. Chem. Phys.*, 43, 1829 (1965).

NOTES

Reactions of Hydrocarbons with Mixtures of Active Nitrogen and Hydrogen Atoms. III. The Reactions of Methylacetylene and Allene

by David R. Safrany[1] and Walter Jaster

Atomic Energy of Canada Limited, Whiteshell Nuclear Research Establishment, Pinawa, Manitoba, Canada
(Received February 6, 1968)

We have recently reported the results of an investigation of the reactions of mixtures of active nitrogen and hydrogen atoms with alkenes, alkanes,[2] and one alkyne, acetylene.[3] In these studies we postulated that the initial reaction of alkenes is addition of atoms by the reaction

$$H + C_nH_{2n} \longrightarrow C_nH_{2n+1} \qquad (1)$$

while the initial reaction of alkanes is abstraction by H atoms

$$H + C_nH_{2n+2} \longrightarrow H_2 + C_nH_{2n+1} \qquad (2)$$

The alkyl radicals produced by reactions 1 and 2 then react rapidly with N atoms to form HCN and the other well-known products of the over-all reactions of active nitrogen with hydrocarbons.[4]

In the reaction of C_2H_2 with active nitrogen, we postulated that N atoms successively replaced the H atoms in the molecule and, thereby, formed $(CN)_2$.[3]

$$C_2H_2 + N \longrightarrow CHCN + H \qquad (3)$$

$$CHCN + N \longrightarrow (CN)_2 + H \qquad (4)$$

The over-all behavior of the reaction of C_2H_2 had been known to exhibit behavior different from that of alkenes with active nitrogen and to more closely resemble the reaction of $(CN)_2$.[3-5] The results of our previous investigation[3] clearly showed that this behavior is due to the large amounts of $(CN)_2$ that are produced by the initial reactions 3 and 4 in the C_2H_2 reaction. We postulated that, once a critical concentration of $(CN)_2$ is produced by these reactions, N atoms react rapidly with $(CN)_2$ by a branching chain reaction so that the over-all reaction appears to be that of $(CN)_2$ with active nitrogen. The mechanism of this chain reaction is also given in our other paper and, for the purposes of this discussion, need not be repeated here.[3]

Replacement of H by N in C_2H_2 is energetically possible because the carbon–nitrogen triple bond in molecules is very strong, $D_{C\equiv N} \approx 210$ kcal/mol.[6] In the case of methylacetylene, it is again energetically possible for N atoms to replace the terminal H atom in the initial attack. To determine, therefore, whether replacement of H by N was unique to C_2H_2 or whether H atoms in other molecules which have appropriate structures might also be replaced by N, we studied the reactions of methylacetylene and its isomer, allene, with mixtures of active nitrogen and H atoms.

If replacement of the terminal H atom in CH_3C_2H by N indeed occurred, $(CN)_2$ might be produced, and the over-all reaction might be expected to display behavior more closely similar to the C_2H_2 reaction than to reactions of alkenes. In the case of allene, replacement of H by N would not be expected but, in view of the double bonds present, addition of H by a reaction analogous to reaction 1, would be anticipated.

The results reported herein were surprising in view of these expectations but clarify considerably the mechanisms of the initial attack of hydrocarbons in hydrocarbon-active nitrogen systems.

Experimental Section

The preparation of gases used in this investigation, as well as apparatus and experimental technique, is given in part I of this series of papers.[2]

Results

The reactions of both methylacetylene and allene with active nitrogen, surprisingly, exhibited behavior typical of alkenes, which is described in detail in our previous publication;[2] CH_3C_2H did not display the anticipated anomalous behavior. A brief summary is given of the observations under conditions when [hydrocarbon] > [N].

(1) The reactions went to *complete* consumption of N atoms in a few milliseconds at room temperature, in agreement with the findings of Schavo and Winkler for the reaction of CH_3C_2H with active nitrogen;[7] short flames (10–30 cm) were formed and the N_2 afterglow downstream was *completely* quenched. (In the reactions of $(CN)_2$ or C_2H_2 with active nitrogen, N atoms are never completely consumed; a faint, pink-white afterglow remains downstream from the reaction

(1) To whom correspondence should be sent.

(2) D. R. Safrany and W. Jaster, *J. Phys. Chem.*, **72**, 518 (1968).

(3) D. R. Safrany and W. Jaster, *ibid.*, **72**, 3305 (1968).

(4) H. G. Evans, G. R. Freeman, and C. A. Winkler, *Can. J. Chem.*, **34**, 1271 (1956).

(5) J. Versteeg and C. A. Winkler, *ibid.*, **31**, 129 (1953).

(6) J. L. Cottrell, "The Strengths of Chemical Bonds," Butterworth and Co. Ltd., London, 1958.

(7) A. Schavo and C. A. Winkler, *Can. J. Chem.*, **37**, 655 (1959).

Table I: Formation of Products in the Reactions of CH_3C_2H and $CH_2{=}C{=}CH_2$ with Active Nitrogen

	Expt	Products, μ: H_2	N_2	HCN	CH_3C_2H	$CH_2{=}C{=}$ CH_2	C_2H_2	CH_4	C_2H_6	NO	HCN: NO
(1)	(a) $N_2 + H_2 + CH_3C_2H$	77.4	32.0	...	20.7	...	...	...	...	...	...
	(b) $N_2 + H + CH_3C_2H$	73.0	30.6	...	16.1	...	2.67	0.27	2.75	...	...
	(c) $N + H_2 + CH_3C_2H$	84.7	27.4	7.06	13.7	...	2.89	0.061	0.21	...	0.52
	(d) $N + H + CH_3C_2H$	78.2	25.8	12.6	7.6	...	7.59	0.30	1.2	...	0.94
	(e) NO titration	...	...	...	...	...	...	...	...	13.5	...
(2)	(a) $N_2 + H_2 + CH_2{=}C{=}CH_2$	82.9	37.4	...	...	9.85	...	...	...	...	...
	(b) $N_2 + H + CH_2{=}C{=}CH_2$	73	36.5	...	...	7.68	1.81	0.25	1.69	...	...
	(c) $N + H_2 + CH_2{=}C{=}CH_2$	100	32.5	6.75	...	5.33	2.35	...	0.13	...	0.63
	(d) $N + H + CH_2{=}C{=}CH_2$	91.2	32.0	9.79	...	2.44	5.95	0.21	0.42	...	0.91
	(e) NO titration	...	...	...	...	...	...	...	...	10.8	...

flame when either of these substances is added to active nitrogen.[3])

(2) Peach colored CN radiation, typical of that from alkene reactions,[2] was emitted. (CN radiation from the $(CN)_2$ or C_2H_2 reactions is emitted much more strongly in the red region of the spectrun.[3-5])

(3) Only about half of the N atoms present, as measured by NO titration,[8,9] formed HCN.

(4) Addition of these hydrocarbons to a stream of H atoms, in the absence of N atoms, led to formation of large quantities of CH_4 and C_2H_6.

Also analogous to the reactions of alkenes, the addition of H atoms to both the $CH_3C{\equiv}CH$ + N and $CH_2{=}C{=}CH_2$ + N systems increased the over-all rates of the reactions and the formation of HCN to the extent that good agreement was obtained between the HCN produced and the N atom concentration measured by NO titration.[2]

Table I, experiments 1a and 2a, shows the composition of the gas mixtures prior to activation of either the N or H atom discharges. At these concentrations of reactants, flames were formed and the reactions went to complete consumption of reactive species. Experiments 1c and 2c, column 3, show the formation of 7.06 and 6.75 μ of HCN, respectively, when only the N atom discharge was activated. Experiments 1d and 2d show that 12.6 and 9.79 μ of HCN were produced when both discharges were activated, while experiments 1e and 2e, column 9, give the NO titration value for N atom concentrations with which these values of HCN formation should be compared. Experiments 1b and 2b, columns 7 and 8, show the formation of CH_4 and C_2H_6 with only the H atom discharge activated.

In striking contrast to the reactions of alkenes and alkanes, however, in which acetylene is only a minor product,[2,4] C_2H_2 was found to be the major hydrocarbon product of the reactions of both CH_3C_2H and $CH_2{=}C{=}CH_2$ with N, H, or, mixtures of, N and H atoms, as shown in Table I, column 6. C_2H_2 is produced in such large quantities, moreover, that it must be produced by a major initial reaction of the hydrocarbon.

The observation that C_2H_2 survived as a product in such large quantities suggests, furthermore, that this substance, subsequent to its formation, must have been relatively inert to reaction with reactive species present in the system. To test this hypothesis, we added C_2H_2 to reacting systems of arbitrarily chosen alkenes with active nitrogen and measured the concentration of C_2H_2. Table II, column 5, shows the anticipated inert behavior of C_2H_2 when added to C_3H_6 + N and *i*-C_4H_8 + N systems under a variety of conditions. Experiments 3c and d and 4c and d are experiments with N atoms alone or with mixtures of N and H atoms. Experiments 3b and 4b are experiments with H atoms alone.

Discussion

In the reactions of both methylacetylene and allene, C_2H_2 is produced in such large quantities that it must be produced by the initial reactions.

In the case of $CH_3C{\equiv}CH$, the reaction almost certainly occurs *via* displacement of a CH_3 radical by an H atom

$$CH_3C_2H + H \longrightarrow CH_3 + C_2H_2 \qquad (5)$$

Replacement of H by N or cracking at the triple bond cannot be the initial reactions, since it would be difficult to explain how C_2H_2 could be formed by subsequent reactions; N atoms or H atoms would almost certainly react rapidly with the hydrocarbon radicals that would be produced.

In the case of $CH_2{=}C{=}CH_2$, the initial reaction appears to be catalyzed isomerization by H atoms, by the exchange reaction

$$CH_2{=}C{=}CH_2 + H \longrightarrow CH_3C_2H + H \qquad (6)$$

since the over-all behavior of the reaction and, especially, the formation of C_2H_2 are so similar to those of

(8) G. B. Kistiakowsky and G. G. Volpi, *J. Chem. Phys.*, **27**, 114 (1957).

(9) P. Harteck, R. R. Reeves, and G. Mannella, *ibid.*, **29**, 608 (1958).

Table II: Consumption of C_2H_2 when Added to the Reactions of C_3H_6 and i-C_4H_8 with Active Nitrogen

	Expt	Products, μ				
		H_2	N_2	C_3H_6	i-C_4H_8	C_2H_2
(3)	(a) $N_2 + H_2 + C_3H_6 + C_2H_2$	87.0	34.7	5.73	...	12.5
	(b) $N_2 + H + C_3H_6 + C_2H_2$	86.8	31.2	2.50	...	12.1
	(c) $N + H_2 + C_3H_6 + C_2H_2$	95.5	30.4	2.70	...	12.4
	(d) $N + H + C_3H_6 + C_2H_2$	94.2	29.9	0.44	...	12.4
(4)	(a) $N_2 + H_2 + i$-$C_4H_8 + C_2H_2$	85.9	39.8	...	4.60	12.8
	(b) $N_2 + H + i$-$C_4H_8 + C_2H_2$	88.0	38.1	...	3.44	12.9
	(c) $N + H_2 + i$-$C_4H_8 + C_2H_2$	102	34.2	...	3.25	12.2
	(d) $N + H + i$-$C_4H_8 + C_2H_2$	94.5	36.0	...	1.93	12.9

the $CH_3C{\equiv}CH$ reaction. Reaction 6 would then be followed by reaction 5 and could be expected to occur readily since methylacetylene is stable by 1.6 kcal/mol with respect to allene: $\Delta H_f(CH_2{=}C{=}CH_2) = 45.02$ kcal/mol *vs.* $\Delta H_f(CH_3C{\equiv}CH) = 43.42$ kcal/mol.[10-12]

It is conceivable that reactions 5 and 6 might take place in one step

$$CH_2{=}C{=}CH_2 + H \longrightarrow CH_3 + C_2H_2 \qquad (7)$$

This reaction, however, involves transfer of an H atom and might, therefore, be less likely to occur than reaction 6 followed by reaction 5.

The significance of these experiments is that the results provide an insight into the mechanisms by which hydrocarbons are cracked in hydrocarbon-active nitrogen systems. Trick and Winkler found that large amounts of C_2H_4 were produced in the reaction of propylene with active nitrogen.[13] The formation of C_2H_4 can readily be explained if cracking is due to H atoms according to the well-known reaction[14]

$$H + CH_3C_2H_3 \longrightarrow CH_3 + C_2H_4 \qquad (8)$$

If, however, reaction 8 is studied directly by adding C_3H_6 to a stream of H atoms produced, as in our experiments, by electrically dissociating H_2, the major product is not C_2H_4, but rather, CH_4 and C_2H_6 are observed.[14] The latter substances are formed because the C_2H_4 product of reaction 8 undergoes the subsequent reactions[14]

$$H + C_2H_4 \longrightarrow C_2H_5 \qquad (9)$$

$$H + C_2H_5 \longrightarrow 2CH_3 \qquad (10)$$

$$(CH_3,\ C_2H_5 \longrightarrow CH_4,\ C_2H_6)$$

with the large concentrations of H atoms that are present in discharge-tube experiments.[14]

In contrast to the $C_3H_6 + H$ system, C_2H_4 *is* observed as a product of the $C_3H_6 + N$ system, because the steady-state H atom concentration in the latter system is lower than in the $C_3H_6 + H$ system, since H atoms are not added initially as a reactant but are produced during the reaction. The only important reaction of the relatively small concentrations of H atoms, compared with the C_3H_6 concentration, therefore, will be the initial cracking of the C_3H_6, reaction 8, since few H atoms will be available for subsequent reactions with C_2H_4, reactions 9 and 10.

Support for the correctness of this conclusion is provided by the results of the present investigation. Clearly, the $CH_3C_2H + N$ and $CH_3C_2H + H$ systems are analogous to the $CH_3C_2H_3 + N$ and $CH_3C_2H_3 + H$ systems. In the $CH_3C_2H + H$ system, cracking again occurs at the single bond, reaction 5. In contrast to the C_2H_4 product of the analogous $CH_3C_2H_3 + H$ reaction, however, the product molecule of the initial reaction in the $CH_3C_2H + H$ reaction, C_2H_2, is inert to further consumption even by the very large concentrations of H atoms present in the discharge-tube experiments and is, therefore, readily detected, as shown by Tables I and II. C_2H_2 survives as a product because (1) the only reactions of C_2H_2 with H atoms are the well-known reactions[14]

$$H + C_2H_2 \longrightarrow C_2H_3 \qquad (11)$$

$$H + C_2H_3 \longrightarrow H_2 + C_2H_2 \qquad (12)$$

whose over-all effect is merely to combine H atoms *without consuming* C_2H_2, and (2) the reactions of C_2H_2 with N atoms to form $(CN)_2$ by reactions 3 and 4 are the slowest reactions in the system[3] and, therefore, cannot compete with the other reactions.

Viewed in this context, it is clear that, if reactions of N atoms are neglected,[15] hydrocarbon–N atom systems are similar to hydrocarbon–H atom systems in which the H atoms are produced by photolytic methods and in which, therefore, H atoms are also present in small concentrations relative to the concentration of hydro-

(10) "American Institute of Physics Handbook," 2nd ed, McGraw-Hill Book Co., Inc., New York, N. Y., 1963.

(11) These results conflict with those of Hughes and Purnell,[12] who found no reaction between allene and H atoms when H atoms were produced by dissociation of H_2 on a tungsten filament but who did observe reaction when H atoms were produced by photolysis of HI.

(12) A. N. Hughes and J. H. Purnell, *Nature*, **210**, 255 (1966).

(13) G. S. Trick and C. A. Winkler, *Can. J. Chem.*, **30**, 915 (1952).

(14) E. W. R. Steacie, "Atomic and Free Radical Reactions," Reinhold Publishing Corp., New York, N. Y., 1954.

(15) It will be shown in another paper that, owing to the stability of the products of N atom reactions, *viz.*, N_2, CN, and HCN, the net effect of N atoms in hydrocarbon-active nitrogen systems is only to produce H atoms.

carbon.[14] The study of hydrocarbon-active nitrogen systems thus provides a kinetic tool by which hydrocarbon–H atom reactions can be studied with concentrations of H atoms intermediate between the low concentrations of photolysis experiments and the high concentrations of discharge-tube experiments. Our conclusions concerning cracking of hydrocarbons by H atoms, as studied in hydrocarbon-active nitrogen systems, will be presented in another paper.

One other point requires presentation. In addition to forming C_2H_2, reaction 5 also produces CH_3 radicals. Since C_2H_2, once produced, moreover, remains an inert constituent of the reaction mixture, the fast reactions that occur subsequent to reaction 5 must be those of CH_3 radicals with N or H atoms and not those of C_2H_2. The complexity of these subsequent reactions of CH_3 radicals is shown by the increased formation of HCN upon addition of H atoms to the CH_3C_2H + N and $CH_2{=}C{=}CH_2$ + N systems. These reactions, however, also require detailed presentation in another paper and are, again, not discussed further here.

The conclusions reached in this investigation also suggest that the addition of CH_3C_2H to a stream of H atoms might have use as a source of CH_3 radicals for kinetic studies because of the inertness of C_2H_2 to subsequent consumption by reactive species. We also plan to investigate this possibility further.

The reaction of CH_3C_2H with H atoms, however, probably could *not* be used to obtain accurate estimates of H atom concentrations (by measuring the C_2H_2 produced), since H atoms will be rapidly combined by the C_2H_2 produced by reaction 5, owing to the occurrence of the fast reactions 11 and 12, $k_{over-all} \approx 10^{-14}$ cm^3/molecule sec,[14,16] in competition with reaction 5.

(16) J. V. Michael and H. Niki, *J. Chem. Phys.*, **46**, 4969 (1967).

Solid-State Reactions of $SrCO_3$ + TiO_2

by N. H. Harris and R. L. Cook

University of Illinois, Ceramic Engineering Department, Urbana, Illinois 61803 *(Received October 6, 1967)*

The reaction kinetics of the formation of $SrTiO_3$ from $SrCO_3$ + TiO_2 (rutile) were studied by Hanykyr[1] in the temperature range of 812–1356°. Activation energies were reported for the formation of $SrTiO_3$ to be 55.4 kcal/mol by reaction of 0.26 μ (average particle size) of $SrCO_3$ with 0.19 μ of TiO_2 and 55.6 kcal/mol with 50–60 μ of TiO_2. Kinetic data were obtained from chemical determination of unreacted $SrCO_3$. Activation energy calculations were based on kinetic models of Jander,[2] Carter,[3] and Dünwald and Wagner.[4] Thermodynamic calculations, thermogravimetric analysis, and X-ray diffraction measurements of the present study have indicated that it is an oversimplification to assign these activation energy values to the formation of $SrTiO_3$.

In solid–solid reactions, according to Garner,[5] a product layer is formed at the contact boundary between reactants. The reactions proceed by diffusion of the reactants through the product layer and by phase-boundary processes which cause consumption of the original crystal lattices. Concentration gradients in the product layer permit the formation of compounds with stoichiometries other than that of the original reactant mixture.

The solid–solid reactions of $BaCO_3$ + TiO_2 were studied by Templeton and Pask.[6] They reported that $BaTiO_3$ was formed by an initial contact reaction, and subsequent diffusion-controlled reactions formed all possible compounds indicated for a given temperature in the phase diagram of Rase and Roy.[7]

The heats of reaction and equilibrium CO_2 pressures for some possible reactions of $SrCO_3$ + TiO_2 were calculated from the data of Coughlin,[8] Lander,[9] and Kelley, Todd, and King.[10] The calculated values are summarized in Table I for the temperatures 1000, 1200, and 1400°K. The calculated equilibrium CO_2 pressures for reactions 1–4 are shown in Figure 1 for the temperature range of 800–1400°K.

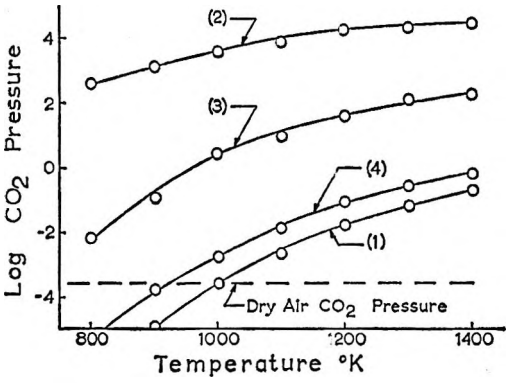

Figure 1. Calculated equilibrium CO_2 pressures *vs.* temperature (°K) for reactions 1–4 of $SrCO_3$ + TiO_2 (1:1 mole ratio).

(1) V. Hanykyr, *Silikaty*, **10**, 17 (1966).

(2) W. Jander, *Z. Anorg. Allgem. Chem.*, **163**, 1 (1927).

(3) R. E. Carter, *J. Chem. Phys.*, **34**, 2010 (1961); **35**, 1137 (1961).

(4) H. Dünwald and C. Wagner, *Z. Physik. Chem.* (Leipzig), **B24**, 53 (1934).

(5) W. E. Garner, "Chemistry of the Solid State," Butterworth and Co. Ltd., London, 1955, p 297.

(6) L. K. Templeton and J. A. Pask, *J. Amer. Ceram. Soc.*, **42**, 212 (1959).

(7) D. E. Rase and R. Roy, *ibid.*, **38**, 102 (1955).

(8) J. P. Coughlin, U. S. Bureau of Mines Bulletin 542, U. S. Government Printing Office, Washington, D. C., 1954.

(9) J. J. Lander, *J. Amer. Chem. Soc.*, **73**, 5794 (1951).

(10) K. K. Kelley, S. S. Todd, and E. G. King, Report of Investigations 5059, Bureau of Mines, Pittsburgh, Pa., Oct 1954.

Table I: Calculated Heats of Reaction and Equilibrium CO_2 Pressures for Reactions of $SrCO_3$ + TiO_2

Reaction	Temp, °K	CO_2 pressure, atm	ΔF,[a] kcal/mol	ΔH,[b] kcal/mol
(1) $SrCO_3(s) \rightarrow SrO(s) + CO_2(g)$	1000	2.98×10^{-4}	16.4	51.5
	1200	1.77×10^{-2}	9.43	46.1
	1400	2.00×10^{-1}	4.48	44.6
(2) $SrCO_3(s) + TiO_2(s) \rightarrow SrTiO_3(s) + CO_2(g)$	1000	3,800	−16.4	21.4
	1200	17,340	−23.3	15.7
	1400	24,600	−28.1	15.8
(3) $2SrCO_3(s) + TiO_2(s) \rightarrow Sr_2TiO_4(s) + 2CO_2(g)$	1000	2.72	−3.96	60.7
	1200	38.9	−17.4	48.6
	1400	126	−26.8	47.1
(4) $SrCO_3(s) + SrTiO_3(s) \rightarrow Sr_2TiO_4(s) + CO_2(g)$	1000	1.91×10^{-3}	12.4	48.5
	1200	8.67×10^{-2}	5.83	42.9
	1400	6.31×10^{-1}	1.28	41.3

[a] ΔF is the free energy of the reaction. [b] ΔH is the heat of the reaction.

The calculated CO_2 pressures of reactions 2 and 3 are much greater than reaction 1, so that formation of a compound would be an easier path for $SrCO_3$ decomposition. However, the formation of SrO as an intermediate step would be thermodynamically possible, as indicated by combination of reactions 1 and 2 and of reactions 1 and 4

$$SrO + TiO_2 \longrightarrow SrTiO_3$$

$$SrO + SrTiO_3 \longrightarrow Sr_2TiO_4$$

According to Figure 1, reaction 1 would not be possible in the temperature range 800–1400°K if the CO_2 pressure were 1 atm or greater. However, under a vacuum or in 1 atm of air or inert gas, reaction 1 could not be ruled out as a necessary intermediate or alternate path. Thermodynamic data are not available to permit calculations for reactions forming $Sr_3Ti_2O_7$ and $Sr_4Ti_3O_{10}$.

In the present study an activation energy of 53.7 kcal/mol was obtained from thermogravimetric analysis of $SrCO_3$ + TiO_2 (1:1 mole ratio) in the temperature range of 950–1100°. The isothermal thermogravimetric measurements were conducted in an ambient air atmosphere. Reagent grade $SrCO_3$ (Mallinckrodt Chemical Works, New York, N. Y., 99.67% pure) and high-purity TiO_2 (National Lead Co., South Amboy, N. J., Lot No. MP–2254 99.98% pure) were used as raw materials. The raw-material impurity contents are shown in Table II. The TiO_2 was determined by X-ray diffractometry to consist almost entirely of the rutile form. The highest intensity anatase line (101) was barely detectable, while that for rutile (110) was observed to be very intense in the TiO_2 sample as received. Average particle sizes of 0.6 μ for $SrCO_3$ and 0.8 μ for TiO_2 were obtained by direct-transmission electron microscope observation.

X-Ray diffraction measurements at 25° for $SrCO_3$ + TiO_2 (1:1 mole ratio) heated 6 hr at 950° showed only phases of $SrCO_3$, TiO_2 (rutile), and $SrTiO_3$. However, the samples heated 6 hr at 1100° indicated the presence of $SrCO_3$, TiO_2 (rutile), $SrTiO_3$, Sr_2TiO_4, $Sr_3Ti_2O_7$, and $Sr_4Ti_3O_{10}$.

Table II: Impurity Content of Raw Materials

	Impurity, %
$SrCO_3$ (99.67% pure)	
Alkali salts (sulfates)	0.300
Ba	0.005
Cl	0.005
Pb	0.002
Fe	0.002
SO_4	0.005
Acetic acid (insoluble)	0.010
TiO_2 (99.98% pure)	
SiO_2	0.003
Fe_2O_3	<0.002
Al_2O_3	0.003
Sb_2O_3	<0.003
Mg	<0.0001
Cu	<0.0001
Pb	<0.0005
Mn	<0.00005
Ni	<0.0009
V	0.0004
Cr	0.0001

On the basis of the observed results and thermodynamic calculations, it is concluded that the reported[1] activation energies for the reaction of $SrCO_3$ + TiO_2 (rutile) in the temperature range of 812–1356° cannot be assigned to the formation of $SrTiO_3$.

$Hg(6^3P_1)$-Photosensitized Isomerization of Octafluorobutene-2[1a]

by D. M. Graham and Takumi Hikida[1b]

Department of Chemistry, University of Western Ontario, London, Ontario, Canada *(Received December 18, 1967)*

It is now reasonably well established that the $Hg(6^3P_1)$-photosensitized isomerization of butene-2 may be explained by the mechanism[2]

$$C + Hg^* \longrightarrow P^* + Hg \qquad (qc)$$

$$T + Hg^* \longrightarrow P^* + Hg \qquad (qt)$$

$$P^* \longrightarrow \rho C + (1 - \rho)T \qquad (i)$$

where C and T refer to the *cis* and *trans* forms, respectively, and P* represents the excited olefin triplet state. The probability factor, ρ, has been shown to be 0.5 from quantum yield measurements, and the ratio of the quenching rate constants is thought to control the photosensitized equilibrium such that

$$K = (T)_e/(C)_e = k_{qc}/k_{qt} = 1.13$$

A recent investigation[3] of the mercury-photosensitized isomerization of the perfluoro compound has indicated the possibility of a much more complex mechanism. The quantum yields reported were less than one-fifth of those reported for the hydrogenated compound, and no definite conclusions were reached concerning the establishment of a photostationary equilibrium. Because of the extensive success of *cis–trans* isomerization reactions in actinometric measurements of triplet quantum yields, it was felt that the isomerization of octafluorobutene-2 warranted further investigation, if only because of its relatively high stability with respect to decomposition at low pressures.

Experimental Section

Octafluorobutene-2 (Matheson Co.) was equilibrated by passing it through a column of activated alumina at 25°. The remaining 13% of the *cis* isomer was separated by glc on a 25-ft, $^1/_4$-in. o.d. pentadecafluorooctyl acrylate column. This column was also used with a flame ionization detector for analysis. Complete baseline resolution of the *cis* and *trans* peaks could not be obtained, and areas were calculated using the Gaussian approximation which was shown to hold for an isolated peak. This procedure required greater than 15% reaction to give reliable results. *cis-Butene*-2 (Phillips Research Grade) was analyzed on a 8 ft × $^3/_{16}$-in. o.d. dimethylsulfolane column at 0°. Tetrafluoromethane (Matheson Co.) was distilled from silica gel at −77° to remove traces of impurities which quenched $Hg(^3P_1)$.

The photolysis apparatus consisted of a cylindrical quartz cell, 250 × 42 mm o.d., illuminated along its length by a U-shaped lamp (Hanovia 87-A-45). This lamp has a Vycor envelope which limits emission to wavelengths above 2200 Å. Both lamp and cell were immersed in a water bath operated at 25.0 ±0.1°.

Results

Since only small amounts of reactants were available, it was necessary to carry out the experiments at pressures where complete quenching of excited mercury atoms could not occur. A technique using *cis*-butene-2 sensitized isomerization as an actinometer under these conditions has been developed and will be discussed more fully in a subsequent publication.[4] Briefly, it is based upon the not unreasonable assumption that the effective lifetime of an excited mercury atom depends primarily upon the rate of quenching in the cell, all external factors remaining constant. In order to eliminate the possibility of pressure-broadening effects, all measurements are carried out in the presence of a constant excess of CF_4 which has been shown to be virtually a nonquencher. Thus, the determination of the quantum yield for a sensitized reaction of octafluorobutene-2 requires an actinometric run using *cis*-butene-2 at a concentration such that the calculated quenching rates are equal for the two experiments; this gives the effective number of quanta (I_{eff}) which are transferred. The required relative quenching rate constant is readily obtained from retardation of *cis*-butene-2 isomerization by the fluorinated olefin. The competitive quenching plot is given in Figure 1, the slope of which gives directly a ratio of 0.15 ± 0.01 for the quenching efficiency of octafluorobutene-2 relative to that for *cis*-butene-2. These measurements were made on a mixture of 13% *cis*- and 87% *trans*-octafluorobutene-2 under conditions such that only slightly better than 1% of the *cis*-butene-2 and virtually none of the perfluoro compound was isomerized.

A number of experiments were carried out to determine the photostationary equilibrium; these are summarized in Table I. Since at pressures less than 0.1 torr some decomposition was observed, the low olefin pressure runs were carried out in the presence of 50 torr of CF_4 which is a very efficient vibrational energy quencher. On the basis of these results there seems to be little doubt that an equilibrium is established, with K = 1.35. This is not too different from that observed for the hydrogenated compound.

The isomerization rate measurements are given in Table II. In calculating the initial quantum yields given in Table II, it is necessary to correct for the high

(1) (a) This work was supported by a grant from the National Research Council of Canada. (b) Province of Ontario Graduate Fellow.

(2) R. B. Cundall and T. F. Palmer, *Trans. Faraday Soc.*, **56**, 121 (1960).

(3) D. Saunders and J. Heicklen, *J. Phys. Chem.*, **69**, 3205 (1965).

(4) D. M. Graham and T. Hikida, to be submitted.

Table I: Photosensitized Equilibrium of Octafluorobutene-2

Initial pressure, torr		Time,	Final %
cis	*trans*	hr	*trans*
0.065	0	2	55.4
0.070	0	3	56.0
0	0.068	2	58.7
0	0.066	3	57.6
1.90	0	2	56.5
0	1.94	0.5	58.0
0	2.00	2	58.4

Table II: Isomerization Quantum Yields of Octafluorobutene-2

Octafluoro-butene-2, torr	Con-version, %	Time, min	$I_{eff} \times 10^9$, einsteins $l.^{-1}$ sec^{-1}	Φ
1.96[a]	19.9	240	8.95	0.22
1.85[a]	18.5	120	12.4	0.26
1.08[a]	18.9	90	10.7	0.26
0.20[a]	15.8	30	4.21	0.30
0.14[a]	18.0	30	3.22	0.32
0.10[a]	19.1	15	3.88	0.43
0.097[a]	33.3	38	3.69	0.43
0.090[a]	16.9	20	2.24	0.41
0.077[b]	16.7	10	3.05	0.36
0.095[a,c]	22.3	40	2.03	0.34
0.077[b,c]	17.7	30	1.72	0.30

[a] *trans*. [b] *cis*. [c] +0.065 torr of butene-2. All experiments were carried out in the presence of 50 torr of CF_4.

degree of conversion required by the analytical technique used. This has been done using an integrated rate equation derived from the mechanism described previously for butene-2. There are two possible ways that this correction may be made depending upon whether the equilibrium constant is a result only of different quenching efficiencies for the *cis* and *trans* isomers, or whether it depends primarily on the ratio of the probability factors, $\rho/(1 - \rho)$. The form of the integrated equation is different in each case, but the initial quantum yields calculated using these equations differ by less than 5%. For reasons given below, the yields given in Table II were calculated assuming $K = k_{qc}/k_{qt} = 1.35$. In determining I_{eff} for these calculations, the measured relative quenching efficiency of 0.15 was used. If the above assumption is valid, relative efficiencies of 0.14 and 0.19 for the *trans* and *cis* isomers, respectively, would be more correct. However, over the pressure range investigated, small changes in quenching rates are, to a certain extent, compensated by a corresponding change in the mean rate of radiative energy loss, and the use of these different quenching efficiencies results in a change of only about 5% in the calculated quantum yields.

Whatever corrections are made, the quantum yields exhibit the same behavior as shown in Figure 2. The

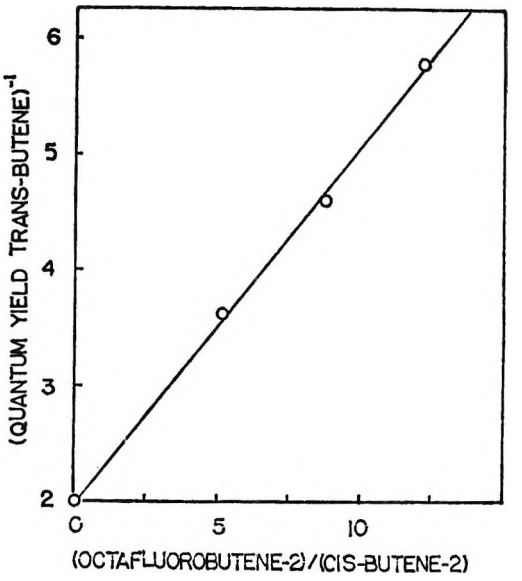

Figure 1. Competitive quenching of octafluorobutene-2 and *cis*-butene-2.

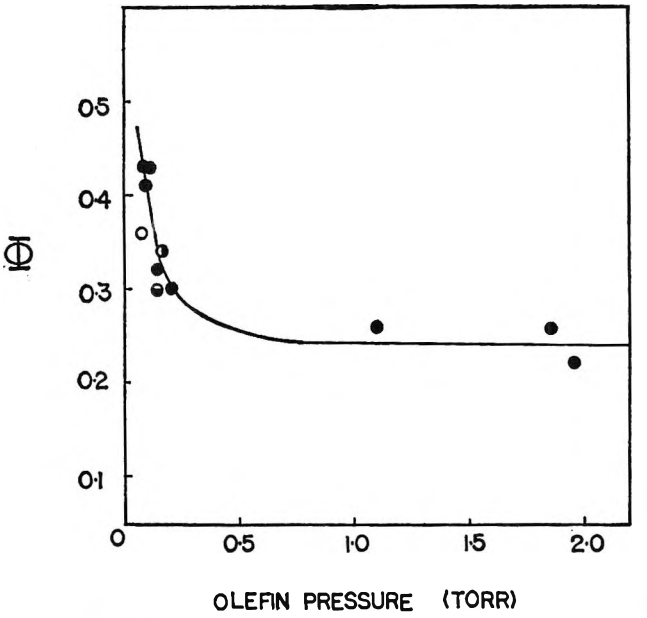

Figure 2. Variation of initial quantum yield with olefin pressure: ●, Φ_{cis}; ◑, Φ_{cis} with 0.065 torr of butene-2; ○, Φ_{trans}; ◒, Φ_{trans} with 0.065 torr of butene-2.

quantum yields decrease with increasing olefin pressure, probably approaching a limiting value. A high concentration limit would be consistent with the results of Saunders and Heicklen,[3] who obtained roughly constant quantum yields from 0.5 to 6 torr. Their values are, however, smaller since they used a different actinometer and did not attempt to allow for incomplete quenching. Their results also indicate (as does the one value of Φ_{trans} which we were able to obtain) that the sum of the quantum yields, $\Phi_{cis} + \Phi_{trans}$, cannot possibly be unity even with any reasonable correction for incomplete quenching. This implies, as these

authors have suggested, a barrier to internal rotation in the excited state (or states) produced by sensitization.

The olefin pressure dependence of the quantum yields must result from efficient deactivation of the excited state by olefin which competes with internal rotation. Butene-2 appears to be about as effective as the perfluoro derivative. Deactivation by olefin has also been shown to be important in the sensitized isomerization of hexafluorocyclobutene[4] and in the photoisomerization of 1,2-dichloroethylene, although the interpretation is less clear in the latter case due to the possibility of chlorine atom catalysis.

Since the equilibrium constant is independent of olefin pressure, it appears most likely that the equilibrium constant depends primarily upon the quenching efficiencies of the *cis* and *trans* isomers. The change in the probability factors with olefin pressure, that is reflected in the change in quantum yields, must occur in such a way that their ratio remains constant. This would be the case if the barrier to internal rotation were symmetrical and should result in limiting low pressure quantum yields of 0.5 which are not inconsistent with possible extrapolations on Figure 2.

Formation Constants of Some 2:2 and 3:3 Ion Pairs

by R. A. Matheson

Chemistry Department, Victoria University of Wellington, New Zealand *(Received February 14, 1968)*

When calculating the formation constant of an ion pair or molecule from cryoscopic, ultraviolet absorption, or conductance measurements, one commonly uses the Debye–Hückel formula

$$-\log \gamma_{\pm} = \frac{Az_1z_2\sqrt{I}}{1 + Bd\sqrt{I}} \quad (1)$$

for the activity coefficient of the free ions and, if necessary, one of the following conductance equations: the Onsager limiting law, the Leist equation

$$\Lambda = \Lambda^0 - \left(\frac{\alpha'\Lambda^0}{(1 + 2^{-1/2}Bd\sqrt{I})} + \beta'\right)\frac{\sqrt{I}}{1 + Bd\sqrt{I}} \quad (2)$$

the Robinson and Stokes (RS) equation (eq 2 without the factor $1 + 2^{-1/2}Bd\sqrt{I}$), or the Fuoss Onsager (FO) equation

$$\Lambda = \Lambda^0 - (\alpha + \beta\Lambda^0)\sqrt{C} + EC \log C - JC \quad (3)$$

in which J is a function of the distance of closest approach parameter d. Sometimes the value of the formation constant K depends on the figure assumed for d. Thus in water at 25°, Covington, *et al.*,[1] obtained for the bisulfate ion $K = 95\ M^{-1}$ when $d = 5.17$ Å and $K = 86\ M^{-1}$ when $d = 3.04$ Å, while Prue and coworkers[2] found larger variations of K with d for several sulfate ion pairs involving divalent cations. The model implicit in the calculation of K from experimental data *via* eq 1 considers pairs of ions of separation[3] less than d to be associated, while those of greater separation are regarded as free. This implies some dependence of K upon d, since when d is increased from d_1 to d_2 a number of pairs of ions formerly considered free become classed associated, thus increasing the value of K. By using Bjerrum's formula to calculate the number of ion pairs having separations between d_1 and d_2, Guggenheim[4] obtained an equation for the variation of K with d which is consistent with Covington's results for the bisulfate ion. We shall examine the implications of this equation in regard to the dissociation of some 2:2 and 3:3 ion pairs.

For a species dissociating into two ions of valency Z, Guggenheim's equation becomes

$$K_2 - K_1 = 4\pi N(Z^2S)^3 \int_{Z^2S/d_2}^{Z^2S/d_1} X^{-4}e^X \, dX \quad (4)$$

where K_i corresponds to a distance of closest approach d_i, N is Avogadro's number, and S is the length e^2/DkT (7.15 Å for water at 25°). A moles per unit volume concentration scale is assumed. In Table I we compare values of $K_2 - K_1$ for $CuSO_4$ and $MgSO_4$ calculated from formation constants obtained from various experimental measurements with those given by eq 4.

Equation 4 gives values of $K_2 - K_1$ consistently larger than the figures obtained from "experimental" formation constants, especially those derived from conductances *via* the Leist and Pitts equations. Although agreement between eq 4 and the other experimental figures is better, there are still discrepancies in excess of the uncertainty in $K_2 - K_1$, when $d_1 < 10$ Å.

Dunsmore, Kelly, and Nancollas[5] reported precise conductance measurements for dilute aqueous solutions of several rare earth cobalticyanides and ferricyanides from which they calculated, *via* the limiting laws, ion pair formation constants of about $5.5 \times 10^3\ M^{-1}$. In the case of such 3:3 aqueous ion pairs, eq 4 requires a substantial variation of K with d, unless d is in the vicinity of the Bjerrum critical distance (32 Å). We have therefore reanalyzed the data for lanthanum ferricy-

(1) A. K. Covington, J. V. Dobson, and W. F. K. Wynne-Jones, *Trans. Faraday Soc.*, **61**, 2057 (1965).

(2) (a) P. G. M. Brown and J. E. Prue, *Proc. Roy. Soc.*, **A232**, 320 (1955); (b) W. G. Davies, R. J. Otter, and J. E. Prue, *Discussions Faraday Soc.*, **24**, 53 (1957); (c) R. J. Otter and J. E. Prue, *ibid.*, **24**, 106, 123 (1957); (d) "Ionic Equilibria," J. E. Prue, Pergamon Press Ltd., London, 1966; (e) R. J. Otter, Ph.D. Thesis, University of Reading, 1960.

(3) By separation, we mean the distance between ionic centers.

(4) E. A. Guggenheim, *Trans. Faraday Soc.*, **62**, 2750 (1966).

(5) H. S. Dunsmore, T. R. Kelly, and G. H. Nancollas, *ibid.*, **59**, 2606 (1963).

Table I: Values of $K_2 - K_1$ for $d_2 = 14$ Å

$CuSO_4$

	$K_2 - K_1$, M^{-1}			
d_1, Å	Eq 4	Uv[2b,e] (K_2 = 286 M^{-1})	Cryoscopic[2a,b] (K_2 = 300 M^{-1})	Conductance (Leist)[2b] (K_2 = 286 M^{-1})
10	47	36	37	6
7	96	36	56	18
4.3	221	161	133	52

$MgSO_4$

	$K_2 - K_1$, M^{-1}				
d_1, Å	Eq 4	Cryoscopic[2a,b] (K_2 = 244 M^{-1})	Conductance (Leist)[2d] (K_2 = 213 M^{-1})	Conductance (Pitts)[2d] (K_2 = 204 M^{-1})	Conductance (FO)[2d] (K_2 = 200 M^{-1})
10	47	...	13	20	30
8.6	67	36	...	...	...
7	96	53	...	...	...
4.3	221	134	33	9	82

anide using the RS and FO equations with $d = 7.5$, 10, 14, and 28 Å. For each value of d, the RS equation (here substantially equivalent to the Leist equation) gives formation constants which differ little from the limiting-law figure of 5.49×10^3 M^{-1}, but the FO equation gives $K = (2.50 \pm 0.09) \times 10^3$ M^{-1} for $d = 7.5$ Å $(3.05 \pm 0.08) \times 10^3$ M^{-1} for $d = 10$ Å, $(3.76 \pm 0.04) \times 10^3$ M^{-1} for $d = 14$ Å, and $(5.29 \pm 0.05) \times 10^3$ M^{-1} for $d = 28$ Å. While formation constants which showed a satisfactorily small variation with concentration could always be obtained from a single value of Λ^0 (169.57 ohm^{-1} cm^2 g-equiv^{-1}) when the RS equation was used, this was not so in the case of the FO equation, in which we used $\Lambda^0 = 165$ ohm^{-1} cm^2 g-equiv^{-1} when $d = 7.5$ Å, 166 ohm^{-1} cm^2 g-equiv^{-1} when $d = 10$ Å, 167.5 ohm^{-1} cm^2 g-equiv^{-1} when $d = 14$ Å, and 170 ohm^{-1} cm^2 g-equiv^{-1} when $d = 28$ Å. Our calculations suggest caution in regard to the view of some workers that the FO equation and the limiting law give very similar formation constants for $K \geq 100$ M^{-1}. While this may be the case for 1:1 electrolytes in many solvents, exceptions appear possible with higher valence type electrolytes (or 1:1 electrolytes in a solvent of very low dielectric constant), since for these E and J may be so large that the two equations differ significantly even at high dilutions.

From eq 4 we calculated for a 3:3 electrolyte $K_{28} - K_{14} = 1.1 \times 10^3$ M^{-1}, $K_{28} - K_{10} = 2.2 \times 10^3$ M^{-1}, and $K_{28} - K_{7.5} = 4.9 \times 10^3$ M^{-1}. Only the last is in serious disagreement with the formation constants calculated with the FO equation. (These give $K_{28} - K_{14} = 1.5 \times 10^3$ M^{-1}, $K_{28} - K_{10} = 2.2 \times 10^3$ M^{-1}, and $K_{28} - K_{7.5} = 2.8 \times 10^3$ M^{-1}.) However, disagreement with the data obtained *via* the RS equation is complete. Since formation constants for $CuSO_4$ and $MgSO_4$ calculated from conductances with the Leist equation show a variation with d which is not consistent with the figures derived from other types of measurements or with eq 4, we are inclined to the view that the RS and Leist equations do not always correctly relate the conductances of free ions to their distance of closest approach and that the d obtained from these equations is not always this distance.

Equation 4 and the methods used to calculate formation constants from experimental data are all based on the model of ion association outlined earlier and all assume a "charged spheres–continuous dielectric medium" view of interactions between certain of the ions (in eq 4, all pairs of ions with separations between d_1 and d_2; in the calculation of K_i from experimental data, all pairs of separation greater than d_i). Discrepancies between eq 4 and formation constants derived from experimental data may imply failure of the model or of this assumption. However, there are other possibilities, such as failure of the Debye–Hückel treatment of interactions between charged spheres and, in the case of data calculated from conductances, failure of the assumption that symmetrical ion pairs do not conduct or of the equation used for the free-ion conductances. The Debye–Hückel expression for the potential due to the ionic atmosphere is used in the derivations of eq 1–3 but not eq 4, which is obtained by equating each formation constant, K_i, to the ratio $(1 - \alpha_i)/C$ (α_i is the degree of dissociation when d is set at d_i) for extremely low concentrations where $1 - \alpha \ll 1$ and the contribution of the ionic atmosphere to the field experienced by an *associated* ion is negligible. It has been shown[6] that the Debye–Hückel potential expression fails for a 2:2 electrolyte at ionic separations ≈ 4 Å. One might expect similar failure at somewhat larger separations in the case of a 3:3 electrolyte. Thus the discrepancies which we find at low values of d are not surprising.

There remains one unsatisfactory feature of our FO analysis of the $LaFe(CN)_6$ data, namely the fact that differing values of Λ^0 were required depending on the value assumed for d. There is no reason why the mobility of two free ions *at infinite dilution* should depend on the separation at which the distinction between free ions and associated ions is drawn. Possibly our adjustments to Λ^0 were necessary to compensate for variation in the adequacy of our assumptions as d was altered. In this connection it is interesting to note that for $K_3Fe(CN)_6$ and $LaCl_3$, respectively, figures of 172.6 and 145.95 ohm^{-1} cm^2 g-equiv^{-1} for Λ^0 have been obtained[7] from an empirical extension of the limiting law which is of a similar form to the FO equation. Thus since Λ^0 for KCl equals 149.95 ohm^{-1} cm^2 g-

(6) E. A. Guggenheim, *Discussions Faraday Soc.*, **24**, 53 (1957).

(7) J. C. Jones and C. B. Monk, *Trans. Faraday Soc.*, **46**, 1046 (1950).

equiv^{-1},[8] Λ^0 for $LaFe(CN)_6$ equals 168.6 ohm^{-1} cm^2 g-equiv^{-1}, which makes the figure of 165 ohm^{-1} cm^2 g-equiv^{-1} for $d = 7.5$ Å seem rather unsatisfactory.

In conclusion, it seems that provided d is not set too small, experimental formation constants for these salts show approximately the variations with d required by the ion-association model. However, in the sole case where a reasonably large variation in K is found to be consistent with eq 4, $LaFe(CN)_6$, only formation constants derived from conductances are available. We consider that other types of experimental measurements which would yield formation constants for this (or a similar) salt are desirable to confirm our conclusions.

(8) R. Fernandez-Prini and J. E. Prue, *Z. Phys. Chem.* (Leipzig), **228**, 373 (1965).

Estimation of the Critical Surface Tension for Polymers from Molecular Constitution by a Modified Hildebrand–Scott Equation

by Souheng Wu

Fabrics and Finishes Department, E. I. du Pont de Nemours Company, Wilmington, Delaware 19898 *(Received March 1, 1968)*

Zisman's critical surface tension[1] has been widely used as an approximate value to the surface free energy of solids. Attempts[2-4] to correlate the critical surface tension with the bulk properties have been reported previously. However, none of these is quantitatively reliable. In this work, we developed a modified Hildebrand–Scott equation[5] that permits prediction of the critical surface tension for polymers from molecular constitution with good accuracy.

Derivation

For spherical molecules with nearest neighbor interaction in a condensed phase, the surface tension γ can be related to the molar cohesive energy ΔE_c and the molar cross-sectional area of the molecule A by[6]

$$\gamma = K(\Delta E_c/A) \tag{1}$$

where K is a constant determined by the coordination number of the lattice. The molar cohesive energy is, by definition, related to the solubility parameter δ by

$$\Delta E_c = V_m\delta^2 \tag{2}$$

where V_m is the molar volume. The molar cross-sectional area for spherical molecules can be written as

$$A = N^{1/3}V_m^{2/3} \tag{3}$$

where N is Avogadro's number. Combination of eq 1–3 leads to the basis of the Hildebrand–Scott equation.[5]

For polymer molecules which are chainlike, eq 3 cannot be used. The significance of A in the case of polymers becomes complicated. However, we will assume that A is the "effective" molar cross-sectional area of a segment (or repeat unit) and is given by

$$A = kN^{1/2}n_s(V_m^s/n_s)^{2/3} \tag{4}$$

where V_m^s is the molar volume of a segment, n_s is the number of atoms in the segment, and k is a parameter determined by the structure and the packing geometry of the polymer molecules. Equation 4 can be obtained by assuming that polymer molecules may be represented by a collection of "equivalent spheres," each sphere being an interacting unit whose volume is V_m^s/n_s. Although this assumption seems artificial, its validity is affirmed by the applicability of the resulting equation, as can be seen later. Combining eq 1, 2, and 4 and considering only the dispersion-force contributions, we obtain

$$\delta_d = \alpha\left[\frac{\gamma^d}{(V_m^s/n_s)^{1/3}}\right]^\beta \tag{5}$$

where δ_d and γ^d are the dispersion-force contributions to δ and γ and α and β ($= 0.5$) are numerical constants.

In order to relate the critical surface tension, γ_c, to the molecular structure, we use γ_c to approximate γ^d, which is closely related,[7] and use Small's equation[8] to evaluate δ_d.

$$\delta_d = (\sum F)^s/V_m^s \tag{6}$$

where $(\sum F)^s$ is the sum of Small's molar attraction constants[8] for a segment and is presumed to give predominantly the dispersion-force contributions.[8] Instead of using the theoretical value of 0.5 for β, we plot log $(\sum F)^s/V_m^s$ *vs.* log $\gamma_c/(V_m^s/n_s)^{1/3}$ for 36 polymers, using the experimental literature values of γ_c, and we obtain $\alpha = 1.83$ and $\beta = 0.54$. Thus

$$\delta_d = 1.83\left[\frac{\gamma_c}{(V_m^s/n_s)^{1/3}}\right]^{0.54} \tag{7}$$

where γ_c is the critical surface tension at 20°, in dyn/cm,

(1) (a) W. A. Zisman in "Contact Angle, Wettability, and Adhesion," Advances in Chemistry Series, No. 43, American Chemical Society, Washington, D. C., 1964, pp 1–51; (b) W. A. Zisman in "Adhesion and Cohesion," P. Weiss, Ed., Elsevier Publishing Co., New York, N. Y., 1962, pp 176–208.

(2) J. L. Gardon, *J. Phys. Chem.*, **67**, 1935 (1963).

(3) (a) I. J. Lee, W. M. Muir, and D. J. Lymann, *ibid.*, **69**, 3220 (1965); (b) R. J. Roe, *ibid.*, **69**, 2809 (1965).

(4) L. H. Lee, Preprints, Division of Organic Coatings and Plastics Chemistry, 154th National Meeting of the American Chemical Society, Chicago, Ill., Sept 1967, pp 61–84.

(5) J. H. Hildebrand and R. L. Scott, 'The Solubility of Nonelectrolytes," 3rd ed, Reinhold Publishing Corp., New York, N. Y., 1950, p 431.

(6) A. S. Michaels in "Symposium on Properties of Surfaces," ASTM Special Technical Publication, No. 340, American Society for Testing and Materials, Philadelphia, Pa., 1963, pp 3–23.

(7) F. M. Fowkes in "Chemistry and Physics of Interfaces," American Chemical Society, Washington, D. C., 1965, pp 1–12.

(8) P. A. Small, *J. Appl. Chem.*, **3**, 71 (1953).

V_m^s is the molar volume of the segment, in cm³/mol, n_s is the number of atoms in the segment, and δ_d is the dispersion-force contribution to the solubility parameter, in (cal/cm.³)$^{1/2}$, to be determined from Small's molar attraction constants.[8] In fact, $\alpha = 2.09$ and $\beta = 0.5$ also give about the same results as eq 7. Combining eq 6 and 7, we obtain

$$\gamma_c = 0.327\left(\frac{(\sum F)^s}{n_s}\right)^{1.85}\left(\frac{n_s}{V_m^s}\right)^{1.52} \quad (8)$$

Results and Discussion

Equation 8 can be used to calculate the critical surface tension for polymers from molecular constitution by using Small's molar attraction constants.[8] Equation 7 resembles but differs from the Hildebrand–Scott equation[5] that is applicable to low molecular weight liquids but inapplicable to polymers. The difference lies mainly in that the former contains an additional parameter, n_s, the number of atoms in a segment, which is necessary for the macromolecules in our model. The γ_c values calculated by eq 8 for 37 polymers agree well with the experimental values, as can be seen in Table I. The experimental values of the critical surface tension in Table I are those reported in the literature.[1,4,9] The density data used are those of the typical solid polymers at 25°.

In calculating the F value for hydroxyl group OH, we used the sum of constants –O– ($F = 70$) and –H ($F = 100$), as suggested by Small.[8] This should be permissible, since we are dealing with the dispersion-force contributions. For the amide group, CONH, Small's table[8] does not allow a similar calculation. Therefore, we evaluated the F value to be 340 by using the dispersion-force contribution to the surface tension of formamide, 39.5 dyn/cm,[7] and the Hildebrand–Scott equation.[5] This F value gave correct γ_c's for poly(6-aminocaproic acid), poly(hexamethyleneadipamide), and urea–formaldehyde resin, as can be seen in Table I. For CFCl, we used the average of CF_2 and CCl_2. For Si (in silicones), an F value of −38, as given by Burrell,[10] was used. For the nitrile group, CN, Small's F value of 410 seems to contain an appreciable amount of contributions from polarity. The γ_c values of poly(methacrylonitrile) and of poly(acrylonitrile) indicate that the dispersion-energy part of F for CN should be 297.

It is interesting to note that eq 8 indicates that the lower critical surface tension of poly(tetrafluoroethylene) (18.5 dyn/cm) than that of polyethylene (31 dyn/cm) is mainly due to its lower packing density (*e.g.*, larger average atomic size). For poly(tetrafluoroethylene), $(\sum F)^s = 300$ and $V_m^s = 45.5$ ($n_s = 6$). For polyethylene, $(\sum F)^s = 266$ and $V_m^s = 30.0$ ($n_s = 6$). Recently, Hoernschemeyer[11] proposed a similar conclusion by a different approach. On the other hand, the increased critical surface tension of poly(chlorotrifluoroethylene) (31 dyn/cm) over that of poly(tetrafluoroethylene) is due to its increased molar attraction constants. For poly(chlorotrifluoroethylene), $(\sum F)^s = 438$ and $V_m^s = 56.2$ ($n_s = 6$).

Newman[12] recently measured γ_c of poly(vinyl butyral)

Table I: The Calculated and the Experimental Values of the Critical Surface Tensions of Polymers at 20°

Polymers	Molar volume of a segment (V_m^s), cm³/mol	Critical surface tensions, dyn/cm Calcd	Exptl
Poly(tetrafluoroethylene)	45.5	21	18.5[a]
Poly(dimethylsiloxane)	65.0	23	24[b]
Poly(vinylidene fluoride)	36.4	26	25[a]
Poly(1,2-butadiene)	56.4	29	25[c]
Poly(2-methylpropene)	63.0	24	27[c]
Poly(vinyl fluoride)	32.0	29	28[a]
Poly(vinyl methyl ether)	55.6	27	29[c]
Polypropylene	46.2	27	29[a]
Poly(4-*t*-butylstyrene)	169	28	29[c]
Poly(*trans*-2-methyl-1,3-butadiene)	72.4	31	30[c]
Poly(*cis*-2-methyl-1,3-butadiene)	75.0	29	31[c]
Poly(chlorotrifluoroethylene)	56.2	31	31[a]
Polyethylene (linear)	29.5	32	31[a]
Polyethylene (branched)	30.8	30	31[a]
Poly(*trans*-1,3-butadiene)	58.2	30	31[c]
Poly(*cis*-1,3-butadiene)	60.1	29	32[c]
Poly(propylene oxide)	58.0	28	32[c]
Poly(*n*-butyl methacrylate)	134	32	32[d]
Poly(ethylene methacrylate)	103	33	33[c]
Polystyrene	100	36	33[a]
Poly(ethyl acrylate)	91.0	35	35[c]
Poly(methylene oxide)	21.0	38	36[c]
Poly(vinyl acetate)	72.4	36	36[d]
Poly(vinyl alcohol)	34.2	37	37[b]
Poly(2-chloro-1,3-butadiene)	72.0	38	38[c]
Poly(methacrylonitrile)	57.3	39	39[d]
Poly(vinyl chloride)	44.6	43	39[a]
Poly(methyl methacrylate)	84.1	36	39[a]
Poly(vinylidene chloride)	58.0	40	40[a]
Poly(methyl acrylate)	70.5	40	41[c]
Polycarbonate (bisphenol-A type)	212	40	42[c]
Poly(2-chlorostyrene)	111	42	42[c]
Poly(6-aminocaproic acid)	100	40	42[b]
Poly(ethylene terephthalate)	143	50	43[a]
Poly(acrylonitrile)	45.4	44	44[c]
Poly(hexamethyleneadipamide)	182	46	46[a]
Urea–formaldehyde resin	40.5	64[e]	61[b]

[a] Data from ref 1. [b] Data from E. G. Shafrin in "Polymer Handbook," J. Brandrup and E. H. Immergut, Ed., Interscience Publishers, New York, N. Y., 1966, pp 111–113. [c] Data from ref 4. [d] Our measurements. [e] Calculation is based on (–NHCONHCH₂–)$_n$.

(9) E. G. Shafrin in "Polymer Handbook," J. Brandrup and E. H. Immergut, Ed., Interscience Publishers, New York, N. Y., 1966, pp 111–113.

(10) H. Burrell, *Offic. Dig. Federation Soc. Paint Technol.*, **27**, 726 (1955); **29**, 1069, 1159 (1957).

(11) D. Hoernschemeyer, *J. Phys. Chem.*, **70**, 2628 (1966).

(12) S. Newman, *J. Colloid Interfac. Sci.*, **25**, 341 (1967).

to be 24–25 dyn/cm which is much lower than those of polyethylene and poly(vinyl alcohol) (37 dyn/cm). He thus proposed that the CH_3 groups appeared to predominate over CH_2, ether oxygen, and OH groups on the poly(vinyl butyral) surface. However, the γ_c value calculated by our eq 8 for a poly(vinyl butyral) containing 35 mol % of poly(vinyl alcohol) and having a density of 1.05[13] is 25 dyn/cm, in good agreement with the experimental value, indicating that the various groups are probably actually randomly distributed on the surface. The low γ_c value of the polymer as compared with those of polyethylene and poly(vinyl alcohol) arises from the presence of three CH groups in the vinyl butyral segment which lower the molar attraction constant.

(13) H. R. Simonds and J. M. Church, "A Concise Guide to Plastics," Reinhold Publishing Corp., New York, N. Y., 1963, p 70.

Absorption Spectra of Sodium–Ammonia Mixtures in the Gas Phase

by Irving Warshawsky

Lewis Research Center, National Aeronautics and Space Administration, Cleveland, Ohio 44135
(Received March 6, 1968)

Gibson and Argo's spectral studies of dilute solutions of alkali metals in liquid ammonia suggest that a common species is present in these solutions.[1] This species has been identified as the "solvated electron." In a more recent investigation, where both the metal concentration and spectral ranges were extended, it was concluded that for the solvated electron Beer's law holds, even at concentrations where ion-pair formation was occurring.[2] Thus the position and shape of the absorption band of the solvated electron are surprisingly insensitive to the changes occurring in the electron's environment.

It is of interest to investigate whether the electron from sodium is delocalized in gaseous ammonia as it is when sodium dissolves in liquid ammonia, in view of Naiditch's demonstration that sodium is soluble in gaseous ammonia.[3] Further, the gaseous medium allows a broad range of relative concentrations of the solvent through the control of pressure.

The purpose of this note is to report some observations of the absorption spectra of gaseous sodium–ammonia mixtures over a range of ammonia pressures from 0 to 6 atm.

A diagram of the optical cell used for the spectral measurements is shown in Figure 1, with the path length between inner windows being 5.00 cm. A trace heater element (consisting of a metal-sheathed oxide-insulated

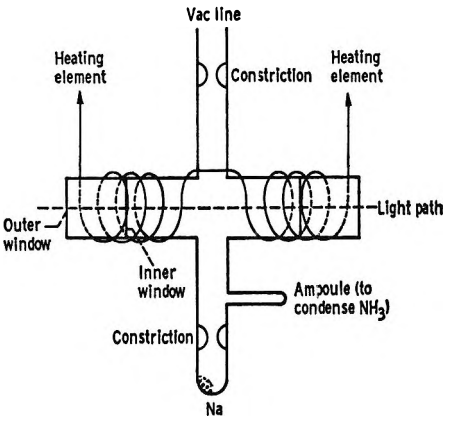

Figure 1. Optical cell used for spectral measurements.

nichrome wire) was wrapped around the inner windows of the vacuum-jacketed wall. The main heat input to the cell was by means of silver-coated copper shavings in thermal contact with the inner walls of a small oven. Temperature regulation was obtained with an Electromax pyrometric controller and an iron–constantan thermocouple which was welded to a copper plate placed in the oven. At 250°, temperature fluctuations near the cell were less than 3°. The outer windows of the optical cell were cooled by flushing with nitrogen gas. A Perkin-Elmer 350 recording spectrophotometer was used to record the spectra.

In a typical run, the optical cell was glass-blown to the vacuum line and pumped on for approximately 1 week at pressures less than 10^{-6} mm. During the final 24 hr of pumping, a liquid nitrogen bath was placed around a trap between the McLeod gauge and the cell in order to minimize mercury contamination of the cell due to its possible catalytic activity.[4] During the distillation of sodium into the cell through the constriction (Figure 1), the inner windows were coated with sodium. This sodium was distilled from the inner windows to the walls of the cell by passing a current through the heating element (Figure 1). The excess sodium was sealed off at the constriction while pumping. A known quantity of dry ammonia was then distilled into the cell. This was done by use of a gas buret (ammonia vapor at a pressure of 4.20 cm was distilled into an ampoule on the vacuum line whose volume had previously been calibrated) along with a liquid nitrogen bath which was placed around the ampoule on the cell shown in Figure 1. With a liquid nitrogen bath around the ampoule, the system was

(1) G. E. Gibson and W. L. Argo, *J. Amer. Chem. Soc.*, **40**, 1327 (1918).

(2) M. Gold and W. L. Jolly, *Inorg. Chem.*, **1**, 818 (1962); M. Gold, W. L. Jolly, and K. S. Pitzer, *J. Amer. Chem. Soc.*, **84**, 2264 (1962).

(3) S. Naiditch in "Metal Ammonia Solutions: Physical-Chemical Properties," G. LePoutre and M. J. Sienko, Ed., W. A. Benjamin, Inc., New York, N. Y., 1964, p 113.

(4) J. F. Dewald and G. Lepoutre, *J. Amer. Chem. Soc.*, **76**, 3369 (1954).

sealed off at the constriction while pumping. After placing the system in the oven described above, the absorption spectrum of the sodium–ammonia mixture was scanned repeatedly from 1000 to 350 mμ in the temperature range from 188 to 205°.

For *pure* sodium or sodium–ammonia mixtures containing smaller initial concentrations of ammonia than 0.11 *M*, no absorption band was observed over the temperature range 188–205°. However, for sodium–ammonia mixtures in which the initial concentration of ammonia was 0.11 *M*, assuming the ideal gas law (the cell volume was 50 ml), a narrow symmetrical absorption band with no fine structure was observed at 587 ± 2 mμ in two of three runs. A similar absorption band was observed in one of two runs where the initial ammonia concentration was 0.13 *M*. In each case where an absorption band was observed, it extended from 590 to 585 mμ, and the band width seemed to be independent of the temperature in the range from 188 to 205°. During a run, the intensity of the peak rose to a maximum, remained constant for about 15 min, and then decreased to zero once again. Where the initial ammonia concentration was 0.11 *M*, the maximum per cent absorptions (the transmittance multiplied by 100) for the three runs were 4, 8, and 0%, respectively. For an initial ammonia concentration of 0.13 *M*, the maximum per cent absorptions for two runs were 4 and 0%, respectively. After each of the runs had been completed, the initial sodium film had disappeared completely. Prior to a run, these films appeared stable to the eye at room temperature in the presence of ammonia. In contrast, potassium films were seen to disappear at room temperature in the presence of ammonia gas at several atmospheres of pressure.

The instability of the intensity of the band is not too surprising, in view of the well-known heterogeneous reaction between sodium and ammonia to form the amide. The constant absorption intensity which holds for approximately 15 min is probably due to the establishment of a steady-state concentration of absorbing species in the gas phase. The rate of formation would be expected to depend on the quantity of sodium and ammonia in the cell and the temperature. The rate of decomposition would depend on the state of the Pyrex surface where decomposition takes place,[5] diffusion from the gas phase to the catalytic sites on the glass surface, and the temperature. The nonreproducibility of the Pyrex surface[5] from run to run may account for the range of absorption intensities (from 0 to 8%) in the five different runs.

The narrow absorption maximum at approximately 587 mμ, which coincides with the $^2S_{1/2} \rightarrow {}^2P_{1/2,\,3/2}$ transition of the gaseous sodium atom, suggests that the absorbing species in the gaseous sodium–ammonia mixtures is one in which the 3s electron of the sodium atom remains essentially unperturbed. The absence of absorption in the 1000-mμ region, which is characteristic of the solvated electron in liquid ammonia,[1,2] indicated no appreciable charge transfer of the type reported in the liquid phase. At higher ammonia concentrations, where the gaseous solvent may be more liquidlike in structure, perhaps close to the critical point of ammonia, the possibility of observing charge-transfer processes may be more likely. Investigation of this effect at higher pressures could not be carried out in the present apparatus due to strength limitations.

(5) I. Warshawsky, *J. Catal.*, **3**, 291 (1964).

Kinetics of the Thermal $\alpha \rightarrow \beta$ Polymorphic Conversion in Metal-Free Phthalocyanine

by James H. Sharp and Roger L. Miller

Xerox Research Laboratories, Rochester, New York
(Received March 21, 1968)

The phthalocyanines are an important class of organic compounds which have been extensively studied for their pigment properties.[1] Moreover, within the last decade these compounds have undergone intensive investigations with respect to their optical, magnetic, and electronic conduction properties. Because of their high thermal stability, the phthalocyanines offer many advantages in the field of molecular electronics. In particular, since several of the phthalocyanines also exhibit photoconductive behavior, there has been wide interest in the use of these materials as photoconductors.

These compounds are known to exist in several polymorphic forms. The β form is the most stable polymorph, and its detailed crystal structure has been reported by Robertson.[2] Other polymorphs designated as the α,[3-10] γ,[10,11] and *x*[12] forms have been characterized by X-ray powder diffraction pattern and infrared or visible spectroscopy. Assour[10] and Sidorov

(1) See, for example, F. H. Moser and A. L. Thomas, "Phthalocyanine Compounds," Reinhold Publishing Corp., New York, N. Y., 1963.

(2) J. M. Robertson, *J. Chem. Soc.*, 615 (1935); 1195 (1936); 219 (1937).

(3) G. Susich, *Anal. Chem.*, **22**, 425 (1950).

(4) F. R. Tarantino, D. H. Stubbs, T. F. Cooke, and L. A. Melsheimer, *Amer. Ink Maker*, **29**, 35, 425 (1950).

(5) A. A. Ebert, Jr., and H. B. Gottlieb, *J. Amer. Chem. Soc.*, **74**, 2806 (1952).

(6) F. W. Karasek and J. C. Decius, *ibid.*, **74**, 4716 (1952).

(7) M. Shigemitsu, *Bull. Chem. Soc. Jap.*, **32**, 607 (1959).

(8) D. N. Kendall, *Anal. Chem.*, **25**, 382 (1953).

(9) A. N. Sidorov and I. P. Kotlyar, *Opt. Spektrosk.*, **11**, 92 (1961).

(10) J. M. Assour, *J. Phys. Chem.*, **69**, 2295 (1965).

(11) J. W. Eastes, U. S. Patent 2,770,620 (1956).

(12) J. F. Byrne and P. F. Kurz, U. S. Patent 3,357,989 (1967); J. H. Sharp and M. Lardon, *J. Phys. Chem.*, **72**, 3230 (1968).

and Kotlyar[9] reported that the α form is converted to the β phase when heated above 300°. The purpose of this work was to investigate the kinetics of the $\alpha \rightarrow \beta$ thermal conversion and the thermal stability of the x-polymorph.

Experimental Section

The samples of α-phthalocyanine were prepared by vacuum evaporation of commercially available phthalocyanine onto 1.5- × 0.75- × 0.045-in. rectangular KBr flats obtained from the Perkin-Elmer Corp., Norwalk, Conn. The evaporations were carried out at 10^{-6} torr in a Bendix Balzers Model BA-3 evaporator.

The prepared samples were mounted in a simply designed furnace which was placed in the sample beam of a Perkin-Elmer Model 337 grating infrared spectrophotometer. The furnace temperature was varied by adjusting the voltage supplied to a heating tape which was uniformly wrapped about the cylindrical furnace. Three thermocouples were situated radially around the sample, and the temperature of the sample could be maintained to within ±2° throughout the temperature range used. Before any conversions were initiated, the samples were held at a temperature of approximately 200° for 8–12 hr.

Results and Discussion

The infrared absorption spectrum of the initial α-polymorph in the 700–800-cm^{-1} region is shown in Figure 1a, and the corresponding spectrum of the β-polymorph, obtained by total thermal conversion of the α film, is shown in Figure 1b. The kinetics of the $\alpha \rightarrow \beta$ thermal conversion were followed by continuously monitoring the change in the infrared spectra at a given temperature. The growth of the 724- and 782-cm^{-1} frequencies, characteristic of only the β-polymorph, were chosen for the kinetic analyses. If first-order kinetics are used to describe the thermal conversion, then the rate constant, k_1, can be obtained from

$$\ln\left(\frac{A^{\infty}}{A^{\infty} - A^{t}}\right) = k_1 t \qquad (1)$$

where A^{∞} is the absorbance of the β-polymorph at total conversion and is A^{t} the absorbance at time t.

The results, at five different temperatures between 260 and 345°, were plotted according to eq 1, and the first-order plots for the 724-cm^{-1} frequency are shown in Figure 2. The calculated first-order rate constants are listed in Table I and a least-squares analysis of the data fits an Arrhenius plot represented by

$$k_1(760 \text{ mm}) = 10^{8.06 \pm 0.08} \times \exp[(-31{,}200 \pm 370)/RT] \text{ sec}^{-1} \qquad (2)$$

These results correspond to a frequency factor of 10^8 sec^{-1} and an activation enthalpy, $\Delta H^{\ddagger}$ of 31.2 kcal/mol. The activation entropy, $\Delta S^{\ddagger}$, of the conversion can be computed from

$$k_1 = \frac{kT}{h} \exp(\Delta S^{\ddagger}/R) \exp(-\Delta H^{\ddagger}/RT) \qquad (3)$$

where $k = 1.38 \times 10^{-16}$ erg/deg and $h = 6.62 \times 10^{-27}$ erg sec and is found to be -23.1 ± 1.0 cal/mol deg at 300°.

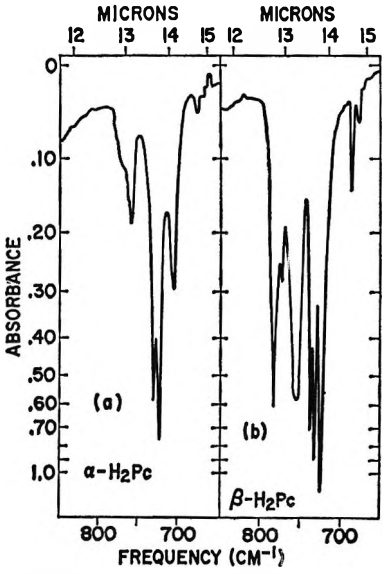

Figure 1. The infrared absorption spectra of metal-free α- and β-phthalocyanine in the 700–800 cm^{-1} absorption region.

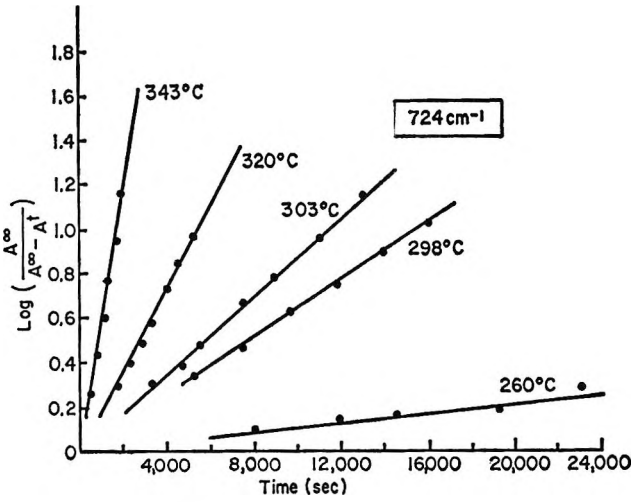

Figure 2. The plots of the first-order rate constant calculated from the 724-cm^{-1} frequency of the β-polymorph.

Table I: Calculated First-Order Rate Constants

Temp, °C	Rate constant, k_1, sec^{-1} 724 cm^{-1}	782 cm^{-1}	(av), k_1 sec^{-1}
260 ± 2	2.12×10^{-5}	2.04×10^{-5}	$(2.08 \pm 0.04) \times 10^{-5}$
298 ± 2	1.50×10^{-4}	1.38×10^{-4}	$(1.44 \pm 0.06) \times 10^{-4}$
303 ± 2	2.03×10^{-4}	2.18×10^{-4}	$(2.10 \pm 0.07) \times 10^{-4}$
320 ± 2	4.22×10^{-4}	4.60×10^{-4}	$(4.41 \pm 0.19) \times 10^{-4}$
343 ± 2	1.35×10^{-3}	1.24×10^{-3}	$(1.30 \pm 0.06) \times 10^{-3}$

Although the rate data do not yield any information on the mechanism of the conversion process, bond rupture in the phthalocyanine molecule is improbable. The activation enthalpy must be associated with the rearrangement of the phthalocyanine molecules in the $\alpha \rightarrow \beta$ polymorphic conversion. The monitored frequencies in the 700–800-cm^{-1} region are associated with the out-of-plane CH-bending absorption of the four peripheral benzene rings of the phthalocyanine molecule. Since phthalocyanine is a planar molecule, these bending modes will be influenced by the orientation of adjacent molecules which determines the polymorphic form.

If the activated complex is similar in structure to the product of the conversion; *i.e.*, β-phthalocyanine, then the negative value of the activation entropy must be associated with an increase in order in the β-polymorph. This is consistent with the fact that single crystals of β-phthalocyanine are easily grown, whereas single crystals of the α-polymorph have not been reported.

A close inspection of the infrared spectra resulting from the continuous monitoring of the $\alpha \rightarrow \beta$ conversion gives no evidence that x-phthalocyanine[12] is an intermediate. Furthermore, an attempt to thermally convert x-phthalocyanine to another polymorph under conditions similar to those used in the $\alpha \rightarrow \beta$ conversion was unsuccessful and the x form was found to be stable up to at least 378°.

Cobalt-60 Radiolysis of Aqueous Eosin[1a]

by A. F. Rodde, Jr., and L. I. Grossweiner[1b]

Department of Radiation Therapy, Michael Reese Hospital and Medical Center, Chicago, Illinois 60616
(Received March 27, 1968)

Organic dyes in aqueous solution are interesting radiolysis systems because of their reactivity with oxidizing and reducing radicals to form strongly colored intermediates which are important also in sensitized photochemical reactions. However, with the exception of methylene blue, limited information on dye radiolysis G values or mechanisms appears in the literature. The only published study on the well-known photosensitizer eosin (tetrabromofluorescein) is the early work of Patti,[2] which reports that X-ray irradiation of air-free or air-saturated solutions produces first a colored, nonfluorescent product followed by eventual decoloration. This note reports initial G values for the decoloration of aqueous eosin in the presence of specific scavengers for hydrated electrons, H atoms, and OH radicals. The results are explained by extending the scheme proposed in recent pulse-radiolysis investigations of eosin[3a] and fluorescein.[3b]

The irradiation source was a cobalt-60 therapy unit providing a uniform dose rate of approximately 1 rad/sec in a reaction vessel which could be positioned accurately. The exact dose was calibrated periodically with the modified Fricke dosimeter[4] and followed the 5.2-year half-life to within 2%. The irradiation vessel was an 8-ml Pyrex ampoule, provided with a 1-cm path side tube for *in situ* optical absorption measurements, which could be evacuated to a partial air pressure of 2×10^{-6} torr. A check of the dosimetry procedure with deaerated methylene blue in the presence of 100 mM sodium formate gave $G(-\mathrm{MB}^+) = 2.85$ (Table I) in agreement with published values of 3.3[5] and 2.75 (15%)[6] and an average of results obtained with different organic reductants of 2.9 ± 0.1.[7] The samples were prepared with 40 μM $Na_2B_4O_7$ buffer in triply distilled water. The dye was purified on an alumina–talc column by the method of Koch[8] to give ϵ_{max} (518 mμ) =

Table I: Initial $G(-\mathrm{S})$ Values for Bleaching of Aqueous Eosin by Cobalt-60 γ Rays

Dye concn, μM	pH	Additive(s)	$G(-\mathrm{S})$[a]
10	8.1	0.02 mM H_2O_2	1.03* (2)
10	8.1	0.2 mM H_2O_2	1.43* (2)
10	8.1	1.0 mM H_2O_2	1.48* (2)
10	8.1	18 mM N_2O	1.70* (2)
10	8.1	0.25 mM O_2	0.85* (2)
10	8.2	1 mM $HCOO^-$	1.64 (2)
10	8.2	100 mM $HCOO^-$	2.06 (2)
50	8.2	100 mM $HCOO^-$	2.08
10 (fluorescein)	8.1	100 mM $HCOO^-$	2.32
10 (methylene blue)	6.9	100 mM $HCOO^-$	2.85
10	8.2	100 mM $HCOO^-$ + 0.25 mM O_2	0.00
10	8.2	100 mM $HCOO^-$ + 1 mM H_2O_2	0.00 (2)
1	8.1	Deaerated	0.33*
10	8.1	Deaerated	0.72*
50	8.7	Deaerated	0.95*

[a] The asterisk indicates correction was made for growth of colored product; (2) indicates average of two determinations.

(1) (a) Based in part on an M.S. thesis submitted by A. F. Rodde, Jr., to the Physics Department, Illinois Institute of Technology, June 1967. (b) Physics Department, Illinois Institute of Technology.

(2) F. Patti, *J. Chim. Phys.*, 52, 77 (1955).

(3) (a) J. Chrysochoos, J. Ovadia, and L. I. Grossweiner, *J. Phys. Chem.*, 71, 1629 (1967); (b) P. Cordier and L. I. Grossweiner, *ibid.*, 72, 2018 (1968).

(4) L. M. Dorfman and M. S. Matheson, *Progr. Reaction Kinetics*, 3, 237 (1965).

(5) E. Hayon, G. Scholes, and J. J. Weiss, *J. Chem. Soc.*, 301 (1957).

(6) J. P. Keene, E. J. Land, and A. J. Swallow in "Pulse Radiolysis," M. Ebert, J. P. Keene, A. J. Swallow, and J. H. Baxendale, Ed., Academic Press, Inc., New York, N. Y., 1965, pp 227–245.

(7) A. J. Swallow, "Radiation Chemistry of Organic Compounds," Pergamon Press, Oxford, 1960, pp 175–185.

$9.6 \times 10^4\ M^{-1}\ cm^{-1}$. Other chemicals were CP grade. The G values were determined from the rate of absorbance decrease at 518 mμ as measured with a Beckman DU spectrophotometer.

The pulse radiolysis studies[3] have shown that the water radiolysis radical products react with eosin (S) by the following fast processes

$$S + e_{aq}^-(H) \longrightarrow R \quad (I)$$

$$S + OH\cdot \longrightarrow X + OH^- \quad (II)$$

$$S + OH\cdot \longrightarrow SOH\cdot \quad (III)$$

where R is the semiquinone, X is a phenoxyl semioxidized radical, and SOH· is the OH adduct. In deaerated solutions the radicals decay predominantly by the back reaction

$$R + X \longrightarrow 2S \quad (IV)$$

accompanied by the slower processes

$$2X \longrightarrow \text{products} \quad (V)$$

$$2R \longrightarrow S + L \quad (VI)$$

where L is the leuco base. The OH adduct decays by a slow, first-order process, which was postulated to be water elimination

$$SOH\cdot \longrightarrow X + OH^- \quad (VII)$$

Radiolysis in Reducing Conditions

The presence of high sodium formate converts OH and H atoms to CO_2^-, which contributes to dye reduction *via*

$$S + CO_2^- \longrightarrow R + CO_2 \quad (VIII)[3]$$

so that the maximum value of $G(-S)$ is $^1/_2\ (G_e + G_H + G_{OH}) = 3.0$ (based on $G_e = 2.8$,[9] $G_H = 0.55$,[4] and $G_{OH} = 2.65$).[4] The spectral data show that the dye is bleached almost to completion (Figure 1b), with an early stage during which the absorption shifts to shorter wavelengths (Figure 1c). The final product matches the absorption spectrum of leuco fluorescein as prepared by reduction with sodium amalgam.[10] Blue shifts have been observed in the photochemical reduction of halogenated fluoresceins and were interpreted as dehalogenation.[11-13] The mechanism in this case is believed to involve reduction and debromination by e_{aq}^- in the early stages, although it was not feasible to identify micromolar quantities of Br^- in the presence of the strongly absorbing dye. In the case of fluorescein, where debromination cannot occur, the difference between the measured $G(-S)$ and the maximum value of 3.0 is attributed to oxidation of the semiquinone by primary H_2O_2

$$2R + H_2O_2 \longrightarrow 2S + 2H_2O \quad (IX)$$

The predicted yield is $^1/_2(G_e + G_H + G_{OH} - 2G_{H_2O_2}) = 2.3$, based on $G_{H_2O_2} = 0.7$,[4] which agrees with the experimental value. The difference between this result and $G(-S) = 2.1$ obtained with eosin can be explained by postulating that 10% of the e_{aq}^- reacts by debromination instead of (I), because the splitting-off of Br^- leaves a tribromo form of X which can react *via* (IV) to lower the reduction yield. The suppression of all bleaching in the presence of high formate and high H_2O_2 (Table I) supports the H_2O_2 step, because the primary radicals are converted entirely to CO_2^- in this case, which would reduce the dye by (VIII) unless (IX) takes place.

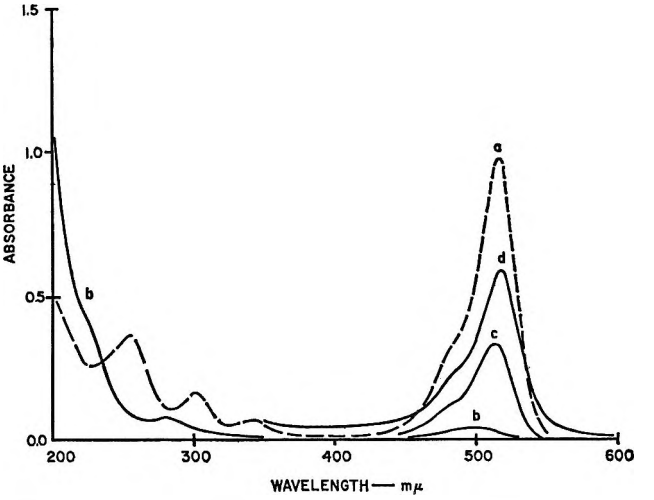

Figure 1. Spectral changes induced by cobalt-60 irradiation of deaerated, 10 μM eosin at pH 8.1: (a) unirradiated (silica cell); (b) after 60,000 rads in the presence of 10 mM sodium formate (silica cell); (c) after 3820 rads in the presence of 100 mM sodium formate (Pyrex irradiation cell); (d) after 5530 rads in the presence of 1 mM hydrogen peroxide (Pyrex irradiation cell).

Radiolysis in Oxidizing Conditions

The radiolysis of deaerated solutions or with e_{aq}^- scavengers such as H_2O_2, N_2O, or O_2 present leads to the colored product reported by Patti.[2] Typical spectral results are shown in Figure 1d. The product was isolated by exposing 10 mM solutions of deaerated eosin to 3×10^6 rads and separating the mixture on an alumina–talc column. The uppermost violet band, which is not present in unirradiated solutions, was dissolved in concentrated NaOH, filtered to eliminate talc, precipitated at pH 1.5 where AlO(OH) and $Mg(OH)_2$ remain in solution, washed, and dried. At pH 9 the product spectrum shows a peak at 520 mμ and a shoulder at 540 mμ. The G values indicated by * in Table I were corrected for product growth from the absorbance changes at 560

(8) L. Koch, *J. Assoc. Offic. Agr. Chemists*, **39**, 397 (1956).

(9) E. M. Fielden and E. J. Hart, *Radiation Res.*, **32**, 564 (1967).

(10) K. Uchida, S. Kato, and M. Koizumi, *Bull. Chem. Soc. Jap.*, **35**, 16 (1962).

(11) M. Imamura and M. Koizumi, *ibid.*, **29**, 913 (1956).

(12) G. Oster, G. K. Oster, and G. Karg, *J. Phys. Chem.*, **66**, 2514 (1962).

(13) E. F. Zwicker and L. I. Grossweiner, *ibid.*, **67**, 549 (1963).

mμ where eosin is colorless. Since the back reaction (IV) cannot take place with e_{aq}^- and H atom scavengers present, the low G values indicate that more than one OH radical is required to decolor a dye molecule. In fact, if n OH are required, then the expected values of $G(-S)$ in air-saturated solutions, in N_2O saturated solutions, and with moderately high H_2O_2 present are: G_{OH}/n, $(G_e + G_{OH})/n$, and $<(G_e + G_{OH} + G_H)/n$, respectively, where the last case applies when H and OH react predominantly with the dye and not H_2O_2. The results in Table I give $n = 3.1$, 3.2, and <4 for each case. A possible mechanism leading to $n = 3$ is disproportionation of X followed with an additional oxidation by OH. The suppression of bleaching when both oxygen and formate are present (Table I) is explained by the reaction

$$R + O_2 \longrightarrow S + O_2^- \qquad (X)$$

which has been identified in the pulse radiolysis work.[3a] Furthermore, it can be concluded that the dye is relatively unreactive with O_2^-. The bleaching yield in deaerated solutions without scavengers cannot be calculated readily because it depends on the relative rates of (IV), (V), and (VI) plus subsequent reactions.

The G values obtained in this work are consistent with the initial reactions deduced from the pulse radiolysis transient spectra and kinetics measurements. The occurrence of (IX) and debromination as a side reaction to (I) were not observed in the pulse radiolysis work. The colored oxidation product has not been identified, but it is not likely to be a stable dimer resulting from (V), which would give $G(-S) \simeq 5.5$ in the presence of high H_2O_2 or N_2O.

Acknowledgment. This work was supported by the National Institutes of Health on Grant No. GM-12716.

Thermodynamic Values for the Dimerization of 2-Pyridone and 2-Thiopyridone

by N. Kulevsky and W. Reineke

Department of Chemistry, University of North Dakota, Grand Forks, North Dakota 58201 *(Received March 29, 1968)*

The dimerization of 2-pyridone and 2-thiopyridone in benzene and dioxane solutions has previously been studied by vapor pressure osmometry.[1] The equilibrium constants for the monomer–dimer equilibrium (K_d) calculated from such data have a good deal of experimental scatter; however, they do indicate that the degree of dimerization for the oxygen compound is about five times greater than that of the sulfur compound. We have recently published the results of a study which conflict with the above report, in that the equilibrium constants for a series of saturated thiolactams are as large or larger than those of the corresponding oxygen compounds.[2] Since the work on the saturated compounds was based upon infrared absorbance measurements on dilute CCl_4 solutions, a comparison of equilibrium constants for the unsaturated species obtained by the same techniques is useful in discussing the effect of thio substitution on H bonding in amides. Furthermore, from the variation of ln K_d with temperature, both the enthalpy and entropy of dimerization, which have not been reported before, are calculated.

The pure compounds were prepared according to standard literature methods.[1] Procedures for making quantitative solutions, measuring the ir absorbance, and temperature control were essentially the same as in our earlier paper.[2] The main difference is that a Beckman IR12 spectrophotometer, operated in the single-beam mode, was used in this work.

The equations used to calculate the equilibrium constants at a given temperature have been discussed previously.[2,3] The absorbance at the maximum of the monomer NH stretching frequency (A) was plotted *vs.* C_0/A (C_0 is the formal concentration of the amide as a monomer), and K_d was then calculated from the slope and intercept of the curve. The measurements were made on solutions where the concentrations varied from 2×10^{-4} to 40×10^{-4} M for 2-pyridone and from 0.8×10^{-4} to 10×10^{-4} for 2-thiopyridone. The data for solutions with concentrations above 25×10^{-4} M show a pronounced curvature and, therefore, were not used in the calculations. The failure of the linear relationship at these concentrations suggests that these solutions may also contain linear dimers or higher polymers or both.[4,5]

The NH stretching frequencies of the monomers appear at 3412 cm^{-1} for 2-pyridone and 3376 cm^{-1} for 2-thiopyridone. This is in good agreement with literature values of 3413 and 3371 cm^{-1}, respectively.[6] The values of K_d obtained for these two compounds at several temperatures are given in Table I. Table II contains values of $\Delta H°$, $\Delta G°_{25}$, and $\Delta S°$ for these compounds as well as for other lactams and thiolactams previously investigated.[2,3,7,8]

From the results given in Table II it is apparent

(1) M. H. Krackov, C. M. Lee, and H. G. Mautner, *J. Amer. Chem. Soc.*, **87**, 892 (1965).

(2) N. Kulevsky and P. M. Froehlich, *ibid.*, **89**, 4839 (1967).

(3) R. C. Lord and T. J. Porro, *Z. Elektrochem.*, **64**, 672 (1960).

(4) E. S. Hanrahan and B. D. Bruce, *Spectrochim. Acta*, **A23**, 2497 (1967).

(5) T. C. Chiang and R. M. Hammaker, *J. Phys. Chem.*, **69**, 2715 (1965).

(6) L. J. Bellamy and P. E. Rogash, *Proc. Roy. Soc.*, **A257**, 98 (1960).

(7) H. E. Affsprung, S. D. Christian, and J. D. Worley, *Spectrochim. Acta*, **20**, 1415 (1964).

(8) M. Tsuboi, *Bull. Chem. Soc. Jap.*, **24**, 75 (1951).

Table I: Equilibrium Constants for the Dimerization of 2-Pyridone and 2-Thiopyridone[a]

Temp, °C	K_d, M^{-1} 2-Pyridone	K_d, M^{-1} 2-Thiopyridone
16.2	10.43×10^3	
20.3		5.35×10^3
26.8		3.93×10^3
30.3	6.27×10^3	
31.9		3.22×10^3
35.3	4.49×10^3	
37.5		2.70×10^3
41.6	2.71×10^3	
42.5		2.30×10^3
45.9	2.80×10^3	

[a] The probable errors in the slope and intercept calculated at the 90% confidence level give standard errors of approximately 10% in the values of K_d.

Table II: Thermodynamic Functions for Dimerization of Thiolactams and Lactams

Name	$\Delta H°$, kcal/mol	$\Delta G°_{25}$, kcal/mol	$\Delta S°$, eu
2-Pyridone[a]	-8.8 ± 0.4[b]	-5.25 ± 0.08	-12.0
2-Thiopyridone[a]	-7.0 ± 0.3[b]	-4.94 ± 0.06	-6.7
Thiobutyrolactam[c]	-5.8 ± 0.7	-3.34 ± 0.06	-8.3
Butyrolactam[d]	-7.0 ± 0.4	-3.32	-12.3
Thiovalerolactam[c]	-3.1 ± 0.4	-3.62 ± 0.06	1.7
Valerolactam[e]	-10.3 ± 1.0	-3.34	-23.4
Thiocaprolactam[c]	-3.9 ± 0.5	-3.52 ± 0.06	-1.6
Caprolactam[f]	-5.5 ± 0.3	-2.77	-9.2

[a] This work. [b] Errors calculated using probable errors in slope and intercept. [c] Reference 2. [d] Reference 7. [e] Reference 8. [f] Reference 3.

that both of these compounds form relatively strong H bonds. In fact, the $\Delta H°$ value for 2-pyridone is about the same as some of the values observed for benzoic acids.[4] Bellamy and Rogash came to a similar conclusion, basing it upon the large shifts of the NH stretching frequencies observed for the dimers of these compounds.[6]

A comparison of the data for the unsaturated and saturated compounds shows that the H bond is strongest for 2-pyridone in the oxygen series and 2-thiopyridone in the sulfur compounds. The one piece of evidence contrary to this is the very high $\Delta H°$ (10 kcal) reported for valerolactam.[8] However, this value is open to question, as the experimental techniques used (measuring the dimer peak instead of the monomer peak) can lead to large errors in $\Delta H°$.[3] That the unsaturated compounds are the more strongly H bonded can be attributed to the higher acidity of the NH groups and the higher basicity of the C=S and C=C groups. The higher acidity and basicity can be caused by contributions of resonance forms in which the amide or thioamide group interacts with the double bonds of the ring.

The $\Delta H°$ of dimerization for the thio compound is about 80% that of the oxygen compound, which is consistent with the ratios found for two out of three saturated systems previously investigated. Valerolactam is again the exception, with a much higher $\Delta H°$ than its thio analog. That the differences in $\Delta H°$ are so small can be explained on the basis of the increased acidity of the NH group in the thioamides partially compensating for the lower basicity of the C=S group.[2] Thioamides would be more acidic, owing to the smaller resonance interaction of sulfur compared with oxygen and a consequent higher polarity.

Finally, the values of K_d calculated at 25° are 7100 M^{-1} for 2-pyridone and 4200 M^{-1} for 2-thiopyridone. Unlike the saturated thiolactams and lactams, the $\Delta H°$ values for these compounds are large enough to dominate the entropy terms which had caused the saturated oxygen and sulfur compounds to have very similar K_d values. The values of K_d reported by Krackov, *et al.*,[1] show larger differences than those given here. This could be due to the different solvents and higher concentrations used in their work.

Acknowledgment. We wish to thank the National Science Foundation for the support of William Reineke as a participant in the Research Participation for High School Teachers Program, Grant No. GW-1702.

Kinetics of the Gas-Phase Reactions of Diborane with Methylphosphines and Trimethylamine

by H. Brumberger and W. H. Smith

Department of Chemistry, Syracuse University, Syracuse, New York 13210 *(Received April 3, 1968)*

The reaction of phosphine with diborane in the gas phase at 0° is relatively slow ($k_1 \cong 2.3$ cc mol^{-1} sec^{-1}) and can be accounted for by the mechanism

$$B_2H_6 + PH_3 \underset{k_{-1}}{\overset{k_1}{\rightleftharpoons}} BH_3PH_3(g) + BH_3$$

$$BH_3 + PH_3 \underset{k_{-2}}{\overset{k_2}{\rightleftharpoons}} BH_3PH_3(g) \underset{\text{equil}}{\overset{\text{rapid}}{\rightleftharpoons}} BH_3PH_3(s)$$

The activation energy $E_1 = 11.4 \pm 2.0$ kcal/mol;[1] the solid product is reversibly dissociated and has a dissociation pressure of 200 mm at 0°.[2]

Observations on the reactions of diborane with

(1) H. Brumberger and R. A. Marcus, *J. Chem. Phys.*, **24**, 741 (1956).

(2) E. L. Gamble and P. Gilmont, *J. Amer. Chem. Soc.*, **62**, 717 (1940).

methyl- and dimethylphosphine (MP and DMP) indicated that these were very fast, comparable in velocity to the reactions of diborane with amines. Some kinetic flow-reactor studies of the competitive reactions of MP and DMP with diborane and of DMP and trimethylamine (TMA) with diborane are reported here.

All materials were purified by degassing and distillation where necessary.[3] Vacuum and flow reactor systems were in all essentials similar to those described by Daen and Marcus,[4] as were the techniques used to measure reaction rates, exchange reactions, etc. It was found by infrared spectroscopy of various reaction mixtures that exchange reactions between adducts and reactants were negligible, and that the pumping system used to collect effluent reactor gases for analysis did not significantly fractionate these gases. Infrared Beer's law curves established for pure components at appropriate absorption peaks were used to determine the composition of reaction mixtures to better than 5% for each component.

All measurements were made under essentially isothermal steady-state flow conditions. An excess of competitors relative to diborane was always present. Flow rates were obtained by dividing the pressure of the reactor effluent gas collected in a standard volume during a run by the elapsed collection time. Such flow rates (mm min^{-1}) were measured for the competitor mixtures under constant driving pressure when diborane was absent from the reactor, and after it was admitted. The difference in flow rates for gas i without and with diborane present, $R_i^\circ - R_i$, is the rate of disappearance of i due to reaction in the reactor volume. The ratio of competitor flow rates during reaction, R_i/R_j, equals the ratio of their steady state pressures P_i/P_j in the reactor in the absence of pump fractionation and assuming complete mixing.

Total steady-state reactor pressures during reaction varied from ~0.009 to ~0.35 mm for DMP–MP runs, and from ~0.03 to ~0.28 mm for DMP–TMA runs. Relative rate measurements were made at 25 ± 2° for both systems, and also at 9 ± 1° for the DMP–TMA reaction with diborane.

Summary of Observations

The raw data are somewhat scattered due to the experimental error with which low-pressure flow rate measurements are afflicted, and due to slight temperature variations over the relatively large vacuum system. Significant trends are nevertheless apparent.

1. No significant correlation is found between diborane inflow rate or various functions of this rate (*i.e.*, $R_{B_2H_6}^{1/2}$ etc.) and the relative reaction rates for either competitor pair. The diborane flow rate was varied by a factor of 10 for the MP–DMP reaction, and by a factor of 3 for the DMP–TMA reaction. The relative rate r_{ij} is computed as $(R_i^\circ - R_i)/(R_j^\circ - R_j)$; a mass balance for each gas gives

$$R_i^\circ = R_i + \int[\text{Rate of reaction per unit volume}]dV \quad (1)$$

i.e., the inflow rate must equal the outflow rate plus the removal due to chemical reaction in the reactor volume, in a steady state.

2. For both sets of competitors, a rough proportionality between relative rate and P_i/P_j is found, which appears unaffected by a change in the total reactor pressure by a factor of 5 or more. If the runs of common relative rate are grouped together (regardless of total reactor pressure) and plotted against the P_i/P_j values averaged within each group, Figures 1 and 2 are obtained.

3. MP and DMP reactions with diborane are of comparable speed, both very much faster than the PH_3–B_2H_6 reaction, and the infrared spectra of the adducts are almost identical.

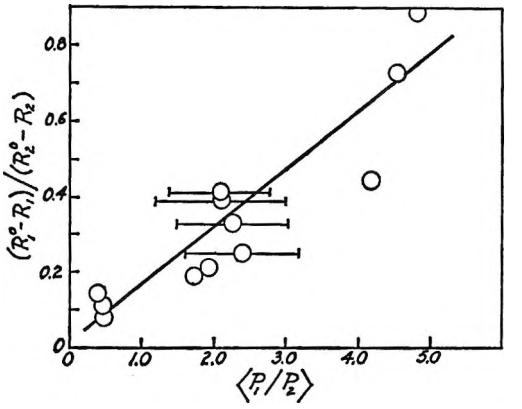

Figure 1. Relative reaction rate for methylphosphine (1) and dimethylphosphine (2) competing for diborane, *vs.* relative steady-state concentration ratio at 25°.

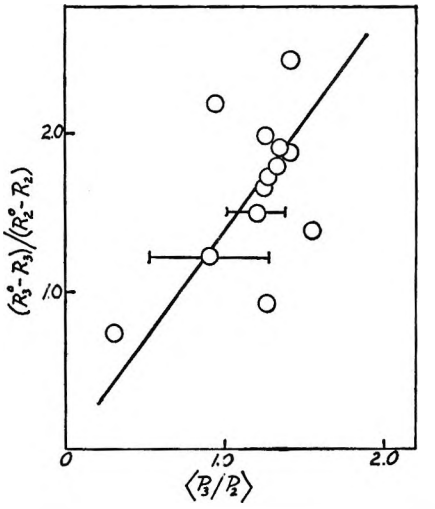

Figure 2. Relative reaction rate for trimethylamine (3) and dimethylphosphine (2) competing for diborane, *vs.* relative steady-state concentration ratio at 25°.

(3) Experimental details may be found in the Ph.D. dissertation of W. H. Smith, Department of Chemistry, Syracuse University, 1965.

(4) J. Daen and R. A. Marcus, *J. Chem. Phys.*, **26**, 162 (1957).

4. Relative rate measurements of TMA–DMP with B_2H_6 at 9° under the same flow and pressure conditions as a set of the 25° runs indicate no substantial change in relative rates within the estimated experimental uncertainties.

Kinetic Analysis

Because of the nature of the data, relatively little insight can be gained into the mechanisms of these reactions. If one assumes that similar mechanisms hold for MP and DMP—a reasonable assumption in view of the similarity in product structure, reaction rate, and lack of systematic effect of the diborane flow rate on the relative rates—then there are several mechanisms which yield rate equations in accord with the observed behavior, *i.e.*, with

$$\frac{-\mathrm{d}(\mathrm{Me_2PH})/\mathrm{d}t}{-\mathrm{d}(\mathrm{MePH_2})/\mathrm{d}t} = \frac{k_{\mathrm{DMP}}(\mathrm{Me_2PH})}{k_{\mathrm{MP}}(\mathrm{MePH_2})} \quad (2)$$

All of these involve the formation of a 1:1 adduct intermediate, or the formation of a product molecule and BH_3, in the first step, but cannot be distinguished by these measurements.

If one accepts the mechanism of Bauer, *et al.*,[5] for the TMA–B_2H_6 reaction in which diborane appears to the first order, then the implication is that the DMP–B_2H_6 reaction is also first order in diborane, since experimentally

$$\frac{-\mathrm{d}(\mathrm{Me_3N})/\mathrm{d}t}{-\mathrm{d}(\mathrm{Me_2PH})/\mathrm{d}t} = \frac{k_{\mathrm{TMA}}(\mathrm{Me_3N})}{k_{\mathrm{DMP}}(\mathrm{Me_2PH})} \quad (3)$$

Our temperature studies indicate that the relative rates of the TMA–B_2H_6 and DMP–B_2H_6 reactions do not change substantially, implying similar (*i.e.*, low) activation energies. These factors would militate against a mechanism incorporating the diborane–borine equilibrium as an important step.

Relative "phenomenological" rate constants can, however, be evaluated without reference to specific mechanisms. Since

$$r_{ij} = \frac{k_i(P_i)}{k_j(P_j)} = \frac{k_iR_i}{k_jR_j} = \frac{R_i^\circ - R_i}{R_j^\circ - R_j} \quad (4)$$

one can write

$$\frac{k_i}{k_j} = \frac{(R_i^\circ/R_i) - 1}{(R_j^\circ/R_j) - 1} \quad (5)$$

We find $k_{\mathrm{MP}}/k_{\mathrm{DMP}} = 0.22 \pm 0.11$, $k_{\mathrm{TMA}}/k_{\mathrm{DMP}} = 1.60 \pm 0.44$, independent of total steady-state reactor pressure, at 25°. Thus $k_{\mathrm{TMA}}:k_{\mathrm{DMP}}:k_{\mathrm{MP}}::8:5:1$.

Acknowledgment. The authors are grateful to the Research Corporation for supporting a portion of this work.

(5) S. H. Bauer, J. V. Martinez, D. Price, and W. D. Jones, "Boron–Nitrogen Chemistry," Advances in Chemistry Series, No. 42, American Chemical Society, Washington, D. C., 1964, pp 35–52.

Contact Angles and Transition Regions in Soap Films

by H. M. Princen

Lever Brothers Company, Research and Development Division, Edgewater, New Jersey 07020 *(Received April 3, 1968)*

Recently, Mysels, *et al.*,[1] described a technique for measuring the "contact angle" between a thin liquid film and its adjoining Plateau border. The possible existence of such discontinuities had been predicted previously[2–4] as a necessary consequence of interaction forces in these thin liquid structures. A reported anomaly in the shape of a drop at a liquid–liquid interface[5] could be explained on this basis.[2,3]

Mysels' technique consists of moving an air bubble at a horizontal air–water interface into such a position that the bulk surface is flat up to the circle of contact with the bubble. From the dimensions of the spherical film above the level of the bulk surface, the contact angle can be readily calculated.

It seemed to us that the contact angle could be measured more conveniently by utilizing the refractive properties of the Plateau border, which acts to a good first approximation like a prism with finite top angle. Figure 1 illustrates the path of a horizontal light beam through the region between a vertical flat soap film and the Plateau border which connects the film to the bulk solution. The upper part of the beam passes through the film undeflected, while the lower part is deflected downward. A screen, placed behind the film at a distance R, shows a bright spot between A and B, a dark region of length D, and a line of light further downward. The angle of deflection is given by

$$\tan \alpha = D/R \quad (1)$$

From Snell's law, applied to the top of the liquid prism, it follows that α is related to the contact angle θ by

$$\alpha = \sin^{-1}\left\{n \sin\left[2\theta - \sin^{-1}\left(\frac{\sin\theta}{n}\right)\right]\right\} - \theta \quad (2)$$

where n is the refractive index of the bulk solution. For small angles (θ), eq 2 reduces to

$$\alpha \simeq 2(n - 1)\theta \quad (3)$$

In real systems the liquid surfaces are bounded by monolayers of stabilizing surfactant molecules. In

(1) K. J. Mysels, H. F. Huisman, and R. I. Razouk, *J. Phys. Chem.*, **70**, 1339 (1966).

(2) H. M. Princen and S. G. Mason, *J. Colloid Sci.*, **20**, 156 (1965).

(3) H. M. Princen, Ph.D. Thesis, University of Utrecht, Utrecht, 1965.

(4) B. V. Deryagin, G. A. Martynov, and Y. V. Gutop, *Colloid J.* (USSR), **27**, 357 (1965).

(5) G. D. M. MacKay, Ph.D. Thesis, McGill University, Montreal, 1962.

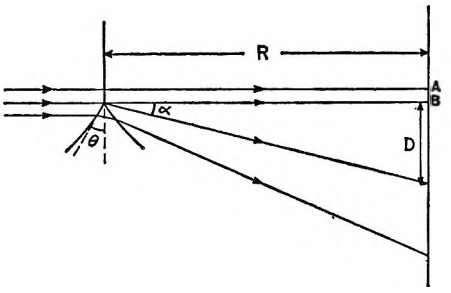

Figure 1. Path of a horizontal light beam through a Plateau border with a contact angle θ.

the optical model these can be incorporated as thin layers of different refractive index. However, when Snell's law is applied to this composite structure, it is found that eq 2 still applies, whatever the thickness and refractive index of these layers, provided n stands for the refractive index of the aqueous core. For lack of better information, it is assumed to be equal to that of the bulk.

In our experiments the film was formed by pulling a thin rectangular glass frame out of the solution, contained in the cavity of a narrow rectangular Teflon block which was filled to overflowing. The system was enclosed in a 3-cm square glass cell to prevent evaporation. The illumination was rather primitive and was provided by a simple microscope lamp. The emerging beam was collimated as well as possible and passed through a stop about 2 mm in diameter before entering the cell. The screen was placed at a distance of 175 cm behind the film. Immediately after formation of the film, the image on the screen was a long vertical line of light from A down (Figure 1). After some time a black film formed at the top of the frame and spread downward. As soon as the black film reached the Plateau border and a contact angle was established, the dark region D developed. It should be mentioned that the top of the deflected beam was not very sharp, so that the error in the reading of D was about 0.5 cm. This results in an error in θ of about 15′.

Some of our results are given in Table I. The surfactants are laboratory prepared and purified sodium dodecylsulfate ($NaC_{12}SO_4$) and sodium decylsulfate ($NaC_{10}SO_4$). Contact angles were observed only at sufficiently high concentrations of added electrolyte, in this case sodium chloride. Although we did not measure the thicknesses of the equilibrated films, there is little doubt that all of them were second black films with a thickness below 50 Å.[6] Our value of 9° 23′ in 0.05% $NaC_{12}SO_4$ + 0.4 M NaCl compares with 8° 50′ reported by Mysels. Another system examined was 0.2% $NaC_{10}SO_4$ in the presence of $MgCl_2$. The contact angle increased from 3° 20′ to 5° 12′ upon raising the $MgCl_2$ concentration from 5×10^{-3} to 2×10^{-2} mol/l.

Phenomenologically, the contact angle results from

Table I: Measured Contact Angles as a Function of Electrolyte Concentration

	Contact angles			
[NaCl], M	0.05% $NaC_{12}SO_4$ (24.3 ± 0.3°)	0.2% $NaC_{12}SO_4$ (22.5 ± 0.2°)	0.2% $NaC_{10}SO_4$ (23.5 ± 0.5°)	$-\Delta F$, ergs/cm²
0.2	...	3° 21′	...	...
0.22	2° 56′	...	...	...
0.25	5° 6′	...	...	...
0.26	5° 36′	...	...	...
0.28	5° 49′	...	...	...
0.30	7° 25′	8° 0′	4° 53′	0.26
0.40	9° 23′	10° 20′	9° 6′	0.90
0.50	11° 28′	11° 18′	10° 17′	1.13
0.60	12° 35′	...	11° 20′	1.36
0.80	...	..	12° 55′	1.72
1.00	...	...	14° 47′	2.16
1.50	...	...	17° 15′	2.78

a force balance between the film tension pulling upward and the two bulk surfaces, making an angle θ with the film, pulling downward. This leads to

$$\gamma_f = 2\gamma_0 \cos\theta \qquad (4)$$

where γ_f is the film tension and γ_0 is the normal surface tension. Therefore, contact angles exist only when $\gamma_f < 2\gamma_0$.

The difference between γ_f and $2\gamma_0$ can be interpreted as the free energy of interaction per square centimeter of the equilibrium film, *i.e.*, the nongravitational work done in bringing the surfaces from infinity to their equilibrium separation. Hence

$$-\Delta F = 2\gamma_0 - \gamma_f = 2\gamma_0(1 - \cos\theta) \qquad (5)$$

The values of ΔF for 0.2% $NaC_{10}SO_4$ + NaCl are given in the last column of Table I. It thus appears that contact angle measurements can give important new information on thin liquid films.

A few observations that were made in the course of these experiments are worth mentioning, although they were not studied in any detail. First, if the frame containing the film was raised at constant speed, so that the area of the film increased, the contact angle dropped below the equilibrium value. The effect increased with increasing rate of expansion of the film. Similarly, the contact angle could be greatly increased upon "compression" of the film by lowering the frame. These dynamic contact angles can be conveniently studied with the technique described above. Secondly, a curious phenomenon was observed during the preparation of the solutions by shaking them in volumetric flasks. Whenever θ was smaller than about 10°, the small bubbles would ascend through the neck of the flask as individual bubbles. On the other hand, for solutions whose contact angle

(6) M. N. Jones, K. J. Mysels, and P. C. Scholten, *Trans. Faraday Soc.*, **62**, 1336 (1966).

exceeded 10°, the hydrodynamic forces were insufficient to separate the individual bubbles, which rose through the neck in large clusters. This "foam coagulation" may warrant more extensive study.

In an effort to improve the optical system, we replaced the light source by a He–Ne gas laser (2 mW, University Laboratories, Model 240). It was thought that monochromaticity and the improved parallelism of the incident beam would enhance the sharpness of the image. This did not occur, but the high intensity of the laser beam did reveal very clearly that light is transmitted at *all* angles of deflection, so that Figure 1 is an oversimplification. This has important implications, since it can, in principle, be explained by noting that the contact angle is a macroscopic concept. On a microscopic scale the transition region between the film and the Plateau border proper must be continuous, and this gives rise to a continuous variation of the intensity with α.

The exact shape of the surfaces in the transition region depends on the variation of the interaction forces with the distance of separation. If this shape could be determined in detail, for example, from the above intensity profile, then the disjoining pressure (or, by integration, the potential energy) would be known for any thickness exceeding that of the film proper by using the Laplace equation in the form

$$p_t = p_h + p_d = \gamma_0/\rho \tag{6}$$

where ρ is the radius of curvature of the surface, p_t is the total pressure in the transition region relative to the atmosphere, p_h is the hydrostatic pressure ($= -zdg$, where z is the height above the bulk surface, d is the density, and g is the acceleration due to gravity), and p_d is the disjoining pressure. Thus a novel and powerful technique would become available for the study of thin liquid films.

It seemed plausible that the profile of the intensity as a function of α could indeed be used for this purpose. From the laws of geometrical optics, with neglect of losses due to reflection at the two surfaces, the relationship between the intensity and the shape parameters can be readily derived (see Figure 2). Conservation of energy for an element dy of the parallel incident beam requires that

$$I_0 dy = I(R + \Delta R)d\alpha$$

or

$$\frac{dy}{d\varphi} = \frac{I}{I_0}(R + \Delta R)\frac{d\alpha}{d\varphi}$$

where I_0 is the incident intensity, I is the transmitted intensity at a distance R behind the film, y is a vertical coordinate measured downward from the lowest point of the film proper, φ is the variable angle between the surfaces and the vertical, and $R + \Delta R$ is the total distance between the virtual source O of the refracted rays

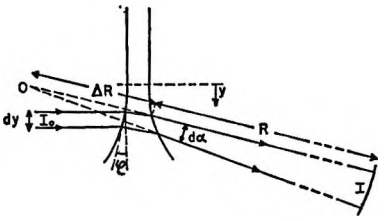

Figure 2. Detailed view of the path of the light beam through an element of the transition region.

and the observer. The angles α and φ are directly related through eq 2 or 3, in which θ is replaced by φ.

When φ and α are not very small, source O coincides with the film for all practical purposes, *i.e.*, $\Delta R \ll R$, so that

$$\frac{dy}{d\varphi} = \frac{I}{I_0}R\frac{d\alpha}{d\varphi}$$

To include the region of very small α, a sufficiently accurate approximation for ΔR is

$$\Delta R \simeq \frac{dy}{\sin(d\alpha)} \simeq \frac{dy}{d\alpha}$$

which leads to the more general expression

$$\frac{dy}{d\varphi} = \frac{I}{I_0 - I}R\frac{d\alpha}{d\varphi} \tag{7}$$

When h is the horizontal distance between the surfaces, we can write $dh = 2 \tan \varphi\, dy$, so that

$$\frac{dh}{d\varphi} = 2\frac{I}{I_0 - I}R \tan \varphi \frac{d\alpha}{d\varphi} \tag{8}$$

On the basis of eq 7 and 8, one would expect to be able to calculate $dy/d\varphi$ and $dh/d\varphi$ from the intensity profile $I(\alpha)$. By integration, the shape of the interfaces would be obtained. Moreover, since the radius of curvature of each interface is given by

$$\rho = -\frac{1}{\cos \varphi}\frac{dy}{d\varphi} \tag{9}$$

the disjoining pressure at each point would be known from eq 6.

The expected profile would show a sharp drop in the intensity near $\alpha = 0$, followed by a region of low intensity where the curvature of the surfaces is large. In the region of α corresponding to the macroscopic contact angle, the intensity would rise sharply and level off to an almost constant value corresponding with the Plateau border proper where interaction forces become negligible. This level is given by

$$\frac{I}{I_0 - I} = \frac{1}{R}\frac{d\varphi}{d\alpha}\left[\frac{\gamma_0(1 + \sin \varphi)}{2dg}\right]^{1/2} \tag{10}$$

which is readily derived from elementary capillary

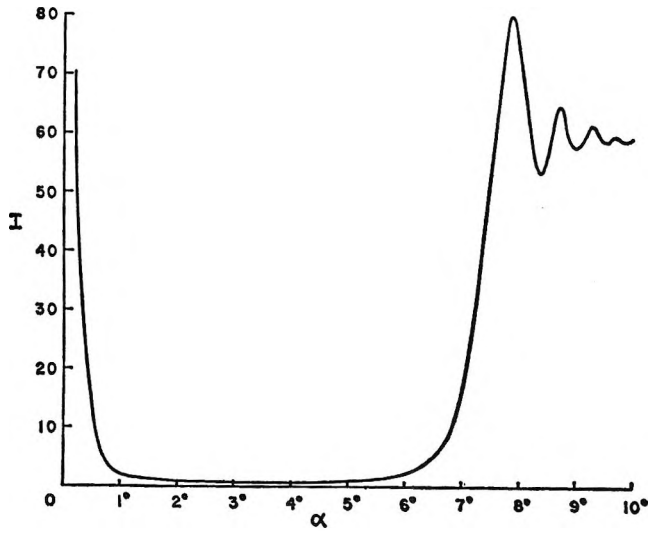

Figure 3. Measured intensity profile for 0.2% $NaC_{12}SO_4$ + 0.4 *M* NaCl.

theory, according to which the radius of curvature of a cylindrical interface in a gravitational field is given by[7]

$$\rho = -\frac{dy}{d \sin \varphi} = -[2dg(1 - \sin \varphi)/\gamma_0]^{-1/2} \quad (11)$$

so that

$$\frac{dy}{d\varphi} = \left[\frac{\gamma_0(1 + \sin \varphi)}{2dg}\right]^{1/2} \quad (12)$$

Substituting for $dy/d\varphi$ in eq 7 yields eq 10, which can be used to obtain I_0 from the measured intensity at large α. This is preferable to measuring I_0 directly in the transmitted beam at $\alpha = 0$.

Experimentally, the intensity was measured with a photomultiplier tube (RCA 6199) which could be moved at constant speed through a circular arc behind the cell. The signal was recorded, and a typical curve is shown in Figure 3. It indicates that geometrical optics is insufficient to describe the system quantitatively. The fringes at large angles are definitely due to diffraction, resulting from the small size of the transition region and the large curvature of the bounding surfaces. This severely complicates the problem and, although we feel that the curve contains, in principle, the necessary information for a complete description of the transition region, we have not yet succeeded in analyzing these diffraction effects satisfactorily. It is also possible that the intensity profile is not sufficiently sensitive to the detailed shape of the transition region. Alternative techniques are being investigated.

Although these initial attempts at studying the transition region have not been successful, we stress again the importance of this region as a potential source of valuable information on interaction forces in thin liquid films.

Acknowledgment. The author expresses his thanks to the Lever Brothers Co. for permission to publish this paper.

(7) For example, by combining eq 25 and 29 in H. M. Princen in "Surface and Colloid Science," Vol. I, E. Matijevic and F. Eirich, Ed., Interscience Publishers, New York, N. Y., in press.

Isobutane Chemisorption on Synthetic Faujasites

by P. Donald Hopkins and R. L. Stoffer

Research and Development Department, American Oil Company, Whiting, Indiana *(Received April 17, 1968)*

In recent years zeolites, particularly synthetic faujasites, have been introduced as catalysts for cracking and other hydrocarbon conversion reactions. Faujasites both by themselves and dispersed in matrices of clay or amorphous silica–alumina have demonstrated marked increases in cracking and isomerization activity over amorphous silica–alumina catalysts; *e.g.*, increases in activity for cracking of hexane by factors of up to 10^4 have been observed.[1] The reasons for these increases are not well understood.

The structure of synthetic faujasite has been determined;[2] the large spherical cavities in faujasite (entrance diameter about 8 Å) are easily accessible to a large variety of hydrocarbon molecules. Cracking is believed to occur primarily within the large cavity system and it has been suggested that the stereoregularity of the faujasite results in a marked increase in the number of catalytically active sites compared to silica–alumina.[3] On the other hand, one active site in every 10^4 cavities has been claimed to be sufficient to explain cumene cracking rates over synthetic hydrogen Y (HY) faujasite.[4]

MacIver, *et al.*,[5] found two types of chemisorbed isobutane on silica–alumina, reversibly adsorbed isobutane which underwent exchange with gas phase isobutane, and irreversibly adsorbed isobutane which could be removed only by burning in oxygen. Larson and Hall[6] further separated reversibly adsorbed isobutane into two types based on rate of exchange. Reversible adsorption reached an equilibrium, but irreversible

(1) J. N. Miale, N. Y. Chen, and P. B. Weisz, *J. Catal.*, **6**, 278 (1966).

(2) L. Broussard and D. P. Shoemaker, *J. Amer. Chem. Soc.*, **82**, 1041 (1960).

(3) J. A. Rabo, P. E. Pickert, D. N. Stamires, and J. E. Boyle, in "Actes du Deuxieme Congres International de Catalyse," Editions Technip, Paris, 1961, p 2055.

(4) J. T. Richardson, *J. Catal.*, **9**, 182 (1967).

(5) D. S. MacIver, P. H. Emmett, and H. S. Frank, *J. Phys. Chem.*, **62**, 935 (1958).

(6) J. G. Larson and W. K. Hall, *J. Amer. Chem. Soc.*, **85**, 3570 (1963).

adsorption was a linear function of time. The amounts adsorbed were very small (<0.02 mg of isobutane/g of silica–alumina).

In order to determine whether differences in catalytic activity are accompanied by changes in the number of chemisorption sites, we have studied the chemisorption of isobutane on some synthetic faujasites and on amorphous silica–alumina using a carbon-14 tracer technique. Isobutane was chosen not only because the previous workers[5,6] used it but also because it is small enough to minimize steric problems associated with the zeolite cavities and contains a reactive tertiary C–H bond which should enhance chemisorption. The conditions of the experiments were chosen to enable comparison with the previous work.

Experimental Section

Apparatus. The adsorption apparatus was similar to that described by MacIver, *et al.*[5] Teflon stopcocks were substituted for some of the mercury cutoffs after gravimetric adsorption studies indicated that isobutane adsorption by Teflon was negligible. The circulating pump was omitted since we felt our system would give rapid circulation by thermal convection; we found that adsorption and exchange equilibria were reached in the same time as in the previous work.[5]

Our radiation counting system was very similar to that described by MacIver, *et al.*[5] A proportional counter (Model D46 gas flow counter with "Micromil" window) manufactured by Nuclear Chicago Corp. was used in place of a Geiger tube. The counting gas was 10% methane in argon obtained from the Matheson Co. The remainder of the counting equipment, consisting of a preamplifier (Model 31-24), a high voltage supply (Model 40-9B), a linear amplifier (Model 30–19), a scaler (Model 49–44), and a timer (Model 54-8003), was obtained from Nuclear Chicago Corp.

Materials. Synthetic faujasite Y was supplied in the sodium form (NaY) by Linde Division of Union Carbide and had an Si/Al ratio of 2.43. The ammonium form (NH_4Y) was prepared from NaY by ion exchange with aqueous NH_4NO_3 and was found by Na analysis to be 74% exchanged. The decationized (DcY) form was obtained from NH_4Y by heating *in vacuo* at 500° for 16 hr after sealing into the adsorption apparatus, a procedure known to remove all ammonia and at least half the hydroxyl groups created by ammonia removal.[7] Z-14US, supplied by Davison Division, W. R. Grace and Co., is a decationized faujasite stabilized by a special procedure.[8] Nalco HA-1 is a high alumina (~25% Al_2O_3) amorphous silica–alumina cracking catalyst.

Fresh catalysts were generally calcined in 160 torr of oxygen for 2 hr and then evacuated overnight at 500° before the adsorption experiment. For repeat runs the catalysts were evacuated at 500° for 16 hr prior to the adsorption experiment. DcY and Z-14US treated in this manner were extremely active (greater than 20% conversion of heptane) in a microcatalytic cracking reactor in which NaY and HA-1 were virtually inactive.[9] The reduced sample of Z-14US was formed by heating in 195 torr of hydrogen at 500° for 6 hr after calcination.

Isobutane-2-C^{14} was supplied by New England Nuclear Corp. Unlabeled isobutane was Phillips Research Grade (99.52 mol.% pure).

Gravimetric Studies. Adsorption of isobutane on the various substrates at 150° was measured gravimetrically with a Cahn RG electrobalance and these results were used to calculate the amount of isobutane to be used to give the proper equilibrium pressures in the chemisorption studies. Weight losses of the catalysts on evacuation were also determined with the electrobalance.

Chemisorption. The procedure followed closely that of MacIver, *et al.*,[5] for the chemisorption of isobutane on silica–alumina. The distinction between physical adsorption and chemisorption is not always unambiguous but the method described previously[5] seemed reasonable. The material assumed to be chemisorbed is that which was adsorbed at the conditions chosen for the experiment but could not be removed by evacuation overnight at room temperature.

Adsorption conditions were 150° and 10 torr of isobutane. Isobutane-2-C^{14} was adsorbed for 90 min on 5.00 g (evacuated weight) of catalyst; the catalyst was then cooled to ambient temperature and evacuated overnight. Exchange with unlabeled isobutane was carried out at 150° for 8 hr; at both 4 and 8 hr a portion of the exchange solution was transferred to the counter and counted. Checks at longer times demonstrated that equilibrium was reached within 8 hr; the material exchanged is reported as reversibly chemisorbed isobutane. Some C^{14}-containing material remained on the catalyst; this was burned off in 160 mm of O_2 at 500° for 20 hr; the CO_2 was condensed to the counter and counted. This is reported as irreversibly chemisorbed isobutane.

Results and Discussion

The amounts of isobutane reversibly and irreversibly adsorbed on the various catalysts are summarized in Table I, where measurements on each new sample are grouped together. Values previously reported[5,6] for a low alumina silica–alumina (Houdry M-46) pretreated in manners similar to our standard and hydrogen reduction methods have been converted to mg/g from ml (STP)/g and are listed in Table II.

Reduction in hydrogen of Z-14US reduced the amount of chemisorption by a factor of 10. Larson and Hall[6] found a comparable (2–3-fold) decrease in

(7) J. B. Uytterhoeven, L. G. Christner, and W. K. Hall, *J. Phys. Chem.*, 69, 2117 (1965).

(8) P. K. Maher and C. V. McDaniel, U. S. patent 3,293,192.

(9) P. D. Hopkins, to be published.

Table I: Chemisorption of Isobutane on Faujasites and HA-1

Catalyst	Amount adsorbed (mg/g) × 10³ Reversible	Irreversible
NaY (sample 1)	3.2	0.68
	1.9	0.48
NaY (sample 2)	3.5	0.07
	1.6	0.33
DcY (sample 1)	3.2	2.8
	3.0	2.2
	3.1	4.5[a]
DcY (sample 2)	1.1	0.23
	1.2	0.52
DcY (sample 3)	0.30	...
Z-14US	2.0	2.2
	2.2	5.3
	0.2[b]	0.51
HA-1 (sample 1)	0.23	0.17[a]
	0.27	0.22
HA-1 (sample 2)	0.09	0.13
	0.28	0.14

[a] Adsorption for 3 hr. [b] Catalyst reduced in H_2 for 6 hr.

Table II: Chemisorption of Isobutane on Houdry M-46 Silica–Alumina

Sample no.	Amount adsorbed (mg/g) × 10² Reversible	Irreversible	Ref
1	0.70	0.15	5
2	1.13	0.41	6
3	1.59	0.30	
	0.53[a]	0.05[a]	6
	0.55[a]	0.06[a]	
	1.12	0.21	
4	1.83	0.66	6
	1.76	0.55	
5	1.79	0.40	6

[a] Reduced in hydrogen at 500° after normal pretreatment of calcination in oxygen at 500°.

isobutane adsorption by M-46 after hydrogen reduction. This demonstrates that pretreatment conditions are critical and may explain the difficulty of obtaining reproducible results. Possibly chemisorbed oxygen is a necessary component of some adsorption sites.

For one adsorption on DcY, the time of adsorption was doubled; the amount of reversibly adsorbed isobutane was not changed but the amount irreversibly adsorbed doubled. This confirms the previous report[5] that equilibrium is established with reversibly adsorbed isobutane but that the amount irreversibly adsorbed increases linearly with time. Since greater amounts of irreversibly adsorbed isobutane were found on DcY and Z-14US than on HA-1 and M-46, the rate of adsorption was greater, and, if irreversibly adsorbed hydrocarbons are coke precursors, one would expect the rate of coke formation to be greater on faujasites than on amorphous silica–aluminas. This is apparently what is found on clean catalyst surfaces.[1]

The amount of isobutane reversibly adsorbed was less on high alumina HA-1 than on the previously reported low-alumina M-46 despite nearly equal surface areas. Possibly, there is a decrease in the number of Lewis acid sites of sufficient strength to abstract a hydride ion from isobutane; if true, this supports previous observations that the number of Lewis sites is not necessarily proportional to the aluminum content.[10]

Essentially the same amount of isobutane was reversibly chemisorbed on the three faujasites studied. Adsorption on the faujasites was greater by an order of magnitude over HA-1 and only slightly greater than on M-46. DcY and Z-14US irreversibly adsorbed isobutane slightly more rapidly than NaY. These differences obviously cannot explain the large differences in catalytic activity between the decationized faujasites on the one hand and NaY and amorphous silica–alumina on the other.

The amount of isobutane adsorbed on the faujasites was extremely small at 150°. The value of 3.2×10^{-2} mg/g on DcY, which was the largest adsorption we measured on catalytically active faujasite, amounts to only one molecule of isobutane in 1270 large cavities of the DcY structure. These low values lead one to suspect that there is no regular structural site in faujasite on which chemisorption of isobutane occurs. More likely chemisorption takes place on irregular features such as crystal interfaces or dislocations.

Chemisorption of isobutane does not differentiate catalytically active materials from inactive ones. Although the number of chemisorption sites on DcY is greater than the minimum number of sites required for catalysis,[4] the fact that the number of sites is not much greater than on silica–alumina suggests that at least some if not all adsorption sites are not cracking sites.

Acknowledgment. The authors wish to thank J. B. Peri for helpful discussions and advice.

(10) J. B. Peri, *J. Phys. Chem.*, **70**, 3168 (1966).

Dielectric Study of the Molecular Complexes Formed between Triethylamine and Acetic and Monochloracetic Acid

by S. R. Gough and A. H. Price[1]

Edward Davies Chemical Laboratory, University College of Wales, Aberystwyth, United Kingdom *(Received April 19, 1968)*

Dielectric titrations provide a convenient method for investigating molecular interactions in solution. The method involves measurement of the permittivity of solutions containing varying molar ratios of the two

(1) Address all correspondence to this author.

interacting solutes. The total solute concentration is kept constant. If the complex formed has a higher dipole moment than the dipole moment of the individual components, then a plot of the solution permittivity against the molar ratio of the solutes shows a maximum at the molar ratio corresponding to that present in the complex.

Barrow and Yerger[2] showed from infrared measurements that triethylamine forms both 1:1 and 1:2 complexes with acetic and with monochloracetic acid. Dipole moments of 6.37[3] and 6.8 D[4] have been reported for the 1:1 triethylamine–monochloracetic acid complex and moments of 3.87[4] and 3.96 D[5] for the 1:1 triethylamine–acetic acid complex.

Dielectric titrations of triethylamine complexes with acetic and with monochloracetic acid in benzene solution at 20° and at a frequency of 159 kHz are reported.

Triethylamine–Acetic Acid System

The experimental results for benzene solutions containing total solute concentrations of 0.470 and 0.235 *M* and for a dioxane solution of total solute concentration of 0.476 *M* are shown in Figure 1, where $\Delta\epsilon$ is the difference between the solution and the solvent permittivity. There is clear evidence for the formation of an A_2B complex (where A refers to the acid and B to the base), whose effective dipole moment may be determined from the variation of the solution permittivity with the total solute concentration (keeping the molar acid–base ratio constant). If the Guggenheim equation[6] is used, an effective dipole moment of 5.5 D is calculated for the A_2B complex in benzene solution and 5.1 D in dioxane solution. These calculations assume no dissociation of the complex. The degree of dissociation may be estimated from the curvature of the $\Delta\epsilon$ *vs.* solute composition plot near the maximum. The sharper the maximum the lower the degree of dissociation. The results shown in Figure 1 indicate a low degree of dissociation for the complex. A quantitative estimate of the degree of dissociation may be obtained if we assume the validity of the Guggenheim equation for each individual species in solution. This equation may be written as $\Delta\epsilon = k\mu^2 c$, where $\Delta\epsilon = \epsilon - \epsilon_0$, ϵ is the solution permittivity, ϵ_0 is the solvent permittivity, μ is the dipole moment of the species of molar concentration c, $k = [\pi N(\epsilon_0 + 2)(n_0^2 + 2)]/6750kT$, and n_0 is the solvent refractive index. For the equilibrium $A_2B \rightleftharpoons 2A + B$, then

$$\frac{\Delta\epsilon}{k} = c_A\mu_A^2 + c_B\mu_B^2 + c_C\mu_C^2 \qquad (1)$$

where the subscripts A, B, and C refer to the acid, base, and complex. If α is the degree of dissociation of the complex, then

$$\frac{\Delta\epsilon}{k} = c\alpha(2\mu_A^2 + \mu_B^2) + c(1 - \alpha)\mu_C^2 \qquad (2)$$

where c is the complex concentration if undissociated.

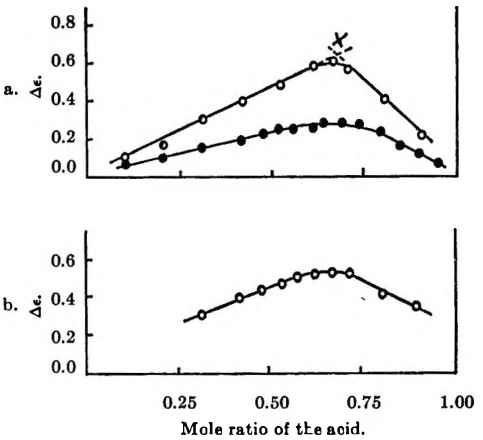

Figure 1. Dielectric titration of triethylamine–acetic acid systems in benzene (a) and in dioxane (b): ○, 0.470 *M*; ●, 0.235 *M*.

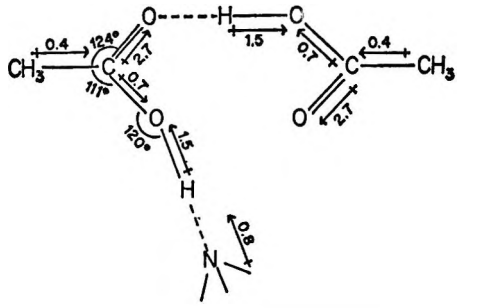

Figure 2. Assumed configuration and bond moments in the triethylamine–acetic acid complex.

Equation 2 contains two unknowns (α and μ_C^2) but may be solved if we write $c\mu_C^2 = \Delta\epsilon_C/k$. The $\Delta\epsilon_C$ value corresponds to the permittivity increment obtained if no dissociation occurred and may be taken as the point of intersection of the linear extrapolation of the wings of the $\Delta\epsilon$ *vs.* molar ratio plot (point X in Figure 1). Thus

$$\frac{\Delta\epsilon}{k} = c\alpha(2\mu_A^2 + \mu_B^2) + (1 - \alpha)\frac{\Delta\epsilon_C}{k} \qquad (3)$$

For the 0.470 *M* triethylamine–acetic acid solution in benzene, $\Delta\epsilon = 0.60$ at the concentration corresponding to the A_2B molar ratio $c = 0.157$ *M* and $\Delta\epsilon_C = 0.64$. Substitution into eq 3 with $\mu_A = 2.31$ D and $\mu_B = 0.8$ D[7] gives $\alpha = 0.1$. In view of the approximations involved in eq 1, no great quantitative significance should be given to this degree of dissociation, but it suffices to establish the low degree of dissociation of the complex.

Adopting the planar model proposed by Barrow and

(2) G. M. Barrow and E. A. Yerger, *J. Amer. Chem. Soc.*, **76**, 5211 (1954).

(3) L. Sobczyk and J. K. Syrkin, *Rocz. Chem.*, **30**, 893 (1956).

(4) J. W. Smith, *J. Chim. Phys.*, **61**, 125 (1964).

(5) H. Tsubomura, *Bull. Chem. Soc. Jap.*, **31**, 435 (1958).

(6) E. A. Guggenheim, *Trans. Faraday Soc.*, **45**, 714 (1949).

(7) A. L. McLellan, "Tables of Experimental Dipole Moments," W. H. Freeman and Co., New York, N. Y., 1963.

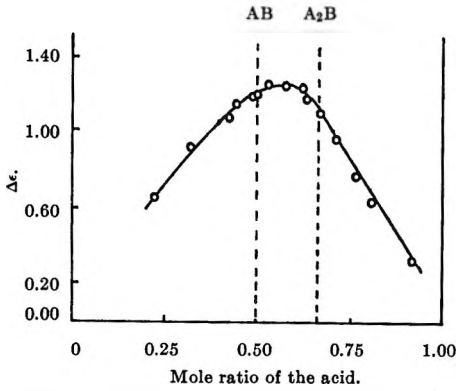

Figure 3. Dielectric titration of triethylamine–monochloracetic acid in benzene. The total solute concentration is 0.470 *M*.

Yerger[2] for the A_2B complex (Figure 2) (and using the bond moments shown), a dipole moment of 2.2 D is calculated for the hydrogen-bonded form of the complex. The group moment of the OH---N group must be increased to 5.9 D to reproduce the measured moment of the complex. If the OH bond distance in the complex is 1.02 Å,[8] the OH dipole carries a charge of 5×10^{-10} esu (*i.e.*, in excess of the electronic charge). This shows that the OH---N group acquires an ion-pair character, and the complex exists in predominantly an ionic form.

Triethylamine–Monochloracetic Acid Complex

The experimental results for total solute concentrations of 0.470 and 0.188 *M* are shown in Figure 3. These show a clear evidence for complex formation, but the maximum occurs at molar ratios intermediate between those required for a 1:1 and a 1:2 complex. The system probably exists in an equilibrium

$$2A + B \rightleftharpoons AB + A \rightleftharpoons A_2B$$

Dipole moments derived from permittivity measurements on this system have limited significance unless the equilibrium is defined. The concentration dependence of the permittivity of a 1:1 molar ratio of solutes yields an effective dipole moment of 6.4 D, in agreement with the values previously mentioned. An effective dipole moment of 7.5 D is calculated for the 1:2 molar ratio.

(8) M. Davies and L. Sobczyk, *J. Chem. Soc.*, 3000 (1962).

Viscosities of Some Organic Glasses Used as Trapping Matrices. II[1]

by A. Campbell Ling and John E. Willard

Department of Chemistry, University of Wisconsin, Madison, Wisconsin 53706 *(Received May 6, 1968)*

For studies of the trapping and decay of electrons, ions, and free radicals produced by radiation in organic glasses[2] and for studies of rheological phenomena[3] in such glasses, more data are needed on the viscosity of the media. In an earlier paper[4] we have reported the viscosities of eight organic glasses as a function of temperature. Similar data are given below for additional glasses of varied molecular structure and polarity.

Experimental Section

Method. Viscosities were determined from the rate of extrusion of a plug of the organic glass from the end of a glass tube to which high pressures of He gas were applied. The temperature was controlled by the rate of flow of gaseous nitrogen which passed over the sample after generation from a liquid nitrogen bath. Full details of the method have been described previously.[4]

Except where noted, a glass viscometer tube of 0.90-cm radius was used. Viscosities were determined at approximately 1°K intervals covering the range of about 10^6 to 10^{10} P.

Materials. All compounds were used as received. 3-Ethylpentane (3EP), 4-methylheptane (4MHp), ethylcyclohexane (ECHx), methylcyclohexane (MCHx), 2,3-dimethylpentane (DMP), and 3-methyloctane (3MO) were from the Aldrich Chemical Co.; 3-methylhexane (3MHx) was from J. T. Baker Chemical Co.; perfluoro-1,2- and perfluoro-1,4-dimethylcyclohexane (PFCHx) isomer mixture and *trans*-1,2-dimethylcyclohexane were from Halogen Chemicals, Inc.; anhydrous methanol and ethanol were from Merck Chemical Co.; 3-methylpentane (3MP) was from the Phillips Petroleum Co.; and totally deuterated 3-methylpentane (3MP-d_{14}) was from Merck Sharp and Dohme. Anhydrous CH_3OH and C_2H_5OH crystallize when cooled to 77°K. Therefore, 4% H_2O by volume was added to each of these compounds to produce glass-forming mixtures.

Results

Data for 11 organic glasses are plotted in Figure 1. Figure 2 gives data for mixtures of MCHx and 3MP. Figure 3 compares results for perdeuterated 3-methylpentane with results for the normal protiated compound measured under the same conditions.

For convenience in comparing different compounds and in extrapolating to temperatures beyond the range

(1) This work has been supported in part by U. S. Atomic Energy Commission Contract AT(11-1)-1715 and by the W. F. Vilas Trust of the University of Wisconsin.

(2) For examples and references, see: (a) W. H. Hamill, "Ionic Processes in γ-Irradiated Organic Solids at −196°," a chapter in "Radical Ions," E. T. Kaiser and L. Kevan, Ed., John Wiley and Sons, Inc., New York, N. Y., 1968; (b) J. E. Willard, "Radiation Chemistry of Organic Solids," a chapter in "Fundamentals of Radiation Chemistry," P. Ausloos, Ed., John Wiley and Sons, Inc., New York, N. Y., in press; (c) B. Wiseall and J. E. Willard, *J. Chem. Phys.*, **46**, 4387 (1967); (d) J. Lin, K. Tsuj., and F. Williams, *J. Amer. Chem. Soc.*, **90**, 2766 (1968).

(3) (a) D. J. Plazek and J. H. Magill, *J. Chem. Phys.*, **45**, 3038 (1966); (b) J. H. Magill, *ibid.*, **47**, 2802 (1967); (c) J. H. Magill and D. J. Plazek, *ibid.*, **46**, 3757 (1967); (d) G. A. von Salis, H. Labhart, *J. Phys. Chem.*, **72**, 752 (1968); (e) for further references see ref 4.

(4) A. C. Ling and J. E. Willard, *J. Phys. Chem.*, **72**, 1918 (1968).

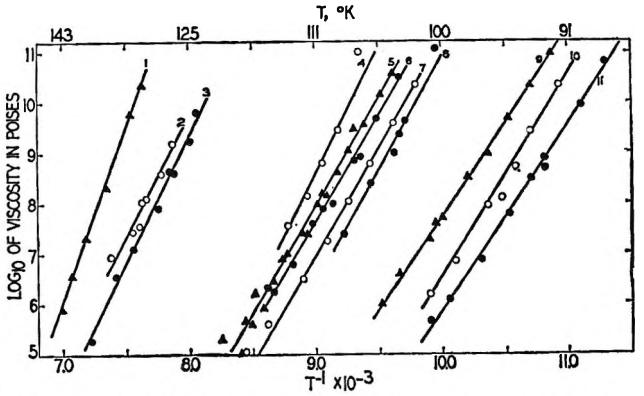

Figure 1. Viscosities of some organic glasses as a function of temperature: (1) perfluorodimethylcyclohexane, (2) isoamyl alcohol, (3) *n*-amyl alcohol, (4) 3-methyloctane, (5) methanol + 4 vol % water, (6) ethanol + 4 vol % water, (7) ethylcyclohexane, (8) 4-methylheptane, (9) 3-ethylpentane, (10) 3-methylhexane, (11) 2,3-dimethylpentane.

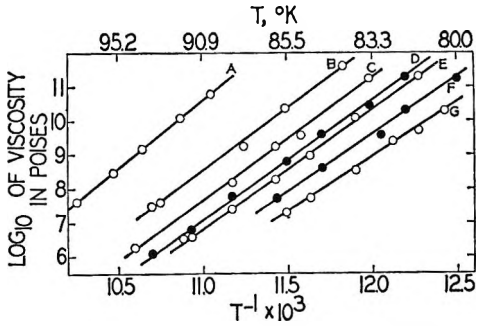

Figure 2. Viscosities of mixtures of methylcyclohexane with 3-methylpentane in the glassy phase as a function of temperature, mole fraction of methylcyclohexane: A, 0.95 mf; B, 0.67 mf; C, 0.50 mf; D, 0.33 mf; E, 0.29 mf; F, 0.17 mf; G, pure 3MP.[4]

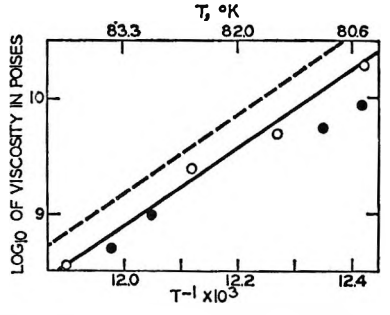

Figure 3. Viscosity of perdeuterated 3-methylpentane glass compared with nondeuterated samples: ●, 3-methylpentane-d_{14}, determined with a 1-g sample; ○, 3-methylpentane-h_{14}, determined with a 1-g sample. Dashed line shows viscosity–temperature dependence determined over more extended range with 5-g samples of 3-methylpentane-h_{14}.

of the current measurements, columns 2 and 3 of Table I give the values of A and B from the equation $\log \eta = AT^{-1} + B$, as obtained from a least-squares fit of the data. Column 5 gives the viscosities at 77°K calculated using this equation. The extrapolation to 77°K has been made for the purpose of obtaining an approximate indication of relative viscosities at a single temperature and some indication of their absolute magnitudes at the temperature most frequently used in matrix trapping studies. The values may deviate considerably from the true values, since the extrapolation from the experimental data crosses the glass transition temperature. Column 4 of Table I gives the Arrhenius E factors.

Table I: Viscosity Parameters for Organic Glasses

	A, °K^{-1} × 10^{-3}	$-B$	E, eV	Viscosity at 77.5°K (extrapolated), P
3-Methylpentane[a]	3.46	32.2	0.69	2.2 × 10^{12}
2-Methylpentane[a]	3.48	31.5	0.69	2.4 × 10^{13}
2-Methylpentene-1[a]	3.96	34.3	0.72	3.8 × 10^{16}
3-Ethylpentane	3.64	28.68	0.72	2.4 × 10^{18}
2,3-Dimethylpentane	3.67	30.91	0.73	3.6 × 10^{16}
3-Methylhexane	4.15	35.06	0.82	3.2 × 10^{18}
4-Methylheptane	4.89	37.82	0.97	2.0 × 10^{25}
3-Methyloctane	5.75	43.05	1.14	1.2 × 10^{31}
Methylcyclohexane[b]	4.16	35.57	0.83	1.2 × 10^{18}
Ethylcyclohexane	3.97	28.64	0.78	4.4 × 10^{22}
Perfluorodimethylcyclohexane	6.99	42.94	1.39	2.4 × 10^{47}
Methanol + 4% water	4.22	29.50	0.84	1.1 × 10^{25}
Ethanol + 4% water	2.95	18.78	0.59	2.1 × 10^{19}
2-Methyltetrahydrofuran[a]	4.93	43.1	0.98	3.7 × 10^{20}
n-Propyl alcohol[a]	2.70	16.35	0.54	3.0 × 10^{18}
n-Amyl alcohol	5.09	31.38	1.01	2.1 × 10^{34}
Isoamyl alcohol	4.79	28.63	0.95	1.6 × 10^{33}
Isopropyl benzene[a]	7.01	43.33	1.39	1.7 × 10^{47}
n-Butylbenzene[a]	6.31	37.98	1.25	3.5 × 10^{43}
Di-*n*-butyl phthalate[a]	7.51	32.08	1.49	8.7 × 10^{64}

[a] Reference 4. [b] By extrapolation from MCHx–3MP mixtures.

As noted earlier,[4] it has not been possible to measure the viscosity of methylcyclohexane glass by the extrusion method because of the tendency for the glass to crack and to crystallize. However, a stable glass is formed from solutions containing 0.98 mol fraction or less of MCHx in 3MP. Extrapolation of the data of Figure 2 for each concentration to 77.5°K gives the following values: 0.95 mf, 4 × 10^{17} P; 0.66 mf, 3 × 10^{15} P; 0.50 mf, 2 × 10^{14} P; 0.33 mf, 4 × 10^{13} P; 0.28 mf, 2 × 10^{13} P; 0.17 mf, 3 × 10^{12} P. Extrapolation of these estimated values to an MCHx mol fraction of unity gives a value of 1.2 × 10^{18} P as the viscosity of of pure MCHx glass at 77.5°K. The value for pure 3MCHx at 77.5°K was previously[4] bracketed as falling between 10^{16} and 10^{21} P.

Plots of viscosity against composition of the 3MP–MCHx mixture appear to have a slight curvature in the direction of more rapidly increasing viscosity as the concentration of MCHx increases, in contrast to 3MP–isopentane mixtures.[4]

Because deuteration has been observed to cause cer-

tain striking effects on the decay rates of radicals in glassy matrices, the viscosity of perdeuterated 3MP was determined. Four measurements on a 1-g sample in a 0.55 cm in diameter viscometer tube were compared with results on an identical sample of the nondeuterated compound (Figure 3). The dotted line in Figure 3 is from measurements[4] with the more accurate 0.9-cm tube. The results indicate that there is no major difference between the viscosities of 3MP-h_{14} and 3MP-d_{14} glasses.

The viscosity of *trans*-1,3-dimethylcyclohexane glass at 112°K is 8.3×10^7 P.

Related Measurements

von Salis and Labhart[5] have recently reported determinations of the viscosities of MCHx in the region 135–205°K and of 3MP in the region 95–120°K, using a commercial rotating cylinder viscometer. The former values are above the glass softening temperature, and the latter span it, so that comparison with extrapolated values of the present work is not meaningful. It appears, however, that their value for pure 3MP at 95°K (10^5 P) is about one order of magnitude higher than that found in our earlier work[4] at this temperature, although our investigations[4] of other highly viscous glasses have agreed well with earlier results extending from lower viscosities.[4]

(5) G. A. von Salis and H. Labhart, *J. Phys. Chem.*, **72**, 752 (1968).

COMMUNICATIONS TO THE EDITOR

Intramolecular Elimination Reactions in the Photolysis of Fluoroaldehydes

Sir: Recently, perfluoroalkyl radicals have been generated by the photolysis of various fluoroaldehydes,[1] and data have been obtained for the abstraction of the aldehydic hydrogen atom by the radical

$$R_f + HCOR_f \xrightarrow{1} R_fH + COR_f$$

The aldehyde has also been used[2] as a radical source to investigate the removal of hydrogen from various substrate molecules, *i.e.*

$$R_f + RH \xrightarrow{2} R_fH + R$$

This technique is satisfactory if there is no other source of R_fH in the reaction system.

In a study of the photolysis of CF_3COCF_3–$HCOC_2F_5$ mixtures it became apparent that although the fluoroform formation could be adequately accounted for by the reactions

$$CF_3 + HCOC_2F_5 \xrightarrow{3} CF_3H + COC_2F_5$$

$$2CF_3 \xrightarrow{4} C_2F_6$$

the pentafluoroethane formation was not similarly expressed by the reactions

$$C_2F_5 + HCOC_2F_5 \xrightarrow{5} C_2F_5H + COC_2F_5$$

$$2C_2F_5 \xrightarrow{6} C_4F_{10}$$

Our evidence for this conclusion was that although a plot of the ratio $R_{CF_3H}/R^{1/2}_{C_2F_6}$ *vs.* aldehyde concentration gave, within experimental error, zero intercept, a corresponding plot for $R_{C_2F_5H}/R^{1/2}_{C_4F_{10}}$ yielded a markedly positive intercept. Analysis of the data published for the $HCOC_2F_5$ system yielded essentially the same conclusion.

When cyclopropanecarboxaldehyde is photolyzed,[3,4] its decomposition has been shown to involve production of free radicals and also the formation of propylene by an intramolecular elimination reaction (8).

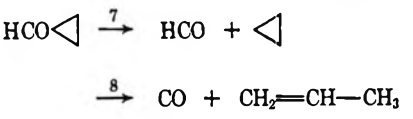

It seemed likely that such an intramolecular elimination reaction was also contributing to pentafluoroethane formation when the fluoroaldehyde was photolyzed; *i.e.*, the primary processes were

$$HCOC_2F_5 \xrightarrow{9} HCO + C_2F_5$$

$$\xrightarrow{10} CO + C_2F_5H$$

We have photolyzed under similar conditions the aldehyde alone and also aldehyde–nitric oxide mixtures. In the latter cases perfluorobutane formation was completely inhibited although extensive pentafluoroethane formation occurred, the yield decreasing by only ~75%

(1) G. O. Pritchard, G. H. Miller, and J. K. Foote, *Can. J. Chem.*, **40**, 1830 (1962).

(2) G. O. Pritchard and J. K. Foote, *J. Phys. Chem.*, **68**, 1016 (1964).

(3) G. Greig and J. C. J. Thynne, *Trans. Faraday Soc.*, **63**, 1369 (1967).

(4) J. J. I. Overwater, H. J. Herman, and H. Cerfontain, *Rec. Trav. Chim.*, **83**, 637 (1964).

at 400°K compared with the experiments performed in the absence of the inhibitor. We therefore conclude that reaction 10 contributes substantially to pentafluoroethane formation. The fact that only such a relatively small degree of C_2F_5H inhibition was observed, particularly with regard to the fact that, in the unscavenged experiments there will be substantial contributions to the C_2F_5 radical concentration by the decarbonylation of the COC_2F_5 radical produced in reaction 5, suggests that photodecomposition of the aldehyde by reactions 9 and 10 must be comparable.

Similar examination of the photolyses of $HCOCF_3$ and $HCOC_3F_7$ showed that the following intramolecular elimination reactions occur appreciably in these systems.

$$HCOCF_3 \longrightarrow CO + CF_3H$$

$$HCOC_3F_7 \longrightarrow CO + C_3F_7H$$

We therefore conclude that fluoroaldehydes are not suitable for use as photochemical sources of fluoroalkyl radicals in connection with hydrogen atom abstraction reactions and that the kinetic data reported[1,2] for such reactions are likely to be significantly in error.

CHEMISTRY DEPARTMENT
EDINBURGH UNIVERSITY
EDINBURGH 9, SCOTLAND
E. R. MORRIS
J. C. J. THYNNE

RECEIVED MAY 10, 1968

A Reply to "Intramolecular Elimination Reactions in the Photolysis of Fluoroaldehydes"

Sir: The point made by Morris and Thynne in the preceding communication[1] is valid, and an examination of the data on C_2F_5CHO photolysis[2] at about room temperature is in accord with their observation. The intramolecular elimination of R_fH (where R_f = CF_3, C_2F_5, or C_3F_7)

$$R_fCHO + h\nu \longrightarrow R_fH + CO \qquad (1)$$

vs. the cleavage into radicals

$$R_fCHO + h\nu \longrightarrow R_f + CHO \qquad (2)$$

is presumably temperature independent, so that the formation of R_fH *via* reaction 1 will be relatively more important than formation by abstraction

$$R_f + R_fCHO \longrightarrow R_fH + CO + R_f \qquad (3)$$

at lower temperatures.[3] The Arrhenius plots used[2] to yield values of $E_3 - {}^1/_2E_4$

$$R_f + R_f \longrightarrow R_{f_2} \qquad (4)$$

will therefore lead to low values ($\sim$4 kcal mol^{-1}) of E_3, assuming that $E_4 = 0$. This is actually the case, as shown by the tabulation of the data[4] and the value of $E_3 = 8.2$ kcal mol^{-1} obtained by Dodd and Smith[5] in CF_3CHO photolysis is now substantiated. These authors made a correction for CF_3H formation *via* mode 1, but found it to be unimportant above 150°; and a plot of their results, $R_{CF_3H}/R^{1/2}_{C_2F_6}$ *vs.* aldehyde pressure, obtained at 209°, passes through the origin.[6] It does not necessarily follow therefore that the data reported on the abstraction reactions with hydrogen and hydrocarbons

$$R_f + RH \longrightarrow R_fH + R \qquad (5)$$

using the aldehydes as sources are significantly in error. The data on H_2 and D_2[7] compare favorably with similar data obtained using perfluoroketones and perfluoroazo compounds as radical sources,[4,7,8] and the collected data on CH_4 and isobutane are similarly self-consistent.[4,7,9] At elevated temperatures the main mode of decomposition of the aldehyde is *via* reaction 3 and a similar chain propagating step involving the atom or radical produced in reaction 5.[10]

A reinvestigation of the photodissociation of these aldehydes is warranted, particularly with regard to the possible difference in multiplicities of the electronic states which lead to the two dissociative modes.

Acknowledgment. We thank the National Science Foundation for financial assistance.

(1) E. R. Morris and J. C. J. Thynne, *J. Phys. Chem.*, **72**, 3351 (1968).

(2) G. O. Pritchard, G. H. Miller, and J. K. Foote, *Can. J. Chem.*, **40**, 1830 (1962).

(3) Reaction 3 assumes that the fluoroacyl radicals decompose, which may not be completely true at room temperature. However, the relative instability of CF_3CO has been noted; J. C. Amphlett and E. Whittle, *Trans. Faraday Soc.*, **63**, 80 (1967).

(4) G. O. Pritchard, J. R. Dacey, W. C. Kent, and C. R. Simonds, *Can. J. Chem.*, **44**, 171 (1966).

(5) R. E. Dodd and J. W. Smith, *J. Chem. Soc.*, 1465 (1957); this is further verified by the value of $E_3 = 9.7$ kcal mol^{-1} obtained for $C_2F_5 + CF_3CHO$ using perfluoroazoethane as the radical source.[4]

(6) Our data[2] are not extensive enough at high temperatures to make this test.

(7) G. O. Pritchard and J. K. Foote, *J. Phys. Chem.*, **68**, 1016 (1964).

(8) With D_2, R_{R_fD} was, in any case, determined directly.

(9) G. O. Pritchard and G. H. Miller, *J. Chem. Phys.*, **35**, 1135 (1961).

(10) In the $C_3F_7 + D_2$ experiments we observed 60 to 100% HD formation based on C_3F_7D produced.[7]

DEPARTMENT OF CHEMISTRY
UNIVERSITY OF CALIFORNIA
SANTA BARBARA, CALIFORNIA 93106
G. O. PRITCHARD
M. J. PERONA

RECEIVED JUNE 11, 1968

Charged Square-Well Model for Ionic Solutions[1]

Sir: The simplest physical model for electrolyte solutions seems to be the charged hard-sphere model

(1) Grateful acknowledgment is made for the support of this research by the Office of Saline Water, U. S. Department of the Interior

(primitive model) for which the potential of the average force between ions i and j in the pure solvent of dielectric constant ϵ is

$$u_{ij}(r) = e_i e_j/\epsilon r + u_{ij}^*(r) \quad (1)$$

$$u_{ij}^*(r) = \infty \quad (r < a_{ij})$$
$$= 0 \quad (a_{ij} < r) \quad (2)$$

where e_i and e_j are the charges and a_{ij} is the sum of the sphere radii. It is well known that values of a_{ij} considerably larger than the sum of crystallographic radii are required to get activity and osmotic coefficients calculated from the model to compare well with experimental data for dilute aqueous solutions of halides of Li, Na, and K. This is attributed to ionic hydration. However, a more realistic way to treat hydration effects is to introduce the charge square-well model for which we have

$$u_{ij}^*(r) = \infty; \quad r < r_i + r_j$$
$$= d_{ij}; \quad r_i + r_j < r < r_i + r_j + 2w \quad (3)$$
$$= 0; \quad r_i + r_j + 2w < r$$

where r_i and r_j are crystallographic radii and $w = 1.36$ Å, the radius of a water molecule. The parameter d_{ij} is a sort of free energy like other terms in a potential of average force. It is negative for a well and positive for a "square mound" such as might represent the reversible work in displacing the hydration layers on the ions.

Computations by the method of the HNC integral equation[2] for this model with parameters[3] chosen to correspond to aqueous NaCl at 25° give the results in Figure 1. It is remarkable that only a very small mound height would be required to give an accurate fit to the osmotic coefficient data at low concentrations. It is also remarkable that $d_{+-} = {}^1/_4 kT$ gives a rather respectable fit up to 1 M. The treatment of the model

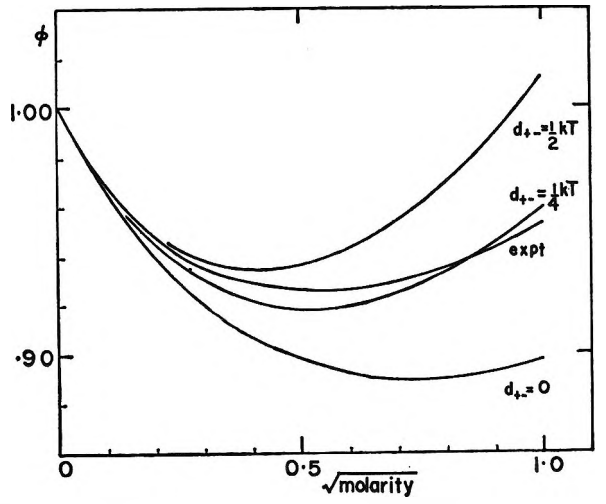

Figure 1. Osmotic coefficients calculated from the HNC equation compared with experiment. All osmotic coefficients are for the McMillan–Mayer reference states which are slightly different from the usual molal, T, P reference states (ref 2). All computations are for $d_{++} = d_{--} = 0$.

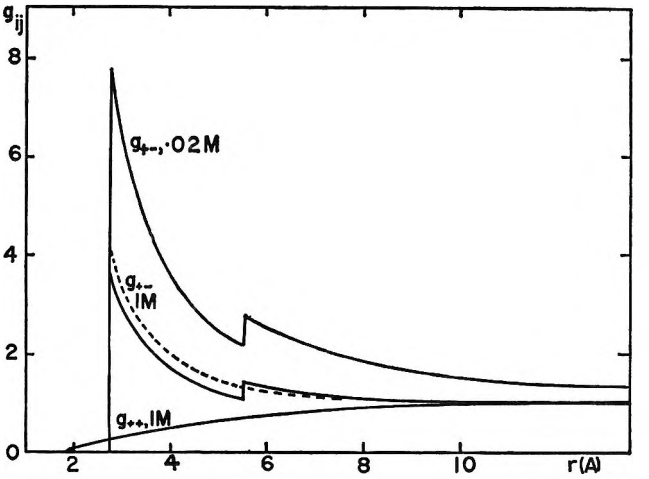

Figure 2. Pair correlation functions for charged hard-sphere model: ———, $d_{+-} = {}^1/_4 kT$; – – – –, $d_{+-} = 0$; $d_{++} = d_{--} = 0$ in each case. If c_j is the bulk concentration of ions of species j, then $c_j g_{ij}(r)$ is the local concentration of j ions at a distance r from an i ion. Discontinuities in g_{ij} coincide with those in u_{ij}.

up to 1 M seems to be accurate judging by the self-consistency test employed for the primitive model.[2] Inclusion of positive d_{++} and d_{--}, as would be required in fitting this model to data for mixtures (Harned's rule data), would likely worsen the fit while it seems clear that the fit could be improved by changing the *shape* of the mound.

The important conclusion that a mound height less than kT is adequate to account for the hydration effects is not likely to be affected by refinements. It has an important implication in aqueous NaCl and similar systems: the ionic distributions at contact are not greatly affected by hydration. This is illustrated clearly by the pair correlation functions g_{ij} computed for this model (Figure 2). It is of course possible that different conclusions will be reached by this method in cases in which the hydration is stronger, *e.g.*, for more highly charged ions.

The charged square-well model invites application to excess enthalpies and volumes as well. In such cases a new set of parameters appears, for example

$$v_{ij} = \partial d_{ij}/\partial P$$

A model which specifies v_{ij} seems much more physical and more amenable to molecular interpretation than one which specifies $\partial a_{ij}/\partial P$, the additional parameter that one needs to fit excess volume data to the primitive model.

(2) J. C. Rasaiah and H. L. Friedman, *J. Chem. Phys.*, 48, 2742 (1968).

(3) $r_+ = 0.95$ Å; $r_- = 1.81$ Å.

DEPARTMENT OF CHEMISTRY
STATE UNIVERSITY OF NEW YORK
AT STONY BROOK
STONY BROOK, NEW YORK 11790

JAYENDRAN C. RASAIAH
HAROLD L. FRIEDMAN

RECEIVED MAY 16, 1968

Experimental Method for Determining the Intersystem Crossing Rate Constant from Lowest Excited Singlet to Lowest Triplet State

Sir: One of the most important, and experimentally elusive, parameters of intramolecular energy transfer is the rate constant for intersystem crossing from lowest excited singlet to lowest triplet state, k_{ISC}.[1] The usual experimentally determinable parameters such as the fluorescence quantum yield, ϕ_F, or experimental fluorescence lifetime, τ_F^e, contain the rate constant for internal conversion from excited to ground singlet, k_{IC}, and the natural rate constant for fluorescence, k_F° as well as k_{ISC}. Therefore, at best these experimental data can give only a maximum value of k_{ISC}. This follows from

$$k_F^\circ = \phi_F/\tau_F^e \quad (1)$$

$$\tau_F^e = 1/(k_F^\circ + k_{ISC} + k_{IC}) \quad (2)$$

and

$$k_{ISC} = 1/\tau_F^e - k_F^\circ - k_{IC} = (1 - \phi_F)/\tau_F^e - k_{IC} \quad (3)$$

Then, since $k_{IC} \geqslant 0$, setting $k_{IC} = 0$ gives the upper limit on k_{ISC}

$$k_{ISC} \leqslant (1 - \phi_F)/\tau_F^e \quad (4)$$

Based upon quantum yield data, this approximation seems to be a good one for some aromatic hydrocarbons,[2] but a more accurate and quantitative method of obtaining k_{ISC} is desirable in order to study its dependence upon temperature, solvent media, and molecular properties.

We wish to propose an experimental method of obtaining numerical values of k_{ISC} involving optical density changes occurring during triplet–triplet absorption under steady-state conditions. Since many aromatic hydrocarbons and heterocyclic compounds exhibit triplet–triplet absorption,[3] this method should be applicable to a wide range of compounds. The equations derived here yield a rate constant k^a_{ISC} which we will call the apparent k_{ISC} constant. This apparent rate constant is equal to k_{ISC} if only one triplet level lies below the lowest singlet. It is a sum of lowest singlet to triplet rate constants for other cases, which will be described in a later paragraph. The analysis given here is not directly applicable to heterocyclic compounds where n,π^* states lie below the π,π^* states. However, the approach given here may easily be extended to such cases.

The optical density *change*, $\rho(\lambda)$, due to triplet–triplet absorption from the lowest triplet state, T_1 to a higher triplet state, T_n, at a wavelength λ is

$$\rho(\lambda) = \epsilon_T(\lambda) l [T_1] \quad (5)$$

where $\epsilon_T(\lambda)$ is the triplet–triplet extinction coefficient at wavelength λ, l is the optical path length, and $[T_1]$ is the concentration in the lowest triplet state, T_1. We shall assume[4] that *steady-state conditions hold with respect to both S_1 and T_1*, (excitation time $\approx$ 10 phosphorescence lifetimes), that no photochemical decomposition occurs, and that no bimolecular quenching occurs. We further assume that all of the exciting light (corresponding to ground singlet-lowest excited singlet absorption only) is absorbed by the sample, that direct population of T_1 by absorption from the ground state is negligible, and that *the rate of absorption of the optical density measuring light, I_T, is very small compared to rate of absorption of exciting light, I_a.*

The differential equation for the lowest triplet state population with respect to time is then

$$d[T_1]/dt = I_a k^a_{ISC} \tau_F^e - [T_1]/\tau_P^e - I_T + [T_n]/\tau_F^{e\prime} \quad (6)$$

where I_a is the rate of absorption into the $S_0 \rightarrow S_1$ band, I_T is the rate of absorption from $T_1 \rightarrow T_n$, T_n is some higher triplet state, $\tau_F^{e\prime}$ is the experimental fluorescence lifetime for $T_n \rightarrow T_1$ emission, and τ_P^e is the experimental phosphorescence lifetime. Both of the last two terms in eq 6 are negligible and/or cancel one another under the assumed conditions of low T_n monitoring light. In this case, after an excitation time, $t \gg \tau_P^e$

$$[T_1]_{SS} = \tau_P^e \tau_F^e k^a_{ISC} I_a \quad (7)$$

then

$$\rho(\lambda)_{SS} = \epsilon_T(\lambda) \tau_P^e \tau_F^e k^a_{ISC} I_a l \quad (8)$$

and

$$k^a_{ISC} = \rho(\lambda)_{SS}/\epsilon_T(\lambda) \tau_P^e \tau_F^e I_a l \quad (9)$$

k^a_{ISC} may be determined from eq 9 since all quantities on the right can be experimentally measured. The most difficult quantities to obtain are $\epsilon_T(\lambda)$ and τ_F^e. However, recently, methods of obtaining τ_F^e[5a,b] and $\epsilon_T(\lambda)$[6] have been improved. It should also be noted that k^a_{ISC} can be calculated from measurements of $\rho(\lambda)_{SS}$ and $\epsilon_T(\lambda)$ at one selected wavelength. Even if only a maximum value of ϵ_T is available, use of the $\epsilon_T(\max)$ in eq 9 will yield a minimum value of k^a_{ISC}. This minimum, together with the maximum from eq 4, will define the range of k^a_{ISC}.

(1) See, for example, N. J. Turro, "Molecular Photochemistry," W. A. Benjamin, Inc., New York, N. Y., 1965, p 74, and S. K. Lower and M. A. El-Sayed, *Chem. Rev.*, **66**, 199 (1966). Usually, estimates of k_{ISC} are made by assuming k_{IC} is negligible or by comparing $\phi_F + \phi_T$ (triplet state quantum yield) with unity.

(2) E. Lim and J. Laposa, *J. Chem. Phys.*, **41**, 3257 (1964).

(3) (a) D. P. Craig and I. G. Ross, *J. Chem. Soc.*, 1589 (1954); (b) B. R. Henry and M. Kasha, *J. Chem. Phys.*, **47**, 3319 (1967); (c) G. Porter and M. W. Windsor, *Proc. Roy. Soc.*, **A245**, 238 (1958); (d) D. S. McClure, *J. Chem. Phys.*, **19**, 670 (1951).

(4) All of the assumptions are controllable by experimental design, *e.g.*, use of proper filters, light intensities, etc.

(5) (a) See I. B. Berlman, "Handbook of Fluorescence Spectra of Aromatic Molecules," Academic Press, New York, N. Y., 1965, p 231, for a bibliography of methods; (b) W. R. Ware and B. A. Baldwin, *J. Chem. Phys.*, **43**, 1194 (1965).

(6) (a) R. A. Keller and S. G. Hadley, *ibid.*, **42**, 2382 (1965); (b) P. G. Bowers and G. Porter, *Proc. Roy. Soc.*, **A296**, 348 (1967); (c) W. R. Dawson, *J. Opt. Soc. Am.*, **58**, 222 (1968).

Table I: Values of Intersystem Crossing Rate Constants for Aromatic Hydrocarbons at 77°K

Compound	$\rho(\lambda)/I_{al}$,[a] einstein^{-1}, sec cm^2 × 10^{-8}	ϵ_T,[a] mol^{-1} cm^{-1} l. × 10^{-4}	τ_F^e,[d] nsec	τ_P^e,[e] sec	ϕ_F[f]	k^a_{ISC},[g] sec^{-1} × 10^{-6}	Max k^a_{ISC},[h] sec^{-1} × 10^{-6}
Naphthalene	0.18	1.3[i]	96[c]	2.25	0.39	6.4 ± 2.0	6.4 ± 1.0
Naphthalene-d_8	0.97	0.87	96[c]	18.3	0.40[j]	6.3 ± 2.0	6.4 ± 1.0
Phenanthrene	0.65	2.1[i]	71[b]	3.68	0.14	12 ± 3.0	12 ± 2.0
Triphenylene	1.08	0.78	37[c]	14.8	0.06	26 ± 8.0	26 ± 3.0

[a] Reference 6a. Data obtained at 77° K in 1-butanol–isopentane glass (3:7). ϵ_T were recalculated using the more accurate τ_F^e and ϕ_F values in this table. Estimated errors by comparison with data in ref 3a, c, and 6b are 20%, except for triphenylene which may have a 30% error. [b] J. D. Laposa, E. C. Lim, and R. E. Kellogg, *J. Chem. Phys.*, **42**, 3025 (1965), in EPA at 77°K. Estimated error is 10%. [c] Reference 5a, obtained in deoxygenated cyclohexane at room temperature. Estimated error is 5%. [d] Data required at 77°K are assumed to be same as those obtained at room temperature. This probably introduces a maximum error of 15%. [e] Reference 2, in EPA at 77°K. [f] See A. A. Lamola and G. S. Hammond, *J. Chem. Phys.*, **43**, 2129 (1965), for references and discussion of the reported values in EPA at 77°K. These values are probably reliable to ±0.02. [g] From eq 9. Estimated errors propagated from other parametric errors are listed. [h] From eq 4. Estimated errors are 15% except for triphenylene which is 11%. [i] This agrees with the average of data reported in ref 3a and 6b.

The experimentally determined value of k^a_{ISC} from eq 9 is equal to the rate of intersystem crossing from S_1 to T_1 when only one triplet state is accessible from S_1. In the case where two triplets are accessible from the lowest singlet state, the experimentally determined k^a_{ISC} is

$$k^a_{ISC} = k^1_{ISC} + k^2_{ISC}(k^{21}_{IC}\tau_P^{e\prime\prime}) \qquad (10)$$

where k^i_{ISC} is the intersystem rate constant from S_1 to T_i, k^{21}_{IC} is the rate constant for internal conversion from T_2 to T_1, and $\tau_P^{e\prime\prime}$ is the experimental lifetime of T_2. If $k^{21}_{IC} \approx 1/\tau_P^{e\prime\prime}$, as is usually assumed

$$k^a_{ISC} = k^1_{ISC} + k^2_{ISC} \qquad (11)$$

For the case where three triplet states are accessible from the lowest singlet state

$$k^a_{ISC} = k^1_{ISC} + k^2_{ISC}(k^{21}_{IC}\tau_P^{e\prime\prime}) + k^3_{ISC}(k^{21}_{IC}\tau_P^{e\prime\prime}k^{32}_{IC}\tau_P^{e\prime\prime\prime} + k_{IC}{}^{31}\tau_P^{e\prime\prime\prime}) \qquad (12)$$

Here $\tau_P^{e\prime\prime\prime}$ is the experimental lifetime of T_3, and k^{3i}_{IC} are internal conversion rate constants from T_3 to T_i. If $k^{21}_{IC} \approx 1/\tau_P^{e\prime\prime}$ and $(k^{31}_{IC} + k^{32}_{IC}) \approx 1/\tau_P^{e\prime\prime\prime}$

$$k^a_{ISC} = k^1_{ISC} + k^2_{ISC} + k^3_{ISC} \qquad (13)$$

Of the existing data on triplet–triplet absorption of aromatic compounds, only that of Keller and Hadley[6a] appears to satisfy the assumptions made in the derivation of eq 9. As an example of the proposed method, these data with values of k^a_{ISC} are collected in Table I along with maximum values of k^a_{ISC} obtained from eq 4. We have recalculated the $\epsilon_T(\lambda)$ values using more accurate ϕ_F and τ_F^e data listed in Table I. Because τ_F^e data at 77°K are not available for most of the compounds, we have assumed that the values obtained at room temperature in cyclohexane are identical with 77°K values in EPA. This introduces an estimated error of 15%.

These limited and not highly precise data allow some interesting conclusions to be made. First, agreement (to within experimental error) between values calculated from 9 and 4 shows that the S_1 to S_0 internal conversion rate constant is negligible compared to those for fluorescence and intersystem crossing, confirming a previous statement to this effect.[2] The data for naphthalene and deuterated naphthalene show no isotope dependence (to within experimental error) for k^a_{ISC} in agreement with previous indirect evidence based on ϕ_F values of phenanthrene, triphenylene, and naphthalene.[2] Since the isotope effect on k^a_{ISC} is expected to be largest for naphthalene[7] (with the largest T_1–S_1 energy difference), there should be no isotope effect on k^a_{ISC} for triphenylene and phenanthrene, both of which have smaller T_1–S_1 energy differences. The values of k^a_{ISC} are 10^6 to 10^7 sec^{-1} and show an inverse dependence upon the T_1–S_1 energy gap as predicted by Kasha.[8] The higher values of k^a_{ISC} for triphenylene and phenanthrene may be due to one or more triplet states lying between S_1 and T_1, since the two compounds are predicted to have three and two triplet states, respectively, below S_1.[9] The precision of k^a_{ISC} could be markedly improved by precise τ_F^e data at 77°K which is not now available.

The proposed method of obtaining k^a_{ISC} should prove invaluable in further studies of the effect of temperature and intramolecular factors on this rate constant. We hope that experimentalists involved in energy transfer studies will use this method to investigate this important parameter. Hopefully, more precise methods of

(7) M. R. Wright, R. P. Frosch, and G. W. Robinson, *J. Chem. Phys.*, **33**, 934 (1960).

(8) M. Kasha, *Radiation Res. Suppl.*, **2**, 243 (1960).

(9) D. R. Kearns, *J. Chem. Phys.*, **36**, 1608 (1962); (assignments I or II).

obtaining ϵ_T will be developed thereby improving the utility of this method.

MATERIALS SCIENCES LABORATORY
LOCKHEED-GEORGIA COMPANY
MARIETTA, GEORGIA 30060

DONALD R. SCOTT
OTTO MALTENIEKS

RECEIVED MAY 10, 1968

A Note on the Dissolving of Stationary Spheres, Especially Gas Bubbles

Sir: Krieger, Mulholland, and Dickey[1] have reported in this journal an elegant experimental method of studying the dissolving of spherical gas bubbles in a liquid. A particularly attractive feature is that the conditions approach very closely the spherical symmetry which is a required condition for obtaining any reasonably straightforward theoretical interpretation.

By analogy with the equivalent problem of heat transfer to a sphere with constant surface temperature,[2] the rate of change of radius (a) with time (t) is[3]

$$\frac{da}{dt} = -\frac{D(C_a - C_\infty)}{\rho}\left[\frac{1}{a} + \frac{1}{(\pi Dt)^{1/2}}\right] \quad (1)$$

where D is the effective diffusivity, ρ the density of the sphere (of pure solute); C_a is the dissolved concentration of solute in equilibrium at the surface of the sphere; and C_∞ is the original uniform concentration of the solute in the solution. Introducing the dimensionless parameters $a^* = a/a_0$, $t^* = Dt/a_0^2$, and $\beta_0 = (C_a - C_\infty)/\rho$, where a_0 is the initial radius, eq 1 becomes

$$\frac{da^*}{dt^*} = -\beta_0\left[\frac{1}{a^*} + \frac{1}{(\pi t^*)^{1/2}}\right] \quad (2)$$

Several authors have assumed that $1/(\pi t^*)^{1/2} \ll 1/a^*$, which leads to

$$a^{*2} = 1 - 2\beta_0 t^* \quad (3)$$

and have used this relation to interpret the dissolving of gas bubbles, particularly to evaluate diffusivities.

Krieger, *et al.* (like Epstein and Plesset,[3] Cable,[4] Frischat and Oel[5]), did not ignore the term involving $1/(\pi t^*)^{1/2}$ and obtained a solution to eq 2 which fitted their observations quite closely (see their Figure 4). They then used their experimental data and theoretical model to evaluate diffusivities in seven gas–liquid systems.

Unfortunately, this theoretical model entirely ignores the effects of the motion of the boundary and the radial velocity of the liquid on the shape of the concentration distribution and hence da/dt. Johns[6] attempted to estimate how big an error in diffusivity resulted from ignoring the velocity terms and using the quasi-static solution described by eq 2. In his analysis he assumed that $\partial C/\partial t$ ($\partial \rho_l/\partial t$ in his notation) equals zero. He concluded that the error was about 1% for air in water and 5% for carbon dioxide in water.

If one assumes a constant partial specific volume ($\bar{V}_A$) for the solute, the diffusion equation including the convective terms is

$$\frac{\partial C^*}{\partial t^*} - \left[\frac{2}{r^*} - (1 - \alpha)\frac{a^{*2}}{r^{*2}}\frac{da^*}{dt^*}\right]\frac{\partial C^*}{\partial r^*} - \frac{\partial^2 C^*}{\partial r^{*2}} = 0 \quad (4)$$

where $C^* = (C - C_\infty)/(C_a - C_\infty)$ and $\alpha = \rho\bar{V}_A$. The problem is completely described by also specifying the relation between da/dt and the flux at the interface (see Readey and Cooper[7])

$$\frac{da^*}{dt^*} = \beta\left.\frac{\partial c^*}{\partial r^*}\right|_{a^*} \quad (5)$$

where $\beta = (C_a - C_\infty)/\rho(1 - C_a\bar{V}_A)$. An analytical solution is possible only for growth from zero size, and this problem was solved by Scriven.[8] By recourse to numerical methods, Cable and Evans[9] solved these equations for both growth and dissolution from finite initial size (a_0) for a wide range of values of α and β. For dissolving spheres it proved possible to plot the results in a way that makes it easy to interpolate the relation between a^* and t^* for any values of α from -0.10 to 2 and β from 0.01 to 4 using the data already available without undertaking further computations. It is therefore easy to produce the theoretical solutions suitable for gases in liquids for which one can usually assume that $\alpha = 0$.

Two important conclusions drawn from this theoretical investigation were that the relation between a^* and t^* varies considerably with solubility (β) and that even for small solubilities it differs considerably from that represented by eq 3 or a full solution of eq 2. Some comparisons showing good agreement between theory and experiment for oxygen and hydrogen bubbles in water have already been published.[10]

For the data shown in Figure 4 of Krieger, *et al.*, $\beta = 0.0267$ and $t^*_{a=0} = 27.37$ according to Cable and Evans (compared with $t^*_{a=0} = 18.7$ according to eq 3). The shape of the curve of a^* *vs.* t^* according to the full solution of eq 2 is expected to be very similar to that of the computed solution of eq 4 and 5, but the time to dissolve is expected to be little over half as big ($t^*_{a=0} <$

(1) I. M. Krieger, G. W. Mulholland, and C. S. Dickey, *J. Phys. Chem.*, **71**, 1123 (1967).

(2) H. S. Carslaw and J. C. Jaeger, "Conduction of Heat in Solids," Oxford University Press, London, 1959, pp 247–248.

(3) P. S. Epstein and M. S. Plesset, *J. Chem. Phys.*, **18**, 1505 (1950).

(4) M. Cable, *Glass Technol.*, **2**, 60 (1961).

(5) G. H. Frischat and H. J. Oel, *Glastechn. Ber.*, **38**, 156 (1965).

(6) L. E. Johns, Jr., *J. Phys. Chem.*, **71**, 4566 (1967).

(7) D. W. Readey and A. R. Cooper, *Chem. Eng. Sci.*, **21**, 917 (1966).

(8) L. E. Scriven, *ibid.*, **10**, 1 (1959).

(9) M. Cable and D. J. Evans, *J. Appl. Phys.*, **38**, 2899 (1967).

(10) M. Cable, *Chem. Eng. Sci.*, **22**, 1393 (1967).

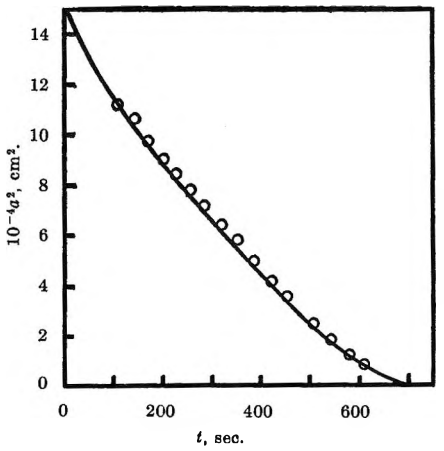

Figure 1. The theoretical relationship of Cable and Evans for $\alpha = 0$ and $\beta = 0.0267$ fitted to the experimental data of Krieger, *et al.*

18.7 sec). The diffusivity obtained by fitting the full quasi-stationary solution to the data is therefore expected to be little over half its correct value (see ref 9, Figure 5).

Figure 1 shows the data of Krieger, *et al.*, taken from their Figure 4 and the computer solution of Cable and Evans for $\alpha = 0$ and $\beta = 0.0267$, assuming that $a_0^2 = 15 \times 10^{-4}$ cm^2 and $t_{a=0} = 700$ sec. Agreement between theory and experiment is good and could be made excellent by slight adjustment to a_0 and $t_{a=0}$. The diffusivity obtained is 5.86×10^{-5} cm^2 sec^{-1}, which is about 1.7 times the value given by Krieger, *et al.* This discrepancy between the solution including convection of the fluid and the quasi-stationary result is of the magnitude expected and far bigger than Johns suggested. It seems paradoxical that inserting the initial limiting slope shown on the original Figure 4 in eq 3 gives $D = 4.5 \times 10^{-5}$ cm^{-2} sec^1, a value nearer to the computed value than that given by the full quasi-stationary solution.

Although the agreement between the data of Krieger, *et al.*, and the theory of Cable and Evans is, by itself, excellent, the diffusivity of 5.8×10^{-5} cm^2 sec^{-1} at 30° for oxygen in water is about twice the value expected on reviewing all the diffusivity values available. The conclusion drawn from this communication therefore is the disappointing one that neither the recommended value for the diffusivity of oxygen in water nor the best technique for measuring it can be proposed with confidence.

DEPARTMENT OF GLASS TECHNOLOGY M. CABLE
SHEFFIELD UNIVERSITY
SHEFFIELD, ENGLAND

RECEIVED APRIL 3, 1968

Reply to Communication by M. Cable

Sir: Since the recession of the bubble surface imposes an inward convection of liquid, the solute must diffuse "upstream." As a result, diffusion coefficients computed without considering this convection will necessarily be low. Whereas Johns estimates an error of *ca.* 1% for the systems studied by Krieger, Mulholland, and Dickey (KMD), the more elaborate analysis by Cable seems to indicate an error of *ca.* 70%. His fit to KMD's data is not optimal; the calculated line shows more curvature than do the data points, and all points except the first and last fall above the line. It is not possible without detailed computer calculations to determine the best fitting set of a_0 and β values, but they would probably not deviate greatly from those which Cable presents.

In the experimental method proposed by KMD, one can determine the time of bubble disappearance very accurately. Data on small bubbles were considered to be intractable, however, for the following reasons: (1) the diameter of the fiber is no longer negligible compared with the bubble diameter; (2) convective effects are presumably more important; (3) any interfacial impurities are more concentrated; and (4) the effect of surface tension on solubility becomes significant. For these reasons, the systematic departures at small bubble size between KMD's calculated line and their data were not considered by them to be serious; indeed, better correspondence can be achieved with their data by systematically ignoring points for $a < 0.3a_0$.

The KMD paper does present a new method of great promise for the study of bubble solution rates, but Cable shows that the analysis of the data to yield diffusion coefficients is beset by unresolved problems. The author is currently engaged in a program to improve the accuracy and reproducibility of the measurements, in the hope that when better data are available the questions which Cable raises can be answered.

DEPARTMENT OF CHEMISTRY IRVIN M. KRIEGER
CASE WESTERN RESERVE UNIVERSITY
CLEVELAND, OHIO 44106

RECEIVED JUNE 5, 1968

A Further Note on the Rate of Dissolving of Spherical Gas Bubbles

Sir: Recently the theoretical interpretation of the experimental method for determining the diffusivities of gases in liquids, reported by Krieger,[1] *et al.*, has been investigated by Johns[2] and Cable.[3] These authors account for the convective transport that is induced by the change of volume that accompanies the phase

(1) J. M. Krieger, G. W. Mulholland, and C. S. Dickey, *J. Phys. Chem.*, 71, 1123 (1967).
(2) L. E. Johns, *ibid.*, 71, 4566 (1967).
(3) M. Cable, *ibid.*, 72, 3356 (1968).

change but disagree over the importance of this factor in the calculation of diffusivities from experimental data. Johns made the stationary approximation and found an analytical solution, whereas Cable made a finite-difference approximation to essentially the same set of equations and found a numerical solution using a computing machine.

Cable fitted his numerical solution to a set of Krieger's data for oxygen dissolving in water and found that $D = 5.86 \times 10^{-5}$ cm^2 sec^{-1}, whereas Krieger, neglecting convection, reported that $D = 3.53 \times 10^{-5}$ cm^2 sec^{-1}, a value that is close to the literature value. Cable concluded therefore that convection is an important factor in Krieger's experiment and, by implication, in the experiments of many others. As reported earlier,[2] however, convection cannot be important in experiments with slightly soluble gases and does not mask the correct value of the diffusivity in these experiments. In order to confirm the earlier estimate, we make an exact calculation of the ratio of the convective mass flux to the diffusive mass flux at the surface of the bubble. For a homogeneous gas bubble at rest dissolving in a large volume of liquid, the balance equations at the bubble surface take the special form

$$\rho^g\dot{R} = \rho^l(\dot{R} - v^l)$$

$$\rho_1{}^g\dot{R} = \rho_1{}^l(\dot{R} - v^l) - j_1{}^l$$

where the superscripts g and l indicate the phase, and the notation of ref 2 is used. We find from these equations that

$$v^l = \epsilon\dot{R}$$

$$j_1{}^l = -\delta\dot{R}$$

where $\epsilon = (\rho^l - \rho^g)/\rho^l$ and $\delta = \rho_1{}^g - (1 - \epsilon)\rho_1{}^l$. If these results are used, the ratio of the convective part of the total flux of species 1 to the diffusive part, evaluated at the bubble surface, is easily seen to be

$$\frac{\rho_1{}^l v^l}{j_1{}^l} = -\frac{\rho_1{}^l\epsilon}{\rho_1{}^g - (1 - \epsilon)\rho_1{}^l}$$

or

$$\frac{\rho_1{}^l v^l}{j_1{}^l} = \frac{-\rho_1{}^l}{\rho_1{}^g} \quad (\text{for } \epsilon = 1)$$

For oxygen dissolving in water at 30° and 1 atm, we get

$$\frac{\rho_1{}^l v^l}{j_1{}^l} = -0.029$$

This calculation is exact and the result holds for all time; moreover, the fluxes are largest in absolute value at the bubble surface where their values must be known most accurately if the value of $\dot{R}$ is to be predicted correctly.

We should also investigate what the stationary approximation means and how solutions derived from it are to be used to interpret experimental data. When we set $\partial\rho_1/\partial t = 0$ in an initial-value problem we must give up the hope of satisfying the initial conditions and look for an asymptotic solution for large t. If we find such a solution, the absolute values of R and t may not be meaningful, but we still may use these values to calculate a parameter in the equation from experimental data taken for large values of t. Whatever the initial state may be, we suspect that after a sufficiently long time the state of the process will change slowly and a balance will be maintained between the moving source of species 1 and the concentration field carrying species 1 away from the surface.

Using the stationary solution[2] to interpret the data of Figure 4 of ref 1, we find that $D = 3.79 \times 10^{-5}$ cm^2 sec^{-1}. Neither the short time data nor the very long time data can be used, because the former reflects the initial conditions while the latter reflects the increased pressure in a small bubble as the surface tension begins to become important. Krieger's interpretation of these data is based upon an equation which reduces to the nonconvective stationary approximation for $R/\sqrt{\pi Dt} \ll 1$; however, only the short-time data are used to calculate the value $D = 3.53 \times 10^{-5}$ cm^2 sec^{-1}. Whatever the physical meaning of the term $R/\sqrt{\pi Dt}$ in Krieger's equation, it causes his value of D to be lower and closer to the literature values than that predicted by a purely stationary theory.

CHEMICAL ENGINEERING DEPARTMENT
UNIVERSITY OF FLORIDA
GAINESVILLE, FLORIDA 32601
L. E. JOHNS, JR.

RECEIVED MAY 8, 1968

The Extent of Association in Liquid Dimethyl Sulfoxide[1]

Sir: In a number of recent reviews on the solvent properties of dimethyl sulfoxide (DMSO), the latter has been described as a strongly associated liquid.[2] It is the purpose of this paper to suggest what local liquid structures are excluded from consideration as a result of calculations based on dielectric measurements. The Kirkwood equation[3]

$$\frac{(\epsilon_0 - \epsilon_\infty)(2\epsilon_0 + \epsilon_\infty)}{\epsilon_0(\epsilon_\infty + 2)^2}\left(\frac{M}{d}\right) = \frac{4\pi N_0\mu_0{}^2}{9kT}g$$

permits a description of those polar liquids which have specific short-range forces which hinder rotation of the

(1) This research was supported by a grant from the Research Corporation of America.

(2) D. Martin, A. Weise, and H. J. Niclas, *Angew. Chem. Int.*, **6**, 318 (1967).

(3) (a) J. G. Kirkwood, *J. Chem. Phys.*, **7**, 911 (1939); (b) A. D. Buckingham, *Discussions Faraday Soc.*, **43**, 205 (1967); J. B. Hasted in "Progress in Dielectrics," Vol. 3, J. B. Birks, Ed., Heywood & Co. Ltd., London, 1961, p 103.

molecule. The limiting dielectric permittivities at low and high frequencies are ϵ_0 and ϵ_∞ respectively; μ_0 is the permanent dipole moment of the free molecule; and d is the liquid density measured at temperature T. The correlation factor g is a measure, through statistical mechanics, of the short-range effects which hinder orientation between a molecule and its surrounding neighbors. For systems in which specific intermolecular forces orient neighboring dipole vectors in a parallel fashion, g is greater than unity; for an antiparallel configuration of dipoles, g is less than unity. For systems in which specific intermolecular forces are absent, g equals unity and Kirkwood's equation reduces to the Onsager expression for a normal polar liquid.[4]

Hence a calculation of g from available dielectric data should provide a measure of the association present in a polar liquid. Three possible association complexes have been proposed to explain the properties of liquid DMSO.[2] The suggested complexes would arise from the formation of O–H, S–H, or S–O intermolecular bridges. It has been convincingly pointed out by Allerhand and Schleyer[5] that hydrogen bonding will not involve C(sp^3)–H as a proton donor unless at least two adjacent electron-withdrawing groups are present on the carbon. This would appear to eliminate the possibility of an O–H bridge occurring in DMSO. Sulfur being less electronegative than oxygen, an S–H bridge seems to be even less likely to occur in DMSO.[2]

In all three cases, one can show that the existence of such association complexes would give rise to a correlation factor greater than unity. The proposal that O–H and S–H bridges are formed in liquid DMSO leads one to a predominately three-dimensional liquid structure. That such a structure would arise follows from both the nonlinearity of the molecule and the multiple proton sites for hydrogen bonding. Kirkwood has shown that structures of this type, if predominant, will produce a correlation factor greater than unity.[3] For example, calculations based on a similar model for water yielded a g value of 2.81, in good agreement with the experimentally determined value.[3a] An S–O intermolecular bridge would generate a linear n-mer. It has been shown that such a parallel arrangement of neighboring dipoles leads also to a correlation factor greater than unity and equal to the average number of monomer units in the chain.[6a] A good example of this is liquid cyanoacetylene, in which g is 2.08 at 281°K.[6b]

From the dielectric data of Schläfer and Schaffernicht,[7] the correlation factor of liquid DMSO has been calculated and plotted in Figure 1 as a function of temperature. Also included are literature values for N,N-dimethylformamide[8] and nitrobenzene,[9] two nonassociated liquids.[10]

It is evident that within experimental error the g values for all these liquids are near unity and have a temperature dependence which is consistent with normal polar-liquid behavior. Hence we conclude that

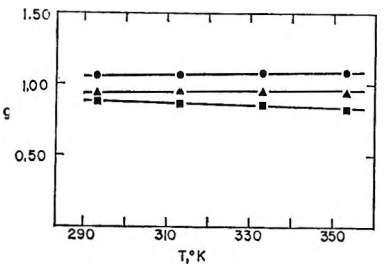

Figure 1. Plot of Kirkwood correlation factor, g as a function of temperature: ●, DMF; ▲, DMSO; ■, nitrobenzene.

the physical properties of DMSO cited as evidence for association in the liquid (boiling point, entropy of vaporization, etc.)[2] are due primarily to its large molecular dipole moment (4.3 D) and to the presence in the liquid of strong but nonspecific dipole–dipole forces.

Acknowledgment. Several helpful discussions with Robert Chang are gratefully acknowledged.

(4) R. H. Cole in "Progress in Dielectrics," Vol. 3, J. B. Birks, Ed., Heywood & Co. Ltd., London, 1961, p 70.

(5) A. Allerhand and P. Schleyer, *J. Amer. Chem. Soc.*, **85**, 1715 (1963).

(6) (a) R. H. Cole, *ibid.*, **77**, 2012 (1955); (b) W. Dannhauser and A. F. Flueckinger, *J. Chem. Phys.* **38**, 69 (1963).

(7) H. L. Schläfer and Schaffernicht, *Angew. Chem.*, **72**, 618 (1960).

(8) R. M. Meighan and R. H. Cole, *J. Phys. Chem.*, **68**, 509 (1964).

(9) J. Timmermans, "Physico-Chemical Constants of Pure Organic Compounds," Vol. 1, Elsevier Publishing Co., New York, N. Y., 1950, pp 591–593.

(10) For comparison purposes, ϵ_∞ was represented in each case by the usual approximation, $\epsilon_\infty = 1.1n^2$, where n is the refractive index measured at optical frequencies. Larger assumed values for ϵ_∞ will result in somewhat reduced g values.

DEPARTMENT OF CHEMISTRY
OCCIDENTAL COLLEGE
LOS ANGELES, CALIFORNIA 90041

RALPH L. AMEY

RECEIVED JUNE 17, 1968

On Radical Recombination Rates in SO_2-Doped Flames

Sir: In recent work on the ternary kinetics of radical recombination in SO_2-doped H_2–air flames, Fenimore and Jones[1] and also Kallend[2] have attributed the accelerated recombination rates to a catalytic mechanism

$$H + SO_2 + M \longrightarrow HSO_2 + M \qquad (1)$$

followed by regeneration of SO_2 by either of the reactions

$$HSO_2 + H \longrightarrow H_2 + SO_2 \qquad (2)$$

$$HSO_2 + OH \longrightarrow H_2O + SO_2 \qquad (3)$$

(1) C. P. Fenimore and G. W. Jones, *J. Phys. Chem.*, **69**, 3593 (1965).

(2) A. S. Kallend, *Trans. Faraday Soc.*, **63**, 2442 (1967).

Reaction 1 is favored because of the work of Webster and Walsh[3] who studied the inhibiting influence of SO_2 on the second explosion limit of H_2–O_2 mixtures as measured in KCl-coated vessels. The lowering of the second pressure limit at 784°K is consistent with step 1 occurring with a ternary constant $k_1 = 4 \times 10^{-32}$ cm^6 molecule^{-2} sec^{-1} (where M is H_2). Fenimore and Jones reported a higher value, $k_1 = 19 \times 10^{-32}$ cm^6 molecule^{-2} sec^{-1}, measured in low-pressure flames at 1550°K, while Kallend found the value $3.5 \times 10^{-32} < k_1 < 4.4 \times 10^{-32}$ (where M is the total flame gases) in atmospheric flames at temperatures ranging from 1620 to 1720°K.

The purpose of this communication is to draw attention to three points regarding this work. First, in flames it is doubtful that reaction 1 is the only catalytic reaction of SO_2 as a scavenger of radical excesses. The hydroxyl addition

$$OH + SO_2 + M \longrightarrow HOSO_2 + M \qquad (4)$$

seems just as likely and in fact would be indistinguishable from reaction 1, owing to the quasi-equilibrium maintained between [OH] and [H] by

$$OH + H_2 \rightleftarrows H_2O + H \qquad (5)$$

About 10 years ago McAndrew and Wheeler[4] made measurements of the effects of various additives on recombination rates in propane–air flames. Their SO_2 results were reported later in terms of a ternary rate constant for an over-all combination of reactions 1–4, *i.e.*, $k_{1+2+3+4} = 1.1 \times 10^{-29}$ cm^6 molecule^{-2} sec^{-1} (where M is SO_2). If we now recalculate these measurements assuming a slow step of either reaction 1 or 4, we find that $k_{1+4} = 11.0 \times 10^{-32}$ cm^6 molecule^{-2} sec^{-1} at 2080°K (where M is the total flame gases). This compares favorably with the later results in H_2–air flames.

Second, it is important to note that the propane-flame value was obtained in direct comparison with other additives to the same flame. There is no doubt of the superiority of SO_2 as a scavenger. If a similar catalytic scheme exists for CO_2, then McAndrew and Wheeler's work shows that the corresponding ternary constant at 2080°K is $k_{1'+4'} = 1.3 \times 10^{-32}$ (where M is the total flame gases).

Finally, the structure of the intermediate radicals is of interest. $HOSO_2$ would be quite probably pyramidal about an apex of the atom S. The S–O bond strength is likely in excess of 100 kcal/mol and for this reason reaction 4 should be considered in any flame system. Webster and Walsh suggested that the HSO_2 radical contains direct S–H bonding because the most weakly held electrons in SO_2 are constrained to an orbital on the S atom. Nevertheless, a structural case can be made for a thionyl form, HOSO, treating OH as a pseudofluorine atom. Also it is known that S–H bonding in most compounds is noticeably weaker (D(S–H) $\sim$ 85 kcal/mol) than S–O bonding in comparable compounds (D(S–O) $\sim$ 115 kcal/mol).

As an additive CO_2 is a good yardstick for comparison with SO_2, because the C and S electronegativities are nearly identical and yet the geometries are decidedly different. The propane-flame work suggests that corresponding CO_2 intermediates just do not form, or if they do there is no regeneration *via* reactions 2′ and 3′ and the CO_2 is lost. Unless some ionization process follows reactions 1′ and 4′ in preference to regeneration of CO_2 by reactions 2′ and 3′ (and this is difficult to believe), the assumption must be that very little HCO_2 or $HOCO_2$ is formed in these flames.

Using any of the empirical methods for estimating bond energies, it is apparent that the C–H or C–OH bond would be stronger than the corresponding S–H and S–OH bonds. Structurally, both HCO_2 and $HOCO_2$ would be probably planar or nearly so. However, in order to form at all, a considerable decrease in bond angle from the stable 180° in CO_2 is necessary. Perhaps this requirement is just too great making for high activation energies in reactions 2′ and 4′. Because SO_2 is already in a triangular configuration, rearrangement to form any of the pyramidal intermediates is much less severe with corresponding lower activation energies in reactions 1 and 4.

It might be easier to make a case for a linear HOCO radical as opposed to a triangular HCO_2, but the lack of efficiency of CO_2 as a scavenger suggests that HOCO is not an important species in flames. The inference here then is that the catalytic effect on recombination is through reaction of the additive with OH (reactions 4 and 4′) rather than with H (reactions 1 and 1′).

(3) P. Webster and A. D. Walsh, *Symp. Combust., 10th, Cambridge, Cambridge, Engl., 1964*, 463 (1965).

(4) T. McAndrew and R. Wheeler, *J. Phys. Chem.*, **66**, 229 (1962).

DEPARTMENT OF CHEMISTRY ROBERT WHEELER
QUEEN'S UNIVERSITY
KINGSTON, ONTARIO, CANADA

RECEIVED JULY 10, 1968